

# Combustion Research Gas Phase Chemical Physics Program

DOE Principal Investigators'  
Abstracts

April, 2013

Chemical Sciences, Geosciences, and Biosciences Division  
Office of Basic Energy Sciences  
Office of Science  
U.S. Department of Energy

The research grants and contracts described in this document are supported by the U.S. DOE Office of Science, Office of Basic Energy Sciences, Chemical Sciences, Geosciences and Biosciences Division.

## Foreword

This collection of active research abstracts illustrates the breadth and depth of basic research supported by the Department of Energy's Office of Basic Energy Sciences (BES) and, in large measure, by the chemical physics program that contributes to the development of a predictive capability for combustion processes. The long-term objective of this effort is the provision of theories, data, and procedures to enable the development of reliable computational models of combustion processes, systems, and devices.

We appreciate the privilege of serving in the management of this research program. In carrying out these tasks, we learn from the achievements and share the excitement of the research of the many sponsored scientists and students whose work is summarized in the abstracts published on the following pages.

We thank all of the researchers whose dedication and innovation have advanced DOE BES research. We look forward to our assembly in 2014 for our 34<sup>th</sup> annual meeting. *A DOE Combustion Research Meeting was not held in 2013.*

Michael Casassa  
Mark Pederson  
Wade Sisk



# *Table of Contents*



# Table of Contents

<b>Foreword</b> .....	iii
<b>Table of Contents</b> .....	v
<b>Abstracts</b> .....	1
<b><u>Principal Investigators' Abstracts</u></b>	
Millard H. Alexander - Kinetic processes of importance in combustion .....	1
Wesley Allen and Henry F. Schaefer III - Theoretical Studies of Elementary Hydrocarbon Species and Their Reactions.....	5
Robert S. Barlow - Turbulence-Chemistry Interactions in Reacting Flows.....	9
Josette Bellan - Modeling Reactions in High-Pressure Turbulence in the Cold Ignition Regime.....	13
Guillaume Blanquart - Towards predictive simulations of soot formation: from surrogate to turbulence.....	17
Joel M. Bowman - Theoretical Studies of Combustion Dynamics.....	21
Nancy J. Brown - Combustion Chemistry.....	25
Laurie J. Butler - Dynamics of Product Branching in Elementary Combustion Reactions: OH + Alkenes and Nitrogen Chemistry.....	29
David W. Chandler - Crossed-Molecular-Beam Studies of Energy Transfer.....	33
Jacqueline H. Chen - Petascale Direct Numerical Simulation and Modeling of Turbulent Combustion.....	37
Robert E. Continetti - Dynamics and Energetics of Elementary Combustion Reactions and Transient Species.....	41
F.F. Crim - Dissociation Pathways and Vibrational Dynamics in Excited Molecules and Complexes.....	45
H. Floyd Davis - Bimolecular Dynamics of Combustion Reactions.....	49
Michael J. Davis - Exploration and validation of chemical-kinetic mechanisms.....	53
Theodore S. Dibble - Dynamics of Radical Reactions in Biodiesel Combustion.....	57
Gary Douberly - Vibrational Spectroscopy of Transient Combustion Intermediates Trapped in Helium Nanodroplets.....	61
Kent M. Ervin - Hydrocarbon Radical Thermochemistry: Gas-Phase Ion Chemistry Techniques.....	65
Robert W. Field - Spectroscopic and Dynamical Studies of Highly Energized Small Polyatomic Molecules.....	69
Jonathan H. Frank - Quantitative Imaging Diagnostics for Reacting Flows.....	73
Michael Frenklach - Mechanism and Detailed modeling of Soot Formation.....	77
William H. Green - Computer-Aided Construction of Chemical Kinetic Models.....	81
Hua Guo - Quantum Dynamics of Elementary Combustion Reactions.....	85

Gregory E. Hall - Gas-Phase Molecular Dynamics: High Resolution Spectroscopy and Collision Dynamics of Transient Species.....	87
Nils Hansen - Flame Chemistry and Diagnostics.....	91
Ronald K. Hanson and Craig T. Bowman - Spectroscopy and Kinetics of Combustion Gases at High Temperatures.....	95
Lawrence B. Harding - Theoretical Studies of Potential Energy Surfaces.....	99
Martin Head-Gordon - Chemical Accuracy from Ab-Initio Molecular Orbital Calculations.....	103
John F. Hershberger - Laser Studies of Combustion Chemistry.....	107
So Hirata - Breakthrough Design and Implementation of Electronic and Vibrational Many-Body Theories.....	111
Mark R. Hoffmann - Generalized Van Vleck Variant of Multireference Perturbation Theory....	115
Ahren W. Jasper - Theoretical Kinetics and Non-Born–Oppenheimer Molecular Dynamics...119	
Ralf I. Kaiser - Probing the Reaction Dynamics of Hydrogen-Deficient Hydrocarbon Molecules and Radical Intermediates via Crossed Molecular Beams.....	123
Michael E. Kellman - Dynamical Analysis of Highly Excited Molecular Spectra.....	127
Christopher J. Kliewer - Time-Resolved Diagnostics.....	131
Stephen J. Klippenstein - Theoretical Chemical Kinetics.....	135
Stephen J. Klippenstein and Craig A. Taatjes et. al - Argonne-Sandia Consortium on High-Pressure Combustion Chemistry.....	139
Anna I. Krylov - Theoretical Modeling of Spin-Forbidden Channels in Combustion Reactions.....	143
Stephen R. Leone – Synchrotron Studies of Gas-Phase and Heterogeneous Chemistry Relevant in Combustion Environments.....	147
Marsha I. Lester - Intermolecular Interactions of Hydroxyl Radicals on Reactive Potential Energy Surfaces.....	151
William A. Lester, Jr. - Theoretical Studies of Molecular Systems.....	155
Joanna Lighty - Development of Kinetics for Soot Oxidation at High Pressures Under Fuel-Lean Conditions.....	159
Tianfeng Lu - Computational Flame Diagnostics for Direct Numerical Simulations with Detailed Chemistry of Transportation Fuels.....	163
Robert P. Lucht - Advanced Nonlinear Optical Methods for Quantitative Measurements in Flames.....	167
R. G. Macdonald - Time-Resolved Infrared Absorption Studies of Radical Reactions.....	171
Alexander M. Mebel - Theoretical Studies of Chemical Reactions Related to the Formation and Growth of PAHs and Molecular Properties of Their Key Intermediates...175	
Joe V. Michael - Flash Photolysis-Shock Tube Studies.....	179
H. A. Michelsen - Particle Diagnostics Development.....	183
Terry A. Miller - Detection and Characterization of Free Radicals Relevant to Combustion Processes.....	187
William H. Miller - Reaction Dynamics in Polyatomic Molecular Systems.....	191
Amy S. Mullin - Dynamics of Activated Molecules.....	195

Habib N. Najm - Reacting Flow Modeling with Detailed Chemical Kinetics.....	199
David J. Nesbitt - Spectroscopy, Kinetics and Dynamics of Combustion Radicals.....	203
Daniel M. Neumark - Radical Photochemistry and Photophysics.....	207
C. Y. Ng - Determination of Accurate Energetic Database for Combustion Chemistry by High-Resolution Photoionization and Photoelectron Methods.....	211
Joseph C. Oefelein - Large Eddy Simulation of Turbulence-Chemistry Interactions in Reacting Multiphase Flows.....	215
David L. Osborn - Kinetics and Dynamics of Combustion Chemistry.....	219
Carol A. Parish - A Theoretical Investigation of the Structure and Reactivity of the Molecular Constituents of Oil Sand and Oil Shale.....	223
David S. Perry - The Dynamics of Large-Amplitude Motion in Energized Molecules.....	227
Piotr Piecuch - New Single- and Multi-Reference Coupled-Cluster Methods for High Accuracy Calculations of Ground and Excited States.....	231
William J. Pitz and Charles K. Westbrook - Kinetic Modeling of Combustion Chemistry.....	235
Stephen B. Pope - Investigation of Non-Premixed Turbulent Combustion.....	239
Stephen T. Pratt - Optical Probes of Atomic and Molecular Decay Processes.....	243
Hanna Reisler - Photoinitiated Reactions of Radicals and Diradicals in Molecular Beams.....	247
Klaus Ruedenberg – Accurate Calculations and Analyses of Electronic Structure, Molecular Bonding and Potential Energy Surfaces.....	251
Branko Ruscic - Active Thermochemical Tables – Progress Report.....	255
Trevor Sears - Gas-Phase Molecular Dynamics: High Resolution Spectroscopy and Collision Dynamics of Transient Species.....	259
Ron Shepard - Theoretical Studies of Potential Energy Surfaces and Computational Methods.....	263
Raghu Sivaramakrishnan - Mechanisms and Models for Combustion Simulations.....	267
M. D. Smooke and M. B. Long - Computational and Experimental Study of Laminar Flames.....	271
John F. Stanton - Quantum Chemistry of Radicals and Reactive Intermediates.....	275
Arthur G. Suits - Universal and State-Resolved Imaging Studies of Chemical Dynamics.....	279
James Sutherland - A Novel Multi-scale Simulation Strategy for Turbulent Reacting Flows.....	283
Craig A. Taatjes - Elementary Reaction Kinetics of Combustion Species.....	287
Robert S. Tranter - Elementary Reactions of PAH Formation.....	291
Donald G. Truhlar - Variational Transition State Theory.....	295
Angela Violi - Developing a predictive model for the chemical composition of soot nanoparticles: Integrating Model and Experiment.....	299
Albert Wagner - Pressure Dependence of Combustion Reactions: Quantum Inelastic Dynamics On Automatically Generated Potential Energy Surfaces.....	303
Peter M. Weber - Ultrafast Structural Dynamics in Combustion Relevant Model Systems.....	307
Curt Wittig - Detailed Studies of Hydrocarbon Radicals: C <sub>2</sub> H Dissociation Dynamics.....	311
Margaret S. Wooldridge - Experimental Ignition Studies of Oxygenated Hydrocarbons.....	313
David R. Yarkony - Theoretical Studies of the Reactions and Spectroscopy of Radical Species Relevant to Combustion Reactions and Diagnostics.....	317

Hua-Gen Yu - Gas-Phase Molecular Dynamics: Theoretical Studies in Spectroscopy and Chemical Dynamics.....	321
Judit Zádor - Chemical Kinetics of Elementary Reactions.....	325
Timothy S. Zwier - Isomer-specific Spectroscopy and Isomerization in Aromatic Fuels.....	329

*Abstracts  
of  
Principal Investigator  
Presentations*



## Kinetic processes of importance in combustion

Millard H. Alexander (mha@umd.edu),<sup>1</sup> Lifang Ma,<sup>†</sup> Jacek Klos<sup>‡</sup>  
Department of Chemistry and Biochemistry, University of Maryland, College Park, MD 20742-2021  
Paul J. Dagdigian<sup>§</sup> and Qianli Ma<sup>†</sup>  
Department of Chemistry, The Johns Hopkins University, Baltimore, MD 21218-2685

### I. Program Scope

Our group studies inelastic and reactive collisions of small molecules, focusing on radicals important in combustion environments. Our goal is the better understanding of kinetic processes which may be difficult to access experimentally. An essential component is the accurate determination of potential energy surfaces (PES's). After fitting<sup>1</sup> the *ab initio* points to obtain global PESs, we treat the dynamics using time-independent (close-coupling) methods. Cross sections and rate constants for collisions of are determined with our Hibridon program suite,<sup>2</sup> which we continue to modify and extend.

### II. DOE Synergy

Alexander and Dagdigian maintain a close interaction with Hall and Sears at Brookhaven. In addition to the work on relaxation of methylene (described below), they have developed together a new Matlab-based algorithm for solving the kinetic master equation.<sup>3</sup> Alexander's group has also collaborated closely with Chandler's group at Sandia Livermore on the inelastic scattering of the NO radical.<sup>4</sup> The work of Dagdigian and Alexander on transport properties (described below) was initiated by extensive discussions with Brown at the Lawrence Berkeley Laboratory. Work on relaxation of the methyl radical has been used by Douberly, in DOE supported work<sup>5</sup> on this radical in He droplets. Also, Alexander and Dagdigian plan to collaborate with Lester in the interpretation of her DOE supported work<sup>6</sup> on electronic quenching of OH.

### III. Recent Progress and future work

This section reports several highlights of the work done so far under the direction of Alexander (as Principal Investigator) and Dagdigian (as Senior Investigator), and the proposed continuations contained in a renewal proposal they have submitted to DOE. Two of the main research thrusts are:

#### a. Inelastic scattering of polyatomic hydrides

Inelastic collisions of the methylene radical ( $\text{CH}_2$ ) are currently under experimental study at Brookhaven.<sup>7-9</sup> Since the inception of our DOE-funded program (fall 2009), we focused on the study of collisions of He with methylene in its  $\tilde{a}^1A_1$  state<sup>10</sup> and, more recently, in its  $\tilde{X}^3B_1$  ground state,<sup>11</sup> as well with the methyl radical ( $\text{CH}_3$ ) in its  $\tilde{X}^2A_2''$  ground electronic state.<sup>12,13</sup> Our work is among the first detailed simulations of state-to-state relaxation of asymmetric and symmetric top molecules.

Most recently, we have extended our earlier investigation in several directions: First, we have determined the  $\text{CH}_3\text{-He}$  and  $\text{CH}_2\text{-He}$  PES's to include the dependence on the umbrella motion (in the case of  $\text{CH}_3$ ) and the bending vibration (in the case of  $\text{CH}_2$ ; the vibrational potential and wave function for the  $v=3$  state are displayed in Fig. 1 on the next page). By averaging the PES's over the vibrational wave functions associated with these low-frequency vibrational modes, we can determine the coupling between the low-lying vibrational levels. This has allowed us to study, for the first time ever, ro-vibrational inelasticity in collisions of polyatomic hydrides.

For  $\text{CH}_3\text{-He}$ , we predict ro-vibrational relaxation to be nearly two orders of magnitude less probable than

---

<sup>1</sup> Principal investigator; <sup>†</sup> Graduate student; <sup>‡</sup> Research Assistant Professor; <sup>§</sup> Senior investigator.

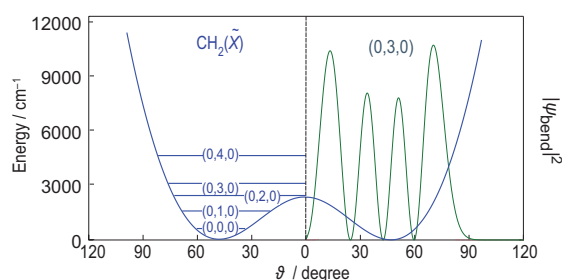


Fig. 1. (Left-hand panel) The dependence on the bending angle of the energies (horizontal lines) and potential for the bending motion in the  $X$  state of  $\text{CH}_2$ . Both bond lengths are frozen at their equilibrium values. (Right-hand panel) The dependence of the bending probability (the square of the bending wave function) on the bending angle for the  $(0,3,0)$  level of the  $X$  state.

rotational relaxation for  $\text{CH}_3$ . This confirms what one might have expected, based on far cruder dynamical models. Notwithstanding, it is important to have a firm prediction for the relative magnitude of vibrational compared to rotational relaxation probabilities, for guidance in developing combustion simulations. In the vibrational relaxation of the  $v=1$  umbrella level of  $\text{CH}_3$ , we find that the relaxation is enhanced by rotational excitation<sup>13</sup>; in most models for vibrational relaxation, the effect of rotation is not included. As seen in Fig. 2, ro-vibrational relaxation is a complex interplay between vibrational energy loss and change in the rotational angular momentum and its projection.

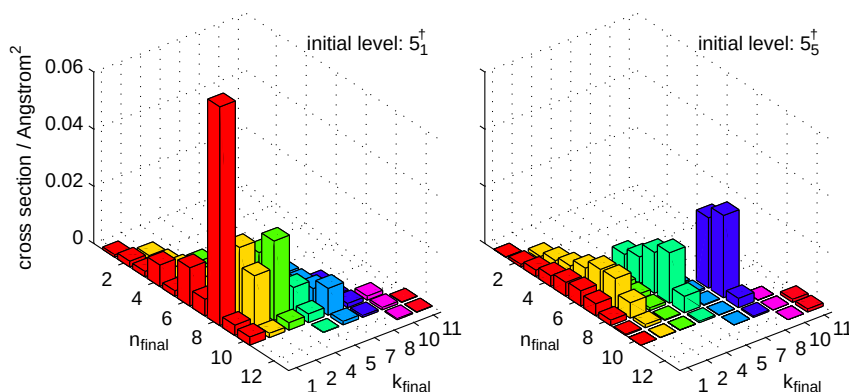


Fig. 2. Bar plot of the integral cross sections for  $v=1 \rightarrow 0$  ro-vibrationally inelastic scattering of *para*  $\text{CH}_3$  ( $k$  not a multiple of 3) in the  $jk_a=5_1$  and  $5_5$  levels of the  $v=1$  state (designated by the dagger) through collision with He at a collision energy of  $300 \text{ cm}^{-1}$ .

The  $(0,0,0)$  vibrational level of the  $\tilde{a}$  state of  $\text{CH}_2$  lies just above several excited bend levels of the electronic ground state. Certain rotational levels of these two electronic-vibrational states are (accidentally) nearly degenerate. Perturbational mixing between these states provides a collisional “gateway” for energy flow from the  $\tilde{a}$  to the  $X$  state. With our highly accurate PES’s and using the experimentally known positions of the ro-vibronic states of  $\text{CH}_2$ , we are now carrying out calculations to quantify the efficiency of this process. Cross sections (and, subsequently, rate constants) can be obtained by taking linear combinations of the  $S$  matrix elements for scattering of the  $\text{CH}_2$  molecule in either one or the other of these two states. Ultimately, we would like to obtain a complete characterization of the collisional relaxation of  $\text{CH}_2$  in its two lowest electronic states. Dagdigian has written a review of our work on inelastic collisions of small polyatomic intermediates.<sup>14</sup>

We will extend our calculations on collisional energy transfer to other polyatomic intermediates, for example, the HCO radical, which is a marker of the flame front.

## ii. Exact determination of transport properties

Chemical kinetic models describing non-homogeneous reacting systems require knowledge of the relevant transport properties for an accurate description of the temporal and spatial dependence of the species concentrations, as well as for the calculation of flame velocities and shapes and the production of pollutants in combustion media. To assess the accuracy of the simple models currently used to model

transport,<sup>15</sup> we have used our accurate *ab initio* PES for collisions of OH and CH<sub>2</sub> in their ground electronic state with He to determine transport cross sections, collision integrals and temperature dependent rates.<sup>16,17</sup>

In the case of OH, inclusion of the full anisotropy leads to differences of only a few percent in the transport properties when compared with spherical averaged potentials or even simple Lennard-Jones potentials. For the case of CH<sub>2</sub>, however, the larger degree of electronic anisotropy, particularly in the excited  $\tilde{a}$  state (due to the Lewis amphotericism of the electronic distribution<sup>10</sup>) results in a substantial deviation from the predictions of a spherical model. This can be seen in Fig. 3.

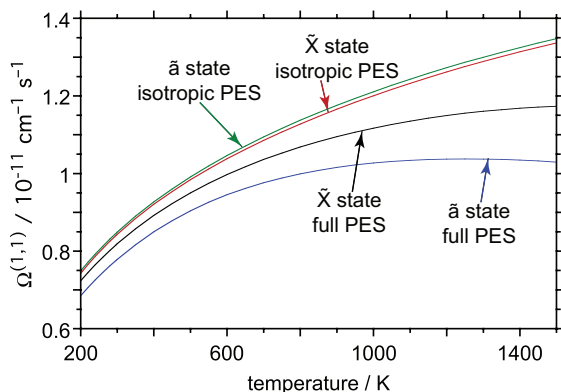


Fig. 3. The collision integral  $\Omega^{(1,1)}$  (which governs the diffusion coefficient) as a function of temperature, computed for the CH<sub>2</sub>( $X, a$ )-He systems. The full PES and the spherical average of the PES's has been used for both electronic states.

We will continue this investigation of the influence of the anisotropy of the PES on transport properties in for collisions of H atoms with H<sub>2</sub>O, a system of some relevance to combustion. In addition, we will investigate transport in collisions in which chemical reaction can occur. Since it is the small-impact-parameter collisions that lead to large-angle inelastic scattering, which make the largest contribution to transport properties, we anticipate that transport properties will be substantially decreased in the presence of a reactive channel. For the calculation of transport properties for systems that have a barrierless insertion pathway, we are adapting the quantum statistical capture theory of Manolopoulos and co-workers.<sup>18</sup>

#### IV. Interaction with other groups

Our work on the interaction of the methyl radical with He has encouraged work in the group of Orr-Ewing in Bristol, UK on the determination of differential cross sections for the scattering CH<sub>3</sub> with He. As mentioned above, our work on the CH<sub>3</sub>-He PES was invaluable to Douberly and co-workers in their analysis of the spectroscopy of CH<sub>3</sub> in He droplets.<sup>5</sup> Our interactions with both of these groups continues.

#### V. Publications and submitted journal articles supported by this project to date

1. L. Ma, M. H. Alexander, and P. J. Dagdigan, "Theoretical investigation of rotationally inelastic collisions of CH<sub>2</sub>( $\tilde{a}$ ) with helium," J. Chem. Phys. **134**, 154307 (13 pages) (2011)
2. M. H. Alexander, G. Hall, and P. J. Dagdigan, "The Approach to Equilibrium: Detailed Balance and the Master Equation," J. Chem. Educ. **88**, 1538-1540 (2011).
3. P. J. Dagdigan and M. H. Alexander, "Theoretical investigation of rotationally inelastic collisions of the methyl radical with helium", J. Chem. Phys. **135**, 064306 (9 pages) (2011).
4. L. Ma, M. H. Alexander, and P. J. Dagdigan, "Theoretical investigation of rotationally inelastic collisions of CH<sub>2</sub>( $\tilde{X}$ ) with helium," J. Chem. Phys. **136**, 224306 (9 pages) (2012).
5. P. J. Dagdigan and M. H. Alexander, "Exact quantum scattering calculation of transport properties for free radicals: OH( $X^2\Pi$ )-helium," J. Chem. Phys. **137**, 094306 (7 pages) (2012).
6. Q. Ma, P. J. Dagdigan, and M. H. Alexander, "Theoretical study of the vibrational relaxation of the methyl radical in collisions with He," J. Chem. Phys. **XXX**, yyyyy (2013).

7. P. J. Dagdigian and M. H. Alexander, "Exact quantum scattering calculations of transport properties:  $\text{CH}_2(X^3B_1, a^1A_1)$ -helium," *J. Chem. Phys.* **XXX**, yyyyy (2013).
8. P. J. Dagdigian, "Theoretical investigation of collisional energy transfer in polyatomic intermediates," *Int. Rev. Phys. Chem.* **32**, xxx-yyy (2013).

## VI. References

1. P. J. Dagdigian and M. Alexander, "Depolarization in  $\text{H}_2\text{O}$ -He collisions," *Mol. Phys.* **108**, 1159-1169 (2010).
2. HIBRIDON is a package of programs for the time-independent quantum treatment of inelastic collisions and photodissociation written by M. H. Alexander, D. E. Manolopoulos, H.-J. Werner, P. J. Dagdigian and others. More information and/or a copy of the code can be obtained from the website <http://www2.chem.umd.edu/groups/alexander/hibridon/hib43>.
3. M. H. Alexander, G. Hall, and P. J. Dagdigian, "The approach to equilibrium: Detailed balance and the master equation," *J. Chem. Educ.* **88**, 1538-1543 (2011).
4. J. J. Kay, J. D. Steill, J. Klos, G. Paterson, M. L. Costen, K. E. Strecker, K. G. McKendrick, M. H. Alexander, and D. W. Chandler, "Collisions of electronically excited molecules: differential cross-sections for rotationally inelastic scattering of  $\text{NO}(A^2\Sigma^+)$  with Ar and He," *Mol. Phys.* **110**, 1693-1703 (2012).
5. A. M. Morrison, P. L. Raston, and G. E. Douberly, "Rotational dynamics of the methyl radical in superfluid  $^4\text{He}$  nanodroplets," *J. Phys. Chem. A* **XXX**, yyyyy-zzzz (2013).
6. L. P. Dempsey, C. Murray, P. A. Cleary, and M. I. Lester, "Electronic quenching of OH  $A^2\Sigma^+$  radicals in single collision events with  $\text{H}_2$  and  $\text{D}_2$ : a comprehensive quantum state distribution of the OH  $X^2\Pi$  products," *Phys. Chem. Chem. Phys.* **10**, 1424-1432 (2008).
7. Y. Kim, A. V. Komissarov, G. E. Hall, and T. J. Sears, "Observation of the  $c^1A_1$  state of methylene by optical-optical double resonance," *J. Chem. Phys.* **123**, 24306 (4 pages) (2005).
8. Z. Wang, Y. Kim, G. E. Hall, and T. J. Sears, "State mixing and predissociation in the  $c\leftarrow a$  band system of singlet methylene studied by optical-optical double resonance," *J. Phys. Chem. A* **112**, 9248-9254 (2008).
9. S. K. Lee, Y. Kim, T. J. Sears, and G. E. Hall, private communication.
10. L. Ma, M. H. Alexander, and P. J. Dagdigian, "Theoretical investigation of rotationally inelastic collisions of  $\text{CH}_2(\tilde{a})$  with helium," *J. Chem. Phys.* **134**, 154307 (13 pages) (2011).
11. L. Ma, P. J. Dagdigian, and M. H. Alexander, "Theoretical investigation of rotationally inelastic collisions of  $\text{CH}_2(X)$  with helium," *J. Chem. Phys.* **136**, 224306 (9 pages) (2012).
12. P. J. Dagdigian and M. H. Alexander, "Theoretical investigation of rotationally inelastic collisions of the methyl radical with helium," *J. Chem. Phys.* **135**, 064306 (9 pages) (2011).
13. Q. Ma, P. J. Dagdigian, and M. H. Alexander, "Theoretical study of the vibrational relaxation of the methyl radical in collisions with He," *J. Chem. Phys.* **XXX**, yyyyy (2013).
14. P. J. Dagdigian, "Theoretical investigation of collisional energy transfer in polyatomic intermediates," *Int. Rev. Phys. Chem.* **32**, xxx-yyy (2013).
15. N. J. Brown and K. L. Revzan, "Comparative sensitivity analysis of transport properties and reaction rate coefficients," *Int. J. Chem. Kinetics* **37**, 538-553 (2005).
16. P. J. Dagdigian and M. H. Alexander, "Exact quantum scattering calculation of transport properties for free radicals: OH( $X^2\Pi$ )-helium," *J. Chem. Phys.* **137**, 094306 (7 pages) (2012).
17. P. J. Dagdigian and M. H. Alexander, "Exact quantum scattering calculations of transport properties:  $\text{CH}_2(X^3B_1, a^1A_1)$ -helium," *J. Chem. Phys.* **XXX**, yyyyy (2013).
18. E. J. Rackham, T. Gonzalez-Lezana, and D. E. Manolopoulos, "A rigorous test of the statistical model for atom-diatom insertion reactions," *J. Chem. Phys.* **119**, 12895-12907 (2003).

# Theoretical Studies of Elementary Hydrocarbon Species and Their Reactions

Wesley D. Allen and Henry F. Schaefer III  
Center for Computational Chemistry and Department of Chemistry  
University of Georgia, Athens, GA 30602-2525  
E-mail: wdallen@uga.edu and sch@uga.edu; Phone: (706) 542-7729

## Methylhydroxycarbene: Tunneling Control of a Chemical Reaction

In joint theoretical and experimental work published in *Science* within the last year,<sup>30</sup> methylhydroxycarbene (**1**, Me–C–OH) was generated for the first time by high vacuum flash pyrolysis (HVFP) of pyruvic acid (at 900 °C) and spectroscopically (IR, UV/Vis) characterized via immediate matrix isolation in solid Ar at 11 K. The identity of **1** was unequivocally confirmed by precise agreement between observed IR bands and theoretical anharmonic vibrational frequencies computed from an all-electron (AE) CCSD(T)/cc-pCVTZ complete quartic force field. The UV/Vis spectrum of **1** displays a broad band with maximum absorption at 393 nm (3.2 eV) that extends to around 460 nm (2.7 eV), in full accord with our aug-cc-pVTZ multireference coupled cluster [Mk-MRCCSD(T)] computations that gave a gas-phase vertical (adiabatic) excitation energy of 3.4 (2.7) eV. Surprisingly, we observed rapid disappearance **1** after cryogenic trapping. Upon standing in Ar at 11 K in the dark, the IR peaks of **1** decayed gradually via first-order kinetics with a half-life of  $t_{1/2} = 66 (\pm 5)$  min. In stark contrast, the bands of the deuterium isotopologue Me–C–OD (**d-1**) did not change under identical conditions for extended periods of time (at least 16 h). The kinetic experiments thus revealed that **1** isolated in its ground vibrational and electronic state exhibits facile [1,2]-hydrogen tunneling and that two conspicuous phenomena occur simultaneously: efficient penetration of a formidable 28.0 kcal mol<sup>-1</sup> barrier to yield acetaldehyde (**3**), and complete obstruction of the formation of vinyl alcohol (**4**) despite a much lower 22.6 kcal mol<sup>-1</sup> barrier.

We established the theoretical basis for the remarkable behavior of methylhydroxycarbene by computing pure tunneling rates for both **1** → **3** and **1** → **4**. The AE-CCSD(T)/cc-pCVTZ method was employed to precisely map out the associated intrinsic reaction paths (IRPs) descending from transition states TS<sub>1t-3</sub> and TS<sub>1t-4t</sub> (Fig. 1) and to determine zero-point vibrational energies (ZPVEs) along these steepest-descent routes. Final potential energy curves for the isomerization paths were then constructed from high-quality AE-CCSD(T)/cc-pCVQZ energy points appended with the ZPVEs. Tunneling probabilities for our high-accuracy IRPs were computed by exact numerical methods and also by WKB theory. This theoretical analysis yielded a tunneling half-life of 71 min for **1** → **3**, in close agreement with the observed rate of decay. Moreover, the computed half-life for **1** → **4** was 190 days, nicely explaining why vinyl alcohol is not the preferred product of methylhydroxycarbene isomerization, despite the lower barrier for formation of **4**.

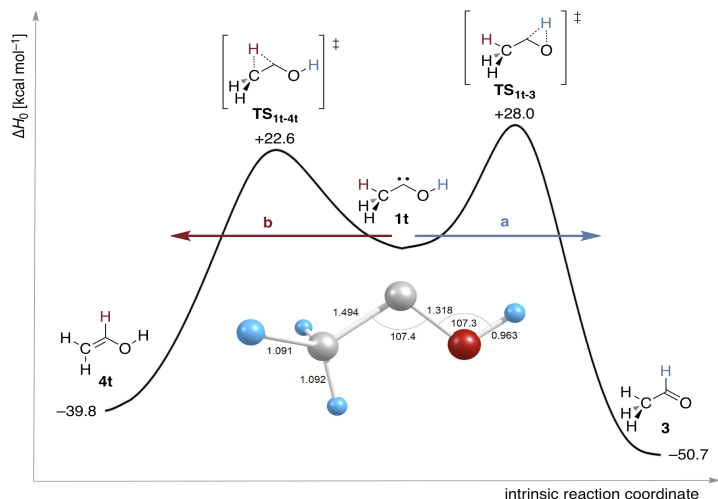


Figure 1. Energetic profiles for [1,2]H-shift isomerizations of *trans*-methylhydroxycarbene (**1t**); relative energies (in kcal mol<sup>-1</sup>) pinpointed from convergent focal-point analysis (FPA) computations. The bond lengths (Å) and angles (°) given for **1t** are ground-state optimum geometrical parameters given by AE-CCSD(T)/cc-pCVQZ theory. The curves are drawn quantitatively with the intrinsic reaction coordinate (IRC) in mass-weighted Cartesian space as the abscissa in order to reflect the proper barrier heights and widths for the two competing reactions. Simple visual inspection thus indicates a higher hydrogen tunneling probability for the more narrow energy profile of path **a**.

Methylhydroxycarbene highlights the possibility of reactions in which the observed product is neither the one requiring the lowest activation barrier nor the one with the lowest free energy but rather the one most readily reached by quantum mechanical tunneling. It is worth emphasizing that the remarkable tunneling behavior of

methylhydroxycarbene is not an isolated occurrence, as our earlier research demonstrated that both hydroxymethylene [*Nature* **453**, 906–909 (2008)] and phenylhydroxycarbene<sup>19</sup> spontaneously isomerize to their respective aldehydes via H-tunneling under large barriers near 30 kcal mol<sup>-1</sup>.

### Explicitly Correlated R12 Methods for Radicals

The Coulomb singularities in the electronic Hamiltonian require the exact wave function to display a cusp and corresponding depletion of electron density (Coulomb hole) when any interelectronic distance ( $r_{12}$ ) approaches zero. Unlike conventional electronic structure methods, approaches using wave functions that depend explicitly on  $r_{12}$  can effectively treat the cusp region without the need for large orbital basis sets. While closed-shell and spin-orbital explicitly correlated (R12) methodologies for coupled-cluster theory have been well developed, open-shell, spin-restricted R12 methods are lacking, which is problematic for the free-radical chemistry predominant in combustion applications. An ideal starting point for open-shell R12 methods is the symmetric exchange or Z-averaged approach. By introducing a symmetric exchange operator for  $\alpha$  and  $\beta$  electrons, the number of wave function parameters is drastically reduced. This formalism has negligible spin contamination compared to unrestricted methods, and the imposed spin constraints do not introduce size-consistency errors as in many other spin-adapted schemes. Building on our previous work on ZAPT2-R12 perturbation theory for open-shell systems,<sup>8</sup> we have now developed capabilities for the more complicated and robust ZA-CCSD-R12 method.<sup>22</sup> We have demonstrated the excellent basis set convergence of our ZA-CCSD-R12 method for a series of atomization energies. Specifically, with only a triple- $\zeta$  (TZ) quality basis, ZA-CCSD-R12 surpasses the accuracy of conventional computations with augmented sextuple- $\zeta$  (aV6Z) basis sets.

### The Propyl + O<sub>2</sub> Reaction System

Reactions of alkyl radicals (R·) with O<sub>2</sub> are ubiquitous in combustion, atmospheric chemistry, and biological processes. As the size of the alkyl radical grows, R + O<sub>2</sub> reactions rapidly become more complex, and isomerizations to hydroperoxyalkyl radicals (QOOH) can increase in importance relative to concerted elimination of HO<sub>2</sub>. The need for definitive *ab initio* theoretical research on propyl + O<sub>2</sub> is demonstrated by the disparity between the reaction energetics from the best existing electronic structure computations and parameters derived from master equation kinetic models that best reproduce the available body of experimental measurements. In a herculean investigation, we have fully optimized geometries at the CCSD(T)/cc-pVTZ level of theory for all chemically relevant minima and transition states of the *n*-propyl and *i*-propyl + O<sub>2</sub> systems (Fig. 2). Final energetics for combustion models were derived from explicit computations with basis sets as large as cc-pV5Z and correlation treatments as extensive as coupled cluster through full triples with perturbative inclusion of quadruple excitations [CCSDT(Q)]. Focal point analyses (FPA) targeting the complete basis set (CBS) limit of CCSDT(Q) theory were executed with inclusion of auxiliary corrections for core correlation and relativistic effects. For the *n*-propyl + O<sub>2</sub> system, the critical transition state (TS1) for concerted elimination of HO<sub>2</sub> lies 3.4 kcal mol<sup>-1</sup> below the reactants and 2.6 kcal mol<sup>-1</sup> lower than the key isomerization transition state (TS2) for CH<sub>3</sub>CHCH<sub>2</sub>OOH radical formation. Even the robust CCSD(T)/cc-pVQZ method yields a concerted elimination barrier that is 1.8 kcal mol<sup>-1</sup> too high, a striking result because such shifts of barrier heights in R + O<sub>2</sub> reactions can change branching fractions by an order of magnitude.

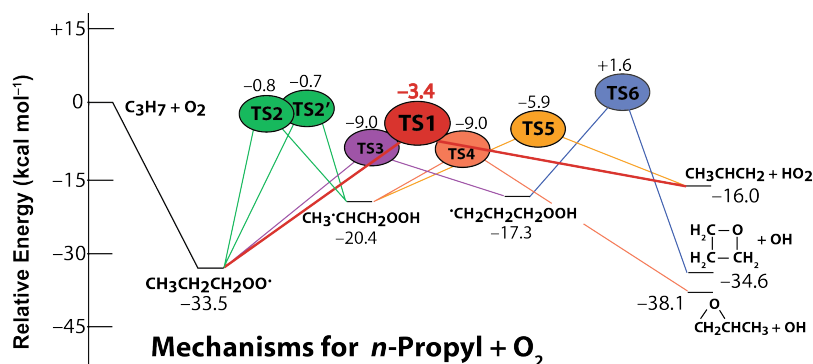


Figure 2. Energetic results from rigorous focal-point analyses (FPA) of the potential energy surfaces for the reactions of *n*-propyl radicals with molecular oxygen.

A new discovery is that two distinct, nearly isoenergetic transition states (Fig. 3; TS2, -0.84 kcal mol<sup>-1</sup>; TS2', -0.71 kcal mol<sup>-1</sup>) exist for producing the CH<sub>3</sub>CHCH<sub>2</sub>OOH radical by hydrogen transfer from the peroxypropyl intermediate. Earlier master equation kinetic models did not include the TS2' path, resulting in an empirically-

adjusted barrier height for  $\text{CH}_3\text{CHCH}_2\text{OOH}$  formation that is too low. Our definitive energetics for propyl +  $\text{O}_2$  provide benchmarks for critical assessment and improvement of current kinetic models.

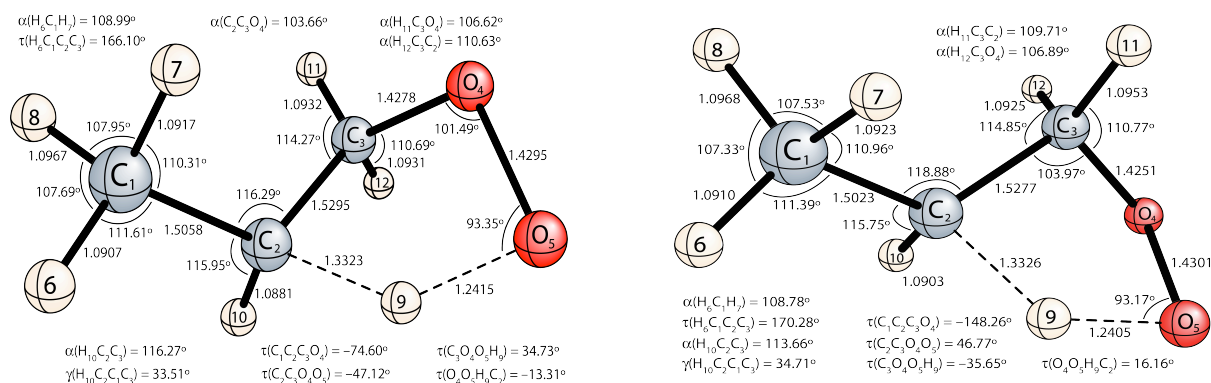


Figure 3. Competing CCSD(T)/cc-pVTZ transition states (**TS2**, left; **TS2'**, right) for formation of hydroperoxypropyl QOOH radicals from peroxypropyl intermediates.

### Vibrational Anharmonicity in Combustion Kinetics; Radical-Radical Abstraction Reactions

Collaborations with Stephen Klippenstein and Larry Harding at Argonne have been undertaken with two primary objectives: (1) Exploration of the effects of vibrational anharmonicity in combustion kinetics by rigorous investigation of the  $\text{H} + \text{H}_2\text{O}_2 \rightarrow \text{H}_2\text{O} + \text{OH}$  and  $\text{H} + \text{H}_2\text{O}_2 \rightarrow \text{H}_2 + \text{HO}_2$  reactions at the highest possible levels of electronic structure theory. Full quartic force fields and vibrational anharmonicity constants ( $x_{ij}$ ) were computed for the reactants and transition states of these two reactions at the coupled-cluster CCSD(T)/aug-cc-pVQZ level of theory. Anharmonic vibrational state counts were employed with various options for computation of rate coefficients. (2) Examination of paradigmatic potential energy surfaces for radical-radical abstractions, a general class of reactions in combustion chemistry. Our multireference coupled cluster methods (Mk-MRCC) were applied to the  $\text{CH}_3 + \text{C}_2\text{H}_5 \rightarrow \text{CH}_4 + \text{C}_2\text{H}_4$  hydrogen-abstraction reaction path, as well as the  $\text{CH}_3 + \text{CH}_3 \rightarrow \text{C}_2\text{H}_6$  recombination curve. These rigorous results provide important benchmarks for validating more approximate electronic structure methods for studying radical-radical abstraction and recombination.

### Publications Supported by DOE: 2009-2012

1. S. E. Wheeler, K. N. Houk, P. v. R. Schleyer, and W. D. Allen, "A Hierarchy of Homodesmotic Reactions," *J. Am. Chem. Soc.* **131**, 2547 (2009).
2. P. R. Schreiner, H. P. Reisenauer, E. Mátyus, A. G. Császár, A. Siddiqi, A. C. Simmonett, and W. D. Allen, "Infrared Signatures of the NCCO Radical," *Phys. Chem. Chem. Phys.* **11**, 10385 (2009).
3. A. C. Simmonett, H. F. Schaefer, and W. D. Allen, "The Enthalpy of Formation and Anharmonic Force Field of Diacetylene," *J. Chem. Phys.* **130**, 044301 (2009).
4. A. C. Simmonett, N. J. Stibrich, B. N. Papas, H. F. Schaefer, and W. D. Allen, "The Barrier to Linearity and Anharmonic Force Field of the Ketenyl Radical," *J. Phys. Chem. A* **113**, 11643 (2009).
5. S. E. Wheeler and H. F. Schaefer, "Thermochemistry of the HOSO Radical, a Key Intermediate in Fossil Fuel Combustion," *J. Phys. Chem. A* **113**, 6779 (2009).
6. Q. Hao, A. C. Simmonett, Y. Yamaguchi, D.-C. Fang, and H. F. Schaefer, "Structures and Energetics of  $\text{H}_6^+$  Clusters," *J. Phys. Chem. A* **113**, 13608 (2009).
7. Q. Cheng, F. A. Evangelista, A. C. Simmonett, Y. Yamaguchi, and H. F. Schaefer, "The Water Dimer Radical Cation: Structures, Vibrational Frequencies, and Energetics," *J. Phys. Chem. A* **113**, 13779 (2009).
8. J. J. Wilke and H. F. Schaefer, "The Subtleties of Explicitly Correlated Z-Averaged Perturbation Theory: Choosing an R12 Method for High-Spin Open-Shell Molecules," *J. Chem. Phys.* **131**, 244116 (2009).
9. J. C. Hargis, H. F. Schaefer, K. N. Houk, and S. E. Wheeler, "Non-Covalent Interactions of a Benzo[a]pyrene Diol Epoxide with DNA Base Pairs: Insight into the DNA Intercalation of (+) - BaP DE-2," *J. Phys. Chem. A* **114**, 2038 (2010).
10. J. A. Miller, S. J. Klippenstein, Y. Georgievskii, L. B. Harding, W. D. Allen, and A. C. Simmonett, "Reactions between Resonance-Stabilized Radicals: Propargyl + Allyl," *J. Phys. Chem. A* **114**, 4881 (2010).

11. T. Lu, Q. Hao, A. C. Simmonett, F. A. Evangelista, Y. Yamaguchi, D.-C. Fang, and H. F. Schaefer, "Low-Lying Triplet States of Diphosphene and Diphosphinylidene," *J. Phys. Chem. A* **114**, 9617 (2010).
12. Q. Wu, A. C. Simmonett, Y. Yamaguchi, Q. Li, and H. F. Schaefer, "Silacyclopropenylidene and its Most Important SiC<sub>2</sub>H<sub>2</sub> Isomers," *Barbara J. Garrison Special Issue, J. Phys. Chem. C* **114**, 5447 (2010).
13. E. Mátyus, C. Fábri, T. Szidarovszky, G. Czákó, W. D. Allen, and A. G. Császár, "Assigning Quantum Labels to Variationally Computed Rotational-Vibrational Eigenstates of Polyatomic Molecules," *J. Chem. Phys.* **133**, 034113 (2010).
14. Q. Wu, Q. Cheng, Y. Yamaguchi, Q. Li, and H. F. Schaefer, "Triplet States of Cyclopropenylidene and its Isomers," *J. Chem. Phys.* **132**, 044308 (2010).
15. U. Bozkaya, J. M. Turney, Y. Yamaguchi, and H. F. Schaefer, "The Barrier Height, Unimolecular Rate Constant, and Lifetime for the Decomposition of HN<sub>2</sub>," *J. Chem. Phys.* **132**, 064308 (2010).
16. H. Feng and W. D. Allen, "The Problematic F<sub>2</sub> + C<sub>2</sub>H<sub>4</sub> Reaction Barrier," *J. Chem. Phys.* **132**, 094304 (2010).
17. Q. Cheng, A. C. Simmonett, F. A. Evangelista, Y. Yamaguchi, and H. F. Schaefer, "Characterization of the BNNO Radical," *J. Chem. Theory Comput.* **6**, 1915 (2010).
18. Q. Wu, Q. Hao, J. J. Wilke, A. C. Simmonett, Y. Yamaguchi, Q. Li, D.-C. Fang, and H. F. Schaefer, "Anharmonic Vibrational Analysis for the Propadienylidene Molecule (H<sub>2</sub>C=C=C)," *J. Chem. Theory Comput.* **6**, 3122 (2010).
19. D. Gerbig, H. P. Reisenauer, C.-H. Wu, D. Ley, W. D. Allen, and P. R. Schreiner, "Phenylhydroxycarbene," *J. Am. Chem. Soc.* **132**, 7273 (2010).
20. Y. Yamaguchi and H. F. Schaefer, "Analytic Derivative Methods in Molecular Electronic Structure Theory and its Applications to Spectroscopy," in *Handbook of High Resolution Spectroscopy*, Editors M. Quack and F. Merkt (Wiley, Chichester, 2011).
21. D. S. Hollman, A. C. Simmonett, and H. F. Schaefer, "The Benzene + OH Potential Energy Surface: Intermediates and Transition States," *Phys. Chem. Chem. Phys.* **13**, 2214 (2011).
22. J. J. Wilke and H. F. Schaefer, "Spin-Restricted Explicitly Correlated Coupled Cluster for High-Spin Open-Shell Molecules. The Z-Averaged CCSD-R12 Approach," *J. Chem. Theory Comput.* **7**, 2416 (2011).
23. P. N. Ascik, J. J. Wilke, A. C. Simmonett, Y. Yamaguchi, and H. F. Schaefer, "The Beryllium Tetramer: Profiling an Elusive Molecule," *J. Chem. Phys.* **134**, 074110 (2011).
24. J. C. Hargis, E. Vöhringer-Martinez, H. L. Woodcock, A. Toro-Labbe, and H. F. Schaefer, "Characterizing the Mechanism of the Double Proton Transfer in the Formamide Dimer," *J. Phys. Chem. A* **115**, 2650 (2011).
25. H. Feng, W. Sun, Y. Xie, and H. F. Schaefer, "Structures and Energetics of the *t*-Butyl Cation: The Final Answer or a Never-Ending Story," *Chem. Eur. J.* **17**, 10551 (2011).
26. H. M. Jaeger, H. F. Schaefer, E. G. Hohenstein, and C. D. Sherrill, "Protonated Benzene Dimer: Demystifying Intermolecular Interactions of Complex Systems," *Computational and Theoretical Chemistry* **973**, 47 (2011).
27. J. M. Turney, A. C. Simmonett, R. M. Parrish, E. G. Hohenstein, F. Evangelista, J. T. Fermann, B. J. Mintz, L. A. Burns, J. J. Wilke, M. L. Abrams, N. J. Russ, M. L. Leininger, C. L. Janssen, E. T. Seidl, W. D. Allen, H. F. Schaefer, R. A. King, E. F. Valeev, C. D. Sherrill, and T. D. Crawford, "Psi4: An Open-Source *Ab Initio* Electronic Structure Program," *Wiley Interdisciplinary Reviews: Computational Molecular Science*, doi: 10.1002/wcms.93, published online, October 31, 2011.
28. J. Agarwal, J. M. Turney, and H. F. Schaefer, "Reaction Energetics for the Abstraction Process C<sub>2</sub>H<sub>3</sub> + H<sub>2</sub> → C<sub>2</sub>H<sub>4</sub> + H," *J. Phys. Chem. Lett.* **2**, 2587 (2011).
29. G. Koleva, B. Galabov, J. Kong, H. F. Schaefer, and P. R. Schleyer, "Electrophilic Aromatic Sulfonation with SO<sub>3</sub>: Concerted or Classical S<sub>E</sub>Ar Mechanism," *J. Am. Chem. Soc.* **133**, 19094 (2011).
30. P. R. Schreiner, H. P. Reisenauer, D. Ley, D. Gerbig, C.-H. Wu, and W. D. Allen, "Methylhydroxycarbene: Tunneling Control of a Chemical Reaction," *Science* **332**, 1300 (2011).
31. H. Feng, W. Sun, Y. Xie, and H. F. Schaefer, "Is There an Entrance Complex for the F + NH<sub>3</sub> Reaction?" *Chem. Asian J.* **6**, 3152 (2011).
32. B. S. Narendrapurapu, A. C. Simmonett, H. F. Schaefer, J. A. Miller, and S. J. Klippenstein, "Combustion Chemistry: Important Features of the C<sub>3</sub>H<sub>5</sub> Potential Energy Surface, Including Allyl Radical, Propargyl + H<sub>2</sub>, Allene + H, and Eight Transition States," *J. Phys. Chem. A* **115**, 14209 (2011).
33. D. S. Hollman and H. F. Schaefer, "In Search of the Next Holy Grail of Polyoxide Chemistry: Explicitly Correlated *Ab Initio* Full Quartic Force Fields for HOOH, HOOOH, HOOOOH, and Their Isotopologues," *J. Chem. Phys.* **136**, 084302 (2012).

## Turbulence-Chemistry Interactions in Reacting Flows

Robert S. Barlow  
Combustion Research Facility  
Sandia National Laboratories, MS 9051  
Livermore, California 94550  
barlow@sandia.gov

### Program Scope

This program is directed toward achieving a more complete understanding of turbulence-chemistry interactions in flames and providing detailed measurements for validation of combustion models. In the Turbulent Combustion Laboratory (TCL) simultaneous line imaging of spontaneous Raman scattering, Rayleigh scattering, and two-photon laser-induced fluorescence (LIF) of CO is applied to obtain spatially and temporally resolved measurements of temperature, the concentrations of all major species, mixture fraction, and reaction progress, as well as gradients in these quantities in hydrocarbon flames. The instantaneous three-dimensional orientation of the turbulent reaction zone is also measured by imaging of OH LIF or Rayleigh scattering at 355 nm in two crossed planes, which intersect along the laser axis for the multiscale measurements. These combined data characterize both the thermo-chemical state and the instantaneous flame structure, such that the influence of turbulent mixing on flame chemistry may be quantified. Our experimental work is closely coupled with international collaborative efforts to develop and validate predictive models for turbulent combustion. This is accomplished through our visitor program and through the TNF Workshop series. Although the past emphasis has been on nonpremixed and partially premixed combustion, the workshop and this program have expanded their scope in recent years to address a broad range of combustion modes, including premixed and stratified flames. We are also working to extend our quantitative multiscale diagnostics to more complex hydrocarbon fuels. Entry into these new research areas has prompted developments in both hardware and methods of data analysis to achieve unprecedented spatial resolution and precision of multiscale measurements. Within the CRF we collaborate with Jonathan Frank, who applies advanced imaging diagnostics to turbulent flames, and with Joe Oefelein, who performs high fidelity large-eddy simulations (LES) of our experimental flames in order to gain greater fundamental understanding of the dynamics of multi-scale flow-chemistry interactions.

### Recent Progress

#### *Multiply Conditioned Statistics on the Structure of Premixed and Stratified Turbulent Flames*

Stratified combustion, in which a flame propagates through non-uniformly mixed reactants, is common in practical systems and is often used to improve flame stability in overall-lean combustion strategies. However, fundamental questions regarding the structure and dynamics of turbulent stratified flames remain unanswered, experimental data for model testing has been limited, and the state of modeling of stratified combustion remains less advanced than that of nonpremixed or fully premixed combustion. In collaboration with Cambridge University (M.S. Sweeney and S. Hochgreb), we have conducted extensive investigations of a series of premixed and stratified turbulent CH<sub>4</sub>/air flames, stabilized on the co-annular bluff-body burner shown in Fig. 1. The test matrix includes fully premixed cases (same equivalence ratio in both annular

streams) and nonswirling cases, as well as two levels of stratification and two levels of swirl. In all 9 cases the global equivalence ratio is the same,  $\phi_g = (\phi_i + \phi_o)/2 = 0.75$ . Axial velocities of the inner flow, outer flow, and coflow were held constant, with  $U_i = 8.31$  m/s,  $U_o = 18.7$  m/s, and  $U_{cf} = 0.4$  m/s, giving Reynolds numbers based on hydraulic diameter of  $Re_i = 5,960$  and  $Re_o = 11,500$  for the annular flows. Even with modest Reynolds numbers, shear-generated turbulence yields relatively high  $u'/S_L$  (up to  $\sim 25$ ) in the region where the flame brush crosses the mixing layer, especially in the higher swirl cases.

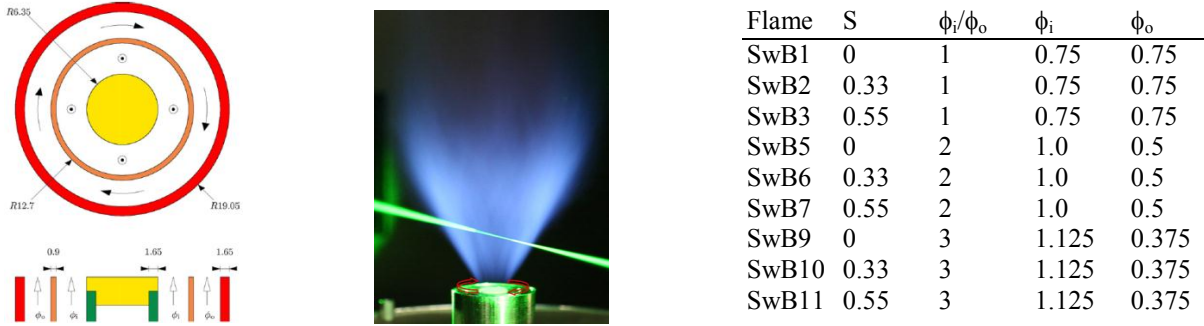


Figure 1. Diagram, photo, and matrix of test parameters for the Cambridge/Sandia stratified swirl burner. Swirl number  $S$  is the ratio of tangential to axial momentum from LDA measurements 2 mm above the exit.

Since our last BES abstract, we have published results on differences in scalar structure of stratified vs. premixed flames (Sweeney et al., *Combust. Flame* 161, 2012), based upon multiply conditioned statistics from large data sets (30,000-shot records) taken with the 6-mm probe centered at the location in each stratified case where the flame brush crosses the center of the mixing layer ( $\bar{\phi} = 0.75$ ). These records were acquired and processed using a method of spatial oversampling ( $\sim 20$   $\mu\text{m}$  spacing) and wavelet filtering, which significantly reduces noise while preserving the  $\sim 60$  mm optical resolution of the line-imaging system. In the conditional analysis we first isolate those realizations in the stratified flames that have a measured equivalence ratio at the location of maximum CO mass fraction,  $\phi_{CO}$ , within  $\pm 2.5\%$  of the average value,  $\bar{\phi}_{CO} = 0.751$ , measured in the turbulent premixed flames. The spatial location of maximum  $Y_{CO}$  is well resolved in these experiments, and it aligns within 10 microns of the location of peak heat release in Chemkin premixed flame calculations for  $0.7 < \phi < 0.8$ . These realizations were further conditioned on the degree of local stratification, which was determined from the change in  $\phi$  across the flame in each realization.

In Fig. 2a pdfs of the stratification metric,  $\Delta\phi/\Delta r$ , are shown for the three high-swirl cases (SwB3, SwB7, and SwB11) at 30 mm above the burner. Results for the two stratified cases are conditioned on  $\phi_{CO} = 0.751 \pm 2.5\%$ . These distributions were separated into bins centered at  $\Delta\phi/\Delta r = 0.0, 0.1, \dots, 0.4$ , and doubly conditioned averages were calculated. Results show that stratification produces significantly higher  $H_2$  and CO mass fractions throughout the flame, compared to the uniformly premixed case. High values of  $\Delta\phi/\Delta r$  produced increases in  $|\nabla T|$  and  $|\nabla c|$  throughout the flame and corresponding decreases in flame thickness, as shown in Fig. 2b. Stratification also causes broadening of the distribution of flame curvature. All of these effects of stratification on scalar structure are present in the unconditioned results, but they are better quantified and more obvious in the conditionally averaged results. In all, this is the most comprehensive data set we have created on any burner.

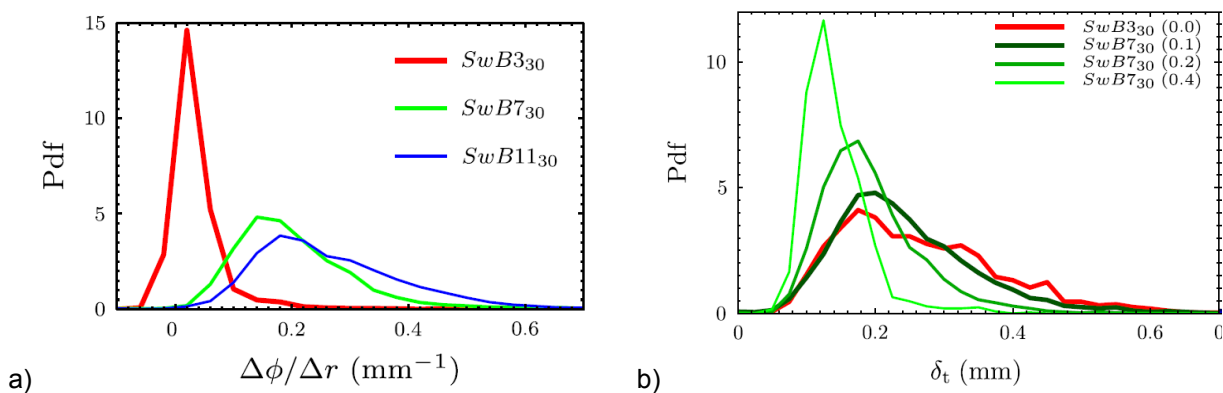


Figure 2. a) Pdfs of  $\Delta\phi/\Delta r$  conditioned on  $\phi_{CO} = 0.751 \pm 2.5\%$ . b) Doubly conditioned distributions of flame thickness,  $\delta_t = (T^* - T_{min})/|\nabla T|_{max}$ , where  $T^*$  is the temperature at the location of angle-corrected maximum gradient,  $|\nabla T|_{max}$ , in each realization.

### Development of Quantitative Raman Scattering Diagnostics for DME Flames

Another research priority identified by the TNF Workshop community is to extend model validation efforts to fuels beyond methane. This presents a significant challenge for Raman/Rayleigh diagnostics because the stable hydrocarbon intermediates in DME flames ( $CH_4$ ,  $C_2H_6$ ,  $C_2H_4$ ,  $C_2H_2$ ,  $CH_2O$ ) have mole fractions that are far from negligible and scattering cross sections very different from the parent fuel. Furthermore, the main C-H vibrational bands overlap for most of these species, theoretical Raman work on these molecules is limited or nonexistent, direct calibrations and spectral measurements on individual species can only be achieved over a limited temperature range, and signals from intermediate species in flames are small. Fuest et al. (*Combust. Flame* 159, 2012) developed a method of Raman/Rayleigh data analysis based on the use of laminar flame calculations to tabulate effective Rayleigh and Raman scattering cross sections for the “hydrocarbon channel” as a function of temperature. This is a reasonable approach for fully connected turbulent jet flames, and it is also likely that an analogous approach would work well for turbulent premixed flames into the regime of thin reaction zones, provided that preferential transport effects, such as reported by Barlow et al. (*Combust. Flame* 159, 2012), are not present. However, it is expected that this approach, based on an assumed flames structure, would be inappropriate for flames with strong turbulence-chemistry interactions, such as localized extinction. Consequently, we are developing methods to directly measure concentrations of the main stable hydrocarbon intermediates.

In collaboration with Isaac Ekoto, (funded by a Sandia Early Career LDRD award with R. Barlow as mentor) and Dirk Geyer, TU Darmstadt, we have developed experimentally based, temperature dependent Raman spectral libraries for  $CH_4$ ,  $C_2H_2$ ,  $C_2H_4$ ,  $C_2H_6$ , DME, and  $C_3H_8$ . Libraries of these relatively low resolution Raman spectra have been represented by skew-normal functions to facilitate interpolation, extrapolation, and tabulation. We will use these spectral libraries in the same way that we currently use theoretically based Raman spectral libraries from the RAMSES code from TU Darmstadt. That is to generate temperature dependent response curves (tabulations) for Raman signals from each molecule collected onto specific binned regions on the Raman detector. A Sandia report is complete, and publication is pending. Measurements on a series of partially-premixed, piloted DME/air jet flames are in progress.

## Future Plans

Experimental priorities for the next year include further developments on data acquisition/analysis methods for extension of spontaneous Raman scattering to achieve quantitative measurements in turbulent DME flames, including direct measurement of some stable intermediates (collaboration with TU Darmstadt, UT Austin, and Ohio State) and completion of experiments on a series of piloted partially premixed DME/air jet flames (collaboration Jonathan Frank and with Jeff Sutton and Frederik Fuest, Ohio State University).

## BES Supported Publications (2011 - present)

F. Fuest, R.S. Barlow, D. Geyer, F. Seffrin, A. Dreizler, "A Hybrid Method for Evaluation of 1D Raman Spectroscopy," *Proc. Combust. Inst.* **33**, 815–822 (2011).

J. Cai, C. Tong, R.S. Barlow, A.N. Karpetsis, "Conditionally filtered diffusion of mixture fraction and temperature in turbulent partially premixed flames," *Proc. Combust. Inst.*, **33**, 1505-1513 (2011).

M.S. Sweeney, S. Hochgreb, R.S. Barlow, "The structure of premixed and stratified low turbulence flames," *Combust. Flame* **158**, 935-948. (2011).

M.S. Sweeney, S. Hochgreb, M.J. Dunn, R.S. Barlow, "A comparative analysis of flame surface density metrics in premixed and stratified flames," *Proc. Combust. Inst.* **33**, 1419-1427 (2011).

F. Fuest, R.S. Barlow, D. Geyer, F. Seffrin, A. Dreizler, "Raman/Rayleigh scattering and CO-LIF measurements in laminar and turbulent jet flames of dimethyl ether," *Combust. Flame* **159**, 2533-2562 (2012).

R.S. Barlow, M.J. Dunn, M.S. Sweeney, S. Hochgreb, "Effects of preferential transport in turbulent bluff-body-stabilized lean premixed CH<sub>4</sub>/air flames," *Combust. Flame* **159**, 2563-2575 (2012).

M.S. Sweeney, S. Hochgreb, M.J. Dunn, R.S. Barlow, "The structure of turbulent stratified and premixed methane/air flames I: Non-swirling flows," *Combust. Flame* **159**, 2896-2911 (2012).

M.S. Sweeney, S. Hochgreb, M.J. Dunn, R.S. Barlow, "The structure of turbulent stratified and premixed methane/air flames II: Swirling flows," *Combust. Flame* **159** 2912-2929 (2012).

A. Sevault, M.J. Dunn, R.S. Barlow and Mario Ditaranto, "On the structure of the near field of oxy-fuel jet flames using Raman/Rayleigh laser diagnostics," *Combust. Flame* **159**, 3342-3352 (2012).

M.S. Sweeney, S. Hochgreb, M.J. Dunn, R.S. Barlow, "Multiply conditioned analyses of stratification in highly swirling methane/air flames," *Combust. Flame* **161**, 322-334 (2012).

M.J. Dunn, R.S. Barlow, "Effects of preferential transport and strain in bluff body stabilized lean and rich premixed CH<sub>4</sub>/air flames," *Proc. Combust. Inst.* **34**, 1411-1419 (2013).

R. Zhou, M.S. Sweeney, R.S. Barlow, S. Hochgreb, "Flow field measurements of a series of turbulent premixed and stratified methane/air flames," *Combust. Flame* (accepted).

**TNF Workshop Information:** <http://www.sandia.gov/TNF>

# Modeling Reactions in High-Pressure Turbulence in the Cold Ignition Regime

Josette Bellan

Mechanical and Civil Engineering Department, California Institute of Technology  
Pasadena, CA 91125

[Josette.Bellan@jpl.nasa.gov](mailto:Josette.Bellan@jpl.nasa.gov)

DOE Award Number: **DE-FG02-09ER16107**

STRIPES award number of **SC0002679**

## I. Program Scope

This study addresses issues highlighted in the Basic Energy Needs for Clean and Efficient Combustion of 21st Century Transportation Fuels (DOE BES, 2006) under the topic of Combustion under Extreme Pressure. It is there noted that “the most basic concepts of thermal autoignition” are “based on experience and theory at near atmospheric pressures” and that “as pressure increases significantly..., many of these conceptual pictures begin to change or disappear”. It is also stated “A better description of the coupling and interaction of high pressure flow and molecular transport processes with chemistry is also necessary”, particularly because “Ignition and flame propagation of alternative and renewable fuels, as well as of the changing feed stocks of conventional fossil-based fuels, are very likely to be much different at very high pressures than under the more familiar, lower pressure conditions of current engines.” Recognizing that “Under such (*increasing pressure*) conditions distinctions between gas and liquid phases become moot, new equations of state must be used...”, it is immediately apparent that there must be “a re-examination of the basic assumptions that govern the physics and chemistry related to combustion; and the need for this type of re-examination increases as the combustion pressure increases.” This recognition is also stated under the topic of Multiscale Modeling since due to the new equations of state “The combination of unexplored thermodynamic environments and new physical and chemical fuel properties results in complex interactions among multiphase (*according to the above, the multiphase distinction becomes moot with increasing pressure*) fluid dynamics, thermodynamic properties, heat transfer, and chemical kinetics that are not understood even at a fundamental level.” From the theoretical viewpoint for “systems at high pressure, fluid dynamic time scales can be comparable to chemical time scales.” and therefore “completely diffusion-controlled reactions ... can become important”.

Thus, the objective of this study is the investigation of the coupling among thermodynamics, transport properties, intrinsic kinetics and turbulence under the high-pressure and the relatively (with respect to combustion) low-temperature conditions typical of the auto-ignition regime, with particular emphasis on the manifestation of this coupling on the effective kinetic rate. As planned, we established collaboration with Dr. Joseph Oefelein of the Combustion Research Facility at Sandia Livermore to work together towards implementing the models developed in this research into the high-pressure Large Eddy Simulation code under development by him at Sandia.

## II. Recent Progress

This report contains results obtained during the last year of study. The focus of this last year was to understand the features of high-pressure multi-species mixing before undertaking

reactive flow simulations. To this end we have performed a suite of Direct Numerical Simulations (DNS) realizations and analyzed them; the eight DNS realizations were obtained in the context of a temporal mixing layer by considering the effect of the initial Reynolds number ( $Re$ ), the effect of pressure and that of the initial composition (various amounts of  $n$ -heptane, nitrogen, oxygen, carbon dioxide and water). The DNSs use accurate transport properties computed according to mixing rules and utilize the Peng-Robinson equation of state [i]. The thermal conductivity and viscosity are computed using the mixing rules described in [ii]. The binary mass-diffusion coefficients are computed according to [iii], and they, together with the EOS, form the building blocks for computing the  $(5 \times 5)$  mass diffusion coefficient matrix according to [iv]. The thermal diffusion factors are also computed according to [iv] mixing rules. For each specified value of  $Re$ , a reference viscosity is obtained to enable DNS at the specified  $Re$  value; the ratio of the reference viscosity to the physical viscosity yields a factor by which all other physical transport properties are scaled so as to maintain the physical values of the Schmidt ( $Sc$ ) and Prandtl ( $Pr$ ) numbers. Each DNS realization reached a state having turbulent characteristics, and the analysis was mainly performed on this particular state. Because each species mass flux depends on the gradients of all species, on the temperature gradient and on the pressure gradient, in order to understand the salient aspects of the flow, a diagonalization has been performed which enabled the definition of an effective mass-diffusion coefficient for each species and an effective  $Sc$ . The same strategy was used for the heat flux to define an effective thermal conductivity and an effective  $Pr$ . Some results from the computations are illustrated in Fig. 1 showing that  $n$ -heptane which was initially segregated in

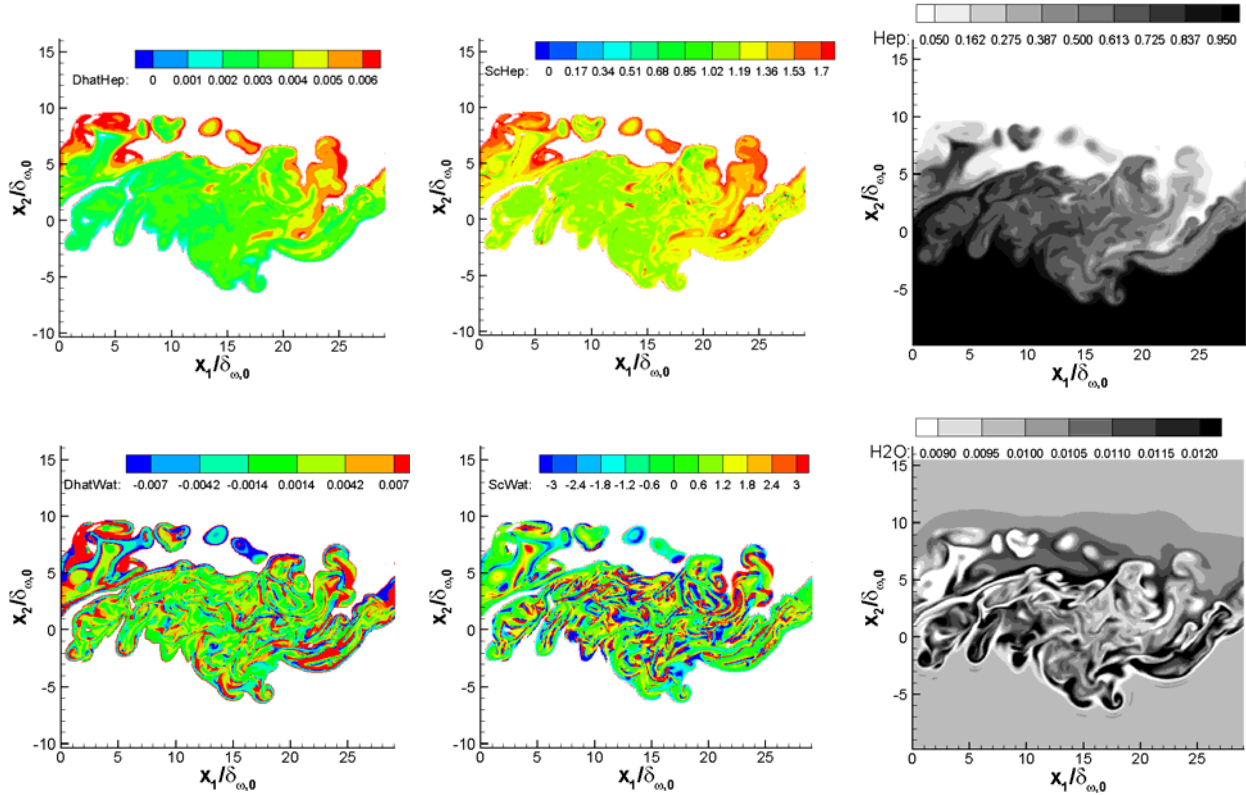


**Figure 1. Effective diffusivities (left column), effective Schmidt numbers (middle column) and mass fractions (right column).  $n$ -Heptane - top row; water - bottom row.  $p=60$  atm in the free stream and  $Re_0=600$ . Results are depicted in a spanwise plane at the transitional time corresponding to  $Re=1264$ , where  $Re$  is based on the momentum thickness.**

the lower stream, and water which was present in both streams behave very differently. Whereas the *n*-heptane effective diffusivity is positive, that of water (and CO<sub>2</sub> which was also initially distributed over the entire field) has both positive and negative values; the negative effective diffusivity values indicates species spinodal decomposition, meaning that the species naturally segregates into regions of high density and low density as seen in the last column of Fig. 1. The effective Sc exceeds unity for all species, as does the effective Pr and the effective Lewis number (Le), this last result being an indicator that if this fact persists for reactive flow simulations, despite the possible evidence of flamelets [v], the flamelet model of Peters [vi] may not apply. The effective values of Pr were generally in the 1-5 range which encompasses the 4-5 range of R-12 liquid refrigerant. We showed that a necessary and sufficient condition for species spinodal decomposition occurrence is that the particular species be initially present in both streams; this is why *n*-heptane, nitrogen and oxygen never experienced spinodal decomposition during the physical time of the simulations. We also found that the typical requirement that each species undergoing spinodal decomposition must be initially uniformly distributed [vii] is not necessary; in fact non-uniformity will promote, through gradients, the diffusion causing spinodal decomposition. At otherwise same initial conditions except for the species distribution, mixtures where spinodal decomposition occurs are more turbulent than those where it does not, this being due to the additional gradients created by the spinodal decomposition; these gradients act akin to a solid mesh in creating turbulence.

We also demonstrated the crucial effect of off-diagonal diffusion in terms of depicting the physics of the problem.

Indeed, a thorough comparison between the diagonal elements of the species mass-diffusion matrix and the corresponding effective species-specific diffusion coefficients, as shown in Fig. 2 for oxygen and *n*-heptane, elucidated the crucial effect of the off-diagonal terms of the species-mass diffusion matrix, all of which are by a factor of O(10<sup>1</sup>)-O(10<sup>2</sup>) smaller than the diagonal terms. If one were to neglect these off-diagonal terms, then (1) a major portion of the diffusivity small-scale structure in the mixing layer would be missed, (2) since all diagonal elements are

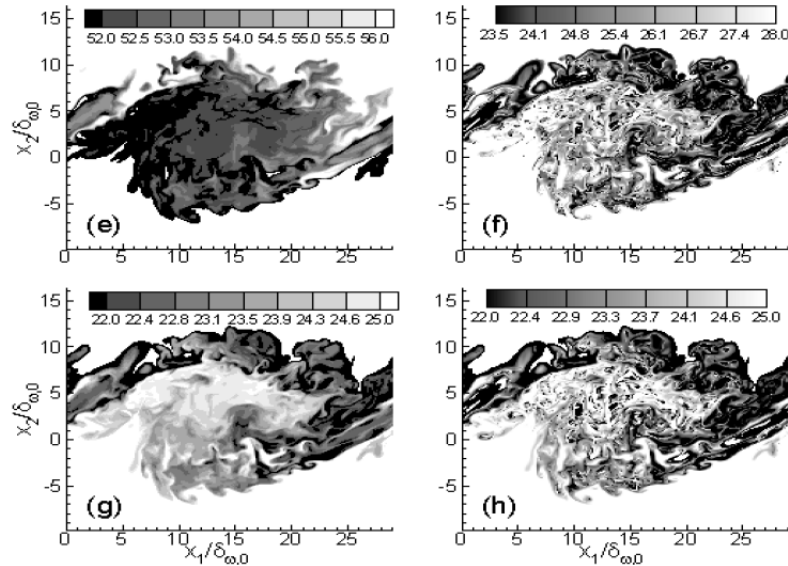


**Figure 2. Product of the density and diagonal diffusion coefficients (left column). Product of the density and effective diffusion coefficients (right column). Units: 10<sup>-6</sup> kg/( m s). Oxygen – top row; *n*-heptane -- bottom row. p=60 atm in the free stream and Re<sub>0</sub>= 2000. Results are depicted at the transitional time when Re based on the momentum thickness is 3804.**

positive, then no species spinodal decomposition would be observed for the species for which it occurs, (3) the qualitative aspect of diffusion would be distorted from reality (i.e. incorrect placement of high and low diffusivity regions) for a species as important as oxygen, and (4) the

magnitude of the diffusivity for light species (e.g. oxygen) could be in error by a factor of 2 implying a correspondingly erroneous mixture ignition-delay time. Clearly, without the off-diagonal terms, the physics of the problem would be entirely missed. Therefore, one must be cautious about utilizing the popular zeroth-order approximation of the diffusion matrix which describes the diffusion of each species into the mixture and results in a diagonal matrix which not only would be entirely inadequate for portraying small-scale molecular mixing but would additionally be unable to describe species spinodal decomposition because all the matrix elements are positive. Mathematically, the importance of the small off-diagonal terms is consistent with asymptotic expansion concepts wherein the crucial behavior is embodied in a small parameter.

We have extended our model and code to reactive flows; the reactive-flow code is operational. We also have defined an appropriate Damköhler number (Da). Currently, the activities are focused on selecting a Da value which will permit reaching ignition at the transitional state, when the flow is turbulent, so as to allow the study of turbulent ignition.

The PI has continued the collaboration with Dr. Oefelein by providing the information developed in [3], and Dr. Oefelein indicated that experiments will focus on this new physics.

### III. Future Plans

The following activities are planned:

- Conduct a series of reactive-flow DNS to examine and understand turbulent ignition.
- Analyze *a priori* the reacting-flow database and propose subgrid-scale models for the turbulent reaction terms.

### IV. References

- Harstad, K.; Miller, R. S.; Bellan, J. *A.I.Ch.E. J.* **1997**, *43*(6), 1605
- Reid, R. C.; Prausnitz, J. M.; Poling, B. E. *The Properties of Gases and Liquids*, 4th edition, McGraw-Hill, NY, **1987**
- Harstad, K.; Bellan, J. *Journal of Chemical Physics* **2004a**, *120*(12), 5664
- Harstad, K.; Bellan, J. *Ind. & Eng. Chem. Res.* **2004b**, *43*(2), 645
- Williams, F A. *Recent advances in the theoretical descriptions of turbulent diffusion flames* (ed. S. Murthy), Plenum, N. Y., **1975**, 189
- Peters, N., *Turbulent Combustion*, Cambridge University Press, **2000**
- Nauman, E. B and He, D. Q., *Chem. Eng. Sci.*, **2001**, *56*, 1999

### V. Publications, presentations and submitted articles supported by this project September 2011-April 2013

- [1] Masi, E.; Bellan, J; Harstad, K. Direct Numerical Simulation of High-Pressure Multispecies Turbulent Mixing in the Cold Ignition Regime, paper AIAA 2012-0351, presented at the 50th Aerospace Sciences Meeting, Nashville, TN, January 9-12, 2012
- [2] Masi, E.; Bellan, J; Harstad, K. Modeling and Direct Numerical Simulation of High-Pressure Multispecies Turbulent Mixing in the Cold Ignition Regime, poster presentation at the 34<sup>th</sup> International Symposium on Combustion, August 2012
- [3] Masi, E.; Bellan, J; Harstad, K.; Okong'o, N., Multi-species turbulent mixing under supercritical-pressure conditions: modeling, Direct Numerical Simulation and analysis revealing species spinodal decomposition, accepted in *J. Fluid Mech.*, 01/25/2013

## Towards predictive simulations of soot formation: from surrogate to turbulence

Guillaume Blanquart  
Department of Mechanical Engineering  
California Institute of Technology  
1200 E. California Blvd., Pasadena, CA 91125

### Objectives

The combustion of hydrocarbon fuels, including kerosene, gasoline, and diesel, leads to the formation of soot particles which are known to be the source of several health problems and environmental issues.

The objective of the proposed work is to reduce the gap in the present understanding and modeling of soot formation both in laminar and turbulent flames. This effort spans several length scales from the molecular level to large scale turbulent transport. More precisely, the objectives are three fold: 1) develop a *single combined chemical and soot model* validated for all relevant components usually found in real fuel surrogates; 2) develop a framework able to *explain the complete evolution of soot particles* from cluster of PAHs to oxidation of large fractal aggregates; 3) *understand and model the interplay* between unsteady chemistry, differential diffusion, and turbulent transport.

### Recent progress

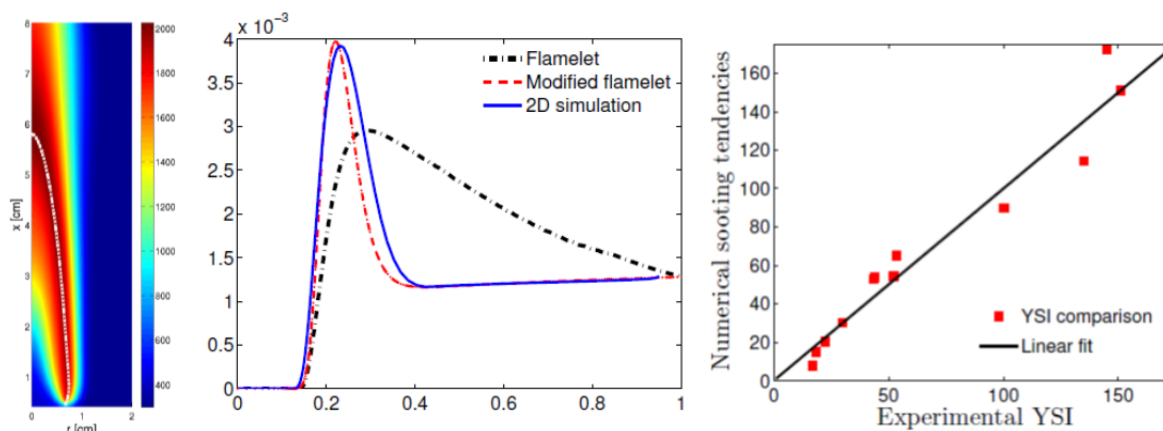


**Figure 1.** Temperature for the 2D coflow diffusion flame (left). Comparison of dopant mass fraction profiles for the conventional and modified flamelet models (center). Linear relation between the measured YSI in the literature and the numerically computed YSI (right).

#### *Predicting sooting tendencies*

The intent of this part is to predict the experimental sooting tendencies [Combust. Flame 148 (2007) 10-222] from a detailed chemical mechanism with relatively low computational cost, using a flamelet-based model. Towards that goal, direct numerical simulations using finite-rate chemistry are conducted on a methane-air confined axisymmetric co-flow diffusion flame to provide reference data. Soot transport model is excluded in these direct simulations for both simplicity and to be unbiased from the choice of soot model used. Sooting tendencies are estimated exclusively from the increment of polycyclic aromatic hydrocarbon (PAH) dimer production rate along the centerline when the flame is doped. Calculations using the conventional steady state diffusion flamelet model are performed and this model

is shown to be inadequate in reproducing the correct species profiles on the centerline of the flame, where the sooting tendencies are defined. The main reason for the failure of the conventional flamelet model is due to the neglect of multidimensional convection and diffusion effects. In an effort to overcome these deficiencies, a new numerical framework based on modified flamelet equations is proposed. The flamelet equations are re-derived for species mass fractions along the centerline of the co-flow diffusion flame considered. These equations take into account the effects of multidimensional diffusion and convection of species in mixture fraction space due to non-unity Lewis numbers. The modified flamelet equations take as input the temperature, convective velocity, and scalar dissipation rate profiles calculated from the direct simulation of the diffusion flame. The numerical sooting tendencies for both non-aromatic and aromatic test species are then calculated using on the PAH dimer production rate generated from the flamelet solutions doped by the test species. These first numerically-computed sooting tendencies are derived from a detailed chemical kinetic mechanism and are in good agreement when compared to experimental values (Figure 1).

This work has been accepted recently for publication in *Combustion and Flame*.

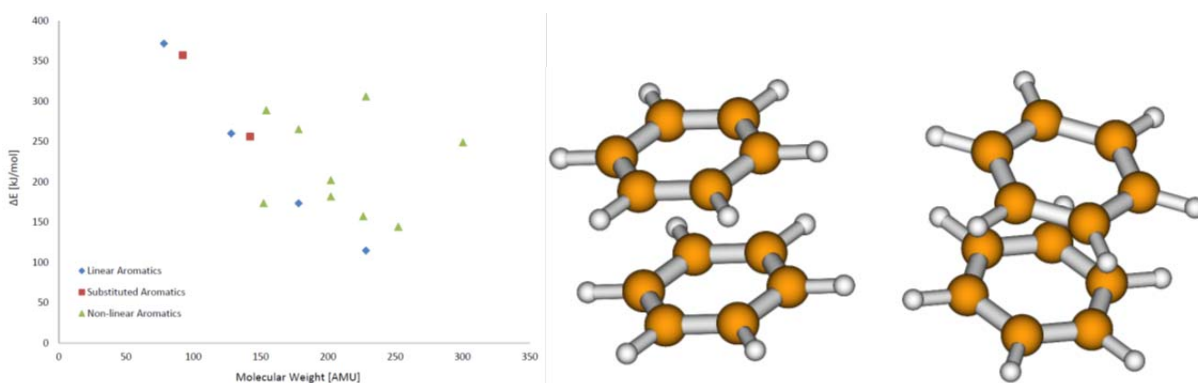


**Figure 2.** Energy difference between ground state and first excited state for a series of PAH molecules (left). Two different configurations of a benzene excimer (parallel – center; rotated – right).

### *Soot nucleation from excimers*

We conducted an ab-initio quantum computational study to address certain issues present in current models of soot nucleation. Most models base soot nucleation upon the dimerization of gas phase polycyclic aromatic hydrocarbons (PAHs) that arises through collisions between these gaseous molecules. These models contain three major flaws and ultimately violate the second law of thermodynamics. Firstly, soot particles are formed at all temperatures, including room temperature, a phenomenon that is not observed experimentally. Secondly, these models predict that collisions between aromatic molecules of any size, including benzene, will form a soot particle. Thirdly, the dimers produced by these collisions are predicted to be infinitely stable. In an attempt to correct for the first two issues, we hypothesized that only collisions that included at least one excited state PAH, which would not be found at low temperatures, could form a stable dimer. The calculations of the excitation energy difference between excited and ground states were performed at the B3LYP level with the Dunning's Correlation Consistent basis sets. The cc-PVDZ basis set proved itself sufficient, as its excitation energy calculations differed from those of higher order Dunning's sets by only a few percent. The results suggest that, while the excitation energy negatively correlated with molecular weight, it was strongly dependent upon the structure of the given PAH (Figure 2). PAHs that more closely resembled the n-

acenes in structure had lower excitation barriers than other PAHs of similar mass. Using the calculated excitation energies, we evaluated the population of excited states at a given temperature assuming a Boltzmann equilibrium distribution. We found that only higher mass PAHs, particularly anthracene and tetracene, form a sufficiently large population of excited molecules at common sooting flame temperatures. Then, to tackle the third issue presented by current models, we used benzene and naphthalene as test cases to determine the stability of any dimers formed from a successful collision. Even though we found such dimers unlikely to form, they provided computationally efficient results that should generalize to higher order PAHs. These calculations were carried out using the MP2/cc-PVDZ level of theory. We compared the energy of two molecules, one in its ground and one in its excited state, an "infinite distance" apart to two in close proximity (3-4 angstroms) and found that, for benzene, dimerization provides significant stabilization to the two molecules (30 kJ/mol) (Figure 2). The present results suggest that a collision based model involving one ground state and one excited state PAH might adequately capture the physics of soot nucleation.

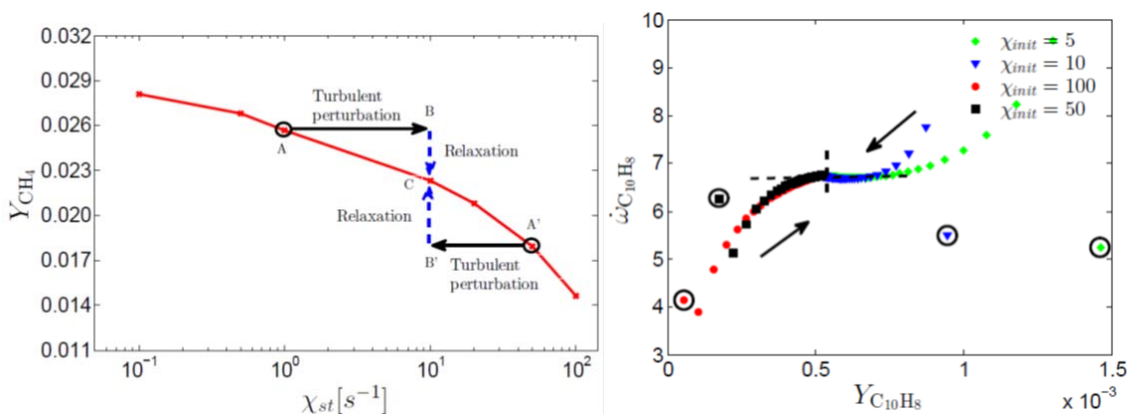


**Figure 3.** Overview of the chemistry relaxation model under turbulent fluctuations (left). Dependence of chemical source term on the species mass fraction for naphthalene for various initial scalar dissipation rates (right).

### *A PAH relaxation model for soot formation in turbulent flames*

In this paper, the response of different species to turbulent unsteadiness is investigated utilizing the 1D unsteady laminar diffusion flamelet model. Turbulent effects are modeled solely through an abrupt change in the scalar dissipation rate. Steady-state flamelets are perturbed by the modeled turbulent effects. One-dimensional flamelet calculations assuming unity-Lewis number for all species are performed. Based on the numerical results, relations between the chemical source terms and species mass fractions are examined for various representative species. It is found that the smallest turbulent time scale remains much larger than that of the gaseous phase chemistry for some small species. The steady state flamelet assumption for these species is well justified and their mass fractions can be pre-tabulated using the flamelet library legibly. On the other hand, PAH chemistry is relatively slow, and these PAH species cannot react instantaneously to the abrupt change in the local scalar dissipation rate. Based on the above considerations, a relaxation model is proposed for the chemical source terms of light species, species of moderate molecular weights, and heavy hydrocarbons. These source terms can be decomposed into a positive production term and a negative consumption term. The production term is observed to be constant for a given mixture fraction value, whereas the consumption term is found to be linearly dependent on the local species concentration. The dependence of the consumption term on

the species mass fraction is found to be determined only by the scalar dissipation rate after its abrupt change (Figure 3). This observation suggests that the relaxation model can be fully pre-tabulated using the results of steady state flamelets. Based on the relaxation results, the validity of different chemistry tabulation models is assessed.

### **Current and future work**

#### *Direct Numerical Simulations of turbulent sooting flames*

Simultaneously to the development of the chemistry and soot models, we have started setting up the Direct Numerical Simulations of soot formation. The first configuration to be analyzed is a diffusion mixing layer. Currently, the focus is placed on two elements: 1) developing an accurate and robust numerical scheme for the transport of soot quantities in a highly turbulent flow field, and 2) identifying the most relevant initial conditions to study the inception of soot in a turbulent flow field.

### **Publications**

Xuan, Y., Blanquart, G. « *Numerical Modeling of Sooting Tendencies in a Laminar Co-flow Diffusion Flame* » Combustion and Flame (2013), accepted.

Bartlett, A., Blanquart, G., « *Investigation into the Mechanism of Soot Deposition from Gaseous Polycyclic Aromatic Hydrocarbons* », Proceedings of 8th US Combustion Meeting, Salt Lake City, Utah (2013)

Xuan, Y., Blanquart, G., Mueller, M., « *Impact of mixture fraction field curvature on chemical species transport in diffusion flames* », Proceedings of 8th US Combustion Meeting, Salt Lake City, Utah (2013)

Xuan, Y., Blanquart, G., « *A flamelet-based relaxation model for polycyclic aromatic hydrocarbons in turbulent flames* », Proceedings of 8th US Combustion Meeting, Salt Lake City, Utah (2013)

## Theoretical Studies of Combustion Dynamics (DE-FG02-97ER14782)

Joel M. Bowman

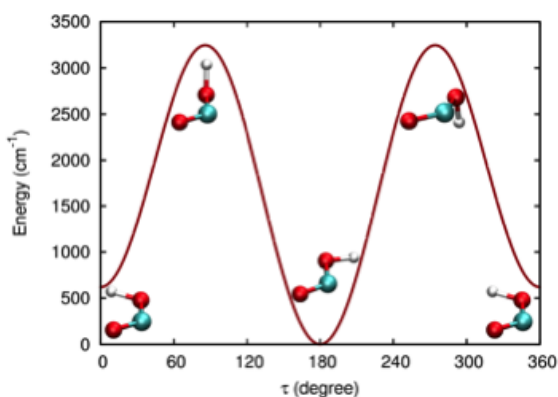
Cherry L. Emerson Center for Scientific Computation and Department of Chemistry,  
Emory University Atlanta, GA 30322, jmbowma@emory.edu

**Program Scope.** The research supported by this Department of Energy grant is focused on development of rigorous computational methods to model and predict the chemical and physical processes of importance in gas-phase combustion reaction dynamics. This includes developing full-dimensional, global *ab initio*-based potential energy surfaces (PESs) that describe complex unimolecular and bimolecular reactions. The dynamics on these potentials, which may contain multiple minima and saddle points, are done mainly using classical trajectories, for long times and can reveal new pathways and mechanisms of chemical reactions. Large amplitude motion, including isomerization, "roaming", energy transfer in collisions with atoms and molecules can be studied with these potentials. The choice of reaction system to study is generally motivated by experiments that challenge and ultimately advance basic understanding of combustion reaction dynamics. Quantum approaches are also employed mainly to study the rovibrational states of polyatomic molecules.

**Recent Progress: Potential Energy Surfaces for F, Cl, and O(<sup>3</sup>P)+CH<sub>4</sub> reactions.** We developed full-dimensional, *ab initio*-based potential energy surfaces (PESs) for the title reactions,<sup>P1-P7</sup> based on fitting roughly 20 000 highly accurate composite electronic energies, using fitting methods developed in the group.<sup>P8</sup> These PESs are the most accurate ones available and have been used in detailed reaction dynamics calculations, motivated by experiments of Lui and co-workers.<sup>1</sup> The PESs have been used by us and by other groups to investigate the applicability of the "Polanyi rules", which state what the effect of vibrational excitation should be in accelerating (or not) a chemical reaction. These rules were formulated based on many experimental and theoretical studies atom-diatom reactions and recently there has been considerable interest in<sup>1</sup> (and some controversy<sup>P6</sup> about) whether these rules apply to these reactions, notably the Cl+CD<sub>3</sub>H reaction. The aspect of these reactions that makes the rules perhaps problematic is the presence of an entrance channel van der Waals well. In some cases this well can steer the reactants away from the reaction saddle point and the issue is whether this steric steering-away increases with vibrational excitation of the CH-bond that is broken in the reaction.

**Three-state surface hopping calculations of acetaldehyde photodissociation to CH<sub>3</sub>+HCO.** We reported three electronic-state surface-hopping calculations of the photodissociation of CH<sub>3</sub>CHO with a particular focus on the S<sub>0</sub>/T<sub>1</sub> branching ratio and final-state distributions of the CH<sub>3</sub>+HCO channel(s) versus photolysis energy using full-dimensional *ab initio* PESs and spin-orbit coupling.<sup>P9</sup> Comparison with experiment<sup>2,3</sup> showed good agreement and provided insight into the detailed multi-surface dynamics.

**Potential Surfaces for HOCO Dynamics and Spectroscopy.** In collaboration with Hua Guo and Richard Dawes, a global, *ab initio* potential energy surface for the OH+CO reaction has been developed and used in several dynamics calculations already.<sup>P10,P11</sup> A



new PES and dipole moment surface, which are focused in the region of the two isomers and barrier separating them has also been developed and employed in exact calculations of vibrational energies and IR intensities.<sup>P12</sup> The potential along the relaxed torsional path is shown to the left. The PES is highly accurate, producing a barrier to isomerization within 6 cm<sup>-1</sup> of direct benchmark calculations. The

vibrational energies for both isomers are in very good agreement with experiment<sup>4</sup> and this PES and dipole moment surface can be used to probe isomerization states with predictive accuracy. **Ro-Vibrational Calculations and Line-list Spectroscopy of C<sub>2</sub>H<sub>4</sub>.** The MULTIMODE code using a very reduced mode coupling scheme was shown to produce vibrational energies in high accuracy<sup>P13</sup> (less than 1 cm<sup>-1</sup>) in comparison to benchmark 12-mode calculations for roughly 120 states.<sup>5</sup> More recent calculations of the “line-list” ro-vibrational IR spectrum were reported, using a new *ab initio* dipole moment surface.<sup>P14</sup> The results agree very well with available experiments.

**Future Plans.** We plan to study collision-induced isomerization, energy transfer, dissociation and recombination in highly energized molecular complexes with rare gases. This will be a major new direction for our research and is aimed at addressing a dearth of research in this very important process in combustion chemistry

## References

1. Vibrational Enhancement Factor of the Cl + CHD<sub>3</sub>( $v_1=1$ ) Reaction: Rotational Probe Effects, F. Wang, J.-S. Lin, Y. Cheng, and K. Liu, *J. Phys. Chem. Lett.* **4**, 323-327 (2013) and references therein.
2. The photodissociation of CH<sub>3</sub>I in the red edge of the A-band: Comparison between slice imaging experiments and multisurface wave packet calculations, L. Rubio-Lago, A. Garcia-Vela, A. Arregui, G. A. Amaral and L. Bañares, *J. Chem. Phys.* **131**, 174309 (2009).
3. Photoisomerisation of acetaldehyde between 310 and 330 nm: using H/D exchange in CH<sub>3</sub>CDO to probe photochemical and photophysical processes, D. U. Andrews, B. R. Heazlewood, A. T. Maccarone, T. Conroy, R. J. Payne, M. J. T. Jordan, and S. H. Kable, preprint.
4. Dynamics and Energetics of Elementary... C. J. Johnson, M. E. Harding, B. L. J. Poad, J. F. Stanton, R. E. Continetti, *Communication: J. Am. Chem. Soc.* **133**, 19606-19609 (2011).

5. Using a pruned basis, a non-product quadrature grid, .... for C<sub>2</sub>H<sub>4</sub>, J. G. Avila and T. Carrington Jr, J. Chem. Phys. **135**, 064101 (2011).

#### **PUBLICATIONS SUPPORTED BY THE DOE (2011-present)**

1. Dynamics of the Reaction of Methane with Chlorine Atom on an Accurate Potential Energy Surface, G. Czako and J. M. Bowman, Science **334**, 343 (2011).
2. An *ab initio* spin-orbit-corrected potential energy surface and dynamics for the F + CH<sub>4</sub> and F + CHD<sub>3</sub> reactions, G. Czako and J. M. Bowman, Phys. Chem. Chem. Phys. **13**, 8306-8312 (2011).
3. Communication: Probing the Entrance Channels of the X + CH<sub>4</sub> → HX + CH<sub>3</sub> (X = F, Cl, Br, I) Reactions via Photodetachment of X<sup>-</sup>-CH<sub>4</sub>, M. Cheng, Y. Feng, Y. Du, Q. Zhu, W. Zheng, G. Czako, and J. M. Bowman, J. Chem. Phys. **134**, 191102 (2011).
4. Accurate *ab initio* potential energy surface, thermochemistry, and dynamics of the Cl(<sup>2</sup>P, <sup>2</sup>P<sub>3/2</sub>) + CH<sub>4</sub> → HCl + CH<sub>3</sub> and H + CH<sub>3</sub>Cl reactions, G. Czako and J. M. Bowman, J. Chem. Phys. **136**, 044307 (2012).
5. Dynamics of the O(<sup>3</sup>P) + CHD<sub>3</sub>(*v*<sub>CH</sub>=0,1) reactions on an accurate *ab initio* potential energy surface, G. Czako and J. M. Bowman, Proc. Natl. Acad. Sci., USA, **109**, 7997-8001 (2012).
6. Theoretical Study of the Validity of the Polanyi Rules for the Late-Barrier Cl+CHD<sub>3</sub> Reaction, Z. Zhang, Y. Zhou, D. H. Zhang, G. Czako, and J. M. Bowman, J. Phys. Chem. Lett. **3**, 3416-3419 (2012).
7. Mode Selectivity for a "Central" Barrier Reaction: Eight-Dimensional Quantum Studies of the O(<sup>3</sup>P) + CH<sub>4</sub> → OH + CH<sub>3</sub> Reaction on an *Ab Initio* Potential Energy Surface, R. Liu, M. Yang, G. Czako, J. M. Bowman, J. Li, and H. Guo, J. Phys. Chem. Lett. **3**, 3776-3780. (2012).
8. Invited Perspective: High-dimensional *ab initio* potential energy surfaces for reaction dynamics calculations, J. M. Bowman, G. Czako, and B. Fu, Phys. Chem. Chem. Phys. **13**, 8094-8111 (2011).
9. Three-State Trajectory Surface Hopping Studies of the Photodissociation Dynamics of Formaldehyde...", B. Fu, B. C. Shepler, and J. M. Bowman, J. Am. Chem. Soc. **133**, 7957 (2011).
10. Communication: A chemically accurate global potential energy surface for the HO + CO → H + CO<sub>2</sub> reaction, J. Li, Y. Wang, B. Jiang, J. Ma, R. Dawes, D. Xie, J. M. Bowman, and H. Guo, J. Chem. Phys. **136**, 041103 (2012).
11. Quasi-Classical Trajectory Study of the HO + CO → H + CO<sub>2</sub> Reaction on a New *ab Initio* Based Potential Energy Surface, J. Li, C. Xie, J. Ma, Y. Wang, R. Dawes, D. Xie, J. M. Bowman, and H. Guo, J. Phys. Chem. A, **116**, 5057-5067 (2012).
12. Variational Calculations of Vibrational Energies and IR Spectra of *trans*- and *cis*-HOCO Using New *ab Initio* Potential Energy and Dipole Moment Surfaces, J. Phys. Chem. A [asap dx.doi.org/10.1021/jp309911w](https://doi.org/10.1021/jp309911w)

13. MULTIMODE Calculations of Rovibrational Energies of C<sub>2</sub>H<sub>4</sub> and C<sub>2</sub>D<sub>4</sub>, S. Carter, J. M. Bowman, and N. C. Handy, *Mol. Phys.* **110**, 775-781 (2012).
14. First-principles calculations of rovibrational energies, dipole transition intensities and partition function for ethylene using MULTIMODE, S. Carter, A. R. Sharma, and J. M. Bowman, *J. Chem. Phys.* **137**, 154301 (2012).
15. The Dynamics of Allyl Radical Dissociation, C. Chen, B. Braams, D. Y. Lee, J. M. Bowman, P. L. Houston, and D. Stranges, *J. Phys. Chem. A* **115**, 6797 (2011).
16. Are Roaming and Conventional Saddle Points for H<sub>2</sub>CO and CH<sub>3</sub>CHO Dissociation to Molecular Products Isolated from Each Other? B. C. Shepler, Y. Han, and J. M. Bowman, *J. Phys. Chem. Lett.* **2**, 834 (2011).
17. Quasiclassical Trajectory Calculations of the Dissociation Dynamics of CH<sub>3</sub>CHO at High Energy Yield Many Products Y-C Han, B. C. Shepler, and J. M. Bowman, *J. Phys. Chem. Lett.* **2**, 1715 (2011).
18. Roaming Radicals, J. M. Bowman and B. C. Shepler, *Annu. Rev. Phys. Chem.* **62**, 531 (2011).
19. Roaming reactions: The third way, J. M. Bowman and A. G. Suits, *Phys. Today* **64**, 33 (2011).
20. Large-amplitude dynamics in vinyl radical: The role of quantum tunneling as an isomerization mechanism, A. R. Sharma, J. M. Bowman, and D. J. Nesbitt, *J. Chem. Phys.* **136**, 034305 (2012).
21. Overtone-induced dissociation and isomerization dynamics of the hydroxymethyl radical (CH<sub>2</sub>OH and CD<sub>2</sub>OH). I. A theoretical study, E. Kamarchik, C. Rodrigo, J. M. Bowman, H. Reisler, and A. I. Krylov. *J. Chem. Phys.* **136**, 084304 (2012)
22. Three-state surface hopping calculations of acetaldehyde photodissociation to CH<sub>3</sub>+HCO on *ab initio* potential surfaces, B. Fu, Y.-C. Han, and J. M. Bowman, *Faraday Disc.* **157**, 27-39 (2012).
23. Intersystem crossing and dynamics in O(<sup>3</sup>P)+C<sub>2</sub>H<sub>4</sub> multichannel reaction: Experiment validates theory, B. Fu, Y.-C. Han, J. M. Bowman, L. Angelucci, N. Balucani, F. Leonori, P. Casavecchia, *Proc. Nat. Acad. Sci., USA*, **109**, 9733-9738 (2012).
24. Quasiclassical trajectory study of fast H-atom collisions with acetylene, Y.-C. Han, A. R. Sharma, and J. M. Bowman, *J. Chem. Phys.* **136**, 214313 (2012).
25. Reactant zero-point energy is needed to access the saddle point in molecular dynamics calculations of the association reaction H + C<sub>2</sub>D<sub>2</sub> → C<sub>2</sub>D<sub>2</sub>H\*, Y. Han and J. M. Bowman, *Chem. Phys. Lett.* **55**, 39–43 (2013).
26. Vibrational Excitation and Product Branching Ratios in Dissociation of the Isotopologs of H<sub>3</sub>O: Experiment and Theory, J. E. Mann, Z. Xie, J. D. Savee, J. M. Bowman, R. E. Continetti, *J. Phys. Chem. A*, accepted for publication.

**COMBUSTION CHEMISTRY**  
**Nancy J. Brown**  
**Environmental Energy Technologies Division**  
**Lawrence Berkeley National Laboratory**  
**Berkeley, California, 94720**  
**510-486-4241 NJBrown@lbl.gov**

**PROJECT SCOPE**

Combustion processes are governed by chemical kinetics, energy transfer, transport, fluid mechanics, and their complex interactions. Understanding the fundamental chemical processes offers the possibility of optimizing combustion processes. The objective of our research is to address fundamental issues of chemical reactivity and molecular transport in combustion systems. Our long-term research objective is to contribute to the development of reliable combustion models that can be used to understand and characterize the formation and destruction of combustion-generated pollutants. We emphasize studying chemistry at both the microscopic and macroscopic levels. Our current work is concerned with improving the calculation of transport properties for combustion modeling.

**RECENT PROGRESS**

In our previous work [Bastien et al., 2010 and Loisy and Brown, 2012], we demonstrated that simple Lennard-Jones potentials are adequate for transport property calculations, which recently has been verified by Dagdigian and Alexander [2012]. Bastien et al. also demonstrated that many which recently has been verified by Dagdigian and Alexander [2012]. Bastien et al. also demonstrated that many that many different ( $\epsilon_{ii}$ ,  $\sigma_{ii}$ ) pairs can yield predicted viscosities that agree with experimental values with less than 1% error over a wide range of temperatures. These results all suggest a surprising insensitivity of the transport properties to the potential, which should be explored further. Since our study of thermal diffusion, thermal diffusion factors (TDFs) revealed some sensitivity to the potential shape, we have conducted a sensitivity study of the TDF to the potential surface using the LJ 9-6 and 12-6 potentials. By conducting the study of TDF sensitivity, we *de facto* conduct a study of the other transport properties because the collision integrals and other parameters required for TDFs include those that are important for diffusion, viscosity, and thermal conductivity.

**Methodology:** The sensitivity study was conducted with classical mechanics by applying a local perturbation to the reduced LJ 9-6 and 12-6 intermolecular potentials. Ideally the perturbation would be a Dirac delta function, but this would cause a discontinuity. This was avoided by approximating the delta function with a Gaussian, and defining the perturbation as:

$$p(r^*) = K e^{-\left(\frac{r^* - r_p^*}{w}\right)^2} \quad (1)$$

where  $p(r^*)$  is the perturbation at the reduced intermolecular distance  $r^*$ ,  $r_p^*$  is the location of the Gaussian maximum,  $K$  is the amplitude of the perturbation, and  $w$  is the width. The parameters of the Gaussian were given fixed values determined by trial and error as  $K=0.05$  and  $w=0.001$ . For a specific reduced energy and reduced impact parameter, the potential was perturbed at a number of  $r^*$  positions between  $r_p^* = r_c^*$ , the

distance of closest approach and  $r_p^* = 10$ , an intermolecular distance where the potential is effectively zero.

**Results:** Fully normalized sensitivity coefficients of the deflection function, cross sections, collision integrals  $\Omega^{(l,s)}$  for  $l=1,2$  and  $s=1-3$ , functionals, TDFs and other transport properties to the intermolecular potential were computed. The deflection function,  $\cos^l X(b^*, G^*)$ , which is the scattering angle as a function of reduced energy and impact parameter, depends on the intermolecular potential, and is evaluated by performing an integral over the reduced intermolecular distance. The cross section is obtained by integrating the cosine of the deflection function (raised to the power 1 or 2) over the reduced impact parameter weighted by it. Collision integrals are obtained by integrating the cross section over a Boltzmann distribution with a weighting factor, which is the reduced energy raised to an appropriate (for the transport property of interest) power. Functionals are ratios of collision integrals or ratios of differences of collision integrals.

The location of the maximum sensitivity of the deflection function,  $\cos^l X(b^*, G^*)$  is located at the distance of closest approach. The maximum sensitivity of the  $\cos^l X(b^*, G^*)$  deflection function versus  $(b^{*2})$  and  $G^*$  and for  $l=2$  is shown in Figure 1:

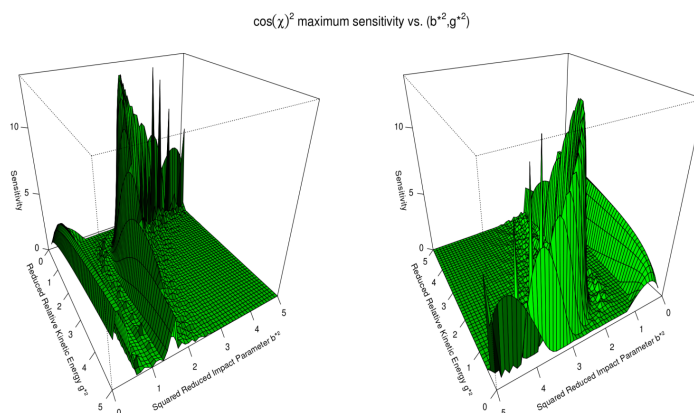


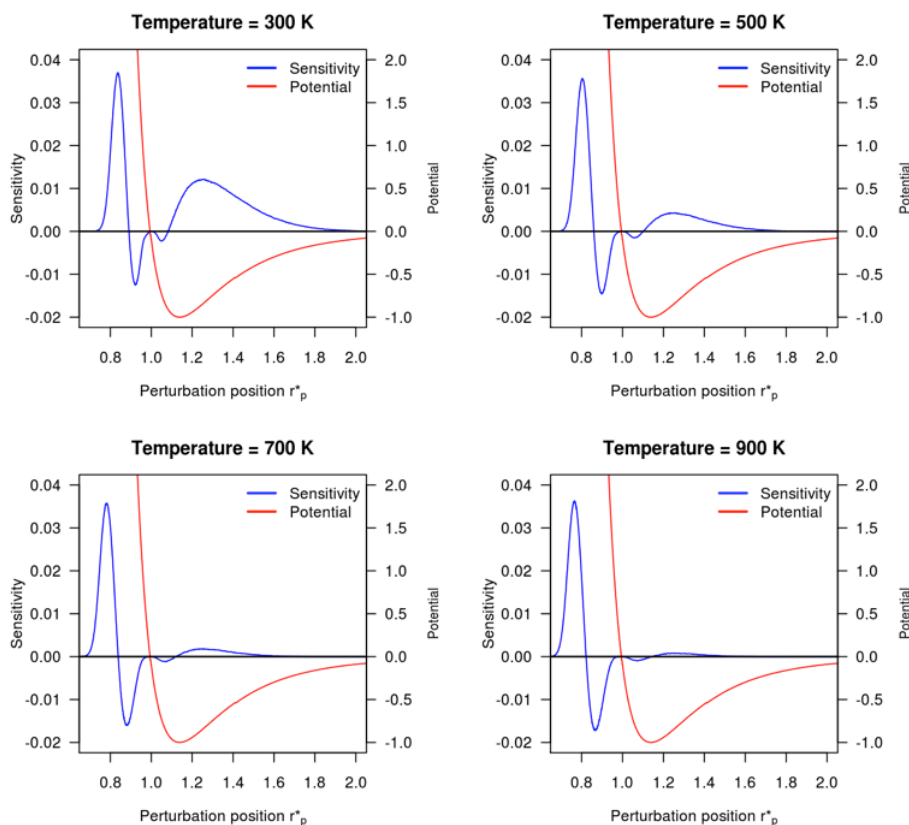
Figure 1 Maximum sensitivity of  $\text{Cos}^2 X$  versus the square of the reduced impact parameter and the reduced energy

where maximum values are between 1 and 12 for small values of  $G^*$  less than 5 and values of  $(b^{*2})$  between 1 and 4. Examination of the maximum cross section sensitivities to the potential as a function of  $G^*$  revealed that they had **decreased by two orders of magnitude** due to the weighting of the integrand by the impact parameter. The integrand of the collision integral was examined for different values of the reduced temperature,  $T^*$  ( $kT/\epsilon$ ); low values of  $T^*$  favored small values of the energy over a limited range of energies, and as  $T^*$  increased, the maximum contribution shifted to higher energies and decreased in magnitude while the range of energies that contributed to the integrand increased. This behavior was manifested in the collision integral sensitivities computed for different values of  $T^*$ , when  $T^* > 1.0$ . The collision integral sensitivities and those associated with the functionals **decreased by another order of magnitude** with maximum values of approximately  $5 \times 10^{-3}$ , and were dominated by the repulsive portion of the potential. The TDF sensitivities as a function of perturbation position for different

temperatures for  $N_2 + H_2$  is shown in Figure 2. The sensitivities have maximum values of  $3.5 \times 10^{-2}$ , and are dominated by the repulsive portion of the potential as the temperature

### Thermal diffusion factor sensitivity vs. perturbation position $r_p^*$

H<sub>2</sub>-N<sub>2</sub> mixture;  $x(H_2)=0.50$ ; LJ 9-6 potential; Kihara's method



increases.

Figure 2 The TDF versus perturbation position for various temperatures. The TDF for the figure was calculated with a LJ 9 6 potential and the Hirshfelder approximation.

**Conclusions:** The conclusions of this study are that transport properties do not constrain the potential at the energies that are important for the temperature range 250 K to adiabatic flame temperatures, considered in our studies. The TDF is an order of magnitude more sensitive to the potential than the other transport properties, but the TDF and the other transport properties are very insensitive  $O(10^{-3})$ . In contrast, flame property sensitivity to rate coefficient and transport properties can achieve values of magnitude 10. The sensitivity is dominated by the repulsive portion of the potential. A parameter, which provides a measure of the steepness of the repulsive portion of the potential, is  $(\sigma/r_m)$ , and this suggests that there is an important relationship between the length and energy scaling parameters. The parameter  $r_m$ , the internuclear separation at the potential minimum, is related to  $\sigma$  for LJ potentials. Of the intermolecular potentials considered in our study, the LJ 9-6 potential is the least repulsive. Bastien et al. found that a curve (trough) exists in  $(\sigma\varepsilon)$  space, which can be approximated as a straight line, where the parameter pairs on the curve generate a calculated viscosity in good agreement with measurements for a pure gas or binary mixture. The low sensitivity, the importance of the repulsive portion of the

potential for transport, and the relationship between  $\sigma$  and  $\varepsilon$  provide an explanation the Bastien et al. finding.

**Publications supported by DOE for last two years:**

Jin, L., Harley, R.A., Brown, N.J., "Meteorology-induced Variations in the Spatial Behavior of Summer Ozone Pollution in Central California" *Atmospheric Environment* 45 pp4704-4718 (2011).

Sharon M. Shearer, S.M., Harley, R.A., Jin L., and Brown, N.J., "Evaluation of the Condensed SAPRC07 Chemical Mechanism: Predictions of Photochemical Air Pollution in Central California," *Atmospheric Environment* 46 (2012) pp205-216.

E.C. McDonald-Buller, D.T. Allen, N. J. Brown, D.J. Jacobs, D. Jaffe, C.E. Kolb, A.S. Lafohn, S. Oltmans, D.D. Parrish, GYarwood, and Lin Zhang."Establishing Policy Relevant Background (PRB) Ozone Concentrations in the United States," *Env. Sci. Tech.* 3011, 45 pp9484-9497.

Loisy, A., and Brown, N.J., "Thermal diffusion and Combustion Modeling," submitted to *Progress in Energy and Combustion Science*, 2012.

Jin, L., and Brown, N.J., "Role of Meteorological Processes in Ozone Responses to Emission Controls in California's San Joaquin Valley," Submitted to *Journal of Geophysical Research Atmospheres*, 2012.

**References**

Bastien, L.A.J., Price, P.N. and Brown, N.J. "Intermolecular Potential Parameters and Combining Rules Determined from Viscosity Data," *International Journal of Chemical Kinetics* 42, DOI 10.1002/kin.20521, pp 713-723 (2010).

Brown, N.J., Bastien, L.A.J., and Price, P.N. "Transport Properties for Combustion Modeling." *Progress in Energy and Combustion Science* [doi.org/10.1016/j.pecs.2010.12.001](https://doi.org/10.1016/j.pecs.2010.12.001) (2010) .

Dagdikian P.J, Alexander M.H. (2012) Exact quantum scattering calculation of transport properties for free radicals: OH( $X^2\Pi$ ) - helium. *J. Chem. Phys.*, in press.

# Dynamics of Product Branching in Elementary Combustion Reactions: OH + Alkenes and Nitrogen Chemistry

Laurie J. Butler

The University of Chicago, The James Franck Institute

5640 South Ellis Avenue, Chicago, IL 60637

L-Butler@uchicago.edu

## I. Program Scope

While the total rate constant for many elementary reactions is well-characterized, understanding the product branching in complex reactions presents a formidable challenge. To gain an incisive probe of such reactions, our experiments directly investigate the dynamics of the product channels that arise from long-lived radical intermediates along the bimolecular reaction coordinates. Our work uses the methodology developed in my group in the last twelve years, using both imaging and scattering apparatuses. The experiments generate a particular isomeric form of an unstable radical intermediate along a bimolecular reaction coordinate and study the branching between the ensuing product channels of the energized radical as a function of its internal rotational and vibrational energy under collision-less conditions.

The experiments use a combination of: 1) measurement of product velocity and angular distributions in a crossed laser-molecular beam apparatus, with electron bombardment detection in my lab in Chicago or 2) with tunable vacuum ultraviolet photoionization detection at Taiwan's National Synchrotron Radiation Research Center (NSRRC), and 3) velocity map imaging using state-selective REMPI ionization and single photon VUV ionization of radical intermediates and reaction products. Our experimental work in the second funding period focused on three systems, the radical intermediate when OH adds to the end carbon of allene, two radical intermediates in the reaction of OH + propene, and the photodissociation of BrCH<sub>2</sub>CH<sub>2</sub>ONO at 351 nm. The last is in collaboration with Terry Miller's group. In collaboration with Joel Bowman, we have also been doing substantial theoretical modeling, described below, of our experiments on the OH + ethene radical intermediate, CH<sub>2</sub>CH<sub>2</sub>OH. We are scheduled for March 10, 2013 to take data on the OH + allene system, so I'll just describe the work on BrCH<sub>2</sub>CH<sub>2</sub>ONO at 351 nm and the classical trajectories on the OH + ethene intermediate below. The results develop insight on product channel branching in reactions that proceed via an addition/elimination mechanism and provide a key benchmark for emerging electronic structure and dynamics calculations on polyatomic reactions that proceed through unstable radical intermediates.

## II. Recent Progress

### A. Photoproduct Channels from BrCH<sub>2</sub>CH<sub>2</sub>ONO at 351 nm

Terry Miller's group has been interested in studying the spectroscopy of substituted alkoxy radicals, so had photolyzed at 351nm a series of substituted alkyl nitrites, XCH<sub>2</sub>CH<sub>2</sub>ONO (X=F, Cl, Br, OH) and obtained spectra of the observed products. They reported (J. Phys. Chem. A, 116, 12032 (2012)) that only for X=F did they observe the spectrum of substituted alkoxy radical, XCH<sub>2</sub>CH<sub>2</sub>O; for all systems they observed electronic transitions of formaldehyde and vinyloxy radical, CH<sub>2</sub>CHO. Our experimental work in this second year of funding characterized the primary photodissociation channels of BrCH<sub>2</sub>CH<sub>2</sub>ONO at 351 nm to help Miller's group to understand the sources of the photoproducts they were detecting. We were particularly interested in whether the vinyloxy product might result from primary HBr photoelimination or from a competing channel in the unimolecular dissociation of the nascent BrCH<sub>2</sub>CH<sub>2</sub>O radicals (most of

those radicals would be expected to dissociate to  $\text{BrCH}_2 + \text{CH}_2\text{O}$ , the source of Miller's formaldehyde signal). We have not yet published our experimental results as we wish to take a spectrum of the  $\text{BrCH}_2$  products from the secondary dissociation of  $\text{BrCH}_2\text{CH}_2\text{O}$  radicals on our velocity map imaging apparatus, but the experimental results on our scattering apparatus are complete. They definitively show that the only primary photodissociation channel of  $\text{BrCH}_2\text{CH}_2\text{ONO}$  at 351 nm is O-NO fission to form  $\text{NO} + \text{BrCH}_2\text{CH}_2\text{O}$  radicals. The upper limit on a potential HBr photoelimination channel is <2%, so any HBr photoelimination co-fragment,  $\text{CH}_2\text{CHONO}$ , would certainly be in too small a yield to be responsible for Miller's vinoxy signal. (This radical would dissociate to vinoxy + NO, but it is not present to do so.) We then turned to characterizing the internal energy distribution of the nascent  $\text{BrCH}_2\text{CH}_2\text{O}$  radicals. Although most of those radicals would be expected to dissociate to  $\text{BrCH}_2 + \text{CH}_2\text{O}$ , there is a higher energy HBr elimination channel from this radical which might produce some vinoxy signal if the radical were formed with high internal energies. Figure 1 shows the internal energy distribution determined in

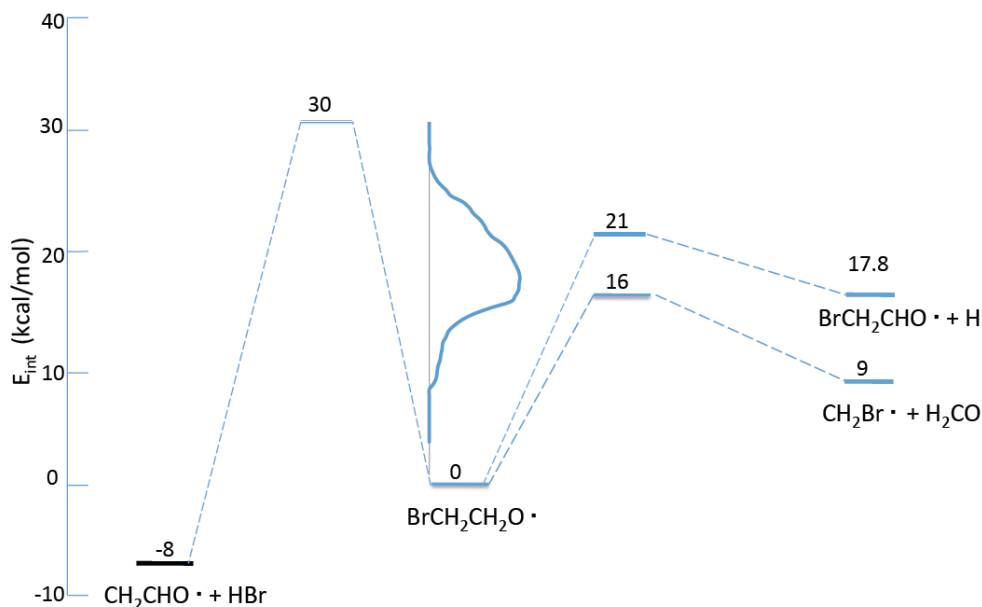


Figure 1. Internal energy distribution of the  $\text{BrCH}_2\text{CH}_2\text{O}$  radicals produced from the 351 nm photodissociation of  $\text{BrCH}_2\text{CH}_2\text{ONO}$ . The internal energy carried away by the NO co-fragment was estimated to be 13.94 kcal/mol (it has been subtracted from the total internal energy).

our experiments. The nascent  $\text{BrCH}_2\text{CH}_2\text{O}$  radicals do not have enough internal energy to dissociate to vinoxy + HBr when they are produced from the 351 nm photodissociation of  $\text{BrCH}_2\text{CH}_2\text{ONO}$ . Thus we cannot determine the source of Miller's vinoxy spectra. We are presently taking data in our velocity map imaging apparatus to characterize the secondary dissociation of  $\text{BrCH}_2\text{CH}_2\text{O}$  radicals to  $\text{BrCH}_2 + \text{H}_2\text{CO}$ . Our new tunable VUV ionization capability can resolve the  $\text{BrCH}_2$  signal from that from dissociative ionization of stable  $\text{BrCH}_2\text{CH}_2\text{O}$  radicals. We plan to write the results up for publication this spring.

## B. Theoretical Study of the Dissociation Dynamics and Product Branching of the Partially Deuterated Radical Intermediate, $\text{CD}_2\text{CD}_2\text{OH}$ , of the OH + ethene reaction

Our prior experimental work on the OH + ethene reaction evidenced four product channels from the  $\text{CH}_2\text{CH}_2\text{OH}$  radical intermediate formed in the addition mechanism of this reaction (Ratliff et al, *J. Phys. Chem. A* **115**, 9097 (2011)). Though the dissociation of the radical

back to ethene + OH and the product channels of ethenol + H and methyl + formaldehyde (with minimal contribution from H + acetaldehyde) were expected based on the RRKM work of Klippenstein and co-workers (Senosian et al., *J. Phys. Chem. A* **110**, 6960 (2006)), our experiments evidenced a surprising branching to water + vinyl. The barrier for this channel is quite high from the radical intermediate (these products are produced in the H atom abstraction channel of the OH + ethene bimolecular reaction via a much lower transition state) so had not been included in Klippenstein's study (or any prior one) as a possible product channel from the radical intermediate. Concurrently with our experimental work, Bowman and co-workers (*J. Phys. Chem. Lett.* **1**, 3058–3065 (2010)) were investigating this reaction with quasiclassical trajectories. Both the experimental results and Bowman's trajectories evidence a H<sub>2</sub>O + vinyl product channel from the radical intermediate. However, his trajectories, calculated with J=0 and 44 kcal/mol of internal energy, show less than a 2% branching to these products, while the experiments detected that 14.5% of the dissociating radicals (from a broad internal energy distribution with high angular momentum J) resulted in water + vinyl. To test the possible role of tunneling, in the last funding period we took data on the partially deuterated radical.<sup>4</sup> We found that the branching to this channel remained high, so tunneling cannot explain the different branching to this channel predicted in the trajectories. Thus, we posited that it may be important to assess the role of angular momentum in the dynamics, as the β-hydroxyethyl radical intermediates in our experiment are produced photolytically rather than from the OH + ethene bimolecular collision (producing the intermediate photolytically allows us to separate the direct abstraction reaction from the addition/elimination reactions). Thus, we sought to run the trajectory calculations appropriately counting for the direction and magnitude of the angular momentum imparted to the radicals.

This year, in collaboration with J. Bowman and E. Kamarchik, my student Ben McKown wrote additional code to allow Bowman's QCT code to correctly include the initial angular momentum imparted to the radical intermediate in the experimental work. We also corrected our model for estimating the rotational energy in the radical from the measured recoil kinetic energy distribution for the C-Br bond photofission that generates the radical. The revised model may be used in the general case where the radical's rotation is not about a principle axis. Figure 2 below shows the derived distribution of J in the nascent radicals from the trans photolytic precursors, with an individual plot at one of the lower recoil kinetic energies that generates radicals with high

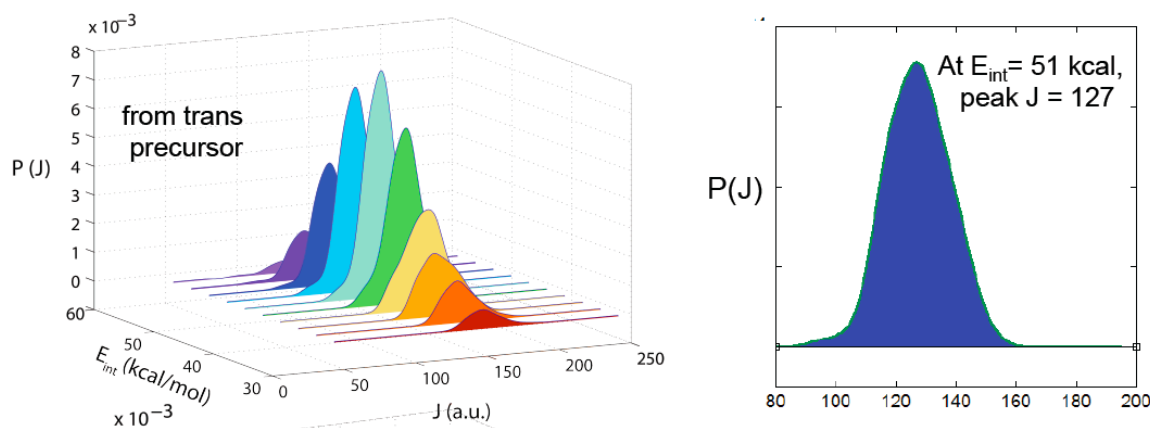


Figure 2: Representative angular momenta derived from expt for classical trajectory calculations.

enough internal energies to dissociate. Our trajectory results thus far give an excellent prediction for the measured recoil kinetic energy between the OH and ethene products from the high rotational energy CD<sub>2</sub>CD<sub>2</sub>OH radicals; this is shown in Figure 3 below. This validates our model

for deriving the distribution of energy between rotation and vibration. The product branching from the rotationally excited radicals interestingly predicts that although the H + ethenol channel would dominate, the surprising water + vinyl channel is comparable in importance to the channel producing methyl + formaldehyde. The branching predicted for the OH + ethene channel is much larger than that measured experimentally, however, so Bowman and co-workers plan to further improve the fitted potential energy surface.

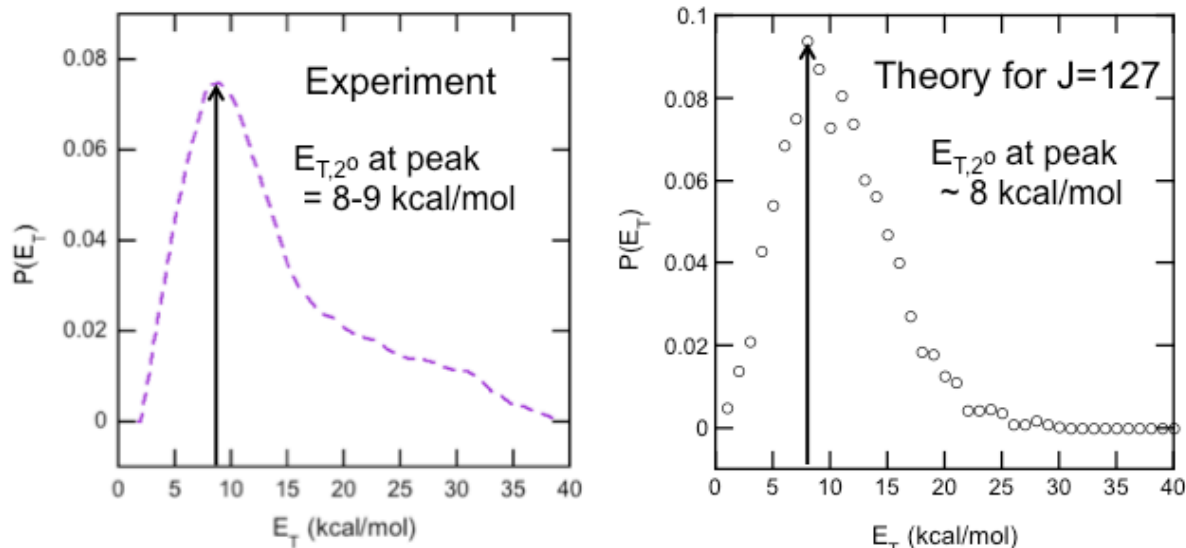


Figure 3: Comparison of the measured energy imparted to recoil kinetic energy when the rotationally excited radicals dissociate to OH + ethene to that predicted by the classical trajectories with  $J=127$ . The prediction for  $J=0$  is much different, peaking near  $E_T=0$ .

We explored three dimensionality reduction methods to understand the trajectory results; we found that Ceriotti's sketch maps (M. Ceriotti et al, PNAS 108, 13023 (2011)), originally developed for protein folding, give new physical insight on the unexpected H<sub>2</sub>O + vinyl product channel from this intermediate. A manuscript describing these results is in preparation.

### III. Publications Acknowledging DE-FG02-92ER14305 (2011 or later)

1. Theoretical Study of Isomerization and Dissociation Transition States of C<sub>3</sub>H<sub>5</sub>O Radical Isomers: Ab Initio Characterization of the Critical Points and Statistical Transition-State Theory Modeling of the Dynamics, B. L. FitzPatrick, J. Phys. Chem. A 115, 1701 (2011). (Work completed as a Ph.D. student with L. J. Butler.)
2. Product Branching from the CH<sub>2</sub>CH<sub>2</sub>OH Radical Intermediate of the OH + Ethene Reaction, B. J. Ratliff, B. W. Alligood, L. J. Butler, S. -H. Lee, and J. J. Lin, J. Phys. Chem. A 115, 9097-9110 (2011).
3. Characterizing the ro-vibrational distribution of CD<sub>2</sub>CD<sub>2</sub>OH radicals produced via the photodissociation of 2-bromoethanol-d<sub>4</sub>, C. C. Womack, R. S. Booth, M. D. Brynteson, L. J. Butler, and D. E. Szpunar, J. Phys. Chem. A 115, 14559-14569 (2011).
4. Photoproduct channels from BrCD<sub>2</sub>CD<sub>2</sub>OH at 193 nm and the HDO + vinyl products from the CD<sub>2</sub>CD<sub>2</sub>OH radical intermediate, C. C. Womack, B. J. Ratliff, L. J. Butler, S. -H. Lee, and J. J. Lin, J. Phys. Chem. A 116, 6394-6407 (2012).

# Crossed-Molecular-Beam Studies of Energy Transfer

David W. Chandler  
Combustion Research Facility, MS 9054  
Sandia National Laboratories  
Livermore, CA 94551-0969  
Email: chand@sandia.gov

## Program Scope:

My research focuses on the field of chemical dynamics of gas phase molecular species. I define chemical dynamics as the detailed study of the motion of molecules and atoms on potential energy surfaces in order to learn about the details of the surface as well as the dynamics of their interactions. We have tested simple bimolecular potential energy surfaces by the careful study of collisional energy transfer processes in crossed molecular beam arrangements utilizing Velocity Mapped Ion Imaging techniques. We use laser light to state-selectively excite the reagents and detect the products of collisional energy transfer processes and therefore we can use the polarization qualities of the light to learn about not only the angular distribution of scattering processes but the alignment and orientation of the angular momentum vector of the products. We attempt to do this with high velocity resolution when possible and with single quantum-state preparation of the reagent molecules. We recently have found that we can use laser excitation to electronic states at the crossing of the molecular beam with either an atomic or molecular beam to create a state-selected transient species for which energy transfer can be studied while in the excited electronic state.

## Chemical Dynamics Progress Report: Electronically excited state scattering:

We first realized that we could record the differential cross section of scattering from electronically excited state species produced at the crossing of two beams when studying elastic collision of Kr atoms [1]. This Kr tagging experiment and the observation of scattering spheres from elastic scattering of metastable Kr atoms at delay times as short as 400 ns implies that a molecule that is in an electronically excited state for only 400 ns could undergo sufficient collisions to generate a scattering image from which a differential cross section and alignment moments could be recovered. NO(A, j=0) state has a lifetime of 200 ns, and we excited it with near-UV light around 226 nm at the crossing of a 5%NO/He beam and a neat beam of He, Ne or Ar atoms [2,3]. A 400-ns delay between the excitation and performing state-selective REMPI of the NO(A) state molecules is sufficient time to allow for collisions in the crossed molecular / atomic beams. During this delay ~90% of the NO(A<sup>2</sup>Σ<sup>+</sup>) state molecules have decayed back to the ground state and of those remaining in the excited state approximately 1% have a collision. Those collisions cause rotational energy transfer to about 20 possible quantum states. Quantum-state resolved ionization detection of the collision products reveals both the differential cross section and the alignment of the angular momentum vector of the product molecule. Ionization is accomplished by selectively ionizing the NO (A, N) molecules by (1 + 1) REMPI through the NO(E) state at ~620 nm, and those ions are velocity-mapped Ion Imaged. In Fig. 1 are sum images (image taken with vertical plus image taken with horizontal polarization of the detection laser) of NO(A, N=4, 5, 7, 9) from such an experiment where the NO(A) collision partner is Ne. Analysis of the sum images gives us information on the differential cross section and the alignment of the angular momentum vector.

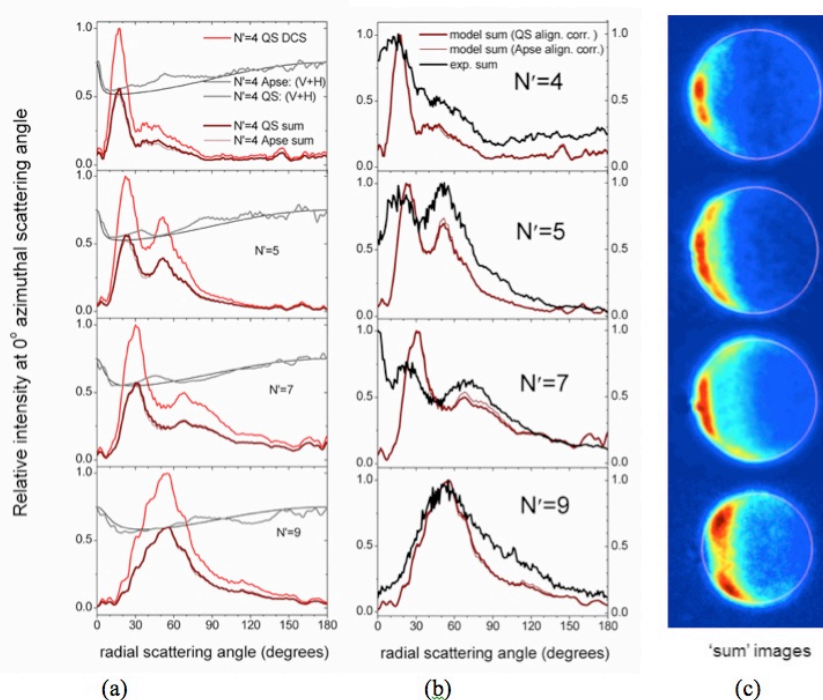


Figure 1: (a) DCS from QS calculations at 543 cm-1 collision energy with correction for detection sensitivity using both QS and KA models. (b) Predicted angular intensities for V + H image from QS and KA models together with experimental angular intensities. (c) Experimental V + H images for  $N' = 4, 5, 7$  and 9.

What we have concluded from this study is that the best potential energy surface for the scattering of NO(A) state molecules from rare gas atoms does accurately reproduce the experimental results for the differential cross section except for the very most forward scattering peak for  $N=7$  [4]. The calculations also reproduce the alignment of the angular momentum vector that is observed. An interesting side note is that there is much more quantum interference in the scattering of NO(A) with rare gas atoms than for scattering of NO(X) with rare gas atoms. Considering the excited state is a more spherical Rydberg,  $^2\Sigma^+$  state and the ground is a more ellipsoidal shaped  $^2\Pi_{1/2}$  state this is a little surprising. The answer, I believe, lies in the softness of the potential energy surface as different scattering interactions actually scatter from different parts of the potential as only the component of velocity along the Apse angle of the collision is useful in the collision dynamics. Analysis of this data has led to a simple classical “Kinetic Apse model”, KA, for the prediction of the alignment of the angular momentum vector upon collision that can predict classically about 80% of the observed alignment that is observed in scattering experiments [5]. This work is being done by postdoctoral fellows Jeffrey Steill and Jeff Kay in collaboration with the groups of Ken McKendrick and Matt Costen (Harriott-Watt Univeristy) and Millard Alexander and Jacek Klos (University of Maryland).

### Present and Future work: Collision Induced Dissociation of NO<sub>2</sub>:

The shape of the collisional energy transfer function,  $P(E, v, j; E', v', j')$ , for a collision of a polyatomic molecule has been the subject of many experiments as this collisional energy transfer process activates and deactivates molecules in real-world collisional environments. Over the years many efforts have been made to measure the average energy transferred in a collision between a hot and a cold molecule as this dictates how fast molecules come to thermal

equilibrium [For example 6,7]. Highly reactive systems such as flames and explosions many times are not in thermal equilibrium since the energy transfer collisions cannot keep up with the reactive collisions that generate heat release.

Collisional stabilization is critical to understanding complex gas phase kinetics of reactions where the potential energy surface has multiple minima [8,9]. Several groups have prepared vibrationally excited ground-state molecules by exciting large aromatic molecules to the first electronically excited state [for example 10]. Internal conversion of the energy generates a translationally and rotationally cold, but vibrationally-excited ground-electronic-state molecule suitable for the study of energy transfer. Much theoretical effort has accompanied these experimental efforts. Much has been learned about the shape of the energy transfer function,  $P(E, v, j; E', v', j')$  from various studies but what has not been measured directly is the collisional energy transfer from highly vibrationally excited states of a molecule into the dissociative continuum: collision induced dissociation (CID). This collision-induced dissociation is the final step in a pyrolysis reaction where a cold molecule is heated in a hot bath and collisionally dissociates. In addition this measurement has direct bearing on three-body recombination reactions as they are related by microscopic reversibility.

In a new set of experiments we have recently started we will measure directly the shape and extent of collisional energy transfer between a highly vibrationally excited triatomic molecule and an atom.  $\text{NO}_2$  seeded into a skimmed supersonic molecular beam is electronically excited to the first electronic  ${}^2\text{B}_2$  state around 398.7 nm. At this wavelength the molecule does not have quite enough energy to dissociate (dissociation energy is 25,129  $\text{cm}^{-1}$  or 397.9 nm). The electronic  ${}^2\text{B}_2$  state is strongly coupled to the ground  ${}^2\text{A}_1$  state and internal conversion is quick, sub-picoseconds. In this manner we are able to generate an  $\text{NO}_2$  molecule with a precise amount of vibrational energy. This hot molecule undergoes a collision with a rare gas atom from a supersonic expansion with a center-of-mass collision energy approximately  $560\text{cm}^{-1}$  for collision with Ar. Any collision transferring more than  $50\text{cm}^{-1}$  of energy will deposit sufficient energy for the  $\text{NO}_2$  molecule to dissociate and form  $\text{NO}(\text{X}) + \text{O}$  atoms. In order to determine the shape of the energy transfer function  $P(E)$  we taken images of many energetically

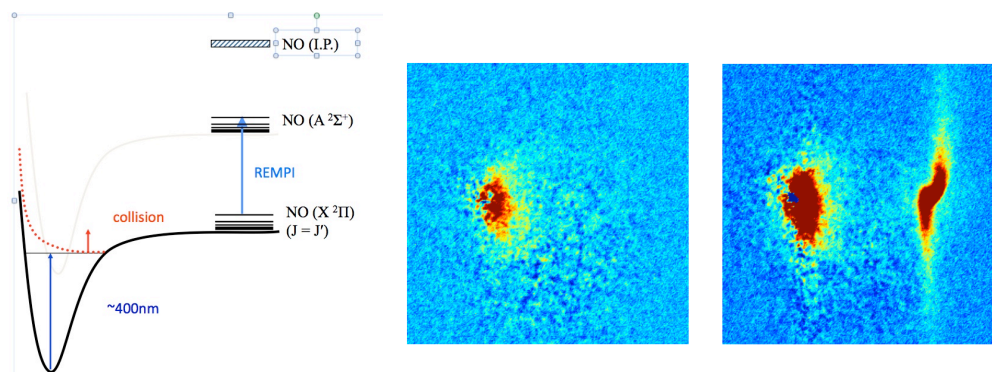


Figure 2: Schematic of  $\text{NO}_2$  collisional dissociation experiment and data on the photo-dissociation of  $\text{NO}_2$  showing that particular quantum states are preferentially formed at certain excitation energies. Images of  $\text{NO}$  ( $J=1.5$  (left) and  $J=7.5$  (right)) produced from collision of hot  $\text{NO}_2$  with Ar atoms. The feature on the right side of the left hand image of the  $\text{NO}$  collision induced dissociation product is  $\text{NO}(J=1.5)$  impurity in the Ar beam used to scatter with the  $\text{NO}_2$ .

accessible quantum states of the product NO molecule a few milliseconds after excitation of the NO<sub>2</sub> molecule, Fig. 4. This data combined with data on the product branching ratio of NO<sub>2</sub> into NO(X, J) as a function of energy will give us a direct measure of the collisionally induced energy transfer process. Theory to compliment our data and help with the analysis is being performed by Dr. Ahren Jasper (Sandia).

### References:

- 1) Cold Atoms by Kinematic Cooling, J.J. Kay, J. Klos, M. H. Alexander, K. E. Strecker, D. W. Chandler, Phys. Rev. A Vol.82 (3), 032709 (2010).
- 2) Direct Angle Resolved Measurements of Collision Dynamics with Electronically Excited State Molecules: NO(A<sup>2</sup>S<sup>+</sup>)+Ar, J. J. Kay, G Paterson, M. L. Costen, K. E. Strecker, K.G. McKendrick, D. W. Chandler., J Chem. Phys. 134, 091101 (2011)
- 3) Collisions of Electronically Excited Molecules: Differential Cross-Sections for Rotationally Inelastic Scattering of NO(A<sup>2</sup>Σ<sup>+</sup>) with Ar and He.; J. J. Kay, J. D. Steill, J. Klos, G. Paterson, M. L. Costen, K. E. Strecker, K. G. McKendrick, M. H. Alexander and D. W. Chandler, Molecular Physics 00268976.2012.670283. (2012)
- 4) Interaction of NO (A<sup>2</sup>Σ<sup>+</sup>) with Rare Gas Atoms: Potential Energy Surfaces and Spectroscopy J. Klos, M. H. Alexander, R. Hernandez-Lamonedá, et al., Journal of Chemical Physics, Vol.: 129 Issue: 24, 244303 (2008)
- 5) Alignment Measurements Following NO(A) + Ne Collisions: J. D. Steill, D. W. Chandler, K. G. McKendrick, M. L. Costen, G. Paterson, J. Klos and M. H. Alexander, Manuscript submitted.
- 6) Rotationally Resolved IR-Diode Laser Studies of Ground-State CO<sub>2</sub> Excited by Collisions with Vibrationally Excited Pyridine. J. A. Johnson, K. Kim, M. Mayhew, D. G. Mitchell, and E. T. Sevy. Journal of Physical Chemistry A, 112(12):2543–2552, (2008).
- 7) Energy-Dependent Dynamics of Large ΔE Collisions: Highly Vibrationally Excited Azulene (E=20,390 and 38,580 cm<sup>-1</sup>) with CO<sub>2</sub>. L. Yuan, J. Du, and A. S. Mullin. ,Journal of Chemical Physics, 129(1), JUL 7 2008.
- 8) Multiple-Well, Multiple-Path Unimolecular Reaction Systems. I. MultiWell computer program suite. International J. R. Barker, Journal of Chemical Kinetics, 33(4):232–245, APR 2001.
- 9) The Recombination of Propargyl Radicals: Solving the Master Equation. S. Klippenstein and J. A. Miller, The Journal of Physical Chemistry A, 105:7254–7266, 2001.
- 10) Energy Transfer of Highly Vibrationally Excited Naphthalene: Collisions with CHF<sub>3</sub>, CF<sub>4</sub>, and K; H. Hsu, M. T. Tsai, Y. A. Dyakov, C. K. Ni, J. Chem. Phys Vol. 135 (5) Article # 054311 (2011)

### BES-Supported Publications, 2010 – present:

- 1) Dual-Etalon Frequency-Comb Cavity-Ring-Down Spectrometer: D. W. Chandler and K. E. Strecker: J. Chem. Phys. 136,154201 (2012).
- 2) Collisions of electronically excited molecules: differential cross-sections for rotationally inelastic scattering of NO(A<sup>2</sup>Σ<sup>+</sup>) with Ar and He.; J. J. Kay, J. D. Steill, J. Klos, G. Paterson, M. L. Costen, K. E. Strecker, K. G. McKendrick, M. H. Alexander & D. W. Chandler, Molecular Physics DOI 10.1080/00268976.2012.670283. (2012).
- 3) Atom-Molecule Interactions Beyond billiard ball collisions: D. W. Chandler Source: Nature Chemistry, Vol. 3(8) 574-575 (2011).
- 4) Direct Angle Resolved Measurements of collision dynamics with electronically excited state molecules: NO(A<sup>2</sup>S<sup>+</sup>)+Ar, Kay J.J., Paterson G., Costgen M.L., Strecker K.E., McKendrick K.G., Chandler D.W., J Chem. Phys. 134,091101 (2011)
- 5) Cold and ultracold molecules: Spotlight on orbiting resonances, Chandler DW, J Chem. Phys. Vol.132 110901 (2010).
- 6) Cold atoms by kinematic cooling, Kay, JJ; Klos, J; Alexander, MH, Strecker KE, Chandler DW, Phys. Rev. A Vol.82(3) 032709 (2010).

## Petascale Direct Numerical Simulation and Modeling of Turbulent Combustion

Jacqueline H. Chen (PI) and Sgouria Lyra

Sandia National Laboratories, Livermore, California 94551-0969

Email: [jhchen@sandia.gov](mailto:jhchen@sandia.gov)

### Program Scope

In this research program we have developed and applied massively parallel three-dimensional direct numerical simulation (DNS) of building-block, laboratory scale flows that reveal fundamental turbulence-chemistry interactions in combustion. The simulation benchmarks are designed to expose and emphasize the role of particular phenomena in turbulent combustion. The simulations address fundamental issues associated with chemistry-turbulence interactions at atmospheric pressure that underly practical combustion devices: extinction and reignition, premixed and stratified flame propagation and structure, flame stabilization in autoignitive coflowing jet flames and reactive jets in crossflow, and flame propagation in boundary layers. In addition to the new understanding provided by these simulations, the resultant DNS data are used to develop and validate predictive mixing and combustion models required in engineering Reynolds-Averaged Navier Stokes (RANS) and large-eddy (LES) simulations.

### Recent Progress

In the past year, computer allocations from a DOE Innovative and Novel Computational Impact on Theory and Experiment (INCITE) grant have enabled us to perform several petascale three-dimensional DNS of turbulent flames with detailed chemistry. These studies focused on understanding: 1) Extinction of stratified counterflow  $H_2$ /air flames under intense turbulence and strain [1], and 2) Lean premixed  $H_2$ /air flames in intense sheared turbulence [2]. DNS data were also used to assess various mixing and flame wrinkling models for RANS and LES [3-6]. Highlights of our accomplishments in the past year are summarized below, followed by a summary of future research directions.

#### *Extinction of stratified counterflow $H_2$ /air flames under intense turbulence and strain*

Highly turbulent lean premixed hydrogen-air flames stabilized against non-adiabatic stoichiometric combustion products in chemical equilibrium are investigated in a joint direct numerical simulation (DNS) and experimental approach [1]. The effects of turbulence, strain rate, non-adiabaticity and composition stratification on flame structure, local flame quenching and re-ignition are studied using three-dimensional DNS and laser induced fluorescence (LIF) imaging of OH. Combustion was established at an elevated turbulent Reynolds number of 1,000 in a compact cylindrical volume delimited by the two co-axial nozzles of diameter 12.7 mm and separation distance 12 mm. The reactant and stoichiometric product streams are specified at temperatures of 294 K and 1475K, respectively, and at 1 atm. The DNS was performed with a detailed chemical kinetics mechanism for hydrogen-air that involves 9 species and 19 elementary reaction steps. The analysis of the combined simulated and measured data quantifies the local extinction levels, and reveals the morphology of the extinguishing and re-light events. The joint approach focuses on the turbulence-flame interactions and assessment of the driving mechanism that leads to local extinction and identifies the main re-ignition patterns and the probability of their occurrence.

A parametric study was performed where two parameters, the equivalence ratio of the reactant stream (Flames A, C, D) and the length scale of the turbulent structures (Flame E), were varied in the DNS. Systematic increase of the reactant mixture equivalence ratio, from 0.2 to 0.6, leads to higher overall burning rate as depicted by a comparison of the heat release rate isocontours between Flame A (equivalence ratio of 0.2) and Flame D (equivalence ratio of 0.6) in Figs. 1a and 1b. Increasing the length scale of the turbulent structure in Flame E by ten-fold over Flame C (ratio of integral turbulence scale to nozzle diameter is 0.3 for Flame E) while maintaining a constant equivalence ratio of 0.4 leads to a significantly thicker flame brush with apparent higher corrugation, as shown in Figs. 1c and 1d.

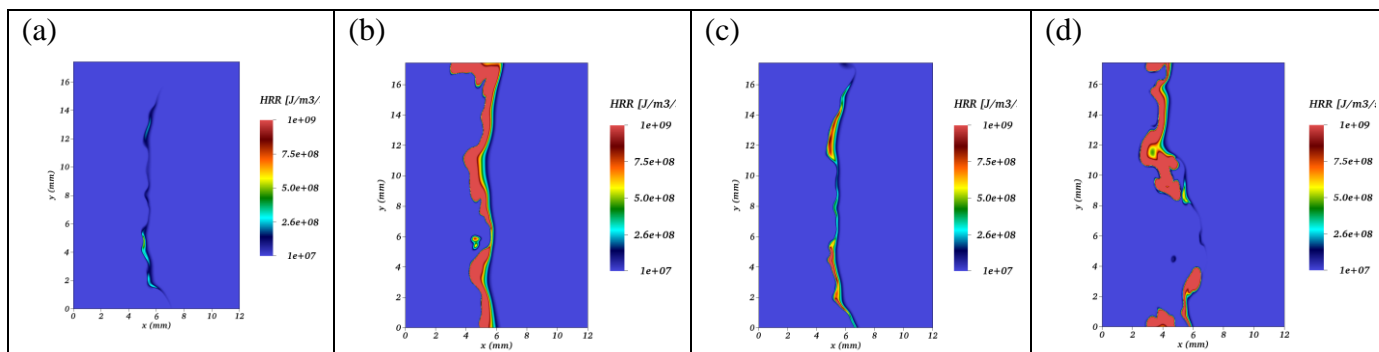


**Figure 1:** (a-d) Heat release rate, in the middle spanwise plane for the simulated flames A,D, C and E (from left to right). The equivalence ratio of flames A,C,D and E is 0.2, 0.4, 0.6 and 0.6, respectively.

Figure 2 shows the mass fraction of OH in the middle spanwise plane between the opposed nozzles at a representative time from the DNS and experiment performed under similar flow/flame conditions in the same counterflow configuration [1]. Both the DNS and experimental data illustrate the presence of a thick flame stabilized approximately 3mm downstream of the tip of the reactants nozzle. The inflowing turbulence interacts with an initially flat laminar flame and induces significant corrugation and a highly curved instantaneous flame surface morphology. Three-dimensional motions contorted by the large scale turbulent eddies aid the formation of flame branches, which in the two dimensional view, appear as detached from the main flame surface indicating the strong effect of turbulence on the flame topology. Successive low heat release rate events occurring on the reactants stream of the configuration characterized by low levels of OH are classified as local extinction events. The extinguished regions appear as holes in the flame structure and are convex towards the counterflowing products gases. This suggests that as the flame is convected downstream by the turbulent straining motions, it is forced to interact with the sub-adiabatic hot product stream and exhibits partial quenching.

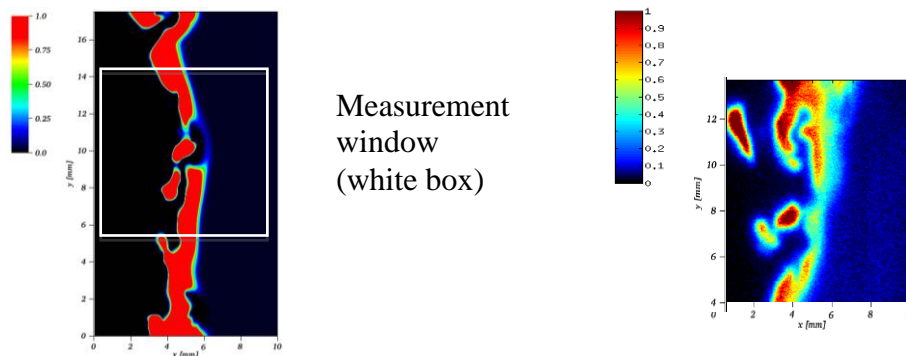


**Figure 2:** a) Instantaneous OH mass fraction from Flame E by DNS (left), and experiments (right).

Once formed, the locally quenched regions grow in physical extent with time; however, full quenching of the reaction zone is not observed. Instead, favorable thermochemical and flow conditions lead to local re-ignition events. The observed recovery modes in the DNS include a combination of edge-flame propagation and expansion of an ignition kernel that forms within the extinguished region.

#### DNS and a priori LES modeling of turbulent premixed flames in intense sheared turbulence

DNS were performed of a lean premixed hydrogen flame with a detailed chemical kinetic model in shear-driven turbulence [2]. The DNS configuration is a canonical flow of two initially planar flames propagating towards each other into a temporally developing plane jet of premixed reactants. The jet Reynolds number of 10,000 necessitates using nearly seven billion grid points to resolve the fine-scale

turbulent structure and obtain reasonable statistical convergence. While the principal novel contribution of the present database is the consideration of a strong mean shear which drives intense turbulent mixing within the flame structure, in addition, the turbulence Reynolds numbers are higher than previous DNS studies (turbulent Reynolds numbers of up to 1000) which have similar resolution of fine-scale structure. The turbulent kinetic energy spectrum exhibits over a decade in the inertial range with Kolmogorov's  $k^{-5/3}$  scaling with wave number  $k$ . Three cases were simulated with different Damköhler numbers, while Reynolds number was held fixed. The flames burn in the thin reaction zones regime where the Karlovitz number is high. The integrated burning rates up to approximately six times the laminar burning rate were obtained. It is shown that increased flame surface area accounts for most of the enhanced burning while increases in the burning rate per unit area also play an important contribution.

The DNS database was then used to assess a new model for the unresolved flame surface area, i.e. the subfilter flame wrinkling, intended for LES. The approach draws on concepts from fractal geometry, requiring the modeling of an inner cut-off scale representing the smallest scale of flame wrinkling, and the fractal dimension controlling the resolution dependence of the unresolved flame surface area. In contrast to previous modeling, it was argued that the inner cut-off should be filter-size invariant in an inertial range. Then, dimensional and physical reasoning together with Damköhler's limiting scaling laws for the turbulent flame speed were used to infer the cut-off and fractal dimension in limiting regimes. Two methods of determining the fractal dimension were proposed: a static, algebraic expression or a dynamic approach exploiting a Germano-type identity. Finally the model was compared against the DNS in *a priori* tests and was found to give excellent results, quantitatively capturing the trends with time, space, filter size, and Damköhler number.

#### **Future Work:**

##### *Flame characterization and blow-off of jet arrays in a turbulent cross-flow*

Reactive transverse fuel jets in cross-flowing turbulent flow are widely encountered in aeronautical and land based combustion devices where they are used to improve mixing and minimize pollutant formation. The designed injection nozzles need to provide the desired rapid mixing between the fuel and the cross-flowing oxidizer stream and prevent flame stabilization in the near field of the fuel injection nozzle, which is challenging for gas turbines operating with hydrogen enriched fuels. Combustion in such flows has been identified to occur in mixed modes downstream of the injector, which poses a significant challenge for modeling. Earlier studies [7,8] have investigated the stabilization of isolated transverse jets injected perpendicularly and at an angle of  $75^\circ$  with the transverse direction.

The proposed research aims to build upon previous findings by investigating the flame structure and stabilization of a) multiple interacting transverse jets, b) isolated jets injected obliquely, at various injection angles in the spanwise direction, and c) isolated jets injected in high pressure environments. The proposed computational study will be performed using high-fidelity direct numerical simulation (DNS) resolving all the relevant time- and length-scales of turbulence and chemical kinetics. The analysis will provide detailed benchmark data augmenting previous parametric studies in the JICF configuration, which will provide in-depth fundamental understanding about mixing processes and flame stabilization.

#### **References:**

1. S. Lyra, H. Kolla, B. Coriton, A. Gomez, J. H. Frank and J. H. Chen, "Extinction of stratified counterflow  $H_2$ /air flames under intense turbulence and strain," accepted to Eighth U.S. National Combustion Meeting, University of Utah, May 19-22, 2013.
2. E. R. Hawkes, O. Chatakonda, H. N. Kolla, and J. H. Chen, "A petascale DNS study of the modelling of flame wrinkling for large-eddy simulations in intense turbulence," *Combust. Flame* **159(8)** (2012), 2690-2703.
3. O. Chatakonda, E. R. Hawkes, M. Talei and J. H. Chen, "A priori assessment of algebraic wrinkling models of premixed turbulent flames in the thin reaction zones for large-eddy simulation," submitted to *Flow Turb. and Comb.*, 2012.

4. O. Chatakonda, E.R. Hawkes, A.J. Aspden, A.R. Kerstein, H. Kolla, J.H. Chen, "On the fractal characteristics of low Damköhler number flames," submitted to *Comb. Flame*, 2012.
5. C. M. Kaul, V. Raman, E. Knudsen, E. S. Richardson, J. H. Chen, "Large eddy simulation of a lifted ethylene flame using a dynamic nonequilibrium model for subfilter scalar variance and dissipation rate," *Proc. Comb. Inst.* **34** (2012), 1289-1296.
6. E. Knudsen, E. S. Richardson, E. M. Doran, H. Pitsch, and J. H. Chen, "Modeling scalar dissipation and scalar variance in LES: algebraic and transport equation closures," *Phys. Fluids* **24** 055103 (2012).
7. R. W. Grout, A. Gruber, J. H. Chen and C. S. Yoo, "Direct numerical simulation of flame stabilization downstream of a transverse fuel jet in cross-flow," *Proc. Combust. Inst.* **33** (2011), 1629-1637.
8. H. Kolla, R. Grout, A. Gruber, J. H. Chen, "Mechanisms of flame stabilization and blowout in a reacting turbulent hydrogen jet in cross-flow," *Combust. Flame* **159(8)** (2012), 2755-2766.

#### **BES Publications (2011-2013):**

1. R. W. Grout, A. Gruber, J. H. Chen and C. S. Yoo, "Direct numerical simulation of flame stabilization downstream of a transverse fuel jet in cross-flow," *Proc. Combust. Inst.* **33** (2011), 1629-1637.
2. C. S. Yoo, E. S. Richardson, R. Sankaran, and J. H. Chen, "A DNS study of the stabilization mechanism of a turbulent lifted ethylene jet flame in highly-heated coflow," *Proc. Combust. Inst.* **33** (2011)1619-1627.
3. L. Wang, E. R. Hawkes, and J. H. Chen, "Flame edge statistics in turbulent combustion," *Proc. Combust. Inst.* **33** (2011) 1439-1446.
4. E. R. Hawkes, R. Sankaran, and J. H. Chen, "Estimates of the three-dimensional flame surface density and all terms in its transport equation from two-dimensional measurements," *Proc. Combust. Inst.* **33** (2011) 1447-1454.
5. N. Punati, J. C. Sutherland, A. R. Kerstein, E. R. Hawkes, and J. H. Chen, "An evaluation of the one-dimensional turbulence model: comparison with direct numerical simulations of CO/H<sub>2</sub> jets with extinction and reignition," *Proc. Combust. Inst.* **33** (2011),1515-1522.
6. J. H. Chen, *Plenary Paper* "Petascale direct numerical simulation of turbulent combustion –fundamental insights towards predictive models," *Proc. Combust. Inst.* **33** (2011), 99-123.
7. D. Lignell and J. H. Chen, and H. Schmutz "Effects of Damköhler number on flame extinction and reignition in turbulent non-premixed flames using DNS," *Combust. Flame* **158** (2011), 949-963.
8. C. S. Yoo, T. Lu, J. H. Chen, and C.K. Law, "Direct numerical simulations of ignition of a lean n-heptane/air mixture with temperature inhomogeneities at constant volume: parametric study," *Combust. Flame* **158** (2011), 1727-1741.
9. Z. Luo, C. S. Yoo, E. Richardson, J. H. Chen, C. K. Law, T. Lu, "Chemical explosive mode analysis for a turbulent lifted ethylene jet flame in highly-heated coflow," *Combust. Flame* **159** (2012), 265-274.
10. E. R. Hawkes, O. Chatakonda, H. N. Kolla, and J. H. Chen, "A Petascale DNS study of the modelling of flame wrinkling for LES in intense turbulence," *Combust. Flame* **159(8)** (2012), 2690-2703.
11. E. S. Richardson and J. H. Chen, "Probability density function modelling of molecular mixing in flames with differential diffusion," *Combust. Flame* **159(7)** (2012), 2398-2414.
12. H. Kolla, R. Grout, A. Gruber, J. H. Chen, "Mechanisms of flame stabilization and blowout in a reacting turbulent hydrogen jet in cross-flow," *Combust. Flame* **159(8)** (2012), 2755-2766.
13. A. Gruber, J. H. Chen, D. Valiev, and C. K. Law, "Direct numerical simulation of premixed flame boundary layer flashback in turbulent channel flow," *J. Fluid Mech.* **709** (2012), 516-542.
14. R. W. Grout, A. Gruber, H. Kolla, P.-T. Bremer, J. C. Bennett, A. Gyulassy and J. H. Chen, "A direct numerical simulation study of turbulence and flame structure in transverse jets analysed in jet-trajectory based coordinates," *J. Fluid Mech.* **706** (2012), 351-383.
15. E. Knudsen, E. S. Richardson, E. M. Doran, H. Pitsch, and J. H. Chen, "Modeling scalar dissipation and scalar variance in LES: algebraic and transport equation closures," *Phys. Fluids* **24** 055103 (2012).
16. Y. Yang, H. Wang, S. B. Pope, J. H. Chen, "Large-eddy simulation/probability density function modeling of a non-premixed CO/H<sub>2</sub> temporally evolving jet flame," *Proc. Comb. Inst.* **34** (2012), 1241-1249.
17. N. Chakraborty, H. Kolla, R. Sankaran, E. R. Hawkes, J. H. Chen, and N. Swaminathan, "Determination of three-dimensional quantities related to scalar dissipation rate and its transport from two dimensional measurements: Direct Numerical Simulation based validation," *Proc. Comb. Inst.* **34** (2012), 1151-1162.
18. C. M. Kaul, V. Raman, E. Knudsen, E. S. Richardson, J. H. Chen, "Large eddy simulation of a lifted ethylene flame using a dynamic nonequilibrium model for subfilter scalar variance and dissipation rate," *Proc. Comb. Inst.* **34** (2012), 1289-1296.

# Dynamics and Energetics of Elementary Combustion Reactions and Transient Species

Grant DE-FG03-98ER14879

Robert E. Continetti (rcontinetti@ucsd.edu)

Department of Chemistry and Biochemistry, University of California San Diego  
9500 Gilman Drive, La Jolla, CA 92093-0340

## I. Program Scope

This research program pursues unique studies of transient neutral species and collision complexes relevant to combustion phenomena. The experimental approach involves photodetachment of precursor molecular and cluster anions, allowing direct measurements of the stability and dissociation dynamics of energy-selected reactive intermediates. This technique combines photoelectron spectroscopy with photofragment translational spectroscopy to yield photoelectron-photofragment coincidence (PPC) spectroscopy to fully characterize dissociative photodetachment (DPD) processes. In the final year of this grant we have continued to exploit a new cryogenic electrostatic ion beam trap (CEIBT) to study the photoelectron spectra and examine the DPD processes of cooled anion precursors of species important to combustion processes. This general experimental advance was described in detail in the *Review of Scientific Instruments* in 2011 [1]. Using this apparatus, we have carried out a number of experiments on reactive intermediates important to combustion processes as discussed below. The primary effort currently underway involves preparation of vibrationally excited anions prior to injection in the CEIBT.

## II. Recent Progress

### A. Studies of the Effects of Vibrational Excitation on the Reactivity of Combustion Intermediates

We are working to demonstrate the ability to selectively vibrationally excite anions prior to injection into the CEIBT. Using a Nd:YAG-pumped mid-IR OPO/OPA system (LaserVision), IR radiation in the 2000 – 5000  $\text{cm}^{-1}$  range is injected into the ion source region and counterpropagates relative to the ion beam using a mirror the ion beam ‘jumps’ over. This allows excitation of the full ensemble of ions produced in the 10 Hz ion source prior to injection into the CEIBT, where the kHz PPC experiment is carried out. We are currently working to demonstrate excitation of  $\text{OH}^-$  using threshold photodetachment to photodetach only  $\text{OH}^-(v=1)$ . In this sets of experiments trapped  $\text{OH}^-$  anions are irradiated with tunable laser light close to the photodetachment threshold around ( $\sim 680$  nm). Since all ions have typical rotational temperatures well below 100 K only a few transitions are allowed in the photodetachment process. A typical photoelectron spectrum that has been obtained from a measurement at 679.7 nm (1.824 eV) is shown in Fig. 1. The two peaks in the spectrum are assigned to P3(2) and Q3(1) rotational branches from  $\text{OH}^-(v=0)$  (for notation see reference [2]) and the arrow denotes where the expected contribution from vibrationally excited anions should appear. To date we have seen no clear evidence for vibrational excitation and are working to optimize IR beam transport and overlap with the ion beam.

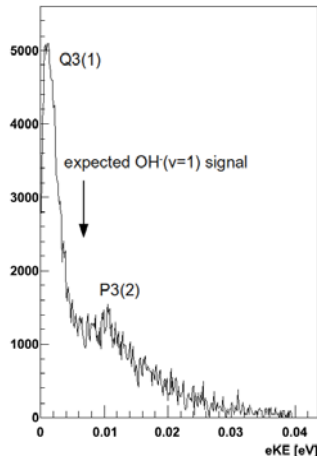


**Figure 1:** Near threshold photoelectron spectrum of  $\text{OH}^-$

Once infrared excitation is optimized we will examine the effects of OH stretch excitation on the dynamics of the  $\text{HOCO}$ ,  $\text{OH}(\text{H}_2\text{O})$  and the  $\text{OH}(\text{OH})$  neutral systems produced by photodetachment of the vibrationally excited anions.

### B. Transition State Dynamics of the $\text{F} + \text{H}_2\text{O} \rightarrow \text{OH} + \text{HF}$ Reaction

A fundamental reaction of particular interest in the scope of vibrationally excited systems is the fluorine-water reaction  $\text{F} + \text{H}_2\text{O} \rightarrow \text{HF} + \text{OH}$ . Crossed beam studies of this reaction have revealed rich reaction dynamics in the fluorine-water system, including an inverted product vibrational distribution and

non-adiabatic surface hopping [3]. From a theoretical point of view, a full six-dimensional treatment of the quantum dynamics of this system, although theoretically challenging, has recently become possible [4].

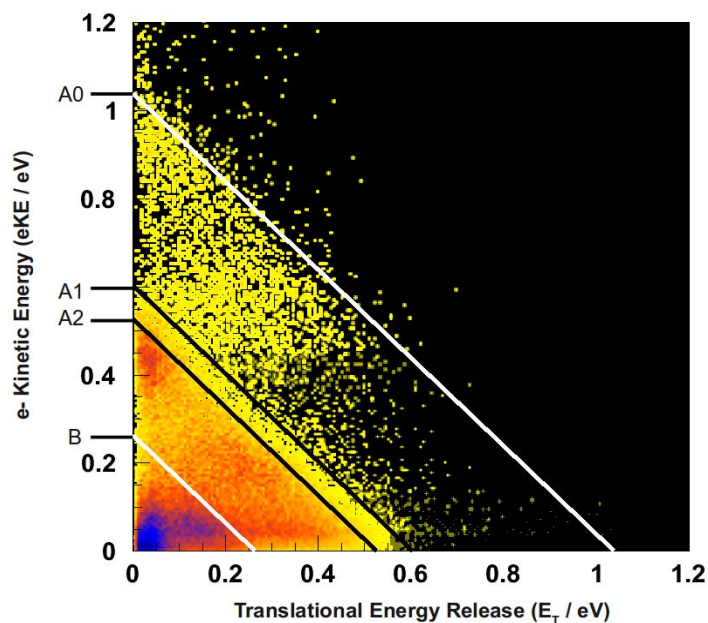


Figure 2: PPC spectrum for the  $F(H_2O)$  dissociation at a photon energy of 4.80 eV. Diagonal limits indicate the energetic thresholds for fragmentation into **A0**)  $HF + OH$ , **A1**)  $OH(v=1) + HF$ , **A2**)  $OH + HF(v=1)$  and **B**)  $F + H_2O$

rotational levels.

Studies of the neutral reaction have shown that the OH products are formed in the two  ${}^2\Pi_{1/2}$  and  ${}^2\Pi_{3/2}$  spin-orbit states. While these two states are only spaced by  $150\text{cm}^{-1}$  in OH they adiabatically belong to two different potential energy surfaces that are separated by several hundred meV along the reaction pathway. Along the diagonal ridge assigned to the  $HF(v=1)$  state (A2) two distinct features can be identified, one with an intensity maximum near  $KER=0.05\text{ eV}$  and the second one near  $KER=0.25\text{ eV}$ . Since both of these features are found on the same diagonal line, they must belong to identical (or in this case nearly degenerate) states. We assign these features to DPD events which end up on the two different surfaces (characterized by different repulsive energies) that lead to the two OH spin-orbit state products.

In a recent study on vibrational predissociation of  $F^-(H_2O)\cdot Ar$  clusters the wavefunction of the  $F^-(H_2O)$  cluster has been analyzed with respect to the role of the shared  $F-H-O$  proton [5]. McCoy *et al.* find that already in the ground state the structure of the anion must be partially described as a  $(FH)OH^-$  cluster. This effect becomes more dominant upon vibrational excitation of the shared proton bond, which would increase the efficiency of dissociation into  $HF + OH$  since the  $(FH)OH^-$  structure has a better Franck-Condon overlap into this reaction channel. This indicates that once the infrared excitation scheme is optimized, the  $F^-(H_2O)$  cluster will be an interesting test case to study mode-selective reaction dynamics.

Using a photon energy of 4.80 eV the DPD of  $F^-(H_2O)$  was studied. In the measured PPC spectra, shown in Fig. 2, the energetic onsets ( $KE_{max}$ ) for two different dissociation pathways are marked: fragmentation into **A**) the lower in energy  $HF + OH + e^-$  products and **B**) the higher lying reactant side asymptote  $F + H_2O + e^-$ . Although the configuration of the nascent  $FH_2O$  is thought to be more “reactant-like” the spectra clearly show that a majority of all events proceed to form  $HF + OH$  products.

Further  $KE_{max}$  limits in the PPC spectrum shown in Fig. 2 (marked as **A1** and **A2** in the plot) denote dissociation into vibrationally excited OH and HF fragments, respectively. For the HF fragments significant vibrational excitation in ( $v=1$ ) is observed, exceeding the population found in the ground state. In comparison the OH fragments show less excitation and can be considered vibrationally cold. All vibrational features show a broad band structure assigned to the population of high

### C. State-Resolved Predissociation Dynamics of the Formyloxy Radical – HCO<sub>2</sub>/DCO<sub>2</sub>

Building on our recent work on the HOCO radical, we have returned to further examine the isomeric formyloxy radical, HCO<sub>2</sub>. Accessing several low-lying electronic states (<sup>2</sup>B<sub>2</sub>, <sup>2</sup>A<sub>1</sub>, and <sup>2</sup>A<sub>2</sub>) [6], photodetachment at 290nm (4.27 eV) yields the neutral formyloxy radical with substantial excitation in the O-C-O bending mode. This O-C-O bending excitation is coupled to bending excitation in the CO<sub>2</sub> product. Each vibrational state in the neutral can predissociate to several CO<sub>2</sub> product states resulting in a series of vertically aligned features in the

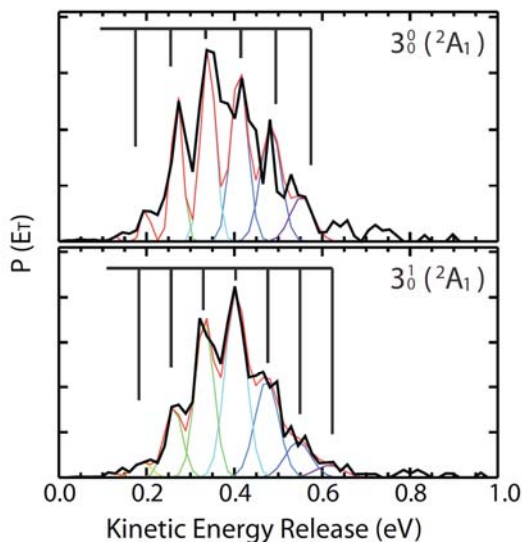


Figure 3: Electron kinetic energy slices for selected peaks corresponding to the O-C-O bending mode in the <sup>2</sup>A<sub>1</sub> state for peaks.

O bending mode in the CO<sub>2</sub> products than predicted, with results peaked around  $\omega_2 = 3$  depending on the available energy as determined by the initial neutral state formed by photodetachment. Even the ground state of the neutral formyloxy radical results in CO<sub>2</sub> products with significant populations (on the order of 20 - 30%) in  $\omega_2 = 2, 3,$  and 4, consistent with our previous findings [6].

### D. Photodetachment and DPD of Alkoxides and Hydroxy Carbanions

More complex oxygenated organic radicals are of considerable interest owing to their role as combustion intermediates in the oxidation of new fuel stocks such as biofuels. In experiments using the CEIBT we have carried out a study on the photodetachment of tert-butoxide with both non-deuterated and deuterated precursors, (CH<sub>3</sub>)<sub>3</sub>CO<sup>-</sup> at m/e = 73 and (CD<sub>3</sub>)<sub>3</sub>CO<sup>-</sup> at m/e = 82 respectively. The experiments provided confirmation that the primary product is the tert-butoxy radical, consistent with prior results by Lineberger and co-workers [8].

However, PPC spectra also revealed a DPD process involving the loss of a methyl radical. There are two possible reaction pathways for dissociation by loss of a methyl radical: from the carbanion isomer: (a) (CH<sub>3</sub>)<sub>2</sub>COHCH<sub>2</sub><sup>-</sup> + hv → CH<sub>3</sub> + CH<sub>3</sub>COHCH<sub>2</sub> or tert-butoxide: (b) (CH<sub>3</sub>)<sub>3</sub>CO<sup>-</sup> + hv → CH<sub>3</sub> + (CH<sub>3</sub>)<sub>2</sub>CO (acetone). The PPC spectrum shown in Figure 5 compares the experimental results at 3.2 eV photon energy with calculated energetics using the CBS-Q//B3 level of theory for the transition state barrier and product energetics for each dissociative pathway. The horizontal lines indicate the maximum eKE expected for dissociation above the transition state barrier for formation of the products (a) or (b). The

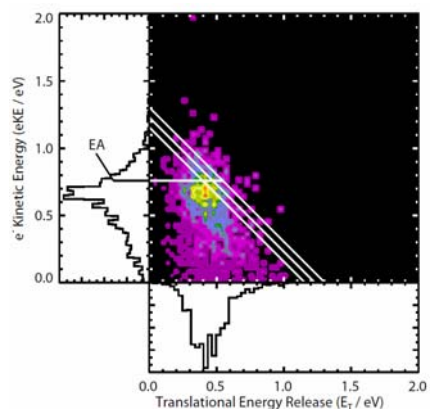


Figure 4: Photoelectron-photofragment coincidence spectrum for the reaction  $\text{DCO}_2^- + h\nu \rightarrow \text{D} + \text{CO}_2 + e^-$  at 290 nm.

spectrum first reported in ref. [6].

These features derive from predissociation sequence bands,

wherein a given bending state of the radical as determined in the photoelectron spectrum can predissociate to form several bending excited states in CO<sub>2</sub>, as determined in the E<sub>T</sub> spectrum. In Figure 3, a coincidence spectrum is shown, wherein the right-most KE<sub>max</sub> corresponds to formation of D + CO<sub>2</sub>(000). The other KE<sub>max</sub> limits at lower total kinetic energy represent sequential excitation in the bending mode of the CO<sub>2</sub> product. While the signal-to-noise in the coincidence spectrum is not great, slices in eKE selecting different predissociated vibrational modes in DCO<sub>2</sub> provide state-resolved CO<sub>2</sub> bending distributions as shown by the fits to the data in Figure 4. These results offer a direct comparison to the much colder bending vibration distributions calculated by Ma and Guo [7]. Our experimental results indicate greater excitation of the O-C-

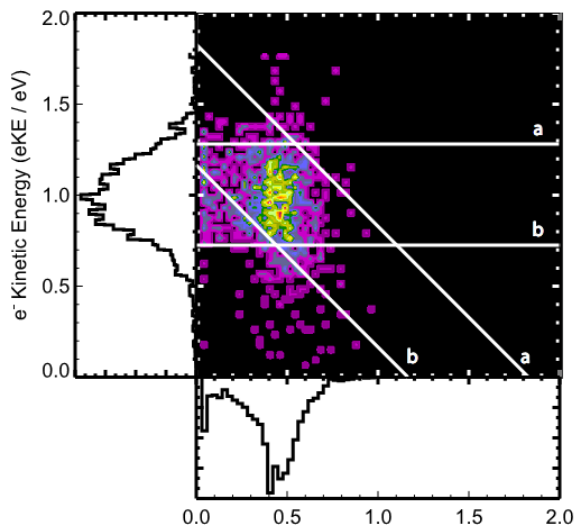


Figure 5: PPC spectrum for  $m/e = 73$  at 3.2 eV photon energy of  $(\text{CH}_3)_2\text{COHCH}_2^-$  with calculated energetics displayed for the pathways (a)  $(\text{CH}_3)_2\text{COHCH}_2^- + h\nu \rightarrow \text{CH}_3 + \text{CH}_3\text{COHCH}_2$  (propen-2-ol) or (b)  $(\text{CH}_3)_3\text{CO}^- + h\nu \rightarrow \text{CH}_3 + (\text{CH}_3)_2\text{CO}$  (acetone). Horizontal lines, at 1.30 eV and 0.73 eV represent the maximum eKE for dissociation over the barriers to yield pathways a and b, respectively.  $\text{KE}_{\text{max}}$  limits at 1.77 eV and 1.16 eV indicate the maximum available energy for pathways a and b, respectively.

important biofuels that are coming into use. This will be an important future direction for this research program.

#### IV. References

1. C.J. Johnson, B.B. Shen, B.L.J. Poad and R.E. Continetti, *Rev. Sci. Instrum.* **82**, 105105 (2011).
2. F. Goldfarb, C. Drag, W. Chaibi, S. Kroger, C. Blondel, and C. Delsart, *J. Chem. Phys.* **122**, 014308 (2005)
3. A. M. Zolot, D. J. Nesbitt, *J. Chem. Phys.* **129**, 184305 (2008)
4. J. Li, R. Dawes, H. Guo, *J. Chem. Phys.* **137**, 094304 (2012)
5. S. Horvath, A.B. McCoy, J.R. Roscioli and M.A. Johnson, *J. Phys. Chem. A* **112**, 12337 (2008)
6. T.G. Clements and R.E. Continetti, *J. Chem. Phys.* **115**, 5345 (2001)
7. J. Ma and H. Guo, *Chem. Phys. Lett.* **511**, 193 (2011).
8. T.M. Ramond, G.E. Davico, R.L. Schwartz and W.C. Lineberger, *J. Chem. Phys.* **112**, 1158 (2000)

#### V. Publications supported by this project 2010-2013

1. C.J. Johnson and R.E. Continetti, *Dissociative photodetachment of cold  $\text{HOCO}^-$  and below-barrier dissociation to  $\text{H} + \text{CO}_2$* , *J. Phys. Chem. Lett.* **1**, 1895-1899 (2010).
2. B.L.J. Poad, C.J. Johnson and R.E. Continetti, *Photoelectron-photofragment coincidence studies of  $\text{NO}^-$ -X clusters ( $X=\text{H}_2\text{O}$ ,  $\text{CD}_4$ )*, *Discussions of the Faraday Society* **150**, 481-492 (2011).
3. C.J. Johnson, B.L.J. Poad, B.B. Shen and R.E. Continetti, *Communication: New insight into the barrier governing  $\text{CO}_2$  formation from  $\text{OH} + \text{CO}$* , *J. Chem. Phys.* **134**, 171106-1-4 (2011).
4. C.J. Johnson, B.B. Shen, B.L.J. Poad and R.E. Continetti, *Photoelectron-photofragment coincidence spectroscopy in a cryogenically cooled electrostatic ion beam trap*, *Rev. Sci. Instrum.* **82**, 105105-1-9 (2011).
5. C.J. Johnson, M.E. Harding, B.L.J. Poad, J.F. Stanton and R.E. Continetti, *Communication: The electron affinities, well depths and vibrational spectroscopy of cis- and trans- $\text{HOCO}$* , *J. Am. Chem. Soc.* **133**, 19606-19609 (2011).

diagonal lines indicate the  $\text{KE}_{\text{max}}$  available assuming ground state products using the calculated reaction enthalpies. The calculated energetics indicate that pathway (b) is not viable as a result of not only the barrier height but also conservation of energy as shown by the diagonal line (b), under the assumption that the parent anions are not vibrationally excited. This leads to the conclusion that photodetachment of the hydroxyl carbanion forms an unstable radical that dissociates to  $\text{CH}_3 + \text{CH}_3\text{COHCH}_2$  (propen-2-ol).

#### III. Future Work

During the final months of the present grant the primary focus will be on pursuing the experiments on vibrational excitation of the precursor anions, as well as obtaining new results on oxygenated radicals such as the carboxyl radical derived from 2-propynoic acid,  $\text{HC}\equiv\text{C-CO}_2\text{H}$  and related unsaturated carboxylic acids. In addition, we are currently completing the develop of an electrospray ionization source with other support (ACS Petroleum Research Foundation New Directions Grant, ending September 2013) that will open up a variety of new systems for study in the future, including large oxygenated organic molecules important to the combustion of the increasingly

## Dissociation Pathways and Vibrational Dynamics in Excited Molecules and Complexes

F.F. Crim  
Department of Chemistry  
University of Wisconsin–Madison  
Madison, Wisconsin 53706  
fcrim@chem.wisc.edu

Our research investigates the chemistry of vibrationally excited molecules. The properties and reactivity of vibrationally energized molecules are central to processes occurring in environments as diverse as combustion, atmospheric reactions, and plasmas and are at the heart of many chemical reactions. The goal of our work is to unravel the behavior of vibrationally excited molecules and to exploit the resulting understanding to determine molecular properties and to control chemical processes. A unifying theme is the preparation of a molecule in a specific vibrational state using one of several excitation techniques and the subsequent photodissociation of that prepared molecule. Because the initial vibrational excitation often alters the photodissociation process, we refer to our double-resonance photodissociation scheme as *vibrationally mediated photodissociation*. In the first step, fundamental or overtone excitation prepares a vibrationally excited molecule, and then a second photon, the photolysis photon, excites the molecule to an electronically excited state from which it dissociates. Vibrationally mediated photodissociation provides new vibrational spectroscopy, measures bond strengths with high accuracy, alters dissociation dynamics, and reveals the properties of and couplings among electronically excited states.

Our recent experiments have used ion imaging to follow the adiabatic and nonadiabatic dissociation pathways in ammonia, to study the influence of vibrational excitation on the dynamics at conical intersections in phenol, and to obtain new vibrational spectroscopy on the formic acid dimer. These studies have set the stage for our newest measurements on the spectroscopy and vibrational predissociation dynamics of ammonia dimers and trimers. Our goal is to understand and prepare vibrations in the ground electronic state, to study the vibrational structure of the electronically excited molecule, and to probe and control the dissociation dynamics of the excited state in clusters.

### Spectroscopy of Ammonia Oligomers

The detailed insights that have come from our experiments on the influence of vibrational excitation on the excited state dynamics of ammonia suggest that the vibrationally mediated photodissociation of ammonia dimers and of complexes of ammonia with other small molecules could reveal novel behavior. Our two central concerns are the influence of complexation on the dynamics at the conical intersection and the changes that complexation produces in the vibrationally mediated photodissociation of ammonia. There are detailed studies of the photodissociation of bare ammonia molecules that provide a starting point for our work. We have studied the vibrational predissociation of ammonia dimers and trimers as a prelude to experiments that add electronic excitation.

A supersonic expansion of ammonia in He produces the oligomers we study. Exciting the N-H stretching vibration in an oligomer produces vibrationally and rotationally excited ammonia fragments that we detect by (2+1) REMPI through the  $\tilde{B}$  state, as illustrated on the left-hand side of Figure 1. The right-hand side of the figure shows the infrared action spectrum obtained by observing NH<sub>3</sub> fragments with one quantum of excitation in the umbrella bending vibration ( $\nu_2$ ). As the lower trace in the figure shows, these features are consistent with the transitions observed in He droplets (Slipchenko *et al.*, J. Phys. Chem. A

111, 7460 (2007)) and show that excitation of either the symmetric N-H stretch or the antisymmetric N-H stretch initiates vibrational predissociation.

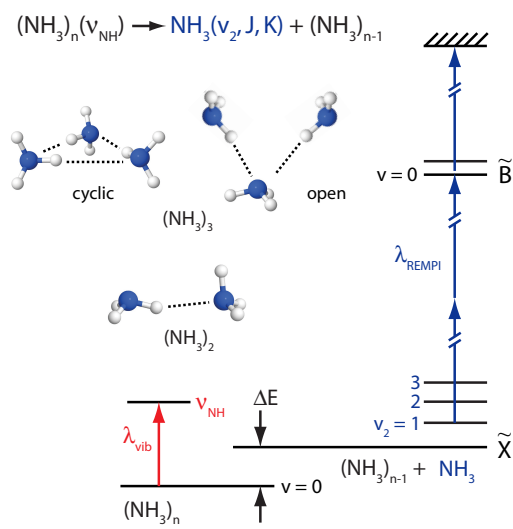
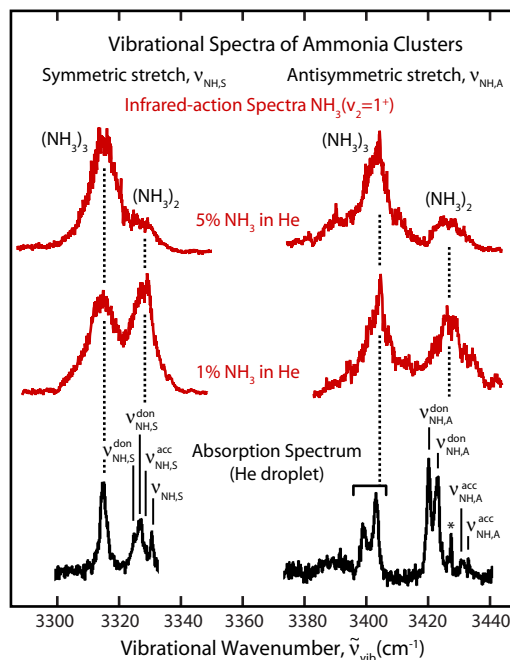


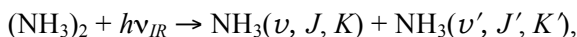
Figure 1



The key to obtaining these action spectra and to the analysis of the predissociation dynamics described below is the ability to interrogate individual vibrational rotational states ( $v, J, K$ ) of the ammonia products using REMPI detection. A collaboration with Dr. Collin Western at the University of Bristol has been critical to simulating and assigning the spectra. Along the way, we have been able to identify new transitions and refine some spectroscopic constants.

### Dissociation Energy and Dynamics of Ammonia Dimers

Velocity-map ion-imaging detection of fragments  $\text{NH}_3(v, J, K)$  directly provides the distribution of recoil speeds of the undetected partner fragment  $\text{NH}_3(v', J', K')$  formed in the vibrational predissociation of the dimer,



where  $J$  and  $K$  are the quantum numbers for the total angular momentum and its projection on the symmetry axis, respectively. Because the distribution of recoil energies mirrors the distribution of internal energies  $E'_{\text{int}}(\text{NH}_3)$  of the undetected fragment, analysis of the recoil distributions yields the binding energy of the dimer.

Even though there are many available states, clear patterns of state population are apparent in the distribution of recoil speeds. For example, Figure 2 shows the distribution extracted from the ion image of the product,  $\text{NH}_3(v_2=2^+, J=6, K=6)$ . As the vertical lines indicate, the maxima in the distribution align with recoil speeds corresponding to the formation of the undetected product in various  $J'$  states with  $K'=0$ . The identification of the features marked in the figure comes from using conservation of energy

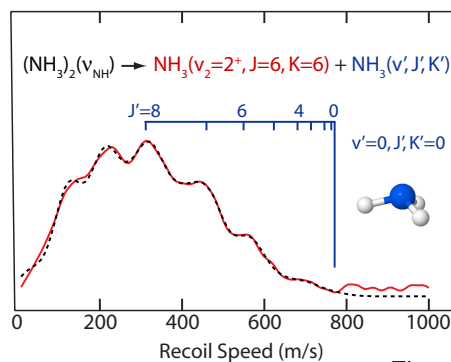


Figure 2

and a dissociation energy of  $658 \text{ cm}^{-1}$ . Introducing all of the possible values of  $K'$  in the analysis produces the simulation of the recoil speed distribution shown as the dashed line in the figure. Performing this same analysis self-consistently for a total of 17 different detected rovibrational states ( $\nu, J, K$ ) produces comparably good fits to all of the data and gives a dissociation energy for the dimer of  $D_0 = 660 \pm 20 \text{ cm}^{-1}$ . This value is much more precise than previous experimental estimates and is consistent with recent calculations. Calculating the dissociation energy is challenging because of the large contribution of zero-point energy (about 40% of the well depth  $D_e$ ) in this loosely bound complex

The analysis of the images also shows that most of the available energy appears as vibrational excitation, with there being at least two quanta of umbrella bending excitation distributed between the fragments. Producing  $\text{NH}_3(\nu_2=3^+)$  requires almost all of the available energy and leaves the undetected partner with no vibrational energy. In many cases,  $\text{NH}_3(\nu_2=2^+)$  appears in partnership with  $\text{NH}_3(\nu=0)$  although there are cases where it is possible to make  $\text{NH}_3(\nu_2=1)$ . In cases where the detected product is  $\text{NH}_3(\nu_2=1^+)$ , the distributions suggest that the partner is born with a quantum of umbrella bending excitation as well, reflecting the transfer of vibrational energy between the two moieties during dissociation. Although the antisymmetric umbrella bending vibration ( $\nu_4$ ) is energetically accessible, we see no evidence of its formation, perhaps reflecting a dynamical bias in the vibrational predissociation.

### Dissociation Energy of Ammonia Trimers

Features corresponding to higher-order clusters appear in the infrared-action spectra in the regions of the intramolecular symmetric N-H stretching vibration ( $\nu_{NH,S}$ ) and the intramolecular antisymmetric N-H stretching vibration ( $\nu_{NH,A}$ ) shown in Figure 1. The spectra illustrate the influence of expansion conditions on the relative intensities of the features in the spectrum. The top trace is for an expansion containing 5%  $\text{NH}_3$  in He and the middle trace is for one containing only 1%  $\text{NH}_3$ . The spectra in both the symmetric and antisymmetric stretching regions differ markedly for the two different expansion conditions, with the lower energy feature being more prominent in the expansions containing more  $\text{NH}_3$ . Because these larger seed ratios should favor the formation of larger clusters, the changes between the spectra suggest that the lower energy feature comes from the trimer and that the higher energy feature comes from the dimer, in agreement with the assignments from the He droplet spectra.

Removing an  $\text{NH}_3$  fragment from the cyclic trimer requires breaking two hydrogen bonds, and, thus, the dissociation into monomer and dimer fragments,



consumes more energy than cleaving the single hydrogen bond of the dimer. Indeed, as the left hand side of Fig. 3 shows, the trimer feature is prominent in the infrared-action spectrum for detection of  $\text{NH}_3(\nu_2 = 1^+, J = 1, K = 0)$  but is essentially absent for detection of  $\text{NH}_3(\nu_2 = 3^+, J = 3, K = 0)$ . The relative intensities of the dimer and trimer features in the infrared-action spectra depend on the amount of energy available for breaking the hydrogen bonds in the cluster, a quantity that depends on the energy content of the detected fragment. Infrared-action spectra for ammonia fragments with large amounts of internal energy have almost no trimer component because there is not enough energy available to break two bonds in the cyclic trimer. By contrast, infrared-action spectra for fragments with low amounts of internal energy have a substantial trimer component. The right-hand side of the figure shows a quantitative analysis of the trimer contribution compared to that of the dimer in the action spectra. The growth in the trimer signal suggests that fragmentation of the trimer into a monomer and dimer requires an energy of 1700 to 1800  $\text{cm}^{-1}$ , a range that is consistent with several theoretical estimates.

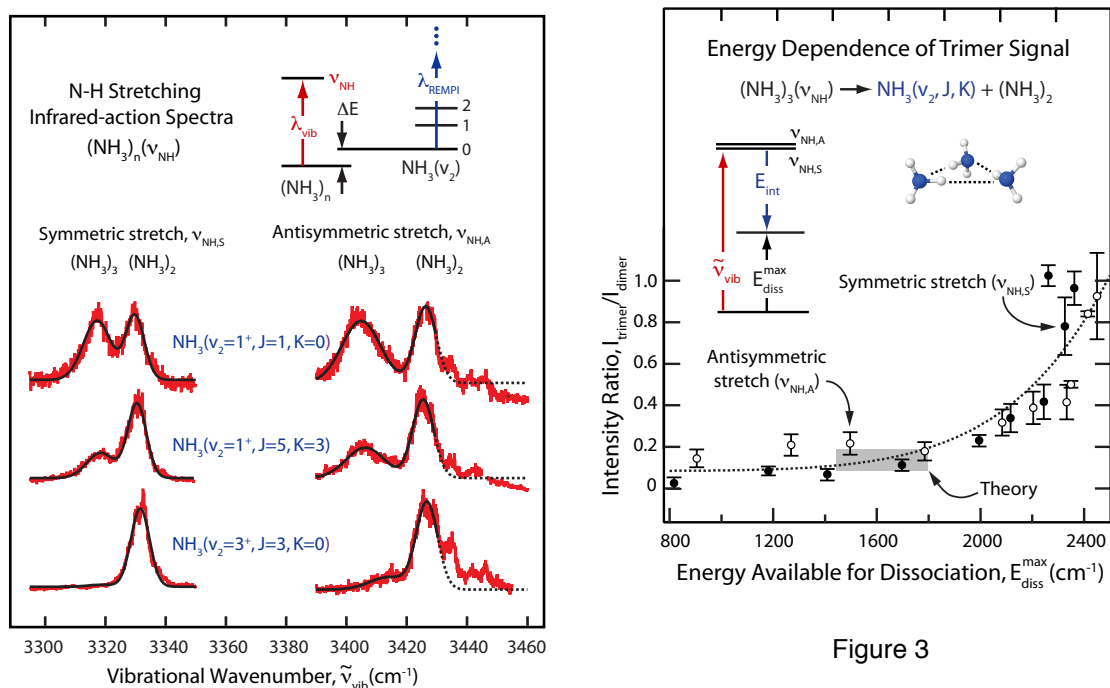


Figure 3

### Mixed Clusters and Future Directions

We have obtained our first results on a mixed cluster containing ammonia. Our first target has been the complex of  $\text{NH}_3$  with 3-aminophenol, on which there is good spectroscopy. We have used ion-dip to monitor the complex and have observed the first evidence of vibrationally induced isomerization in the complex. Our goal is to study complexes where we can use vibrational excitation to drive the isomerization and predissociation and where we can influence the passage through conical intersections. The variety of complexes available, including ones with different bonding motifs, offers a rich array of possibilities in which to study the influence of an adduct and initial vibrational excitation.

### PUBLICATIONS SINCE 2010 SUPPORTED BY DOE

*Reactive Scattering: Quantum-State-Resolved Chemistry*, F. Fleming Crim, in *Tutorials in Molecular Reaction Dynamics*, Eds. Mark Brouard and Claire Vallance (Royal Society of Chemistry, London, 2010).

A. S. Case, C. G. Heid, S. H. Kable, and F. F. Crim, *Dissociation energy and vibrational predissociation dynamics of the ammonia dimer*, *J. Chem. Phys.* **135**, 084312 (2011).

A. S. Case, C. G. Heid, C. M. Western, and F. F. Crim, *Determining the dissociation threshold of ammonia trimers from action spectroscopy of small clusters*, *J. Chem. Phys.* **136**, 124310 (2012).

*Molecular Reaction Dynamics Across the Phases: Similarities and Differences*. F. Fleming Crim, *Faraday Discussions* **157**, 1 (2012).

# Bimolecular Dynamics of Combustion Reactions

H. Floyd Davis

Department of Chemistry and Chemical Biology  
Baker Laboratory, Cornell University, Ithaca NY 14853-1301  
hfd1@Cornell.edu

## I. Program Scope:

The aim of this research program is to better understand the mechanisms and product energy disposal in elementary bimolecular reactions fundamental to combustion chemistry. Using the crossed molecular beams method, the angular and velocity distributions of neutral products from single reactive collisions are measured using “universal” mass spectrometry with single photon pulsed vacuum ultraviolet (VUV) photoionization, or for reactions leading to H, D, or O products, by Rydberg tagging time-of-flight (TOF) methods.

## II. Recent Progress:

### i. Crossed Beam Dynamics Using Pulsed Tabletop VUV Light Sources:

We have recently completed a PCCP perspective article<sup>1</sup> describing work in our laboratory on the development and application of pulsed photoionization detection employing high intensity vacuum-ultraviolet (VUV) radiation produced by tabletop light sources. This method employs four-wave mixing of collimated (unfocussed) commercial nanosecond dye lasers in mercury vapor.<sup>2</sup> This is an extremely valuable alternative to the use of synchrotron light sources for sensitive universal photoionization detection of products from crossed molecular beam reactions employing pulsed beam sources. Several examples involving combustion-related reactions are provided, and future prospects for the use of tabletop short-wavelength radiation applied to studies of chemical reaction dynamics are discussed.

### ii. Coherent XUV Light Source:

We have extended our high intensity VUV light source to the 12.5 eV range by developing what we believe is a very important method using noncollinear phasematching of tunable lasers in mercury vapor produced by pulsed laser vaporization of liquid mercury (Hg). As in our previous work involving VUV generation of unfocussed lasers in 1 m long Hg cells, the two photon states of Hg at  $71,333\text{ cm}^{-1}$  ( $^1D_2$ ) or  $63,928\text{ cm}^{-1}$  ( $^1S_0$ ) are employed. However, because of the use of laser vaporization, this method facilitates windowless operation, so wavelengths ( $\lambda$ ) in the region where even lithium fluoride (LiF) windows absorb strongly (the LiF cutoff is at  $\lambda = 105\text{ nm}$ ) are easily generated. Because Hg has a much higher nonlinear response than noble gases commonly employed for VUV generation, the efficiency is vastly higher, *i.e.*, by a factor of 10 or more. Also, due to the noncollinear nature of the four

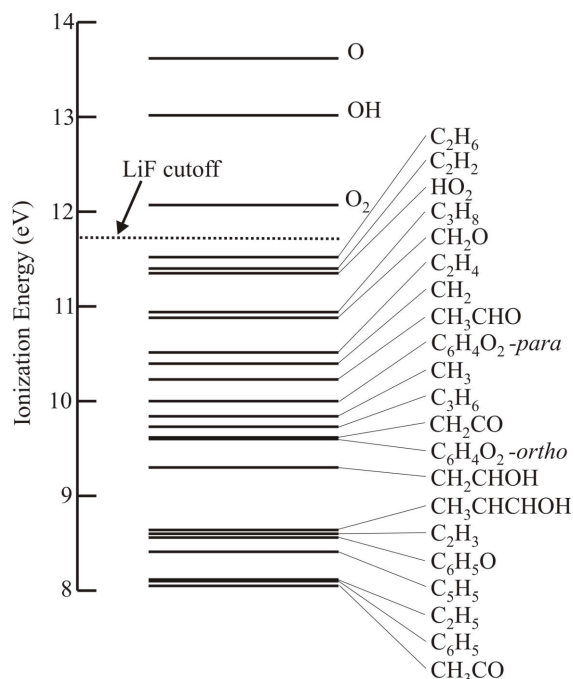


**Fig. 1:** Ionization energies of some molecules relevant to combustion.

wave mixing process, the VUV is spatially separated from the incident beams without need for gratings, prisms, lenses or other dispersive elements, yielding much higher usable intensities than is possible from other approaches. However, unlike generation of light near 10 eV, which is most efficient using *collimated* laser beams<sup>1</sup>, it is necessary to use *focused* configurations in noncollinear mixing. We have found that the XUV radiation may be easily refocused or recollimated into the ionization region using a concave silicon mirror at near-normal angle of incidence.

### iii. Reaction Dynamics of Phenyl Radicals:

Over the past year, we completed additional studies of reactions of phenyl radicals  $C_6H_5$  with  $O_2$ <sup>3</sup> as well as with propene and butene<sup>4</sup>. An important question that remains unanswered for  $C_6H_5 + O_2$  is what role, if any, does the isomerization of the initially-formed phenyl peroxy radical  $C_6H_5OO$  to the 2-oxepinyloxy radical<sup>5</sup> play in the dynamics. This species is expected to decompose to several different product channels, including  $C_5H_5 + CO_2$ ,  $C_6H_4O_2 + H$ , and  $C_5H_5O + CO$ , but to date, none of these have been detected directly either in our work or in the work of Kaiser and coworkers.<sup>6</sup>

### iv. Experimental Studies of the $H + O_2$ Reaction:

The  $H + O_2 \rightarrow OH(^2\Pi) + O(^3P_1)$  reaction is generally considered to be among the most important in combustion.<sup>7</sup> It is well-known that the OH is preferentially formed in high-N levels in  $v = 0$  and 1. Employing our high-intensity VUV pulsed laser system and ORTOF<sup>8</sup>, we have been able to achieve sensitivity levels sufficient to study this reaction under single crossed beam conditions. As indicated in the recent literature, a particularly interesting feature of this system is that while complex-forming dynamics play an important role, there is strong evidence for nonstatistical behavior. In our studies, fast ( $> 15,000$  m/s) H atoms are produced by photodissociation of either HI or HBr. Because HI is not commercially available, we have primarily used 193 nm photodissociation of HBr in our experiments. One complication is that the bandwidth of a free-running 193 nm excimer laser is large ( $\sim 100$   $cm^{-1}$ ), leading to broadening of the H atom beam velocity distribution. To date, this has been the limiting factor in our ability to achieve resolution sufficient to resolve OH rotational structure in the O atom velocity distributions. This difficulty can be surmounted using a Nd:YAG laser at 266 nm for photodissociation of HI as the H atom source. These studies are currently underway.

## III. Future Plans:

### i. Coaxial “Universal” VUV/XUV Photoionization in Crossed Beams Experiments:

For many years, we employed pulsed 157 nm radiation (7.9 eV) from a commercial  $F_2$  excimer laser for photoionization detection of products from transition metal + hydrocarbon reactions.<sup>9</sup> However, for most combustion-related systems, product ionization energies lie well above 7.9 eV, and pulsed tabletop VUV sources may be used for universal photoionization detection.<sup>1</sup>

While imaging detection may be applied for product detection using state-specific REMPI methods, a significant limitation of imaging methods for “universal detection” is that it generally requires that ionization using VUV radiation be carried out in the beam-crossing region where the pressure is high ( $> 10^{-5}$  Torr). Under such conditions, photodissociation of reactant molecules or bimolecular reactions of photoions produced in the detection step are difficult to avoid. Such VUV

laser-induced processes can greatly complicate the interpretation of experimental data, and could potentially cause experimental artifacts leading to erroneous conclusions.

While the approach used in our laboratory for product detection involving photoionization *outside of the beam-crossing region* is more difficult than imaging, artifacts due to unintended VUV-induced processes are unlikely. A significant experimental issue, making our approach particularly challenging, results from the fact that we employ an orthogonal ionization configuration similar to that used in crossed-beam machines employing synchrotron light sources.<sup>10</sup> Because synchrotrons are quasi-continuous, time-of-flight (TOF) data may be recorded continuously using pulsed molecular beams or continuous molecular beams with a slotted chopper wheel inserted into the product beam path. However, using pulsed laser-based VUV light sources, the determination of product TOF spectra requires that the photoionization laser delay be stepped in time relative to time zero for reaction. Depending upon the reaction kinematics, a TOF spectrum typically requires stepping the delay in 3-5 microsecond increments over ~25 channels. This factor of 25 reduction in duty cycle, as well as pulse to pulse VUV intensity fluctuations, has limited the signal to noise ratio attainable in our experiments.

We have recently proposed an experimental approach that promises to improve our experimental signal to noise ratios by up to *two orders of magnitude*.<sup>1</sup> It involves photoionization using a *coaxial* rather than an *orthogonal* VUV laser configuration. In order to test the method, we have recently assembled a single beam apparatus equipped with a conventional on-axis quadrupole mass spectrometer similar to that used in our rotatable source - fixed detector crossed beams machine. The apparatus includes a second quadrupole ion guide where coaxial photoionization is carried out.

After characterizing coaxial photoionization detection using this single beam apparatus, the method will be implemented in crossed beam experiments as follows: Using a rotatable source machine with fixed detector, products from bimolecular crossed beam reactions are produced as usual at the beam-crossing region, with time zero for reaction defined by the photolytic pulsed radical beam. Reaction products drift away from the crossing region as usual, spreading out spatially due to their different nascent velocities. A fraction of the products pass through several defining apertures into the first quadrupole field, about 20 cm long, held at  $<10^{-9}$  Torr. A pulsed counterpropagating and collimated VUV laser is then fired along the beam axis, ionizing a column of neutral products without significantly perturbing their nascent velocities. The ions then continue their motion along the beam axis and are mass filtered by the second quadrupole and counted as usual, producing a TOF spectrum. In this way, a much larger fraction (factor of 25) of reaction products are detected in each VUV laser pulse. This method holds great promise for opening up studies of a wide variety of combustion systems not previously amenable to the crossed beams method. We believe that only a few relatively straightforward technical issues need to be overcome in order to implement this approach.

#### **IV. Publications (published or accepted) citing DOE Support since 2010:**

1. D. R. Albert and H. Floyd Davis, "Collision Complex Lifetimes in the Reaction  $C_6H_5 + O_2 \rightarrow C_6H_5O + O$ ", *J. Phys. Chem. Lett.* **1**, 1107 (2010).
2. D. L. Proctor, D. R. Albert and H. F. Davis, "Improved piezoelectric actuators for use in high-speed pulsed valves", *Rev. Sci. Instrum.* **81**, 023106 (2010).

## V. References:

---

1. D.R. Albert and H. F. Davis, "Experimental Studies of Bimolecular Reaction Dynamics Using Pulsed Tabletop Vacuum Ultraviolet Photoionization Detection", invited perspective article, submitted to *Phys. Chem. Chem. Phys.*
2. D.R. Albert, D.L. Proctor, and H.F. Davis, "Efficient Production of VUV Pulses Using Unfocussed Laser Beams", submitted to *Rev. Sci. Instrum.*
3. D.R. Albert, M. Todt, and H.F. Davis, "The Role of Collision Energy in the  $C_6H_5 + O_2$  Reaction", to be submitted to *J. Phys. Chem. A*.
4. D.R. Albert, M. Todt, and H.F. Davis, "Competing Reaction Pathways in Phenyl Radical Reactions with Propene and Butene", to be submitted to *J. Phys. Chem. A*.
5. I.V. Tokmakov, G.S. Kim, V.V. Kislov, A.M. Mebel, and M.C. Lin, "The Reaction of Phenyl Radical with Molecular Oxygen: A G2M Study of the Potential Energy Surface", *J. Phys. Chem. A* **109**, 6114 (2005).
6. Parker, D.S., Zhang, F.; Gu, X; Kaiser, R.I. "Phenoxy Radical Formation under Single Collision Conditions from Reaction of the Phenyl Radical with Molecular Oxygen: The Final Chapter?", *J. Phys. Chem. A* **115**, 11515 (2011).
7. Z. Sun, D.H. Zhang, C. Xu, S. Zhou, D. Xie, G. Lendvay, H. Guo, "State-to-State Dynamics of  $H + O_2$  Reaction, Evidence for Nonstatistical Behavior", *J. Am. Chem. Soc.* **130**, 14962 (2008).
8. C. Lin, M.F. Witinski, and H.F. Davis, "Oxygen Atom Rydberg Time-of-Flight spectroscopy-ORTOF", *J. Chem. Phys.* **119**, 251 (2003).
9. P.A. Willis, H.U. Stauffer, R.Z. Hinrichs, H.F. Davis, "Rotatable Source Crossed Molecular Beams Apparatus with Pulsed VUV Photoionization Detection", *Rev. Sci. Instrum.* **70**, 2606 (1999).
10. X. Yang, J. Lin, Y.T. Lee, D.A. Blank, A.G. Suits, A.M. Wodtke, "Universal crossed molecular beams apparatus with synchrotron photoionization mass spectrometric product detection", *Rev. Sci. Instrum.* **68**, 3317 (1997).

# Exploration and validation of chemical-kinetic mechanisms

Michael J. Davis

Chemical Sciences and Engineering Division  
Argonne National Laboratory  
Argonne, IL 60439  
Email: davis@tcg.anl.gov

The focus of the work is on exploration and theoretical validation of chemical-kinetic mechanisms, which combines global sensitivity analysis with the exploration of the characteristics of the sensitivity analysis over the physical and chemical parameters. We have made modifications to our algorithm for global sensitivity analysis so that it is accurate with small sample sizes, allowing for its use in device modeling.

## Recent Progress

### Global Sensitivity Analysis with Small Sample Sizes

In collaboration with W. Liu, a project was initiated in the past year to improve our algorithm for doing global sensitivity analysis. It was made more efficient, so that smaller sample sizes could be used. We extended this further by incorporating sparse regression

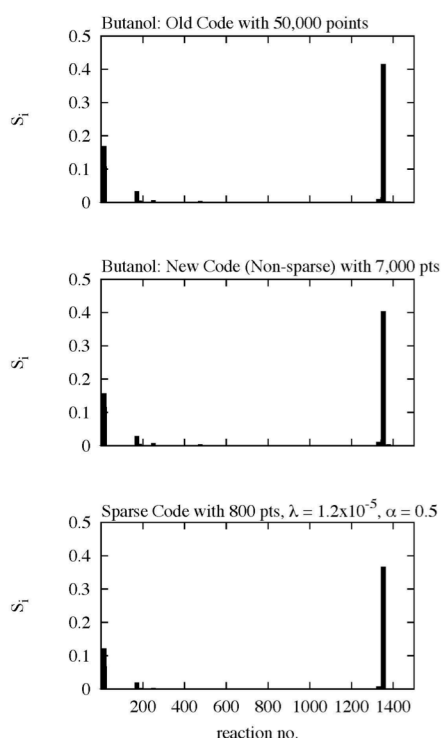


Fig. 1. The top shows sensitivity coefficients for butanol ignition with the old algorithm, the middle panel with the modified algorithm and the bottom with the sparse algorithm.

## Butanol Selection (Ignition)

Rxn	No	$S_i$	Rank	400	800	1200
NC4H9OH+HO2 = C4H8OH-1+H2O2	1353	0.403	1	1	1	1
H2O2+O2 = HO2+HO2 (dupl.)	14	0.158	2	2	2	2
H2O2(+M) = OH+OH(+M)	16	0.116	3	3	3	3
NC4H9OH+HO2 = C4H8OH-3+H2O2	1351	0.055	4	4	4	4
NC4H9OH+HO2 = C4H8OH-2+H2O2	1352	0.032	5	5	5	5
C2H5+HO2 = C2H5O+OH	171	0.0290	6	6	7	7
H2O2+O2 = HO2+HO2 (dupl.)	15	0.0287	7	7	6	6
NC4H9OH+HO2 = C4H8OH-4+H2O2	1350	0.018	8	8	8	8
NC4H9OH+HO2 = C4H8OH-4+H2O2	1329	0.011	9	9	9	9

## Butanol Selection: C<sub>2</sub>H<sub>4</sub>

Rxn	No	$S_i$	Rank	400	800	1200
NC4H9OH+OH = C4H8OH-4+H2O	1340	0.341	1	1	1	1
NC4H9OH+OH = C4H8OH-3+H2O	1341	0.222	2	2	2	2
NC4H9OH+HO2 = C4H8OH-1+H2O2	1353	0.102	3	3	3	3
NC4H9OH+HO2 = C4H8OH-4+H2O2	1350	0.032	4	4	4	4
C4H8OH-4 = C2H4+PC2H4OH	1388	0.022	5	5	5	6
C2H4+OH = C2H3+H2O	251	0.019	6	10	7	5
C2H5+HO2 = C2H5O+OH	171	0.013	7	6	6	7

Fig. 2. High sensitivity reactions.

techniques to limit the sample size even more. A summary of this approach is given in [P10].

Results for the new non-sparse and sparse computer codes are shown in Fig. 1, for n-butanol ignition [P9]. The old algorithm typically needed sample sizes of  $\sim 40$ /reaction. The n-butanol reaction mechanism has 1446 reactions and the sample size in the top panel of Fig. 1 is 50,000. The top panel of Fig. 2 lists all reactions with sensitivity coefficients greater than 0.01. The middle panel of Fig. 1 shows results using the new algorithm with a sample size of only 7000 and shows good agreement with the top panel.

The sample size can be reduced further using sparse regression techniques, as shown in the bottom panel of Fig. 1, where only 800 samples were used, which is less than the number of reactions. The accuracy of the sparse regression technique is tested in Fig. 2, where comparisons with the non-sparse algorithm are made. The top panel shows that for the ignition delay target sample sizes as low as 400 give a reasonable ordering of the reactions. The mis-orderings are shown in red, and in all columns there is accurate ordering down to a sensitivity coefficient of 0.02. For a sample size of 1200 there is accurate ordering except for the sixth and seventh most sensitive reactions, whose sensitivity coefficients are very close.

The bottom panel of Fig. 2 shows results for a species target. The reactions listed in the bottom panel are those for which the concentration of ethylene is most sensitive at  $\frac{1}{2}$  the ignition delay time. Once again there is very good agreement between sparse algorithm and the non-sparse algorithm, where the sample size is 10,000.

### *The Role of Individual Rate Coefficients in the Performance of Compression Ignition Engine Models*

In collaboration with Sivaramakrishnan, W. Liu (CSE Div., Argonne), Som, Longman (ES Div., Argonne), Zhou, and Skodje (Colorado), a set of calculations have been completed to investigate how the uncertainty of individual reaction coefficients affect engine performance, particularly the ignition delay time. The engine simulations are high fidelity, three-dimensional computations and include detailed chemistry (140 – 160 species and 800 – 1000 reactions), using a model for a biodiesel surrogate developed in [p8].

One of the goals of this work is to do global sensitivity analysis for the engine model, and the motivation for developing the sparse algorithm in the previous subsection was to make such calculations tractable, as each engine simulation takes several processor weeks.

Figure 3 presents ignition delay results for engine simulations for eight sets of reactions

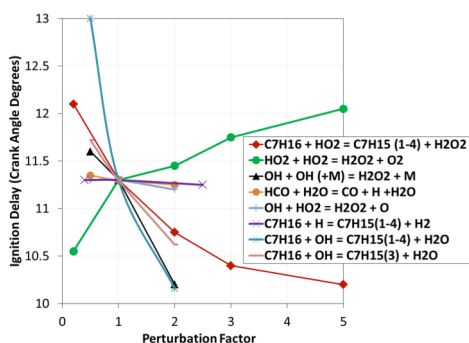


Fig. 3. Ignition delay for a series of engine simulations where rate coefficients of select reactions have been increased and decreased by their uncertainty factors are presented here.

chosen based on their sensitivities in constant-volume, 0-D ignition. 1 CA° is approximately 0.1ms at an engine speed of 1600 rpm. The results in Fig. 3 demonstrate that variations of rate coefficients of individual reactions can have a significant impact on engine performance, as a difference of 1 – 2 CA° can lead to misfiring if the engine is operating near the stability limit. In general, the sensitivity coefficients we calculated in 0-D were a good indication of the effect of the uncertainties of a given reaction under engine conditions.

However the ordering of the reactions can be different, with the caveat that there are ranges of conditions in the engine that are not encapsulated by any of our 0-D calculations.

The major difference between the engine simulations and the 0-D simulations is the sensitivity of ignition to the OH + n-heptane reactions.

Simulation	Ignition Delay HRR-based (CA°)	Ignition Delay Temperature-based (CA°)
Original	11.28	10.6
No Tunneling	11.08	10.4
Tunneling	11.31	10.6
+ 1 Kcal - No Tunneling	10.7	9.75
+ 1 Kcal - Tunneling	11.05	10.4
- 1 Kcal - No Tunneling	11.4	10.56
- 1 Kcal - Tunneling	11.45	10.75

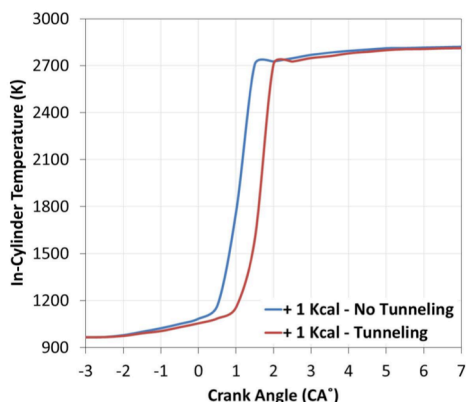
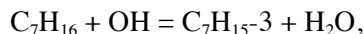


Fig. 4. A list of ignition delay times for the biodiesel surrogate is shown in the top panel for several different calculations of the rate coefficient for the HO<sub>2</sub> self-reaction. The bottom panel shows the maximum temperature as a function of crank angle. Total time is ~ 1 ms (initial CA is -9, and 1 CA is ~ 0.1 ms

These reactions were chosen for study because ignition is not generally sensitive to them in 0-D constant volume ignition calculations, although species concentrations can be very sensitive to their rates. Figure 3 indicates that the total variation of all four of these abstraction reactions has the strongest effect on ignition of any of the sets we studied, even though its uncertainty factor is set to 2. What is most interesting to us is that ignition delay times are sensitive to the single abstraction reaction:



which has a very small sensitivity coefficient in 0-D. Obviously the complexity of the engine simulation compared to the constant-volume ignition makes the cause of this difference difficult to ascertain without further study, which we plan to do. An important conclusion from comparison of Fig. 3 to 0-D calculations is that a global sensitivity analysis within the engine cylinder is liable to yield some significant differences and is motivating us to complete such a study.

In addition to the uncertainty calculations in Fig. 3, we studied how the features of a given reaction would affect ignition delay times, choosing the self-reaction of HO<sub>2</sub>, whose rate coefficient was recently calculated [P6]. We examined how barrier height and tunneling affected the ignition delay time. The results are summarized in Fig. 4. The top

### H<sub>2</sub>CO Glob. Sensitivity for MF Pyrolysis

Reaction	No.	S <sub>i</sub>	S <sub>i,373</sub>
CH <sub>3</sub> OCHO=CH <sub>3</sub> +HCO <sub>2</sub>	358	0.25	0.019
CH <sub>3</sub> OCHO+H=CH <sub>3</sub> OCO+H <sub>2</sub>	373	0.18	—
CH <sub>3</sub> OCO=CH <sub>3</sub> +CO <sub>2</sub>	385	0.18	0.0005
CH <sub>3</sub> OCHO+H=CH <sub>2</sub> OCHO+H <sub>2</sub>	362	0.051	0.0058
CH <sub>3</sub> OCO=CH <sub>3</sub> O+CO	386	0.035	0.00025
CH <sub>2</sub> O+HCO=CH <sub>2</sub> OCHO	388	0.029	0.014
CH <sub>3</sub> OCHO+CH <sub>3</sub> =CH <sub>3</sub> OCO+CH <sub>4</sub>	375	0.017	0.0002
CH <sub>3</sub> OCHO+CH <sub>3</sub> =CH <sub>2</sub> OCHO+CH <sub>4</sub>	364	0.014	0.0003
CH <sub>2</sub> OCHO=CH <sub>3</sub> OCO	387	0.011	0.0079
CH <sub>3</sub> OCHO=CH <sub>3</sub> OH+CO	355	0.010	0.0023

The modeling presented in Figs. 3 and 4 demonstrate that a detailed understanding of molecular motion is crucial for the accurate modeling of the ignition characteristics of realistic devices.

### Global Sensitivity Analysis for Methyl Formate Pyrolysis

panel shows the ignition delay time for two different definitions of ignition and the bottom panel demonstrates that whether tunneling is included or not in the rate calculation can have a noticeable affect on ignition delay times. The bottom panel demonstrates that there is a 6% affect on ignition delay time whether tunneling is included or not.

In collaboration with Sivaramakrishnan and Liu, global sensitivity analysis for speciation in methyl formate pyrolysis has been undertaken. The new non-sparse computer code allowed for the accurate calculation of first and second order sensitivity coefficients, with the latter unattainable with our previous algorithm without very large sample sizes. Some of our results are summarized in the table.

### Future Plans

Using our new sparse algorithm we will do global sensitivity analysis in engine simulations. We will extend this work to a different fuel, dimethyl ether, which will allow for incorporation of recent experimental and theoretical chemical kinetics information into the engine modeling. A new project has been initiated to compare reaction pathway analysis to global sensitivity analysis. This is a collaboration with Skodje (Colorado).

In the previous year we initiated a new project on dimension reduction using machine learning techniques, particularly unsupervised regression. This project is meant to be a nonlinear version of principal components analysis, which has recently been implemented in reactive flow simulations (Sutherland and Parrente).

### Publications

1. S. J. Klippenstein, L. B. Harding, M. J. Davis, R. T. Skodje, and A. S. Tomlin, "Uncertainty driven theoretical kinetics studies of  $\text{CH}_3\text{OH}$  ignition:  $\text{HO}_2 + \text{CH}_3\text{OH}$  and  $\text{O}_2 + \text{CH}_3\text{OH}$ ", *Proc. Combust. Inst.* 33, 351-357 (2011).
2. M. J. Davis, R. T. Skodje, and A. S. Tomlin, "Global sensitivity analysis of chemical-kinetic reaction mechanisms: Construction and deconstruction of the probability density function", *J. Phys. Chem A* 115, 1556-1578 (2011).
3. R. Sivaramakrishnan, D. Y. Zhou, R. T. Skodje, and M. J. Davis, "A comprehensive mechanism for ethanol combustion", *Proceedings of the 7<sup>th</sup> US National Technical Meeting of the Combustion Institute, Georgia Institute of Technology, Atlanta, GA* (2011).
4. R. Sivaramakrishnan, W. Liu, M. J. Davis, S. Som, and D. E. Longman, "A high temperature model for the combustion of methylbutanoate", *East. States Section of the Comb. Instit.* (2011).
5. R. L. Miller, L. B. Harding, M. J. Davis, and S. K. Gray, "Bi-fidelity fitting and optimization", *J. Chem. Phys.* 136, 074102-1 – 074102-11 (2012).
6. D. D. Y. Zhou, K. Han, P. Zhang, L. B. Harding, M. J. Davis, and R. T. Skodje, "Theoretical Determination of the Rate Coefficient for the  $\text{HO}_2 + \text{HO}_2 \rightarrow \text{H}_2\text{O}_2 + \text{O}_2$  Reaction: Adiabatic Treatment of Anharmonic Torsional Effects", *J. Phys. Chem.* 116, 2089-2100 (2012).
7. W. Liu, R. Sivaramakrishnan, M. J. Davis, S. Som, and D. E. Longman, "Development of a Reduced Biodiesel Surrogate Model for Compression Ignition Engine Modeling", *Central States Section of the Combustion Institute* (2012).
8. W. Liu, R. Sivaramakrishnan, M. J. Davis, S. Som, D. E. Longman and T. F. Lu, "Development of a reduced biodiesel surrogate model for compression ignition engine modeling", *Proc. Combust. Inst.* 34 401-409 (2013).
9. D. D. Y. Zhou, M. J. Davis, and R. T. Skodje, "Multi-Target Global Sensitivity Analysis of n-Butanol Combustion", *J. Phys. Chem. A*, submitted.
10. D. D. Y. Zhou, R. T. Skodje, W. Liu, and M. J. Davis, "Multi-Target Global Sensitivity Analysis of n-Butanol Combustion", *Proceedings of the 8<sup>th</sup> US National Technical Meeting of the Combustion Institute, University of Utah* (2013).
11. W. Liu, S. Som, D. D. Y. Zhou, R. Sivaramakrishnan, D. E. Longman, R. T. Skodje, and, M. J. Davis, "The Role of Individual Rate Coefficients in the Performance of Compression Ignition Engine Models", *Proceedings of the 8<sup>th</sup> US National Technical Meeting of the Combustion Institute, University of Utah* (2013). (2013)

# Dynamics of Radical Reactions in Biodiesel Combustion

Theodore S. Dibble

Department of Chemistry, SUNY-Environmental Science and Forestry

Syracuse, NY, 13210

[tsdibble@esf.edu](mailto:tsdibble@esf.edu)

## I. Program Scope

The ignition of diesel fuel depends on isomerization of peroxy radicals ( $\text{ROO}\bullet$ ) via a hydrogen shift reaction:



Production of OH radicals (chain propagation and branching) following reaction (1) leads to autoignition. Processes such as reaction (2):



compete with chain branching. Experimentalists face several difficulties in gaining an understanding of this chemistry, and no QOOH species has ever been detected by experiment! This has inspired many computational studies of these processes.

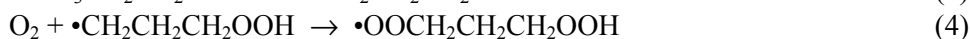
Biodiesel fuel is increasingly being used worldwide. Although we have a fair understanding of the molecular details of the chemistry of peroxy radicals derived from alkanes, biodiesel fuels contain ester and olefin groups which significantly impact the thermodynamics and kinetics of biodiesel ignition.<sup>1</sup> The broader goal of this research is to carry out systematic computational studies of the elementary kinetics of peroxy radical chemistry from compounds that are models for biodiesel ignition. This includes not only reactions (1) and (2), but also reactions leading to chain branching. In addition, the research will:

- include rigorous treatments of tunneling effects
- quantify the effect of chemically activated processes
- synthesize the results into structure-activity relations (SARs)

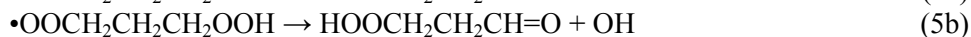
## II. Recent Progress

### A) Tunneling in the 1,5 H-shift of the a Model Second-Generation Peroxy Radical

Consider the sequence of reactions starting from propylperoxy radical and the 1,5 H-shift of the  $\bullet\text{OOQOOH}$  radical (reaction 5):



The species  $\text{HOOCH}_2\text{CH}_2\text{CH}\bullet\text{OOH}$  may or may not be a minimum on the potential energy surface, but even if it is, it likely lives for picoseconds or less.<sup>2</sup>



Reaction (5b) and analogous reactions are very exothermic on account of the loss of OH radical and formation of a carbonyl compound. Tunneling calculations in such cases commonly invoke the asymmetric Eckart formula and use this large exothermicity as a parameter which influences the extent of tunneling. As part of our study of tunneling in this autoignition archetype, we will explore the sensitivity of different tunneling treatments to assumptions about the stability of  $\text{HOOCH}_2\text{CH}_2\text{CH}\bullet\text{OOH}$

We have computed tunneling effects within the framework of two different semiclassical theories: the semiclassical transition state theory (SCTST) of Miller and coworkers,<sup>3</sup> and multidimensional tunneling as implemented by Truhlar and coworkers in Polyrate. The latter has been used by several research groups and has proven fairly accurate. The former approach (SCTST) has been less widely used because it was computationally inefficient for molecules of more than four atoms. A new algorithm applied by

Barker and co-workers makes SCTST much more efficient.<sup>4</sup> SCTST relies upon the coupling of anharmonic vibrational modes (including the imaginary frequency) to compute the extent of tunneling.

Polyrate calculations require calculation of Hessians at many points along the reaction path. By comparison, SCTST has the potential to be more efficient because, like TST, only the reactant and saddle point need to be characterized. However, SCTST is less well-tested than Polyrate. In addition to SCTST and SCT and LCT calculations, comparison was made to the asymmetric Eckart tunneling approach.

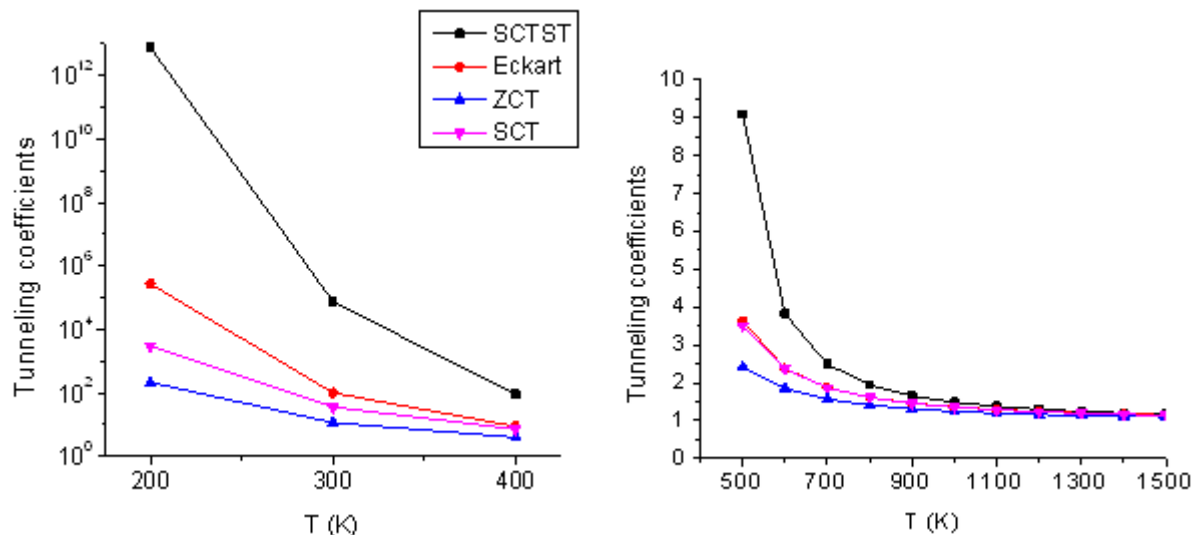
We started by characterizing the stationary points using density functional theory. As can be seen from Table 1, the results are in very good agreement with the QCISD(T) results of Goldsmith et al. Torsional motions were treated as separable hindered rotors. We then proceeded to use compute tunneling corrections to the canonical (high-pressure limiting) rate constant for reactions (5a) and (5b) using SCTST, ZCT, SCT, LCT, and Eckart tunneling.

**Table 1.** Comparison of relative energies from the present work and the literature for reaction (5).

Species	M05-2X/6-311+g(2df,2p)	M05-2X/6-31+g(d,p)	Goldsmith et al (Ref 5) QCISD(T)/CBS//B3LYP/6-31G(d)
•OOCH <sub>2</sub> CH <sub>2</sub> OOH	0.00	0	0.0
TS for 1,5 H-shift (v*, cm <sup>-1</sup> )	21.5 (1769i)	21.4 (1805i)	21.6 (Not listed)
HOOCH <sub>2</sub> CH <sub>2</sub> CH•OOH	12.1	11.2	NA
HOOCH <sub>2</sub> CH <sub>2</sub> CH=O + OH	-27.1	-22.6	-27.1

Results of tunneling calculations are shown in Figure 1. Result for LCT are not shown because tunneling was dominated by SCT at all temperatures shown. At temperatures relevant to autoignition (700-900 K) the difference between SCTST and ZCT with respect to SCT are of opposite sign, and modest in size. The Eckart approach seems to work very well. At lower temperatures, Eckart diverges from the SCT results, and SCTST tunneling corrections are much larger than predicted based on SCT. While reaction (7) is not expected to be important at such low temperatures, the discrepancy between the results of the methods calls into question the accuracy of at least one of them. Both are numerical methods, subject to

**Figure 1.** Tunneling coefficients ( $\kappa(T)$ ) for reaction (5a) by SCTST, Eckart tunneling, ZCT and SCT at (a) 200-400 K on a log scale, (b) 500-1500 K on a linear scale.



failure when used outside the area in which their assumptions and approximations are valid. We are in the process of investigating the source(s) of this discrepancy.

### B) Autoignition Mechanism of Methyl Butanoate (MB)

Methyl butanoate (MB) is composed of a methyl ester group and a short alkyl group (see Figure 2). MB oxidation mechanism has been studied as the starting point for understanding biodiesel combustion for a decade.<sup>6</sup> The CBS-QB3 composite method is used to determine reaction energies and activation barriers to reactions of peroxy radicals and the corresponding QOOH species. We include all four peroxy radicals formed subsequent to H-atom abstraction from MB (sites 1-3 and 5 in Figure 2). Reactions treated include H-shift and HO<sub>2</sub> elimination of ROO•, and decomposition of QOOH by C-C, C-O, and O-O scission.

Potential energy profiles have been obtained for all four peroxy radicals. Where one of these peroxy radicals isomerizes to form a carbon-centered radical, the chemistry of the second-generation peroxy radical has been investigated. Results are shown in Figure 4 for a single case.

Some models of autoignition chemistry of MB describe unimolecular reactions of QOOH as competing with subsequent O<sub>2</sub> addition. Therefore, we sought to thoroughly investigate the unimolecular reactions of all four QOOH from MB. The potential energy profile in Figure 3 depicts the eight reactions with the lowest barriers for the QOOH formed following 1,5 H-shift from OOC<sub>2</sub>H<sub>2</sub>CH<sub>2</sub>C(=O)OCH<sub>3</sub> (the peroxy radical formed following H-abstraction from site 1 of MB). The analogous studies have been carried out for the other three isomeric primary peroxy radicals from MB

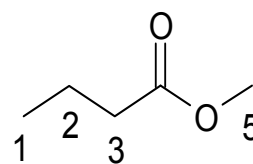


Figure 2. Methylbutanoate

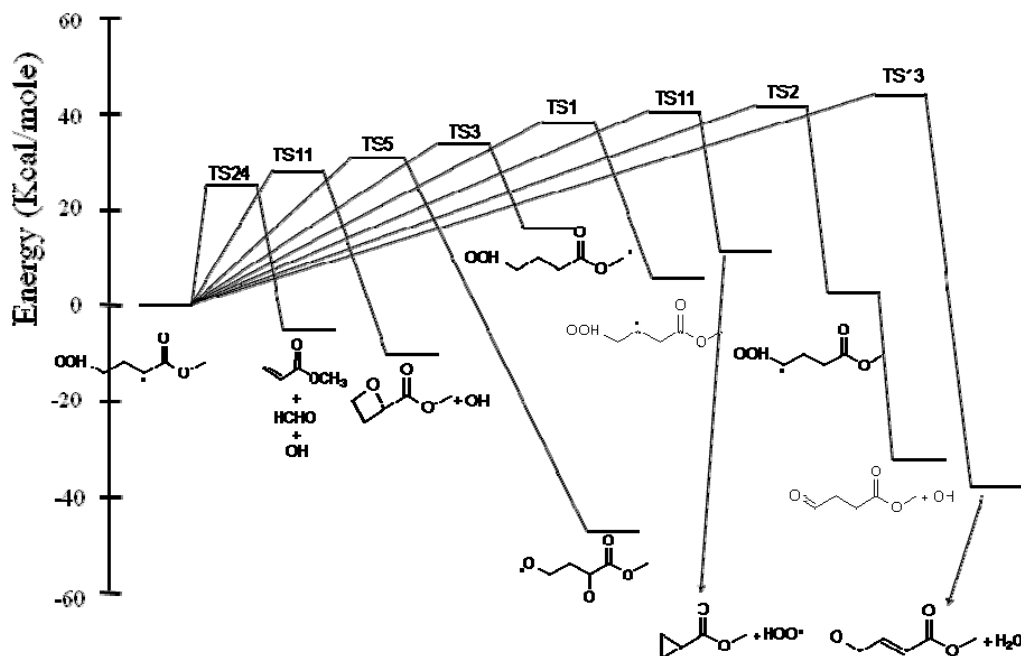
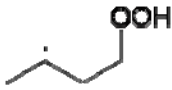
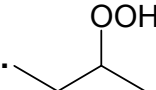


Figure 3. Potential energy profile for the most favorable unimolecular reactions of the QOOH species HOOC<sub>2</sub>CH<sub>2</sub>CHC(=O)OCH<sub>3</sub>. Energies in kcal/mol at M05-2X/6-311+G(2df,2p) with ΔZPE.

### C) Benchmark Quantum Calculations on Model QOOH Systems

The studies of unimolecular reactions of QOOH from methyl butanoate inspired us to investigate a range of unimolecular reactions of simpler QOOH. Selected results of these calculations are presented in Table 2. Different computational methods give rather different results, but the concerted OH loss is clearly the low-energy reaction pathway.

**Table 2.** Comparison of relative energies (kcal/mol) for two (lowest barrier) unimolecular reactions of two different 4-carbon QOOH formed by 1,5 H-shift from the corresponding peroxy radicals. CCSD(T)/ aug-cc-pVTZ //M052x/6-311++G(2df,2p) of the present work and M052x/6-311++G(2df,2p) (in parentheses).

Reactant			Method
Concerted elimination	OH		
	17.6 (22.1)	19.5 (23.5)	Present work
	17.1	19.7	CBS-QB3
	21.3	22.5	BHandHLYP
	14.3	22.2	QCISD(T)
C-C scission			Present work
	26.5 (28.1)	28.7 (28.4)	

### III. Future Work

We will refine the results of calculations on the QOOH and peroxy radicals from methylbutanoate, based in part on the insights from QOOH from n-butane. We will then proceed with RRKM/Master Equation Calculations on the QOOH from methylbutanoate.

We are in the process of investigating the source(s) of the discrepancy between SCTST and SCT tunneling predictions.

### IV. References

- [1] Sumathi, R.; Green W. H., *Phys. Chem. Chem. Phys.*, **2003**, 5, 3402-17.
- [2] Andersen, A.; Carter, E. A. *J. Phys. Chem. A*, **2006**, 110, 1393-1407.
- [3] Miller, W. H. *Faraday Discuss. Chem. Soc.*, **1977**, 62, 40-46
- [4] Nguyen, T. L.; Stanton, J. F.; and Barker, J. R. *Chem. Phys. Lett.*, **2010**, 499, 9-15
- [5] Goldsmith, C.F.; Green, W.H.; Klippenstein, S. J. *J. Phys. Chem. A*, **2012**, 116, 3325-3346.
- [6] Dooley, S.; Curran, H. J.; and Simmie, J. M. *Combust. Flame*, **2008**, 153, 2–32.

### V. Publications and submitted journal articles supported by this project 2010-2012

- T. S. Dibble, Y. Sha, W. F. Thornton, and F. Zhang. Cis-trans isomerization of chemically activated 1-methylallyl radical and fate of the resulting 2-buten-1-peroxy radical, *J. Phys. Chem. A* **2012**, 116, 7603–7614.
- F. Zhang and T. S. Dibble. Impact of Tunneling on hydrogen-migration of n-propylperoxy radical. *Phys. Chem. Chem. Phys.*, **2011**, 13, 17969-77.
- F. Zhang and T. S. Dibble, Effects of ester and olefin functional groups on kinetics of unimolecular reactions of peroxy radicals, *J. Phys. Chem. A* **2011**, 115, 655-663.
- T. S. Dibble and Yue Zeng, Potential energy profiles for the N + HOCO reaction and products of the chemically activated reactions N + HOCO and H + HOCO. *Chem. Phys. Letts.*, **2010**, 495, 170-174.

## Grant No. DE-FG02-12ER16298

Title: Vibrational Spectroscopy of Transient Combustion Intermediates Trapped in Helium Nanodroplets

PI: Gary E. Douberly  
University of Georgia  
Chemistry Department  
1001 Cedar St.  
Athens, GA 30602-1546

### 2012 Progress Report:

We have made tremendous progress towards the design, construction and optimization of an instrument to carry out low-temperature, high-resolution spectroscopy of transient species of fundamental importance to combustion science. Since the beginning of this funding period, we have constructed and implemented a high temperature pyrolysis source for the generation of hydrocarbon radicals, and we have demonstrated that we can record spectra of these species once they have been isolated in He nanodroplets. We reported the ro-vibrational spectrum of the  $\nu_3(e')$  band of the He-solvated methyl radical ( $\text{CH}_3$ ) (Ref. 1). Five allowed transitions produce population in the  $N_K = 0_0, 1_1, 1_0, 2_2$  and  $2_0$  rotational levels. The observed transitions exhibit variable Lorentzian line shapes, consistent with state specific homogeneous broadening effects. Population relaxation of the  $0_0$  and  $1_1$  levels is only allowed through vibrationally inelastic decay channels, and the  $^P P_1(1)$  and  $^R R_0(0)$  transitions accessing these levels have 4.12(1) and 4.66(1) GHz full-width at half-maximum linewidths, respectively. The linewidths of the  $^P R_1(1)$  and  $^R R_1(1)$  transitions are comparatively broader (8.6(1) and 57.0(6) GHz, respectively), consistent with rotational relaxation of the  $2_0$  and  $2_2$  levels within the vibrationally excited manifold. The nuclear spin symmetry allowed rotational relaxation channel for the excited  $1_0$  level has an energy difference similar to those associated with the  $2_0$  and  $2_2$  levels. However, the  $^P Q_1(1)$  transition that accesses the  $1_0$  level is 2.3 and 15.1 times narrower than the  $^P R_1(1)$  and  $^R R_1(1)$  lines, respectively. This is taken as evidence that the symmetry and anisotropy of the He- $\text{CH}_3$  intermolecular potential plays an important role in the rate of population relaxation of the rotational levels within the excited vibrational manifold. The anisotropy in the potential

necessary for coupling the  $1_0$  and  $0_0$  levels in the vibrationally excited level is by symmetry much less than the coupling associated with the rotational relaxation of the excited  $2_0$  and  $2_2$  levels. Only because the  $\text{CH}_3$  radical is an oblate top with two nuclear spin modifications were we capable of probing such high lying rotational levels with such large rotational relaxation energy gaps. Indeed, as a result of this work, the  $\text{CH}_3$  radical will be an interesting benchmark for theoretical calculations that aim to provide insight into the rotational and vibrational relaxation dynamics of He-solvated molecules that are classified as “light” rotors.

The vinyl radical ( $\text{H}_2\text{C}_\beta=\text{C}_\alpha\text{H}$ ) has been produced by the pyrolysis of di-vinyl sulfone and trapped in liquid He nanodroplets (Ref. 2). At 0.4 K, the entire population of nuclear spin isomers is cooled to either the  $0_{00}^+$  (ortho) or  $0_{00}^-$  (para) roconvibrational level. Survey scans in the fundamental CH stretch region reveal three bands that are assigned to the symmetric  $\text{CH}_2$  ( $\nu_3$ ), antisymmetric  $\text{CH}_2$  ( $\nu_2$ ) and lone  $\alpha\text{-CH}$  ( $\nu_1$ ) stretch bands. The assignments are based on comparisons to the jet-cooled vinyl radical spectrum of the  $\nu_3$  mode (from D.J. Nesbitt and co-workers), vibrational configuration interaction (VCI) calculations (from J.M. Bowman and co-workers), and the observed rotational fine structure for each band. The vinyl radical CH stretch band origins in He droplets differ from the VCI calculations by  $\approx 1$ , 2 and  $10\text{ cm}^{-1}$  for the  $\nu_3$ ,  $\nu_2$  and  $\nu_1$  modes, respectively. Each band consists of *a*-type and *b*-type transitions from the  $0_{00}$  level, and each of these is split by either the *difference in* or *sum of* the  $v=0$  and  $v=1$  tunneling splittings. From the separation between and splitting within these *a*- and *b*-type components, we obtain an *A'-B'* constant and the tunneling splittings in both  $v=0$  and  $v=1$  for each observed band. Comparing the He droplet spectra to previous high-resolution spectroscopy of the  $\nu_3$  band, we find that the *A'-B'* rotational constant for this mode is reduced to 89% of its gas phase value, and the tunneling splittings (ground and  $\nu_3$  excited states) are both reduced by  $\approx 20\%$ . In addition, the relative intensities of the  $\nu_3$  transitions seem to indicate 4:4 spin statistics for ortho and para nuclear spin isomers, suggesting a facile interchange mechanism for all *three* H atoms within the  $\approx 1200\text{ K}$  pyrolysis source, prior to the pick-up and cooling of the hot vinyl radical by the He droplet. The tentative upper state tunneling splittings extracted from the  $\nu_1$  and  $\nu_2$

bands are qualitatively inconsistent with those predicted using 1D vibrationally adiabatic potentials along the tunneling coordinate. We currently do not have a clear understanding of this apparent discrepancy, the resolution of which will require high-resolution jet-cooled spectra of these higher frequency bands. The  $\approx 20\%$  reduction in the ground and  $\nu_3$  excited state tunneling splittings is most likely due to two contributing effects from the He solvent. The He droplet can in principle modify both the tunneling barrier and the effective reduced mass for motion along this coordinate. We have estimated that either an  $\approx 40 \text{ cm}^{-1}$  increase in the effective barrier height or an  $\approx 5\%$  increase in the effective mass of the tunneling particles (both as upper limits) is sufficient to account for the observed  $\approx 20\%$  tunneling splitting reduction. Future theoretical work will be required to assess the extent to which each of these effects contribute to the overall modification of the vinyl radical tunneling dynamics upon solvation in liquid He.

The ethyl radical has been isolated and spectroscopically characterized in He droplets (Ref. 3). The five fundamental CH stretch bands are observed near  $3 \mu\text{m}$  and have band origins shifted by  $< 1 \text{ cm}^{-1}$  from those reported for the gas phase species [S. Davis, D. Uy and D. J. Nesbitt, *J. Chem. Phys.* **112**, 1823-1834 (2000); T. Häber, A. C. Blair, D. J. Nesbitt and M. D. Schuder, *J. Chem. Phys.* **124**, 054316 (2006)]. The symmetric  $\text{CH}_2$  stretching band ( $\nu_1$ ) is rotationally resolved, revealing nuclear spin statistical weights predicted by  $G_{12}$  permutation-inversion group theory. The first measurement of this radical's permanent electric dipole moment ( $0.28(2) \text{ D}$ ) is obtained via the Stark spectrum of the  $\nu_1$  band. The four other CH stretch fundamental bands are broadened in He droplets and lack rotational fine structure. The approximately  $1\text{-}2 \text{ cm}^{-1}$  line widths for these bands are attributed to the homogeneous broadening associated with solvent-mediated rovibrational relaxation dynamics. In addition to the five fundamentals, three  $A_1'$  overtone/combination bands are observed and have resolved rotational substructure. These are assigned to the  $2\nu_{12}$ ,  $\nu_4+\nu_6$ , and  $2\nu_6$  bands through comparisons to anharmonic frequency computations at the CCSD(T)/cc-pVTZ level of theory.

In addition to the fundamental spectroscopy described above for methyl, ethyl and vinyl radicals, we have demonstrated that hydrocarbon radical +  $\text{O}_2$  reactions can

be carried out within the low temperature, He droplet environment. For example, the sequential addition of a methyl radical and molecular oxygen to He nanodroplets leads to the barrierless reaction,  $\text{CH}_3 + \text{O}_2 \rightarrow \text{CH}_3\text{OO}$ . The reaction enthalpy is  $\sim 30$  kcal/mol and therefore requires the dissipation of  $\sim 2000$  He atoms to cool the  $\text{CH}_3\text{OO}$  to 0.37 K. The product  $\text{CH}_3\text{OO}$  radical remains in the droplet and is observed downstream with IR laser beam depletion spectroscopy. All three CH stretch bands of  $\text{CH}_3\text{OO}$  are observed, and rotational fine structure is partially resolved for the  $\nu_2$  totally symmetric CH stretch band, indicating complete internal cooling of the product to the droplet temperature. Electron impact ionization of the droplets containing  $\text{CH}_3\text{OO}$  results in the charge transfer reaction  $\text{He}^+ + \text{CH}_3\text{OO} \rightarrow \text{CH}_3\text{O}_2^+ + \text{He}$ , which is followed by the fragmentation of the  $\text{CH}_3\text{O}_2^+$  ion. The major fragmentation channel is the production of  $\text{HCO}^+$  and  $\text{H}_2\text{O}$ . The outcome of this work is encouraging and suggests that infrared laser spectroscopy can be employed as a selective probe of the outcome of organic radical-radical reactions in which multiple products may be formed. By integrating the total ion signal arising from the ionization of the droplet beam, the relative IR beam depletion band intensities associated with the various possible products can be used directly to determine product branching ratios.

**There will be no unexpended funds at the end of this budget period.**

**Publications acknowledging DOE support (from start date, 7/1/12, to present, 3/1/13):**

1. Alexander M. Morrison, Paul L. Raston and Gary E. Douberly, "Rotational Relaxation Dynamics of the Methyl Radical in Helium Nanodroplets" *Journal of Physical Chemistry A*, (2013), in press. DOI: 10.1021/jp310083j
2. Paul L. Raston, Tao Liang and Gary E. Douberly, "Infrared Spectroscopy and Tunneling Dynamics of the Vinyl Radical in  $^4\text{He}$  Nanodroplets" *Journal of Chemical Physics*, submitted.
3. Paul L. Raston, Jay Agarwal, Justin M. Turney, Henry F. Schaefer III and Gary E. Douberly, "The Ethyl Radical in Superfluid Helium Nanodroplets: Rovibrational Spectroscopy and Ab Initio Calculations" *Journal of Chemical Physics*, submitted.

# Hydrocarbon Radical Thermochemistry: Gas-Phase Ion Chemistry Techniques

Kent M. Ervin  
Department of Chemistry and Chemical Physics Program  
University of Nevada, Reno  
Reno, NV 89557-0216  
ervin@unr.edu

## I. Program Scope

Gas-phase ion chemistry and mass spectrometry techniques are employed to determine energetics of hydrocarbon radicals that are important in combustion processes and to investigate the dynamics of ion–molecule reactions. Tandem mass spectrometry is used to measure the activation of endoergic ion-molecule reactions as a function of kinetic energy. Modeling the measured reaction cross sections using statistical rate theory or empirical reaction models allows extraction of reaction threshold energies. These threshold energies yield relative gas-phase acidities, proton affinities or hydrogen atom affinities, which may then be used to derive neutral R–H bond dissociation enthalpies using thermochemical cycles involving established electron affinities or ionization energies. The reactive systems employed in these studies include endoergic bimolecular proton transfer reactions, hydrogen-atom transfer reactions, and collision-induced dissociation of heterodimer complex anions and cations. Electronic structure calculations are used to evaluate the possibility of potential energy barriers or dynamical constrictions along the reaction path, and as input for RRKM and phase space theory calculations.

## II. Recent Progress

### A. Enthalpy of formation of peroxyformyl radical, $\text{HCO}_3^\bullet$

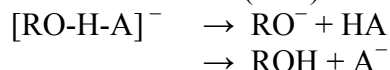
In recently published work,<sup>1</sup> we have determined the enthalpy of formation of the peroxyformyl radical,  $\text{HCO}_3^\bullet$ , which is an intermediate in the oxidation of  $\text{HCO}^\bullet$ . We use the guided ion beam tandem mass spectrometry technique to measure the energy-resolved collision-induced dissociation of the peroxyformate anion,



The threshold energy for this process can be used to determine the energetics of peroxyformate anion, not previously established experimentally, relative to the known enthalpy of formation of formate anion,  $\text{HCO}_2^-$ . Our measured energy for oxygen (<sup>3</sup>P) loss from the peroxyformate anion is  $126 \pm 12$  kJ/mol.<sup>1</sup> Combined with literature thermochemical values, we obtain the first experimental measurements of the enthalpies of formation of peroxyformyl radical,  $\Delta_f H(\text{HCO}_3^\bullet) = -98 \pm 12$  kJ/mol, of gas-phase peroxyformic acid,  $\Delta_f H(\text{HCO}_3\text{H}) = -287 \pm 19$  kJ/mol,<sup>1</sup> which is a high-energy isomer of carbonic acid.

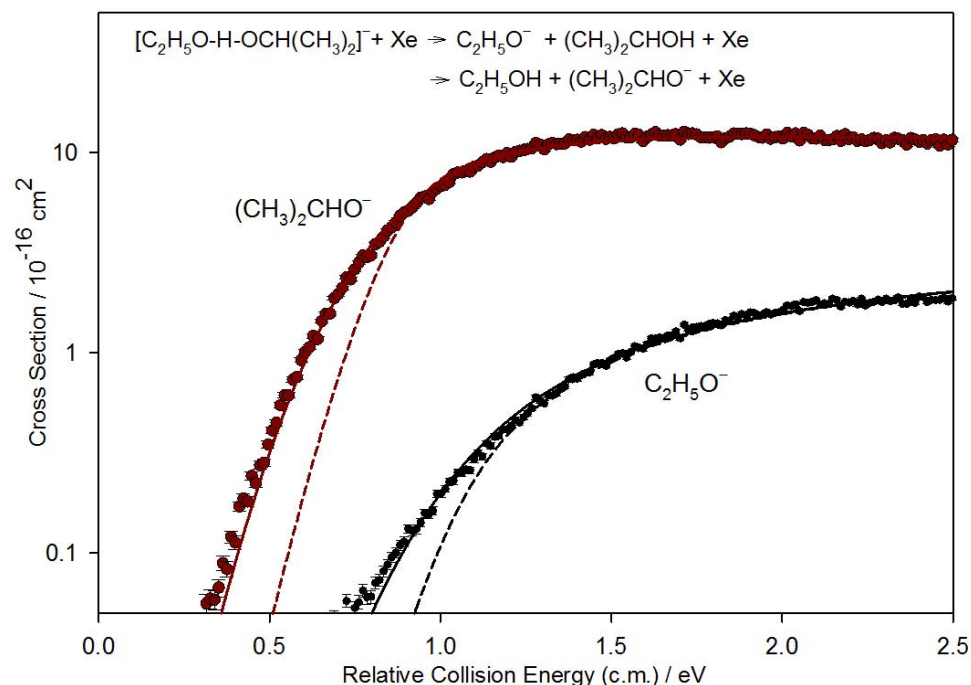
## B. Gas-phase acidities and bond dissociation energies of isomeric alcohols

We have previously developed<sup>2-3</sup> methods for determining accurate relative gas-phase acidities of alcohols (ROH) using competitive collision-induced dissociation of proton-bound complexes of the alkoxide anion ( $\text{RO}^-$ ) with a reference acid (HA),



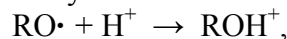
where the difference in energies between the two product channels yields the gas-phase acidity difference,  $\Delta E_0 = \Delta_{\text{acid}}H(\text{ROH}) - \Delta_{\text{acid}}H(\text{HA})$ . The gas-phase acidity then yields the neutral O–H bond dissociation energy using the negative ion thermochemical cycle,  $D(\text{RO-H}) = \Delta_{\text{acid}}H(\text{ROH}) + \text{EA}(\text{RO}\cdot) - \text{IE}(\text{H})$ , where the  $\text{RO}\cdot$  radical electron affinity may be obtained precisely from photoelectron spectroscopy.

Our previous work<sup>2-3</sup> focused on the alkanol series methanol, ethanol, iso-propanol, and tert-butanol. Because of recent interest in combustion of butanol as a biofuel, we are currently extending this work to the other three isomers of butanol and also n-propanol. The key to this method is to obtain relative acidities between various pairs of acids to create a ladder of gas-phase acidities with extra redundancy. Then a least-squares optimization is used to obtain the absolute unknown acidities from the relative acidities. For example, the figure below shows initial experiments performed recently on collision-induced dissociation of iso-propoxide complexed with ethanol,<sup>4</sup> a complex that was not included in the previous gas-phase acidity ladder. The preliminary fits (not including full treatment of the hindered rotors and conformations) use RRKM theory to model the product branching fractions as a function of the energy provided by the collision with the xenon target gas.



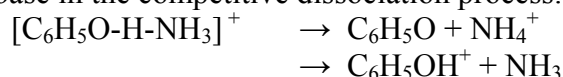
### C. Proton affinity measurements

An alternative thermochemical route to O–H and C–H bond dissociation energies of hydrocarbons uses the proton affinity of the radical. For example, for an alkoxy radical the proton affinity is defined by formation of the alcohol cation,



where  $\text{PA}(\text{RO}\cdot) = -\Delta H$  for the reaction. The bond dissociation energy of the neutral is then given by the thermochemical cycle  $D(\text{RO–H}) = \text{PA}(\text{RO}\cdot) + \text{IE}(\text{ROH}) - \text{IE}(\text{H})$ .

Analogously to the negative ion method described in the previous section to obtain relative gas-phase acidities, we have begun new experiments using collision-induced dissociation of the hydrocarbon cation complexed with a gas-phase base to obtain relative proton affinities. For example, to obtain the proton affinity of phenol, we can use ammonia as the reference base in the competitive dissociation process:



Preliminary experiments<sup>5</sup> on this system show that the cationic complexes can be synthesized in our flow tube reactor in sufficient quantities and that the expected product masses are produced. Further experiments are underway to evaluate the relative proton affinities.

### D. Franck-Condon analysis of photoelectron and photoionization spectra

Determination of hydrocarbon R–H bond dissociation energies from our measured gas phase acidities require accurate electron affinities, which can be measured accurately using negative ion photoelectron spectroscopy. Our PESCAL software for simulating the Franck-Condon profiles for photoelectron spectra, as well as for photoionization threshold experiments, has been further developed through this grant project and has enjoyed increasing use in the community, including since 2012 in references 6-17.

## III. References

- (1) Nickel, A. A.; Lanorio, J. G.; Ervin, K. M. *J. Phys. Chem. A* **2013**, *117*, 1021-1029.
- (2) DeTuri, V.F; Ervin, K. M. *J. Phys. Chem. A* **1999**, *103*, 6911-6920.
- (3) Ervin, K. M.; DeTuri, V.F. *J. Phys. Chem. A* **2002**, *106*, 9947-9956.
- (4) Nickel, A. A.; Lanorio, J. G.; Ghale, S.; Ervin, K. M. (work in progress).
- (5) Ghale, S.; Nickel, A. A.; Lanorio, J. G.; Ervin, K. M. (work in progress).
- (6) Liu, Z. L.; Xie, H.; Qin, Z. B.; Cong, R.; Wu, X.; Tang, Z. C. Lu, X. He, J.; *J. Chem. Phys.* **2012**, *137*, 204302.
- (7) Xie, H.; LI, X.; Zhao, L.; Qin, Z.; Wu, X.; Tang, Z.; Xin, X. *J. Phys. Chem. A* **2012**, *116*, 10365-10370
- (8) Waller, S. E.; Mann, J. E.; Rothgeb, D. W.; Jarrold, C. C. *J. Phys. Chem. A* **2012**, *116*, 9639-9652.
- (9) Mann, J. E.; Waller, S. E.; Jarrold, C. C. *J. Chem. Phys.* **2012**, *137*, 044301.

- (10) Goulay, F.; Trevitt, A. J.; Savee, J. D.; Bouwman, J.; Osborn, D. L.; Taatjes, C. A.; Wilson, K. R.; Leone, S. R. *J. Phys. Chem. A* **2012**, *116*, 6091-6106
- (11) Xie, H.; Xing, X.; Liu, Z.; Cong, R.; Qin, Z.; Wu, X.; Tang, Z.; Fan, H. *J. Chem. Phys.* **2012**, *136*, 184312.
- (12) Mann, J. E.; Waller, S. E.; Rothgeb, D. W.; Jarrold, C. C. *J. Chem. Phys.* *135*, 104317.
- (13) Ray, A. W.; Taatjes, C. A.; Welz, O.; Osborn, D. L.; Melon, G. *J. Phys. Chem. A* **2012**, *116*, 6720-6730.
- (14) Bouwman, J.; Goulay, F.; Leone, S. R.; Wilson, K. R. *J. Phys. Chem. A* **2012**, *116*, 3907-3917.
- (15) Wren, S. W.; Vogelhuber, K. M.; Garver, J. M.; Kato, S.; Sheps, L.; Bierbaum, V. M.; Lineberger, W. C. *J. Am. Chem. Soc.* **2012**, *134*, 6584-6595.
- (16) Wren, S. W.; Vogelhuber, K. M.; Ichino, T.; Stanton, J. F.; Lineberger, W. C. *J. Phys. Chem. A* **2012**, *116*, 3118-3123.
- (17) Adams, C. L.; Knurr, B. J.; Weber, J. M. *J. Chem. Phys.* **2012**, *136*, 064307.

#### IV. Recent publications supported by this project

1. Dangi, B. B.; Sassin, N. A.; Ervin, K. M. "Pulsed ion extraction diagnostics in a quadrupole ion trap linear time-of-flight mass spectrometer", *Rev. Sci. Instrum.* **2010**, *81*, 063302/1-10.
2. K. M. Ervin, PESCAL, Fortran program for Franck-Condon simulation of photoelectron spectra, <http://wolfweb.unr.edu/~ervin/pes/> (revised 2010).
3. Vogelhuber, K. M.; Wren, S. W.; McCoy, A. B.; Ervin, K. M.; Lineberger, W. C. "Photoelectron spectra of dihalomethyl anions: Testing the limits of normal mode analysis", *J. Chem. Phys.* **2011**, *134*, 184306/1-13.
4. Dangi, B. B.; Ervin, K. M. "Optimization of a quadrupole ion storage trap as a source for time-of-flight mass spectrometry", *J. Mass Spectrom.* **2012**, *47*, 41-48.
5. Nickel, A. A.; Lanorio, J. G.; Ervin, K. M. "Energy-resolved collision-induced dissociation of peroxyformate anion: Enthalpies of formation of peroxyformic acid and peroxyformyl radical", *J. Phys. Chem. A* **2013**, *117*, 1021-1029.

Robert W. Field  
 Massachusetts Institute of Technology  
 Cambridge, MA 02139  
[rwfield@mit.edu](mailto:rwfield@mit.edu)

## I. Program Scope

The fundamental goal of this program is to develop the experimental techniques, diagnostics, interpretive concepts, spectrum-assignment strategies, and pattern-recognition schemes needed to reveal and understand how large-amplitude motions are encoded in the vibration-rotation energy level structure of small, gas-phase, combustion-relevant polyatomic molecules. We are focusing our efforts on unimolecular isomerization in several prototypical systems, including the  $\text{HNC} \leftrightarrow \text{HCN}$  and  $\text{HCCH} \leftrightarrow \text{CCH}_2$  isomerization systems. We are developing chirped-pulse millimeter wave (CPmmW) spectroscopy as a technique that can be used in conjunction with Stimulated Emission Pumping (SEP) and the measurement of hyperfine structure and Stark effect to populate and identify molecular states with high excitation in *local* large-amplitude vibrational modes, which are of key importance in isomerization processes. In addition, we are attempting to demonstrate the capability of CPmmW spectroscopy to determine reaction mechanisms and the structures of molecular fragmentation transition states by measurement of fragment species/vibrational level populations.

## II. Recent Progress

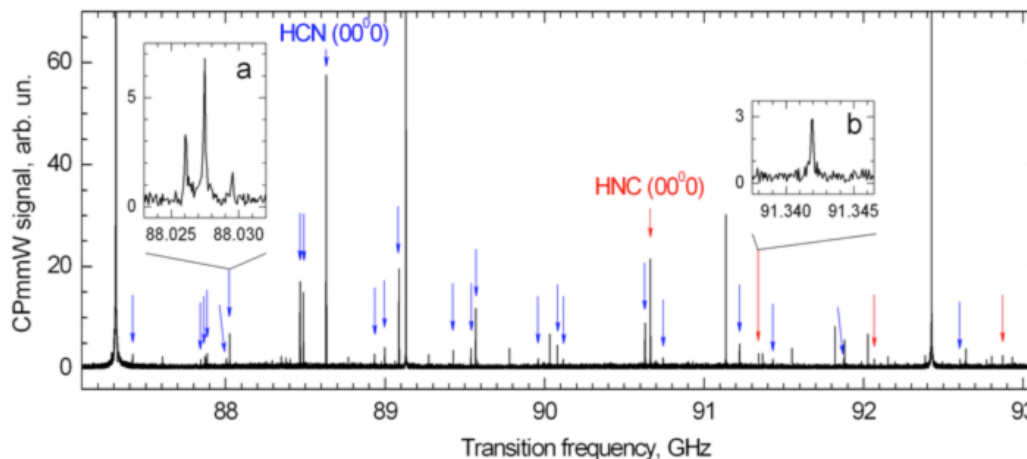


Figure 1: The CPmmW spectrum of products of 193 nm photolysis of VCN. The  $J = 0-1$  transitions in more than 25 HCN, HNC vibrational levels are identified. The insets show the characteristic eqQ hyperfine structure of HCN vs. HNC.

### A. CPmmW Spectroscopy

#### 1. Chirped Pulse/Slit jet spectrometer

Chirped-Pulse Millimeter-Wave (CPmmW) spectroscopy is the first truly broadband and high resolution technique for spectroscopy in the millimeter wave region. We have built and tested a CPmmW spectrometer that operates in the 70–102 GHz frequency range. The spectrometer can acquire up to 12 GHz of spectral bandwidth at better than 100 kHz resolution in a single shot. As part of our search for mm-wave transitions in vinylidene and highly excited local-bender acetylene we have expanded the lower-frequency limit of our CPmmW spectrometer to 58 GHz and implemented a slit-jet source. The slit-jet apparatus has increased the sensitivity of our CPmmW experiments by a factor of 10, due to increased number of molecules in the interaction region and reduced Doppler profile. The collisional region of the slit-jet supersonic expansion extends to up to 2 cm downstream from the slit-jet source, allowing for precise control over the number of cooling collisions that the photolysis products experience in the expansion. This control over the extent of rotational thermalization could be crucial in distinguishing between rotationally highly excited

and unexcited nascent reaction products. The CPmmW/slit-jet spectrometer is now fully operational and we have observed beautiful spectra of the HCN, HNC photolysis products of vinyl cyanide (Fig. 1).

## 2. 193 nm Photolysis of Vinyl Cyanide

Vinyl cyanide 193 nm photodissociation has been studied using CPmmW spectroscopy. Figure 1 shows  $J = 0-1$  transitions of more than 30 vibrationally excited states of the HCN and HNC products that have been recorded and assigned within the 7 GHz wide chirp range. Bending excitations of HCN up to  $\nu_2 = 14$ , leading toward the HCN-HNC isomerization transition state, are detected and interpreted in terms of their electric quadrupole,  $(eQq)_N$ , and rotational,  $B_\nu$ , constants. The photolysis reaction transition states were probed using both normal vinyl cyanide,  $\text{CH}_2=\text{CHCN}$ , and its singly-deuterated isotopologue,  $\text{CH}_2=\text{CDCN}$ . The observed difference in the vibrational population distribution (VPD) obtained from the integrated intensities of the HCN and DCN products from the  $\text{CH}_2=\text{CHCN}$  vs.  $\text{CH}_2=\text{CDCN}$  photolysis reactions, suggests the relative unimportance of the three-center elimination mechanism for HCN production. On the other hand, the similarity in the observed VPD and overall intensities of HCN from  $\text{CH}_2=\text{CHCN}$  and  $\text{CH}_2=\text{CDCN}$  photolysis suggests four-center elimination as the major mechanism leading to the HCN product. Additional  $(J + 1)-J$  transitions would be required to characterize both the vibrational and the rotational state distributions of the products, which would permit more complete characterization of the transition state(s).

## 3. Multiplexed MODR

Application of broadband chirped-pulse technology to Millimeter-wave-Optical Double Resonance (MODR) allows simultaneous acquisition of MODR spectra for multiple millimeter-wave transitions. This new multiplexed implementation, Millimeter-wave-Optical Multiplexed Double Resonance (MOMDR), is capable of resolving and rotationally assigning complicated and congested spectral regions in only a single laser scan and serves as a powerful complement to Laser Induced Fluorescence (LIF). We have applied the technique to several vibrational bands of the  $\tilde{C} \leftarrow \tilde{X}$  transition in  $\text{SO}_2$ . Five millimeter-wave transitions within the bandwidth of the millimeter-wave spectrometer were excited by back-to-back single-frequency pulses with a total duration of  $\sim 1 \mu\text{s}$ . After the Free Induction Decay (FID), a pulsed dye laser excites the sample and a second microwave pulse identical to the first induces another FID. The MOMDR spectrum is obtained by comparing the two FID intensities at each millimeter-wave transition frequency.

In the  $(\nu_1, \nu_2, \nu_3) = (1, 3, 2)$  band, we used the technique to increase the number of rotationally assigned term values from 7 to 17 (Fig. 2). Most of the rotational lines in the LIF spectrum of this region were previously unassigned due to spectral congestion and strong Fermi and  $c$ -axis Coriolis interactions. We have also measured MOMDR for predissociated bands of the  $\tilde{C}$  state. MOMDR is well suited to predissociated states because its intensity is proportional to absorption rather than fluorescence and broadened features can be resolved and rotationally assigned by the two-dimensional nature of the experiment. The technique may also be well suited to a simultaneous search for rotational transitions between electronically-excited levels.

## B. High- and low-barrier unimolecular isomerization in $S_0$ and $S_1$ HCCH

The goal of our studies of the acetylene  $\leftrightarrow$  vinylidene system is to observe barrier-proximal vibrational states. Many studies have demonstrated that the vibrational eigenstates of acetylene and similar molecules undergo a normal-to-local transition in which the normal modes appropriate to describe small displacements from the equilibrium geometry evolve into local modes in which the excitation is isolated in a single large-amplitude C-H bond stretch or  $\angle\text{CCH}$  bend. The evolution of vibrational character is of particular interest in the acetylene bending system, because the local-bending vibration bears a strong resemblance to the reaction coordinate for isomerization from acetylene to vinylidene, where one hydrogen moves a large distance off of the C-C bond axis while the other hydrogen remains nearly stationary. In the first singlet excited state of acetylene, we find ourselves in the unique situation of being close to characterizing the complete rovibronic level structure up to the transition state energy in a system exhibiting conformational change.

### 1. Observation and theoretical treatment of vibrational levels of $S_1$ *cis* acetylene

The  $S_1$  *cis-trans* isomerization has been the focus of many theoretical studies, but has been difficult to study experimentally because transitions from the ground electronic state to the  $S_1$ -*cis* geometry are

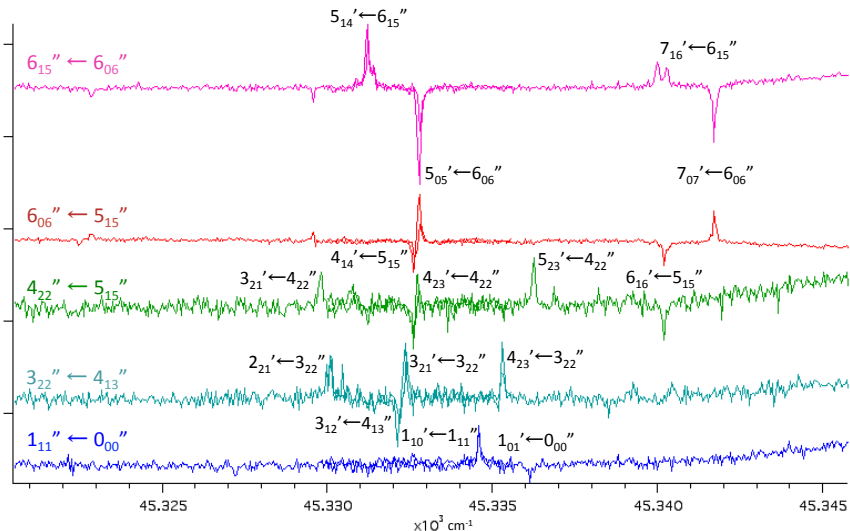


Figure 2: MOMDR spectrum of the  $\tilde{C}(1, 3, 2) \leftarrow \tilde{X}(0, 0, 0)$  transition in  $\text{SO}_2$ . The spectrum was obtained from two overlapping scans of the etalon chamber pressure of our pulsed dye laser, scanned at the same rate that we use for LIF spectroscopy. Upward and downward peaks in the MOMDR spectrum correspond to depletion of the upper and lower levels, respectively, of the rotational transitions monitored in  $\tilde{X}(0, 0, 0)$  (labeled on the left side of the figure). Rotational assignments in the  $\tilde{C}$  state were made on the basis of selection rules and combination differences in the LIF spectrum. Several weak transitions have not been assigned and may arise from a perturbing band.

electronically forbidden. We have made the first definitive observation and identification of levels belonging to  $S_1$ -*cis*, and surprisingly, these levels were observed below the energy of the calculated barrier to *trans-cis* isomerization, and must therefore owe their observed intensity to mixing via tunneling with *trans*-geometry-localized states.

We now find ourselves in possession of a complete set of vibrational assignments for both the *trans* and *cis* conformers up to the expected transition state energy, with few exceptions. Our comprehensive examination of the *cis-trans* isomerization in  $S_1$  acetylene has led to the development of a universal, model-independent spectroscopic diagnostic of transition state energies in systems that exhibit conformational change. We believe that it is possible to extend the concept of effective frequency as an indicator of qualitative dynamical changes, previously used for dissociation in diatomics (Birge-Sponer, LeRoy-Bernstein) and the bent-linear transition in quasilinear triatomics (“Dixon dip”), to determine the isomerization barrier height in asymmetric double minimum potentials (Fig. 3). We can determine the transition state energy to high accuracy by fitting the observed pattern to the empirical formula  $\omega^{\text{eff}} = \omega_0(1 - \frac{E}{E_{ts}})^{1/n}$ , where  $E_{ts}$  is the transition state energy.

One major qualitative consequence of *cis-trans* isomerization is the tunneling staggering of rotational sublevels with different  $K$  quantum numbers *within* a given vibrational state (as opposed to tunneling *splittings* in other isomerizing systems such as ammonia or internal rotors). The size and direction of these staggers serve as a sensitive probe of isomerization and tunneling, as well as a complicating factor in spectral assignment. In order to quantitatively understand and predict these staggers, we are conducting reduced dimension rovibrational variational calculations on a high accuracy *ab initio* potential surface. Our results have aided in rationalizing observed  $K$ -staggering, identifying new *cis* vibrational levels, and assigning complicated near-barrier features. The calculations enable us to move beyond low-energy theoretical models, which fail to capture the effects of isomerization on the high-energy rovibrational level structure.

To overcome predissociation in high energy regions, we have constructed and begun optimizing a velocity-map-imaging style REMPI-TOF detection system that will allow us to record the first high resolution H-atom action spectra of  $S_1$  acetylene. The combination of two distinct complementary data channels (LIF and H-atom action) will not only advance the spectroscopy of the  $\tilde{A}$  state, but also provide valuable information about the mode- and conformer-specific influence of vibrations on the predissociation mechanism.

### III. Future Work

We expect to achieve a >100-fold improvement of the signal:background ratio of our CPmmW spectrometer by taking advantage of new millimeter-wave technology. These enhancements will enable us to

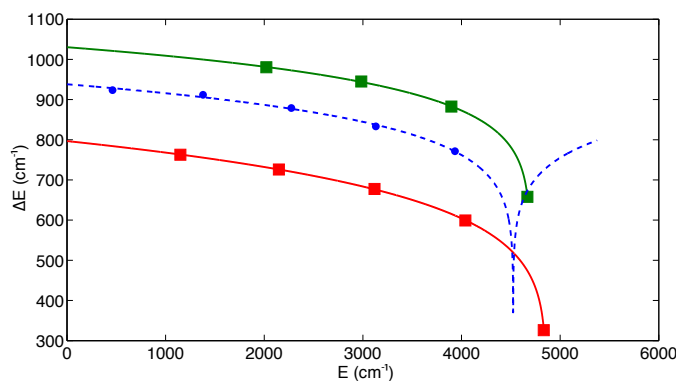


Figure 3: Determination of transition state energy from the pattern of vibrational level spacings. Demonstrated here by a simple one dimensional minimum energy isomerization path (MEIP) calculation, shown in blue (dashed line), the minimum in the pattern of vibrational level spacings reveals, in a model-independent way, the transition state energy for any asymmetric double minimum potential. Experimental values for the vibrational level spacings in the  $3^1B^2$  series are overlaid on the *ab initio* results, showing remarkable agreement between the average of the experimental  $\omega_3^{\text{eff}}$  (green) and  $\omega_6^{\text{eff}}$  (red) normal mode spacings and those found in the 1D MEIP local Bender calculation. The highest energy points in the experimental traces are based on preliminary, unpublished assignments. The solid lines are fits to the equation  $\omega^{\text{eff}} = \omega_0(1 - \frac{E}{E_{ts}})^{1/n}$ , as described in the text.

measure the populations of vibrationally-excited photolysis and pyrolysis products and locate additional acetylene local-bender vibrational states. The combination of our  $S_1$  results with the high resolution/survey capability of CPmmW/DF spectra will guide us towards conclusive SEP experiments that sample levels proximal to the acetylene–vinylidene isomerization barrier. We plan to record Stark effect spectra of the  $S_0$  highly vibrationally excited levels, in order to measure the large predicted dipole moments, which are a measure of progress along the large amplitude local-bender isomerization coordinate. CPmmW measurements of product state distributions will allow us to extract information about the structures of transition states for fragmentation and photodissociation.

## Publications supported by this project 2011–2013

- [1] G. Barratt Park, Adam H. Steeves, Kirill Kuyanov-Prozument, Justin L. Neill, and Robert W. Field. Design and evaluation of a pulsed-jet chirped-pulse millimeter-wave spectrometer for the 70–102 GHz region. *The Journal of Chemical Physics*, 135(2):024202, 2011.
- [2] J. H. Baraban, A. R. Beck, A. H. Steeves, J. F. Stanton, and R. W. Field. Reduced dimension discrete variable representation study of *cis*–*trans* isomerization in the  $S_1$  state of  $C_2H_2$ . *The Journal of Chemical Physics*, 134(24):244311, 2011.
- [3] Anthony J. Merer, Adam H. Steeves, Joshua H. Baraban, Hans A. Bechtel, and Robert W. Field. *cis*–*trans* isomerization in the  $S_1$  state of acetylene: Identification of *cis*-well vibrational levels. *The Journal of Chemical Physics*, 134(24):244310, 2011.
- [4] Joshua H. Baraban, Anthony J. Merer, John F. Stanton, and Robert W. Field. Anharmonic Force Fields for *cis* and *trans*  $S_1$   $C_2H_2$ . *Molecular Physics*, 110(21-22):2725–2733, 2012.
- [5] Joshua H. Baraban, P. Bryan Changala, Anthony J. Merer, Adam H. Steeves, Hans A. Bechtel, and Robert W. Field. The  $\tilde{A}^1A_u$  state of acetylene: *ungerade* vibrational levels in the region 45800–46500  $cm^{-1}$ . *Molecular Physics*, 110(21-22):2707–2723, 2012.
- [6] Kirill Prozument, Rachel Glyn Shaver, Monika Ciuba, G. Barratt Park, John Stanton, John S. Muentner, Hua Guo, Bryan M. Wong, David S Perry, and Robert W. Field. A New Approach toward Transition State Spectroscopy. *Faraday Discuss.*, 2013, accepted.
- [7] Hyunwoo Lee, Joshua H. Baraban, Robert W. Field, and John F. Stanton. High-Accuracy Estimates for the Vinylidene-Acetylene Isomerization Energy and the Ground State Rotational Constants of  $:C=CH_2$ . *The Journal of Physical Chemistry A*, 2013, accepted.

# Quantitative Imaging Diagnostics for Reacting Flows

Jonathan H. Frank  
Combustion Research Facility  
Sandia National Laboratories  
Livermore, CA 94551-0969  
jhfrank@sandia.gov

## Program Scope

The primary objective of this project is the development and application of quantitative laser-based imaging diagnostics for studying the interactions of fluid dynamics and chemical reactions in reacting flows. Imaging diagnostics provide temporally and spatially resolved measurements of species, temperature, and velocity distributions over a wide range of length scales. Multi-dimensional measurements are necessary to determine spatial correlations, scalar and velocity gradients, flame orientation, curvature, and connectivity. Current efforts in the Advanced Imaging Laboratory focus on studying the detailed structure of both isolated flow-flame interactions and turbulent flames. The investigation of flow-flame interactions is of fundamental importance in understanding the coupling between transport and chemistry in turbulent flames. These studies require the development of imaging diagnostic techniques to measure key species in the hydrocarbon-chemistry mechanism as well as mixture fraction, rates of reaction and dissipation. Recent studies on flow-flame interactions have focused on localized extinction and re-ignition as well as effects of stratification. Diagnostic development includes efforts to extend measurement capabilities to a broader range of flame conditions and combustion modes, including combustion of hydrocarbon fuels beyond methane and stratified premixed combustion. We are also expanding our diagnostic capabilities for probing the temporal evolution of turbulent flames using high-repetition rate imaging techniques.

## Recent Progress

### *Non-adiabatic interaction of turbulent premixed counterflow flames with combustion products*

We conducted a series of detailed experimental studies of turbulence-flame interactions in stratified premixed counterflow flames using the Yale counterflow burner in collaboration with Prof. A. Gomez. This burner enables studies of premixed flames at turbulence Reynolds numbers on the order of 1000, which produces strong interactions resulting in localized extinction. Parametric studies were performed by independently varying the global strain rate, turbulent Reynolds number, temperature of the product stream, and stratification between the equivalence ratios of the reactant and product streams. The impact of these effects on the flame depends on the particular reactant and product mixtures as well as the proximity between the turbulent flame front and the stream of combustion products. Figure 1a shows the burner configuration and illustrates the measurements of the interaction distances that were performed using OH-LIF imaging. The degree of interaction undergoes large fluctuations and depends on the distance  $\Delta_f$  between the instantaneous flame front and the interface between the lower stream of combustion products and the products that are formed in the vicinity of the turbulent flame front, which we refer to as the gas mixing layer interface (GMLI).

The interaction between the flame front and the product stream involves a complex combination of variations in local strain rate and dilution by mixing with gases from the product

stream. Figure 1b shows the mean velocity gradient normal to the instantaneous flame front for flames in the near field ( $\Delta_f < 1.5$  mm) and far field ( $\Delta_f > 1.5$  mm) of the GMLI. On average, the flames in the near field experience significantly larger velocity gradients. Flames located in the near field thus have a greater probability of experiencing larger strain rates, which can increase their susceptibility to heat losses and dilution by the stream of combustion products. The distributions of flame front locations for lean and rich flames are shifted significantly closer to the GMLI relative to the locations of stoichiometric flames, regardless of the product stream temperature,  $T_b = 1700$  K-1950 K, as shown in Fig. 1c. The non-stoichiometric flames thus have a greater probability of being extinguished by mixing and heat loss. Indeed, probabilities of localized extinction for the stoichiometric flames in these data sets are insensitive to the product stream temperature, whereas the lean and rich flames encounter significant localized extinction. The observed coupling between effects of stratification, strain, and heat losses in these parametric studies indicate the need to develop a more general regime diagram for characterizing turbulent premixed combustion using additional dimensionless parameters to account for different modes of combustion and a broader range of turbulence-flame interactions.

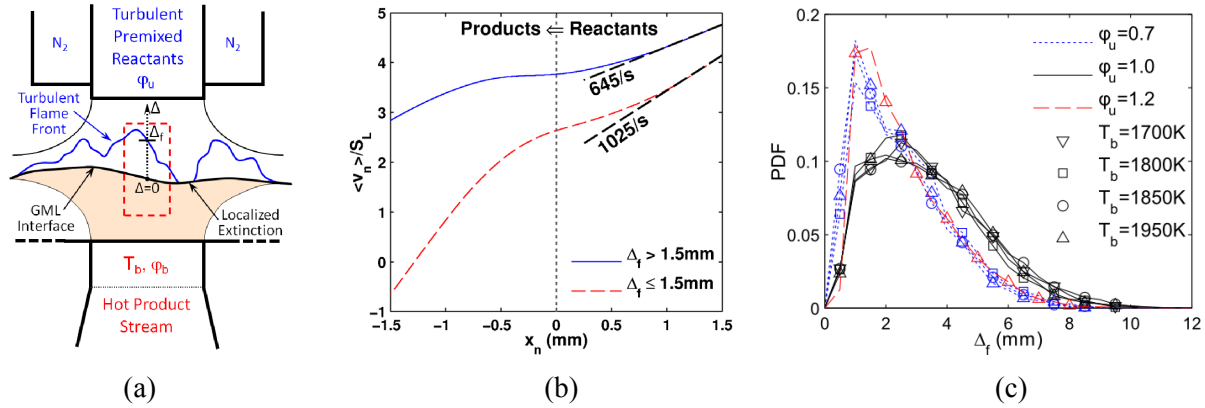


Fig. 1: (a) Schematic diagram of a turbulent premixed counterflow flame with a reactant mixture of equivalence ratio  $\phi_u$  and a stream of combustion products at equivalence ratio  $\phi_b$  and temperature  $T_b$ .  $\Delta_f$  is the separation distance between the instantaneous flame front and the gas mixing layer interface (GMLI), which is the boundary between the lower stream of combustion products and the products formed in the vicinity of the turbulent flame front. (b) Mean velocity profiles across the flame front in the flame normal direction of a lean flame ( $\phi_u = 0.85$ ), parameterized on whether the flame front is in the near field ( $\Delta_f < 1.5$  mm) or far field ( $\Delta_f > 1.5$  mm) relative to the GMLI. Velocities are normalized by the laminar flame speed,  $S_L = 72$  cm/s.  $x_n$  is the distance along the local normal to the flame front contour. (c) probability density function of the local separation distance between flame front and GMLI,  $\Delta_f$ . For all flames,  $\phi_b = 1.0$ ,  $Re_t = 1050$ ,  $K_{bulk} = 1400$ /s.

### Soft x-ray absorption spectroscopy of flames

We continue to investigate the development of in situ soft x-ray measurement techniques for combustion with the eventual goal of studying flames under conditions that are not amenable to traditional diagnostic techniques. X-rays promise advantages over traditional laser diagnostic techniques that use UV and visible radiation to probe flame species via laser-induced fluorescence and Raman scattering. X-ray absorption is not subject to temperature-dependent variations in Boltzmann fraction populations since it probes core-level electrons rather than valence electrons. Core-level spectroscopy probes all carbon containing molecules, providing a spatial map of carbon concentration. Experimental studies of soft x-ray absorption spectroscopy

in flames are performed at the Molecular Science Beamline of the Advanced Light Source (ALS) synchrotron of LBNL in collaboration with David Osborn (Sandia), Hendrik Bluhm (LBNL), and Andrey Shavorskiy (LBNL).

In the most recent experiments, two-dimensional absorption measurements of major carbonaceous species were demonstrated in a low-pressure methane jet flame using the carbon K-edge region of the absorption spectrum. The x-ray beam traversed the axisymmetric jet flame, which was stabilized on a 3-mm diameter nozzle, as shown in Fig. 2a. By tuning the x-ray radiation to strong  $\pi^*$  transitions in the near-edge region of the carbon K-edge spectrum and raster scanning the flame across the x-ray beam, we were able to perform 2D absorption imaging measurements of CO, CH<sub>4</sub>, and CO<sub>2</sub>, as demonstrated in Fig. 2b. Results from this experiment show promise for quantitative absorption tomography and spectroscopy in flames. Plans for developing this capability involve a progression from diagnostic technique development in steady low-pressure methane flames to detailed studies of transient flow-flame interactions with increasingly complex fuels. This diagnostic capability may enable key measurements of flow-flame interactions in flame conditions for which interferences prohibit the use of laser-based techniques. Experimental results will be closely coupled with Habib Najm's (Sandia) numerical simulations and uncertainty quantification techniques to develop computations that accurately capture the coupling between transport and combustion chemistry.

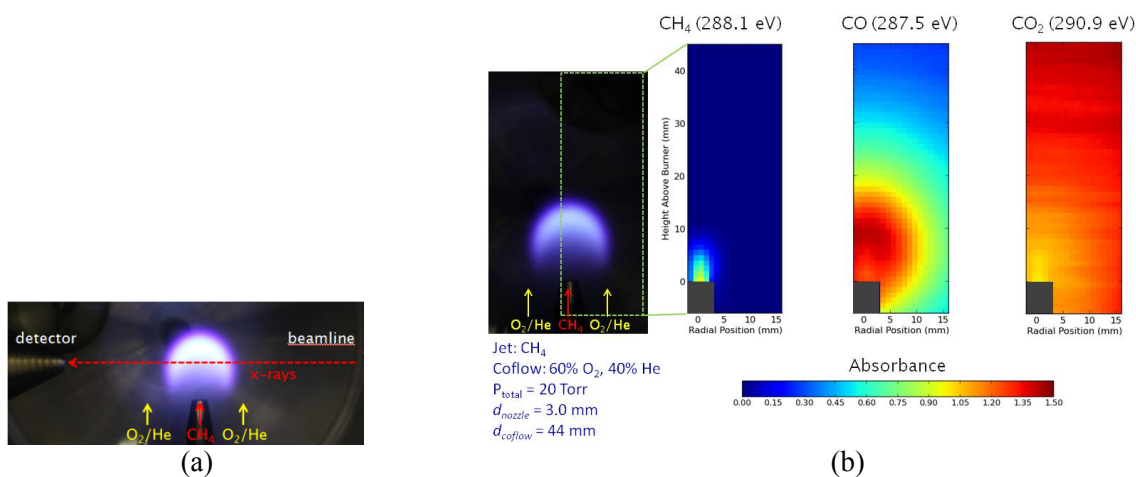


Fig. 2: (a) Chemiluminescence image of the low-pressure non-premixed methane jet flame during a proof-of-principle experiment at the ALS Molecular Science Beamline. (b) Two-dimensional absorbance measurements of the major carbonaceous species (CH<sub>4</sub>, CO, CO<sub>2</sub>) acquired at the corresponding peaks of the near-edge absorption features.

## Future Plans

The recent acquisition of a high-repetition rate stereoscopic particle image velocimetry (PIV) system coupled with our existing high-speed LIF imaging capability enables new studies of flame dynamics. The PIV system provides three-component cinematic imaging of the velocity field within a plane illuminated by a laser sheet. We plan to use this facility to investigate the dynamics of flow-flame interactions in turbulent premixed, non-premixed, and stratified modes of combustion. In particular, we are planning a series of turbulent flame studies that will focus on the dynamics of localized extinction and re-ignition in jet and counterflow flames, stabilization mechanisms in lifted jet flames, turbulent transport of combustion intermediates and turbulent mixing in stratified combustion. We will also conduct a series of studies comparing the

temporal evolution of turbulent non-reacting jets and jet flames to elucidate the effects of heat release on the dynamics of the turbulent flow.

We plan to expand our ability to use a noble gas as a chemically inert tracer for mixing studies to a broad range of combustion environments. Most previous mixture fraction imaging techniques have used combined measurements of chemically reactive species and temperature to construct a conserved scalar. The advantage of this new approach is that the tracer gas remains chemically inert in a wide range of conditions. We plan to refine this diagnostic technique for a broader range of flame conditions and fuel mixtures. A key refinement will be extending measurements of collisional quenching rates for krypton LIF over a wider range of temperatures and for additional collisional partners. Similar quenching rate measurements will be used for improving formaldehyde LIF measurements, which are relevant to our studies of DME flames.

We plan to continue companion experimental and computational studies of the coupling between transport and chemistry in isolated flow-flame interactions in collaboration with J. Chen (Sandia). We are investigating the ability of different chemical mechanisms and transport models to capture the wide range of thermochemical states involved in extinction and re-ignition. Ongoing studies focus on oxygenated fuels, such as dimethyl ether.

We have established a new series of piloted partially-premixed dimethyl ether/air jet flames as target flames for the TNF Workshop. Initial measurements have included particle imaging velocimetry and laser-induced fluorescence of OH and CH<sub>2</sub>O. Plans include refining the LIF measurements, analyzing the velocity-scalar field coupling, and performing high-speed imaging measurements to study dynamics of localized extinction and re-ignition in these flames. Results will be coupled with complementary species and temperature measurements by R. Barlow (Sandia) and large eddy simulations (LES) performed at Sandia by J. Oefelein and at U. Stuttgart by O. Stein and A. Kronenburg. These collaborations will expand our ongoing efforts to couple imaging measurements with LES to advance numerical simulation capabilities and to develop new methods for comparing simulations and experiments.

### **BES-supported publications and submitted journal articles (2011-present)**

J.H. Frank, S.A. Kaiser, J.C. Oefelein, "Analysis of scalar mixing dynamics in LES using high-resolution imaging of laser Rayleigh scattering in turbulent non-reacting jets and non-premixed jet flames," *Proc. Combust. Inst.* **33**, 1373-1381 (2011).

A.G. Hsu, V. Narayanaswamy, N.T. Clemens, J.H. Frank, "Mixture fraction imaging in turbulent non-premixed flames with two-photon LIF of krypton," *Proc. Combust. Inst.* **33**, 759-766 (2011).

B. Böhm, J.H. Frank, A. Dreizler, "Temperature and mixing field measurements in stratified lean premixed turbulent flames," *Proc. Combust. Inst.* **33**, 1583-1590 (2011).

A.M. Steinberg, I. Boxx, C.M. Arndt, J.H. Frank, W. Meier, "Experimental study of flame-hole re-ignition mechanism in a turbulent non-premixed jet flame using sustained multi-kHz PIV and crossed-plane OH PLIF," *Proc. Combust. Inst.* **33**, 1663-1672 (2011).

B. Coriton, J.H. Frank, A.G. Hsu, M.D. Smooke, A. Gomez, "Effect of quenching of the oxidation layer in highly turbulent counterflow premixed flames," *Proc. Combust. Inst.* **33**, 1647-1654 (2011).

S.A. Kaiser and J.H. Frank, "The effects of laser-sheet thickness on dissipation measurements in turbulent non-reacting jets and jet flames," *Meas. Sci. Technol.*, **22**, 045403 (2011).

B. Coriton, J.H. Frank, A. Gomez, "Parametric study of the non-adiabatic interaction of turbulent premixed flames with counterflowing combustion products," *Combust. Flame*, submitted.

## MECHANISM AND DETAILED MODELING OF SOOT FORMATION

Principal Investigator: Michael Frenklach

Department of Mechanical Engineering

The University of California

Berkeley, CA 94720-1740

Phone: (510) 643-1676; E-mail: myf@me.berkeley.edu

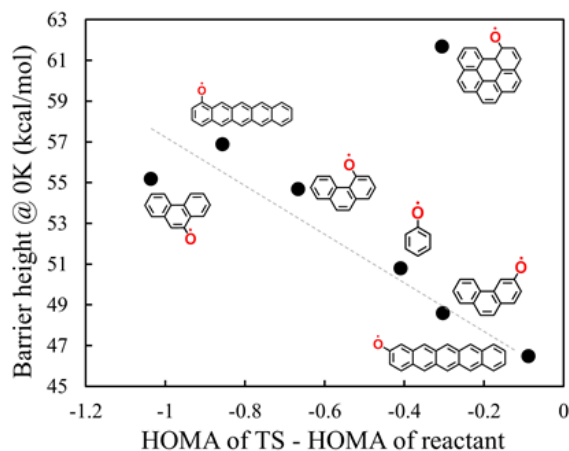
**Project Scope:** Soot formation is one of the key environmental problems associated with the operation of practical combustion devices. Mechanistic understanding of the phenomenon has advanced significantly in recent years, shifting the focus of discussion from conceptual possibilities to specifics of the reaction kinetics. However, along with the success of initial models comes the realization of their shortcomings. This project focuses on fundamental aspects of physical and chemical phenomena critical to the development of predictive models of soot formation in the combustion of hydrocarbon fuels, as well as on computational techniques for the development of predictive reaction models and their economical application to CFD simulations. This work includes theoretical and numerical studies of gas-phase chemistry of gaseous soot particle precursors, soot particle surface processes, particle aggregation into fractal objects, development of economical numerical approaches to reaction kinetics, and construction of a framework for predictive models and modeling.

### Recent Progress:

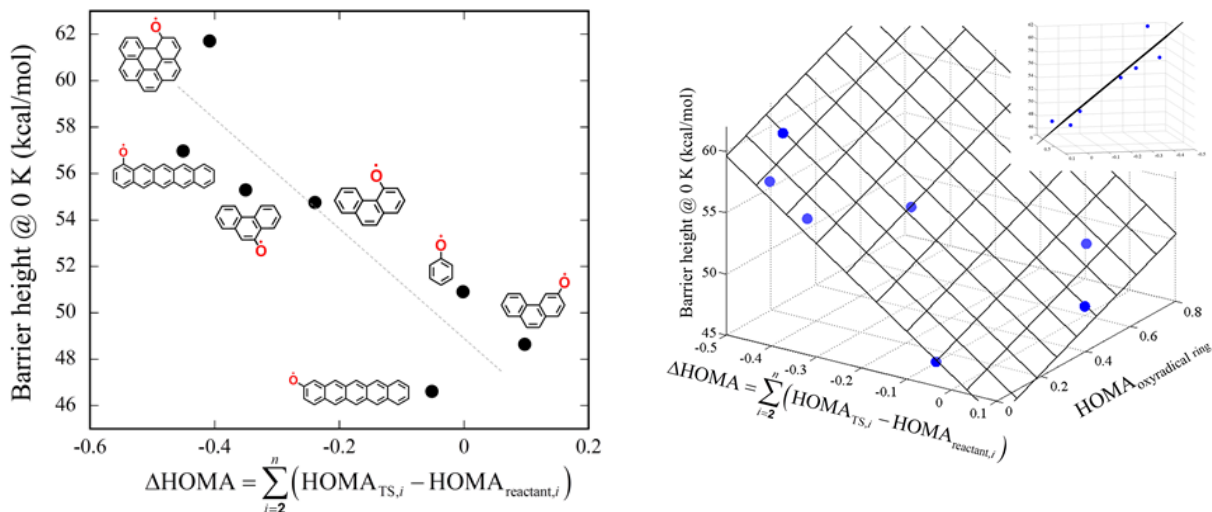
*Correlation of Oxiradical Kinetics with Aromaticity* (with D. E. Edwards, X. You, D. Yu. Zubarev, and W. A. Lester, Jr.)

We have recently reported the correlation of energies and reaction barriers computed for a series of polycyclic oxyradicals with aromaticity (Refs 2,3,6-8 in Publications). The aromaticity of these compounds was evaluated in our studies by employing the Harmonic Oscillator Model of Aromaticity (HOMA). HOMA evaluates the mean deviation of bond lengths in a system under consideration with respect to the bond length in benzene. It is scaled such that HOMA = 0 for the Kekule form of benzene and HOMA = 1 for the aromatic form. We first identified a correlation relating HOMA to energies of pentacene oxyradicals with the oxygen placed at different sites on the pentacene edge. This study was extended to larger polycyclic aromatic hydrocarbons (PAH), up to those composed of 5 by 5 ring structures (Ref 2). It was shown that in both cases the thermodynamic stability of the oxyradicals depends critically on the position of oxygen in the PAH edge.

A correlation of reaction barriers with aromaticity was less successful (Ref 8): while a general trend was clearly observed, the correlation exhibited an outlier, as can be seen in the figure on the right. This figure displays the first barrier height on the potential energy surface (PES), generally rate controlling, against the difference in HOMA ( $\Delta$ HOMA) between the transition and reactant structures. In this original correlation,  $\Delta$ HOMA was calculated by using the HOMA values of just a single ring of the oxyradical, the ring with oxygen attached, i.e., the one being transformed due to the reaction.



In a follow-up study, the one reported here, a closer correlation between reaction barriers and aromaticity was identified. In the new correlation,  $\Delta\text{HOMA}$  was calculated as the aggregate change in HOMA for all rings of the oxyradical, *excluding* the ring with oxygen attached. In this way, the effect of the distortion in the ring undergoing the transformation on the rest of the rings is measured. The new correlation, shown below in the figure on the left, has no major outliers. A further improvement is obtained when an additional factor is included in the correlation, the HOMA value of the reacting oxyradical ring. A 3-D plot, seen below in the figure on the right, shows a best-fit plane to the data (the inset shows the same data but rotated to demonstrate the quality of fit.)



### *Oxidation of Phenanthrene Radicals by OH* (with D. E. Edwards, X. You, D. Yu. Zubarev, and W. A. Lester, Jr.)

In our efforts to elucidate reaction mechanisms for the oxidation of soot, we initially focused on decomposition of oxyradicals, presumably key intermediates in the oxidation pathways. In pursuit of this objective, we determined reaction rates for the thermal decomposition of oxyradicals located on the zigzag (Ref 3) and armchair (Ref 8) edges. Now, we have turned attention to the oxidation of soot by OH.

OH is the primary oxidant of soot in rich and slightly lean conditions. However, to our knowledge, no atomistically resolved pathways leading to the removal of carbon by OH have been identified. Experimental studies reported a relatively high rate of soot oxidation by OH, roughly one tenth of its collisional rate with soot surface. Based on these experimental reports, it is common to use such generic collisional efficiency to characterize soot oxidation by OH in models of soot formation.

Here, we present results of our initial efforts directed towards identifying reaction pathways responsible for oxidation of soot by OH.

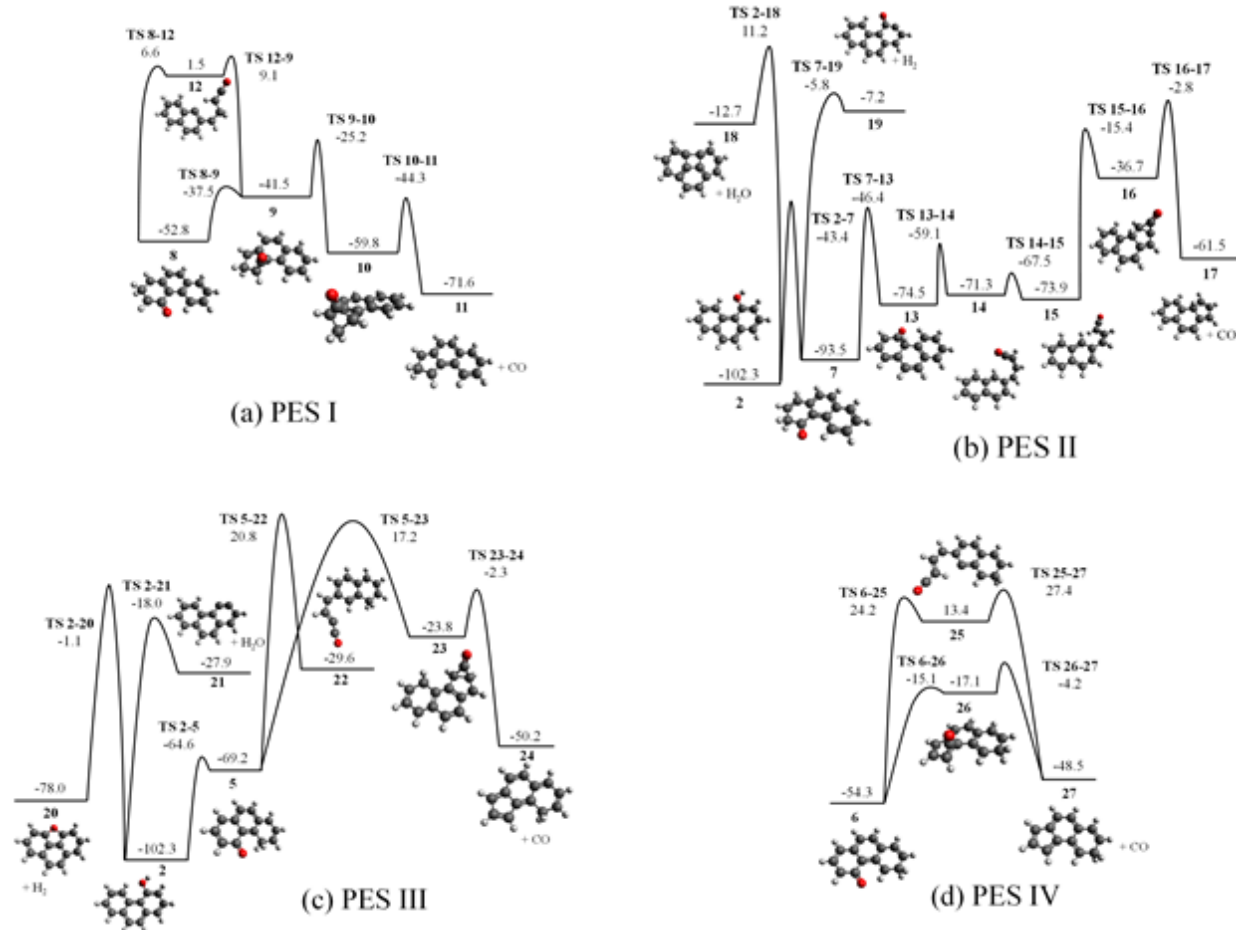
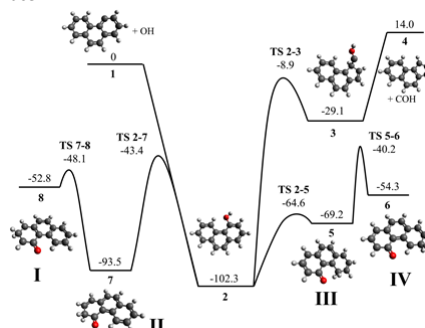
Density functional theory (DFT) was employed to calculate potential energy surfaces of all stable species and transition states for the oxyradical systems. Geometry optimization and vibrational frequency calculations were performed to identify all stationary points on the reaction pathways using the B3LYP hybrid functional and a 6-311G(d,p) basis set.

Soot surface sites can be fundamentally divided into two types,  $\text{C}_{\text{surface-H}}$  and  $\text{C}_{\text{surface}\bullet}$ . We looked into the oxidation of both types by OH. We began the investigation by examining OH attacks on  $\text{C}_{\text{surface-H}}$  sites. No pathways leading to CO expulsion with the rates commensurate with the high experimental values were found. Next, OH reacting with multiple layers of soot was studied to see if the oxidation of soot by OH may be related to the interaction of graphene layers. This too proved to be fruitless. Finally

we examined OH attacking a  $C_{\text{surface}}\bullet$  site. Many of them were, again, too slow. However, those accompanied by hydrogen migration appear to be suitable candidates for the elimination of CO. During these studies we identified over 80 different species and transition states. Below we present some of the main results.

A phenanthrene radical was selected as the surrogate for a  $C_{\text{surface}}\bullet$  site. The adduct and initial wells of the PES for the phenanthrene radical reacting with OH are shown in the figure on the right. This figure shows the PES leading to the formation of four oxyradicals: **8**, **7**, **5**, and **6**, associated with channels I, II, III, and IV, shown below in the figures (a)-(d), respectively. The formation of these oxyradicals is facilitated by the migration of H atoms. Each of these oxyradicals can continue to isomerize down their respective pathways, eventually eliminating CO.

Pathways I-IV are oxyradical decompositions, similar in general features to those of the phenanthrene oxyradicals studied by us previously (Ref 8). Each of these pathways, however, has distinctive reactions and varying barrier heights. For instance, PES I, III, and IV have similar transitions from oxyradical to cyclic intermediate. The barrier heights for these transitions are 15.3, 86.4, and 39.2 kcal/mol for PES I, III, and IV, respectively. In the previous studies of armchair oxyradicals, the barrier height for the similar transition was 54.7 kcal/mol. This wide range of barrier heights is related to the location of a hydrogen



atom with respect to the chemisorbed oxygen atom. In all of the cases, oxygen was located on the same

site of the phenanthrene oxyradical. The relative location of the hydrogen atom and consequently the “ease” of its migration is the primary cause for all of the differences between the four oxyradicals observed in the present study.

### Future Plans

*Graphene Layer Growth and Oxidation Chemistry:* We have completed exploration of the energetics for a set of potential oxidation pathways of soot by OH and identified several promising pathways leading to CO expulsion. Our next objective is to compute the associated rate coefficients for the identified reaction channels. The reaction kinetics will be investigated using MultiWell solving the master equations. We will also investigate the importance of the triplet potential energy surface. All the computations reported here were performed for the singlet potential energy surface, but there exists a triplet surface for the OH + phenanthrene radical reaction. The work will be performed in collaboration with William Lester’s group.

*Graphene Layer Evolution:* Now that we have established the thermodynamic stability of oxyradicals, the kinetics of their decomposition, and have preliminary results on oxidation by OH, we will be adding oxidation reaction steps to the growth mechanism with the objective of performing kinetic Monte-Carlo (KMC) simulations to examine the influence of the oxidation steps on the patterns of graphene-edge evolution. The modification of our KMC code required to accommodate the oxidation reactions of PAHs is in progress.

*Methodology of Predictive Models and Modeling:* We are in the process of a rigorous numerical comparison between our deterministic approach to uncertainty quantification (UQ), Bound-to-Bound DataCollaboration, with the fully-resolved Bayesian-statistics method. We continue collaborative studies with Phillip Westmoreland’s group and his colleagues on the development and automation of the UQ-based framework of ALS data analysis. We will initiate, in collaboration with Nancy Brown, development of data models and data sets for transport properties with the objective of performing a rigorous and systematic UQ analysis of transport data.

### DOE-BES Supported Publications (2011-2013)

1. “Bay-capping reactions: Kinetics and influence on graphene-edge growth,” X. You, R. Whitesides, D. Zubarev, W. A. Lester, Jr., and M. Frenklach, *Proc. Combust. Inst.* **33**, 685-692 (2011).
2. “Patterns of local aromaticity in graphene oxyradicals,” D. Yu. Zubarev, X. You, J. McClean, W. A. Lester, Jr., and M. Frenklach, *J. Mater. Chem.* **21**, 3404-3409 (2011).
3. “Thermal decomposition of pentacene oxyradicals,” X. You, D. Yu. Zubarev, W. A. Lester, Jr., and M. Frenklach, *J. Phys. Chem. A* **115**, 14184-14190 (2011).
4. “Uncertainty-quantified analysis of complex experimental data,” D. R. Yeates, W. Li, P. R. Westmoreland, T. Russi, A. Packard, and M. Frenklach, *Proceedings of the 7<sup>th</sup> U.S. National Combustion Meeting*, Atlanta, GA, 2011, Paper No. 2D01.
5. “Process informatics tools for predictive modeling: Hydrogen combustion,” X. You, A. Packard, and M. Frenklach, *Int. J. Chem. Kinet.* **44**, 101-116 (2012).
6. “Delocalization effects in pristine and oxidized graphene substrates,” D. Yu. Zubarev, X. You, M. Frenklach, and W. A. Lester, Jr., in *Advances in the Theory of Quantum Systems in Chemistry and Physics* (P. E. Hoggan, E. J. Brändas, J. Maruani, P. Piecuch, and G. Delgado-Barrio, Eds.), Progress in Theoretical Chemistry and Physics, Vol. 22, Springer, Dordrecht, 2012, Chapter 29, pp. 553-569.
7. “From aromaticity to self-organized criticality in graphene,” D. Yu. Zubarev, M. Frenklach, and W. A. Lester, Jr., *Phys. Chem. Chem. Phys.* **14**, 12075-12078 (2012).
8. “Thermal decomposition of graphene armchair oxyradical,” D. E. Edwards, X. You, D. Yu. Zubarev, W. A. Lester, Jr., and M. Frenklach, *Proc. Combust. Inst.* **34**, 1759-1766 (2013).
9. Oxidation of phenanthrene radicals by OH,” D. E. Edwards, X. You, D. Yu. Zubarev, W. A. Lester, Jr., and M. Frenklach, *8<sup>th</sup> U.S. National Combustion Meeting*, Salt Lake City, UA, 2013, accepted.

# Computer-Aided Construction of Chemical Kinetic Models

William H. Green  
Department of Chemical Engineering, M.I.T.  
Cambridge, MA 02139  
whgreen@mit.edu

## I. Program Scope

The combustion chemistry of even simple fuels can be extremely complex, involving hundreds or thousands of kinetically significant species. The most reasonable way to deal with this complexity is to use a computer not only to numerically solve the kinetic model, but also to construct the kinetic model in the first place. Because these large models contain so many numerical parameters (e.g. rate coefficients, thermochemistry) one never has sufficient data to uniquely determine them all experimentally. Instead one must work in “predictive” mode, using theoretical values for many of the numbers in the model, and as appropriate refining the most sensitive numbers through experiments. Predictive chemical kinetics is exactly what is needed for computer-aided design of combustion systems based on proposed alternative fuels, particularly for early assessment of the value and viability of proposed new fuels. Our research effort is aimed at making accurate predictive chemical kinetics practical; this is a challenging goal which necessarily includes a range of science advances. Our research spans a wide range from quantum chemical calculations on individual molecules and elementary-step reactions, through the development of improved rate/thermo calculation procedures, the creation of algorithms and software for constructing and solving kinetic simulations, the invention of methods for model-reduction while maintaining error control, and finally comparisons with experiment. Many of the parameters in the models are derived from quantum chemistry, and the models are compared with experimental data measured in our lab or in collaboration with others.

## II. Recent Progress

### A. Methodology for Computer-Aided Kinetic Modeling

The main focus of this research project continues to be the development of methodology for automatically constructing, reducing, and solving combustion simulations. We are constantly adding functionality and additional types of chemistry to the open-source Reaction Mechanism Generator (RMG) software package. Very recently we distributed RMG version 4.0, which includes organosulfur chemistry, a new method for computing thermochemistry of fused cyclic molecules [9], an improved method for automatically identifying and computing the rates of chemically-activated reactions [4,5], and automatic estimation of solvent effects for reactions in liquid phase [i]. We continue to make progress on improved numerical methods to make it easier to use high-fidelity chemistry models in combustion simulations.[ii,iii,iv]

This computer-aided kinetic modeling approach is having an impact beyond MIT. We continue to distribute the mechanism construction software to many research groups, and to train and support the new users. In the past year researchers from LLNL, Belgium, Brazil, China, France, Germany, Spain, and Turkey have visited our group for training in how to use the RMG software. Developers outside of my research group have begun to add functionality to this open-source software; among the most active are researchers at Northeastern University, Oak Ridge National Laboratory, and the University of Ghent. This independently funded external effort leverages the funding provided by this program.

### RMG applications funded separately

The work described above which is funded by this grant is even more heavily leveraged by large application-oriented projects funded separately, which provide demonstrations of the utility of computer-aided modeling of combustion chemistry and tests of the accuracy of RMG. Some of these projects fund addition of new features to RMG.

The largest and most important of these related projects is the DOE Combustion Energy Frontier Research Center, which funded development of models for all four isomers of butanol, many experimental tests of the predictions of these models by other researchers, and many quantum chemistry calculations by our collaborators or by us which have been incorporated into the RMG database. That project has provided excellent comprehensive tests of the capabilities and accuracy of RMG; in several cases the model predictions are quantitatively accurate [v]. Discrepancies observed in other cases have led to the identification and correction of flaws in some of the rate and thermochemistry estimates or databases.[vi] We also participate in a DOE-funded collaboration with Craig Taatjes involving researchers at Aachen and in China, building kinetic models for the chemistry of ketones and other proposed alternative fuels synthesized from biomass by fungi.[vii]

With separate industrial funding, the new capability of RMG to handle sulfur chemistry was tested by building models for fuel desulfurization in supercritical water, and comparisons with experimental data on those systems. Industrial funding also allowed us to include solvent effects in RMG.[i]

## B. Quantum Calculations of Reaction Rates

This year we created an efficient software implementation of the RPMD method for computing reaction rates, which corrects many of the deficiencies of conventional transition state theory.[viii] We collaborated with Hua Guo to test this high accuracy approach on  $\text{OH}+\text{CH}_4$  [10] and  $\text{H}+\text{CH}_4$  [11], and are now collaborating with Al Wagner to couple our RPMDrate software with his rapid method for generating interpolated PES's.

In collaboration with Alexander Mebel, we published computed the rates for  $\text{C}_6\text{H}_5 + \text{C}_3\text{H}_6$ . [8] Some of this forms allyl directly, but much of it reacts via an adduct. We have computed the subsequent chemically-activated isomerizations and dissociations, and compared them with Ralf Kaiser's experimental data in a jointly authored manuscript.[7]

In collaboration with Piotr Piecuch (whose work was funded by the BES Chemical Physics program), and leveraging separate funding, we performed high level calculations on the intramolecular disproportionation reactions of the biradicals formed by unimolecular ring-opening. Most conventional methods say these reactions have significant barriers (e.g. 7 kcal/mole barrier is reported in the literature for disproportionation of the biradical derived from the synthetic fuel JP-10), but our high level calculations show that these reactions are actually barrierless.[ix] Based on these results we have significantly revised the rate estimation rules for intramolecular disproportionations.

## III. Future Work

We are currently adding nitrogen (e.g.  $\text{NO}_x$ , cetane improver) chemistry to RMG. Nitrogen chemistry is trickier than C/H/O chemistry, because changes in valence are more common and important, this has required us to use a more general approach in representing molecules and reactions in the software.

We continue to work on improving the treatment of coupled hindered rotors, which is a major issue in the ignition chemistry of oxygenated fuels, where intramolecular hydrogen bonds are common.

In existing kinetic models, including those generated by RMG, most of the rate coefficients are estimated by functional group analogies. We have recently assessed existing functional-group rate-estimation procedures by using them to predict rate coefficients for hundreds of reactions archived in the NIST database. This comparison revealed many problems with conventional rate-estimation procedures, as well as some discrepancies in the database.

As we push to higher molecular weight fuels, we are running into the limits of our current serial model-construction algorithm. We will parallelize the model construction process, and also develop new methods that naturally apply tighter tolerances to the sensitive chain-branching reactions than to the

ordinary propagation reactions. We are also developing improved graphical interfaces to make it easier for humans to understand and use large kinetic models.

#### IV. References

- i. A. Jalan, R.H. West, and W.H. Green, "An Extensible Framework for Capturing Solvent Effects in Computer Generated Kinetic Models", *J. Phys. Chem. B* (2013, accepted).
- ii. Y. Shi, W.H. Green, H.-W. Wong, and O.O. Oluwole, "Accelerating multi-dimensional combustion simulations using GPU and hybrid explicit/implicit ODE integration", *Combust. Flame* (2012).
- iii. O.O. Oluwole, Yu Shi, Hsi-Wu Wong, and William H. Green, "An Exact-Steady-state Adaptive Chemistry method for combustion simulations: combining the efficiency of reduced models and the accuracy of the full model", *Combustion & Flame* (2012)
- iv. R. Speth, W.H. Green, S. MacNamara, and G. Strang, "Balanced Splitting and Rebalanced Splitting", *SIAM Journal on Numerical Analysis* (submitted, in revision)
- v. N. Hansen, S.S. Merchant, M.R. Harper, and W.H. Green, "The Predictive Capability of an Automatically Generated Combustion Chemistry Mechanism: Chemical Structures of Premixed *iso*-Butanol Flames," *Combustion and Flame* (submitted, in revision).
- vi. N. Hansen, M.R. Harper, and W.H. Green, "High-Temperature Oxidation Chemistry of *n*-butanol: Experiments in Low-Pressure Pre-Mixed Flames and Detailed Modeling", *Phys. Chem. Chem. Phys.* **13**, 20262 - 20274 (2011).
- vii. J.W. Allen, C. Gao, S.S. Merchant, A.M. Scheer, S.S. Vasu, O. Welz, J.D. Savee, D.L. Osborn, C. Lee, S. Vranckx, Z. Wang, F. Qi, R.X. Fernandes, W.H. Green, M.Z. Hadi, C.A. Taatjes, "Concerted Development of Biofuel Production and Utilization: A Coordinated Investigation of Diisopropyl Ketone, a Prototypical Biofuel", *Angew. Chemie* (submitted).
- viii. Y.V. Suleimanov, J.W. Allen, and W.H. Green, "RPMRate: bimolecular chemical reaction rates from ring polymer molecular dynamics", *Comp. Phys. Comm.* (2013, in press).
- ix. Greg Magoon, Jorge Aguilera-Iparraguirre, William H. Green, Jesse J. Lutz, Piotr Piecuch, Hsi-Wu Wong, and O.O. Oluwole, "Detailed Chemical Kinetic Modeling of JP-10 (exotetrahydrodicyclopentadiene) High Temperature Oxidation: Exploring the Role of Biradical Species in Initial Decomposition Steps", *Int. J. Chem. Kinet.* **44**, 179-193 (2012).

#### V. Publications and submitted journal articles supported by this project 2011-2013

1. C.F. Goldsmith, S.J. Klippenstein, and W.H. Green, "Theoretical rate coefficients for allyl + HO<sub>2</sub> and allyloxy decomposition", *Proc. Combust. Inst.* **33**(1), 273-282 (2011).
2. J.D. Mo, E. Kosovich, H.-H. Carstensen, W.H. Green, A.M. Dean, "Thermodynamic properties and kinetic parameters of reactions involving O<sub>2</sub> + substituted allylic radicals", *7<sup>th</sup> US Mtg. Combust. Inst.*, paper 1A05 (2011).
3. R.H. West, C.F. Goldsmith, M.R. Harper, W.H. Green, L. Catoire, and N. Chaumeix, "Kinetic Modeling of Methyl Formate Oxidation", *7<sup>th</sup> US Mtg. Combust. Inst.*, paper 1A06 (2011).
4. J.W. Allen, C.F. Goldsmith, and W.H. Green, "Automatic Estimation of Pressure-Dependent Rate Coefficients", *Physical Chemistry Chemical Physics* **14**, 1131 - 1155 (2012).
5. J.W. Allen and W.H. Green, 'Reply to Comment on "Automatic estimation of pressure-dependent rate coefficients" (J.W. Allen, C. F. Goldsmith, and W. H. Green, *Phys. Chem. Chem. Phys.*, 2012, **14**, 1131-1155)', *Physical Chemistry Chemical Physics* **14**, 8434 (2012)
6. C.F. Goldsmith, W.H. Green, & S.J. Klippenstein, "On the Role of O<sub>2</sub> + QOOH in low-temperature ignition of propane I: Temperature and Pressure Dependent Rate Coefficients", *Journal of Physical Chemistry A* **116**, 3325-3346 (2012).

7. R. Kaiser, M. Goswami, F. Zhang, D. Parker, V.V. Kislov, A.M. Mebel, J. Aguilera-Iparraguirre, W.H. Green. "Crossed Beam Reaction of Phenyl and D5-Phenyl Radicals with Propene and Deuterated Counterparts – Competing Atomic Hydrogen and Methyl Loss Pathways", *Physical Chemistry Chemical Physics* **14**, 720–729 (2012).
8. V. Kislov, A. Mebel, J. Aguilera-Iparraguirre, and W.H. Green, "Reaction of Phenyl Radical with Propylene as a Possible Source of Indene and Other Polycyclic Aromatic Hydrocarbons: An Ab Initio/RRKM-ME Study", *Journal of Physical Chemistry A* **116**, 4176-4191 (2012).
9. G.R. Magoon and W.H. Green, "Design and implementation of a next-generation software system for on-the-fly quantum and force field calculations in automated reaction mechanism generation", *Computers in Chemical Engineering* (2013, in press).
10. Y. Li, Y.V. Suleimanov, M.-H. Yang, W.H. Green, and H. Guo, "Ring Polymer Molecular Dynamics Calculations of Thermal Rate Constants for the  $O(^3P) + CH_4 \rightarrow OH + CH_3$  Reaction: Contributions of Quantum Effects", *Journal of Physical Chemistry Letters* (2013, in press).
11. Y. Li, Y.V. Suleimanov, J. Li, W.H. Green, and H. Guo, "Rate coefficients and kinetic isotope effects of the  $X + CH_4 \rightarrow CH_3 + HX$  ( $X = H, D, Mu$ ) reactions from ring polymer molecular dynamics", *Journal of Chemical Physics* (2013, in press).

# Quantum Dynamics of Elementary Combustion Reactions

Hua Guo ([hguo@unm.edu](mailto:hguo@unm.edu))

*Department of Chemistry and Chemical Biology, University of New Mexico*

Our major efforts in the past year have focused on the elucidation of dynamics of several prototypical reactions with three-four atoms. For example, we have developed accurate PESs for the O + NH reaction and carried out state-to-state QM dynamics studies of this complex-forming reaction.<sup>1</sup> A review on quantum dynamics<sup>2</sup> and another on complex-forming reactions<sup>3</sup> were published.

To continue our work on the "second most important combustion reaction", namely  $\text{HO} + \text{CO} \rightarrow \text{H} + \text{CO}_2$ , we have performed extensive quasi-classical trajectory (QCT) studies of the forward<sup>4</sup> and reverse directions<sup>5</sup> on our newly developed global potential energy surface (PES).<sup>6</sup> These QCT results have shown improved agreement with many experimental findings, validating the accuracy of the PES. We have also performed quantum mechanical (QM) calculations on the rate constant in the forward direction, and a better agreement with experimental rate constants was achieved.<sup>7</sup> To provide a better theoretical understanding of the recent  $\text{HOCO}^-$  photo-detachment experiment of Continatti,<sup>8-9</sup> we have performed reduced- and full-dimensional calculations using both the anion and neutral PESs.<sup>10</sup> The agreement with experiment was excellent, as shown in Fig. 1, confirming the tunneling nature of the dissociation into the  $\text{H} + \text{CO}_2$  channel.

Another tetratomic system we have investigated is the  $\text{F} + \text{H}_2\text{O} \rightarrow \text{HF} + \text{OH}$  reaction. To this end, an accurate global PES for the ground electronic state has been determined<sup>11</sup> using Bowman's permutation invariant polynomial method.<sup>12</sup> Due to multiple low-lying excited state, a dynamically weighted multi-reference configuration interaction (DW-MRCI) scheme<sup>13</sup> was used. The state-to-state QCT calculations on this PES<sup>11</sup> reproduced satisfactorily the experimental observations of Nesbitt.<sup>14-16</sup> Interestingly, our further QCT and full-dimensional QM calculations have found that an entrance channel complex provides anisotropic forces that steer the trajectories towards the transition state, thus enhancing reactivity at low collision energies.<sup>17</sup> To our best knowledge, this is the first time such effect has been observed. Perhaps more interesting, we have found that this early-barrier reaction is significantly enhanced by vibrational excitation of the water reactant, as shown in Fig. 2, in contrast to the well-known Polanyi's rules.<sup>18</sup> This

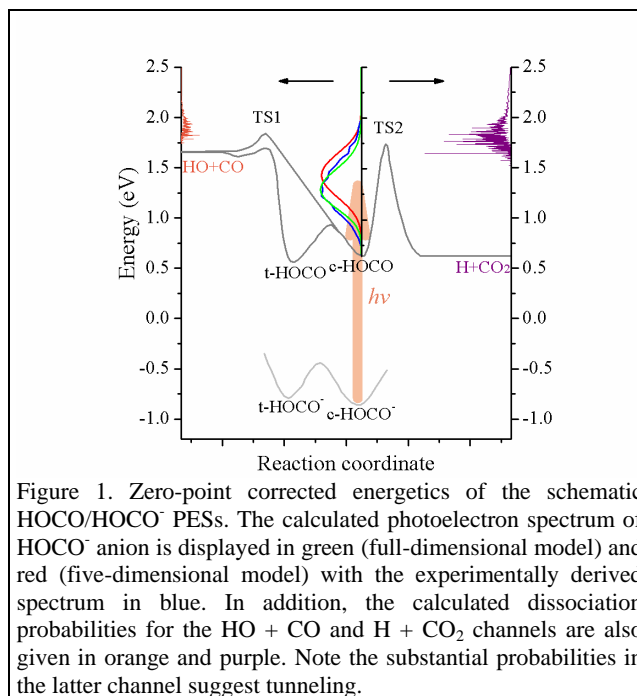


Figure 1. Zero-point corrected energetics of the schematic  $\text{HOCO}/\text{HOCO}^-$  PESs. The calculated photoelectron spectrum of  $\text{HOCO}^-$  anion is displayed in green (full-dimensional model) and red (five-dimensional model) with the experimentally derived spectrum in blue. In addition, the calculated dissociation probabilities for the  $\text{HO} + \text{CO}$  and  $\text{H} + \text{CO}_2$  channels are also given in orange and purple. Note the substantial probabilities in the latter channel suggest tunneling.

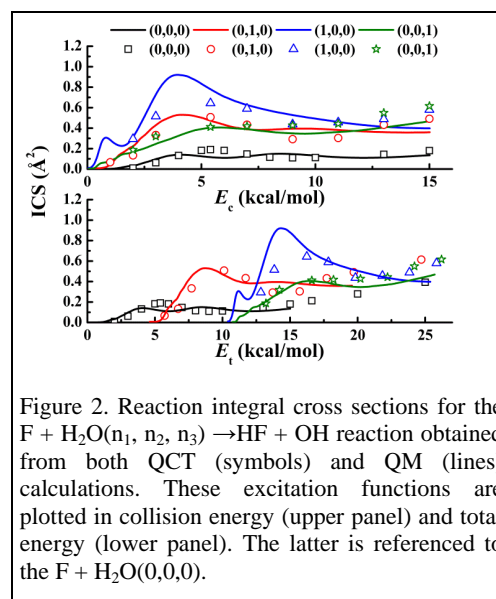


Figure 2. Reaction integral cross sections for the  $\text{F} + \text{H}_2\text{O}(n_1, n_2, n_3) \rightarrow \text{HF} + \text{OH}$  reaction obtained from both QCT (symbols) and QM (lines) calculations. These excitation functions are plotted in collision energy (upper panel) and total energy (lower panel). The latter is referenced to the  $\text{F} + \text{H}_2\text{O}(0,0,0)$ .

surprising effect was explained with a vibrationally adiabatic model, which suggests that the enhancement is better described as the coupling of the vibrational modes to the reaction coordinate, rather than the position of the barrier. These unusual behaviors were found to be minimally impacted when the spin-orbit corrections of both  $F(^2P)$  and  $OH(^2\Pi)$  are added.<sup>19</sup>

In addition to these reaction dynamics studies, we have performed rate constant calculations for a number of important reactive systems. For example, we have used a capture model to estimate the rate constants and temperature dependence for the barrierless  $N + CN$  reaction.<sup>20</sup> In collaboration with Bill Green group, we have also applied the recently proposed ring-polymer molecular dynamics (RPMD) method to the  $O + CH_4$ <sup>21</sup> and  $H + CH_4$  reactions.<sup>22</sup> The RPMD approach was found to give good agreement with the full-dimensional multi-configuration time-dependent Hartree (MCTDH) results on the same PESs, as shown in Fig. 3, thus validating its accuracy. It also gives a good agreement with variational transition-state theory with semi-classical tunneling corrections, except for the  $Mu + CH_4$  case. The discrepancy there is presumably due to the large anharmonicity for this ultralight isotope of hydrogen.

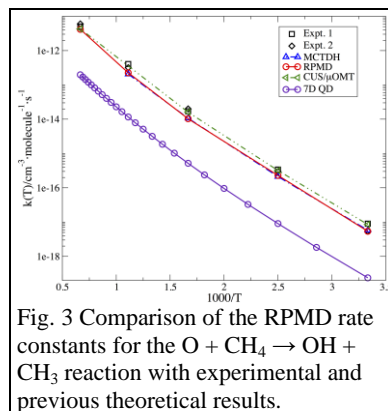


Fig. 3 Comparison of the RPMD rate constants for the  $O + CH_4 \rightarrow OH + CH_3$  reaction with experimental and previous theoretical results.

Finally, we have collaborated with David Yarkony to further our understanding on non-adiabatic dynamics in photodissociation. Full-dimensional quantum dynamics has been performed on accurate non-adiabatically coupled PESs for the photodissociation of ammonia in its A band.<sup>23-24</sup> Unprecedented agreement with experimentally determined line positions, widths and intensity as well as product branching ratios was achieved, validating the accuracy of the PESs and their couplings.

In the next year, we plan to continue to pursue our proposed research in the areas of chemical dynamics and kinetics.

#### References (\* indicates DOE funded work in the past year):

- \*1 A. Li, C. Xie, D. Xie and H. Guo, *J. Chem. Phys.* **138**, 024308 (2013).
- \*2 H. Guo, *Theo. Chem. Acc.* **131**, 1077 (2012).
- \*3 H. Guo, *Int. Rev. Phys. Chem.* **31**, 1 (2012).
- \*4 J. Li, C. Xie, J. Ma, Y. Wang, R. Dawes, D. Xie, J. M. Bowman and H. Guo, *J. Phys. Chem. A* **116**, 5057 (2012).
- \*5 C. Xie, J. Li, D. Xie and H. Guo, *J. Chem. Phys.* **127**, 024308 (2012).
- 6 J. Li, Y. Wang, B. Jiang, J. Ma, R. Dawes, D. Xie, J. M. Bowman and H. Guo, *J. Chem. Phys.* **136**, 041103 (2012).
- \*7 J. Ma, J. Li and H. Guo, *J. Phys. Chem. Lett.* **3**, 2482 (2012).
- 8 C. J. Johnson and R. E. Continetti, *J. Phys. Chem. Lett.* **1**, 1895 (2010).
- 9 C. J. Johnson, B. L. J. Poad, B. B. Shen and R. E. Continetti, *J. Chem. Phys.* **134**, 171106 (2011).
- \*10 J. Ma, J. Li and H. Guo, *Phys. Rev. Lett.* **109**, 063202 (2012).
- \*11 J. Li, R. Dawes and H. Guo, *J. Chem. Phys.* **137**, 094304 (2012).
- 12 J. M. Bowman, G. Czako and B. Fu, *Phys. Chem. Chem. Phys.* **13**, 8094 (2011).
- 13 M. P. Deskevich, D. J. Nesbitt and H.-J. Werner, *J. Chem. Phys.* **120**, 7281 (2004).
- 14 M. Ziemkiewicz, M. Wojcik and D. J. Nesbitt, *J. Chem. Phys.* **123**, 224307 (2005).
- 15 A. M. Zolot and D. J. Nesbitt, *J. Chem. Phys.* **129**, 184305 (2008).
- 16 M. Ziemkiewicz and D. J. Nesbitt, *J. Chem. Phys.* **131**, 054309 (2009).
- \*17 J. Li, B. Jiang and H. Guo, *Chem. Sci.* **4**, 629 (2013).
- \*18 J. Li, B. Jiang and H. Guo, *J. Am. Chem. Soc.* **135**, 982 (2013).
- \*19 J. Li, B. Jiang and H. Guo, *J. Chem. Phys.* **138**, 074309 (2013).
- \*20 J. Ma, H. Guo and R. Dawes, *Phys. Chem. Chem. Phys.* **14**, 12090 (2012).
- \*21 Y. Li, Y. V. Suleimanov, M. Yang, W. H. Green and H. Guo, *J. Phys. Chem. Lett.* **4**, 48 (2013).
- \*22 Y. Li, Y. V. Suleimanov, J. Li, W. H. Green and H. Guo, *J. Chem. Phys.* **138**, 094307 (2013).
- \*23 X. Zhu, J. Ma, D. R. Yarkony and H. Guo, *J. Chem. Phys.* **136**, 234301 (2012).
- \*24 J. Ma, X. Zhu, H. Guo and D. R. Yarkony, *J. Chem. Phys.* **137**, 22A541 (2012).

# Gas-Phase Molecular Dynamics: High Resolution Spectroscopy and Collision Dynamics of Transient Species

Gregory E. Hall  
Chemistry Department, Brookhaven National Laboratory  
Upton, NY 11973-5000  
[gehall@bnl.gov](mailto:gehall@bnl.gov)

## Program Scope

This research is carried out as part of the Gas-Phase Molecular Dynamics program in the Chemistry Department at Brookhaven National Laboratory. Chemical intermediates in the elementary gas-phase reactions involved in combustion chemistry are investigated by high resolution spectroscopic tools. Production, reaction, and energy transfer processes are investigated by transient, double resonance, polarization and saturation spectroscopies, with an emphasis on technique development and connection with theory, as well as specific molecular properties.

## Recent Progress

### A. Collision-induced broadening, shifting, and narrowing in the CN A-X (1-0) band by Ar

Quantitative pressure-dependent line shape studies are of importance both for converting spectroscopic probe measurements into usable concentration data, and for the insights they may provide

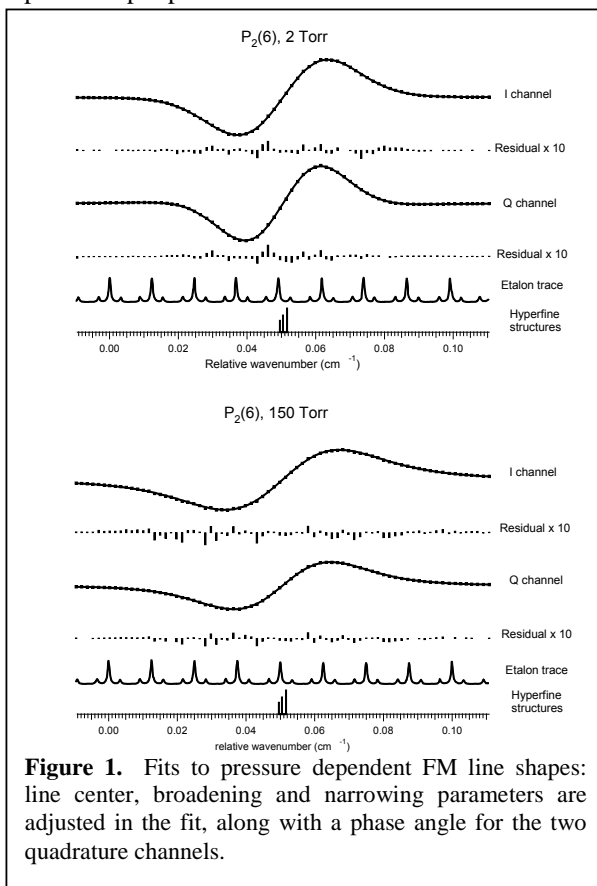


**Figure 1.** Fits to pressure dependent FM line shapes: line center, broadening and narrowing parameters are adjusted in the fit, along with a phase angle for the two quadrature channels.

into collision dynamics and intermolecular potentials. In particular, the deviations from Voigt line shapes (an uncorrelated convolution of Gaussian Doppler width with a pressure-dependent Lorentzian line shape) are typically observed in high-precision line shape measurements, and may be attributed to several effects. Speed-dependent relaxation rates increase the effective Lorentzian broadening for those velocity groups sampled at larger Doppler shifts (and thus higher average collision velocities). Elastic velocity changing collisions can also cause phenomenologically similar narrowing effects through a totally different mechanism: averaging the Doppler shift of individual molecules during multiple elastic velocity-changing collisions prior to the next inelastic collision that terminates the coherent interaction with the optical field. Pressure-induced frequency shifts can be considered the consequence of a differential interaction of the perturber with upper and lower states of the transition, causing a transient shift in the vertical transition energy during the perturbation.

We have measured accurate room temperature line shapes of selected rotational

transitions in the CN  $A^2\Pi-X^2\Sigma^+$  (1-0) band near 900 nm in the presence of argon. Measurements were performed with FM spectroscopy, recording two channels in quadrature, sampling a phased combination of absorption and dispersion signals. The linear pressure dependence of all fit parameters gives accurate experimental values for collision-induced broadening, shifting, and narrowing. No systematic asymmetry in the line shapes was observed. Interesting contrasts can be drawn between the present results and previous measurements by the Hanson group<sup>1-3</sup> on pressure broadening of CN ( $B^2\Sigma^+-X^2\Sigma^+$ ), OH ( $A^2\Sigma^+-X^2\Pi$ ) and NO ( $B^2\Sigma^+-X^2\Pi$ ) by rare gases, and related pressure broadening and shifting in vibrational spectra<sup>4</sup> of the same systems. Understanding trends and relative contributions of rotational energy transfer collisions on ground and excited state surfaces, and the competition between elastic velocity-changing, elastic depolarizing and inelastic collisions in such atom-radical systems is a feasible target for experimental and theoretical comparison.<sup>5-6</sup> Features of rare-gas-CN collisions probed by our recent double-resonance studies of rotationally inelastic collisions, speed-dependent inelastic collision rates, elastic depolarization and elastic velocity-changing collisions are the same ones that play a central role in the interpretation and modeling of pressure-broadening of isolated spectroscopic lines.

## **B. Dual-beam FT spectroscopy with a supercontinuum and single-detector balanced detection**

We have been exploring methods to combine fiber laser frequency comb sources with commercial FTIR instrumentation to provide sensitive and accurate measurements of weak absorption features, for example, in attenuated reflection spectroscopy of surface species. Last year we reported on a general dual-beam method, compatible with commercial FTIR instrumentation that combines strong suppression of source noise with continuous correction for background drift. The method was demonstrated with a mode locked Er fiber laser centered at 1560 nm and a balanced detector consisting of two InGaAs photodiodes, with interferograms simultaneously recorded from the reference path detector and from the differential output of the balanced detectors, producing absorption sensitivity near the shot noise limit.

Matching the broadband capabilities of Fourier transform spectroscopy with supercontinuum sources based on mode locked pump sources and highly nonlinear fibers is an attractive goal, previously limited in practice by excessive spectral and amplitude noise in the broadband output, making sensitive absorption measurements difficult with these sources. The dual beam designs are capable of noise rejection to help this problem, but only at wavelengths for which matched detector pairs can be found that are well matched in amplitude and spectral sensitivity, and display well matched phase shifts and partial saturation in the conversion of repetitively pulsed ultrafast optical pulse trains into photocurrent outputs. We have made progress on two fronts in the past year. Careful temperature stabilization of the fiber laser oscillator produces a supercontinuum with substantially less noise than several commercially produced supercontinuum sources, placing more modest demands on the differential noise cancellation scheme. Furthermore, we have implemented a novel means of performing dual beam balanced detection *with a single detector*. After a spectrally filtered portion of the supercontinuum is modulated in a Fourier transform interferometer, the output beam is split into sample and reference paths with polarizing optics, and then recombined with a half-cycle delay. In this way, interleaved even and odd numbered pulses arriving at twice the repetition rate of the supercontinuum pulse train constitute collinear sample and reference beam paths that can be focused onto a single detector. Phase sensitive detection at the repetition rate isolates the differential interferogram, while the average, low frequency signal monitors the interferogram of the source, in a way that permits excellent cancellation of both source noise and any slow drift in the spectral content of the source on the timescale of the interferometer sweep. We

anticipate that this single detector balanced detection scheme should be particularly attractive for applications at longer wavelengths, into the mid-infrared, where the detectors are slower and harder to match, and the noise reduction advantages of high-frequency phase sensitive detection persist.

## Future Work

### A. Double resonance studies of collision dynamics in CN radicals

We have been studying inelastic collisions of CN ( $X^2\Sigma^+$ ,  $v=0$ ,  $J$ ) with Ar, using transient, polarized, sub-Doppler FM spectroscopy to monitor saturation recovery, following bleaching of selected rotational states. Analysis of the “hole” kinetics yields results identical to what could be observed following pulsed creation of a single state in an otherwise empty rotational manifold. The kinetics of hole-filling gives a rate equivalent to the total inelastic decay rate. Depolarization kinetics allow for a comparison of elastic  $m$ -changing rates and total rotational energy transfer rates. The recovery kinetics are observed to vary with Doppler detuning, a direct measure of the variation of the inelastic collision rate as a function of the average relative velocity of collisions. The relatively rapid filling of depletion in the Doppler wings, compared to the line center provides complementary information on the speed-dependent collision rates, a topic of key relevance to the pressure-broadening studies cited above. Indeed, the entanglement of velocity changing collisions with speed-dependent collision rates that confound pressure-dependent line shape studies makes a parallel appearance in the Doppler-resolved saturation recovery kinetics, as velocity-changing collisions tend to restore a normal thermal Gaussian line shape during the latter stages of depletion recovery. The connections between second-order effects in pressure broadening and aspects of collision dynamics addressed through double resonance studies are a topic of continuing interest.

### B. Sub-Doppler saturation recovery in CN radicals

Future studies with sub-Doppler saturation recovery kinetics, probed by independently tunable sub-Doppler probe spectroscopy can more directly address the conditions under which velocity changing collisions contribute to pressure broadened line shapes. Preliminary work performed with one laser, split into counterpropagating amplitude modulated bleach and frequency modulated probe beams, has shown that the dark recovery rate of a sub-Doppler bleach signal is dominated by rotationally inelastic collisions, at least for low rotational states. One-color saturation spectroscopy is generally sensitive to the collision dynamics on both upper and lower potential energy surfaces, complicating the interpretation of the saturation recovery kinetics. The use of hyperfine crossover resonances, (a three-level, one color, double resonance condition) selectively isolates upper or lower state effects, but only for low rotational states where crossover resonances have significant intensity, and only for the Doppler-free velocity group near line-center. Using an independently tunable and rapidly extinguished bleach laser will allow analogous measurements of sub-Doppler saturation recovery for different velocity groups and any rotational state, and specifically sensitive to either  $A$  state or  $X$  state collisions, for example, with pump laser saturation on the (2-0) band and the probe laser measurement by either gain on the (2-1) band or absorption on the (1-0) band of the red  $A$ - $X$  system. Having access to a range of rotational states will be important, as the relative contribution of velocity changing collisions is expected to increase as the rotational spacing increases and the inelastic cross sections decrease. Comparison with scattering calculations on realistic potentials will be an important part of the program.

### Cited References

- [1] S. T. Wooldridge, R. K. Hanson, and C. T. Bowman, *J. Quant. Spectrosc. Radiat. Transfer* **53**, 481 (1995).
- [2] E. C. Rea, A. Y. Chang, and R. K. Hanson, *J. Quant. Spectrosc. Radiat. Transfer* **37**, 117 (1987).
- [3] M. D. Di Rosa, and R. K. Hanson, *J. Mol. Spectrosc.* **164**, 97 (1994).
- [4] Y. Sakamoto, D. Yamano, T. Nakayama, M. Kawasaki, I. Morino, and G. Inoue, *Chem. Lett.* **38**, 1000 (2009), and references therein.
- [5] M. Brouard *et al.*, *J. Chem. Phys.* **130**, 044306 (2009).
- [6] P. J. Dagdigian, and M. H. Alexander, *J. Chem. Phys.* **130**, 204304 (2009).

### Publications supported by this project since 2011

- Transient laser absorption spectroscopy of CH<sub>2</sub> near 780 nm. C.-H. Chang, Z. Wang, G. E. Hall, T. J. Sears and J. Xin, *J. Molec. Spectrosc.* **267**, 50-57 (2011)
- CH<sub>2</sub> band origin at 1.20 μ. C.-H. Chang, J. Xin, T. Latsha, E. Otruba, Z. Wang, G. E. Hall, T. J. Sears and B.-C. Chang, *J. Phys. Chem. A*, **115**, 9440-9446 (2011)
- The Approach to Equilibrium: Detailed Balance and the Master Equation. M. H. Alexander, G. E. Hall and P. J. Dagdigian, *J. Chem. Educ.* **88**, 1538-1543 (2011)
- What is the best DFT function for vibronic calculations? A comparison of the calculated vibronic structure of the S<sub>1</sub> – S<sub>0</sub> transition of phenylacetylene with accurate experimental band intensities, G. V. Lopez, C.-H. Chang, P. M. Johnson, G. E. Hall, T. J. Sears, B. Markiewicz, M. Milan and A. Teslja, *J. Phys. Chem. A* **116** 6750-6758 (2012).
- Broadband laser-enhanced dual-beam interferometry. V. V. Goncharov and G. E. Hall, *Optics Letters* **37** 2406-2408 (2012).
- Hyperfine structures in the v=1-0 vibrational band of the B<sup>3</sup>Π<sub>g</sub> – A<sup>3</sup>Σ<sub>u</sub><sup>+</sup> of N<sub>2</sub>. D. Forthomme, C. P. McRaven, G. E. Hall, and T. J. Sears, *J. Mol. Spectr.* **282**, 50-55 (2012).
- Argon-induced pressure broadening, shifting and narrowing in the CN A<sup>2</sup>Π – X<sup>2</sup>Σ<sup>+</sup> (1-0) band, D. Forthomme, C. P. McRaven, T. J. Sears and G. E. Hall, (submitted).

# Flame Chemistry and Diagnostics

Nils Hansen

Combustion Research Facility, Sandia National Laboratories, Livermore, CA 94551-0969

Email: nhansen@sandia.gov

## SCOPE OF THE PROGRAM

In this program, we seek to understand the detailed chemistry of combustion through a unique scheme of diagnostics development and experimental studies of simple flames. Our goal is to provide reliable experimental data on the chemical composition of laboratory-scale model flames through state-of-the-art diagnostics. The experiments are designed to serve as benchmarks for the development and validation of detailed chemical kinetic models. In particular, we study laminar premixed flames, which are stabilized on a flat-flame burner under a reduced pressure of ~15-30 Torr and laminar opposed-flow diffusion flames at low and atmospheric pressure. We implement mainly mass spectrometer techniques and our experimental data in the form of species identification and quantification serve as stringent tests for the development and validation of any detailed chemical kinetic mechanisms. Over the past years, the overall objective of this program has been to elucidate the chemistry of soot precursors in hydrocarbon flames. Studying this complex combustion chemistry with an unprecedented level of detail requires determining the chemical structures and concentrations of species sampled from sooting or nearly-sooting model flames.

## PROGRESS REPORT

**Exploring Formation Pathways of Aromatic Compounds in Laboratory-Based Model Flames of Aliphatic Fuels:** During the previous years, we showed how detailed characterization of chemical species in laboratory-scale model flames facilitated our chemical understanding of the formation of the so-called “first aromatic ring”. There is now a general agreement that the first step towards soot formation from non-aromatic fuels is the formation of this “first aromatic ring”, probably - but not necessarily - benzene ( $C_6H_6$ ) or phenyl ( $C_6H_5$ ). Under most combustion conditions, much of the benzene/phenyl was shown to form through combination of two propargyl ( $C_3H_3$ ) radicals. We provided evidence that contributions from reactions of other resonance-stabilized free radicals including allyl ( $C_3H_5$ ), *i*- $C_4H_5$ , and cyclopentadienyl (*cycl.*- $C_5H_5$ ) are partially fuel-dependent and that dissociation and isomerization can be important fuel-decomposition pathways. Even without detailed modeling, experimental data alone indicated that the fuel-structure has an influence on the benzene formation processes. Details of our findings and the eminent role of resonance-stabilized free radicals in the ring formation process were discussed in a review paper for “*Combustion, Explosion, and Shockwaves*”.

**Studies of Laminar Opposed-Flow Diffusion Flames:** With the chemistry of benzene/phenyl formation in flames well understood, the time has come to shift the emphasis to a fundamental chemical understanding of the molecular-growth mechanisms that are responsible for the formation of the large polycyclic aromatic hydrocarbons (PAH's). Recognizing this opportunity, we have recently designed and built an opposed-flow flame system to investigate the chemical composition of slightly-sooting non-premixed flames using *in-situ* flame-sampling molecular-beam mass spectrometry. This project, which was funded through DOE's SISGR program, was done in collaboration with H. A. Michelsen (Sandia). To test the system, we have investigated the chemical composition of three low-pressure (30-50 Torr), non-premixed, opposed-flow acetylene(Ar)/O<sub>2</sub>(Ar) flames.

Funded through the Alexander von Humboldt-Foundation, I was able to set-up and test a flame-sampling molecular-beam mass spectrometer combined with an atmospheric-pressure opposed-flow flame in the labs of Prof. Kohse-Höinghaus at the Universität Bielefeld in Germany. The scientific goal of that extended research stay was to study the molecular-growth chemistry of soot precursors in combustion environments. To this end, we investigated the chemical structures of atmospheric-pressure, non-premixed, opposed-flow flames of *n*-butane, *i*-butane, *i*-butene, and *i*-butanol under slightly sooting conditions using *in situ* flame-sampling molecular-beam mass spectrometry with electron ionization (EI). The quantitative mole-fraction profiles for the major species and several intermediates, measured as function of the distance from the fuel outlet, are currently used to elucidate the influence of the fuel structure on the chemical composition of the flames with a particular emphasis on well-known soot precursors. Isomer-specific measurements of the PAH's formed in these flames were accomplished by flame-sampling *in situ* gas chromatography (GC) with mass spectrometry detection. In addition, we sampled nascent soot particles from laminar premixed atmospheric-pressure flames of the same fuels and studied the impact of the fuel structures on particle size and morphology using Helium Ion Microscopy (HIM), a newly developed charged-particle imaging technique. All data is currently being analyzed and prepared for publication. We anticipate two papers to be submitted within the course of this year.

**Near-Threshold Photoionization Mass Spectra of Combustion-Generated High-Molecular-Weight Soot Precursors:** In collaboration with H. A. Michelsen (Sandia), and K. R. Wilson (Berkeley), we recorded the aerosol mass spectra of organic species having mass-to-charge ratios between 15 and 900 sampled from near-atmospheric pressure, non-premixed, opposed-flow flames of acetylene, ethylene, and propane using an aerosol mass spectrometer with flash vaporization. Near-threshold photoionization was achieved by synchrotron-generated tunable-vacuum-ultraviolet (VUV) light. The contrasting characteristics of the aerosol mass spectra for three different flames suggested that the relative amounts and compositions of soot precursor species were dependent on the chemical structure of the fuel.

Our results provided evidence that the widely accepted H-abstraction-C<sub>2</sub>H<sub>2</sub>-addition (HACA) mechanism cannot explain all observed PAH's. Contributions towards PAH formation and the isomeric content of the soot-precursor species are likely to depend on the fuel structure and/or flame conditions. In addition, spatial profiles indicated the presence of oxygen containing species. A comparison of PIE curves among the three flames suggested the presence of species with higher ionization thresholds than would be expected for the most thermodynamically stable PAH's commonly identified in flames. Their presence provided some evidence for kinetically, as opposed to thermodynamically, driven soot precursor formation mechanisms.

## OUTLOOK

### **Experimental Studies on the Molecular-Growth Chemistry of Soot Precursors in**

**Combustion Environments:** Now that the goal of the research program is shifting towards the formation of larger species in combustion environments, it will be the goal of our future studies to directly address the molecular-growth chemistry from small combustion intermediates to larger and larger PAH's. The underlying chemistry will be investigated by a combination of different experiments. The centerpiece of all experiments is a simple, *i.e.* laminar, model flame, and analyzing the chemical composition of such model flames will provide guidance and benchmarks needed to improve and test theoretical models describing soot-formation chemistry with predictive capabilities. We plan to investigate the chemical composition of these flames in unprecedented detail by flame-sampling mass spectrometry with electron ionization (EI), resonance-enhanced multiphoton ionization (REMPI), single-photon VUV ionization, and gas chromatography (GC/MS). REMPI experiments can be used to great benefit in the flame-structure analysis, as it usually causes less ion fragmentation than electron ionization. In addition, REMPI processes are wavelength-dependent and molecule-specific and can therefore be used for selective and sensitive detection of a given species. In an additional experimental approach, it is proposed to analyze the chemical structure of the opposed-flow flames by gas chromatography equipped with mass spectrometry (GC/MS). The coupling of MBMS with GC is very promising. In spite of its inability to detect reactive compounds, its potential of detailed, even isomer-specific, separation of stable compounds is remarkable. Its sensitivity and its selectivity are very well suited to access small and large aromatics. It is the intention to provide isomer-specific information for PAH species, which is not available from the other MBMS experiments alone.

From the experiments in Bielefeld we learned that a setup with one stage of differential pumping can only be used for non-sooting atmospheric-pressure flames. Although our current set-up allows for a pressure between 30 and 700 Torr, sampling from sooting flames at atmospheric pressure will immediately lead to

clogging of the small opening (a few  $\mu\text{m}$ ) in the microprobe. We therefore propose to rebuild the mass spectrometer and to add an additional stage of pumping and at the same time install a reflectron to achieve a mass resolution that is sufficient to separate PAH's of up to 1000 amu.

#### **PUBLICATIONS ACKNOWLEDGING BES SUPPORT 2011-PRESENT**

1. N. Hansen, T. Kasper, B. Yang, T. A. Cool, W. Li, P. R. Westmoreland, P. Oßwald, K. Kohse-Höinghaus, "Fuel-Structure Dependence of Benzene Formation Processes in Premixed Flames Fueled by  $\text{C}_6\text{H}_{12}$  Isomers", *Proc. Combust. Inst.*, **33**, 585-592 (2011).
2. S. Dooley, F. L. Dryer, B. Yang, J. Wang, T. A. Cool, T. Kasper, N. Hansen, "An Experimental and Kinetic Modeling Study of Methyl Formate Low-Pressure Flames", *Combust. Flame*, **158**, 732-741 (2011).
3. B. Yang, T. A. Cool, C. K. Westbrook, N. Hansen, K. Kohse-Höinghaus, "Fuel-Specific Influences on the Composition of Reaction Intermediates in Premixed Flames of Three  $\text{C}_5\text{H}_{10}\text{O}_2$  Ester Isomers", *Phys. Chem. Chem. Phys.*, **13**, 7205-7217 (2011).
4. W. Li, M. E. Law, P. R. Westmoreland, T. Kasper, N. Hansen, K. Kohse-Höinghaus, "Multiple Benzene-Formation Paths in a Fuel-Rich Cyclohexane Flame", *Combust. Flame*, **158**, 2077-2089 (2011).
5. N. Hansen, M. R. Harper, W. H. Green, "High-Temperature Oxidation Chemistry of n-Butanol – Experiments in Low-Pressure Premixed Flames and Detailed Kinetic Modeling", *Phys. Chem. Chem. Phys.*, **13**, 20262-20274 (2011).
6. B. Yang, C. K. Westbrook, T. A. Cool, N. Hansen, K. Kohse-Höinghaus, "The Effect of Carbon-Carbon Double Bonds on the Combustion Chemistry of Small Fatty Acid Esters", *Z. Phys. Chem.*, **225**, 1293-1314 (2011).
7. T. Kasper, A. Lucassen, A. W. Jasper, W. Li, P. R. Westmoreland, K. Kohse-Höinghaus, B. Yang, J. Wang, T. A. Cool, N. Hansen, "Identification of Tetrahydrofuran Reaction Pathways in Premixed Flames", *Z. Phys. Chem.*, **225**, 1237-1270 (2011).
8. S. A. Skeen, B. Yang, A. W. Jasper, W. J. Pitz, N. Hansen, "Chemical Structures of Low-Pressure Premixed Methylcyclohexane Flames as Benchmarks for the Development of a Predictive Combustion Chemistry Model", *Energy Fuels*, **25**, 5611-5625 (2011).
9. B. Yang, J. Wang, T. A. Cool, N. Hansen, S. Skeen, D. L. Osborn, "Absolute Photoionization Cross-Sections of Some Combustion Intermediates", *Int. J. Mass Spectrom.*, **309**, 118-128 (2012).
10. F. Zhang, R. I. Kaiser, A. Golan, M. Ahmed, N. Hansen, "A VUV Photoionization Study of the Combustion-Relevant Reaction of the Phenyl Radical ( $\text{C}_6\text{H}_5$ ) with Propylene ( $\text{C}_3\text{H}_6$ ) in a High-Temperature Chemical Reactor", *J. Phys. Chem. A*, **2012**, 116(14), 3541-3546.
11. N. Hansen, J. A. Miller, S. J. Klippenstein, P. R. Westmoreland, K. Kohse-Höinghaus, "Exploring Formation Pathways of Aromatic Compounds in Laboratory-Based Model Flames of Aliphatic Fuels", *Combust. Expl. Shock Waves*, **2012**, 48(5), 508-515.
12. C. K. Westbrook, B. Yang, T. A. Cool, N. Hansen, K. Kohse-Höinghaus, "Photoionization Mass Spectrometry and Modeling Study of Premixed Flames of Three Unsaturated  $\text{C}_5\text{H}_8\text{O}_2$  Esters", *Proc. Combust. Inst.*, **2013**, 34(1), 443-451.
13. A. W. Jasper and N. Hansen, "Hydrogen-Assisted Isomerizations of Fulvene to Benzene and of Larger Cyclic Aromatic Hydrocarbons", *Proc. Combust. Inst.*, **2013**, 34(1), 279-287.
14. S. A. Skeen, B. Yang, H. A. Michelsen, J. A. Miller, A. Violi, N. Hansen, "Studies of Laminar Opposed-Flow Diffusion Flames of Acetylene at Low Pressures with Photoionization Mass Spectrometry", *Proc. Combust. Inst.*, **2013**, 34(1), 1067-1075.
15. N. J. Labbe, V. Seshadri, T. Kasper, N. Hansen, P. Oßwald, K. Kohse-Höinghaus, P. R. Westmoreland, "Flame Chemistry of Tetrahydropyran as a Model Heteroatomic Biofuel", *Proc. Combust. Inst.*, **2013**, 34(1), 259-267.
16. S. A. Skeen, H. A. Michelsen, K. R. Wilson, D. M. Popolan, A. Violi, N. Hansen, "Near-threshold photoionization mass spectra of combustion-generated high-molecular-weight soot precursors", *J. Aerosol Sci.*, **2013**, 58(1), 86-102.

# Kinetics and Spectroscopy of Combustion Gases at High Temperatures

R. K. Hanson, C. T. Bowman

Department of Mechanical Engineering, Stanford University

Stanford, CA 94305-3023

[rkhanon@stanford.edu](mailto:rkhanon@stanford.edu), [ctbowman@stanford.edu](mailto:ctbowman@stanford.edu)

## I. Program Scope

This program involves two complementary activities: (1) development and application of cw laser absorption methods for the measurement of concentration time-histories and fundamental spectroscopic parameters for species of interest in combustion; and (2) shock tube studies of reaction kinetics relevant to combustion.

Species currently being investigated in the spectroscopic portion of the research include several species with strong UV or IR absorption features including: formaldehyde ( $\text{CH}_2\text{O}$ ) acetaldehyde ( $\text{CH}_3\text{HCO}$ ), methyl radical ( $\text{CH}_3$ ), hydroxyl radical ( $\text{OH}$ ), water ( $\text{H}_2\text{O}$ ), carbon monoxide ( $\text{CO}$ ), ethylene ( $\text{C}_2\text{H}_4$ ), and oxygenates including alcohols, methyl ester, aldehydes, and ketones.

Recent reaction kinetics work has advanced on two fronts. First, we are continuing direct high-temperature shock tube/laser absorption measurements of the reaction rate constants for  $\text{OH} +$  oxygenates, including small ketones, methyl esters, butanol isomers and a high-precision study of  $\text{OH} + \text{H}_2$ . Second, we are investigating the decomposition and oxidation of oxygenated fuels including 3-pentanone using a multi-species approach.

## II. Recent Progress: Spectroscopy

### Aldehyde Detection using 306 nm UV and 3.4 micron IR Laser Absorption

Formaldehyde and acetaldehyde can be detected in both the IR and the UV. The aldehyde IR spectrum is discrete but densely populated near  $3.5 \mu\text{m}$ , and overlapping lines provide an opportunity for stronger absorption and more sensitivity than with fully isolated lines. This wavelength range is also away from the dominant absorption feature of many fuel-relevant alkanes such as n-heptane. Using this IR wavelength range and a ring dye laser operating near 306.7 nm, a multi-color combined UV/IR laser absorption scheme has been developed for simultaneous formaldehyde and acetaldehyde detection in the presence of OH. Absorption measurements indicated that the aldehydes cross-sections were the same both on and off the OH  $R_1(5)$  line of the A-X (0,0) transition, at  $32606.50 \text{ cm}^{-1}$  and  $32601.10 \text{ cm}^{-1}$ . Together with two IR wavelengths, absorption measurements at these four colors enabled complete separation of formaldehyde, acetaldehyde and OH from interfering species. Important applications of these diagnostics include monitoring formaldehyde and acetaldehyde during pyrolysis and oxidation of oxygenated fuels. Further details can be found in Publication 1.

### Multi-Species Time-History Measurements of Oxygenate Pyrolysis and Oxidation

To assist in the refinement of the detailed mechanism for the pyrolysis and oxidation of 3-pentanone, a multi-species, multi-wavelength shock tube/laser absorption campaign was undertaken to characterize major reactant, intermediate and product species in these systems. Species time-history measurements of 3-pentanone,  $\text{CH}_3$ ,  $\text{C}_2\text{H}_4$  and  $\text{CO}$  during 3-pentanone pyrolysis, when analyzed, provided accurate measurements of the overall decomposition rate (from the 3-pentanone and  $\text{CH}_3$  time-histories), and identified the need to include a methyl ketene decomposition pathway in the Serinyel et al. (2010) mechanism (evident from the  $\text{CO}$  time-history). Measurements of the species time-histories of  $\text{CO}$ ,  $\text{H}_2\text{O}$  and  $\text{OH}$  during 3-pentanone oxidation confirm these conclusions. Representative oxidation data are shown in Fig. 1 along with the modified Serinyel et al. (2010) mechanism simulations. (Z. Serinyel, N. Chaumeix, G. Black, J. M. Simmie, H. J. Curran, *J. Phys. Chem A* 114 (2010) 574-587.) Further details may be found in Publication 10.

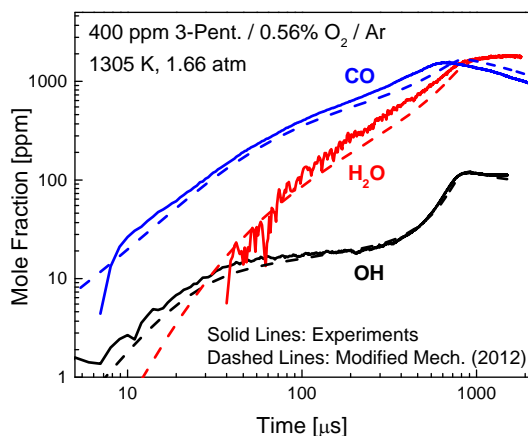


Figure 1. Multi-species time-history measurements during 3-pentanone oxidation. Simulations using the modified Serinyel et al. (2010) mechanism are from Lam et al. (2012).

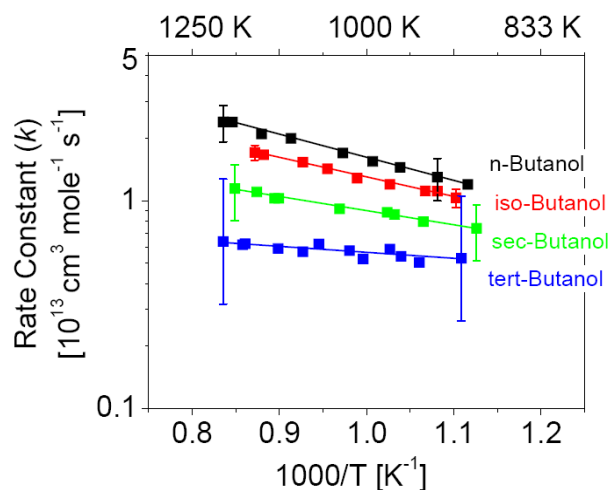


Figure 2. Reaction rate constants for OH + butanol isomers  $\rightarrow$  all products and least-squares fits. Error bars include experimental and modeling uncertainties. (From Pang et al. 2012.)

## II. Recent Progress: Chemical Kinetics

### Rate Constant Measurement: OH + Butanol Isomers $\rightarrow$ Products

The rate constants for the reaction OH plus each of the four butanol isomers, n-butanol, iso-butanol, sec-butanol and tert-butanol, were measured in experiments behind reflected shock waves at temperatures from 900 to 1200 K using tertbutylhydroperoxide (TBHP) as a fast source of OH radicals with the butanol isomer in excess. Narrow-linewidth laser absorption at 306.7 nm was employed for quantitative OH concentration measurements. A detailed mechanism describing the kinetics for each butanol isomer and TBHP was constructed to facilitate the rate constant determinations and account for secondary chemistry influences on the pseudo-first order OH concentration decays. Representative rate constant data determined for the reactions OH + butanol isomers  $\rightarrow$  all products are shown in Fig. 2. The current work extends the temperature range of high-temperature measurements of the rate constant in the literature to 900 to 1200 K. A detailed uncertainty analysis was performed yielding an overall uncertainty in the measured rate constant of between  $\pm 20\%$  and  $\pm 30\%$  depending on the isomer and the temperature. The results were compared with previous experimental and theoretical studies and reasonable agreement was found. Further details can be found in Publications 6-9.

### Rate Constant Measurement: OH + Methyl Esters $\rightarrow$ Products

The overall rate constants for the reactions of hydroxyl radicals (OH) with four small methyl esters, namely methyl formate ( $\text{CH}_3\text{OCHO}$ ), methyl acetate ( $\text{CH}_3\text{OC(O)CH}_3$ ), methyl propanoate ( $\text{CH}_3\text{OC(O)C}_2\text{H}_5$ ), and methyl butanoate ( $\text{CH}_3\text{OC(O)C}_3\text{H}_7$ ), were investigated behind reflected shock waves using UV laser absorption of OH radicals. Again, test gas mixtures used tert-butyl hydroperoxide (TBHP) as a fast source of OH at elevated temperatures. The overall rate constants were determined by matching the measured OH time-histories with the computed profiles from the comprehensive chemical kinetic mechanisms of Dooley et al. (2010) and Dooley et al. (2008), which were originally developed for the oxidation of methyl formate and methyl butanoate, respectively. Detailed error analyses were performed to estimate the overall uncertainties of these reactions, and the estimated ( $2\sigma$ ) uncertainties were found to be typically  $\pm 25\%$  near 900 K and  $\pm 17\%$  near 1300 K. We believe these are the first direct high-temperature rate constant measurements for the reactions of OH with these small methyl esters. These measured rate constants were also compared with the estimated values employed in different

comprehensive kinetic mechanisms. Additionally, the structure-activity relationship from Kwok and Atkinson (1995) was used to estimate these four rate constants, and the estimations from this group-additivity model are in good agreement with the measurements (within ~25%) at the present experimental conditions. Representative data are shown in Fig. 3. (Dooley et al., *Intl. J. Chem. Kinet.* 42 (2010) 527-549; E. S. C. Kwok, R. Atkinson, *Atmos. Environ.* 29 (1995) 1685-1695.) Further details can be found in Publication 4.

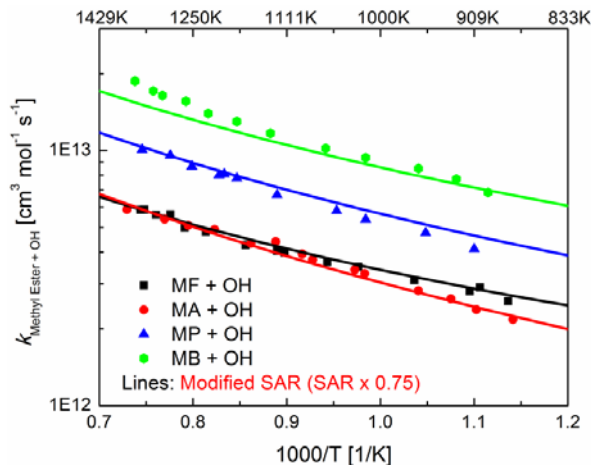


Figure 3. Comparison of the present OH+Methyl Ester rate constant measurements with the modified SAR estimations by Kwok and Atkinson (1995).

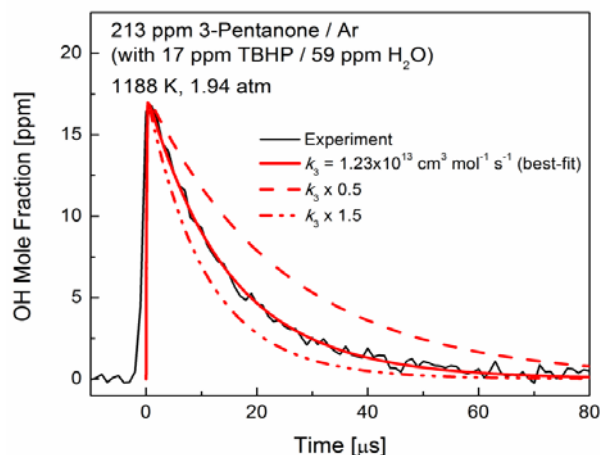


Figure 4. Example 3-pentanone + OH rate constant measurement using a mixture of 213 ppm 3-pentanone with ~17 ppm TBHP (and 59 ppm water) in Ar at 1188 K and 1.94 atm. Simulation from the Serinyel et al. mechanism for the best-fit rate constant, along with perturbations of  $\pm 50\%$ , is also shown.

#### Rate Constant Measurement: OH + Ketones $\rightarrow$ Products

The overall rate constants for the reactions of hydroxyl radicals (OH) with a series of ketones, namely acetone ( $\text{CH}_3\text{COCH}_3$ ), 2-butanone ( $\text{C}_2\text{H}_5\text{COCH}_3$ ), 3-pentanone ( $\text{C}_2\text{H}_5\text{COC}_2\text{H}_5$ ), and 2-pentanone ( $\text{C}_3\text{H}_7\text{COCH}_3$ ), were studied behind reflected shock waves over the temperature range of 870-1360 K at pressures of 1-2 atm. Here also, OH radicals were produced by rapid thermal decomposition of tert-butyl hydroperoxide (TBHP) and monitored by the narrow-linewidth ring dye laser absorption near 306.7 nm. A representative OH time-history is shown in Fig. 4. The overall rate constants were inferred by comparing the measured OH time-histories with simulated profiles from the detailed mechanisms of Pichon et al. (2009) and Serinyel et al. (2010).

The measured rate constant for acetone + OH reaction from the current study is consistent with previous experimental studies within  $\pm 20\%$ . We also reported the first direct high-temperature rate constant measurements of 2-butanone + OH, 3-pentanone + OH and 2-pentanone + OH reactions. The measured values for 2-butanone + OH reaction are in close accord with the theoretical calculation from Zhou et al. (2011), and the measured values for 3-pentanone + OH reaction are in excellent agreement with the estimates (by analogy with the H-atom abstraction rate constants from alkanes) from Serinyel et al. Finally, the structure-reactivity relationship from Kwok and Atkinson (1995) was used to estimate these four rate constants, and the estimated values from this group-additivity model show good agreement with the measurements (within ~25%) at the present experimental conditions. Further details can be found in Publication 5.

### III. Future Work

Spectroscopic experimental work continues on the development of the multi-color IR-UV aldehyde laser absorption diagnostic, and exploration of mid- and far-IR detection of acetylene and larger alkenes (e.g. propene and butene) respectively. Reaction kinetics studies are focusing on two areas: using isotopic labeling (e.g. C<sub>4</sub>H<sub>9</sub><sup>18</sup>OH) to isolate attack sites during the reaction with OH, and extending our OH measurements to other alcohols including methanol.

### IV. Publications and submitted journal articles supported by this project 2012

1. S.K. Wang, D.F. Davidson and R.K. Hanson, "Laser Absorption Diagnostics for Aldehydes in Shock Tube Kinetics Studies," submitted to Intl. Symp. Shock Waves 29, Madison, WI, 10/12.
2. R.K. Hanson, S. Chakraborty, W. Ren, S.K. Wang and D.F. Davidson, "Constrained Reaction Volume: A New Approach to Studying Reactive Systems in Shock Tubes," submitted to ISSW 29, Madison, WI, 10/12.
3. K.-Y. Lam, D.F. Davidson and R.K. Hanson, "A Shock Tube Study of H<sub>2</sub>+OH → H<sub>2</sub>O+H using Laser Absorption," Int. J. Chem. Kinetics, in press. (With additional support from NSF.)
4. K.-Y. Lam, D. F. Davidson, R. K. Hanson, "High-Temperature Measurements of the Reactions of OH with small Methyl Esters: Methyl Formate, Methyl Acetate, Methyl Propanoate, and Methyl Butanoate," J. Phys. Chem. A 116 (2012) 12229-12241.
5. K.-Y. Lam, D.F. Davidson and R.K. Hanson, "High Temperature Measurements of the Reaction of OH with a Series of Ketones: Acetone, 2-Butanone, 3-Pentanone and 2-Pentanone," J. Phys. Chem. A 116 (2012), 5549–5559.
6. G.A. Pang, R. K. Hanson, D. M. Golden and C. T. Bowman, "Experimental Determination of the High-Temperature Rate Constant for the Reaction of OH with sec-Butanol," J. Phys. Chem. A, 116 (2012), 9607-9613.
7. G. A. Pang, R. K. Hanson , D. M. Golden and C. T. Bowman, "High-Temperature Rate Constant Determination for the Reaction of OH with iso-Butanol," J. Phys. Chem. A 116 (2012) 4720-4725.
8. G.A. Pang, R.K. Hanson, D.M. Golden and C.T. Bowman, "Rate Constant Measurements of the Overall Reaction of OH+1-Butanol→ Products from 900 to 1200K," J. Phys. Chem. A 116 (2012) 2475-2483. (With additional support from DOE-EFRC.)
9. G.A. Pang, "Experimental determination of rate constants for reactions of the hydroxyl radical with alkanes and alcohols," Ph.D. Thesis, Mechanical Engineering Dept. Stanford University, CA (2012).
10. K.-Y. Lam, W. Ren, Z. Hong, D.F. Davidson and R.K. Hanson, "Shock Tube Measurements of 3-Pentanone Pyrolysis and Oxidation," Comb.and Flame 159 (2012) 3251-3263.

# Theoretical Studies of Potential Energy Surfaces\*

Lawrence B. Harding  
Chemical Sciences and Engineering Division  
Argonne National Laboratory, Argonne, IL 60439  
harding@anl.gov

## Program Scope

The goal of this program is to calculate accurate potential energy surfaces for both reactive and non-reactive systems. Our approach is to use state-of-the-art electronic structure methods (CASPT2, MR-CI, CCSD(T), etc.) to characterize multi-dimensional potential energy surfaces. Depending on the nature of the problem, the calculations may focus on local regions of a potential surface or may cover the surface more globally. A second aspect of this program is the development of techniques to fit multi-dimensional potential surfaces to convenient, global, analytic functions suitable for use in dynamics calculations.

## Recent Progress

**$^1\text{CH}_2$ +unsaturated hydrocarbons:** Reactions of singlet methylene with unsaturated hydrocarbons are thought to be important pathways to the formation of polycyclic aromatic hydrocarbons. For example the reaction of singlet methylene with acetylene leads to propargyl radical and it is thought that the recombination of propargyl radicals is the most important pathway to the formation of the first aromatic ring. In a collaboration with Klippenstein and Polino we have examined the reactions of singlet methylene with a number of unsaturated hydrocarbons including acetylene, ethylene, propyne, propene, 2-butyne, butene, butadiene, allene and benzene. Plots of the interaction potentials for  $^1\text{CH}_2$  with acetylene, propyne and

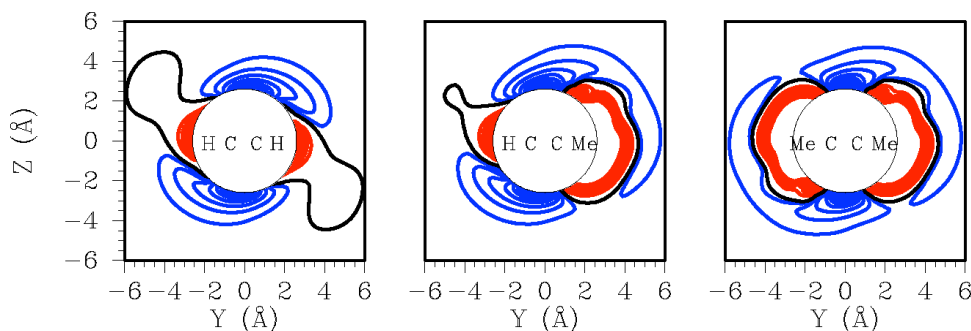


Figure 1

2-butyne are shown in Figure 1. The dominant process in almost all cases is found to be insertion into the  $\pi$ -bond forming three-membered rings. Insertion into CH bonds is also possible. The latter is a relatively minor channel for acetylene, becoming more important for propyne and butyne both because the  $\pi$ -bond insertion path becomes more constrained and the methyl CH bonds are easier insertion targets. For benzene the calculations predict CH bond insertion to be much more important primarily because three-membered ring formation is quite slow.

**Comparisons of the MOLPRO and COLUMBUS implementations of MR-CI:** The two most often used multi reference, configuration interaction programs are MOLPRO and COLUMBUS. There are differences between these two programs, the most significant of which is that MOLPRO uses an *internal contraction* scheme to reduce the number of variational parameters while COLUMBUS does not. Some years ago Georgievskii and Miller<sup>1</sup> noted that the H+O<sub>2</sub> interaction potential they obtained using MOLPRO is significantly less attractive than a potential reported earlier by Harding et al<sup>2</sup> using COLUMBUS even though both calculations employed the same active space and the same basis set. They suggested that this might be attributable to MOLPRO's internal contraction scheme. This year we have begun a systematic comparison of reactive potential surfaces obtained from MR-CI calculations using MOLPRO and COLUMBUS. In Figure 2 we show (9E, 7O)-CAS+1+2/aug-cc-pvtz potential surfaces for

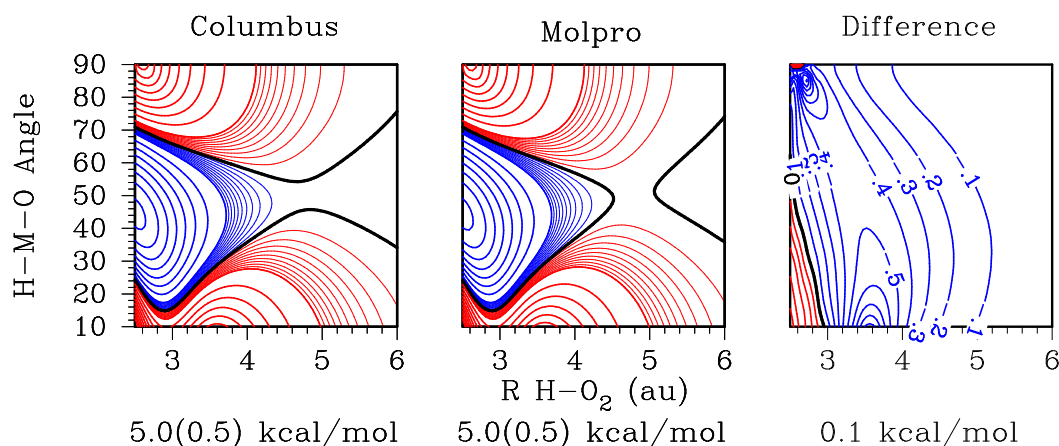


Figure 2

the H+O<sub>2</sub> reaction obtained with COLUMBUS (on the left) and MOLPRO (in the center) along with the difference between the two (on the right). What we find is that although the difference for the overall heat of reaction is small, there are significant differences in the vicinity of the reaction bottleneck with the COLUMBUS energies being up to ~0.5 kcal/mol more attractive

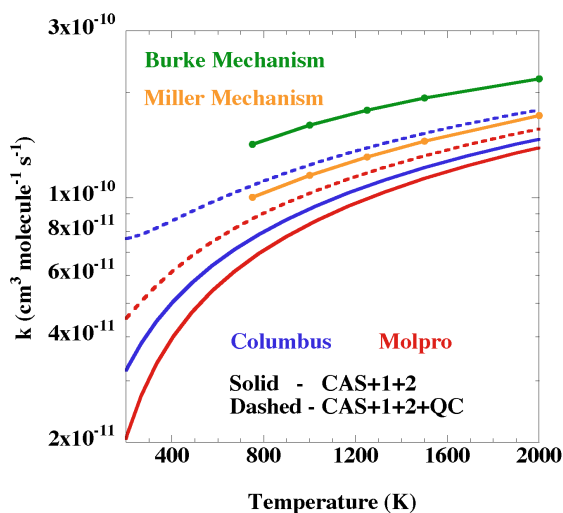


Figure 3

in this region. To determine the effect of this difference on the kinetics, we first evaluated identical, 9x30x21 grids with both programs and fit these grids using three-dimensional splines. Klippenstein then used these surfaces in Variable Reaction Coordinate Transition State Theory (VRCTST) calculations to determine the high-pressure limit rate of reaction. The results are shown in Figure 3 along with the rates employed in two recently reported H<sub>2</sub>/O<sub>2</sub> mechanisms by Miller<sup>1,3</sup> and Burke<sup>4</sup>. The rates obtained using the COLUMBUS energies are shown in blue and those from the MOLPRO energies in red. Because the COLUMBUS potential surfaces are more attractive, they yield higher rates

order excitations increases the differences at all temperatures. Two possible causes for the differences between MOLPRO and COLUMBUS are MOLPRO's use of an internal contraction scheme and its use of an interacting space restriction. The COLUMBUS calculations used neither. We have repeated the COLUMBUS calculations including an interacting space restriction and find the differences between the surfaces with and without the interacting space restriction are very small (less than 0.1 kcal/mol in the bottleneck region). This suggests then that the differences we observe are due to the internal contraction scheme used in MOLPRO.

**Novel Water Elimination Pathway for  $\alpha$ -hydroxy, QOOH Species:** The formation and subsequent decomposition of QOOH species is of key importance in low temperature combustion. The QOOH species are formed when an alkyl-peroxy radical undergoes an intramolecular hydrogen abstraction. In a collaborative effort with Klippenstein, Taatjes and Zador, we have discovered a novel, low energy, water elimination pathway for QOOH radicals in which there is an OH group attached to the radical site. The simplest example is the decomposition of 2-hydroperoxy-1-hydroxy-1-ethyl formed in the reaction of  $O_2$  with the  $\beta$ -hydroxy-ethyl radical. In this case as the OO bond starts to break the hydroxy hydrogen transfers to the departing OH leading to the formation of water and the  $OHCCH_2O$  radical. Accurate treatment of the transition state region for this reaction is found to be quite challenging owing to a strong interaction between two electronic states of very different character (one biradical-like and the other zwitterionic).

### Future Plans

We plan to continue our comparisons of MOLRO and COLUMBUS MRCI calculations with studies of a number of other small reactive systems such as  $H+CO$  and  $OH+H_2$ . We also plan to continue our studies of roaming radical pathways in hydrocarbons, ethers and peroxides.

**Acknowledgement:** This work was performed under the auspices of the Office of Basic Energy Sciences, Division of Chemical Sciences, Geosciences and Biosciences, U.S. Department of Energy, under Contract DE-AC02-06CH11357.

### References:

- (1) S. R. Sellevag, Y. Georgievskii, J. A. Miller, *J. Phys. Chem. A* **112**, 5085 (2009)
- (2) L. B. Harding, J. Troe, V. G. Ushakov, *Phys. Chem. Chem. Phys.* **2**, 631 (2000)
- (3) J. A. Miller (private communication)
- (4) M. P. Burke, M. Chaos, Y. G. Yu, F. L. Dryer, S. J. Klippenstein, *Int. J. Chem. Kinetics* **44**, 444 (2012)

### PUBLICATIONS (2011 - Present):

#### Uncertainty Driven Theoretical Kinetics Studies for $CH_3OH$ Ignition: $HO_2+CH_3OH$ and $O_2+CH_3OH$

S. J. Klippenstein, L. B. Harding, M. J. Davis, A. S. Tomlin, R. T. Skodje  
33<sup>rd</sup> Symposium (International) on Combustion, **33**, 351-357 (2011)

### **The Role of NNH in NO Formation and Control**

S. J. Klippenstein, L. B. Harding, P. Glarborg, J. A. Miller  
Combustion and Flame, **158**, 774-489 (2011)

### **Roaming Radicals in the Thermal Decomposition of Dimethyl Ether: Experiment and Theory**

R. Sivaramakrishnan, J. V. Michael, A. F. Wagner, R. Dawes, A. W. Jasper, L. B. Harding, Y. Georgievskii, S. J. Klippenstein, Combustion and Flame, **158**, 618-632 (2011)

### **Shock Tube and Theoretical Studies on the Thermal Decomposition of Propane: Evidence for a Roaming Radical Channel**

R. Sivaramakrishnan, M.-C. Su, J. V. Michael, L. B. Harding, S. J. Klippenstein  
J. Phys. Chem. A **115**, 3366-3379 (2011)

### **Near-threshold H/D Exchange in CD<sub>3</sub>CHO Photodissociation**

B. R. Heazlewood, A. T. Maccarone, D. U. Andrews, D. L. Osborn, L. B. Harding, S. J. Klippenstein, M. J. T. Jordan, and S. H. Kable, Nature Chemistry **3**, 443-448 (2011)

### **A Statistical Theory for the Kinetics and Dynamics of Roaming Reactions**

S. J. Klippenstein, Y. Georgievskii and L. B. Harding  
J. Phys. Chem. A **115**, 14370-14381(2011)

### **Bi-fidelity Fitting and Optimization**

R. L. Miller, L. B. Harding, M. J. Davis, and S. K. Gray, J. Chem. Phys. **136**, 074102(2012)

### **Theoretical Determination of the Rate Coefficient for the HO<sub>2</sub>+HO<sub>2</sub>→ H<sub>2</sub>O<sub>2</sub>+O<sub>2</sub> Reaction: Adiabatic Treatment of Anharmonic Torsional Effects**

D. D. Y. Zhou, K. Han, P. Zhang, L. B. Harding, M. J. Davis and R. T. Skodje  
J. Phys. Chem. A **116**, 2089-2100 (2012)

### **Shock Tube Explorations of Roaming Radical Mechanisms: The Decomposition of Isobutane and Neopentane**

R. Sivaramakrishnan, J. V. Michael, L. B. Harding and S. J. Klippenstein  
J. Phys. Chem. A **116**, 5981-5989 (2012)

### **Separability of Tight and Roaming Pathways for Molecular Decomposition**

L. B. Harding, S. J. Klippenstein, and A. W. Jasper  
J. Phys. Chem. A **116**, 6967-6982 (2012)

### **A Quantitative Explanation for the Apparent Anomalous Temperature Dependence of OH + HO<sub>2</sub> → H<sub>2</sub>O + O<sub>2</sub> through Multi-Scale Modeling**

M. P. Burke, S. J. Klippenstein, L. B. Harding, Proc. Comb. Inst. **34**, 547-555 (2013)

### **Unconventional Peroxy Chemistry in Alcohol Oxidation: The Water Elimination Pathway**

O. Welz, S. J. Klippenstein, L. B. Harding, C. A. Taatjes, J. Zador  
J. Phys. Chem. Letters **4**, 350-354 (2013)

# CHEMICAL ACCURACY FROM AB INITIO MOLECULAR ORBITAL CALCULATIONS

Martin Head-Gordon

Department of Chemistry, University of California, Berkeley, and,  
Chemical Sciences Division, Lawrence Berkeley National Laboratory,  
Berkeley, CA 94720.  
mhg@cchem.berkeley.edu

## 1. Scope of Project.

Short-lived reactive radicals and intermediate reaction complexes play central roles in combustion, interstellar and atmospheric chemistry. Due to their transient nature, such molecules are challenging to study experimentally, and our knowledge of their structure, properties and reactivity is consequently quite limited. To expand this knowledge, we develop new theoretical methods for reliable computer-based prediction of the properties of such species. We apply our methods, as well as existing theoretical approaches, to study prototype radical reactions, often in collaboration with experimental efforts. These studies help to deepen understanding of the role of reactive intermediates in diverse areas of chemistry. They also sometimes reveal frontiers where new theoretical developments are needed in order to permit better calculations in the future.

## 2. Summary of Recent Major Accomplishments.

### 2.1 *Improved density functionals.*

Self-interaction errors in density functional theory can be as large as 50 kcal/mol for as simple a molecule as  $\text{H}_2^+$ , treated by the widely used B3LYP functional. We have been interested in the use of range-separation to reduce self-interaction, and have developed the  $\omega$ B97 family of functionals, that yield a reduction of roughly 2/3 in self-interaction errors, relative to e.g B3LYP. A recent comprehensive set of benchmarks has further established the good performance of these functionals for both ground and excited state properties that involve significant self-interaction effects [7], as well as cation radicals [4], and water clusters [15]. Like all density functionals, there are still significant limitations and thus potentially significant scope for further improvements. Present work is trying to assess the extent of potential improvements.

### 2.2 *Approximate Brueckner Orbital Methods.*

It is most common to perform correlation treatments such as second order Moller-Plesset (MP2) theory or coupled cluster theory using reference mean field orbitals from e.g. Hartree-Fock calculations. However, in a well-defined sense, the best orbitals are those that minimize the energy in absence of single excitations, which are termed Brueckner orbitals. For high levels of correlation (e.g. CCSDT), it doesn't matter greatly whether or not single excitations are included versus finding the Brueckner orbitals. But for more approximate methods like MP2, it can make a very large difference. This is illustrated by our recent study of the soliton defect in polyene radicals [11], where use of Brueckner orbitals is essential to obtain realistic estimates of the size of the radical defect, as well

reasonable values of  $\langle S^2 \rangle$ . For example, for the ground doublet state of C<sub>41</sub>H<sub>43</sub>,  $\langle S^2 \rangle = 6.8$  for MP2, versus 0.78 for a Brueckner orbital based MP2 method (the O2 approach), versus the exact value of 0.75. The same effect also turns out to be important in fullerenes such as C<sub>36</sub> and C<sub>60</sub> [8].

### 2.3 *Intermolecular interactions.*

It is well known that second order Moller-Plesset (MP2) theory in finite basis sets typically overestimates intermolecular binding energies due to basis set superposition error (BSSE). Even at the complete basis set (CBS) limit, MP2 theory often overestimates interactions because of known deficiencies in the associated C<sub>6</sub> coefficients. Motivated by these facts, we have explored the effect of attenuating the Coulomb operator in MP2 theory, using a single parameter for the attenuation length scale. In the small aug-cc-pVDZ basis, with the attenuation parameter set to 1.05Å, errors in calculated intermolecular interactions can be reduced by about a factor of 5 (!) relative to conventional MP2/aug-cc-pVDZ [17]. For many intermolecular interactions, particularly dispersion-sensitive systems, the attenuated aug-cc-pVDZ results are better than MP2/CBS [17], as well as being hundreds of times faster. This method appears very promising for inter and intra-molecular interactions in large systems where benchmark quality calculations are not feasible. Additional recent work on intermolecular interactions includes obtaining benchmark results for sulfate-water interactions [14], and efforts to improve methods for energy decomposition analysis [10,19].

### 2.4 *Valence bond vs coupled cluster for strong electron correlations.*

Spin-coupled valence bond (SCVB) theory takes a simple product of  $n$  non-orthogonal spatial orbitals and spin-couples those orbitals together in all possible ways (the number grows exponentially with  $n$ ). We have shown that it is possible to exactly reproduce the SCVB limit for fully broken bonds with only quadratic degrees of freedom (provided that the final state is describable by spin-projected unrestricted Hartree-Fock). Taking this limit as a model defines what we call the coupled cluster valence bond (CCVB) method [6]. CCVB is very well-suited for describing strong spin correlations such as those associated with the antiferromagnetic coupling of high spin electrons at two different centers. Bond dissociations and some types of metal complexes are in this class. Lack of ionic excitations in CCVB leads to symmetry-breaking in cases such as resonance-stabilized molecules [6].

To address this problem, we have developed interesting and quite exciting new theory [13] that re-expresses the CCVB model in molecular orbital terms, as a form of coupled cluster doubles theory. However, CCVB expressed as a CCD model has a very interesting difference relative to conventional coupled cluster theory: the doubles operator is complex. Its real part involves the singlet coupling between two pairs of electrons, whilst the imaginary part contains quintet coupling between two pairs of electrons. The latter affects the quadruples, and allows correct separation of two electron pairs within a spin-restricted theory. This suggests a generalization of CCVB as a coupled cluster theory, CCVBSD, that recovers all the usual orbital invariances and ionic excitations of CCSD, whilst retaining the beautiful ability of CCVB to correctly separate multiple electron pairs within a spin-restricted active space.

## 2.5 *New algorithms.*

A variety of interesting novel algorithms for electronic structure calculations have been explored. First, we have reported possibly the most efficient implementation to date of the problem of computing the Cholesky decomposition and inversion associated with the overlap matrix [1]. This is essential for large-scale DFT calculations. Second, in collaboration with Bill Miller, we have explored a very interesting operator identity that permits the two-electron integrals of quantum chemistry to be replaced by products of overlap and kinetic energy integrals [2].

## 2.6 *Fundamental studies of chemical bonding.*

In addition to studies of hydrocarbon polyene radicals [11] to explore the soliton defect, we have also explored electron correlations in the fullerenes, comparing C<sub>36</sub> and C<sub>60</sub> [8]. Other applications have recently been completed, including the tetraradicaloid states associated with the singlet fission process in polycyclic aromatic hydrocarbons such as pentacene [12], and the association process for C<sub>2</sub> hydrocarbons and their cations [18].

## 3. **Summary of Research Plans.**

- Formulation of improved density functionals: There is a clear need for improvements to the functionals we've previously developed, through improving the treatment of long-range correlations associated with van der Waals interactions, to replace simple damped dispersion potentials.
- Intermolecular interactions involving radicals: We are interested in extending theory previously developed for closed shell systems to enable the description of intermolecular interactions involving radicals. We hope this will be of both formal and practical value.
- Extensions of attenuated electron correlation methods: The very encouraging results reported in Sec. 2.3 above suggest that it is worthwhile to explore the effect of attenuation in larger basis sets, and, possibly, for double hybrid density functionals.
- New studies of the properties of reactive radicals and radical reactions will be pursued as opportunities arise. A joint study on the photoionization of glycerol with the groups of Musa Ahmed and Steve Leone is nearly completed.

## 4. **Publications from DOE Sponsored Work, 2011-present.**

- [1] "Fast Sparse Cholesky Decomposition and Inversion using Nested Dissection Matrix Reordering", K. Brandhorst and M. Head-Gordon, *J. Chem. Theor. Comput.* 7, 351-368 (2011).
- [2] "A new fitting metric for resolution of the identity second-order Møller-Plesset perturbation theory", D.S. Lambrecht, K. Brandhorst, W.H. Miller, and M. Head-Gordon *J. Phys. Chem. A* 115, 2794-2801 (2011).
- [3] "The formulation and performance of a perturbative correction to the Perfect Quadruples model", J.A. Parkhill, J. Azar, and M. Head-Gordon, *J. Chem. Phys.* 134, 154112 (2011).
- [4] "Ground Electronic State of Peptide Cation Radicals: A Delocalized Unpaired Electron?" A.I. Gilson, G. van der Rest, J. Chamot-Rooke, W. Kurlancheek, M. Head-Gordon, D. Jacquemin, and G. Frison, *J. Phys. Chem. Lett.* 2, 1426-1431 (2011).
- [5] "Approximate spin-projected broken symmetry energies from optimized orbitals that are unrestricted in active pairs", A.M. Mak, K.V. Lawler, and M. Head-Gordon, *Chem. Phys. Lett.* 515, 173-178 (2011).

- [6] “Post-modern valence bond theory for strongly correlated electron spins”, D.W. Small and M. Head-Gordon, *Phys. Chem. Chem. Phys.* 13, 19285-19297 (2011).
- [7] “How well do post-GGA density functionals perform on molecular problems where self-interaction effects are significant?” N. Mardirossian, J.A. Parkhill and M. Head-Gordon, *Phys. Chem. Chem. Phys.* 13, 19325-19337 (2011).
- [8] “On the Nature of Correlation in  $C_{60}$ ”, D. Stück, T. Baker, P. Zimmerman, W. Kurlancheek, and M. Head-Gordon, *J. Chem. Phys.* 135, 194306 (2011) (5 pages).
- [9] “Mechanism for Singlet Fission in Pentacene and Tetracene: From Single Exciton to Two Triplets”, P.M. Zimmerman, F. Bell, D. Casanova, and M. Head-Gordon, *J. Am. Chem. Soc.* 133, 19944-19952 (2011).
- [10] “An energy decomposition analysis for intermolecular interactions from an absolutely localized molecular orbital reference at the coupled-cluster singles and doubles level”, R.J. Azar and M. Head-Gordon, *J. Chem. Phys.* **136**, 024103 (2012)
- [11] “Exploring the competition between localization and delocalization of the neutral soliton defect in polyenyl chains with the orbital optimized second order opposite spin method”, W. Kurlancheek, R. Lochan, K.V. Lawler, and M. Head-Gordon, *J. Chem. Phys.* 136, 054113 (2012) (11 pages).
- [12] “A computational and experimental study of the mechanism of hydrogen generation from water by a molecular molybdenum-oxo pentapyridine catalyst”, E.J. Sundstrom, X. Yang, V.S. Thoi, H.I. Karunadasa, C.J. Chang, J.R. Long and M. Head-Gordon, *J. Am. Chem. Soc.* 134, 5233-5242 (2012).
- [13] “A fusion of the closed-shell coupled cluster singles and doubles method and valence-bond theory for bond breaking”, D.W. Small and M. Head-Gordon, *J. Chem. Phys.* 137, 114103 (2012) (13 pages).
- [14] “Refined energetic ordering for sulfate-water ( $n=3-6$ ) clusters using high-level electronic structure calculations”, D.S. Lambrecht, L. McCaslin, S.S. Xantheas, E. Epifanovsky, and M. Head-Gordon, *Mol. Phys.* 110, 2513-2521 (2012).
- [15] “Examination of the Hydrogen-Bonding Networks in Small Water Clusters ( $n=2-5,13,17$ ) using Absolutely Localized Molecular Orbital Energy Decomposition Analysis”, Erika A. Cobar, Paul R. Horn, R.G. Bergman, and M. Head-Gordon, *Phys. Chem. Chem. Phys.* 14, 15328-15339 (2012).
- [16] “Restricted Active Space Spin-Flip Configuration Interaction: Theory and Examples for Multiple Spin Flips with Odd Numbers of Electrons”, P.M. Zimmerman, F. Bell, M. Goldey, A.T. Bell, and M. Head-Gordon, *J. Chem. Phys.* 137, 164110 (2012) (11 pages).
- [17] “Attenuating away the errors in inter and intra-molecular interactions from second order Møller-Plesset calculations in the small aug-cc-pVDZ basis set”, Matt Goldey and M. Head-Gordon, *J. Phys. Chem. Lett.* 3, 3592–3598 (2012).
- [18] “Association Mechanisms of Unsaturated  $C_2$  Hydrocarbons With Their Cations: Acetylene and Ethylene”, P.P. Bera, M. Head-Gordon, and T.J. Lee, *Phys. Chem. Chem. Phys.* 15, 2012-2023 (2013).
- [19] “Useful lower limits to polarization contributions to intermolecular interactions using a minimal basis of localized orthogonal orbitals: Theory and analysis of the water dimer”, R. Julian Azar, Paul R. Horn, Eric J. Sundstrom, and M. Head-Gordon, *J. Chem. Phys.* 134, 084102 (2013).

# Laser Studies of Combustion Chemistry

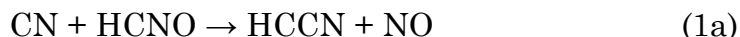
John F. Hershberger

Department of Chemistry and Biochemistry  
North Dakota State University  
NDSU Dept. 2735, PO Box 6050  
Fargo, ND 58108-6050  
john.hershberger@ndsu.edu

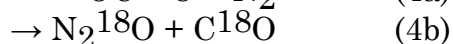
Time-resolved infrared diode laser absorption and laser-induced fluorescence spectroscopy are used in our laboratory to study the kinetics and product channel dynamics of chemical reactions of importance in the gas-phase combustion chemistry of nitrogen-containing species. This program is aimed at improving the kinetic database of reactions crucial to modeling of combustion processes, with emphasis on NO<sub>x</sub> chemistry. When feasible, we perform quantitative measurement of both total rate constants and product branching ratios.

## 1) CN + HCNO Reaction.

Several years previously, we had studied this reaction as part of a survey of radical-molecule kinetics involving HCNO, the fulminic acid molecule.<sup>1</sup> Out of a total of nine exothermic possible channels, the two most likely are:



In the earlier study, we had measured total rate constants, finding this to be a fast reaction. We proposed HCCN + NO to be the dominate product channel, based on experimental measurements of <sup>18</sup>OC<sup>18</sup>O and OC<sup>18</sup>O formed by secondary chemistry when N<sup>18</sup>O reagents were included. The idea was that NCO products from (1b) would lead to singly labeled OC<sup>18</sup>O, while HCCN from (1a) would lead to doubly labeled <sup>18</sup>OC<sup>18</sup>O:



Our observation of much higher <sup>18</sup>OC<sup>18</sup>O yield than OC<sup>18</sup>O yield led us to conclude that HCCN + NO (channel 1a), was the dominant product channel.

A subsequent ab initio study of Pang et al, however, found a somewhat lower barrier to HCN + NCO products, and suggested that channel (1b) dominates, and that our measurement was perhaps contaminated by secondary chemistry.<sup>2</sup> We have therefore re-investigated this reaction. Using CCSD(T) ab initio methods, we do indeed confirm the barrier height calculations of Pang et al at the exact basis set they used. We find, however, that the relative barrier heights to the two channels are quite close and sensitive to the specific theory method/basis set used. We also note that if the energetics are close, entropic factors favor channel (1a). It appears that this system may be too close to call by common single reference methods, and that a multireference treatment may be required to characterize the potential energy surface to sufficient accuracy.

In addition, we have performed several new experiments. Firstly, we have recently acquired an infrared laser diode in the 3250 cm<sup>-1</sup> region, which allows us to probe directly for HCN. We find only a small background signal (due to HCNO photodissociation), and estimate from this result that  $\phi_{1b} < 0.07$ . Secondly, we have measured the yield of NO as a function of added <sup>15</sup>N<sup>18</sup>O reagent (which removes NCO without affecting our NO yield measurement). We find that the NO yield is independent of added <sup>15</sup>N<sup>18</sup>O, which implies that the NO originated from the title reaction, and not from secondary chemistry involving NCO, suggesting that channel (1b) is insignificant. Thirdly, we have directly detected the HCCN radical in this reaction, using spectral data of Curl et al.<sup>3</sup> Although we cannot quantify HCCN yields from this signal, this clearly indicates the presence of channel (1a). Finally, we have detected HC<sup>15</sup>N when the experiment is performed with added <sup>15</sup>N<sup>18</sup>O reagent. We attribute this to



In summary, we have obtained multiple independent pieces of new experimental evidence, all of which confirm our earlier conclusion that HCCN + NO is the dominant product channel.

## 1) C<sub>2</sub>H + NO<sub>x</sub> Reactions

We have recently begun our study of reactions of C<sub>2</sub>H radicals, using CF<sub>3</sub>CCH as a radical precursor. We believe this is a cleaner precursor than C<sub>2</sub>H<sub>2</sub>, which we tried some years ago but ran into difficulties with secondary chemistry. Total rate constants of the C<sub>2</sub>H + NO reaction have been measured by other workers.<sup>4</sup> Possible product channels include:



Previous ab initio work has indicated that channel (6b) dominates.<sup>5</sup>

We have successfully detected CO, HCN, and CN products as well as HNO secondary products from the HCO+NO reaction. Our results confirm the ab initio predictions that HCN+CO is the dominant product channel, but we have several pieces of evidence that HCO + CN is a significant (~20%) minor channel, previously unreported in the literature. Firstly, we detect a 20% excess of CO formation over HCN formation, suggesting additional CO is formed by



We have also, by direct detection, quantified the HNO yield from (7) and the CN yield from (6a), with equivalent results.

Ab initio calculations confirm previous calculations that show that (6b) is the only accessible channel on the singlet potential energy surface, but we note a triplet potential energy surface correlates to both reactants and product channel (6a). CCSD(T) calculations on the triplet surface show only small barriers to (6a) (the exact barrier heights are quite basis set dependent). The calculations therefore suggest that channel (6a) is at least plausible on the triple surface.

Future plans include investigation of the C<sub>2</sub>H + NO<sub>2</sub> reaction.

## References

1. W. Feng and J.F. Hershberger, *J. Phys. Chem A* 110, 12184 (2006).
2. J.-L. Pang, H.-B. Xie, S.-W. Zhang, Y.-H. Ding, and A.-Q. Tang, *J. Phys. Chem. A* 112, 5251 (2008).
3. C.L. Morter, S.K. Farhat, and R.F. Curl, *Chem. Phys. Lett.*, 207, 153 (1993).
4. J. Peeters, H. Van Look, and B. Ceusters, *J. Phys. Chem.* 100, 15124 (1996).
5. D. Sengupta, J. Peeters, and M.T. Nguyen, *Chem. Phys. Lett.* 283, 91 (1998).

## Publications acknowledging DOE support (2010-present)

1. "Infrared Diode Laser Study of the Kinetics of the NCCO + O<sub>2</sub> Reaction", W. Feng and J.F. Hershberger, *Chem. Phys. Lett.* 488, 140 (2010).
2. "Kinetics and Mechanism of the NCCO + NO Reaction", W. Feng and J.F. Hershberger, *J. Phys. Chem. A* 114, 6843 (2010).
3. "Kinetics of the CN + CS<sub>2</sub> and CN + SO<sub>2</sub> Reactions", W. Feng and J.F. Hershberger, *J. Phys. Chem. A* 115, 286 (2011).
4. "Kinetics of the NCCO + NO<sub>2</sub> Reaction", W. Feng and J.F. Hershberger, *J. Phys. Chem. A* 115, 12173 (2011).
5. "Kinetics of the O + ICN Reaction", W. Feng and J.F. Hershberger, *J. Phys. Chem. A* 116, 4817 (2012).
6. "Product Channels of the CN + HCNO Reaction", W. Feng and J.F. Hershberger, *J. Phys. Chem. A* 116, 10285 (2012).
7. "Experimental and Theoretical Study of the Product Channels of the C<sub>2</sub>H + NO Reaction", W. Feng and J.F. Hershberger, *J. Phys. Chem. A*, submitted.

# Breakthrough Design and Implementation of Electronic and Vibrational Many-Body Theories

So Hirata (principal investigator: DE-FG02-11ER16211; formerly DE-FG02-04ER15621)  
Department of Chemistry, University of Illinois at Urbana-Champaign,  
600 South Mathews Avenue, Urbana, IL 61801  
[sohirata@illinois.edu](mailto:sohirata@illinois.edu)

## Program Scope

Predictive chemical computing requires hierarchical many-body methods of increasing accuracy for both electrons and vibrations. Such hierarchies are established, at least conceptually, as configuration-interaction (CI), many-body perturbation (MP), and coupled-cluster (CC) methods, which all converge at the exact limit with increasing rank of a hierarchical series. These methods can generate results of which the convergence with respect to various parameters of calculations can be demonstrated and which can thus be predictive in the absence of experimental information.

The wide use of the hierarchical electronic and vibrational many-body methods has, however, been hindered (1) by the immense cost of *executing* the calculations with these methods and, furthermore, the nonphysical rapid increase of the cost with increasing molecular size, (2) by the complexity and cost of *developing* some of the high-rank members of these methods, and (3) by the slow convergence of electronic energies and wave functions with respect to one-electron basis set sizes, which further drives up the cost of execution. For applications to large molecules and solids, the additional difficulties arise by the lack of (4) size consistency in some methods (whose energies and other observables scale non-physically with size) and of (5) efficient methods that work for strong correlation.

The overarching goal of our research is to address all three difficulties for electrons and vibrations in small molecules in the gas phase and all five for solids and molecules in condensed phases. We have eradicated the second difficulty (the complexity of equations and cost of implementations) for electrons by developing a computerized symbolic algebra system that completely automates the mathematical derivations of electron-correlation methods and their implementation. For vibrations, an assortment of vibrational many-body methods has been implemented in the general-order algorithm that allows us to include anharmonicity and vibrational mode-mode couplings to any desired extent. We have also addressed the third difficulty (the slow convergence with respect to basis set) by departing from the conventional Gaussian basis sets and introduce a new hierarchy of converging electron-correlation methods with completely flexible but rational (e.g., satisfying asymptotic decay and cusp conditions) basis functions such as numerical basis functions on interlocking multicenter quadrature grids and explicit  $r_{12}$  (inter-electronic distance) dependent basis functions.

Our current research focus is to address the first (the cost of execution) and fourth (the size consistency) difficulties to make the hierarchical electronic and vibrational methods applicable to solids.

## Recent Progress

We have made important advances to the fundamental theories and algorithms of electronic and vibrational many-body methods of molecules and solids. Some of these are published, while others are still in various stages of investigation. We have obtained an easily understandable and pedagogical, if not completely rigorous, proof of extensivity of energy in metallic and non-metallic crystals by analyzing the distance decay of chemical interactions. On this basis, we have shown that the conventional definitions of the Fock and two-electron integrals need to be revised. This does not alter the Hartree–Fock (HF) orbitals, energies, electron-correlation energies, or excitation energies, but it does alter the orbital energies and indeed accelerate the convergence of their lattice sums. We have also proposed a number of theorems pertaining to the size consistency of electronic and vibrational methods. We have extended diagrammatic size-extensive vibrational self-consistent field (XVSCF) method to anharmonic geometry corrections.

Since the 32<sup>nd</sup> Annual Combustion Research Meeting, 6 peer-reviewed papers<sup>5-10</sup> and one book chapter<sup>1</sup> in *Annual Reviews of Physical Chemistry* have been published and two more papers<sup>20,21</sup> are currently under review. In total, 21 publications<sup>1-21</sup> (including two submitted) have resulted from this grant in 2010–2012. During the same period, the PI was an invited speaker at 14 international and domestic conferences and gave 11 invited talks at universities and national laboratories including the Moskowitz Memorial Lecture at The University of Minnesota. The PI received a Scialog Award from the Research Corporation for Science Advancement. The PI served as a member of the editorial boards of *Physical Chemistry Chemical Physics*, *Theoretical Chemistry Accounts*, *The Journal of Chemical Physics*, and *International Journal of Quantum Chemistry*. The PI was a guest editor of the 50<sup>th</sup> Year Anniversary Issue (with the regular editors, Christopher Cramer and Donald Truhlar as well as five other guest editors) of *Theoretical Chemistry Accounts* and of the Special Issue (with Gregory Beran) on Fragment and Local Orbital Methods in Electronic Structure Theory in *Physical Chemistry Chemical Physics*.

**Thermodynamic limit of the energy density in a crystal** (Hirata and Ohnishi).<sup>1,5,10</sup> A thermodynamic observable of a chemical system is said to be either extensive or intensive. Extensive quantities include energy ( $E$ ), entropy, mass, and so forth. They increase asymptotically linearly as we increase the volume ( $V$ ) of the system while maintaining the particle density and composition unchanged. Intensive quantities such as temperature, chemical potential, and pressure are asymptotically independent of  $V$ . The assumption that  $E$  is extensive or, equivalently,  $E/V$  converges at a finite value in the thermodynamic (infinite- $V$ ) limit is one of the foundations of chemical thermodynamics. Yet, proving this (“the stability of matter of the second kind”) mathematically turns out to be extremely difficult, taking the finest mathematicians forty years to accomplish. The proof for electrically neutral matter consisting of mobile electrons and nuclei was obtained by Lebowitz and Lieb. The proof for electrically neutral perfect crystals was presented by Fefferman. Only in 2009 was the proof completed by Hainzl *et al.*, who reported those for perfect crystals and crystals with defects. We have presented a pedagogical, semi-rigorous proof of the existence of the thermodynamic limit of  $E/V$  in an electrically neutral perfect crystal, which is an alternative to that of Fefferman’s. Our shorter, simpler proof consists in showing the existence of thermodynamic limits for individual components of exact  $E/V$  in the spirit of Harris, of Lieb and Simon, of Catto *et al.*, and of Pisani *et al.*, who considered the Hartree or HF energy components. Our work is concerned with the whole, exact energy of an electrically neutral metallic or nonmetallic crystal. We have also addressed the issue of divergences of correlation energies in metals obtained by a perturbation theory in relation to the validity of this proof for such systems.

**Charge-consistent redefinition of Fock and two-electron integrals** (Ohnishi and Hirata).<sup>6</sup> The Fock and two-electron integrals as defined and used by chemists involve the lattice sums of electron-electron repulsion that are not compensated by the corresponding lattice sums of nucleus-nucleus repulsion and electron-nucleus attraction. Consequently, some of them diverge in the thermodynamic limit. Solid-state physicists’ definitions of these quantities are different, carefully balancing the repulsive and attractive interactions. We thus redefine the Fock and two-electron integrals such that they contain the lattice sums of the electrostatic interactions between the net neutral charge densities by subtracting appropriate portion of the nuclear charge density in the unit cell from the electronic orbital pair density. These charge-consistent definitions are necessary to maintain the consistent size dependence of these integrals. We show that (1) the diagonal Fock integrals in the new definition converge more rapidly than the conventional Fock integrals as the former contain no charge-multipole interactions (see **Figure**); (2) the new and conventional definitions of the Fock integrals in the canonical HF orbital basis differ only in the diagonal elements merely by a constant and, hence,

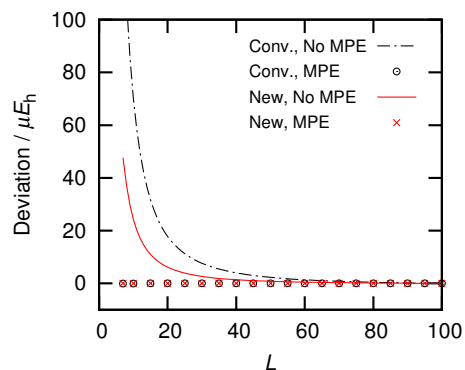


**Fig.** Convergence of orbital energies as a function of the number ( $L$ ) of unit cells included in the lattice sums. MPE stands for multipole expansion corrections.

the HF energy, orbitals, correlation energies, etc. are not altered by the redefinition; and (3) the multipole expansion (MPE) corrections to the lattice sums of the charge-consistent Fock integrals are derived and shown to be simpler than the conventional counterparts because some of the multipole–multipole interactions are no longer there in the charge-consistent definition of the Fock integrals.

**Size-consistency theorems** (Hirata).<sup>1,10</sup> On the basis of the above analysis of extensivity, I have derived some theorems pertaining to size consistency of electronic and vibrational methods. For example, the *normalization theorem* states that the excitation amplitudes of an extensive operator are subject to intermediate normalization and scale as  $V^{1-n/2}$  where  $V$  is the volume and  $n$  is the number of edges of the corresponding vertex, whereas the amplitudes of an intensive operator are normalized and scale as  $V^{1/2-n/2}$ . The *intensive diagram theorem* (which complements the extensive diagram theorem of Goldstone) states that the equations defining an intensive quantity of a size-consistent method consist of connected diagrams with two intensive vertexes. The equations that determine the intensive amplitudes do not need to be connected or linked insofar as they have a prescribed number of intensive vertexes. I have also introduced the *extensive-intensive consistency theorem* which characterizes the methods that are size consistent for extensive and intensive quantities simultaneously.

**Size-extensive vibrational self-consistent field method with anharmonic geometry corrections** (Hermes, Keçeli, and Hirata).<sup>21</sup> In the XVSCF method introduced earlier [M. Keçeli and S. Hirata, *J. Chem. Phys.* **135**, 134108 (2011)] in support of this grant, only a small subset of even-order force constants that can form connected diagrams has been used to compute extensive total energies and intensive transition frequencies. The mean-field potentials of XVSCF formed with these force constants have been shown to be effectively harmonic, in accordance with Makri’s theorem, making basis functions, quadrature, or matrix diagonalization in the conventional VSCF method unnecessary. We introduce two size-consistent VSCF methods, XVSCF( $n$ ) and XVSCF[ $n$ ], for vibrationally averaged geometries in addition to energies and frequencies including anharmonic effects caused by up to the  $n$ th-order force constants. The methods are based on our observations that a small number of odd-order force constants of certain types can form open, connected diagrams isomorphic to the diagram of the mean-field potential gradients and that these nonzero gradients shift the potential minima by intensive amounts, which are interpreted as anharmonic geometry corrections. XVSCF( $n$ ) evaluates these mean-field gradients and force constants at the equilibrium geometry and estimates this shift accurately, but approximately, neglecting the coupling between these two quantities. XVSCF[ $n$ ] solves the coupled equations for geometry corrections and frequencies with an iterative algorithm, giving results that should be identical to those of VSCF when applied to an infinite system. We present the diagrammatic and algebraic definitions, algorithms, and initial implementations as well as numerical results of these two methods. The results show that XVSCF( $n$ ) and XVSCF[ $n$ ] reproduce the vibrationally averaged geometries of VSCF for naphthalene and anthracene in their ground and excited vibrational states accurately at fractions of the computational cost.

## Future Plans

For the electronic structure theory, we will explore the following ideas: (1) the finite-temperature extension of the second- and higher-order MP for molecules and polymers; (2) the use of Monte Carlo integrations with the Metropolis sampling scheme for second- and higher-order MP for molecules and polymers; (3) the use of Wannier functions for MP2 and CCSD for polymers.

For the vibrational structure theory, we pursue (3) the extension of XVSCF( $n$ ) and XVSCF[ $n$ ] for one-dimensional solids and the calculation of anharmonic phonon dispersion curves of polymers; (4) the vibrational Dyson equation at the second order perturbation level for molecules and one-dimensional solids; (5) the anharmonic vibrational theory for thermal expansions.

## Publications of DOE Sponsored Research (2010–Present)

### Book chapters

1. S. Hirata, M. Keçeli, Y.-Y. Ohnishi, O. Sode, and K. Yagi, "Extensivity of energy and size-consistent electronic and vibrational structure methods for crystals," *Annual Reviews of Physical Chemistry* **63**, 131-153 (2012).
2. S. Hirata, O. Sode, M. Keçeli, and T. Shimazaki, "Electron correlation in solids: Delocalized and localized orbital approaches," a chapter in *Accurate Condensed-Phase Quantum Chemistry* edited by F. Manby, p.129–161 (CRC Press, Boca Raton, 2010).
3. S. Hirata, T. Shiozaki, E. F. Valeev, and M. Nooijen, "Eclectic electron-correlation methods," a chapter in *Recent Progress in Coupled-Cluster Methods: Theory and Application* edited by P. Carsky, J. Paldus, and J. Pittner, p.191–217 (Springer, Dordrecht, 2010).
4. S. Hirata, P.-D. Fan, M. Head-Gordon, M. Kamiya, M. Keçeli, T. J. Lee, T. Shiozaki, J. Szczepanski, M. Vala, E. F. Valeev, and K. Yagi, "Computational interstellar chemistry," a chapter in *Recent Advances in Spectroscopy: Astrophysical, Theoretical and Experimental Perspective* edited by R. K. Chaudhuri, R. K. Mekkaden, M. V. Raveendran, A. S. Narayanan, p.21–30 (Springer-Verlag, Berlin, 2010).

### Refereed articles (reviews, perspectives, and editorials in bold letters)

5. S. Hirata and Y.-Y. Ohnishi, *Physical Chemistry Chemical Physics* [Special Issue on "Fragment and Local Orbital Methods in Electronic Structure Theory"] (in press, 2012), "Thermodynamic limit of the energy density in a crystal."
6. Y.-Y. Ohnishi and S. Hirata, *Chemical Physics* [Debashis Mukherjee Special Issue] (in press, 2012), "Charge-consistent redefinition of Fock integrals."
7. **S. Hirata, *Theoretical Chemistry Accounts* [an introductory article in the 50th Anniversary Issue] **131**, 1071 (2012) (4 pages), "Electronic structure theory: Present and future challenges."**
8. M. Keçeli and S. Hirata, *The Journal of Chemical Physics* **135**, 134108 (2011) (11 pages), "Size-extensive vibrational self-consistent field method."
9. Y.-Y. Ohnishi and S. Hirata, *The Journal of Chemical Physics* **135**, 094108 (2011) (10 pages), "Hybrid coupled-cluster and perturbation method for extended systems of one-dimensional periodicity."
10. **S. Hirata, *Theoretical Chemistry Accounts* [an invited Feature Article] **129**, 727-746 (2011), "Thermodynamic limit and size-consistent design."**
11. D. G. Patel, Y.-Y. Ohnishi, Y. Yang, S.-H. Eom, R. T. Farley, K. R. Graham, J. Xue, S. Hirata, K. S. Schanze, and J. R. Reynolds, *Journal of Polymer Science Part B: Polymer Physics* **49** 557-565 (2011), "Conjugated polymers for pure UV light emission: Poly(*meta*-phenylenes)."
12. I. Grabowski, V. Lotrich, and S. Hirata, *Molecular Physics* [QTP Special Issue] **108**, 3313-3322 (2010), "Ab initio DFT--the seamless connection between WFT and DFT."
13. **S. Hirata, *Molecular Physics* [QTP Special Issue] **108**, 3113–3124 (2010), "Bridging quantum chemistry and solid-state physics."**
14. M. Keçeli and S. Hirata, *Physical Review B* **82**, 115107 (2010) (6 pages), "Fast coupled-cluster singles and doubles for extended systems: Application to the anharmonic vibrational frequencies of polyethylene in the  $\Gamma$  approximation."
15. O. Sode and S. Hirata, *The Journal of Physical Chemistry A* [Klaus Ruedenberg Special Issue] **114**, 8873–8877 (2010), "Second-order many-body perturbation study of solid hydrogen fluoride."
16. M. Keçeli, S. Hirata, and K. Yagi, *The Journal of Chemical Physics* **133**, 034110 (2010) (6 pages), "First-principles calculations on anharmonic vibrational frequencies of polyethylene and polyacetylene in the  $\Gamma$  approximation."
17. S. Hirata, M. Keçeli, and K. Yagi, *The Journal of Chemical Physics* **133**, 034109 (2010) (14 pages), "First-principles theories for anharmonic lattice vibrations."
18. Y.-Y. Ohnishi and S. Hirata, *The Journal of Chemical Physics* **133**, 034106 (2010) (8 pages), "Logarithm second-order many-body perturbation method for extended systems."
19. T. Shiozaki and S. Hirata, *The Journal of Chemical Physics (Communications)* **132**, 151101 (2010) (4 pages), "Explicitly correlated second-order Møller–Plesset perturbation method for extended systems."

### Submitted articles

20. R. D. Thomas, I. Kashperka, E. Vigren, W. Geppert, M. Hamberg, M. Larsson, M. af Ugglas, V. Zhaunerchyk, N. Indriolo, K. Yagi, S. Hirata, and B. J. McCall, *Astrophysical Journal* (submitted, 2012), "Dissociative recombination of vibrationally cold  $\text{CH}_3^+$  and interstellar implications."
21. M. R. Hermes, M. Keçeli, and S. Hirata, *The Journal of Chemical Physics* (submitted, 2012), "Size-extensive vibrational self-consistent field method with anharmonic geometry corrections."

# Generalized Van Vleck Variant of Multireference Perturbation Theory

Mark R. Hoffmann  
University of North Dakota  
Chemistry Department  
Grand Forks, ND 58202-9024  
Email: mhoffmann@chem.und.edu

## I. Project Scope

There is a continuing need to develop new, cutting edge theoretical and computational electronic structure methods to support the study of complex potential energy surfaces (PESs). While standard methods of computational chemistry are usually adequate for studying the ground electronic states of molecular species near their equilibrium geometries, reaction intermediates, transition states and excited states generally require advanced methods that take into account their multiconfigurational nature. Multireference (MRPT) and quasidegenerate (QDPT) perturbation theories have been demonstrated to be efficient and effective for the description of electron correlation in essentially arbitrarily complex molecules. Recent work demonstrated that the mathematically robust and physically correct structures in our MRPT, called Generalized van Vleck Perturbation Theory (GVVPT), are amenable to highly efficient algorithms. Specifically, second- and third-order approximations of GVVPT (i.e., GVVPT2 and GVVPT3) utilize routines in common with our efficient macroconfiguration-based, configuration-driven MRCISD<sup>1</sup>. Consequently, theoretical and computational development can proceed by first addressing the structurally simpler equivalent CI problem. Chemical problems that are not addressed readily by other theoretical methods become accessible to MRPT or QDPT: problems such as the descriptions of large regions of excited electronic state PESs of polyatomics, especially when the characters of the excited states are doubly excited relative to the ground state, and the characterizations of multiple PESs of the same symmetry in close proximity. Within the scope of this grant, we apply these theoretical techniques primarily to combustion-relevant Group 15 and 16 oxides, and to develop their descriptions of derivative and spin-orbit nonadiabatic couplings.

## II. Recent Progress

A.1. GVVPT2 Molecular Derivatives and Nonadiabatic Coupling Terms. The fully variational Lagrangian functional formalism<sup>2</sup> provided, in past reporting periods, the framework to construct analytical formulas for GVVPT2<sup>LoP5, LoP7</sup> and MRCISD<sup>LoP2</sup> molecular gradients and nonadiabatic coupling terms. Pilot computer programs for the gradients had been realized, and demonstrated to be correct even for difficult problems. However, efforts to scale-up beyond transformation-based approaches, to iterative techniques, were faced with puzzling convergence issues that manifested themselves in the need to use unfeasibly large Lanczos or Arnoldi subspaces. Ultimately, it was realized that the source of the instability was the commonly used parameterization of the CI vectors in the MCSCF space and the affiliated constraint equation. In the past year, an alternative in which the MCSCF space responses are parameterized in terms of state rotations, with generator

$$R(\mathbf{x}) = \sum_I^{N_P} \sum_{\Lambda(>I)}^{all} R_{\Lambda I}(\mathbf{x}) \left[ |\tilde{\Phi}_{\Lambda}(\mathbf{x})\rangle \langle \tilde{\Phi}_I(\mathbf{x})| - |\tilde{\Phi}_I(\mathbf{x})\rangle \langle \tilde{\Phi}_{\Lambda}(\mathbf{x})| \right], \quad (1)$$

has been derived. While conceptually straightforward, this change in parameterization required a corresponding change in constraint equations. It should be realized that such change also required re-examination of the representation of the MCSCF secondary space, which is decidedly not straightforward for multidimensional primary spaces. Moreover, only formulations that support iterative solutions, and are thus amenable to essentially arbitrary scale-up, were of interest. Computational equations of the form

$$\left(\mathbf{G}_{R, \nu \Delta} \mathbf{x}^{\nu \Delta}\right)_{\Lambda} = \sum_{G_i > G_{i'}} \sum_{\substack{i \in G_i \\ j \in G_{i'}}} \frac{\partial e_{ij}^{\nu \Delta}}{\partial R_{\Lambda}} \quad (2a)$$

$$= (w_I - w_{\Lambda}) \sum_{m,n} C_{m\Lambda} C_{nl} \sum_{G_i > G_{i'}} \sum_{\substack{i \in G_i \\ j \in G_{i'}}} \langle F_m | [H, E_{ij} - E_{ji}] | F_n \rangle x_{ij}^{\nu \Delta} \quad (2b)$$

are found, in which  $i$  and  $j$  represent molecular orbitals belonging to two different orbital groups ( $G_i$  and  $G_{i'}$ , respectively) so that their rotation is nonredundant,  $C_{nl}$  and  $C_{m\Lambda}$  are MCSCF state vectors for primary state  $I$  and state  $\Lambda$ ,  $E_{ij}$  and  $E_{ji}$  are unitary group generators,  $F_m$  and  $F_n$  are configuration state functions (CSFs) in the MCSCF space,  $w_I$  and  $w_{\Lambda}$  are predetermined weights that allow for arbitrary state averaging, and  $x_{ij}^{\nu \Delta}$  is an element of an expansion vector from which solution vectors are obtained. Computational realization of the new formulation is in progress.

**A.2. Relativistic Effects.** Two types of relativistic effects are considered within the scope of this project. One is the scalar (or spin-free) contribution and the other is spin-orbit coupling. The standard approach starts with approximations to the spin-free relativistic Hamiltonian (such as the second-order Douglas-Kroll-Hess (DKH) approximation or the zero-order regular approximation (ZORA)), and grafts onto such calculations spin-orbit coupling (often using some approximation to the Breit-Pauli operator). This protocol, while useful in many respects, is not entirely satisfactory for two distinct reasons. First, the two parts do not have any formal relation to each other; i.e., there is little to guide the relative degrees of approximation made in the spin-free and spin-dependent parts. While this situation might be tolerable when one knows *a priori* that a specific problem requires careful consideration of e.g. contraction of  $s$ - and  $p$ -orbitals (arising from kinematic spin-free relativistic effects) but spin-orbit coupling is not expected to make a significant contribution (i.e., due to either experimental or earlier theoretical treatments), this two-part approach can be problematic for novel systems. Second, the Breit-Pauli operator is not variationally stable, which limits its use to perturbative corrections on previously obtained one-component wave functions. Moreover, even the DKH approximations for the spin-free parts are being increasingly viewed as limited compared to the treatment of kinematic effects in exact transformations, such as in the exact two-component (X2C) approach.<sup>3</sup> However, up to recently<sup>4</sup> there has not been a spin-free formulation of X2C that would preserve the useful one-component spin-free plus later spin-dependent paradigm, which preserves use of high performance computational chemistry codes for dynamic electron correlation. A spin-free X2C has been computationally realized and incorporated into relativistic GVVPT2 calculations. Replacing the DKH approximation for the kinematic effects by a spin-free X2C variant has however introduced an additional complication. Specifically, the use of contracted basis functions in relativistic calculations can be problematic, because of requirements for restricted kinetic balance between large and small components of the wave function, and there is no *a priori* reason to expect that contractions that proved to be practically effective in DKH schemes will necessarily be useful in the context of calculating spin-free X2C. This in turn requires calculation of the so-called pVp-type integrals,

$$\langle \mathbf{a} | pVp | \mathbf{b} \rangle = \int d\mathbf{r} \nabla \varphi(\mathbf{r}; \xi_a, \mathbf{a}, \mathbf{A}) \cdot \frac{1}{|\mathbf{r} - \mathbf{C}|} \nabla \varphi(\mathbf{r}; \xi_b, \mathbf{b}, \mathbf{B}) \quad (3)$$

in an uncontracted basis set, followed by a transformation which involves conventional overlap, kinetic energy and potential energy integrals. Contraction of the atomic basis integrals, critical for efficient calculation of molecular electronic structure, can proceed only then.

In current work, an effective one-electron spin-orbit operator for use in GVVPT2 that is derived from rigorous separation of the spin-dependent from the spin-independent parts of the X2C operator is being pursued. It is conjectured that an effective one-electron spin-orbit operator can be developed that is related to the full spin-dependent component of X2C in much the same manner that atomic mean field

integrals<sup>5</sup> (AMFI) are derived from the Breit-Pauli operator. Calculation of the true one-electron contribution (i.e., essentially the pVp-type integral described above with the scalar product replaced by a vector product) using efficient Obara-Saika recursion has been developed for our software platform. Particular attention was paid to the symmetry properties, as the effective one-electron integrals that include the two-electron contributions through AMFI will have the same symmetries.

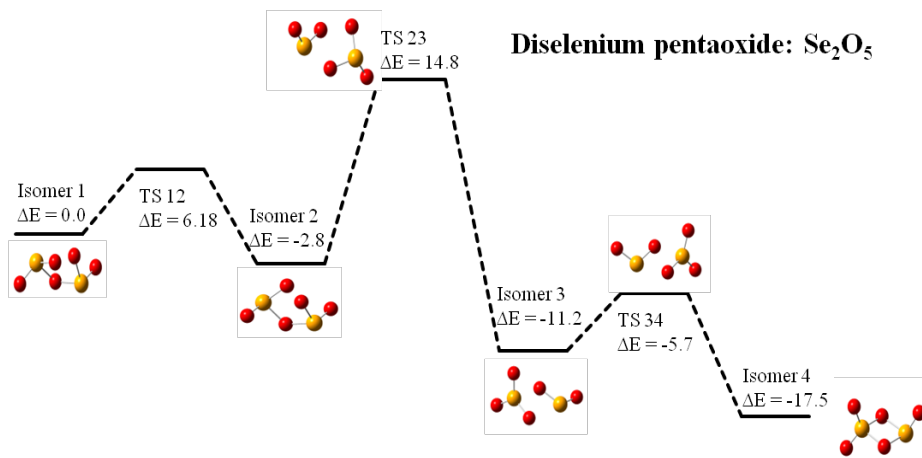
**B. Selenium Oxides** GVVPT2 calculations were performed to determine the relative stabilities of the smaller selenium oxides (SeO, SeO<sub>2</sub> and SeO<sub>3</sub>) and some of their dimers that could potentially be formed during the combustion of coal.<sup>10p8</sup> Initial active spaces were derived from a simple valence picture, but needed to be expanded for SeO<sub>3</sub>. Geometries predicted using the B3LYP DFT method agree fairly well with GVVPT2 optimized values and with experimental data, except for SeO<sub>3</sub> which is disputed.

	Symmetry	Parameters	B3LYP	GVVPT2	Exp.
SeO	$C_{\infty v}$	$r_e(\text{Se-O})$	1.663	1.638	1.6393 <sup>a</sup>
SeO <sub>2</sub>	$C_{2v}$	$r_e(\text{Se-O})$	1.622	1.612	1.607 <sup>b</sup>
		$\angle\text{O-Se-O}$	115.1	115.2	113.50 <sup>b</sup>
SeO <sub>3</sub>	$D_{3h}$	$r_e(\text{Se-O})$	1.613	1.598	1.6878 <sup>c</sup>

<sup>a</sup> Ref. 6. <sup>b</sup> Ref. 7. <sup>c</sup>  $r_0(\text{Se-O})$  from Ref. 8.

For example, for SeO<sub>2</sub> the GVVPT2 value of  $r_e(\text{O-Se})$  and bond angle agree with experimental values, based on microwave spectroscopy data, to within 0.005 Å and 1.7°, respectively. The B3LYP/6-311G\* method leads to the same bond angle as GVVPT2, and the values of  $r_e(\text{O-Se})$  predicted by these methods agree within 0.01 Å. Similarly, harmonic frequencies of SeO<sub>2</sub> in its ground state predicted by the CASSCF, GVVPT2, and B3LYP methods<sup>10p8</sup> are in good agreement with experimental data.

Based on the close agreement obtained for the monomers, geometries of the oxygen-bridged dimers (specifically Se<sub>2</sub>O<sub>3</sub> and Se<sub>2</sub>O<sub>5</sub>) were obtained using B3LYP/6-311G\*. Accurate energies were obtained from GVVPT2 calculations, which differed, in some cases strongly (ca. 20-30 kcal/mol), from the B3LYP results. GVVPT2 energies were corroborated for select structure with CCSD(T) calculations. These predictions are, to our knowledge, the first theoretical or experimental results obtained for these species. While the diselenium trioxide exhibits several energetically close minima (with many of them connected by low barriers), the pentoxide has better separated minima. Perhaps most interesting, the global minimum on the diselenium pentoxide surface is a four-membered cyclic structure.



### III. Future Work

We expect continued progress in both the advancement of nuclear derivative and relativistic effects for GVVPT2 and MRCISD in applications to primarily Group 15 and 16 oxides. The highest priority vis-à-vis GVVPT2 is to resolve the scale-up issue for gradients, which uses the reparametrization of the state space rotations. Progress on scale-up of determination of the GVVPT2 nonadiabatic coupling matrix elements is expected to follow, since the response matrix is identical between GVVPT2 gradients and nonadiabatic couplings. Using the in-house configuration-driven UGA code, spin-dependent X2C effective one-electron spin-orbit coupling matrix elements should become available. This framework should provide a theoretically more consistent alternative to the widely used Breit-Pauli operator based approach, and will be compared. Together with the recently realized inclusion of spin-free exact two-component (X2C) treatment of kinematic effects, robust relativistic MRCISD and GVVPT2 computer programs, appropriate for much of the periodic table, should be operational before too long. As production computer codes become available, we intend to refine the  $\text{Se}_m\text{O}_n$  potential energy surfaces, and develop corresponding  $\text{Sb}_m\text{O}_n$  surfaces, with inclusion of nuclear derivative and spin-orbit nonadiabatic coupling. Similarly, we also intend to further studies on  $\text{O}_3$  and the  $\text{NO}+\text{NO}$  surfaces, which were examined earlier by us at the GVVPT2 level, as the new spin-orbit and nonadiabatic coupling codes become available.

### IV. References

- <sup>1</sup> W. Jiang, Y. G. Khait, and M. R. Hoffmann, *J. Phys. Chem. A* **113**, 4374 (2009).
- <sup>2</sup> T. Helgaker and P. Jørgensen, *Adv. Quantum Chem.* **19**, 183 (1988); *Theor. Chim. Acta* **75**, 111 (1989).
- <sup>3</sup> W. Liu, *Mol. Phys.* **108**, 1679 (2010).
- <sup>4</sup> Z. Li, Y. Xiao, and W. Liu, *J. Chem. Phys.* **137**, 154114/1-18 (2012).
- <sup>5</sup> B. A. Hess, C. M. Marian, U. Wahlgren, and O. Gropen, *Chem. Phys. Lett.* **251**, 365 (1996).
- <sup>6</sup> D. R. Lide, *CRC Handbook of Chemistry and Physics*; CRC Press: Boca Raton, FL., 2005.
- <sup>7</sup> H. Takeo, E. Hirota, and Y. Morino, *J. Mol. Spectrosc.* **34**, 370 (1970).
- <sup>8</sup> N. J. Brassington, H. G. M. Edwards, D. A. Long, and M. Skinner, *J. Raman Spectrosc.* **7**, 158 (1978).

### V. Publications and Submitted Journal Articles Supported by this Project 2010-2012

- <sup>1</sup> D. P. Theis, Y. G. Khait, S. Pal, and M. R. Hoffmann, Molecular dipole moments using the GVVPT2 variant of multireference perturbation theory, *Chem. Phys. Lett.* **487**, 116–121 (2010).
- <sup>2</sup> Y. G. Khait, D. Theis, and M. R. Hoffmann, Lagrangian approach for geometrical derivatives and nonadiabatic coupling terms in MRCISD, *Mol. Phys.* **108**, 2703–2716 (2010).
- <sup>3</sup> Y. E. Bongfen Mbote, Y. G. Khait, C. Hardel, and M. R. Hoffmann, Multireference Generalized Van Vleck Perturbation Theory (GVVPT2) Study of the  $\text{NCO} + \text{HCNO}$  Reaction: Insight into Intermediates, *J. Phys. Chem. A* **114**, 8831–8836 (2010).
- <sup>4</sup> R. M. Mokambe, Y. G. Khait, and M. R. Hoffmann, Ground and Low-Lying Excited Electronic States of  $[3,3']$  Bidiazirinylidene ( $\text{C}_2\text{N}_4$ ), *J. Phys. Chem. A* **114**, 8119–8125 (2010).
- <sup>5</sup> D. Theis, Y. G. Khait, M. R. Hoffmann, GVVPT2 energy gradient using a Lagrangian formulation, *J. Chem. Phys.* **135**, 044117/1–14 (2011).
- <sup>6</sup> T. J. Dudley, J. J. Howard, and M. R. Hoffmann, Generalized Van Vleck Perturbation Theory Study of Chlorine Monoxide, *AIP Conf. Proc.* **1504**, 582–585 (2012).
- <sup>7</sup> Y. G. Khait, D. Theis, and M. R. Hoffmann, Nonadiabatic coupling terms for the GVVPT2 variant of multireference perturbation theory, *Chem. Phys.* **401**, 88–94 (2012).
- <sup>8</sup> R. M. Mokambe, J. M. Hicks, D. Kerker, W. Jiang, D. Theis, Z. Chen, Y. G. Khait, and M. R. Hoffmann, *Mol. Phys.* (submitted).

# Theoretical Kinetics and Non-Born–Oppenheimer Chemistry

Ahren W. Jasper  
Combustion Research Facility, Sandia National Laboratories  
Livermore, CA 94551-0969  
ajasper@sandia.gov

## I. Program Scope

In favorable cases, theoretical chemical kinetics calculations are capable of producing quantitative rate coefficients that can aid in the interpretation of experimental kinetics and inform the development of comprehensive and detailed models of combustion. More broadly, chemical kinetics calculations are approaching so-called “kinetic accuracy,” defined as a factor of  $\sim 2$ . This term may be compared with the 1990s realization of “chemical accuracy” ( $\sim 1$  kcal/mol) in thermochemistry, when calculated thermochemistry began to be accurate enough to be used alongside experimental values. A similar situation is emerging in chemical kinetics thanks to recent and ongoing improvements in computer hardware and theoretical methods. The principal goal of this project is to develop and validate new theoretical methods designed to broaden the applicability and improve the accuracy of theoretical chemical kinetics and to aid in the general realization of kinetic accuracy for applications throughout combustion. The model developments we are presently focused on are: (1) predicting pressure dependence from first principles, (2) more accurately characterizing multistate non-Born–Oppenheimer (e.g., spin-forbidden) kinetics, and (3) predicting vibrational anharmonicity for highly excited systems.

## II. Recent Progress

The weakest link in many theoretical chemical kinetics applications is the treatment of collisional energy transfer, which gives rise to pressure dependence. We have continued our efforts to develop predictive models for pressure dependent kinetics, which include trajectory calculations, potential energy surface development, and master equation model development. The trajectory ensembles produce low-order moments of the total energy and total angular momentum transferred due to the collisions, which are then used to parameterize master equation models of collisional energy transfer. As we are principally interested in low-order moments, we may expect the classical approximation to be a good one. The dominant source of uncertainty in these calculations instead likely arises from the choice of the potential energy surface. We have carried out direct dynamics trajectory calculations, where, instead of a fitted potential energy surface, the potential energy surface is calculated “directly” via quantum chemistry. These full-dimensional direct dynamics studies have been used to test the accuracy of a widely-employed “separable pairwise” approximation, where the total potential energy is written as a sum of the intramolecular potential energies of the target and bath gas and the intermolecular target–bath gas interaction. We quantified that the use of an exponential repulsive wall in the intermolecular term can allow for accurate separable pairwise applications, with differences in the predicted moments of only 10% relative to the results of our direct dynamics calculations. For some anisotropic systems, however, the interaction potential cannot be well described when nonpairwise interactions are neglected, leading to errors in the predicted moments of up to 50% for diatomic baths, for example.

We have used these detailed comparisons to validate more efficient strategies suitable for treating larger systems. We developed “universal” C–M and H–M pairwise interaction parameterizations (where M is an atomic or diatomic bath gas atom) for use with an efficient semiempirical model for the target potential energy surface. This strategy provides an accurate picture of collisional dynamics for hydrocarbon targets and is capable of calculations for atomic and diatomic

baths and hydrocarbon targets with up to dozens of carbon atoms that are many orders of magnitude more efficient than the direct dynamics approach discussed above.

We have used our calculated low-order moments to parameterize collisional energy transfer models for use in master equation calculations, and we have compared our parameter-free kinetics predictions with pressure-dependent experimental kinetics. For example, we tested the use of the popular “single-exponential-down” model for  $P(E,E')$  with  $\alpha$  set to the calculated average energy transferred in deactivating collisions for  $\text{CH}_4$  dissociation in several baths. The first principles kinetics agreed well with available experimental results, and the uncertainty associated with this approach was found to be less than the uncertainty associated with other aspects of the calculation such as the neglect of vibrational anharmonicity. For radical targets with weaker bonds, however, we found that the use of the simple single-exponential-down model resulted in an overprediction of the rate coefficient by a factor of 2–3. As discussed below, we can attribute this to the neglect of angular momentum in  $P$ , and we are developing more detailed models of  $P$  that include angular momentum dependence based on these trajectory studies.

In collaboration with Argonne theorists Harding and Klippenstein, we have applied and analyzed the applicability of transition state theory (TST) to the nontrivial case of roaming radical reactions. The conditions under which competing tight processes (e.g., those with conventional 3-center transition state geometries) and roaming processes for molecular elimination may be accurately treated as dynamically separable were analyzed, and a formal foundation for understanding this separability was developed. We showed that tight and roaming mechanisms may be treated as separable to a good approximation, and we identified features of the potential energy landscape that serve as mechanism dividers (second order saddle points or minimum energy points on conical intersections). Importantly, competing mechanisms may be *dynamically* separable even when the two regions are not energetically separated and even when there is no intrinsic feature of the potential energy surface associated with the mechanism divider. In collaboration with Argonne experimentalists (Michael, Sivaramakrishnan) and theorists (Klippenstein, Harding, Wagner), the importance of roaming to molecular products in the thermal decomposition of dimethyl ether was studied. A strategy for obtaining analytic six-dimensional interaction potentials for studying roaming radical dynamics was developed and applied in reduced dimensional trajectory calculations. Roaming was identified as a minor channel both theoretically and experimentally, although the theory underpredicted the measured molecular branching fractions.

In collaboration with Sandia experimentalist Hansen, dissociation thresholds and ionization energies were calculated for species relevant to the chemistry of tetrahydrofuran and methylcyclohexane flames. These joint theoretical/experimental studies revealed the presence of competing cyclic and ring-opening pathways for fuel decomposition and oxidation. We also characterized the H-assisted isomerization kinetics of fulvene  $\rightarrow$  benzene in detail and discussed the importance of similar processes for the so-called “second-ring” isomers of naphthalene. The fast isomerizations occur via a cyclopropylcarbanyl intermediate—a substituted cyclopropyl group adjacent to a radical carbon—that provides a facile route for carbon bonding rearrangements. If sufficiently fast, such processes may promote thermodynamic equilibria among some isomeric PAHs, thus simplifying the development of detailed reaction mechanisms for PAH growth. Our joint experimental/theoretical studies of unimolecular decomposition kinetics with Tranter were continued. Dioxane decomposition was studied theoretically using a combination of single reference and multireference quantum chemistry calculations. Four low-energy ring-opening pathways were found, and three of these involved a concerted H-atom transfer across the ring as it opens. For each of the concerted pathways, related stepwise pathways were found with weakly-bound diradical intermediates. The major immediate products of dioxane ring opening were shown to be  $\text{CH}_2\text{CHOCH}_2\text{CH}_2\text{OH}$  and  $\text{CH}_3\text{CH}_2\text{OCH}_2\text{CHO}$ , which subsequently decompose at the central bond to radical and molecular products.

### III. Future Work

We propose to continue our development of predictive models for pressure dependence in chemical kinetics. We will apply our direct dynamics methods to new classes of targets, including CH<sub>3</sub>OH and CH<sub>3</sub>Cl. Enhanced energy transfer for halogens and alcohols has been reported, and the trajectory studies will be used to elucidate the dynamical mechanisms of these enhancements. We will also carry out direct dynamics trajectory calculations for two bath gases that were previously not included in our tests: O<sub>2</sub> and H<sub>2</sub>O. H<sub>2</sub>O is an especially important collider, which has been shown experimentally to be up to ~20x more efficient than N<sub>2</sub>. In parallel work, we will continue developing and testing efficient semiempirical potential energy surfaces, with an initial goal of adapting our successful hydrocarbon strategy to include O atoms. As discussed above, existing models for collisional energy transfer used in master equation calculations ignore the effect of changes in angular momentum due to collisions or use simple models to describe this dependence. We will explicitly include this effect in new models for use in master equation calculations, with parameters obtained via our classical trajectory methods and validated potential energy surfaces. This work is being carried out in collaboration with Miller and Klippenstein at Argonne.

We propose to continue to develop and validate theoretical methods for studying electronic state transitions in chemistry. Our initial goals are to apply our multistate trajectory methods to spin-forbidden reactions relevant to combustion and to develop new statistical models for these systems. The trajectory calculations will be used to benchmark the statistical models and to elucidate the underlying multistate physics. In both the trajectory and statistical calculations, we will evaluate the coupled potential energy surfaces directly using ab initio methods to retain broad general applicability.

One goal of the proposed work is to critically evaluate the appropriateness of the TST picture (i.e., the picture that one can obtain accurate dynamical information from a reduced-dimensional crossing seam) for spin-forbidden processes. Specifically, we note that the fundamental assumption of TST (Wigner's third assumption) is that once the system reaches the transition state dividing surface, its fate is decided—namely that it reacts with unit probability. The dynamical bottleneck in conventional TST is therefore access to the dividing surface. For spin-forbidden reactions, the physical picture is very different. Even when electronic transitions are localized at the crossing seam (as is the case for spin-orbit coupled systems involving light atoms), the probability of switching states at each seam crossing is not unity and is instead very small—the transition is “forbidden,” after all. The system is likely to access the seam many times before undergoing a reactive event. The dynamical bottleneck for spin-forbidden reactions is not access to the seam but rather the nonadiabatic event itself. Spin-forbidden reactions therefore violate the fundamental assumption of TST, and we highlight two ways in which this has important consequences for statistical calculations. First, in conventional TST one relies on the assumption of unit reactivity at the seam to derive the variational principle and thus the formal equivalence of TST and trajectory-based implementations of classical dynamics. No analogous formal foundation exists for nonadiabatic implementations of TST or for nonadiabatic statistical theories. Second, electronically nonadiabatic dynamics, unlike adiabatic dynamics, is nonlocal. Therefore, in principle, not only do we need to account for multiple passes through the crossing seam, but we must also keep track of the time-history of subsequent surface crosses. This latter effect is related to electronic decoherence. There is some timescale  $\tau_{\text{deco}}$  on which the electronic variables “reset” or decohere between electronic events. If this timescale is shorter than the time between electronic events, then one can treat the electronic events as independent from one another. If, on the other hand, the time between events is shorter than or similar to  $\tau_{\text{deco}}$ , then the outcome of successive electronic events will depend on the recent history of the system and nonlocal models for decoherence are required. A semiclassical model we developed predicts  $\tau_{\text{deco}}$  to be ~5–100 fs for spin-forbidden systems involving first-row atoms; this timescale is likely similar to the time intervals for seam crossings in many systems, thus motivating the development of nonlocal models.

We propose to develop improved statistical models that include these “missing physics.” Specifically, we will use short-time multistate trajectories to calculate improved spin-forbidden

transition probabilities that, unlike the Landau-Zener approximation, include multidimensional dynamical effects. This proposed work is entirely analogous to the development of modern treatments of tunneling, where it was recognized that there are significant differences in one-dimensional and multidimensional models of this quantum effect. Our preliminary calculations suggest that these missing effects can contribute up to an order of magnitude of uncertainty in the spin-forbidden models. Initial studies are underway for the reactions:  $O + CO$ ,  $H + HO_2$ ,  $H + NCO$ , and  $O +$  alkenes.

The harmonic oscillator approximation is often used in practical applications of TST as it greatly simplifies the evaluation of partition functions and state counts. Thanks to improvements to a variety of aspects of theoretical chemical kinetics, the harmonic approximation is now often the dominant source of uncertainty in many applications, particularly at elevated temperatures where tunneling is not expected to be important and where an exponential dependence mitigates the uncertainty associated with the barrier height. Numerous useful methods have been proposed for calculating anharmonic state counts and partition functions, but none is both widely applicable and nonempirical, particularly for systems with high internal energies. We propose to implement Monte Carlo phase space integration in arbitrary coordinates to obtain fully anharmonic (but classical) state counts and partition functions. The use of arbitrary (e.g., curvilinear Z-matrix) coordinates instead of rectilinear Cartesian normal mode coordinates allows for more efficient sampling as well as useful separable approximations (e.g., one could freeze C–H stretches more usefully in curvilinear coordinates than in Cartesian ones). The critical advance in this work is the use of numerical coordinate transformation matrices, which avoids the cumbersome step of deriving system-dependent analytic transformations. The goal of this work is the development of useful strategies for calculating anharmonic corrections for use in kinetics applications, where existing methods cannot be applied. Examples include crossing seams for spin-forbidden reactions and systems with coupled bends and torsions, such as ring opening reactions. This approach is intended to be complementary to the existing approaches, as it is capable of producing exact (though classical) fully anharmonic properties and is generally applicable.

#### IV. Publications supported by this project since 2011

1. A. W. Jasper and N. Hansen, Hydrogen-assisted isomerizations of fulvene to benzene and of larger cyclic aromatic hydrocarbons. *Proc. Combust. Inst.* 34, 279 (2013).
2. L. B. Harding, S. J. Klippenstein, and A. W. Jasper, Separability of tight and roaming pathways to molecular decomposition. *J. Phys. Chem. A* 16, 6979 (2012).
3. S. A. Skeen, B. Yang, A. W. Jasper, W. J. Pitz, and N. Hansen, Chemical structures of low-pressure premixed methylcyclohexane flames as benchmarks for the development of a predictive combustion chemistry model. *Energy & Fuels* 25, 5611 (2011).
4. T. Kasper, A. Lucassen, A. W. Jasper, W. Li, B. Yang, P. R. Westmoreland, K. Kohse-Höinghaus, B. Yang, J. Wang, T. A. Cool, and N. Hansen, Identification of tetrahydrofuran reaction pathways in premixed flames. *Z. Phys. Chem.* 225, 1237 (2011).
5. A. W. Jasper and J. A. Miller, Theoretical unimolecular kinetics for  $CH_4 + M \rightarrow CH_3 + H + M$  in eight baths,  $M = He, Ne, Ar, Kr, H_2, CO, N_2,$  and  $CH_4$ . *J. Phys. Chem. A* 115, 6438 (2011).
6. X.-G. Wang, T. Carrington, Jr., R. Dawes, and A. W. Jasper, The vibration–rotation–tunneling spectrum of the polar and T-shaped-N-in isomers of  $(NNO)_2$ . *J. Mol. Spectrosc.* 53, 6438 (2011).
7. A. W. Jasper and D. G. Truhlar, Non-Born–Oppenheimer molecular dynamics for conical intersections, avoided crossings, and weak interactions. *Adv. Ser. Phys. Chem.* 17, 375 (2011).
8. R. Sivaramakrishnan, J. V. Michael, A. F. Wagner, R. Dawes, A. W. Jasper, L. B. Harding, Y. Georgievskii, and S. J. Klippenstein, Roaming radicals in the thermal decomposition of dimethyl ether: Experiment and theory. *Combust. Flame* 158, 618 (2011).
9. X. Yang, A. W. Jasper, B. R. Giri, J. H. Kiefer, and R. S. Tranter, A shock tube and theoretical study on the pyrolysis of 1,4-dioxane. *Phys. Chem. Chem. Phys.* 13, 3686 (2011).

# Probing the Reaction Dynamics of Hydrogen-Deficient Hydrocarbon Molecules and Radical Intermediates via Crossed Molecular Beams

Ralf I. Kaiser

Department of Chemistry, University of Hawai'i at Manoa, Honolulu, HI 96822

[ralfk@hawaii.edu](mailto:ralfk@hawaii.edu)

## 1. Program Scope

The major goals of this project are to explore experimentally in crossed molecular beams experiments the reaction dynamics and potential energy surfaces (PESs) of hydrocarbon molecules and their corresponding radical species which are relevant to combustion processes. The reactions are initiated under single collision conditions by crossing two supersonic reactant beams containing radicals and/or closed shell species under a well-defined collision energy and intersection angle. By recording angular-resolved time of flight (TOF) spectra, we obtain information on the reaction products, intermediates involved, on branching ratios for competing reaction channels, on the energetics of the reaction(s), and on the underlying reaction mechanisms. These data are of crucial importance to understand the formation of resonantly stabilized free radicals (RSFRs) and of polycyclic aromatic hydrocarbons (PAHs) together with their hydrogen deficient precursors in combustion flames.

## 2. Recent Progress

### 2.1. Formation of Monocyclic Aromatic Molecules

We elucidated the formation route to the toluene molecule ( $C_6H_5CH_3$ ;  $C_7H_8$ ) and to the benzyl radical ( $C_6H_5CH_2$ ;  $C_7H_7$ ) under single collision conditions via the reactions of the D1-ethynyl radical (CCH) and of dicarbon molecules (CC) with isoprene ( $C_5H_8$ ) (Fig. 1). Combining the scattering experiments with electronic structure and RRKM calculations (Alexander Mebel, FIU), our investigations revealed the very first experimental evidence – contemplated by theoretical studies – that under single collision conditions a methyl substituted aromatic hydrocarbon molecule (toluene) and its corresponding radical (benzyl) can be formed via reaction of two acyclic molecules involving cyclization processes at collision energies relevant to combustion flames. These studies are currently being prepared for publication.

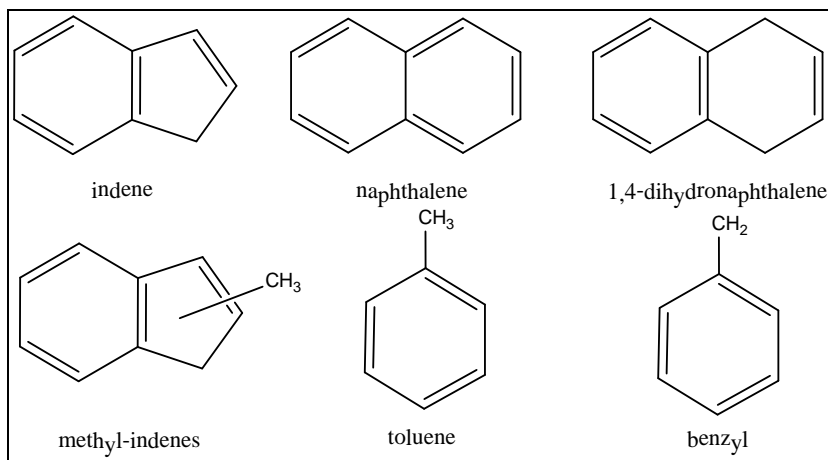


Fig. 1: Structures of the indene ( $C_9H_8$ ), naphthalene ( $C_{10}H_8$ ), and of 1,4-dihydronaphthalene ( $C_{10}H_{10}$ ) formed under single collision conditions via reactions of the phenyl radical ( $C_6H_5$ ) with methylacetylene/allene ( $CH_3CCH/H_2CCCH_2$ ), vinylacetylene ( $C_2H_3CCH$ ), and 1,3-butadiene ( $C_2H_3-C_2H_3$ ). Additionally, indene ( $C_9H_8$ ) and methyl-indenes ( $C_{10}H_{10}$ ) are formed in the crossed beam reactions of phenyl radicals with 1,2-butadiene ( $H_2CCCH(CH_3)$ ) demonstrating that different structural isomers of  $C_4H_6$  lead to distinct reaction products. This highlights the necessity to incorporate isomer-specific reactions into combustion models. Toluene and the benzyl radical can be formed in the reactions of ethynyl and dicarbon with isoprene ( $C_5H_8$ ).

## 2.2. Formation of Bicyclic Aromatic Hydrocarbon Molecules

Based on our unique capabilities to synthesize bicyclic PAH molecules (indene (P10), naphthalene (P14), dihydronaphthalene (P17)) under single collision conditions, we expanded our studies to the next level and probed the formation of methyl-substituted PAHs. Here, crossed beam reactions of phenyl and D5-phenyl with 1,2-butadiene ( $\text{H}_2\text{CCCH}(\text{CH}_3)$ ) provided evidence on the formation of indene and of methyl-indenes via competing methyl and hydrogen loss channels. These studies are currently being prepared for publication.

## 2.3. Formation of Tricyclic Aromatic Hydrocarbon Molecules

We have also probed the potential formation of two tricyclic polycyclic aromatic hydrocarbons, anthracene and phenanthrene ( $\text{C}_{14}\text{H}_{10}$ ), in the crossed beam reactions of the phenyl radical ( $\text{C}_6\text{H}_5$ ) and of the D5-phenyl radical ( $\text{C}_6\text{D}_5$ ) with phenylacetylene ( $\text{C}_6\text{H}_5\text{CCH}$ ) and D1-phenylacetylene ( $\text{C}_6\text{H}_5\text{CCD}$ ) under single collision conditions. The experiments have been just completed and, hence, the data analysis is still ongoing.

## 2.4. PAH Species – Photoionization Studies at the ALS

To yield further insights on the formation of PAHs under combustion relevant conditions (pressure, temperature, reactant molecules), we commissioned in collaboration with Musa Ahmed (LBNL) at the Chemical Dynamics Beamline a high temperature ‘chemical reactor’. A ‘directed synthesis’ of the PAHs is performed *in situ* in a supersonic molecular beam through reaction of pyrolytically generated phenyl radicals ( $\text{C}_6\text{H}_5$ ) with hydrocarbons inside a heated silicon carbide tube (‘chemical reactor’) (P7). The PAHs together with their acyclic isomers formed are then photoionized by vacuum ultraviolet (VUV) light from the Advanced Light Source at various photon energies from 7.5 to 12 eV to record photoionization efficiency (PIE) curves. Based on known (calibrated, computed) PIE curves of the individual PAHs and their acyclic isomers, the recorded PIE curves are then simulated theoretically to extract the nature of the products formed and their branching ratios over a range of combustion-relevant reaction vessel temperatures (1,000-2,000 K) and pressures (few 100 Torr to a few 1,000 Torr). By selecting the reactants allene ( $\text{H}_2\text{CCCH}_2$ ) (P7), methylacetylene ( $\text{CH}_3\text{CCH}$ ) (P7), propylene ( $\text{CH}_3\text{C}_2\text{H}_3$ ) (P16), and 1,3-butadiene ( $\text{C}_2\text{H}_3\text{C}_2\text{H}_3$ ) (P18), these studies access the important  $\text{C}_9\text{H}_x$  ( $x=8,10$ ) and  $\text{C}_{10}\text{H}_x$  ( $x=6,8,10$ ) potential energy surfaces (PESs), among them are the crucial combustion intermediates with indene and naphthalene cores. To date, no experiment has been conducted in which an individual PAH (like) species is formed via a gas phase reaction under well-defined conditions in a high temperature chemical reactor.

**Phenyl–Allene/Methylacetylene (P7):** The aromatic indene molecule ( $\text{C}_9\text{H}_8$ ) together with its acyclic isomers (phenylallene, 1-phenyl-1-propyne, and 3-phenyl-1-propyne) were formed via a ‘directed synthesis’ *in situ* utilizing a high temperature chemical reactor under combustion-like conditions (300 Torr, 1,200-1,500 K) through the reactions of the phenyl radical ( $\text{C}_6\text{H}_5$ ) with propyne ( $\text{CH}_3\text{CCH}$ ) and allene ( $\text{H}_2\text{CCCH}_2$ ). The isomer distributions were probed utilizing tunable vacuum ultraviolet (VUV) radiation from the Advanced Light Source by recording the photoionization efficiency (PIE) curves at mass-to-charge of  $m/z = 116$  ( $\text{C}_9\text{H}_8^+$ ) of the products in a supersonic expansion for both the phenyl-allene and phenyl-propyne systems; branching ratios were derived by fitting the recorded PIE curves with a linear combination of the PIE curves of the individual  $\text{C}_9\text{H}_8$  isomers. Our data suggest that the formation of the aromatic indene molecule via the reaction of the phenyl radical with allene is facile and enhanced compared to the phenyl–propyne system by a factor of about seven. Reaction mechanisms and branching ratios are explained in terms of new electronic structure calculations. Our newly developed high temperature chemical reactor presents a versatile approach to study the formation of combustion-relevant polycyclic aromatic hydrocarbons (PAHs) under well-defined and controlled conditions.

**Phenyl–Propylene (P16):** We studied the reaction of phenyl radicals ( $\text{C}_6\text{H}_5$ ) with propylene ( $\text{C}_3\text{H}_6$ ) exploiting a high temperature chemical reactor under combustion-like conditions (300 Torr, 1200–1500 K). The reaction products were probed in a supersonic beam by utilizing tunable vacuum ultraviolet

(VUV) radiation from the Advanced Light Source and recording the photoionization efficiency (PIE) curves at mass-to-charge ratios of  $m/z = 118$  ( $C_9H_{10}^+$ ) and  $m/z = 104$  ( $C_8H_8^+$ ). Our results suggest that the methyl and atomic hydrogen losses are the two major reaction pathways with branching ratios of  $86 \pm 10\%$  and  $14 \pm 10\%$ . The isomer distributions were probed by fitting the recorded PIE curves with a linear combination of the PIE curves of the individual  $C_9H_{10}$  and  $C_8H_8$  isomers. Styrene ( $C_6H_5C_2H_3$ ) was found to be the exclusive product contributing to  $m/z = 104$  ( $C_8H_8^+$ ), whereas 3-phenylpropene, cis-1-phenylpropene, and 2-phenylpropene with branching ratios of  $96 \pm 4\%$ ,  $3 \pm 3\%$ , and  $1 \pm 1\%$  account for signal at  $m/z = 118$  ( $C_9H_{10}^+$ ). No evidence of the bicyclic indane molecule could be provided. The reaction mechanisms and branching ratios are explained in terms of electronic structure calculations nicely agreeing with a recent crossed molecular beam study on this system.

**Phenyl-1,3-Butadiene (P18):** We studied the reaction of phenyl radicals ( $C_6H_5$ ) with 1,3-butadiene ( $H_2CCHCHCH_2$ ) exploiting a high temperature chemical reactor under combustion-like conditions (300 Torr, 873 K). The reaction products were probed in a supersonic beam by utilizing tunable vacuum ultraviolet (VUV) radiation from the Advanced Light Source and by recording the experimental photoionization efficiency (PIE) curves at mass-to-charge ratios of  $m/z = 130$  ( $C_{10}H_{10}^+$ ), 116 ( $C_9H_8^+$ ), and 104 ( $C_8H_8^+$ ). Our data suggest that the atomic hydrogen (H), methyl ( $CH_3$ ), and vinyl ( $C_2H_3$ ) losses are open with estimated branching ratios of about  $86 \pm 4\%$ ,  $8 \pm 2\%$ , and  $6 \pm 2\%$ , respectively. The isomer distributions were probed further by fitting the experimentally recorded PIE curves with a linear combination of the PIE curves of individual  $C_{10}H_{10}$ ,  $C_9H_8$ , and  $C_8H_8$  isomers. These fits indicate the formation of three  $C_{10}H_{10}$  isomers (trans-1,3-butadienylbenzene, 1,4-dihydronaphthalene, 1-methylindene), three  $C_9H_8$  isomers (indene, phenylallene, 1-phenyl-1-methylacetylene), and a  $C_8H_8$  isomer (styrene). A comparison with results from recent crossed molecular beams studies of the 1,3-butadiene – phenyl radical reaction and electronic structure calculations suggests that trans-1,3-butadienylbenzene (130 amu), 1,4-dihydronaphthalene (130 amu), and styrene (104 amu) are reaction products formed as a consequence of a bimolecular reaction between the phenyl radical and 1,3-butadiene. 1-methylindene (130 amu), indene (116 amu), phenylallene (116 amu), and 1-phenyl-1-methylacetylene (116 amu) are synthesized upon reaction of the phenyl radical with three  $C_4H_6$  isomers 1,2-butadiene ( $H_2CCCH(CH_3)$ ), 1-butyne ( $HCCC_2H_5$ ), and 2-butyne ( $CH_3CCCH_3$ ); these  $C_4H_6$  isomers can be formed from 1,3-butadiene via hydrogen atom assisted isomerization reactions or via thermal rearrangements of 1,3-butadiene involving hydrogen shifts in the high temperature chemical reactor.

### 3. Future Plans

Having established that PAH molecules with indene and naphthalene cores are formed under single collision conditions via phenyl radical reactions with C3 to C5 hydrocarbons, we are aiming to unravel in the coming year the formation mechanisms of prototype bicyclic polycyclic aromatic hydrocarbons via reactions of *aromatic* and *resonantly stabilized*  $C_7H_7$  radicals (benzyl; o-, m-, and p-methylphenyl) with C2 – C4 hydrocarbons (acetylene, methylacetylene, allene, and vinylacetylene). These studies also monitor the formation of methyl-substituted PAHs as detected in oxygen-deficient combustion flames.

### 4. Acknowledgements

This work was supported by US Department of Energy (Basic Energy Sciences; DE-FG02-03-ER15411).

### 5. Publications Acknowledging DE-FG02-03ER15411 (1/2010 – now)

P1 R.I. Kaiser, A.M. Mebel, O. Kostko, M. Ahmed. *On the Ionization Potentials of  $C_4H_3$  Isomers*. Chemical Physics Letters 485, 281-285 (2010).

P2 R.I. Kaiser, *Reaction Dynamics of Carbon-Centered Radicals in Extreme Environments Studied by the Crossed Molecular Beams Technique*. in: Carbon-Centered Radicals: Structure, Dynamics and Reactivity. Malcolm D. E. Forbes, Editor, Wiley, p. 221-248 (2010).

- P3 F. Zhang, B. Jones, P. Maksyutenko, R.I. Kaiser, C. Chin, V.V. Kislov A.M. Mebel, *Formation of the Phenyl Radical [ $C_6H_5(X^2A_1)$ ] under Single Collision Conditions – A Crossed Molecular Beam and Ab Initio Study*. Journal of the American Chemical Society 132, 2672-2683 (2010).
- P4 O. Kostko, J. Zhou, B.J. Sun, J.S. Lie, A.H.H. Chang, R.I. Kaiser, M. Ahmed, *Determination of ionization energies of  $C_nN$  ( $n=3-14$ ) clusters: Vacuum-ultraviolet (VUV) photoionization experiments and theoretical calculations*, The Astrophysical Journal 717, 674-682 (2010).
- P5 P. Maksyutenko, F. Zhang, X. Gu, R.I. Kaiser, *A Crossed Molecular Beam Study on the Reaction of Methylidyne Radicals [ $CH(X^2\Pi)$ ] with Acetylene [ $C_2H_2(X^1\Sigma_g^+)$ ] – Competing  $C_3H_2 + H$  and  $C_3H + H_2$  Channels*. Physical Chemistry Chemical Physics 13, 240-252 (2011).
- P6 D.S.N. Parker, F. Zhang, Y.S. Kim, R.I. Kaiser, A.M. Mebel. *On the Formation of the Resonantly Stabilized  $C_3H_3$  Radicals - A Crossed Beam and Ab Initio Study of the Reaction of Ground State Carbon Atoms with Vinylacetylene*. The Journal of Physical Chemistry A 115, 593-601 (2011).
- P7 F. Zhang, R.I. Kaiser, V. Kislov, A.M. Mebel, A. Golan, M. Ahmed, *A VUV Photoionization Study of the Formation of the Indene Molecule and its Isomers*. The Journal of Physical Chemistry Letters 2, 1731-1735 (2011).
- P8 R.I. Kaiser, M. Goswami, P. Maksyutenko, F. Zhang, Y.S. Kim, A.M. Mebel, *A Crossed Molecular Beams and Ab Initio Study on the Formation of  $C_6H_3$  Radicals - An Interface between Resonantly Stabilized (RSFRs) and Aromatic Radicals (ARs)*. The Journal of Physical Chemistry A 115, 10251-10258 (2011).
- P9 D.S.N. Parker, F. Zhang, R.I. Kaiser, *Phenoxy Radical ( $C_6H_5O$ ) Formation under Single Collision Conditions from Reaction of the Phenyl Radical ( $C_6H_5$ ,  $X^2A_1$ ) with Molecular Oxygen ( $O_2$ ,  $X^3\Sigma_g^-$ ) – The Final Chapter?* The Journal of Physical Chemistry A 115, 11515-11518 (2011).
- P10 D.S.N. Parker, F. Zhang, R. I. Kaiser, V. Kislov, A.M. Mebel, *Indene Formation under Single Collision Conditions from Reaction of Phenyl Radicals with Allene and Methylacetylene – A Crossed Molecular Beam and Ab Initio Study*. Chemistry – An Asian Journal 6, 3035-3047 (2011).
- P11 A.V. Wilson, D.S.N. Parker, F. Zhang, R.I. Kaiser, *Crossed Beam Study of the Atom-Radical Reaction of Ground State Carbon ( $C(^3P_j)$ ) with the Vinyl Radical ( $C_2H_3$ ,  $X^2A'$ )*. Physical Chemistry Chemical Physics 14, 477-481 (2012).
- P12 R.I. Kaiser, X. Gu, F. Zhang, P. Maksyutenko, *Crossed Beams Reactions of Methylidyne [ $CH(X^2\Pi)$ ] with D2-Acetylene [ $C_2D_2(X^1\Sigma_g^+)$ ] and of D1-Methylidyne [ $CD(X^2\Pi)$ ] with Acetylene [ $C_2H_2(X^1\Sigma_g^+)$ ]*. Physical Chemistry Chemical Physics 14, 575-588 (2012).
- P13 R.I. Kaiser, D.S.N. Parker, M. Goswami, F. Zhang, V. Kislov, A.M. Mebel, *Crossed Beam Reaction of Phenyl and D5-Phenyl Radicals with Propene and Deuterated Counterparts – Competing Atomic Hydrogen and Methyl Loss Pathways*. Physical Chemistry Chemical Physics 14, 720-729 (2012).
- P14 D.S.N. Parker, F. Zhang, R.I. Kaiser, V. Kislov, A.M. Mebel, A.G.G.M. Tielens, *Low Temperature Formation of Naphthalene and Its Role in the Synthesis of PAHs in the Interstellar Medium*. Proceedings National Academy of Sciences USA (PNAS) 109, 53-58 (2012).
- P15 D.S.N. Parker, F. Zhang, Y. S. Kim, R. I. Kaiser, A. Landera, A. M. Mebel, *On the Formation of Phenylacetylene ( $C_6H_5CCCH$ ) and D5-Phenylacetylene ( $C_6D_5CCCH$ ) Studied under Single Collision Conditions*. Physical Chemistry Chemical Physics 14, 2997-3003 (2012).
- P16 F. Zhang, R.I. Kaiser, A. Golan, M. Ahmed, N. Hansen, *A VUV Photoionization Study of the Combustion-Relevant Reaction of the Phenyl Radical ( $C_6H_5$ ) with Propylene ( $C_3H_6$ ) in a High Temperature Chemical Reactor*. The Journal of Physical Chemistry A 116, 3541-3546 (2012).
- P17 R.I. Kaiser, D.S.N. Parker, F. Zhang, A. Landera, V.V. Kislov, A.M. Mebel, *Formation of PAHs and their Derivatives under Single Collision Conditions - The 1,4-Dihydronaphthalene Molecule as a Case Study*. The Journal of Physical Chemistry A 116, 4248-4258 (2012).
- P18 A. Golan, M. Ahmed, A.M. Mebel, R.I. Kaiser, *A VUV Photoionization Study on the Formation of Primary and Secondary Products in the Reaction of the Phenyl Radical with 1,3-Butadiene under Combustion Relevant Conditions*. Physical Chemistry Chemical Physics 15, 341-347 (2013).

## DYNAMICAL ANALYSIS OF HIGHLY EXCITED MOLECULAR SPECTRA

Michael E. Kellman

Department of Chemistry, University of Oregon, Eugene, OR 97403

[kellman@uoregon.edu](mailto:kellman@uoregon.edu)

### PROGRAM SCOPE:

Highly excited vibration-rotation dynamics of small molecular species, including those approaching the threshold of reaction, are crucial to understanding fundamental processes important for combustion. Our goal is to develop theoretical tools to analyze spectra and dynamics of these highly excited systems. A persistent theme is the use of effective spectroscopic fitting Hamiltonians to make the link between experimental data and theoretical dynamical analysis. There are three areas currently under investigation. (1) The role of bifurcations and the "birth of new modes in bifurcations from the low energy normal modes." (2) A new focus has been systems approaching and undergoing intramolecular isomerization reactions. We have been developing new generalizations of the effective Hamiltonian, called "polyad-breaking Hamiltonians," to deal with spectra of isomerizing systems. In our most recent work we have extended these investigations to consider time-dependent dynamics, including the isomerization process. (3) We have begun an investigation of the "quantum thermodynamics" of a small quantum molecular system immersed in a quantum heat bath.

**RECENT PROGRESS AND FUTURE PLANS:** The progress described below has been in collaboration with postdoctoral associates George Barnes (now at Siena College) and Vivian Tyng. Our current research is pursuing three main directions.

### CRITICAL POINTS BIFURCATION ANALYSIS OF EFFECTIVE SPECTROSCOPIC HAMILTONIANS.

This work continues with Dr. Vivian Tyng. Ref. 7 was done in collaboration with DOE Combustion PI Hua Guo of the University of New Mexico.

Our emphasis on the critical points bifurcation analysis of effective spectroscopic Hamiltonians has continued in recent years [1,2,7]. In a longstanding project, conducted with Dr. Vivian Tyng who is now a 1/3-time postdoctoral researcher, we are completing our first bifurcation analysis for a rotation-vibration effective Hamiltonian, using a recent spectroscopic Hamiltonian for CO<sub>2</sub> fit to experimental data.

For some time we have had in hand the successful critical points analysis of rotation-vibration dynamics of CO<sub>2</sub> on the effective Hamiltonian fit to experimental data. The analysis gives relatively simple, intelligible dynamics, comparable to but significantly extending what has been obtained with pure vibrational dynamics. At  $J = 0$  there is only the bifurcation tree of normal modes and Fermi resonance modes. Then, as  $J$  increases, we find a principal "Coriolis mode" that bifurcates out of one of the Fermi resonance modes at very low  $J$ , with further finer branching of the tree into Coriolis modes with increasing  $J$ .

The challenge to completing this work has been the physical interpretation of the results of the critical points analysis. What is the physical nature of the rotation-vibration motion in the new bifurcation rotation-vibration "modes" of the molecule? The natural starting point is the standard picture of the rotation-vibration motion of a symmetric top. In the new Coriolis modes of CO<sub>2</sub>

determined in the bifurcation analysis, things will be somewhat but not altogether different from the symmetric top; and also with some similarities to the asymmetric top. In the critical points Coriolis modes, the molecule “locks” into certain configurations that involve combinations of the zero-order vibrational angle variables. The full motion of the molecule separates into a resonant periodic vibration (due to the combined effects of Fermi and Coriolis couplings); and a periodic precession-like rotational motion. In the body-fixed frame, the resonant periodic vibration involves the four vibrational modes including vibrational angular momentum and, unlike the pure Fermi resonance problem, the antisymmetric stretch. We are working on animations that we hope will dramatically simplify the visualization, following the example of our animations of the new bending modes born in bifurcations of acetylene.

In addition, we are newly working to identify patterns in the rotation-vibration spectrum that will be markers of the bifurcations that give the new rotation-vibration modes. This will complete the linking of the effective Hamiltonian, the critical points bifurcation analysis, the visualization of the result new rotation-vibration motions, and the connection of these with observable spectral patterns.

### **POLYAD BREAKING GENERALIZED EFFECTIVE HAMILTONIANS.**

**Generalized spectroscopic Hamiltonian with polyad breaking.** This work has been primarily in collaboration with Dr. George Barnes. The recent focus of our work is systems in which the standard spectroscopic polyad approximation breaks down. This involves a major extension of the standard effective spectroscopic fitting Hamiltonian. The Hamiltonian used in virtually all existing spectral fits invokes an approximate conserved quantity known as the polyad or total quantum number. In a recent step, initiated with two papers [3,4], we showed that it is possible to construct an effective Hamiltonian to encompass multiple potential energy minima, especially in a system that does not have two simple uncoupled modes as a zero-order limit. As our exemplar, we used one of the most important elementary combustion species is the hydroperoxyl radical  $\text{HO}_2$ . I will not describe this work in any more detail, moving instead to our most recent work, an investigation of the time-dependent dynamics of the basis set of the generalized effective Hamiltonian.

**Time dependent dynamics of the generalized effective Hamiltonian.** In the latest phase of our work on generalized effective Hamiltonians, we are investigating the physical nature of the quantum mechanical states [5,6]. The problem is that the effective Hamiltonian uses an abstract zero-order basis – by itself, it gives no way of describing the states in the physical coordinate space of the system. In recent work [6] we have presented a method of obtaining the coordinate space representation of the abstract zero order basis (ZOB) of a spectroscopic effective Hamiltonian. This paper has undergone significant revision, as follows. One referee for the original submission of the paper called our results “miraculous” and “revolutionary,” and urged us to revise the manuscript to bring out these characteristics more boldly! We put in a lot of care to revise the manuscript accordingly, resulting in figures such as the characteristic example shown below. The ZOB is an abstract basis which is the “ideal” basis for a given form and parameterization of the spectroscopic Hamiltonian. Without a physical model there is no way to transform this abstract basis into a coordinate representation. In Ref. [6] we present a method that relies on a set of converged eigenfunctions obtained from a variational calculation on a potential surface. We make a one-to-one correspondence between the energy eigenfunctions of the effective Hamiltonian and those of a model potential surface. Through this correspondence we construct a physical representation of the abstract ZOB. The ZOB basis is a *time-dependent* basis – a point which is obvious from the fact that the ZOB states are superpositions of the energy eigenfunctions – but also something that is not widely thought about. We find that the time

dependent ZOB basis shows states with both conventional low-energy characteristics, with little time-dependence, in terms of wavefunctions assignable with zero-order quantum numbers; and unconventional wildly time-varying “gnarly” ZOB states at higher energies – see Fig. 2 bottom left – that reflect the highly chaotic, multiple-well nature of the potential in regions of the isomerization process. It is this automatic built-in flexibility that allows extension of the effective Hamiltonian to polyad-breaking and highly chaotic multiple well behavior. The “gnarly” state at bottom left in Fig. 2 actually shows regular, “understandably conventional” behavior at certain later times – see Fig. 2 right.

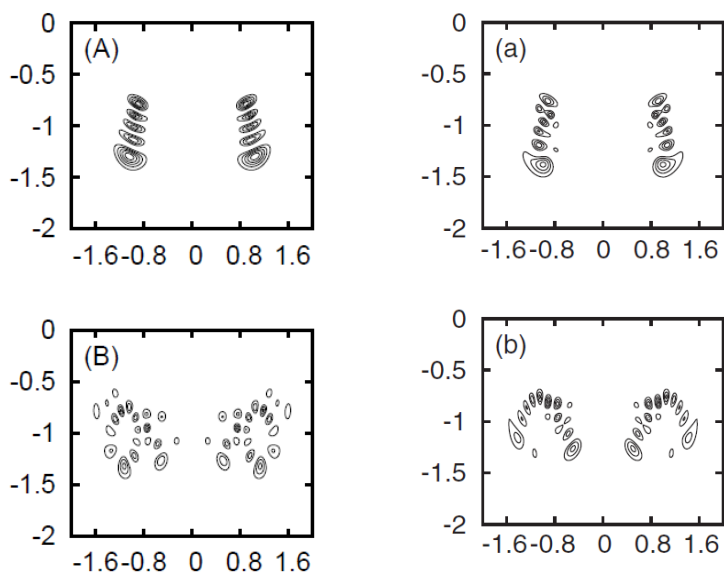


Fig. 2. Left: The squared amplitude of the  $|4\ 0\rangle$  and  $|5\ 0\rangle$  spectroscopic Hamiltonian ZOB functions in panels A and B, respectively.  $|4\ 0\rangle$  illustrates a “conventional” basis function, while  $|5\ 0\rangle$  illustrates an “unconventional” basis function. Right: Two snapshots of the time evolution of the squared amplitude of the  $|5\ 0\rangle$  spectroscopic ZOB function as propagated on the potential surface. The  $t = 0$  snapshot of this state is shown in Left (B). The snapshots on right are at  $t = 0.765$  ps and  $t = 0.830$  ps for panels (a) and (b), respectively. These plots show that although the ZOB at  $t = 0$  appears unconventional, in truth it contains a linear combination of a conventional form and a form understandable in terms of a “horseshoe” shape periodic orbit.

## QUANTUM THERMODYNAMICS OF SMALL MOLECULAR SYSTEMS.

This work is with Dr. George Barnes. The behavior of small quantum entangled systems is of great interest in many areas of fundamental and applied physics and physical chemistry. One area of interest is the “quantum thermodynamics” of small molecular systems. This is of obvious relevance to combustion systems, where small molecular species are embedded in an environment. Our DOE work for many years has focused on the dynamics of highly excited molecular systems in isolation. We have recently turned our attention to embedding these systems in an environment.

We examine the behavior of a model oscillator system – a set of normal mode states of two coupled oscillators – interacting with a finite quantum thermal bath. We examine the time-dependent quantum behavior of various initially prepared pure states as the oscillator system interacts with the quantum environment. The total system + environment “universe” is in a pure

state described by the density matrix  $\rho_{\text{se}}$ . The statistical behavior of the system is described by the reduced density matrix (RDM)  $\rho_s = \text{Trace } \rho_{\text{se}}$ . Visual insight into the dynamics of the system is obtained by examining spatial density distributions of the system RDM  $\rho_s$ .

We chose to examine the time evolution of the zero order (i.e. isolated) system energy eigenstates as well as the system time dependent local mode state. All states reach approximately the same final entropy as well as the same final fitted temperature, the later of which is in good agreement with the temperature expected from the analytic degeneracy formula. An examination of the time dependent dynamics of the system spatial density reveals that each state quickly loses “memory” of its initial density and is rapidly driven to approximately the same fluctuating equilibrium state. The quantum coherences present at time zero have also essentially vanished due to dephasing and population transfer. Contrary to common understanding, quantum coherence in the sense of “interference effects” vanish only with maximal von Neumann entropy, which in turn corresponds to the infinite temperature limit.

Perhaps the most interesting result of this investigation is the phenomenon of each initial state being driven to equilibrium at essentially the same rate. The symmetric normal mode overtone state, which looks most like the equilibrium distribution, is essentially no different in this regard than the antisymmetric mode, which is orthogonal in coordinate space; or the local mode state, which undergoes oscillations between the two local mode overtones in the pure system initial state. An interesting question is whether this behavior will persist for systems with more complex dynamics than the simple normal mode system considered here. Nonlinear systems with strong resonance couplings, such as coupled stretch normal modes in 2:2 resonance, or 2:1 Fermi resonance systems, have marked phase space structure, including stable and unstable modes born in bifurcations. These might be expected to have significantly different dynamics, including decoherence behavior and rates of approach to equilibrium. The results here suggest that this might not be the case, but clearly detailed investigation of these nonlinear systems is warranted.

#### **Recent publications related to DOE supported research:**

1. S. Yang and M.E. Kellman, “Resonance induced spectral tuning”, *Phys. Rev. A.* 81, 062512 (2010).
2. V. Tyng and M.E. Kellman, “The Bifurcation Phase Diagram For  $\text{C}_2\text{H}_2$  Bending Dynamics Has A Tetracritical Point With Spectral Patterns”, *J. Phys. Chem. A.* 114, 9825–9831 (2010).
3. G. L. Barnes and M.E. Kellman, “Effective Spectroscopic Hamiltonian for Multiple Minima with Above Barrier Motion: Isomerization in  $\text{HO}_2$ ”, *J. Chem. Phys.* 133, 101105 (2010).
4. G.L. Barnes and M.E. Kellman, “Detailed Analysis of Polyad-Breaking Spectroscopic Hamiltonians for Multiple Minima with Above Barrier Motion: Isomerization in  $\text{HO}_2$ ”, *J. Chem. Phys.* 134, 074108 (2011).
5. G.L. Barnes and M.E. Kellman, “Effective Hamiltonian for femtosecond vibrational dynamics” *J. Chem. Phys.* 135, 144113 (2011).
6. G.L. Barnes and M.E. Kellman, “Visualizing the Zero Order Basis of the Spectroscopic Hamiltonian,” *J. Chem. Phys.* 136, 024114 (2012).
7. J. Ma, D. Xu, H. Guo, V. Tyng, and M.E. Kellman, “Isotope effect in normal-to-local transition of acetylene bending modes” *J. Chem. Phys.* 136, 014304 (2012).

# Time-Resolved Optical Diagnostics

Christopher J. Kliewer (PI)  
Combustion Research Facility, Sandia National Laboratories  
P.O. Box 969, MS 9055  
Livermore, CA 94551-0969  
cjkliew@sandia.gov

## Program Scope

This program focuses on the development of innovative laser-based techniques for measuring temperature and concentrations of important combustion species as well as the investigation of fundamental physical and chemical processes that directly affect quantitative application of these techniques. Our development efforts focus on crossed-beam approaches such as time-resolved nonlinear wave-mixing. A critical aspect of our research includes the study of fundamental spectroscopy, energy transfer, and photochemical processes. This aspect of the research is essential to the development of accurate models and quantitative application of techniques to the complex environments encountered in combustion systems. These investigations use custom-built tunable picosecond (ps) and commercial femtosecond lasers, which enable efficient nonlinear excitation, provide high temporal resolution for pump/probe studies of collisional processes, and are amenable to detailed physical models of laser-molecule interactions.

## Recent Progress

***Single-laser-shot in-situ measurements of total collisional broadening:*** Accurate time- and spatially resolved measurement of temperature remains a critical focus of combustion diagnostics. The local temperature field and gradient not only govern chemical reaction rates but also physical quantities such as gas expansion and heat transfer.<sup>A</sup> Coherent anti-Stokes Raman spectroscopy (CARS) has been applied for concentration measurements and ro-vibrational thermometry in gas-phase applications for more than three decades. While CARS has often been held as the gold standard for gas-phase thermometry, practical combustion environments lead to greater uncertainty in the interpretation of CARS signals for a variety of reasons. In pure-rotational CARS (RCARS), S-branch transitions are coherently excited in molecules of interest by the difference frequency between photons in pump and Stokes laser pulses. A probe pulse scatters from these coherences to create the signal, which may be spectrally dispersed to form a rotational spectrum of the probed molecules. By fitting theoretically calculated spectra to an experimental spectrum, the gas-phase temperature can be estimated, as the relative line intensities are highly temperature dependent. The temperature sensitivity of the CARS line intensities mainly originates from the thermal population of ro-vibrational levels in a Boltzmann distribution. But the line-intensities are also quite dependent on the rotational-level-specific collisional broadening coefficients. In nanosecond CARS, for example, signal from a resonant transition scales as  $1/(\Gamma_{J''})^2$ , where  $\Gamma_{J''}$  is the Raman linewidth.

We developed and applied a novel capability, enabling direct time-domain measurement of S-branch collisional broadening coefficients and accurate analysis of CARS spectra even when broadening is not known a priori. In these experiments, rotational coherences are excited by either a ps broadband dye laser or transform-limited fs excitation pulses. The coherence is allowed to collisionally dephase for some time delay, and then a ps probe beam scatters from the manifold of excited rotational coherences and a frequency-resolved spectrum is recorded as a function of probe delay time. By monitoring the exponential decrease in the dispersed CARS signal as a function of probe delay, the  $J$ -dependent decay time constants,  $\tau_{CARS,J''}$ , are extracted. The Raman Lorentzian linewidth (FWHM) is given by:

$$\Gamma_{J''} = (2\pi c \tau_{CARS,J''})^{-1} \quad (1)$$

where  $c$  is the speed of light (cm/s),  $\tau_{CARS,J''}$  is the exponential decay time constant for the coherence decay (s), and  $\Gamma_{J''}$  is the Raman linewidth (FWHM,  $\text{cm}^{-1}$ ). In the previous year, we showed that this technique for the determination of Raman broadening coefficients is accurate and reported a

complete data set of self-broadening coefficients for  $N_2$  from 295-1500K as well as the  $N_2$ - $H_2$  broadening coefficient from 295-1500K up to  $J''=44$ .<sup>4,5</sup> While the presented technique yields highly accurate broadening coefficients, it is not a single-laser-shot technique as the experiment requires that the probe delay be set to a range of different values to monitor the coherence decay. Single-laser-shot measurements are important for the analysis of unsteady flows and turbulent combustion where the relative concentration of species in the probe volume changes rapidly.

We recently developed a single-laser shot implementation of this technique for the accurate determination of total broadening coefficients in-situ. The CARS probe beam is separated into four separate beams and each of the four probe beams is sent to a mechanical delay stage so that the relative timing can be adjusted. Figure 1a displays the experimental arrangement of beams leading up to the probe volume. Because each of the four probe beams comes to the CARS probe volume with differing folded BOXCARS angles, there is a vertical separation between the signal beams arising from each probe. This allows for the separation of the four signals on the vertical dimension of a CCD and the time delay between probes allows for the time-domain mapping of the coherence dephasing. Figure 1b compares the evaluated single-shot determination of  $N_2$  Raman broadening coefficients for three of the rotational lines in the spectrum to those reported in the literature using high resolution techniques, and excellent accuracy and precision is shown for the technique.

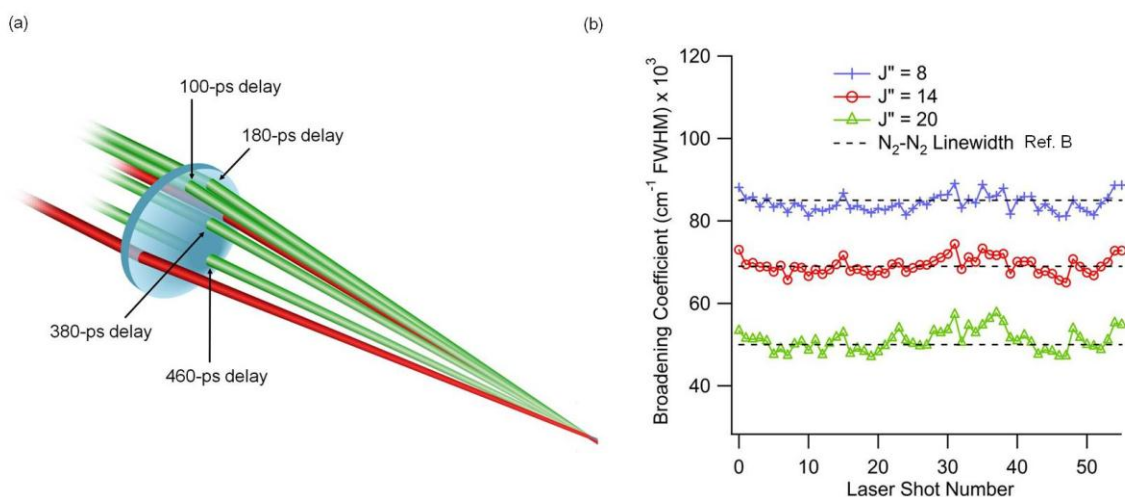
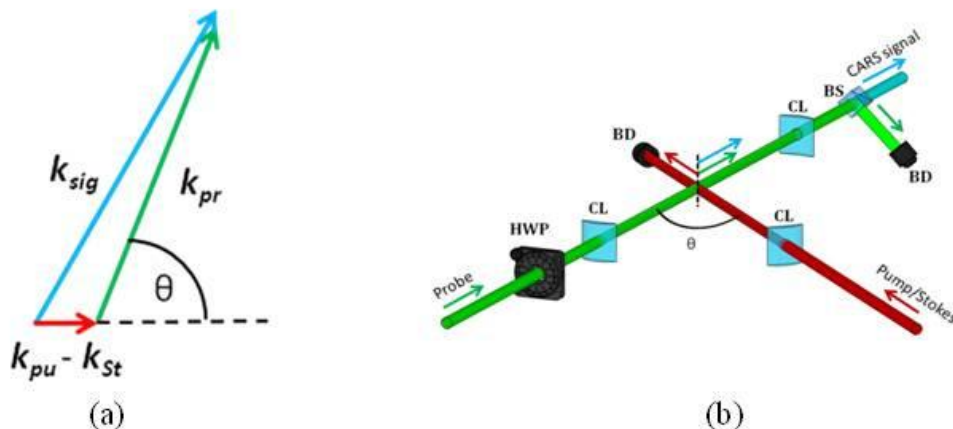


Figure 1. Panel (a) displays the experimental arrangement of laser beams leading to the probe volume where the beams cross for single-shot determination of Raman broadening coefficients. Panel (b) shows evaluated single-shot measurements of the total Raman broadening coefficient as compared with literature values (dashed line, Ref. B). As is shown, good accuracy and single-shot precision is obtained using this single-shot method.

**Two-beam CARS:** We have discovered a new phase matching scheme for rotational CARS that significantly simplifies the way the technique has been done for over 30 years, and opens up several new research directions for probing turbulent combustion environments, probing with extremely high spatial resolution, and for 2-dimensional spectrally resolved CARS plane imaging.<sup>7</sup> The scheme is depicted in Figure 2. Two laser beams, one broadband and one narrowband, are crossed at arbitrary angle, and the generated rotational CARS signal, co-propagating with the probe beam, is isolated using a polarization gating technique. Both pump and Stokes photons originate from the broadband excitation beam. The intrinsic overlap in time of the pump and Stokes photons is a large advantage when using transform-limited fs pulses to efficiently drive the rotational transitions. Such pulses can be difficult to otherwise keep overlapped in time given small temperature fluctuations in the lab. The probe beam crosses at an angle  $\theta$  to the combined pump/Stokes beam. The angle of intersection between the beams can be varied from the small angles typical of the BOXCARS scheme to orthogonal crossing. However, crossing angles greater than  $45^\circ$  overly restrict the phase-matched

excitation bandwidth for application to combustion diagnostics, where rotational transitions up to  $\sim 350$   $\text{cm}^{-1}$  should be acquired.



**Figure 2.** (a) The novel phase-matching scheme displayed as a function of intersection angle. (b) Actual experimental arrangement. HWP: half-wave plate, CL: cylindrical lens, BD: beam dump, BS: polarizing beam splitter cube.

## Future Work

**Two-beam CARS development for turbulent combustion applications.** Because both pump and Stokes photons are derived from the same pulse, they are automatically overlapped in both space and time. This intrinsic spatial overlap makes the technique more amenable towards turbulent environments than standard CARS. For instance, if the technique is implemented in a 1D geometry, both laser beams are focused to sheets using cylindrical lenses and crossed in the probed region. Even in a turbulent environment with some beam steering acting on the beams, the sheets will generally still cross and form a signal, which copropagates with the probe. In some of our initial data taken over a turbulent combusting flow of methane impinging on a steel wall, the signal stability in the two-beam CARS geometry was significantly improved when compared to the standard three-beam geometry. The frequency of laser shots where the signal disappeared as observed in the three-beam case was dramatically reduced in the two-beam scheme. This indicates that this new phase-matching scheme may make rotational CARS a more robust diagnostic for probing turbulent combustion.

**2-dimensional coherent Raman scattering: CARS plane imaging.** The two-beam rotational CARS scheme described above opens the possibility for the first time for generating a two-dimensional rotational CARS signal within a single laser shot. Such spatially correlated single-shot data could provide significant datasets and scientific insight for comparison to turbulent combustion models. For instance, at conditions far from extinction, the thermal mixing field is typically proportional to the scalar dissipation rate.<sup>A</sup> In order to perform frequency-resolved 2D rotational CARS measurements, the probe beam (Fig. 2) remains unfocused and crosses the excitation beam sheet at a large angle, such as  $33^\circ$ . This arrangement provides high spatial resolution (less than  $70 \mu\text{m}$  in the longest probe volume dimension) as well as adequate phase-matched excitation bandwidth ( $> 350 \text{ cm}^{-1}$ ) to cover the  $\text{N}_2$  S-branch. To detect the signal, a new spectrometer needs to be implemented. In a preliminary demonstration, we relay imaged the 2D CARS signal generation plane through a transmission grating to the face of a CCD, producing the 2D image shown in Fig. 3. In this case, the sample was simply  $\text{N}_2$  at 295K. This represents the first ever 2-dimensional rotational CARS measurement. As shown in the bottom of Fig. 3, to analyze such a CCD image, the intensity at a given point within the image of each rotational line is used to construct an intensity spectrum corresponding to a point in the imaged 2D signal generation plane, and this intensity spectrum may be fitted for rotational temperature. We propose to further develop the technique of 2D rotational CARS measurements. Further work must be

done to characterize the current detection scheme and the accuracy obtained by fitting such intensity spectra. A challenge in analyzing such data will be the careful calibration of the dispersion of the system and vectorization to each point of a  $J$ -specific image (Fig. 3, bottom). In the current implementation, the slit function and the line-spread function were both evaluated to be 1-2 pixels, but a model for analyzing the data will need to be developed which takes into account both the slit function and line-spread function in the horizontal dimension of the image. New 2D frequency resolved detection possibilities will be explored. The realization of signal levels high enough to permit 2D CARS measurements in a flame on a single-shot basis requires the use of our high energy fs laser for the pump/Stokes beam, and a time-synchronized ps laser system to provide the probe.

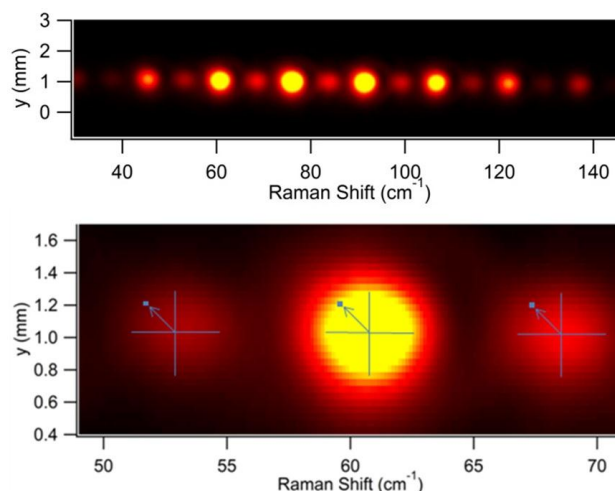


**Figure 3.** (Top) CCD image of the two-beam 2D rotational CARS signal of  $N_2$  at room temperature in a single laser shot. (Bottom) Point-wise analysis of the 2D image produces a rotational CARS spectrum at each point in the probe volume plane.

## References

- A. Patton, R. A.; Gabet, K. N.; Jiang, N.; Lempert, W. R.; Sutton, J. A., *Appl. Phys. B* **2012**, *108* (2), 377-392.  
 B. Koszykowski, M.L.; Rahn, L.A.; Palmer, R.E.; Coltrin, M.E., *J. Chem. Phys.* **91**, 41–46 (1987).

## Publications and submitted journal articles supported by this BES project (2011-present)

1. Kliewer, C. J.; Gao, Y.; Seeger, T.; Kiefer, J.; Patterson, B. D.; Settersten, T. B., Picosecond time-resolved pure-rotational coherent anti-Stokes Raman spectroscopy in sooting flames. *Proceedings of the Combustion Institute* **2011**, *33*, 831-838.
2. Kliewer, C. J.; Gao, Y.; Seeger, T.; Patterson, B. D.; Farrow, R. L.; Settersten, T. B., Quantitative one-dimensional imaging using picosecond dual-broadband pure-rotational coherent anti-Stokes Raman spectroscopy. *Applied Optics* **2011**, *50* (12), 1770-1778.
3. Kliewer, C. J., High-spatial-resolution one-dimensional rotational coherent anti-Stokes Raman spectroscopy imaging using counterpropagating beams. *Optics Letters* **2012**, *37* (2), 229-231.
4. Bohlin, A.; Nordstrom, E.; Patterson, B. D.; Bengtsson, P.-E.; Kliewer, C. J., Direct measurement of S-branch  $N_2$ - $H_2$  Raman linewidths using time-resolved pure rotational coherent anti-Stokes Raman spectroscopy. *The Journal of Chemical Physics* **2012**, *137* (7), 074302.
5. Kliewer, C. J.; Bohlin, A.; Nordstrom, E.; Patterson, B. D.; Bengtsson, P. E.; Settersten, T. B., Time-domain measurements of S-branch  $N_2$ - $N_2$  Raman linewidths using picosecond pure rotational coherent anti-Stokes Raman spectroscopy. *Appl. Phys. B-Lasers Opt.* **2012**, *108* (2), 419-426.
6. Gao, Y.; Bohlin, A.; Seeger, T.; Bengtsson, P.-E.; Kliewer, C. J., In situ determination of  $N_2$  broadening coefficients in flames for rotational CARS thermometry. *Proceedings of the Combustion Institute* **2013**, *34* (2), 3637-3644.
7. Bohlin, A.; Patterson, B.D.; Kliewer, C.J., Simplified two-beam rotational CARS signal generation demonstrated in 1D. *Journal of Chemical Physics* **2013**, *138*, 081102.
8. Kliewer, C.J.; Gao, Y.; Patterson, B.D., Split-probe rotational CARS for single-shot determination of broadening coefficients. *Optics Letters*, submitted

## THEORETICAL CHEMICAL KINETICS

Stephen J. Klippenstein  
Chemical Sciences and Engineering Division  
Argonne National Laboratory  
Argonne, IL, 60439  
[sjk@anl.gov](mailto:sjk@anl.gov)

### Program Scope

The focus of this program is the theoretical estimation of the kinetics of elementary reactions of importance in combustion chemistry. The research involves a combination of *ab initio* electronic structure calculations, variational transition state theory (TST), classical trajectory simulations, and master equation calculations. We apply these methods to reactions of importance in various aspects of combustion chemistry including (i) polycyclic aromatic hydrocarbon (PAH) formation, (ii) hydrocarbon oxidation, and (iii) NO<sub>x</sub> chemistry. The specific reactions studied are generally motivated by our interactions with combustion modeling efforts. We are also interested in a detailed understanding of the limits of validity of and, where feasible, improvements in the accuracy of specific implementations of transition state theory. Detailed comparisons with experiment and with other theoretical methods are used to explore and improve the predictive properties of the transition state theory models. Dynamics simulations are performed as a means for testing the statistical assumptions, for exploring reaction mechanisms, and for generating theoretical estimates where statistical predictions are clearly inadequate. Master equation simulations are used to study the pressure dependence of the kinetics and to obtain phenomenological rate coefficients for use in kinetic modeling.

### Recent Progress

#### *Reaction of <sup>1</sup>CH<sub>2</sub> with Unsaturated Hydrocarbons*

The addition of singlet methylene (<sup>1</sup>CH<sub>2</sub>) to unsaturated hydrocarbons is an important class of reactions in combustion chemistry as they play a key role in the formation and growth of polycyclic aromatic hydrocarbons (PAH). For example, the addition to acetylene is generally the dominant path to formation of propargyl radical, whose self-recombination in turn is most often the dominant route to formation of benzene. Meanwhile, the addition to benzene radical yields toluene and or benzyl radicals, which are also key cyclic intermediates.

In collaboration with Polino (Milan) and Harding, we have studied the <sup>1</sup>CH<sub>2</sub> addition kinetics for a wide variety of unsaturated hydrocarbons including acetylene, ethylene, propene, propyne, allene, butene, butadiene, 2-butyne, tetramethyl-ethylene, and benzene. We find two important pathways for these reactions: addition across the π-bond to yield 3-membered cyclic compounds and insertion into a CH bond to yield CH<sub>3</sub> substituents. The cyclic addition is predicted to generally be the dominant pathway, although the insertion pathway becomes increasingly important with increasing molecular size due in part to the increased number of CH bonds available for insertion.

Our kinetic analysis accounts for the presence and interplay between the multiple transition states for the different regions using the formalism developed as part of our recent statistical theory analysis for roaming radical reactions. A long-range transition state accounts for

the formation of an entropically bound van der Waals complex. Two physically distinct inner transition states account for the formation of either the cyclic addition complex or alternatively the insertion product. Our direct CASPT2 variable reaction coordinate transition state theory approach is used to predict the transition state fluxes for the long-range transition state and for the inner transition state that correlates with the cyclic addition products. Meanwhile, the insertion transition state is treated with reaction path methods. The reaction paths for both the cyclic addition and insertion paths are studied with basis set extrapolated CCSD(T) calculations.

The predicted rate coefficient for the addition to acetylene is illustrated in Fig. 1, where the agreement with experiment is seen to be excellent. In contrast, prior theoretical studies had failed to reproduce the observed decline in the rate coefficient with increasing temperature. For this reaction, the contribution from the insertion channel is minor.

The predicted rate coefficient for the addition to benzene is illustrated in Fig. 2, where the agreement with experiment is again seen to be excellent. In this case, the cyclic addition and insertion paths contribute more or less equivalently to the rate. This is partly due to the need to break the benzene  $\pi$ -resonances during the formation of the cyclic addition complex.

Overall, it appears that our theoretical approach yields quantitatively accurate predictions for the addition kinetics and can be used with confidence to predict the kinetics of related reactions.

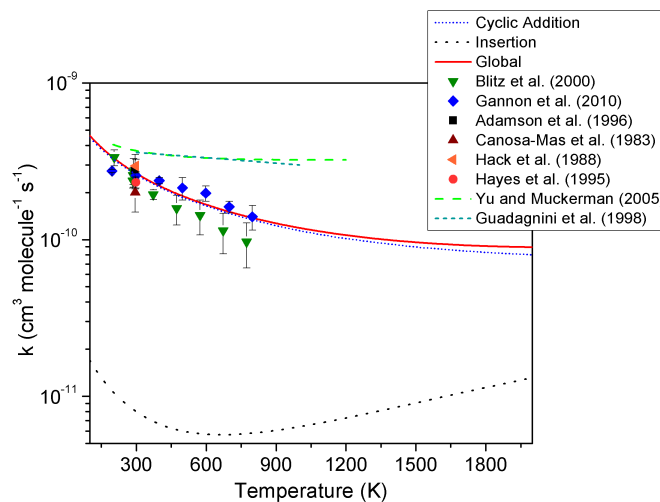


**Fig. 1:** Plot of the  $^1\text{CH}_2 + \text{C}_2\text{H}_2$  rate coefficient.

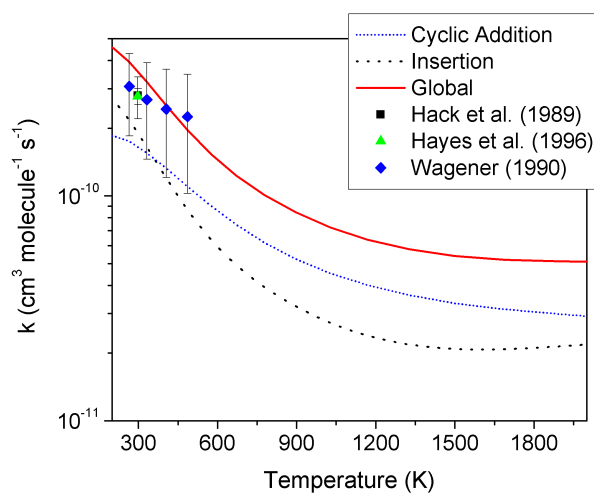


**Fig. 2:** Plot of the  $^1\text{CH}_2 + \text{C}_6\text{H}_6$  rate coefficient.

### High Level *Ab Initio* Thermochemistry and Kinetics

Recent work in a number of groups has demonstrated the feasibility of obtaining *ab initio* predictions for the heat of formation with accuracies on the order of 0.1 kcal/mol. The various methods (e.g., the Wn method of Martin, the HEAT method of Stanton, the focal point method of Allen) rely on the addition of a number of corrections to reference CCSD(T)/CBS energies. We have begun to explore the broad applicability of these methods to combustion thermochemical kinetics.

As a first step, we are collaborating with Allen (Georgia) on a study of the reaction of H

with  $\text{H}_2\text{O}_2$ . This reaction, which can yield either  $\text{H}_2 + \text{HO}_2$  or  $\text{H}_2\text{O} + \text{OH}$ , is found to be significant in  $\text{H}_2/\text{O}_2$  combustion models. A high level focal point analysis, including a detailed study of anharmonic effects, is yielding predictions with greatly reduced uncertainties.

In a separate large scale effort, we are collaborating with Ruscic and Harding in a comparison of high level predictions with a large set of high accuracy values from the active thermochemical tables (ATcT) approach. Using  $\text{H}_2$ ,  $\text{CH}_4$ ,  $\text{H}_2\text{O}$ , and  $\text{NH}_3$  as reference species we have generated *ab initio* values for the majority of hydrocarbon combustion relevant three heavy atom species, as well as a number of four and five heavy atom species. The analysis indicates that the CCSDT(Q), core-valence, and anharmonicity correction are each quite significant with average corrections of about -0.5, 0.5, and 0.5 kcal/mol, respectively. The CCSDT(Q) correction has the greatest variance, and this variance is expected to be even larger for transition states where the chemical bonding is often more multi-reference in nature. Interestingly, the anharmonicity correction, which is the most poorly determined parameter in our and other works, correlates quite closely with the number of  $\text{H}_2$  molecules in the reference thermochemical system. The diagonal Born-Oppenheimer (DBOC) and relativistic corrections are of only minor significance, with average values of 0.1 and -0.1 kcal/mol, respectively. However, in a few instances the DBOC is much larger and very sensitive to electronic structure method, which appears to indicate the presence of a nearby conical intersection.

The predicted 0 K heats of formation are generally within 0.2 kcal/mol of the ATcT values. Larger deviations suggest the need for further theoretical and/or experimental study. The particular scheme we employed in this analysis was designed to be readily applicable to systems with up to five heavy atoms, which allows for the study of a large array of prototype combustion reactions. We are now in the process of employing this approach in *ab initio* transition state theory studies of the kinetics for a number of systems. Preliminary results suggest, via comparison with experimental data, that predicted saddle point energies are similarly accurate. Notably, this then implies that the uncertainties in our kinetics predictions are now largely due to other aspects of the calculations.

## Future Directions

One focus of our continuing work involves the implementation of the abovedescribed high accuracy thermochemical methods in predicting the kinetics of a number of key reactions in the core combustion mechanism for small hydrocarbons. We also continue to explore methods for reducing the uncertainties in other aspects of the calculations and improving the efficacy of our analyses. These efforts will include advanced treatment of the torsional mode contributions via path integral methods coupled to large-scale potential samplings and novel tunneling treatments focussing on local expansions of the potential energy surface about the saddle point.

## DOE Supported Publications, 2011-Present

1. **Roaming Radicals in the Thermal Decomposition of Dimethyl Ether: Experiment and Theory**, R. Sivaramakrishnan, J. V. Michael, A. F. Wagner, R. Dawes, A. W. Jasper, L. B. Harding, Y. Georgievskii, and S. J. Klippenstein, *Comb. Flame*, **158**, 618-632 (2011).
2. **The Role of NNH in NO Formation and Control**, S. J. Klippenstein, L. B. Harding, P. Glarborg, and J. A. Miller, *Comb. Flame*, **158**, 774-789 (2011).

3. **Near-Threshold H/D Exchange in CD<sub>3</sub>CHO Photodissociation** B. R. Heazlewood, A. T. Maccarone, D. U. Andrews, D. L. Osborn, L. B. Harding, S. J. Klippenstein, M. J. T. Jordan, and S. H. Kable, *Nature Chem.*, **3**, 443-448 (2011).
4. **Insights into the Role of PAH Condensation in Haze Formation in Jupiter's Atmosphere**, L. Biennier, H. Sabbah, V. Chandrasekaran, S. J. Klippenstein, I. R. Sims, and B. R. Rowe, *Astronomy and Astrophysics*, **532**, A40, 10.1051, (2011).
5. **Long-Range Interaction Potential of Open Shell Atoms with Neutral Molecules: Application to the Calculation of the Rate Constant for the C<sub>2</sub>H + O(<sup>3</sup>P) Reaction** Y. Georgievskii and S. J. Klippenstein *IAU Symp. 280 (The Molecular Universe), Proceedings*, Eds. J. Cernicharo and R. Bachiller, doi:10.1017/S1743921311025129 (2011).
6. **Combustion Chemistry: Important Features of the C<sub>3</sub>H<sub>5</sub> Potential Energy Surface, Including Allyl Radical, Propargyl + H<sub>2</sub>, Allene + H, and Eight Transition States** B. S. Narendrapurapu, A. C. Simmonett, H. F. Schaefer III, J. A. Miller, and S. J. Klippenstein, *J. Phys. Chem. A*, **115**, 14209-14214 (2011).
7. **Statistical Theory for the Kinetics and Dynamics of Roaming Reactions** S. J. Klippenstein, Y. Georgievskii, and L. B. Harding, *J. Phys. Chem. A*, **115**, 14370-14381 (2011).
8. **Uncertainty Driven Theoretical Kinetics Studies for CH<sub>3</sub>OH Ignition: HO<sub>2</sub> + CH<sub>3</sub>OH and O<sub>2</sub> + CH<sub>3</sub>OH**, S. J. Klippenstein, L. B. Harding, M. J. Davis, A. S. Tomlin, and R. T. Skodje, *Proc. Comb. Inst.*, **33**, 351-357 (2011).
9. **Ab Initio Kinetics for the Decomposition of Monomethylhydrazine (CH<sub>3</sub>NHNH<sub>2</sub>)**, P. Zhang, S. J. Klippenstein, H. Sun, and C. K. Law, *Proc. Comb. Inst.*, **33**, 425-432 (2011).
10. **Rapid Association Reactions at Low Pressure: Impact on the Formation of Hydrocarbons on Titan**, V. Vuitton, R. V. Yelle, P. Lavvas, and S. J. Klippenstein, *Astrophys. J.*, **744**, 11:1-7 (2012).
11. **Exploring Formation Pathways of Aromatic Compounds in Laboratory-Based Model Flames of Aliphatic Fuels**, N. Hansen, J. A. Miller, S. J. Klippenstein, P. R. Westmoreland, and K. Kohse-Hoinghaus, *Combust. Expl. and Shockwaves*, **48**, 508-515 (2012).
12. **Comment on "Automatic Estimation of Pressure-Dependent Rate Coefficients"**, J. A. Miller, S. J. Klippenstein, *Phys. Chem. Chem. Phys.*, **14**, 8431-8433 (2012).
13. **Separability of Tight and Roaming Pathways to Molecular Decomposition**, L. B. Harding, S. J. Klippenstein, and A. W. Jasper, *J. Phys. Chem. A*, **116**, 6967-6982 (2012).
14. **Comprehensive H<sub>2</sub>/O<sub>2</sub> Kinetic Model for High-Pressure Combustion**, M. P. Burke, M. Chaos, Y.-G. Ju, F. L. Dryer, S. J. Klippenstein, *Int. J. Chem. Kinet.*, **44**, 444-474 (2012).
15. **Interception of Excited Vibrational Quantum States by O<sub>2</sub> in Atmospheric Association Reactions**, D. R. Glowacki, J. Lockhart, M. A. Blitz, S. J. Klippenstein, M. J. Pilling, S. H. Robertson, P. W. Seakins, *Science*, **337**, 1066-1069, (2012).
16. **A Quantitative Explanation for the Apparent Anomalous Temperature Dependence of OH + HO<sub>2</sub> = H<sub>2</sub>O + O<sub>2</sub> through Multi-Scale Modeling**, M. P. Burke, S. J. Klippenstein, L. B. Harding, *Proc. Comb. Inst.*, **34**, 547-555 (2013).

## ARGONNE-SANDIA CONSORTIUM ON HIGH-PRESSURE COMBUSTION CHEMISTRY

Stephen J. Klippenstein (PI), Michael J. Davis, Lawrence B. Harding, Joe V. Michael,  
James A. Miller, Branko Ruscic, Raghu Sivaramakrishnan, Robert S. Tranter  
*Chemical Sciences and Engineering Division, Argonne National Laboratory, Argonne, IL, 60439*  
[sjk@anl.gov](mailto:sjk@anl.gov)

Craig A. Taatjes (PI), Ahren W. Jasper, David L. Osborn, Leonid Sheps, Judit Zádor  
*Combustion Research Facility, Mail Stop 9055, Sandia National Laboratories*  
*Livermore, CA 94551-0969*  
[cataatj@sandia.gov](mailto:cataatj@sandia.gov)

### Program Scope

The goal of this project is to explore the fundamental effects of high pressure on the chemical kinetics of combustion and to use that knowledge in the development of accurate models for combustion chemistry at the high pressures of current and future engines. We design and implement novel experiments, theory, and modeling to probe high-pressure combustion kinetics from elementary reactions, to submechanisms, to flames. The work focuses on integrating modeling, experiment, and theory (MET) through feedback loops at all levels of chemical complexity. We are currently developing and testing the methodology for propane and 1-butanol as key prototype fuels. The consortium expands and enhances collaborations between Argonne's Dynamics in the Gas Phase Group and the Combustion Chemistry Group in Sandia's Combustion Research Facility and also interacts closely with the Princeton-led Combustion Energy Frontier Research Center (CEFRC).

### Recent Progress

#### Experimental Developments

*Experimental studies of propyl oxidation:* During the past year we initiated an extensive experimental investigation of propyl radical oxidation, focusing on direct time-resolved measurement of chemical species concentrations, as shown in Fig. 1, over a broad range of pressures, 0.005 – 20 bar. In the low pressure regime, we used synchrotron photoionization mass spectrometry (PIMS) to probe the main reaction channels, including the formation of propene and oxygenated species  $C_3H_6O$ , along with many minor products and intermediates. Isomer-selective species detection, enabled by the tunable synchrotron ionization radiation, allowed separate measurement of the time-histories for the four different  $C_3H_6O$  products: acetone, propanal, trimethylene oxide, and propylene oxide. In the high pressure regime (up to 10 bar) we probed the kinetics with both PIMS measurements and time-resolved laser-induced fluorescence (LIF) detection of OH radicals.

This extensive experimental dataset forms the basis of ongoing work to develop optimized *ab initio* transition-state-theory master equation based submechanisms for propyl radical oxidation (discussed below). The observed strong temperature dependence of the cyclic ether concentration helps constrain the barrier heights on the calculated potential energy surface. Meanwhile, time-dependent probing of acetone and propanal concentrations indicates that they are primary products of QOOH decomposition. Our data suggest that direct production of carbonyl compounds may be underestimated in current combustion models. Both PIMS and LIF results indicate a sharp increase in the radical yield between 600 and 670 K. Many of the product species show a competition between well-skipping and sequential formation even at the highest pressures we surveyed.

*Combustion chemistry of furan-based species:* In collaboration with R. Fernandes (Aachen) we have begun an investigation of low-temperature autoignition behavior of tetrahydrofuran (THF) and 2-methyl THF – two compounds in a class of recently identified potential biofuels with high energy content and effective means of production from organic feedstocks. We have collected time-resolved LIF and PIMS measurements at pressures

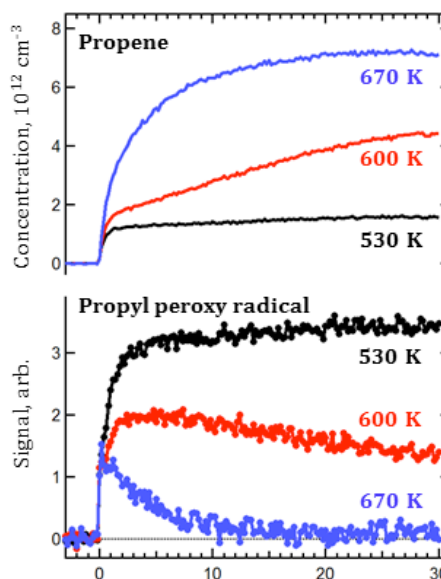


**Fig. 1:** Propyl radical oxidation at 4 Torr: time evolution of propene and propyl peroxy radicals.

from 0.005-20 bar and up to 700 K. These first direct measurements in the low-temperature autoignition range show the presence of chain-terminating HO<sub>2</sub> production, as well as production of cyclic ethers + OH. The photoionization spectra of the products associated with HO<sub>2</sub> formation cannot be explained purely by HO<sub>2</sub> elimination from the parent peroxy radical, which indicates that isomerization (such as furan ring opening) pathways are also active.

**High pressure, miniature high repetition rate shock tube (HRRST):** The HRRST is a unique, miniature shock tube designed to be fired at repetition rates up to 4 Hz and generate reproducible reaction conditions of  $P < 100$  bar

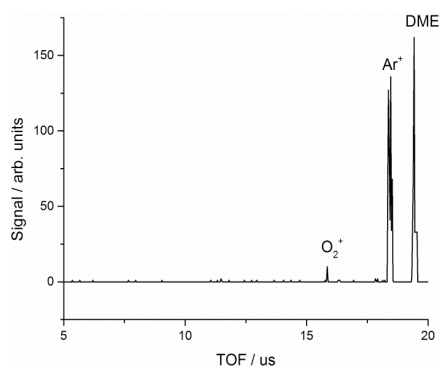


**Fig. 2:** PIMS from a non-reacting mixture of 2% DME/Ar.

and  $600 < T < 3000$  K. A prototype of the HRRST was described in a previous abstract. Based on the results of testing with the prototype, the HRRST was modified to improve shock strength and repeatability. Additionally, a new version was constructed for use in the laboratory and with an existing PIMS apparatus at the Advanced Light Source. Recently, experiments were conducted at the T1 and T3 endstations of the 9.0.2 beamline and a sample mass spectrum is shown in Fig. 2. The mass spectrum is from shocks with 2% dimethyl ether (DME) dilute in argon and is composed of ~400 consecutive, near identical shocks summed together. Under the conditions of these experiments DME did not dissociate. The repeatability of the HRRST is good, but not quite as good as desired and in the future a binning strategy may be employed to obtain the desired error in T5 of <1%. In a separate set of 500 experiments at the T3 endstation, reflected shock, reaction, conditions of  $T5 = 1593 \pm 53$  K and  $P5 = 6754 \pm 367$  Torr, were

obtained, with this P5 likely one of the highest used in a reactor at this beamline.

### Theory Developments

**Energy Transfer:** We have developed a completely *a priori* procedure for predicting the pressure dependence of chemical kinetics. This procedure couples trajectory simulations of the collision induced transition probabilities in  $E$  and  $J$ , with the solution of the two-dimensional master equation, employing state-of-the-art *ab initio* transition state theory predictions for the microcanonical rate coefficients. The  $C_2H_2 + H = C_2H_3$  reaction system has been used to illustrate the approach with comparisons to both room temperature recombination rate measurements and 1000 K dissociation rate measurements. The *a priori* predictions are found to accurately reproduce the full set of experimental data. This case study illustrates the level of agreement that might generally be expected, and also provides a roadmap for future studies of more complex reactions, such as multichannel reactions with competing decomposition processes, where the details of the energy transfer process might be expected to have an even more dramatic effect. For the latter reactions, it is likely that prior model-based master equation calculations have largely yielded a poor representation of the kinetics. A manuscript describing this work is now in preparation.

**Propyl Radical Decomposition:** We have now completed an *ab initio* transition state theory based master equation theoretical study of reactions on the  $C_3H_7$  potential energy surface including a number of dissociation and abstraction reactions. The agreement between our theory and the experimental results available is remarkably good. The final results have been cast in a form that is convenient for chemical kinetics modeling, and which has been incorporated into the chemical kinetic model that we are developing for propane combustion.

### Theory/Experiment Collaborations

**Abstraction Reactions:** We have utilized our detailed chemical kinetics models for simple  $C_3$ - $C_4$  alkanes and  $C_1$ - $C_2$  alcohols to design simple experiments aimed at probing H-atoms (formed as a product in these bimolecular reactions) using the sensitive H-ARAS technique to directly obtain branching ratios for H atom abstractions at high temperatures. As an example, in our recent study on  $C_3H_8$ , we monitored the decay of D-atoms (using  $C_2D_5I$  as a source for D-atoms) with atomic resonance absorption spectrometry (ARAS) to obtain total rate constants for  $D + C_3H_8$ . In our current study, we utilized H-atom ARAS (in similar mixtures of  $C_2D_5I/C_3H_8$ ) to selectively probe abstraction from the secondary site, which is the only source of H-atoms formed at early times in the experiment.

We have also used this methodology to determine rate constants and branching ratios for  $OH + C_3H_8/n-C_4H_{10}/i-C_4H_{10}$ ,  $D + C_3H_8$  and  $D + n-C_4H_{10}/i-C_4H_{10}$ . These reactions were also studied with *ab initio* TST at the CCSD(T)/cc-pv $\infty$ z//M062X/cc-pvtz level of theory. The theoretical rate constants are in good agreement with the present experiments. The present experimental effort represents the first direct measurements at combustion relevant temperatures (>1000 K) for  $D + n-C_4H_{10}/i-C_4H_{10}$ . The same methodology was also applied to mixtures of  $CH_3OH$  and biacetyl (as a source of  $CH_3$  radicals); H-atom formation was monitored to obtain direct determinations for  $CH_3 + CH_3OH$ . The present experimental effort is among a very limited set of unambiguous rate constant measurements for a  $CH_3 +$  molecule reaction at high temperatures.

*Water Elimination Pathway in Peroxy Chemistry:* As described in more detail in Zádor's abstract, we have characterized a low-lying water elimination pathway that involves the interaction of radical and zwitterionic electronic states. These zwitterionic pathways, which appear to be ubiquitous in both alcohol and alkane oxidations, are expected to have a significant impact on current low temperature oxidation mechanisms.

### Modeling Developments

*Multiscale modeling:* We have extended our recently developed multi-scale informatics modeling strategy to treat the much more complex propyl radical oxidation submechanism. In general, the multi-scale model is assembled and informed by a wide variety of targets that include *ab initio* calculations of molecular properties, rate constant measurements of isolated reactions, and complex systems measurements. The current implementation required the treatment of multi-well reactions, the potential for missing reactions, non-statistical product branching ratios, and non-Boltzmann reactant distributions. Optimization variables are chosen to accommodate both "parametric" and "mechanistic" uncertainties. For example, barrier heights of transition states, collisional energy transfer parameters, transition state partition function scaling factors, and other theoretical parameters are included as optimization variables to account for parametric uncertainties in the theoretical treatment; initial temperatures, mixture compositions, absorption cross-sections, and other experimental parameters are included to account for parametric uncertainties in the physical models of the experiments. Additionally, branching ratios among various product channels are included as optimization variables to account for mechanistic uncertainties related to difficulties in modeling sequences of multiple chemically activated steps. RMG software is used to assess potential mechanistic uncertainties due to missing reactions. In this context, multi-scale informatics is employed to 1) extract information from complex systems in the presence of both parametric and mechanistic uncertainties and 2) allow greater utilization of the high information content of ongoing Multiplexed-Synchrotron Photo-Ionization Mass Spectrometry (MPIMS) experiments. Preliminary results in Fig. 3 show that the multi-scale-informed model produced in this way exhibits significant improvements over the *a priori* model and appears to be predictive.

*Comprehensive mechanism:* We have made significant progress towards the development of a rigorous, comprehensive chemical kinetic model for the combustion of propane. Our current model accurately accounts for the complex temperature and pressure dependence exhibited by the rate coefficients of reactions that involve multiple, interconnected potential wells. The source of most of this information is our own theoretical analyses, which necessarily agree with reliable experimental results where they exist. Our model has gone through a number of versions since last year, the most important of which was a merging with the small-alcohol mechanism. We have made comparisons of our model predictions with high-temperature macroscopic experiments, namely flame speeds and ignition delay times. The agreement between the model predictions and experiment for the low-molecular-weight hydrocarbon fuels (methane, ethane, ethylene, acetylene, propene, and propane) is considerably better than we expected. High pressure (at least up to  $\sim 20$  atm) seems not to be a problem. We anticipate having completed a manuscript on this work before the end of the year.

### Future Directions

*HRRST Developments:* The HRRST is currently setup to determine the full range of operating conditions and will be coupled once more to an electron impact TOF-MS for kinetic studies similar to those performed with the full size diaphragmless shock tube. In the near future, additional experiments will be performed at the APS to study jet formation from the nozzle at the end of the HRRST and more experiments are planned at the ALS to investigate chemical kinetics of dimethyl ether pyrolysis and oxidation at engine relevant temperatures and pressures.

*Development of high-pressure (HP)-PIMS:* We plan two major improvements through the design of a new apparatus. First, to suppress heterogeneous chemistry that inevitably occurs on reactor walls, we will optimize the sampling geometry to only probe the core of the reacting flow. In addition, the metal wetted parts of the reactor will be replaced with more chemically inert fused silica, minimizing sample degradation before the reaction chamber. Second, we plan to transfer the ionization region closer to the sampling nozzle (into the area of higher sample density) and use electrostatic optics to guide a large fraction of the resulting ions into the mass spectrometer region. This revision should yield significantly higher signal levels, thereby extending the accessible range of pressures.

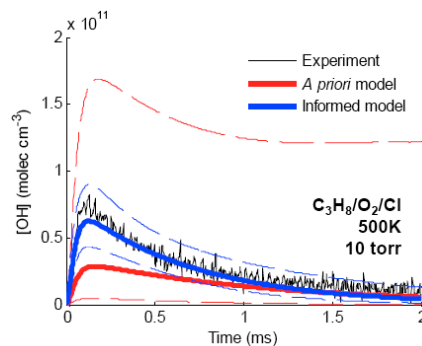


**Fig. 3:** Comparison of the multi-scale model with experimental data that was *not* used as an optimization target. The dashed lines denote the uncertainty in the model predictions.

*Low-temperature autoignition chemistry:* In collaboration with other ongoing projects at Sandia, we will explore the low-temperature alkyl oxidation reactions for longer-chain and branched alkanes, such as methyl cyclohexane. We will continue our current work on butanol and furanic species combustion using both HP-MPIMS and LIF techniques, with an eye on extending the accessible range of experimental conditions to higher pressures. In addition, we plan to investigate the reaction of OH with 2-butene, focusing on the temperature-dependent competition between hydrogen abstraction, addition of OH to the double bond, and back-dissociation of the resulting  $\beta$ -hydroxyalkyl radical adduct in the 600 – 750 K temperature range. The results will be interpreted in the context of a comprehensive model for butanol combustion.

*Theoretical Reaction Kinetics:* Our core mechanism modeling efforts have highlighted a number of reactions of importance for further study. Our modeling of flame speeds identified the reactions  $H + HCO$ ,  $OH + HCO$ ,  $H + C_2H_3$ , and  $H + C_2H_5$  to be worthy of high-level theoretical investigation. The reactions  $C_3H_8 + O_2$ , and  $C_3H_8 + HO_2$ , are of importance to ignition delays. Meanwhile, the low temperature oxidation kinetics is sensitive to the possibility of secondary dissociation, prior to thermalization, for chemically activated reactions. We will also further explore the predictive nature of our coupled energy transfer/two-dimensional master equation approach.

### DOE Supported Publications, 2011-Present

1. **Theoretical Rate Coefficients for Allyl + HO<sub>2</sub> and Allyloxy Decomposition**, C. F. Goldsmith, S. J. Klippenstein, and W. H. Green, *Proc. Comb. Inst.*, **33**, 273-282 (2011).
2. **Role of Peroxy Chemistry in the High Pressure Ignition of n-Butanol - Experiments and Detailed Kinetic Modelling**, S. Vranckx, K. A. Heufer, C. Lee, H. Olivier, L. Schill, W. A. Kopp, K. Leonhard, C. A. Taatjes, and R. X. Fernandes, *Combust. Flame* **158**, 1444-1455 (2011).
3. **Shock Tube and Theoretical Studies on the Thermal Decomposition of Propane: Evidence for a Roaming Radical Channel**, R. Sivaramakrishnan, M.-C. Su, J. V. Michael, S. J. Klippenstein, L. B. Harding, and B. Ruscic, *J. Phys. Chem. A*, **115**, 3366-3379 (2011).
4. **Theoretical Unimolecular Kinetics for CH<sub>4</sub> + M → CH<sub>3</sub> + H + M in Eight Baths, M = He, Ne, Ar, Kr, H<sub>2</sub>, N<sub>2</sub>, CO, and CH<sub>4</sub>**, A. W. Jasper and J. A. Miller, *J. Phys. Chem. A*, **115**, 6438-6455 (2011).
5. **Competing channels in the propene + OH reaction: Experiment and validated modeling over a broad temperature and pressure range**, C. Kappler, J. Zádor, O. Welz, R. X. Fernandes, M. Olzmann, and C. A. Taatjes, *Z. Phys. Chem.* **225**, 1271-1293 (2011).
6. **Pressure Dependent OH Yields in Alkene + HO<sub>2</sub> Reactions: A Theoretical Study**, J. Zádor, S. J. Klippenstein, and J. A. Miller, *J. Phys. Chem. A*, **115**, 10218-10225 (2011).
7. **Combustion Chemistry: Important Features of the C<sub>3</sub>H<sub>5</sub> Potential Energy Surface, Including Allyl Radical, Propargyl + H<sub>2</sub>, Allene + H, and Eight Transition States**, B. S. Narendrapurapu, A. C. Simmonett, H. F. Schaefer, III, J. A. Miller, and S. J. Klippenstein, *J. Phys. Chem. A* **115**, 14209-14214 (2011).
8. **High-Temperature Rate Constants for H/D + C<sub>2</sub>H<sub>6</sub> and C<sub>3</sub>H<sub>8</sub>**, R. Sivaramakrishnan, J. V. Michael, and B. Ruscic, *Int. J. Chem. Kinet.* **44**, 194-205 (2012).
9. **On the Role of O<sub>2</sub> + QOOH in Low-Temperature Ignition of Alkanes I: Temperature and Pressure Dependent Rate Coefficients**, C. F. Goldsmith, W. H. Green, and S. J. Klippenstein, *J. Phys. Chem. A*, **116**, 3325-3346 (2012).
10. **Shock Tube Explorations of Roaming Radical Mechanisms: The Decompositions of Iso-Butane and Neo-Pentane**, R. Sivaramakrishnan, J. V. Michael, L. B. Harding, and S. J. Klippenstein, *J. Phys. Chem. A*, **116**, 5981-5989 (2012).
11. **Exploring Formation Pathways of Aromatic Compounds in Laboratory-Based Model Flames of Aliphatic Fuels**, N. Hansen, J. A. Miller, S. J. Klippenstein, P. R. Westmoreland, and K. Kohse-Höinghaus, *Combustion, Explosions, and Shock Waves* **48**, 508-515 (2012).
12. **Comment on ‘Automatic estimation of pressure-dependent rate coefficients’** (J.W. Allen, C. F. Goldsmith, and W. H. Green, *Phys. Chem. Chem. Phys.*, 2011, **14**, 1131-1155), J. A. Miller and S. J. Klippenstein, *Phys. Chem. Chem. Phys.* **14**, 8431-8433 (2012).
13. **Uncertainty Propagation in the Derivation of Phenomenological Rate Coefficients from Theory: A Case Study of Propyl Radical Oxidation**, C. F. Goldsmith, A. S. Tomlin, and S. J. Klippenstein, *Proc. Comb. Inst.*, **34**, 177-185 (2013).
14. **Unimolecular Dissociation of Hydroxypropyl and Propoxy Radicals**, J. Zádor and J. A. Miller, *Proc. Comb. Inst.* **34**, 519-526 (2013).
15. **Studies of Laminar Opposed-Flow Diffusion Flames of Acetylene at Low Pressures with Photoionization Mass Spectrometry**, S. A. Skeen, B. Yang, H. A. Michelsen, J. A. Miller, A. Violi, N. Hansen, *Proc. Comb. Inst.* **34**, 1067-1075 (2013).
16. **Unconventional Peroxy Chemistry in Alcohol Oxidation – The Water Elimination Pathway**, O. Welz, S. J. Klippenstein, L. B. Harding, C. A. Taatjes, and J. Zádor, *J. Phys. Chem. Lett.*, **4**, 350-354 (2013).
17. **Determining Phenomenological Rate Coefficients from a Time-Dependent, Multiple-Well Master Equation: “Species Reductions” at High Temperatures**, J. A. Miller and S. J. Klippenstein, *Phys. Chem. Chem. Phys.*, *in press* (2013).
18. **The Dissociation of Propyl Radicals and Other Reactions on a C<sub>3</sub>H<sub>7</sub> Potential**, J. A. Miller and S. J. Klippenstein, *J. Phys. Chem. A*, *in press* (2013).

# Theoretical modeling of spin-forbidden channels in combustion reactions

Anna I. Krylov

Department of Chemistry, University of Southern California,  
Los Angeles, CA 90089-0482  
krylov@usc.edu

## 1 Scope of the project

The goal of our research is to develop predictive theoretical methods, which can provide crucial quantitative data (e.g., rate constants, branching ratios, heats of formation), identify new channels and refine reaction mechanisms. Specifically, we are developing tools for computational studies of spin-forbidden and non-adiabatic pathways of reactions relevant to combustion, and applying these tools to study electronic structure, reactions, and spectroscopy of open-shell and electronically excited species involved in these processes.

## 2 Summary of recent major accomplishments

During the past year, we conducted several computational studies of open-shell and electronically excited species. The common theme in these studies is interactions between states of different character and intersections between the corresponding potential energy surfaces. We also continued to develop and benchmark computational methods for modeling electronic structure and spectroscopy of open-shell species. Particular emphasis was placed on determining spectroscopic signatures of transient species, to facilitate comparisons with experimental data. In particular, we have been motivated by photoionization and photodetachment experiments that are broadly used in the combustion community, e.g., photoionization is used as a tool to identify transient reaction intermediates in combustion processes, whereas photodetachment is often employed to create radicals implicated in combustion in order to study their properties and spectroscopic signatures. Interpretation of the photoionization/photodetachment measurements requires information about ionization/detachment energies, cross-sections, and Franck-Condon factors of different species.

In 2012-2013, the DOE support has been acknowledged in two papers;<sup>1,2</sup> one paper is under review,<sup>3</sup> and two more — in final stages of preparation. Some of the recent results are highlighted below.

## 2.1 Ionization-induced proton transfer in microsolvated clusters

Excited-state proton transfer (PT) is ubiquitous in chemistry, materials, and biology. Ionization also increases proton-donating ability of molecules facilitating PT in ionized clusters. Protonated species are commonly observed in molecular beam experiments that are using VUV ionization as a probe, such as experiments at Advanced Light Source at LBNL. In collaboration with Dr. M. Ahmed, we found that water has dramatic effect on PT in ionized species. We investigated this phenomenon in methylated uracil (mU) clusters; however, similar trends were observed in other microhydrated species. We found that microsolvation changes the branching ratio between different relaxation channels and entirely shuts down PT between the mU fragments. Instead, a new pathway opens up in which protonated nucleobases are produced by PT from the ionized water molecule and elimination of the hydroxyl radical. Electronic structure calculations reveal that the shape of the potential energy profile along the PT coordinate depends strongly on the character of molecular orbital from which electron is removed, i.e., the PT from water to mU becomes barrierless when an ionized state localized on water is accessed (see Fig. 1). The computed energetics of PT is in excellent agreement with the experimental appearance energies. We also note that possible adiabatic process, which becomes energetically accessible at lower energies, is not efficient. Thus, in this system PT is controlled electronically, by the character of the ionized state, rather than statistically, by simple energy considerations.

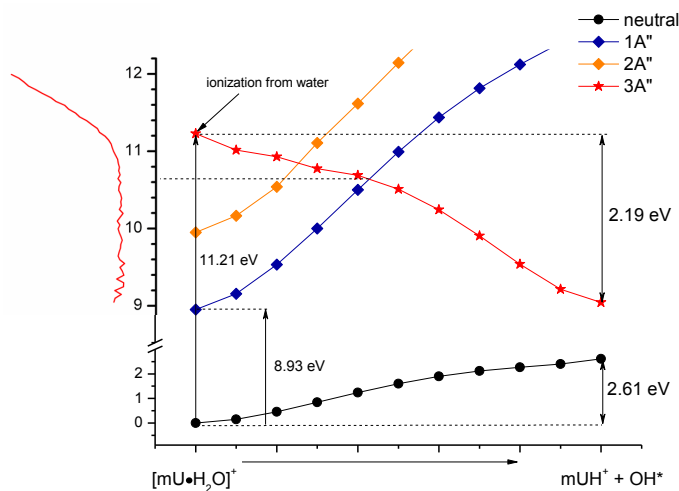


Figure 1: Potential energy profiles for low-lying states of  $mU-H_2O^+$  along the PT reaction coordinate. The proton is moved from the water molecule to the mU oxygen site. The 5th ionized state,  $3A''$ , in which the hole is located on the water molecule, shows no barrier facilitating downhill PT. PT from lower ionized states is possible, but involves changes in electronic wave function character and requires more than 10.2 eV photon energy. The left panel shows the experimental ratio between the  $[mU(D_2O)_2]^+$  and  $[mU(D_2O)_2D]^+$  signals; it shows dramatic enhancement in PT when the  $3A''$  state is accessed.

## 2.2 Modeling photodetachment spectra

Calculations of photoionization/photodetachment energies and photoelectron spectra is instrumental for interpretation of experimental studies that are using photoionization as a diagnostic tool. This study was motivated by the discrepancies between three experimental studies aiming to measure photodetachment spectrum and detachment energy of HBDI. We first performed careful benchmarking of a smaller system, phenolate anion, and found that theory can accurately reproduce both energetics and the spectrum (see Fig. 2). The important results are: (i) DFT using  $\omega$ B97X-D functional agrees well with coupled-cluster and

equation-of-motion methods; (ii) both diffuse functions and high level of polarization are important, for example, Dunning basis sets are superior to similar quality Pople basis sets, i.e., the aug-cc-pVTZ and 6-311+,+G\*\* results differ by 0.3 eV; (iii) the maximum in the spectrum corresponds to the 00 transition — therefore, the computed vertical detachment energy differs considerably from the spectrum maximum. The computed and experimental 00 transitions differ by 0.06 eV. The computed spectrum of HBDI has the same feature — the most intense transition is 00; thus, the computed vertical detachment energy should not be compared with the experimental maximum. Our calculations of HBDI suggested a possible cause of the discrepancies between different experiments.

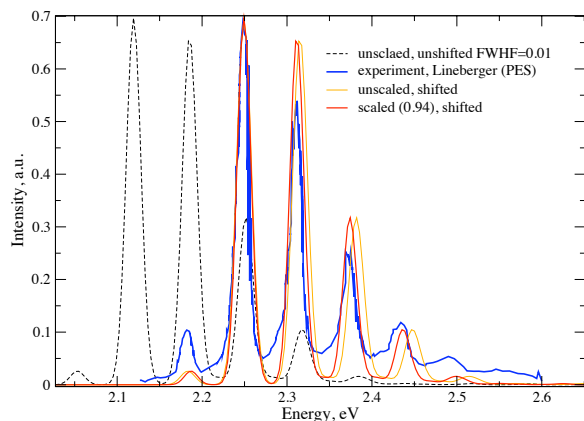


Figure 2: Comparison of the computed ( $\omega$ B97X-D/aug-cc-pVTZ) and experimental photoelectron spectrum of phenolate. The computed spectrum is shifted by +0.06 eV to match the experimental 00 transition. The  $\omega$ B97X-D/aug-cc-pVTZ value of detachment energy is within 0.05 eV from the CCSD(T) and EOM-IP-CCSD results.

## 2.3 Benchmarking of non-collinear SF-TDDFT

Many of the so-called “multi-reference” situations, which are common in molecules with stretched bonds and unpaired electrons, can be efficiently described by robust and efficient single-reference approaches based on equation-of-motion or linear response formalisms. In particular, electronic states of polyradicals can be described as spin-flipping excitation from well-behaved high-spin reference states, which is exploited in the spin-flip (SF) approach.

When implemented within DFT, the SF method extends DFT to systems with extensive electronic degeneracies, such as diradicals, triradicals, and even transition metals. We implemented<sup>1</sup> a general non-collinear variant of SF-TDDFT, which improved the accuracy of original (collinear) SF-TDDFT. The initial study<sup>1</sup> focused on energy gaps in a variety of organic diradicals and open-shell atoms (41 energy gaps). Recently, we extended our benchmark studies to species containing transition metals, such as organometallic molecules considered as building blocks for molecular magnets. We find that SF-TDDFT performs consistently well for this extended set and reproduces small energy gaps ranging from 0 to 800  $\text{cm}^{-1}$ . As in the case of purely organic molecules, B5050LYP and PBE50 show the best performance. Currently, we are investigating the effect of ECP on the overall performance (Fig. 3).

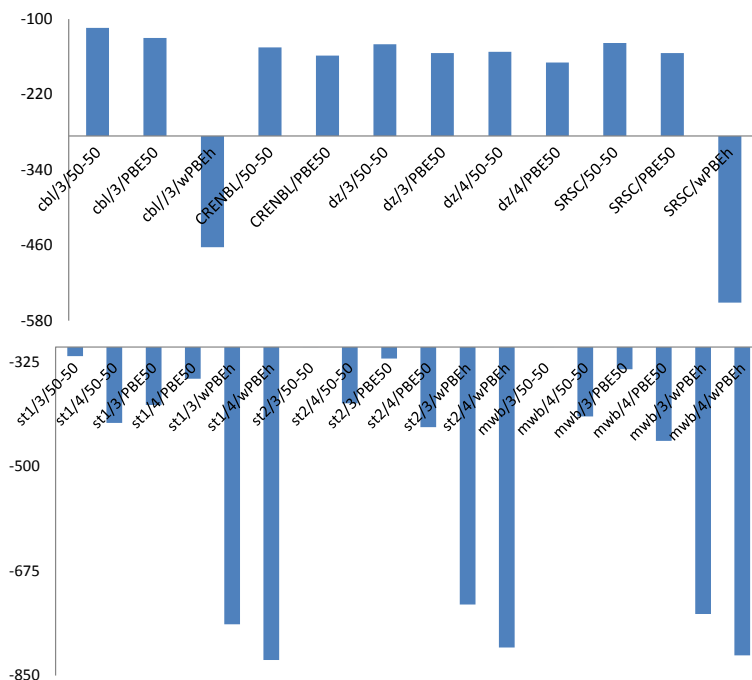
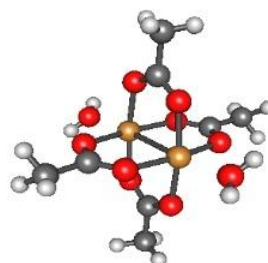


Figure 3: Singlet-triplet gaps ( $\text{cm}^{-1}$ ) in a di-copper compound (shown below). The experimental value is  $-286 \text{ cm}^{-1}$ . We observe that using triple-zeta quality basis set on light atoms (denoted by 3) is important. Furthermore, Stuttgart's ECPs (lower panel) perform better than LANL2Z, CRENBL, and SRSC (upper panel). B5050LYP and PBE50 show the best performance for this and seven other copper-containing complexes that we considered so far.



### 3 Current developments and future plans

Currently, we are pursuing modeling of electronic structure and dynamics of several radicals relevant to combustion. We are working on improving numeric stability of analytic gradients for non-collinear SF-TDDFT. We are also working on improving our Dyson orbital formalism for quantitative calculations of photoionization cross sections.

### References

- [1] Y.A. Bernard, Y. Shao, and A.I. Krylov, General formulation of spin-flip time-dependent density functional theory using non-collinear kernels: Theory, implementation, and benchmarks, *J. Chem. Phys.* **136**, 204103 (2012).
- [2] T. Kuś and A.I. Krylov, De-perturbative corrections for charge-stabilized double ionization potential equation-of-motion coupled-cluster method, *J. Chem. Phys.* **136**, 244109 (2012).
- [3] X. Yang, J. Walpita, D. Zhou, H.L. Luk, S. Vyas, R.S. Khnayzer, S.C. Tiwari, K. Diri, C.M. Hadad F.N. Castellano, A.I. Krylov, and K.D. Glusac, Towards organic photohydrides: Excited-state behavior of 10- methyl-9-phenyl-9, 10-dihydroacridine, *J. Phys. Chem. B* (2013), submitted.

## SYNCHROTRON STUDIES OF GAS-PHASE AND HETEROGENEOUS CHEMISTRY RELEVANT IN COMBUSTION ENVIRONMENTS

Stephen R. Leone, Kevin R. Wilson, Musahid Ahmed, Jessica F. Lockyear,  
Denisia M. Popolan-Vaida, Theodora Nah, Amir Golan, Michael D. Ward and Tyler P. Troy  
Lawrence Berkeley National Laboratory and Departments of Chemistry and Physics  
University of California, Berkeley, California 94720  
(510) 643-5467 srl@berkeley.edu

### I. Scope of the Project

Understanding the fundamental chemical processes that govern combustion phenomena offers the opportunity to optimize combustion for improved engine efficiency and minimization of pollutant formation. Combustion is a complex process involving short-lived radicals, highly excited states, transport processes, heterogeneous chemistry, fluid dynamics, and energy transfer. Vacuum ultraviolet (VUV) light from the Chemical Dynamics Beamline of the Advanced Light Source is a powerful tool to selectively investigate the individual component processes involved in combustion with the aim of improving understanding as a whole. Several experimental techniques are used to work towards this goal; one such apparatus for gas-phase reactions is a multiplexed photoionization mass spectrometer (MPIMS), which was co-constructed with David Osborn and Craig Taatjes of the Sandia Combustion Research Facility. Another is an aerosol mass spectrometer, and a third is a molecular beam source for VUV probing of radical species. Coupling of a shock tube to the beamline, with Robert Tranter of Argonne National Laboratory, as well as a jet-stirred reactor with Craig Taatjes, provide original platforms for innovative investigations.

### II. Recent Progress

#### A. Gas-Phase Chemistry

During the combustion process a multitude of gas-phase species are formed, react with others and are destroyed. The molecules produced at the end of this chain process are dependent on the isomers formed at each stage. Recently, the MPIMS was employed to study the reaction between CH and acrolein. It was found that H-loss from the adduct between the reactants is the dominant reactive pathway and that the principal product is 1,3-butadienal, with a branching fraction of  $51 \pm 36\%$ . Significantly, the second most abundant product isomer is furan, an oxygen heterocycle, with a branching fraction of  $30 \pm 26\%$ . Currently, the reactive pathways that lead to oxygen-heterocycles in combustion environments are not well understood and so the result is significant for an awareness of this class of compounds in combustion environments. Moreover, the cyclization step competes effectively with more entropically, but less energetically, favorable pathways such as direct H-loss. More generally, the CH + propanal and CH + butanal reactions have been investigated as part of a project to understand CH reactivity with the aldehyde functional group. The goal is to be able to predict the products that are likely to be formed in the reaction of CH with larger aldehydes.

#### B. Heterogeneous Chemistry

In order to understand the elementary heterogeneous processes that govern the performance of a combustion system, model systems are required that can successfully reproduce the primary characteristics of larger molecules. The reactions of organic aerosol particles with radicals such as OH, and halogen atoms in the presence of oxygen represent such model systems, which allow the complex radical chain chemistry associated with combustion reactions to be studied under

ambient conditions. The role of heterogeneous chemistry will occupy a greater prominence as low volatility oxygenated fuels are direct-injected into combustion chambers, coating cylinder walls, injectors and valves. The reaction of I atoms with sub-micron droplets composed of squalene and squalane was investigated in an atmospheric pressure flow tube in order to examine how hydrogen abstraction competes with radical addition when C=C bonds are present. The results show no evidence of product formation with squalane droplets (no C=C bonds), but with unsaturated squalene droplets (6 C=C bonds) new peaks appear in the spectrum that can be attributed to iodated squalene. Clear evidence that I atoms add sequentially to the squalene double bond during the reaction is found, and the number of adsorbed I atoms appears to correlate the number of C=C bonds present. The reaction of OH radicals, in the presence of O<sub>2</sub>, with sub-micron oleic acid, linoleic acid and linolenic acid particles has been measured in a photochemical flow reactor. Oleic acid, linoleic acid, and linolenic acid have one, two, and three double bonds, respectively. Kinetic measurements find that the uptake coefficient for OH on these unsaturated fatty acid particles in the absence and presence of O<sub>2</sub> is larger than unity, providing clear evidence for particle phase secondary radical chain chemistry that accelerates the rate of particle oxidation. In addition, the uptake coefficient is inversely proportional to the concentration of OH, signaling a chain termination step by OH that competes with the chain propagation steps. Using a sequential oxidation model, it is found that non-oxidative secondary chain reactions accelerate the reactive depletion rate of the molecular species. In an investigation to probe how molecular structure influences the reaction rates and chemical mechanism in the OH-initiated reaction, it was found that the reactive uptake coefficient for OH + squalene is smaller than those measured for linoleic and linolenic acid. This suggests that the chemical mechanism for branched unsaturated organic particles may be different from that of linear unsaturated organic particles. In another study, the effect of O<sub>2</sub> concentration on the reaction kinetics of squalane aerosol particles with OH radicals has been investigated using a continuous flow stirred tank reactor (CFSTR). The CFSTR allows for much longer interaction times between the radicals and the aerosol particles than would typically be found in flow tube experiments. Preliminary results suggest that the OH uptake coefficient decreases substantially when the O<sub>2</sub> concentration is increased from 5 to 10%. This important finding indicates that high O<sub>2</sub> concentrations effectively suppress radical chain cycling chemistry within the droplet.

### ***C. Collaborations at the Beamline***

With Barney Ellison (Univ. of Colorado, Boulder), John Daily (Univ. of Colorado, Boulder), John Stanton (Univ. of Texas, Austin) and David Osborn (Sandia), the unimolecular dissociation and bimolecular reactions in acetaldehyde decomposition were characterized. These studies were extended to furan and methyl furan, and experiments are underway to quantify branching ratios as a function of reaction temperature. Ralf Kaiser (U Hawaii, Manoa) and Alex Mebel (Florida International Univ.) investigated the formation mechanisms of polycyclic aromatic hydrocarbons (PAHs) with an indene core in hydrocarbon-based combustion processes. ‘Directed synthesis’ of the PAHs was performed in situ in a supersonic molecular beam through reaction of pyrolytically generated phenyl radicals (C<sub>6</sub>H<sub>5</sub>) with hydrocarbons inside the heated microtubular reactor. By selecting the reactants, allene (H<sub>2</sub>CCCH<sub>2</sub>), methylacetylene (CH<sub>3</sub>CCH), propylene (CH<sub>3</sub>C<sub>2</sub>H<sub>3</sub>), diacetylene (HCCCCH), vinylacetylene (HCCC<sub>2</sub>H<sub>3</sub>), and 1,3-butadiene (C<sub>2</sub>H<sub>3</sub>C<sub>2</sub>H<sub>3</sub>), these studies access the important C<sub>9</sub>H<sub>x</sub> (x=8,10) potential energy surfaces; among them are the crucial combustion intermediates with an indene core. A very recent effort to probe high pressure-high temperature chemistry at the beamline involved the coupling of a novel miniature high repetition rate shock tube (HRRST) developed by Rob Tranter (ANL). The

scientific driver for this particular project is to examine the existence of roaming pathways that lead to molecular rather than radical products when a molecule (acetaldehyde, dimethyl ether) thermally dissociates.

#### ***D. Development of a Jet-Stirred Reactor***

A high temperature (500-1100 K) and high pressure (1-10 atm) jet-stirred reactor (JSR) system, which can be used to investigate the chemical transformations in well-defined conditions comparable to those occurring in combustion engines, was designed and is being built. In conjunction with the VUV photoionization aerosol and molecular beam mass spectrometers, the JSR will be used to investigate hydrocarbon oxidation reactions in the gas and particle phase, in addition to biofuel droplet evaporation, differential evaporation, and decomposition. The main innovation of the designed experimental setup consists of the application of aerosol mass spectrometry and analysis techniques to probe high pressure- and temperature-dependent particle formation and destruction chemistry.

### **III. Future Plans**

Future directions in the gas-phase combustion project involve studying the reaction of CH with methanol, which has been the subject of computational research and yet experimental results regarding the isomers formed in the reaction are not known. Understanding the reaction of CH with such a fundamental small molecule, the smallest alcohol, will be important for combustion modelling. In addition, the reaction of CH with oxygen-heterocycles and branched aldehydes will be probed. Cyclic compounds play an important role in combustion and the insights obtained on the branched aldehydes can be compared to those for the linear aldehydes and analogies drawn. The heterogeneous studies will extend several aspects of existing work. Recent improvements of the experimental setup are expected to reduce the amount of residual O<sub>2</sub> to a limit that will allow the study of hydrocarbon radicals with aerosols. The JSR will be utilized for studying heterogeneous chemistry of methyl esters, for example, methyl stearate, methyl oleate, and methyl linoleate. This series of molecules, differing by the number of unsaturated bonds, will be used to investigate the dependence of differential evaporation and oxidation pathways on molecular structure for a range of droplet-oxidizer concentrations. Other future systems to be studied include polycyclic aromatic hydrocarbon (PAH) particle formation chemistry. The phenyl radical is a key intermediate in the PAH formation process and its reactions will be investigated to better understand particle formation. The mass yields and chemical composition of particles formed will be studied. In addition, the reaction of methyl substituted phenyl radicals with O<sub>2</sub> will also be studied to understand how the presence of methyl side groups may influence PAH particle formation. To develop an overall understanding of combustion processes it is helpful to combine experimental studies with kinetic modeling. However, traditional kinetic models based on coupled differential equations become unwieldy when treating complex systems such as heterogeneous oxidation reactions. To this end, a stochastic model is being developed that will treat all mechanistic pathways of the reaction in addition to adsorption onto, and diffusion within, aerosol droplets. Such a model for heterogeneous oxidation reactions will allow the effect of a range of parameters on the oxidation process to be efficiently tested and will ultimately better inform future experimental studies.

### **IV. Recent Publications Citing DOE Support (2011-2013)**

S. A. Skeen, H. A. Michelsen, K. R. Wilson, D. M. Popolan, A. Violi and N. Hansen, "Near-Threshold Photoionization Mass Spectra of Combustion-Generated High-Molecular-Weight Soot Precursors", *J. Aerosol Sci.*, 58, 86 (2013)

- L. Lee, P. Wooldridge, T. Nah, K. R. Wilson, and R. Cohen, "Observation of Rates and Products in the Reaction of  $\text{NO}_3$  with Submicron Squalane Aerosol", *Phys. Chem. Chem. Phys.*, 15, 882 (2013).
- A. Golan, M. Ahmed, A. M. Mebel, and R. I. Kaiser, "A VUV Photoionization Study on the Formation of Primary and Secondary Products in the Reaction of the Phenyl Radical with 1,3-Butadiene under Combustion Relevant Conditions," *Phys. Chem. Chem. Phys.*, 15, 341 (2013).
- A. G. Vasiliou, K. M. Piech, B. Reed, X. Zhang, M. R. Nimlos, M. Ahmed, A. Golan, O. Kostko, D. L. Osborn, J. W. Daily, J. F. Stanton, and G. B. Ellison, "Thermal Decomposition of  $\text{CH}_3\text{CHO}$  Studied by Matrix Infrared Spectroscopy and Photoionization Mass Spectroscopy", *J. Chem. Phys.* 137, 164308 (2012).
- G. Isaacman, A. W. H. Chan, T. Nah, D. R. Worsnop, C. R. Ruehl, K. R. Wilson, and A. Goldstein, "Heterogeneous OH oxidation of motor oil particles causes selective depletion of branched and less cyclic hydrocarbons", *Environ. Sci. Technol.* 46, 10632 (2012).
- J. H. Kroll, J. D. Smith, D. R. Worsnop, and K. R. Wilson, "Characterization of lightly oxidized organic aerosol formed from the photochemical aging of diesel exhaust particles", *Environ. Chem.* 9, 211 (2012).
- S. H. Kessler, T. Nah, K. E. Daumit, J. D. Smith, S. R. Leone, C. E. Kolb, D. R. Worsnop, K. R. Wilson and J. H. Kroll, "OH-Initiated Heterogenous Aging of Highly Oxidized Organic Aerosol", *J. Phys. Chem. A* 116, 6358 (2012).
- J. Bouwman, F. Goulay, S. R. Leone and K. R. Wilson, "Bimolecular Rate Constant and Product Branching Ratio Measurements for the Reaction of  $\text{C}_2\text{H}$  with Ethene and Propene at 79 K", *J. Phys. Chem. A*, *J. Phys. Chem. A* 116, 3907 (2012).
- F. Goulay, A. J. Trevitt, J. D. Savee, J. Bouwman, D. L. Osborn, C. A. Taatjes, K. R. Wilson and S. R. Leone, "Product Detection of the CH Radical Reaction with Acetaldehyde", *J. Phys. Chem. A* 116, 6091 (2012)
- F. Zhang, R. I. Kaiser, A. Golan, M. Ahmed and N. Hansen, "A VUV Photoionization Study of the Combustion-Relevant Reaction of the Phenyl Radical ( $\text{C}_6\text{H}_5$ ) with Propylene ( $\text{C}_3\text{H}_6$ ) in a High Temperature Chemical Reactor", *J. Phys. Chem. A* 116, 3541 (2012).
- F. Zhang, R. I. Kaiser, V. V. Kislov, A. M. Mebel, A. Golan and M. Ahmed, "A VUV Photoionization Study of the Formation of the Indene Molecule and Its Isomers", *J. Phys. Chem. Lett.* 2, 1031 (2011).
- A. G. Vasiliou, K. M. Piech, X. Zhang, M. R. Nimlos, M. Ahmed, A. Golan, O. Kostko, D. L. Osborn, J. W. Daily, J. F. Stanton, and G. B. Ellison, "The Products of the Thermal Decomposition of  $\text{CH}_3\text{CHO}$ ", *J. Chem. Phys.* 135, 014306 (2011).
- F. Goulay, S. Soorkia, G. Meloni, D. L. Osborn, C. A. Taatjes and S. R. Leone, "Detection of Pentatetraene by Reaction of the Ethynyl Radical ( $\text{C}_2\text{H}$ ) with Allene ( $\text{CH}_2=\text{C}=\text{CH}_2$ ) at Room Temperature", *Phys. Chem. Chem. Phys.* 13, 20820 (2011).
- A. J. Trevitt, S. Soorkia, J. D. Savee, T. S. Selby, D. L. Osborn, C. A. Taatjes, and S. R. Leone, "Branching Fractions of the  $\text{CN} + \text{C}_3\text{H}_6$  Reaction Using Synchrotron Photoionization Mass Spectrometry: Evidence for the 3-Cyanopropene Product", *J. Phys. Chem. A* 115, 13467 (2011).
- S. Soorkia, C.-L. Liu, J. D. Savee, S. J. Ferrell, S. R. Leone, and K. R. Wilson, "Airfoil Sampling of a Pulsed Laval Beam with Tunable Vacuum Ultraviolet Synchrotron Ionization Quadrupole Mass Spectrometry: Application to Low Temperature Kinetics and Product Detection", *Rev. Sci. Instrum.* 82, 124102 (2011).
- S. H. Kessler, T. Nah, A. J. Carrasquillo, J. T. Jayne, D. R. Worsnop, K. R. Wilson and J. H. Kroll, "Formation of Secondary Organic Aerosol from the Direct Photolytic Generation of Organic Radicals", *J. Phys. Chem. Lett.* 2, 1295 (2011).
- C.-L. Liu, J. D. Smith, D. L. Che, M. Ahmed, S. R. Leone, and K. R. Wilson, "The Direct Observation of Secondary Radical Chain Chemistry in the Heterogeneous Reaction of Chlorine Atoms with Submicron Squalane Droplets", *Phys. Chem. Chem. Phys.* 13, 8993 (2011).

# INTERMOLECULAR INTERACTIONS OF HYDROXYL RADICALS ON REACTIVE POTENTIAL ENERGY SURFACES

Marsha I. Lester  
Department of Chemistry  
University of Pennsylvania  
Philadelphia, PA 19104-6323  
milester@sas.upenn.edu

## I. Program Scope

Hydroxyl radicals are important in combustion and atmospheric environments, where they are often detected by laser-induced fluorescence (LIF) on the  $A^2\Sigma^+ - X^2\Pi$  band system. However, collision partners known to quench electronically excited OH  $A^2\Sigma^+$  radicals are ubiquitous in these environments. Thus, great effort has been made to quantify the rates and/or cross sections for collisional quenching, so that its effects on LIF signals may be taken into account to allow an accurate determination of OH concentrations. Despite extensive kinetic measurements, fundamental questions remain regarding the fate of the collisionally quenched molecules and the *mechanism* by which these nonadiabatic processes occur. The experimental work carried out under DOE-BES funding in the Lester laboratory is aimed at understanding the fundamental chemical dynamics governing quenching of OH  $A^2\Sigma^+$  by molecular partners ( $M = H_2, N_2, O_2, CO, CO_2, H_2O$ ) of significance in combustion environments.

## II. Recent Progress

### A. A new spectroscopic window on hydroxyl radicals using UV+VUV resonant ionization

Although OH is readily detected using LIF on the  $A^2\Sigma^+ - X^2\Pi$  transition, a quantum state-selective ionization scheme has been a long-standing goal. We have developed a new UV+VUV ionization scheme: the UV photon prepares the  $A^2\Sigma^+$  valence state as the resonant intermediate state and a subsequent fixed frequency VUV photon at 118.2 nm (10.490 eV) provides sufficient energy to ionize.<sup>1</sup> The UV+VUV scheme accesses autoionizing Rydberg states that converge on the  $OH^+ A^3\Pi$  ion state. The onset of ionization with the A-X (1,0) band is attributed to an energetic threshold to accessing this Rydberg series. Recent studies have focused on a detailed comparison of REMPI vs. LIF intensities for various OH A-X (1,0) lines, which avoids complications due to temperatures (population) or line strengths (saturation). The ratio of REMPI to LIF yields an enhancement profile for A-X (1,0) excitation that coincides with the OH [ $A^3\Pi, 3d$ ],  $v = 0$  Rydberg feature. This sensitive ionization scheme for OH radicals is applicable to velocity-map ion imaging of fundamental reaction, photodissociation and inelastic collision dynamics, as will be demonstrated in future research.

### B. Outcomes of collisional quenching of electronically excited OH $A^2\Sigma^+$ radicals

#### 1. Reactive quenching of OH $A^2\Sigma^+$ by $O_2$ and CO

We have examined the outcomes following collisional quenching of electronically excited OH  $A^2\Sigma^+$  by  $O_2$  and CO in a combined experimental and theoretical study.<sup>2</sup> The atomic H- and O-atom products from reactive quenching were probed using two-photon laser-induced fluorescence to obtain the relative yields of these products. Doppler profiles of the H-atom fragments are analyzed to obtain the average kinetic energy and, as indicated, the percentage of available energy released as translation to  $H + O_3$  (35%) or  $H + CO_2$  (6%) products. For O-atom products, we lack the laser resolution required for Doppler measurements, but we are able to show a nearly statistical fine structure distribution. Most interesting is the branching fraction: The experimental product branching ratios show that the O-atom producing pathways are the dominant outcomes of quenching: the  $OH A^2\Sigma^+ + O_2 \rightarrow O + HO_2$  channel accounts for 48(3)% of products and the  $OH A^2\Sigma^+ + CO \rightarrow O + HCO$  channel yields 76(5)% of products. Theoretical studies also characterized the properties of energy minimized conical intersections in regions of strong

nonadiabatic coupling accessible from the OH  $A^2\Sigma^+$  + CO asymptote. Energy minimized points were located on a seam of conical intersection from the OH  $A^2\Sigma^+$  + CO asymptote to a conical intersection with an extended OH bond length and the H-side of OH pointing towards CO in a bent configuration. This region, exoergic with respect to the reaction asymptote, is likely to be the origin of the dominant O + HCO product channel.

## 2. Nonreactive quenching of OH $A^2\Sigma^+$ by Kr

Finally, we have examined the OH  $X^2\Pi$  ( $v''=0-2$ ) products from quenching of OH  $A^2\Sigma^+$  ( $v'=0$ ) by Kr; notably He, Ne, and Ar do not quench OH  $A^2\Sigma^+$ . As observed previously with H<sub>2</sub>, N<sub>2</sub>, and O<sub>2</sub> partners, we find highly rotationally excited OH  $X^2\Pi$  ( $v''=0$ ) products. Ongoing theoretical work by Millard Alexander and coworkers has shown strong nonadiabatic coupling between the OH ( $A^2\Sigma^+$ ,  $X^2\Pi$ ) + Kr potentials of A' symmetry for a crossing (linear) or avoided crossing (non-linear) in Kr-O-H orientations, but not in Kr-H-O configurations where the crossing lies at much higher energy. This 3D system seems to mirror many of the nonadiabatic effects we have unraveled in HO-H<sub>2</sub> (6D), making it more tractable for dynamical calculations.

## C. New velocity map imaging apparatus: Calibration and first results

DOE provided supplementary equipment funds that enabled us to construct a new velocity map imaging (VMI) apparatus, an experimental method first developed by Chandler and Houston<sup>3</sup> and further expanded by Eppink and Parker.<sup>4,5</sup> Sydor Instruments designed and constructed the coupled detector, CCD camera, and MCP gating module system based on our specifications along with a custom light-tight camera enclosure with access for lens focusing. The ion optics assembly is based on the modified design of Suits and coworkers.<sup>6</sup>

The new VMI instrument has been calibrated using photolysis of O<sub>2</sub> around 226 nm. In a one-color experiment, O<sub>2</sub> is photodissociated into O ( $^3P_2$ ) + O ( $^3P_1$ , where J=2,1,0) and O ( $^3P_2$ ) is subsequently ionized via (2+1) REMPI.<sup>7</sup> The known kinetic energy release corresponds to the radial distribution of the image; the raw image is reconstructed using pBASEX.<sup>8</sup> Our velocity resolution of ~4% is excellent compared with previous studies, which reported resolution of 10% or less. Our apparatus also has 2D slicing capability with a 10 ns temporal width, which will yield even better velocity resolution.

First new scientific results using VMI: The photodissociation dynamics of CH<sub>2</sub>I<sub>2</sub> in the ultraviolet range of 277-305 nm via the two lowest B<sub>1</sub> excited states has been well studied using one-color velocity map ion imaging and photofragment translational spectroscopy.<sup>9</sup> We have carried out a two-color experimental study in which CH<sub>2</sub>I<sub>2</sub> is photodissociated by 248 nm via the B<sub>2</sub> or A<sub>1</sub> excited states to give CH<sub>2</sub>I and I ( $^2P_{3/2}$ ) or I\* ( $^2P_{1/2}$ ). The iodine atoms are then state selectively ionized using a (2+1) resonance-enhanced multiphoton ionization process near 310 nm and detected by VMI. Preliminary results show about 85% of the available energy is being funneled into the internal energy of the CH<sub>2</sub>I fragment, consistent with prior infrared emission results of Baughcum and Leone.<sup>10</sup> The anisotropy parameter derived from the image indicates this is a fast dissociation process and reflects the character of the electronic transition. The internal energy distribution of the CH<sub>2</sub>I fragment is of particular interest because of its subsequent reaction with O<sub>2</sub> in a near thermo-neutral reaction to produce the smallest Criegee intermediate, CH<sub>2</sub>OO.<sup>11-13</sup> We anticipate that the internal energy contained in CH<sub>2</sub>I will likely be carried forward into CH<sub>2</sub>OO.

## III. Future Work

Our ongoing research is focused on the *outcomes* of collisional quenching of electronically excited OH  $A^2\Sigma^+$  radicals. Specifically, the experimental studies are examining reactive quenching processes that generate chemically distinct products as well as nonreactive quenching processes that return OH  $A^2\Sigma^+$  radicals to their ground  $X^2\Pi$  electronic state, the latter with an emphasis on the energy transferred to the collision partner. The observed product state distributions from reactive and nonreactive quenching

processes are used to identify the forces acting on the nuclei as the system switches from the electronically excited to ground state potential energy surface. The systems investigated and experimental methods utilized are being expanded to probe previously unobserved outcomes of collisional quenching. Finally, collaborations are being developed with theoretical groups to obtain a comprehensive model for quenching consistent with kinetic rate measurements, product branching ratios, quantum state distributions, and kinetic energy release.

#### IV. References

1. J. M. Beames, F. Liu, M. I. Lester and C. Murray, *J. Chem. Phys.* **134**, 241102 (2011).
2. J. H. Lehman, M. I. Lester, and D. H. Yarkony, *J. Chem. Phys.* **137**, 094312 (2012).
3. D. W. Chandler and P. L. Houston, *J. Chem. Phys.* **87**, 1445 (1987).
4. A. T. J. B. Eppink and D. H. Parker, *Rev. Sci. Instrum.* **68**, 3477 (1997).
5. D. H. Parker and A. Eppink, *J. Chem. Phys.* **107**, 2357 (1997).
6. D. Townsend, M. P. Minitti and A. G. Suits, *Rev. Sci. Instrum.* **74**, 2530 (2003).
7. B. Buijsse, W. J. van der Zande, A. Eppink, D. H. Parker, B. R. Lewis and S. T. Gibson, *J. Chem. Phys.* **108**, 7229 (1998).
8. G. A. Garcia, L. Nahon and I. Powis, *Rev. Sci. Instrum.* **75**, 4989 (2004).
9. H. F. Xu, Y. Guo, S. L. Liu, X. X. Ma, D. X. Dai, and G. H. Sha, *J. Chem. Phys.* **117**, 5722 (2002).
10. S. L. Baughcum and S. R. Leone, *J. Chem. Phys.* **72**, 6531 (1980).
11. O. Welz, J. D. Savee, D. L. Osborn, S. S. Vasu, C. J. Percival, D. E. Shallcross and C. A. Taatjes, *Science* **335**, 204 (2012).
12. E. P. F. Lee, D. K. W. Mok, D. E. Shallcross, C. J. Percival, D. L. Osborn, C. A. Taatjes and J. M. Dyke, *Chem. Eur. J.* **18**, 12411 (2012).
13. J. M. Beames, F. Liu, L. Lu and M. I. Lester, *J. Am. Chem. Soc.* **134**, 20045 (2012).

#### V. Publications supported by this project 2010-2012

1. J. H. Lehman, M. I. Lester, and D. H. Yarkony, "Reactive quenching of OH  $A^2\Sigma^+$  by O<sub>2</sub> and CO: Experimental and nonadiabatic theoretical studies of H- and O-atom product channels", *J. Chem. Phys.* **137**, 094312 (2012).
2. J. M. Beames, F. Liu, M. I. Lester, and C. Murray, "Communication: A new spectroscopic window on hydroxyl radicals using UV+VUV resonant ionization", *J. Chem. Phys.* **134**, 241102 (2011).
3. J. H. Lehman, J. Bertrand, T. A. Stephenson, and M. I. Lester, "Reactive quenching of OD  $A^2\Sigma^+$  by H<sub>2</sub>: Translational energy distributions for H- and D-atom product channels", *J. Chem. Phys.* **135**, 144303 (2011).
4. J. H. Lehman, L. P. Dempsey, M. I. Lester, B. Fu, E. Kamarchik, and J. M. Bowman, "Collisional quenching of OD  $A^2\Sigma^+$  by H<sub>2</sub>: Experimental and theoretical studies of the state-resolved OD  $X^2\Pi$  product distribution and branching fraction", *J. Chem. Phys.* **133**, 164307 (2010).
5. P. Soloveichik, B. A. O'Donnell, M. I. Lester, A. B. McCoy, and J. S. Francisco, "Infrared spectrum and stability of the H<sub>2</sub>O-HO complex: Experiment and theory", *J. Phys. Chem. A* **114**, 1529-1538 (2010).



# Theoretical Studies of Molecular Systems

William A. Lester, Jr.  
Chemical Sciences Division,  
Ernest Orlando Lawrence Berkeley National Laboratory and  
Kenneth S. Pitzer Center for Theoretical Chemistry  
Department of Chemistry, University of California, Berkeley  
Berkeley, California 94720-1460  
walester@lbl.gov

## Program Scope

This research program is directed at extending fundamental knowledge of atoms and molecules. The approach combines the use of ab initio basis set methods and the quantum Monte Carlo (QMC) method to describe the electronic structure and energetics of systems of primarily combustion interest.

Recent Progress

*a) Classification of Nodal Pockets in Many-Electron Wave Functions via Machine Learning* (with E. LeDell, Prabhat, D. Yu. Zubarev, and B. M. Austin)

The accurate treatment of electron correlation in quantum chemistry requires solving the many-electron problem. If the nodal surface of a many-electron wave function is available even in an approximate form, the fixed-node diffusion Monte Carlo (FNDMC) approach from the family of quantum Monte Carlo (QMC) methods can be successfully used for this purpose. The issue of description and classification of nodal surfaces of fermionic wave functions becomes central for understanding the basic properties of many-electron wave functions and for the control of accuracy and computational efficiency of FNDMC computations. In a recent study, we began to explore the approach of automatic classification of nodal pockets of many-electron wave functions. We formulated this problem as that of binary classification and applied a number of techniques from the machine learning literature. We implemented these techniques on a range of atoms of light elements and demonstrated the capability of each. We observed that classifiers with relatively simple geometry performed poorly on the classification task; methods based on a

random collection of tree-based classifiers appeared to perform best. We identified computational challenges and complexity associated with applying these techniques to heavier atoms.

*b) From Aromaticity to Self-Organized Criticality in Graphene* (with D. Yu. Zubarev and M. Frenklach)

The unique properties of graphene are rooted in its peculiar electronic structure where effects of electron delocalization are pivotal. We have shown<sup>6</sup> that the traditional view of delocalization as formation of a local or global aromatic bonding framework has to be expanded for these systems. A modification of the p-electron system of a finite-size graphene substrate results in a scale-invariant response in the relaxation of interatomic distances and reveals self-organized criticality as a mode of delocalized bonding. Graphene is shown to belong to a diverse class of finite-size extended systems with simple local interactions where complexity emerges spontaneously under very general conditions that can be a critical factor controlling observable properties such as chemical activity, electron transport, and spin-polarization.

*c) Correlation of Oxiradical Kinetics with Aromaticity* (with D. E. Edwards, X. You, D. Yu. Zubarev, and M. Frenklach) See the Frenklach abstract in this book.

*d) Oxidation of Phenanthrene Radicals by OH* (with D. E. Edwards, X. You, D. Yu. Zubarev, and M. Frenklach) See the Frenklach abstract in this book.

## **Future Plans**

The present level of development of the two central QMC approaches, variational Monte Carlo (VMC) and FNDMC, is sufficiently high that they can be used routinely to compute ground state energies of molecular systems. Certain basic and methodological aspects of QMC still need refinement and development, especially for electronically excited states and open-shell systems. Future research incorporates these aspects. The first direction is system-specific research that aims to address issues relevant to experimental investigations carried out by CSD PIs.

This direction is primarily dedicated to utilization of existing QMC methodology for computations of various energetic characteristics of molecules, such as reaction energies, reaction barriers, electron affinities and detachment energies. FNDMC is a reliable source of these values even with the simplest available trial wave functions of Hartree-Fock (HF) or Kohn-Sham (KS-DFT) quality. The second direction is directed at the extension of the FNDMC method to the domain of problems that previously have not been addressed by the approach.

Exploration of reactions on graphene will continue in collaboration with Michael Frenklach's group. One of the immediate goals is investigation of the triplet potential energy surface for the phenanthrene + OH reaction.

### DoE Supported Publications (2011-2013)

1. X. You, R. Whitesides, D. Zubarev, W. A. Lester, Jr., and M. Frenklach, "Bay-capping Reactions: Kinetics and Influence on Graphene-Edge Growth," *Proc. Combust. Inst.* **33**, 685 (2011).
2. D. Yu. Zubarev, X. You, J. McClean, W. A. Lester, Jr., and M. Frenklach, "Patterns of local aromaticity in graphene oxyradicals," *J. Mater. Chem.* **21**, 3404 (2011).
3. X. You, D. Yu. Zubarev, W. A. Lester, Jr., and M. Frenklach, "Thermal decomposition of pentacene oxyradicals," *J. Phys. Chem. A* **115**, 14184 (2011).
4. D. Yu. Zubarev, X. You, M. Frenklach, and W. A. Lester, Jr., "Delocalization effects in pristine and oxidized graphene substrates," in *Advances in the Theory of Quantum Systems in Chemistry and Physics* (P. E. Hoggan, E. J. Brändas, J. Maruani, P. Piecuch, and G. Delgado-Barrio, Eds.), Progress in Theoretical Chemistry and Physics, Vol. 22, Springer, Dordrecht, (2012), Chapter 29, p. 553.
5. D. Yu. Zubarev, M. Frenklach, and W. A. Lester, Jr., "From Aromaticity to Self-Organized Criticality in Graphene," *Phys. Chem. Chem. Phys.* **14**, 12075 (2012). (Communication).
6. E. LeDell, Prabhat; D. Yu. Zubarev, B. M. Austin, and W. A. Lester, Jr., "Classification of Nodal Pockets in Many-Electron Wave Functions via Machine Learning," *J. Math. Chem.* **50**, 2043 (2012).
7. D. Yu. Zubarev, B. M. Austin, and W. A. Lester, Jr., "Quantum Monte Carlo for the X-Ray Absorption Spectrum of Pyrrole at the Nitrogen K-Edge", *J. Chem. Phys.* **136**, 144301 (2012).
8. D. Yu. Zubarev, and W. A. Lester, Jr., "Beyond a Single Solvated Electron: Hybrid Quantum Monte Carlo and Molecular Mechanics Approach," ACS Symposium Series "Advances in Quantum Monte Carlo," **1094**, 201 (2012).
9. D. Yu. Zubarev, B. M. Austin, and W. A. Lester, Jr., "Practical Aspects of Quantum Monte Carlo for the Electronic Structure of Molecules," in *Practical Aspects of Computational Chemistry: Methods, Concepts and Applications*, J. Leszczynski and M. K. Shukla, Eds., Springer, 2012, p. 255.

10. B. M. Austin, D. Yu. Zubarev, and W. A. Lester, Jr., "Quantum Monte Carlo and Related Approaches," *Chem. Rev.* **112**, 263 (2012).
11. D. E. Edwards, X. You, D. Yu. Zubarev, W. A. Lester, Jr., and M. Frenklach, "Thermal Decomposition of Graphene Armchair Oxyradical," *Proc. Combust. Inst.* **34**, 1759 (2013).
12. D. E. Edwards, D. Yu. Zubarev, W. A. Lester, Jr., and M. Frenklach, "Oxidation of Phenanthrene Radicals by OH," 8<sup>th</sup> U.S. National Combustion Meeting, Salt Lake City, UA, 2013, accepted

# Development of Kinetics for Soot Oxidation at High Pressures Under Fuel-Lean Conditions

JoAnn S. Lighty

Department of Chemical Engineering, University of Utah, [jlighty@utah.edu](mailto:jlighty@utah.edu)

Randall Vander Wal

Dept. of Energy and Mineral Engineering, Pennsylvania State University, [ruv12@psu.edu](mailto:ruv12@psu.edu)

## I. Project Scope

The focus of the proposed research is to develop kinetic models for soot oxidation with the hope of developing a validated, predictive, multi-scale, combustion model to optimize the design and operation of evolving fuels in advanced engines for transportation applications. The work focuses on the relatively unstudied area of the fundamental mechanism for soot oxidation. The objectives include understanding of the kinetics of soot oxidation by O<sub>2</sub> under high pressure which require: 1) development of intrinsic kinetics for the surface oxidation, which takes into account the dependence of reactivity upon nanostructure and 2) evolution of nanostructure and its impact upon oxidation rate and 3) inclusion of internal surface area development and possible fragmentation resulting from pore development and /or surface oxidation. These objectives will be explored for a variety of pure fuel components and surrogate fuels.

This project is a joint effort between the University of Utah (UU) and Pennsylvania State University (Penn State). The work at the UU focuses on experimental studies using a Two-Stage burner and high-pressure TGA. Penn State will provide HRTEM images and guidance in the fringe analysis algorithms and parameter quantification for the images.

## II. Recent Progress

### A. Fuel components

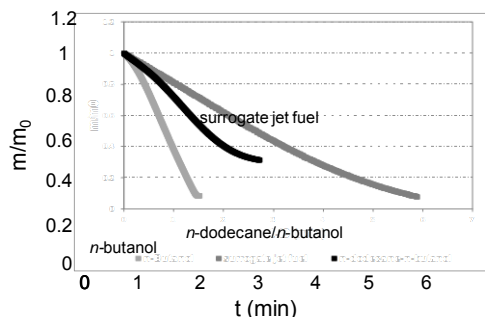
Soot samples from pure fuels and surrogates were studied. For this study, a mixture of n-dodecane/m-xylene was used as a surrogate for jet fuel. Normal-butanol and n-dodecane were chosen as an oxygenated surrogate fuel. A commercial black carbon, Carboxen 1000, was used as a reference. Three model black carbons, ranging from amorphous to onion-like structures are currently being evaluated to obtain a better understanding of the role of nanostructure on oxidation.

### B. Oxidation Studies

The estimation of the kinetic parameters for a variety of fuels and pressures was completed by utilizing a high-pressure thermogravimetric analyzer (HTGA), Cahn TherMax 500. The first step was to find the most favorable experimental conditions such as initial sample mass and the oxidizer gas flow rates to minimize the diffusional limitations.<sup>1-5</sup> An inert material was added to “fill” the crucible to reduce the film diffusion thickness between the top of the crucible and the sample.<sup>3,4</sup> In addition, an algorithm was developed to account for the actual rates versus those rates obtained from the experiment.<sup>6,7</sup> Corrections to kinetic parameters obtained from the mass data Arrhenius plots<sup>8</sup> were found from these effectiveness factors. Multiple isothermal tests were performed at varying temperatures (from 550 to 650°C, with increments of 25°C). A heating rate of 10°C/min was used to reach the oxidation temperature under a controlled gas environment. Nitrogen flowed at 0.55 L/min through the microbalance to protect it. The oxidizer, a mixture of O<sub>2</sub>/N<sub>2</sub>, flowed at 1 L/min.

The activation energy values estimated in this work for m-xylene, n-dodecane, and surrogate jet fuel mixture soot samples were found to range between 154 and 165, which are in the range reported by Ciampelli et al.<sup>9</sup>, Otto et al.<sup>10</sup> and Neeft et al.<sup>11</sup> Carboxen results were also found to be in the range previously reported, approximately 140 kJ/mol.<sup>12</sup> Results were not dependent upon pressure and the pure fuels had similar results as compared to the mixture.

To study the effect of oxygenated fuels on the kinetic parameters, a variety of tests were carried out with n-butanol and with a 40/60 (molar base) mixture of n-butanol/n-dodecane. The experiments were conducted at atmospheric pressure, 21% O<sub>2</sub> in N<sub>2</sub>, and temperature range from 400 to 625°C. The activation energy values were found to be 114 kJ/mol for n-butanol and 129 kJ/mol for the mixture of n-butanol/n-dodecane. Figure 1 shows the mass loss for these fuels, and the surrogate jet fuel, based on the kinetic parameters obtained. As seen in this figure, the kinetics for the pure butanol are the fastest,



followed by butanol/dodecane, and the slowest is the surrogate jet fuel. For butanol, contrary to the surrogate jet fuel, the mixture did not behave in a manner similar to the pure components.

**Figure 1** Mass-based oxidation rate for three different soot samples at 600 °C and air.

### C. Nanostructure Comparison of Various Soots

Penn State performed HR-TEM analysis for the above-referenced soots to explore the effect of nanostructure. The nanostructure analysis was performed by using a custom algorithms developed by Dr. Vander Wal's group for fringe length and tortuosity.<sup>13,14</sup> The HR-TEMs and fringe analyses are shown in Figure 2.

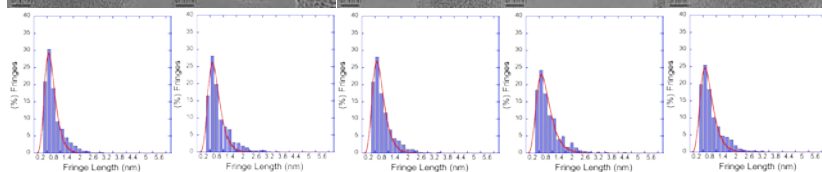
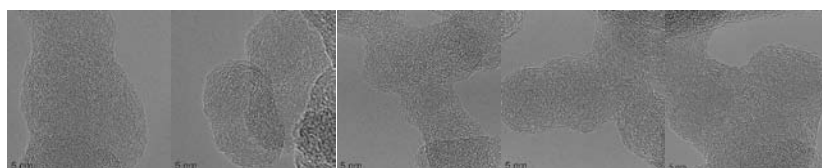


**Figure 2.** HRTEM of nascent soot of (left to right) butanol/n-dodecane, butanol, n-dodecane, m-xylene and m-xylene/n-dodecane.

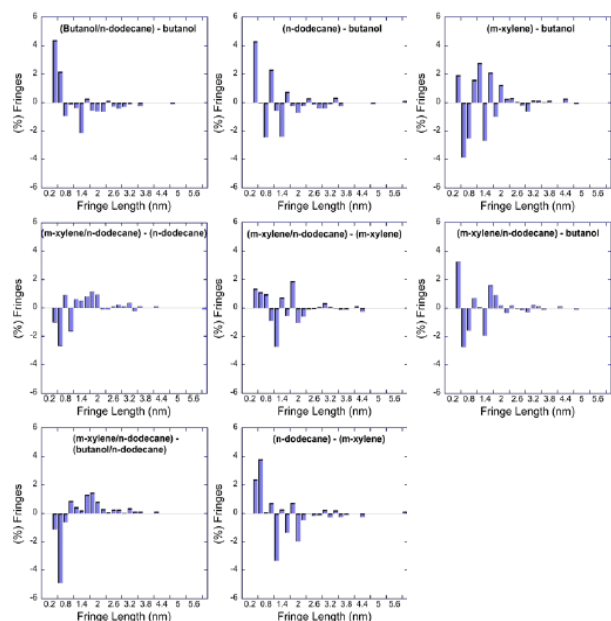
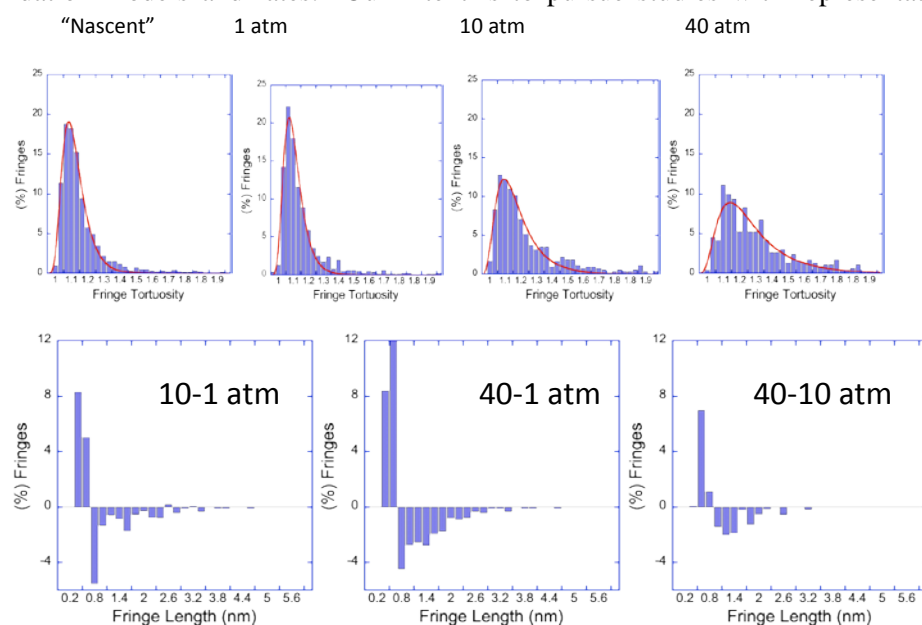


**Figure 3.** Fringe length differences for the difference fuels.

The fringe analysis shows that the fringe length, in nm, is approximately the same for each fuel (see Figure 3), with the exception of the xylene/dodecane mix (surrogate jet fuel) and the butanol/dodecane. The butanol/dodecane had a notably shorter fringe length as compared the surrogate jet fuel mix lower panel of Figure 3, far left). This might explain the differences in the kinetics found above, with shorter fringe lengths exhibiting a more amorphous structure with more end sites, which have been found to be easier to burn.

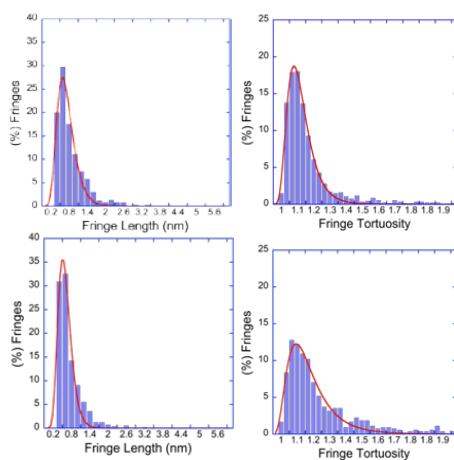
#### D. Effect of Pressure on the Nanostructure of Oxidized Soot

For these studies, soot was collected for the various fuels and then oxidized in the HTGA at 575°C, 21% oxygen, until 50% mass loss. Three pressures were studied: 1 atm, 10 atm, and 40 atm. For pure fuels, butanol and n-dodecane did not show a change in the fringe length with a change in pressure. However, m-xylene exhibited some change in structure with oxidation pressure. The fringe length increased and (not shown here) the tortuosity became broader, suggesting more curvature in the structure. Butanol and n-dodecane did show some differences between the “nascent” soot and the 10 atm oxidation. No real differences were identified between oxidation at 10 and 40 atm. The butanol showed longer fringe lengths and more curvature, while dodecane exhibited the opposite behavior. For the mixtures, the most prominent fringe-length differences were found for the butanol/dodecane mixture. As seen in Figure 4, the fringe length decreases with pressure and the tortuosity increases, suggesting a more curved structure. This unique observation could be a hybrid of external surface oxidation, or shrinking core oxidation, and internal burning of the particle. This is relevant to transportation fuels, such as gasoline and diesel, since these fuels are blends of petroleum-based components and oxygenates, in the form of either ethanol or biodiesel. These results suggest that synergies between fuel components might account for different oxidation models and rates. Our intent is to pursue studies with representative aromatic components



followed by ternary mixtures of all three chemical classes: oxygenates, paraffins, and aromatics.

**Figure 4. HR-TEM and fringe length and tortuosity for the butanol/dodecane mixture.**



Further investigation of the butanol/dodecane mixture is warranted. The structure of the “nascent” butanol/dodecane is slightly different from the pure components. However, upon oxidation (Figure 5), the structures diverge quite dramatically with the mixture (bottom) exhibiting a more fractured structure at the surface. In addition, other studies completed by the Utah group show that, while additional butanol decreases the amount of soot, it appears as though higher concentrations lead to more stable soot particles. These differences are likely due to chemistry.

**Figure 5. 50% extent of oxidation, fringe and tortuosity analysis: butanol (top) and butanol/dodecane (bottom).**

### III. Future Plans

We have just started to look at the oxidation kinetic and nanostructure of model carbons, ranging from amorphous to onion-like nanostructures. These carbons feature uniform morphology and homogeneous edge versus basal plane sites, and can form a baseline by which to gauge rates and activation energies towards mechanistic models and more understanding of the role of nanostructure.

Also, we will continue with our work on butanol as an additive to dodecane to explore the oxidation kinetics with a focus on the amount of the oxygenated fuel and nanostructure.

### IV. References

- [1] P. Gilot, A. Brillard, and B.R. Stanmore. Geometric effects on mass transfer during thermogravimetric analysis: Application to reactivity of diesel soot. *Combustion and Flame*, 102 (4):471-480, 1995.
- [2] N. Zouaoui, J. Brilhac, F. Mechat, M. Jeguirim, B. Djellouli, and P. Gilot. Study of experimental and theoretical procedures when using thermogravimetric analysis to determine kinetic parameters of carbon black oxidation. *Journal of Thermal Analysis & Calorimetry*, 102 (3): 837-849, 2010.
- [3] M. Kalogirou, and Z. Samaras. A thermogravimetric kinetic study of uncatalyzed diesel soot oxidation. *Journal of Thermal Analysis & Calorimetry*, 98 (1):215-224, 2009.
- [4] M. Kalogirou, and Z. Samaras. Soot oxidation kinetics from TG experiments. *Journal of Thermal Analysis & Calorimetry*, 99 (3): 1005-1010, 2010.
- [5] P. Gilot, F. Bonnefoy, F. Marcuccilli, and G. Prado. Determination of kinetic data for soot oxidation. Modeling the competition between oxygen diffusion and reaction during thermogravimetric analysis. *Combustion and Flame*, 95 (1-2):87-100, 1993.
- [6] J. Rodriguez-Fernandez, F. Oliva, and R.A. Vazquez. Characterization of the diesel soot oxidation process through an optimized thermogravimetric method. *Energy & Fuels*, 25 (5):2039-2039, 2011.
- [7] J. Song, J. Chung-Hwan, and A. Boehman. Impacts of Oxygen Diffusion on the Combustion Rate of In-Bed Soot Particles. *Energy Fuels*, 24:2418-2428, 2010.
- [8] Q. Song, B. He, Q. Yao, Z. Meng, and C. Che. Influence of Diffusion on Thermogravimetric Analysis of Carbon Black Oxidation. *Energy Fuels*, 20: 1895-1900, 2006.
- [9] P. Ciambelli, P. Corbo, M. Gambino, V. Palma, and S. Vaccaro. Catalytic combustion of carbon particulate. *Catalysis today*,53:99, 1996.
- [10] K.Otto, M.H. Sieg, M. Zinbo, and L. Baartosiewz. The oxidation of soot deposits from Diesel engines, SAE paper 1981.
- [11] J.P. A. Neeft, T.X. Nijhuis, M. Makkee, and J.A. Moulijn. Kinetics of the oxidation of diesel soot. *Fuel*, 76:1129-36, 1997.
- [12] L.H. Sorensen, E. Gjernes, T. Jessen, and J. Fjellerup. Determination of reactivity parameters of model carbons, cokes and flame-chars. *Fuel*, 75: 31-38, 1996.
- [13] R.L. Vander Wal, A.J. Tomasek, K. Street, D. R. Hull, and W. K. Thompson. Carbon Nanostructure Examined by Lattice Fringe Analysis of High-Resolution Transmission Electron Microscopy Images. *Applied Spectroscopy*, 58 (2):230-237, 2004.
- [14] R.L. Vander Wal, and C.J. Mueller. Initial Investigation of Effects of Fuel Oxygenation on Nanostructure of Soot from Direct-Injection Diesel Engine. *Energy & Fuels*, 20:2364-2369, 2006.

### V. Publications in preparation or submitted

1. I. C. Jaramillo, J. Levinthal, J. S. Lighty, "Soot Oxidation Kinetics: Pressure and Fuel Comparisons," in preparation (2013).
2. P. Toth, A. B. Palotas, T. A. Ring, E. G. Eddings, J.S. Lighty, "Detailed investigation of soot nanostructure: effect of pressure," in preparation (2013).

# Computational Flame Diagnostics for Direct Numerical Simulations with Detailed Chemistry of Transportation Fuels

Tianfeng Lu

Department of Mechanical Engineering, University of Connecticut

Storrs, CT 06269-3139

tlu@engr.uconn.edu

## I. Program Scope

The goal of the proposed research is to create computational flame diagnostics (CFLD) that are rigorous numerical algorithms for systematic detection of critical flame features, such as ignition, extinction, and premixed and non-premixed flamelets, and to understand the underlying physicochemical processes controlling limit flame phenomena, flame stabilization, turbulence-chemistry interactions and pollutant emissions etc. The computational diagnostics will be based on quantitative information extracted using CFLD from high-fidelity datasets generated from direct numerical simulations (DNS). The goal will be accomplished through an integrated approach combining mechanism reduction, DNS of flames at engine conditions, computational diagnostics, turbulence modeling, and DNS data mining and data reduction. Specifically, non-stiff reduced mechanisms for transportation fuels that are amenable for three-dimensional DNS will be derived through rigorous algorithmic development for detailed chemical kinetics that can be highly nonlinear, chemically stiff and extremely large in size. DNS for premixed and non-premixed flames at diesel and homogeneous charge compression ignition (HCCI) engine conditions using non-stiff reduced chemistry will be performed through a collaborative effort with Sandia (Dr. J.H. Chen). The resulting DNS data will be systematically diagnosed with CFLD, e.g. based on chemical explosive mode analysis (CEMA) [i], to systematically extract and understand the critical flame features, and to validate and improve mixing and combustion models for turbulent flame simulations. Systematic methods for DNS data reduction/reconstruction, without significant loss of chemical kinetic information, will be developed to improve the efficiencies of data storage, transfer and processing for petascale DNS.

## II. Recent Progress

The program started on Sept. 1, 2012. During the reporting period, reduced mechanisms for transportation fuels, including primary reference fuels (PRF) and n-dodecane, were being developed and validated for DNS and other flame simulations. Development and validation of computational diagnostic algorithms based on CEMA and bifurcation analysis is in progress, as summarized in the following.

### A. Development of non-stiff reduced mechanisms for DNS and other flame simulations

Detailed mechanisms for transportation fuels involve a large number of species and reactions and can induce severe chemical stiffness, and thus are computationally expensive for DNS and other flame simulations. A systematic approach based on the directed relation graph (DRG) method, analytically solved linearized quasi steady state approximations (LQSSA) and dynamic chemical stiffness removal [ii] was employed to obtain an accurate reduced mechanism for PRF that is suitable for DNS of HCCI combustion. The reduction was based on a detailed LLNL mechanism (ver. 3) for PRF with 1271 species [iii]. The non-stiff reduced mechanism consists of 116 species, while it's comparable to the detailed mechanism in comprehensiveness and accuracy, as demonstrated in Fig. 1 for ignition and extinction for selected parameter ranges.

The non-stiff reduced mechanism was then employed in a 2-D DNS of HCCI with PRF (collaboration with C.S. Yoo). The DNS results (Fig. 2a) were diagnosed with CEMA to identify the auto-igniting mixtures (red), near-equilibrium combustion products (blue), and propagating flame fronts (black isocontour) as shown in Fig. 2b. The relative importance of auto-ignition and premixed flame propagation in controlling the HCCI combustion rate was quantified.

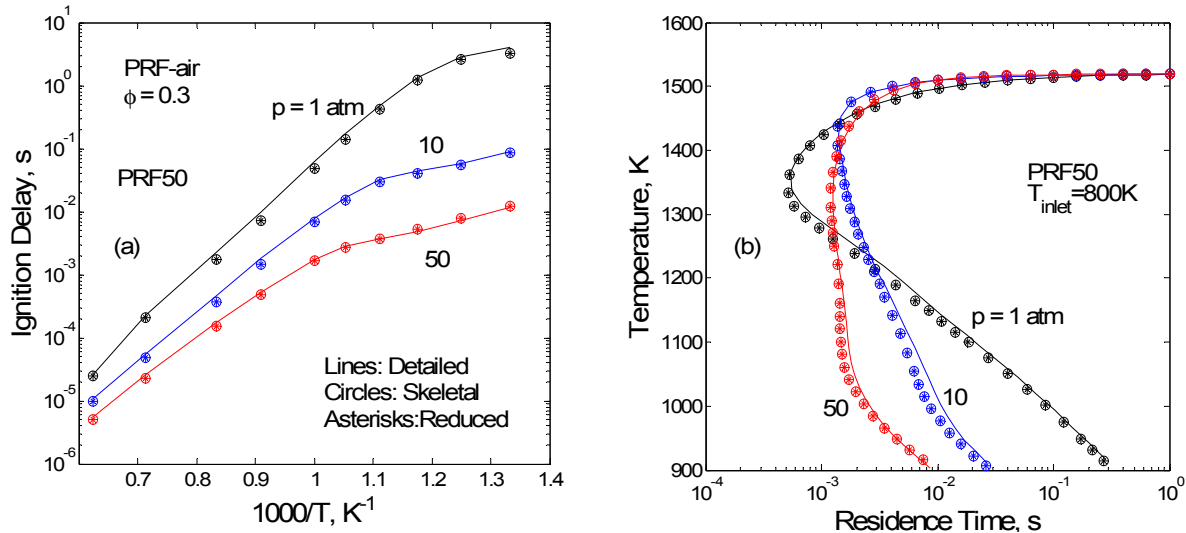


Figure 1. Comparison of the 171-species skeletal and 116-species reduced mechanisms with the detailed mechanism for a) constant-pressure ignition delays, b) extinction temperatures in PSR [1].

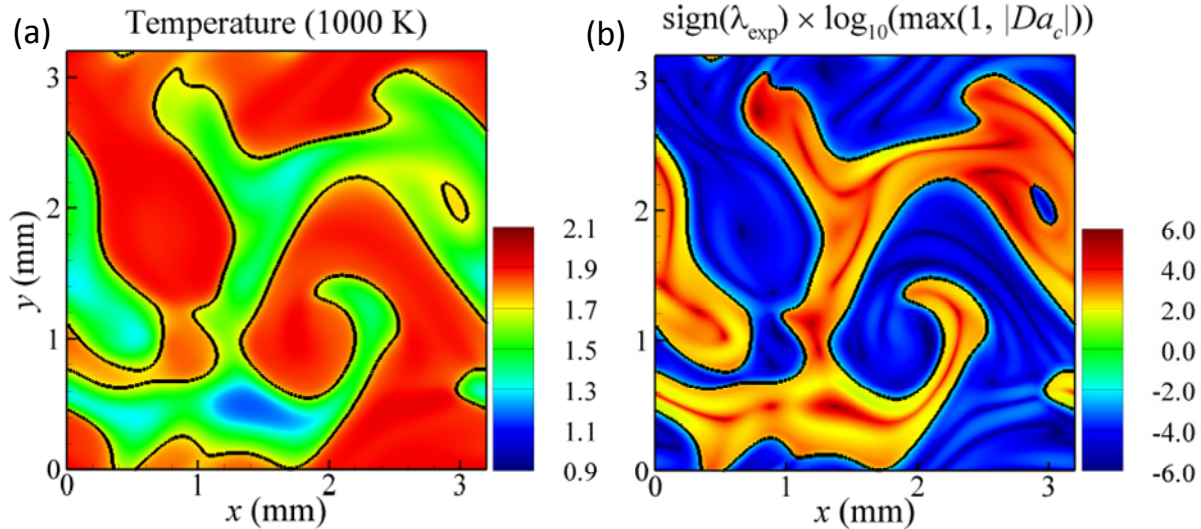


Figure 2. Isocontour of (a) temperature, and (b) a Damköhler number defined on CEMA, for a 2-D DNS of HCCI with PRF/air at  $\tau/\tau_{ig} = 0.95$  with 15K RMS initial temperature fluctuations (Simulation by C.S.Yoo) [1].

To simulate lifted jet flame combustion at diesel engine conditions, a detailed mechanism for n-dodecane was updated, reduced and integrated into diesel engine simulations (collaboration with W.J. Pitz and S. Som) [2]. The updated detailed mechanism consists of more than 2000 species involving the negative temperature coefficient (NTC) chemistry. A 106-species skeletal mechanism was derived and employed to simulate a lifted diesel jet flame as shown in Fig. 3. The skeletal mechanism was comprehensively validated in 0-D, 1-D and 3-D combustion systems. Good agreement was observed in the flame lift-off length (LOL) as shown in Fig. 3, which compared the simulated temperature isocontour (by S. Som) and experimentally measured OH chemiluminescence data [iv].

### B. A bifurcation analysis to identify important reactions for limit flame phenomena

A bifurcation analysis was developed (manuscript in preparation) to systematically identify limit flame phenomena, including ignition, extinction and changes in flame stability, and to understand the underlying physicochemical processes controlling the limit phenomena of steady state flames. A

bifurcation index was further defined to quantify the importance of the reactions and the mixing/transport process to the limit phenomena. Figure 4a shows the *S*-curve for a rich DME/air mixture with NTC behaviors in a steady state perfectly stirred reactor (PSR). The actual flame ignition and extinction states, which may be different from the conventionally regarded turning points, were rigorously detected by bifurcation analysis as the transition states between the stable (solid lines) and unstable (dashed lines) states.

Controlling reactions for the ignition and extinction states were identified by the bifurcation indices as shown in Fig. 4b for the extinction state of the strong flames ( $E_2'$  in Fig. 4a) and that of the cool flames ( $E_1'$ ), respectively. It was found that the strong flame extinction was primarily controlled by the reactions relevant to CO formation, while the extinction of the cool flames involves the NTC chemistry, as expected.

The importance of the reactions in Fig. 4b identified with the bifurcation analysis was verified by perturbing the “A”-factors and recalculating the extinction states with the perturbed mechanisms. It was found that uncertainties (or perturbations) in the “A”-factors of such identified reactions have significant effects on the corresponding extinction states as shown in Fig. 5, and thus their rate parameters should be determined with high accuracy in detailed kinetics. In reduced chemistry, the “A”-factors of these reactions can be slightly tuned to obtain highly reduced mechanism that can accurately predict ignition, extinction and onset of flame instabilities.

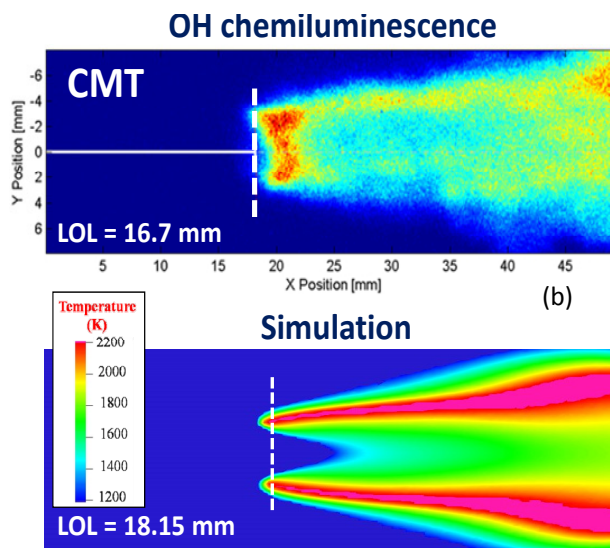
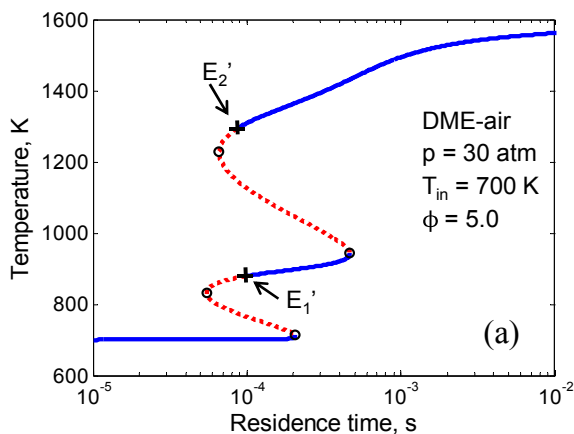


Figure 3. OH chemiluminescence image [iv] and simulated temperature contour plot for a lifted jet flame of n-dodecane into heated air (RANS simulation by S. Som).

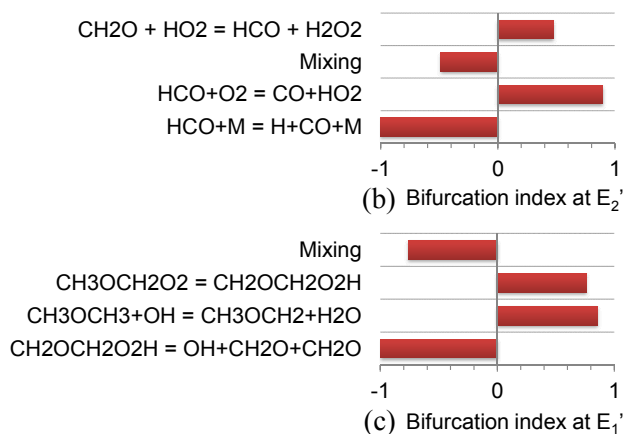


Figure 4. (a) The *S*-curve for a rich DME/air mixture in PSR (solid lines: stable, dashed: unstable). (b) and (c) the important reactions identified with bifurcation indices for the extinction of strong and cool flames, respectively.

### III. Future Work

In the next stage of the proposed research, we plan to further validate and finalize the reduced chemistry for gasoline and diesel surrogates and generate 2-D and 3-D DNS data with the reduced

mechanisms. Dynamic adaptive chemistry and other reduction algorithms will be further investigated to achieve highly efficient flame simulations. Computational diagnostic methods will be created by extending CEMA and the bifurcation analysis for both spatially homogenous and diffusive flames for systematic identification and modeling of the critical flame features in complex turbulent flames. DNS data reduction will also be investigated.

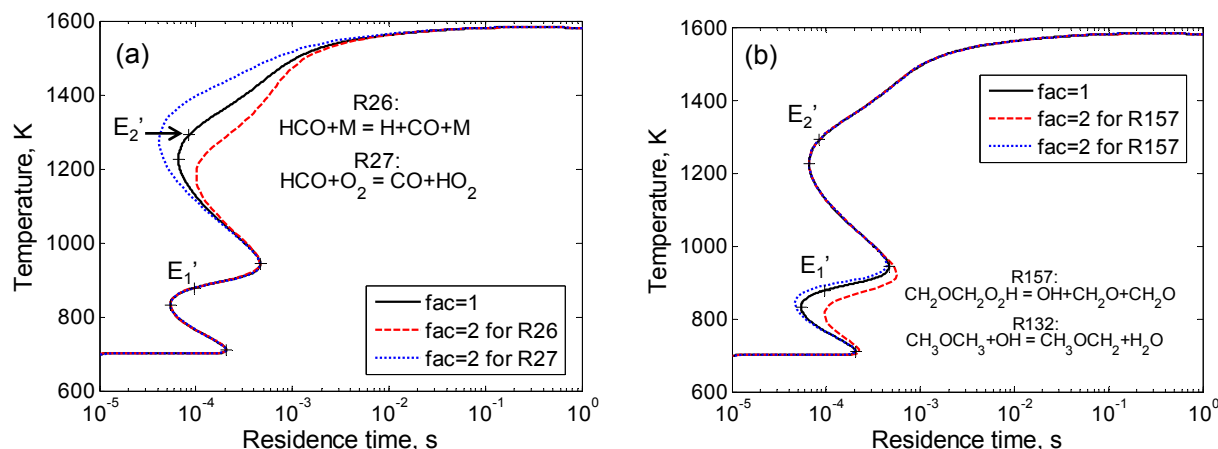


Figure 5. S-curves for DME/air with different perturbations in the “A”-factors of the important reactions for (a) the extinction of strongly burning flames,  $E_2'$  and (b) the extinction of cool flames,  $E_1'$ . “fac” represents the factor multiplied to the “A”-factors.

#### IV. References

- i. Lu, T.F.; Yoo, C.S.; Chen, J.H.; Law, C.K. *J. Fluid Mech.*, **2010** 652 (1) 45–64.
- ii. T. Lu, C. K. Law; *Prog. Energy Combust. Sci.* **2009**, 35(2), 192-215.
- iii. Mehl, M.; Pitz, W.J.; Westbrook, C.K.; Curran, H. *J. Proc. Combust. Inst.* **2011** 33, 193-200.
- iv. Payri F. et al. Engine Combustion Network (ECN), available at <http://www.cmt.upv.es/ECN07.aspx>

#### V. Publications and submitted journal articles supported by this project 2010-2012

1. M.B. Luong, Z. Luo, T.F. Lu, S.H. Chung, C.S. Yoo, "Direct numerical simulations of the ignition of lean primary referencefuel/air mixtures under HCCI condition," *Combust. Flame*, submitted
2. Z. Luo, S. Som, S.M. Sarathy, M. Plomer, W.J. Pitz, D.E. Longman, T.F. Lu, "Development and Validation of an n-Dodecane Skeletal Mechanism for Diesel Spray-Combustion Applications," *Combust. Theory Model.*, submitted.

# Advanced Nonlinear Optical Methods for Quantitative Measurements in Flames

Robert P. Lucht

School of Mechanical Engineering, Purdue University

West Lafayette, IN 47907-2088

Lucht@purdue.edu

## I. Program Scope

Nonlinear optical techniques such as laser-induced polarization spectroscopy (PS), resonant wave mixing (RWM), and electronic-resonance-enhanced (ERE) coherent anti-Stokes Raman scattering (CARS) are techniques that show great promise for sensitive measurements of transient gas-phase species, and diagnostic applications of these techniques are being pursued actively at laboratories throughout the world. The objective of this research program is to develop and test strategies for quantitative concentration and temperature measurements using nonlinear optical techniques in flames and plasmas. We have continued our fundamental theoretical and experimental investigations of these techniques. We have also initiated both theoretical and experimental efforts to investigate the potential of femtosecond (fs) laser systems for sensitive and accurate measurements in gas-phase media. Our initial efforts have been focused on fs CARS, although the systems will be useful for a wide range of future diagnostic techniques involving two-photon transitions.

Over the past year we have continued our PS measurements of atomic hydrogen in flames. We developed and optimized a new laser system for the PS measurements of atomic hydrogen featuring two injection-seeded optical parametric generator/pulsed dye amplifier (OPG/PDA) systems at 656 nm and 486 nm. We are now in the process of developing and aligning a system with OPG/PDA stages for generation of 460.2 nm and 480 nm beams for PS measurements of carbon monoxide. The 460.2 nm beam will be frequency-doubled to provide the 230.1 nm excitation beam for the two-photon X-B transition, and the 480 nm beam will be used to probe the B-A transition.

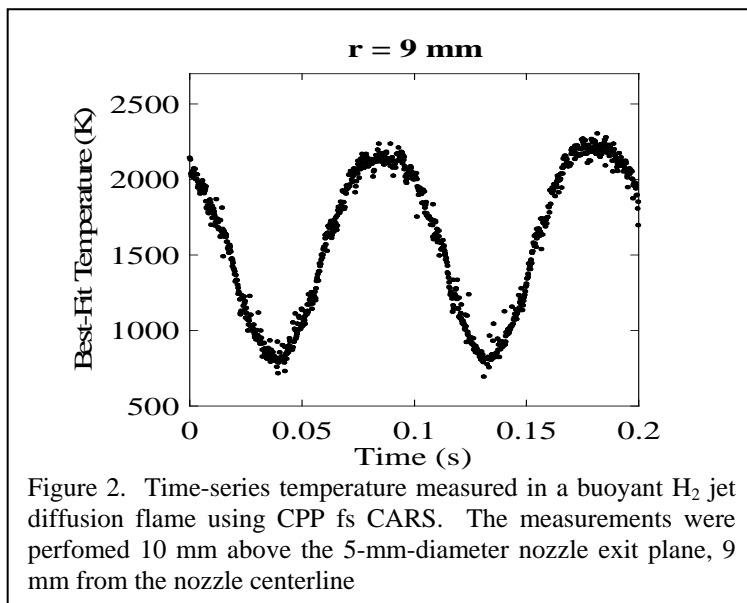
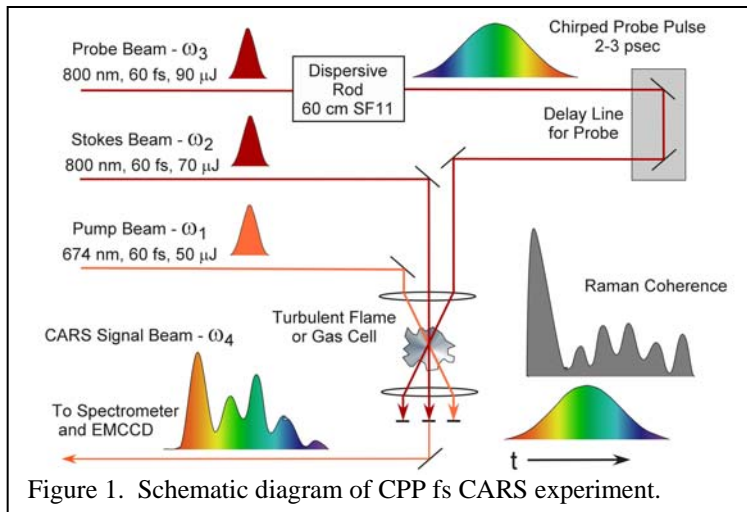
We are investigating the physics of these processes by direct numerical integration (DNI) of the time-dependent density matrix equations for the resonant interaction. Significantly fewer restrictive assumptions are required using this DNI approach compared with the assumptions required to obtain analytical solutions. Inclusion of the Zeeman state structure of degenerate levels has enabled us to investigate the physics of PS and of polarization effects in DFWM and ERE CARS. We are concentrating on the accurate simulation of two-photon processes, including Raman transitions, where numerous intermediate electronic levels contribute to the two-photon transition strength. We also have modified the code to calculate PS and 6WM signal intensities based on spatial integration along the signal beam path.

We also developed a new technique for simultaneous pure rotational and vibrational CARS during the past year. This method takes advantage of a newly discovered two-beam phase-matching scheme for pure rotational CARS.

## II. Recent Progress

### A. Femtosecond CARS Calculations and Experiments

Fs CARS offers several major potential advantages compared with nanosecond (ns) CARS; i.e., CARS as usually performed with nanosecond pump and Stokes lasers. These potential advantages include an elimination of collisional effects in the signal generation and the capability of performing real-time temperature and species measurements at data rates of 1 kHz or greater as compared to 10-50 Hz for ns CARS. Our Coherent ultrafast laser system operates at 5 kHz with a fundamental pulse width of 60 fs and energy of over 2 mJ. The fundamental 800-nm pulse is Fourier-transform-limited to within a few percent. The fundamental 800-nm beam is used as the probe beam for our chirped-pulse-probe (CPP) fs CARS experiments as shown in Fig. 1. The greatly increased pulse energy of the



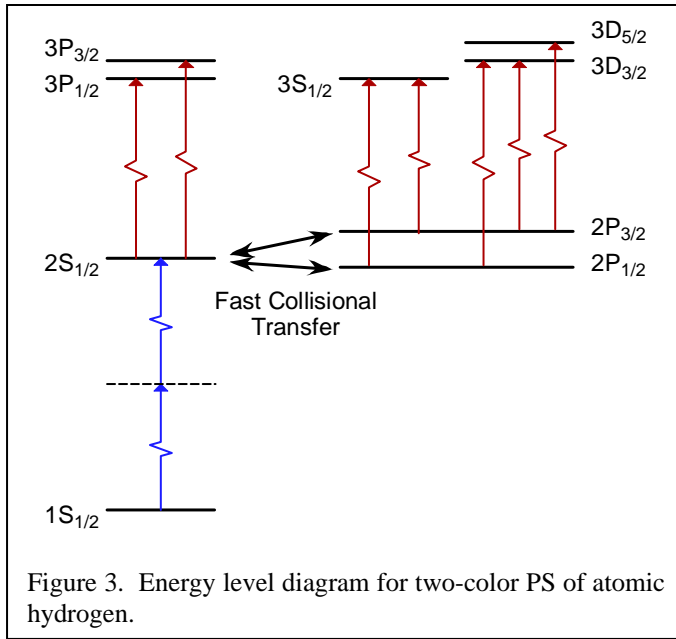
chirped-pulse-probe beam results in a significant increase in the signal-to-noise ratio of the single-pulse measurements.

During the past year single-laser-shot temperature measurements at a data rate of 5 kHz were performed in near-adiabatic laminar flames and in a buoyant turbulent jet diffusion flame. Measurements were performed in the near-nozzle region of a hydrogen jet diffusion flame. The near-nozzle region has buoyant instabilities, so it is unsteady, but the structures are very repeatable so it is not really turbulent in this region. This allowed us to test the dynamic range of the single-shot fs CARS measurements in a system where the temperature fluctuations should be smooth and bounded between room temperature (300 K) and the adiabatic flame temperature (~2400 K). A typical time series from the near-nozzle region is shown in Fig. 2. The precision of the measurement is on the order of 50 K and the dynamic range extends from 400 K to 2400 K, limited at the lower end by camera saturation. At the upper end, the signal-to-noise ratio is still acceptable but decreases rapidly as the temperature increases.

The physics of the CPP fs CARS process was previously analyzed using a time-dependent density matrix analysis. The time-dependent density matrix equations for the fs CARS process were formulated and manipulated into a form suitable for solution by direct numerical integration (DNI). The temporal shapes of the pump, Stokes, and probe laser pulses are specified as an input to the DNI calculations. Based on these numerical results, a much faster fitting code was developed to generate synthetic CPP fs CARS spectra. The parameters in the fitting code were varied to obtain the best fit theoretical spectrum for a given experimental spectrum, and temperature was determined as one of the best-fit parameters. This code is described in detail in publication P3.

### B. Polarization Spectroscopy and Six-Wave Mixing: Experiments and Modeling Efforts

We developed and have continued to apply a new experimental apparatus for high-spectral-resolution PS measurements. The system features two OPG stages that injection seeded at the idler wavelength and pumped by the 355-nm third harmonic radiation from an injection-seeded Nd:YAG laser. The signal radiation from OPGs is then amplified using two separate pulse dye amplifier stages. The first species of interest for us was atomic hydrogen experiments featuring OPGs seeded at 1313 nm and 772 nm with signal outputs at 486 nm and 656 nm, respectively. This system is described in



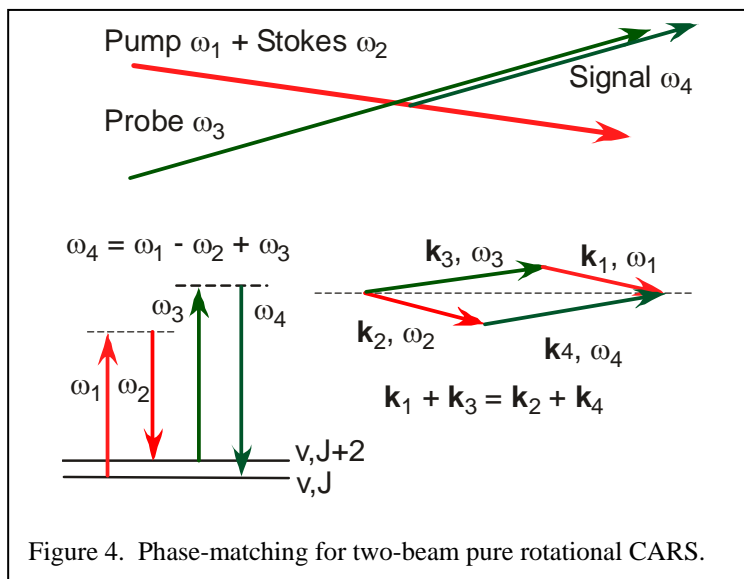
detail in P4. The 486-nm beam is then frequency-doubled to 243 nm for two-photon excitation of the 1S-2S resonance. The 656-nm beam is used to probe the 2S-3P transition using polarization spectroscopy. The 656-nm beam is split into a relatively strong circularly polarized pump beam and a linearly polarized probe beam. This energy level structure for this process is depicted schematically in Fig. 3. We have used this system in the past year for an extensive investigation of atomic hydrogen PS line shapes in near-adiabatic hydrogen-air flames, and investigated the accuracy and precision of concentration measurements of atomic hydrogen in these flames. The system is in the process of being modified for planned measurements of CO; this requires the new injection

seeding sources for the OPGs to produce signal wavelengths of 460.2 nm and 480 nm, and some reconfiguration of the PDA stages for the 480-nm probe beam.

We are continuing our collaborative efforts with Dr. Thomas B. Settersten at Sandia's Combustion Research Facility on six-wave mixing (6WM) spectroscopy and PS of atomic hydrogen. The DNI computer code for the calculation of 6WM and PS signals from atomic hydrogen was significantly modified to incorporate all of the different possible photon mixing processes that can potentially contribute to both the 6WM and PS signals. The computer code has been modified recently to compute the PS signal by integrating over the path length of the PS probe beam, a modification that was necessary to account for the saturation of the 2S-3P transition in the experiments.

### C. Development of a New System for Combined Pure Rotational and Vibrational CARS

We have developed a new scheme for simultaneous generation and detection of pure rotational and vibrational N<sub>2</sub> CARS using two 532-nm pump beams and a 607-nm dye laser beam. The generation of both the pure rotational and the vibrational CARS signals is advantageous because pure rotational CARS is an excellent



thermometry technique for temperatures below 1000 K, and vibrational CARS is most accurate for temperatures above 1000 K. The pure rotational CARS signal is generated by the interaction of either 532-nm beam with the 607-nm beam, and is essentially collinear with either 532-nm beam. The phase-matching scheme for the two-beam pure rotational CARS is shown in Fig. 4. Recent developments in short-wave pass filters allow us to detect the pure rotational CARS signal in the presence of the very strong 532-nm

beam. We have demonstrated the simultaneous detection of both pure rotational and N<sub>2</sub> vibrational CARS in near adiabatic hydrogen/air flames; these measurements and the experimental system are discussed in P7.

### III. Future Work

We will continue to perform fs CARS experiments in our laboratory using the Coherent ultrafast laser system. Our studies of concentration measurements using CPP fs CARS will continue. We will explore the potential for using CPP fs CARS for accurate concentration measurements for water vapor, a very hard species to measure using ns CARS. We will also investigate the potential for measuring mixtures of hydrocarbon species.

Our investigation of the physics of two-photon, two-color PS and 6WM measurements of species such as CO will continue. We have developed a new experimental apparatus for these measurements and collected extensive line shape and concentration data for atomic hydrogen. We have nearly completed the installation and alignment of the optics needed for two-color PS and/or 6WM studies of CO. We will be able to explore collisional effects on the PS and 6WM processes in much more detail using a low-pressure cell filled with CO and different buffer gases. We will continue to use the density matrix code for comparison with and interpretation of the data, and to gain insight into the physics of the PS and 6WM processes.

In the future we plan to introduce a dual-pump CARS variant of the technique for sensitive detection of three or more species along with the temperature measurement from both pure rotational and vibrational CARS. We plan to combine the two-beam pure rotational CARS with a dual-beam CARS system where the vibrational spectra for H<sub>2</sub> and N<sub>2</sub> are detected simultaneously.

### IV. Refereed publications and submitted journal articles supported by this project 2011-2013

- P1. D. R. Richardson, R. P. Lucht, S. Roy, W. D. Kulatilaka, and J. R. Gord, "Single-Laser-Shot Femtosecond Coherent Anti-Stokes Raman Scattering Thermometry at 1000 Hz in a Driven H<sub>2</sub>-Air Flame," *Proc. Combust. Inst.* **33**, 839-845 (2011).
- P2. S. Roy, R. P. Lucht, and J. R. Gord, "Orientation and Alignment Dynamics During Generation of Laser-Induced Polarization Spectroscopy (LIPS) Signal," *JOSA B* **28**, 208-219 (2011).
- P3. D. R. Richardson, R. P. Lucht, S. Roy, W. D. Kulatilaka, and J. R. Gord, "Theoretical Modeling of Single-Laser-Shot, Chirped-Probe Pulse Femtosecond Coherent Anti-Stokes Raman Scattering Thermometry," *Applied Physics B* **104**, 699-714(2011).
- P4. A. H. Bhuiyan, A. Satija, S. V. Naik, and R. P. Lucht, "Development of a Two-Color Laser System for High-Resolution Polarization Spectroscopy Measurements of Atomic Hydrogen," *Optics Letters* **37**, 3564-3566 (2012).
- P5. D. R. Richardson, D. Bangar, and R. P. Lucht, "Polarization Suppression of the Nonresonant Background in Femtosecond Coherent Anti-Stokes Raman Scattering for Flame Thermometry at 5 kHz," *Optics Express* **20**, 21495 (2012).
- P6. D. R. Richardson, R. P. Lucht, S. Roy, W. D. Kulatilaka, and J. R. Gord, "Chirped-Probe-Pulse Femtosecond Coherent Anti-Stokes Raman Scattering Concentration Measurements," *Journal of the Optical Society of America B* **30**, 188-196 (2013).
- P7. A. Satija and R. P. Lucht, "Development of a New Combined Pure Rotational and Vibrational Coherent Anti-Stokes Raman Scattering (CARS) System," *Optics Letters*, submitted for publication (2013).

### V. PhD theses completed by students supported by this project 2011-2013

- T1. Aizaz Bhuiyan, "Polarization Spectroscopy Measurements of Atomic Hydrogen in Flames," Purdue University, May 2012.
- T2. Daniel R. Richardson, "Femtosecond CARS Spectroscopy for High-Data-Rate Temperature Measurements," Purdue University, July 2012.

# Time-Resolved Infrared Absorption Studies of Radical-Radical Reactions

R. G. Macdonald  
Chemistry Division  
Argonne National Laboratory  
Argonne, IL 60439  
Email: rgmacdonald@anl.gov

## Background

Information about the dynamics of radical-radical reactions is sparse. However, these processes are important in combustion being either chain propagating or terminating steps as well as potentially producing new molecular species. For almost all radical-radical reactions, multiple product channels are possible, and the determination of product channels will be a central focus of this experimental effort. In the current experiments, both transient species are produced by excimer laser photolysis of suitable photolytes, and if possible, two species are detected simultaneously using different continuous-wave laser sources operating in the red, near infrared and infrared spectral regions. This approach allows for the direct determination of the second-order rate constant under any concentration conditions if the appropriate absorption cross sections have been measured. The time dependence of individual ro-vibrational states of the reactants and/or products is followed by frequency- and time-resolved absorption spectroscopy. The simultaneous detection of multiple species ensures that species concentration profiles can be normalized to a common set of reaction conditions. In order to determine branching ratios and second-order rate constants, it is necessary to measure state-specific absorption coefficients and transition moments of radicals. These measurements play an important role in this experimental study.

## Recent Results

The old rectangular reaction chamber has been replaced by a new stainless steel cylindrical chamber, approximately 120 x 15 cm. The new chamber is heated by 6 barrel heaters divided into 3 zones. Three PID controllers provide uniform heating along the length of cylinder. Brewster-angle CaF<sub>2</sub> windows admit the UV laser photolysis and probe laser radiation. The window holders are heated by separate heating elements. The laser radiation passes through the center of the chamber remote from the walls. Temperatures over 400 C can be obtained with a uniformity of about 3 Celsius degrees over the length of the 150 cm optical path. The gas mixtures are injected into the chamber through a series of fine holes evenly spaced along the length of the chamber by a 1/4 inch diameter stainless steel tube. The gases are preheated by placing another 1/8 inch diameter tube inside the first. This injection arrangement reduces the possibility of back flow of chamber gases into the injection region by creating a large pressure differential between the injection region and the chamber. Thus, measurements of rate constants can be made over a large pressure range, from a few Torr to over several hundred Torr.

## **NH<sub>2</sub>(X<sup>2</sup>B<sub>1</sub>) + NH<sub>2</sub>(X<sup>2</sup>B<sub>1</sub>) Recombination**

Work is continuing on the study of  $\text{NH}_2 + \text{NH}_2$  and  $\text{NH}_2 + \text{H}$  radical-radical recombination reactions over an extended temperature and pressure ranges. The  $\text{NH}_2 + \text{NH}_2$  system is an ideal system to study the influence of different third bodies on a simple radical-radical recombination reaction. The theoretical calculations of Klippenstein *et al* (*J. Phys. Chem. A* **2009**, *113*, 10241) show that near 300 K bimolecular rate processes make little contribution to the removal process of  $\text{NH}_2$ ; furthermore, these workers have calculated the low and high pressure limits for this system. The reaction system is quite straightforward:



Both  $\text{NH}_2$  and  $\text{NH}_3$  are monitored simultaneously following the photolysis laser pulse. The loss of  $\text{NH}_3$  provides a direct measure of the  $\text{NH}_2$  radical concentration. With the extended mode hop free tuning range of the new dual cavity OPO laser, it is straightforward to determine the  $\text{NH}_3$  concentration by recording on and of line laser intensity.

As the pressure increases, the  $\text{NH}_3$  temporal profiles are sensitive to the recombination rate reaction:



and it is possible to measure the recombination rate constant for reaction 2. To date, the temperature and pressure dependence of reactions 1 and 2 have been made with  $\text{CF}_4$  as the third body over a temperature range of 295 to 450 K and pressure range of 2 to 100 Torr.

The pressure and temperature dependence of the  $\text{NH}_2$  self-recombination reaction rate constant was fit to Troe parameters by fixing  $k_\infty$  to the theoretical estimate of Klippenstein *et al* *J. Phys. Chem A* *113*, 10241 (2009) and varying  $k_0(T)$  and  $F_e$ , assuming  $F_e$  is independent of temperature. With the extended pressure range the determination of these parameters is better defined. At 295 K, the value of  $F_e$  was found to be slightly reduced from the previous measurement to 0.50 and  $k_0(295) = 7.4 \times 10^{-29} \text{ cm}^6 \text{ molecule}^{-1} \text{ s}^{-1}$ , 10 % smaller. The temperature dependence of  $k_0$  was surprising large, decreasing a factor of 5.5 over the temperature range. For  $\text{CF}_4$  as third body,  $k_0$  had a  $T^{-4.0}$  dependence compared to the theoretical prediction for  $k_0$  with  $\text{N}_2$  as collision partner of  $T^{-2.7}$ . For  $\text{NH}_2 + \text{H}$ , the measurements appeared to be in the low pressure regime even up to 100 Torr and the bimolecular rate constants were linear with third body pressure. The slope provided an improved measurement of  $k_0(\text{NH}_3)$  to be  $5.7 \times 10^{-30} \text{ cm}^6 \text{ molecule}^{-1} \text{ s}^{-1}$  at 296 K. The temperature dependence for  $k_0(\text{NH}_3)$  was found to be  $T^{-1.0}$ . There are no previous temperature measurements for this rate constant. Work is continuing to further extend these measurements to both higher temperatures and pressures.



Work has been started on the study of the OH + OH abstraction reaction as a function of temperature. This reaction has important consequences in combustion processes in its own right but also has been treated as a test case for the study of radical-radical reactions in general. It is important to establish the rate constant for the abstraction channel in order to determine accurate measurements of the recombination rate constant for the OH + OH → H<sub>2</sub>O<sub>2</sub>. Previous work from this laboratory, (Bahng and Macdonald, J. Phys. Chem. **111**, 3850 (2007)) measured a rate constant at 295 K that was almost a factor of two greater than the IUPAC recommended value. Recent work from another laboratory (Sangwan and Krasnoperov, J. Phys. Chem. **116**, 11817 (2012)), seemed to confirm the IUPAC value and extended the temperature measurement to 400 K. However, these workers used an indirect method to determine the rate constant in contrast to the direct measurements of Bahng and Macdonald. Besides the inherent difficulty in measuring rate constants for radical-radical reaction, this reaction is difficult to study because the rate constant is much smaller than typical radical-radical reactions near 300 K.

In the present experiments, the OH radical was produced by the reaction of O(<sup>1</sup>D) with H<sub>2</sub>O, following the 193 nm photolysis of N<sub>2</sub>O. The carrier gas was CF<sub>4</sub>, chosen to lower the diffusion rate of OH and not quench O(<sup>1</sup>D). The OH radical was monitored on the P<sub>1e/1f</sub>(4.5) line of the fundamental vibrational transition. The measurements were made over the pressure range of 3 -12 Torr and temperature range of 295 – 647 K. First-order loss by diffusion and flow play an important role in these measurements. Generally, at initial OH radical pressures < 2x10<sup>12</sup> molecules cm<sup>-3</sup>, the abstraction reaction accounts for less than 5% of the loss of OH and the diffusion/flow rate constant can be estimated. The rate constants are determined by profile simulations of the reaction system. At low temperatures, recombination contributes to loss of OH but the rate constant decreases significantly with increasing temperature. The results of the measurements so far are summarized in Figure 1.

### **Publications 2009-present.**

*Determination of the rate constants for the radical-radical reactions NH<sub>2</sub>(X<sup>2</sup>B<sub>1</sub>) + NH<sub>2</sub>(X<sup>2</sup>B<sub>1</sub>) Recombination Reaction with Collision Partners He, Ne, Ar, and N<sub>2</sub> at Low Pressures and 296 K. Part 1, G. Altinay and R. G. Macdonald, J. Phys. Chem. **2012**, *116*, 1353-1367.*

*Determination of the rate constants for the radical-radical reactions NH<sub>2</sub>(X<sup>2</sup>B<sub>1</sub>) + NH<sub>2</sub>(X<sup>2</sup>B<sub>1</sub>) and NH<sub>2</sub>(X<sup>2</sup>B<sub>1</sub>) + H Recombination Reactions with Collision Partners CH<sub>4</sub>, C<sub>2</sub>H<sub>6</sub>, CO<sub>2</sub>, CF<sub>4</sub>, and SF<sub>6</sub> at Low Pressures and 296 K. Part 2, G. Altinay and R. G. Macdonald, J. Phys. Chem. A, **2012**, *116*, 2161-2176.*

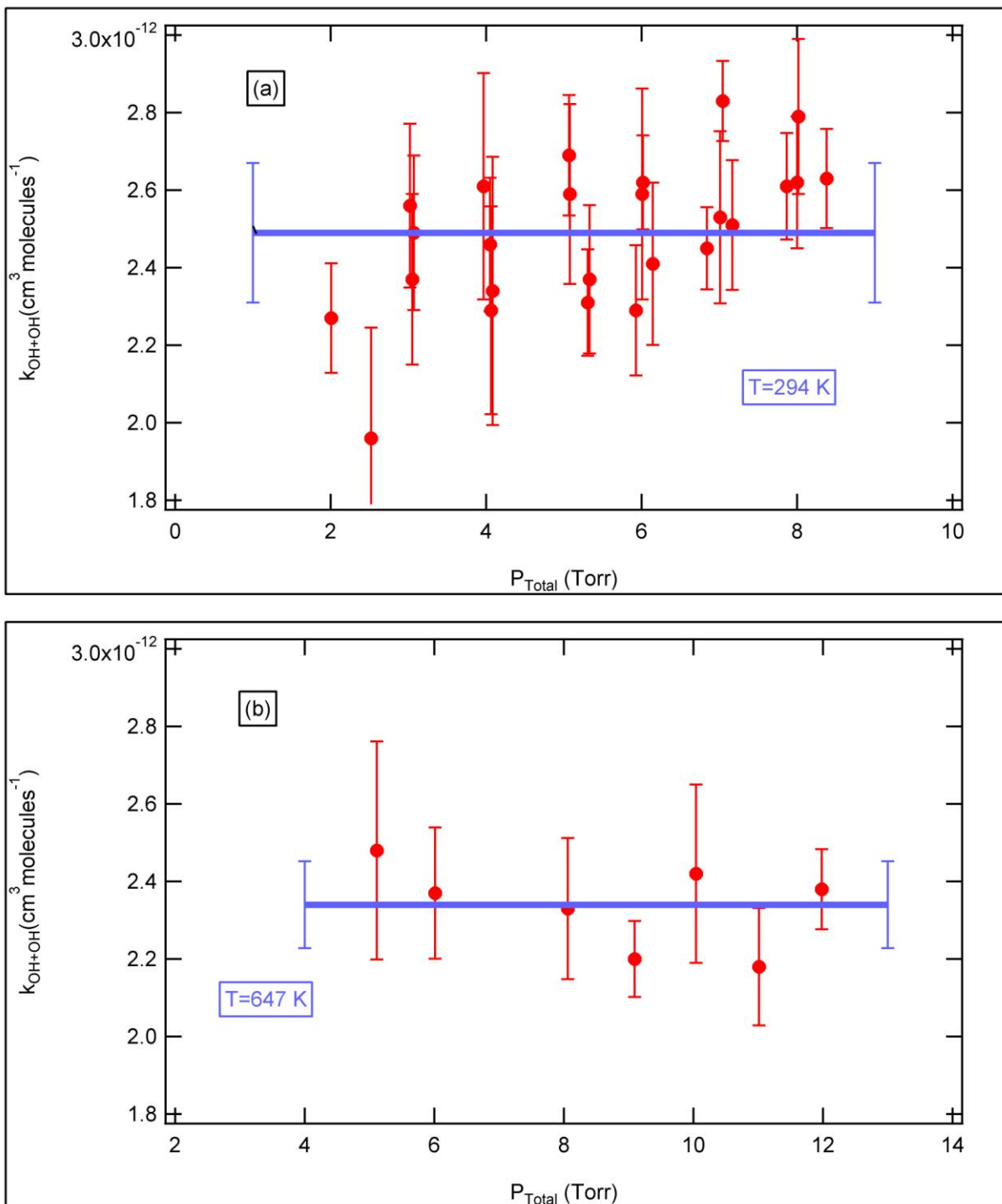


Figure 1. The results for the determination of the rate constant for the abstraction channel for the OH + OH reaction at 294 and 647 K. Each red dot is the average of at least 6 separate measurements of  $k_{\text{OH}+\text{OH}}$  at the indicated pressure but different initial OH concentrations. The error bars indicate the scatter in the experimental measurement at the  $\pm 1\sigma$  level. The blue lines are the average of all the data at that temperature. The data at 294 K is in good agreement with previous measurements from this laboratory using different laser systems, OH transitions and reaction chambers. Measurements at intermediate temperatures are in progress.

# Theoretical studies of chemical reactions related to the formation and growth of polycyclic aromatic hydrocarbons and molecular properties of their key intermediates

Alexander M. Mebel

Department of Chemistry and Biochemistry, Florida International University  
Miami, Florida 33199. E-mail: mebela@fiu.edu

## Program Scope

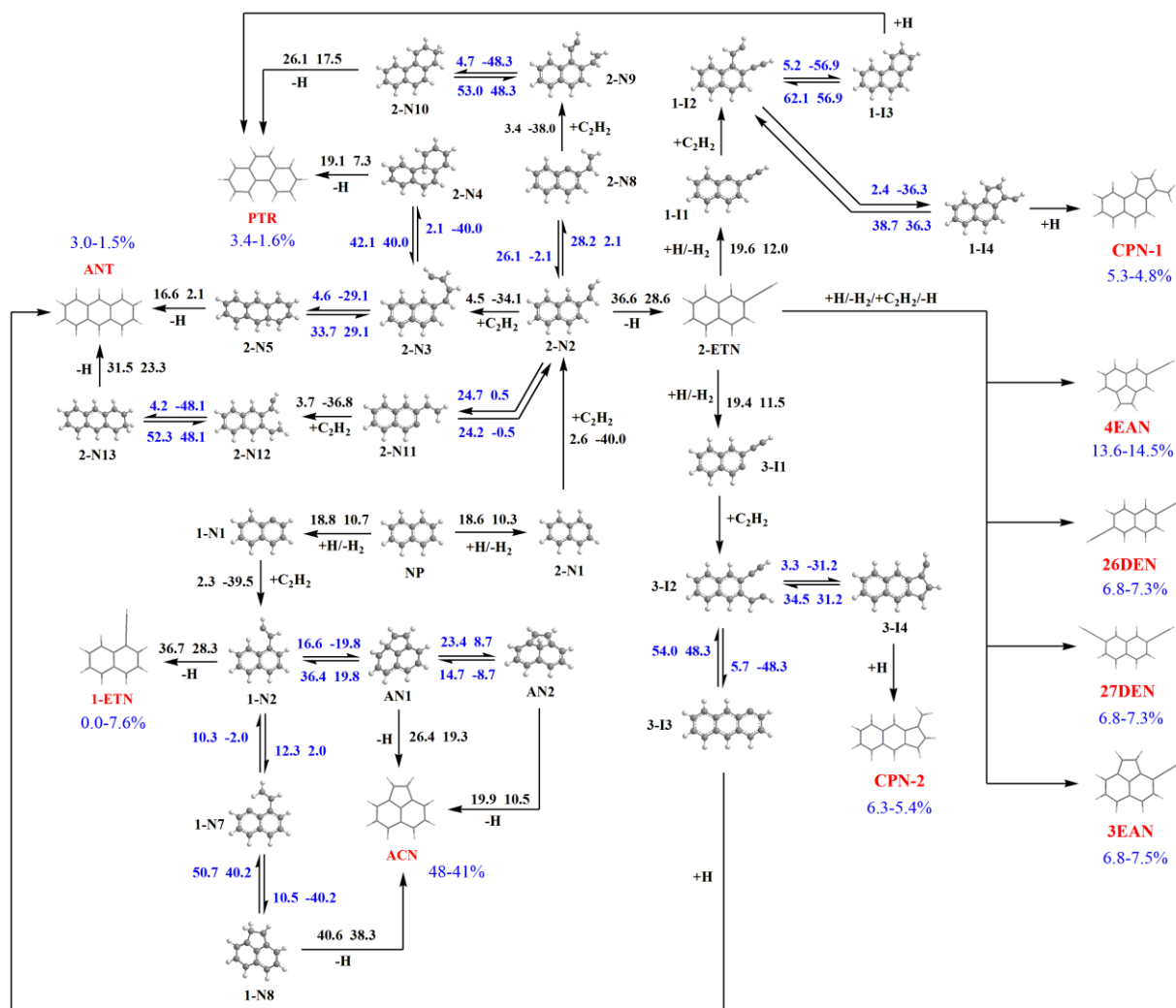
In this project, we investigate complex chemical mechanisms of PAH formation and growth via theoretical studies of their critical elementary reactions. Our primary objectives include (i) to unravel reaction mechanisms through detailed, accurate, and reliable calculations of pertinent potential energy surfaces (PESs); (ii) to compute rate constants for individual reaction steps and total absolute reaction rate constants and product branching ratios depending on reaction conditions, such as collision energy or temperature and pressure; (iii) to characterize molecular, energetic, and spectroscopic parameters of various possible reaction intermediates and products including their enthalpies of formation, geometric structure, vibrational frequencies and rotational constants, as well as photoionization and photoexcitation spectra. To achieve these goals, we employ chemically accurate ab initio and density functional calculations (using CCSD(T)/CBS, G3, G4, and explicitly correlated methods) of the PESs of these reactions which are then utilized for statistical (TST and RRKM/Master Equation) computations of absolute reaction rate constants and product branching ratios. The underlying theme of the current project period concerns the reactions of phenyl and cyclopentadienyl radical, which are able to produce the smallest PAH and CP-PAH molecules, naphthalene and indene, respectively. In addition, we investigate reactions of dicarbon  $C_2$  with unsaturated hydrocarbons producing resonance-stabilized free radicals (RSFR), which in turn can contribute to the formation of aromatic species and also a variety of oxidation reactions competing with the PAH growth.

## Recent Progress

*Product branching ratios in photodissociation of phenyl radical.* Ab initio CCSD(T)/CBS//B3LYP/6-311G\*\* calculations of the potential energy surface for possible dissociation channels of the phenyl radical were combined with microcanonical RRKM calculations of reaction rate constants in order to predict statistical product branching ratios in photodissociation of *c*- $C_6H_5$  at various wavelengths. The results indicate that at 248 nm the photodissociation process is dominated by the production of *ortho* benzyne via direct elimination of a hydrogen atom from the phenyl radical. At 193 nm, the statistical branching ratios are computed to be 63.4%, 21.1%, and 14.4% for the *o*- $C_6H_4 + H$ , *l*- $C_6H_4$  ((*Z*)-hexa-3-ene-1,5-diyne) + H, and *n*- $C_4H_3 + C_2H_2$  products, respectively, in a contradiction with recent experimental measurements, which showed  $C_4H_3 + C_2H_2$  as the major product. Although two lower energy pathways to the *i*- $C_4H_3 + C_2H_2$  products are identified, they appeared to be kinetically unfavorable and the computed statistical branching ratio of *i*- $C_4H_3 + C_2H_2$  does not exceed 1%. To explain the disagreement with experiment, we optimized conical intersections between the ground and the first excited electronic states of  $C_6H_5$  and, based on their structures and energies, suggested the following photodissociation mechanism at 193 nm: *c*- $C_6H_5$  **1** → absorption of a photon → electronically excited **1** → internal conversion to the lowest excited state → conversion to the ground electronic state via conical intersections at **CI-2** or **CI-3** → non-statistical decay of the

vibrationally excited radical favoring the formation of the  $n\text{-C}_4\text{H}_3 + \text{C}_2\text{H}_2$  products. This scenario can be attained if the intramolecular vibrational redistribution in the **CI-2** or **CI-3** structures in the ground electronic state is slower than their dissociation to  $n\text{-C}_4\text{H}_3 + \text{C}_2\text{H}_2$  driven by the dynamical preference.

*Formation mechanism of polycyclic aromatic hydrocarbons beyond the second aromatic ring.* The formation mechanism of polycyclic aromatic hydrocarbons (PAH) containing three rings starting from naphthalene has been studied using accurate ab initio G3(MP2,CC)//B3LYP/6-311G\*\* calculations followed by kinetic analysis of various reaction pathways and computation of relative product yields. The results reveal new insights into the classical Hydrogen Abstraction aCetylene Addition (HACA) scheme of PAH growth. The HACA mechanism has been shown to produce mostly cyclopentafused PAHs instead of PAHs with six-member rings only, in contrast to the generally accepted view on this mechanism. For naphthalene, the HACA-type synthesis of higher PAHs with all six-member rings, anthracene and phenanthrene, accounts only for 3-6% of the total product yield at temperatures relevant to combustion (1000-2000 K), whereas cyclopentafused PAHs, including acenaphthalene (41-48%), 4-ethynylacenaphthalene (~14%), 3-ethynylacenaphthalene (~7.5%), 1-methylene-1H-cyclopenta[b]naphthalene (~6%), and 3-methylene-3H-cyclopenta[a]naphthalene (~5%) account for another ~75%. It has been shown that acetylene addition to the radical site adjacent to the bay region in naphthalene (as in 1-naphthyl



radical) or other similar PAH with a bay region is highly unlikely to be followed by the addition of a second acetylene molecule; alternatively, the bay region closure with a build-up of a new five-member ring occurs. Acetylene addition to a non-bay carbon atom (as in 2-naphthyl radical) can be followed by the second acetylene addition only at  $T < 1000$  K and lead to anthracene and phenanthrene. However, at temperatures relevant to combustion such pathways give negligible contributions to the total product yield, whereas the dominant reaction product, 2-ethynyl-naphthalene, is formed by simple hydrogen atom elimination from the attached ethenyl group. An additional six-member ring build-up may occur only after intermolecular hydrogen abstraction from ethynyl-substituted PAH (2-ethynyl-naphthalene), in particular, from the carbon atoms adjacent to the existing ethynyl ( $C_2H$ ) fragment, followed by  $C_2H_2$  addition producing adducts with two ethynyl  $C_2H$  and ethenyl  $C_2H_2$  groups next to each other, which then undergo a fast six-member ring closure. Nevertheless, this process has been shown to be relatively minor (~25%), whereas the major process is a five-member ring closure involving the same  $C_2H$  and  $C_2H_2$  groups and leading to a cyclopentafused PAH molecule. Although the computed product yields show a good agreement with experimentally observed concentrations of acenaphthalene and anthracene in various aliphatic and aromatic flames, the yield of phenanthrene, which exhibits an order of magnitude higher concentrations than anthracene both in combustion flames and environmental mixtures, via the considered pathways is significantly underpredicted. This result points at possible existence of another mechanism responsible for the formation of phenanthrene and other all-six-member-ring PAHs. The overall kinetic scheme for the HACA build-up process leading to various three-ring PAHs (both with six-member rings only and cyclopentafused) from naphthalene, which can be included in flame kinetic models, has been constructed, with rate constants for all individual reaction steps provided.

### Future Plans

We continue investigating PESs relevant to the formation of larger PAH molecules (anthracene, phenanthrene, chrysene, pyrene, benzopyrene, etc.) via HACA sequences and other possible mechanisms with the goal to understand relative abundances of various PAH molecules in different isomeric forms in combustion flames and environmental samples. The PES calculations will be followed by kinetic computations of reaction rate constants and product branching ratios at various combustion conditions. RRKM-ME calculations are underway for the reactions of oxidation of phenyl and naphthyl radicals,  $C_6H_5/C_{10}H_7 + O_2$ , employing MultiWell and MESMER codes for solving Master Equations. Finally, we study the mechanism and product branching ratios of the reactions of dicarbon,  $C_2(^1\Sigma_g^+ / ^3\Pi_u)$ , with propene  $C_3H_6$  and  $C_4H_6$  isomers 1,2-butadiene and 1- and 2-butyne, in collaboration with Ralf Kaiser's group at the University of Hawaii, who explore these reactions under single-collision conditions of crossed molecular beams. The reactions may potentially lead to the formation of cyclopentadienyl and phenyl radicals as well as to a variety of RSFR, including chain  $C_6H_5$ ,  $C_5H_5$ ,  $C_5H_3$ , and  $C_4H_3$  isomers.

### DOE/BES sponsored publications (2010-2013)

1. Kaiser R.I., Mebel A.M., Kostko O., Ahmed M., "On the Ionization Energies of  $C_4H_3$  Isomers", Chem. Phys. Lett., 2010, 485, 281-285.
2. Zhang F., Jones B., Maksyutenko P., Kaiser R.I., Chin C., Kislov V.V., Mebel A.M., "Formation of the Phenyl Radical [ $C_6H_5(X^2A_1)$ ] under Single Collision Conditions – A Crossed Molecular Beam and Ab Initio Study", J. Am. Chem. Soc., 2010, 132, 2672-2683.
3. Sebree J.A., Kislov V.V., Mebel A.M., Zwier T.S., "Spectroscopic and Thermochemical Consequences of site-specific H-atom addition to Naphthalene", J. Phys. Chem. A, 2010, 114, 6255–6262.

4. Kislov V.V., Mebel A.M., “Ab Initio/RRKM-ME Study on the Mechanism and Kinetics of the Reaction of Phenyl Radical with 1,2-Butadiene”, *J. Phys. Chem. A*, 2010, 114, 7682-7692.
5. Sebree J.A., Kislov V.V., Mebel A.M., Zwier T.S., “Isomer Specific Spectroscopy of C<sub>10</sub>H<sub>n</sub>, n = 8-12: Exploring Pathways to Naphthalene in Titan’s Atmosphere”, *Faraday Disc.*, 2010, 147, 231-249.
6. Parker D.S.N., Zhang F., Kim, Y.S. Kaiser R.I., Mebel A.M., “On the Formation of Resonantly Stabilized C<sub>5</sub>H<sub>3</sub> Radicals -A Crossed Beam and Ab Initio Study of the Reaction of Ground State Carbon Atoms with Vinylacetylene”, *J. Phys. Chem. A*, 2011, 115, 593-601.
7. Zhang F., Kaiser R.I., Kislov V.V., Mebel A.M., Golan A., Ahmed M., “A VUV Photoionization Study of the Formation of the Indene Molecule and Its Isomers”, *J. Phys. Chem. Lett.*, 2011, 2, 1731-1735.
8. Kaiser R.I., Goswami M., Maksyutenko P., Zhang F., Kim Y.S., Landera A., Mebel A.M., “A Crossed Molecular Beams and Ab Initio Study on the Formation of C<sub>6</sub>H<sub>3</sub> Radicals - An Interface between Resonantly Stabilized (RSFRs) and Aromatic Radicals (ARs)”, *J. Phys. Chem. A.*, 2011, 115, 10251-10258.
9. Parker D.S.N., Zhang F., Kaiser R.I., Kislov V.V., Mebel A.M., “Indene Formation under Single Collision Conditions from Reaction of Phenyl Radicals with Allene and Phenylacetylene – A Crossed Molecular Beam and Ab Initio Study”, *Chem. Asian J.*, 2011, 6, 3035-3042.
10. Kaiser R.I., Goswami M., Zhang F., Parker D., Kislov V.V., Mebel A.M., Aguilera-Iparraguirre J., Green W.H., “Crossed Beam Reaction of Phenyl and D5-Phenyl Radicals with Propene and Deuterated Counterparts – Competing Atomic Hydrogen and Methyl Loss Pathways”, *Phys. Chem. Chem. Phys.*, 2012, 14, 720-729.
11. Parker D.S.N., Zhang F., Kaiser R.I., Landera A., Kislov V.V., Mebel A.M., Tielens A.G.G.M., “Low Temperature Formation of Naphthalene and its Role in the Synthesis of PAH in the Interstellar Medium”, *Proc. Nat. Acad. Sci.*, 2012, 109, 53-58.
12. Parker D.S.N., Zhang F., Kim Y.S., Kaiser R.I., Landera A., Mebel A.M., “On the Formation of Phenyl diacetylene (C<sub>6</sub>H<sub>5</sub>CCCCH) and D5-Phenyl diacetylene (C<sub>6</sub>D<sub>5</sub>CCCCH) Studied under Single Collision Conditions”, *Phys. Chem. Chem. Phys.*, 2012, 14, 2997-3003.
13. Zhou C.-W., Kislov V.V., Mebel A.M., “The Reaction Mechanism of Naphthyl Radicals with Molecular Oxygen. I. A Theoretical Study of the Potential Energy Surface”, *J. Phys. Chem. A*, 2012, 116, 1571–1585.
14. Kislov V.V., Mebel A.M., Aguilera-Iparraguirre J., Green W.H., “The Reaction of Phenyl Radical with Propylene as a Possible Source of Indene and Other Polycyclic Aromatic Hydrocarbons: An Ab Initio/RRKM-ME Study”, *J. Phys. Chem. A*, 2012, 116, 4176-4191.
15. Kaiser R.I., Parker D.S.N., Zhang F., Landera A., Kislov V.V., Mebel A.M., “PAH Formation under Single Collision Conditions - Reaction of Phenyl Radical and 1,3-Butadiene to Form 1,4-Dihydronaphthalene”, *J. Phys. Chem. A*, 2012, 116, 4248-4258.
16. Mebel A.M., Landera A., “Product branching ratios in photodissociation of phenyl radical: A theoretical Ab initio/RRKM study”, *J. Chem. Phys.*, 2012, 136, 234305 (9 pp.).
17. Kaiser R.I., Mebel A.M., Golan A., Ahmed M., “A VUV Photoionization Study on the Formation of Primary and Secondary Products in the Reaction of the Phenyl Radical with 1,3-Butadiene under Combustion Relevant Conditions”, *Phys. Chem. Chem. Phys.*, 2013, 15, 341-347.
18. Kislov V.V., Sadovnikov A.I., Mebel A.M., “Formation Mechanism of Polycyclic Aromatic Hydrocarbons Beyond the Second Aromatic Ring”, *Carbon*, submitted.

## FLASH PHOTOLYSIS-SHOCK TUBE STUDIES

Joe V. Michael

Chemical Sciences and Engineering Division  
Argonne National Laboratory, Argonne, IL 60439  
E-mail: jmichael@anl.gov

The scope of the program is to measure, with the ANL flash photolysis reflected shock tube technique, high-temperature thermal rate constants for use in high-temperature combustion. This year we have concentrated on reactions where H(or D) is either a reactant or product. We have also evaluated the viability of using O<sub>3</sub> as a thermal source of O-atoms for use in kinetics studies involving molecules of interest to combustion. For both types of studies we used H/D- and O-atom atomic resonance absorption spectrometry (ARAS) as detection techniques.<sup>1,2</sup> In this work, we are responding to the specific need to develop chemical mechanisms for biofuels. We have already presented results for two such molecules, methylformate and methylacetate.<sup>3</sup> The current emphasis is on CH<sub>3</sub>OC(O)OCH<sub>3</sub> (dimethyl carbonate, DMC).

**The Thermal Decomposition of DMC and H(D) + DMC:**<sup>4</sup> The shock tube technique was used to study the high temperature thermal decomposition of DMC. The formation of H-atoms was measured behind reflected shock waves by using the H-atom ARAS technique. The experiments span a T-range of 1053–1157 K at pressures ~ 0.5 atm. The H-atom profiles were simulated using a detailed chemical kinetics mechanism for thermal decomposition. Simulations indicate that the formation of H-atoms is sensitive to the rate constants for the energetically lowest-lying bond fission channel,



where H-atoms form instantaneously at high temperatures from the sequence of radical  $\beta$ -scissions,  $\text{CH}_3\text{OC}(\text{O})\text{O} \rightarrow \text{CH}_3\text{O} + \text{CO}_2 \rightarrow \text{H} + \text{CH}_2\text{O} + \text{CO}_2$ . A master equation analysis was performed using CCSD(T)/cc-pv $\infty$ z//M06-2X/cc-pvtz energetics and molecular properties for all thermal decomposition processes in DMC. The theoretical predictions were found to be in good agreement with the present experimentally derived rate constants for the bond fission channel (A). The theoretically derived rate constants for this important bond-fission process in DMC can be represented by a modified Arrhenius expression at 0.5 atm over the  $T$ -range 1000–2000 K as,

$$k_{\text{A}}(T) = 6.85 \times 10^{98} T^{-24.239} \exp(-65250 \text{ K}/T) \text{ s}^{-1}$$

The H-atom temporal profiles at long times show only minor sensitivity to the abstraction reaction,



However, H + DMC is an important fuel destruction reaction at high temperatures in oxidative systems. Consequently, measurements of D-atom profiles using D-ARAS allowed unambiguous rate constant measurements for the deuterated analog of reaction (B)



Reaction (C) is a surrogate for H + DMC since the theoretically predicted kinetic isotope effect at high temperatures (1000 - 2000K) is close to unity,  $k_C \approx 1.2 k_B$ . TST calculations employing CCSD(T)/cc-pv $\infty$ z//M06-2X/cc-pvtz energetics and molecular properties for reactions (B) and (C) are in good agreement with the experimental rate constants. The theoretical rate constants for these bimolecular processes can be represented by modified Arrhenius expressions over the  $T$ -range 500–2000 K as,

$$k_B(T) = 1.45 \times 10^{-19} T^{2.827} \exp(-3398 \text{ K}/T) \text{ cm}^3 \text{ molecule}^{-1} \text{ s}^{-1}$$

$$k_C(T) = 2.94 \times 10^{-19} T^{2.729} \exp(-3215 \text{ K}/T) \text{ cm}^3 \text{ molecule}^{-1} \text{ s}^{-1}$$

Both expressions (two bottom lines) are plotted along with the experimental data in Fig. 1. The top line in the figure is from ref. 5.

**The Bimolecular Reactions, O + DMC and H(D) + DMC:**<sup>6</sup> The shock tube technique was used to study the thermal decomposition of ozone, O<sub>3</sub>, with a view to using this as a thermal precursor of O-atoms at high temperatures. The formation of O-atoms was measured behind reflected shock waves by using atomic resonance absorption spectrometry (ARAS). The experiments span a  $T$ -range,  $819 \text{ K} \leq T \leq 1166 \text{ K}$ , at pressures  $0.13 \text{ bar} \leq P \leq 0.6 \text{ bar}$ . Unimolecular rate theory provides an excellent representation of the fall-off characteristics from the present and literature data on ozone decomposition at high temperatures. The present decomposition study on ozone permits its usage as a thermal source for O-atoms allowing measurements for,



Reflected shock tube experiments monitoring the formation and decay of O-atoms were performed on reaction (A) using mixtures of O<sub>3</sub> and DMC, in Kr bath gas over the  $T$ -range,  $862 \text{ K} \leq T \leq 1167 \text{ K}$ , and pressure range,  $0.15 \text{ bar} \leq P \leq 0.33 \text{ bar}$ . A detailed model was used to fit the O-atom temporal profile to obtain experimental rate constants for reaction (A). Rate constants from the present experiments for O + DMC are plotted in Fig. 2 and can be represented by the Arrhenius expression

$$k_A(T) = 2.70 \times 10^{-11} \exp(-2725 \text{ K}/T) \text{ cm}^3 \text{ molecule}^{-1} \text{ s}^{-1} \quad (862 - 1167 \text{ K}).$$

Transition State Theory calculations employing CCSD(T)/cc-pv $\infty$ z//M06-2X/cc-pvtz energetics and molecular properties for reaction (A) are in good agreement with the

experimental rate constants. The theoretical rate constants can be well represented (to within  $\pm 10\%$ ) over the 500 – 2000 K temperature range by,

$$k_A(T) = 1.87 \times 10^{-20} T^{2.924} \exp(-2338 \text{ K}/T) \text{ cm}^3 \text{ molecule}^{-1} \text{ s}^{-1}$$

The present study represents the first experimental measurement and theoretical study on this bimolecular reaction, and this reaction is undoubtedly important in the high temperature oxidation of DMC.

Experiments and kinetics modeling on the thermal decomposition of isopropanol and its reaction with D-atoms are already complete. We also have extensive data on the pyrolysis of three partially deuterated iso-propanes in an attempt to understand branching ratios for radical decompositions. This work is still in progress. With additional experiments, we are also carrying out ab initio electronic structure calculations in support of the isopropanol reaction system.

This work was supported by the U. S. Department of Energy, Office of Basic Energy Sciences, Division of Chemical Sciences, Geosciences, and Biosciences, under Contract No. DE-AC02-06CH11357.

## References

- <sup>1</sup> S.L. Mielke, K.A. Peterson, D.W. Schwenke, B.C. Garrett, D.G. Truhlar, J.V. Michael, M.-C. Su, J.W. Sutherland, Phys. Rev. Lett. **91**, 063201 (2003).
- <sup>2</sup> J.V. Michael, S.S. Kumaran, M.-C. Su, J. Phys. Chem. A **103**, 5942-5948 (1999).
- <sup>3</sup> S. Peukert, R. Sivaramakrishnan, M.-C. Su, and J. V. Michael, Combust. and Flame, **159**, 2312-2323 (2012).
- <sup>4</sup> S. Peukert, R. Sivaramakrishnan and J.V. Michael, J. Phys. Chem. A, in press (2013).
- <sup>5</sup> P.A. Glaude, W.J. Pitz, and M.J. Thompson, Proc. Combust. Inst. **30**, 1111 (2005).
- <sup>6</sup> S. Peukert, R. Sivaramakrishnan, and J.V. Michael, J. Phys. Chem. A, in press (2013).

## PUBLICATIONS FROM DOE SPONSORED WORK FROM 2011-2013

- *H- and D-atom Formation from the Pyrolysis of C<sub>6</sub>H<sub>5</sub>CH<sub>2</sub>Br and C<sub>6</sub>H<sub>5</sub>CD<sub>2</sub>Br: Implications for High-Temperature Benzyl Decomposition*, R. Sivaramakrishnan, M.-C. Su, and J.V. Michael, Proc. Combust. Inst. **33**, 243-250 (2011).
- *Pyrolysis of C<sub>6</sub>D<sub>5</sub>CH<sub>3</sub>: Rate Constants and Branching Ratios in the High Temperature Thermal Decomposition of Toluene*, R. Sivaramakrishnan and J.V. Michael, Proc. Combust. Inst. **33**, 225-232 (2011).
- *Roaming Radicals in the Thermal Decomposition of Dimethyl Ether: Experiment and Theory*, R. Sivaramakrishnan, J.V. Michael, A.F. Wagner, R. Dawes, A.W. Jasper, L.B. Harding, Y. Georgievskii, and S.J. Klippenstein, Combust. and Flame **158**, 618-632 (2011).

- *Experiment and Theory on Methyl Formate and Methyl Acetate Kinetics at High Temperatures: Rate Constants for H-atom Abstraction and Thermal Decomposition*, S. Peukert, R. Sivaramakrishnan, M.-C. Su, and J. V. Michael, *Combust. and Flame*, **159**, 2312-2323 (2012).
- *High Temperature Rate Constants for H/D + Methylformate and Methylacetate*, S. Peukert, R. Sivaramakrishnan, M.-C. Su, and J.V. Michael, *Proc. Combust. Inst.* **34**, 463-471 (2013).
- *High Temperature Shock Tube and Theoretical Studies on the Thermal Decomposition of Dimethyl Carbonate and its Bimolecular Reactions with H and D -Atoms*, S. Peukert, R. Sivaramakrishnan and J.V. Michael, *J. Phys. Chem. A*, in press.
- *High Temperature Shock Tube Studies on the Thermal Dissociation of O<sub>3</sub> and the Reaction of Dimethyl Carbonate with O-atoms*, S. Peukert, R. Sivaramakrishnan, and J.V. Michael, *J. Phys. Chem. A*, in press.
- *The Decomposition Kinetics of Xylyl Radicals*, D. Polino, C. Cavallotti, R. Sivaramakrishnan, S.J. Klippenstein, and J.V. Michael, *J. Phys. Chem. A*, preparation.

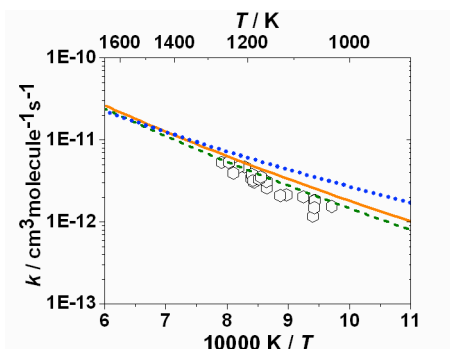


Fig. 1 Arrhenius plot for D + DMC

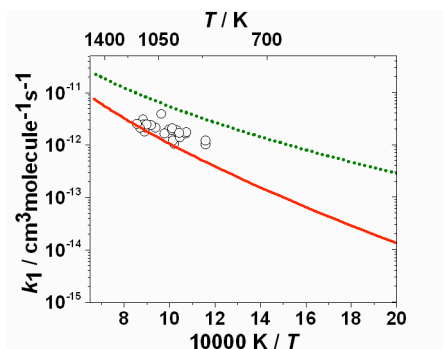


Fig. 2 Arrhenius plot for O + DMC

# Particle Diagnostics Development

H. A. Michelsen

Sandia National Labs, MS 9055, P. O. Box 969, Livermore, CA 94551

hamiche@sandia.gov

## I. Program Scope

Combustion processes often produce solid carbon particles, i.e., soot. These particles may be oxidized to form gas-phase species or released into the exhaust stream, where they can be coated with liquid coatings. These coatings can be comprised of any of a number of components, including unburned fuel, lube oil, sulfuric acid, water, and other combustion by-products.<sup>1</sup> The research program described here focuses on the development of optical diagnostics for soot particles in combustion environments and combustion exhaust plumes. The goal of this work is *in situ* measurements of volume fraction, size, composition, and morphology of combustion-generated particles with fast time response and high sensitivity. Measurement techniques are targeted for studies of soot formation and evolution and must be versatile enough to probe particles throughout their entire life cycle. Techniques are being developed for detection and characterization of particles in combustion environments from incipient particles that are 2-10 nm in diameter and composed of condensed large organic species to mature soot particles composed of aggregates of carbonaceous primary particles resembling polycrystalline graphite. Diagnostics are also being developed for characterization of inhomogeneous exhaust particles.

## II. Recent Progress

Our work has focused on developing a detailed understanding of the chemical and physical mechanisms that influence the applicability of laser-based techniques for soot detection under a wide range of conditions. In recent work, for instance, we have investigated the optical properties of soot in a flame. Using a combination of laser-induced incandescence (LII), extinction, and particle temperature measurements from spectrally and temporally resolved radiative emission, we have studied the wavelength and temperature dependence of the scattering and absorption cross-sections of soot. We have used these results in a model that describes the energy- and mass-balance equations for laser-heated soot and compared the model predictions of time-resolved incandescence signals and particle temperatures to observed LII and temperature temporal profiles. We have also built a particle-beam chamber for focusing and coating soot particles and measuring their optical properties under controlled conditions. We have used this chamber to measure LII of flame-generated soot under low-pressure conditions.

We are also working on a SISGR project led by Prof. Angela Viola to develop a validated predictive multiscale model to describe the chemical composition of soot nanoparticles in premixed and diffusion flames. This project closely couples experimental investigations of soot precursors and incipient particle characteristics with the development of a predictive model for the chemical composition of soot nanoparticles. The co-investigators on the project are Profs. Angela Violi (University of Michigan) for model development and Drs. Hope Michelsen (Sandia), Nils Hansen (Sandia), and Kevin Wilson (LBNL ALS) for experimental investigations.

Experimental and modeling studies have been carried out for several low- and atmospheric pressure flames fueled by acetylene, ethylene, and propane. We designed and built a new counter-flow burner and sampling probe for this project. Polycyclic aromatic hydrocarbons (PAHs) and small soot particles are extracted from the counter-flow flames via a microprobe. The flames vary from lean to rich conditions in order to cover a wide range of practical conditions. The composition of incipient particles is measured using the aerosol mass spectrometer developed by Kevin Wilson and coworkers at the ALS. The corresponding particle size distributions are measured using an SMPS. Angela Violi and coworkers use the experimental results in the development and validation of a predictive multiscale soot model.

### A. Composition of Incipient Soot Particles

The goal of these studies was to measure incipient soot particle sizes and composition in a counterflow diffusion flame at atmospheric pressure. These measurements were intended to inform, constrain, and test the nanoparticle formation model. We designed and built a counterflow burner for measurements of incipient soot particle distributions in these flames at pressures close to atmospheric. We also designed and built a microprobe that would allow dilution of the flow after sampling from the flame

to reduce particle coagulation. We coupled this extraction line to the aerosol mass spectrometer (AMS) developed at the ALS by Kevin Wilson and coworkers. This AMS uses an aerodynamic-lens system to focus an ensemble of particles, sampled at atmospheric pressure, into the high vacuum region of a time-of-flight mass spectrometer. The particle beam is directed onto a heated target, which flash vaporizes the non-refractory components of the particle beam. The resulting vapor plume is photoionized by high-flux tunable VUV radiation ( $\sim 10^{16}$  photons/s) produced by the ALS, and the ions are detected with a time-of-flight mass spectrometer. An illustration of the experimental apparatus is shown in Fig. 1. As with the gas-phase experiments above, the burner was translated relative to the sampling probe for particle profile measurements in the flame, and we scanned the VUV photon energy to measure photoionization efficiency (PIE) curves for isomer identification. We also performed experiments in which we diverted the extraction line to a Scanning Mobility Particle Sizer (SMPS) for particle size distribution measurements.

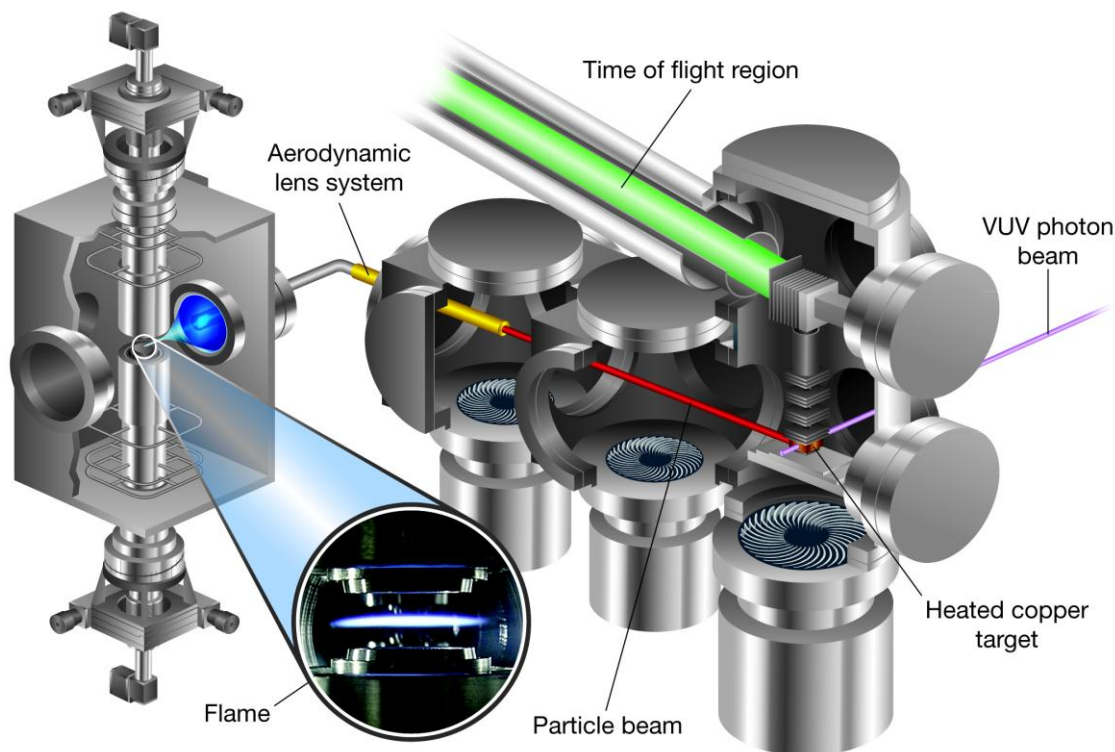


Figure 1. Illustration of the experimental apparatus. Incipient soot particles and their precursors are generated in a counter-flow diffusion flame, extracted through a microprobe into an aerodynamic lens system. Incipient particles condense semi-volatile PAHs and other soot precursors and grow sufficiently in size to make it through the aerodynamic lens system to a heated target where they are flash vaporized and ionized by the VUV beam and detected in the mass spectrometer.

The novelty of this instrument lies in its ability to measure tunable VUV photoionization mass spectra of sub-nanometer particles in real time. Unlike conventional electron impact (EI) ionization sources, which produce many small fragment ions in a mass spectrum, VUV photoionization yields enhanced molecular ion signals that are necessary to analyze chemically complex particle types. We made measurements for several fuels (acetylene, propane, and ethylene) with an opposing flow of  $O_2$ . Both fuel and  $O_2$  were diluted with argon. We presented some of the results in a paper that is currently in press.<sup>2</sup>

Particle-growth mechanisms, such as nucleation, condensation, and coagulation, work to our advantage in the particle-composition experiments. The aerodynamic-lens system used to focus the particles onto the heated target is optimized for focusing particles in the size range of 90-500 nm in diameter and will efficiently focus particles as small as 50 nm.<sup>3</sup> Particles in our size range of interest (1-10 nm) are not focused and are not expected to make it to the heated target. Condensation of gas-phase species onto incipient particles and coagulation of these tiny particles, however, leads to particle-size growth and generates particles large enough for us to detect. We find that, if we send the particles through a thermodenuder (heated to 400°C) to remove the volatile portion prior to the AMS, the particle

composition changes; some of the smaller species are removed from the mass spectra recorded, suggesting that these species were not in particulate form in the flame.

Flame-sampled mass spectra for three fuels are shown in Fig. 2. The samples were extracted from the flames, and the mass spectra were recorded with a heated target temperature of 300 °C and a photon energy of 9.0 eV. Under these conditions, we observed ion signal for species with mass-to-charge ratios ( $m/z$ ) ranging from 15 to >900 with a peak  $m/z$  of 202 or 226 ( $C_{16}H_{10}$  or  $C_{18}H_{10}$ ). This figure shows an example of some of the differences seen between fuels. These spectra mainly consist of regular progressions of groups of  $C_xH_y^+$  ions (with  $x = 14-24$  and  $y = 10-16$ ). Groups of  $C_x$  appear to alternate in intensity, with the even carbon numbers being favored. These results are consistent with previous work,<sup>4</sup> but quantitative comparisons are difficult because the AMS ion signals are not easily calibrated. A comparison of PIE curves among the three flames suggested the presence of species with higher ionization thresholds than would be expected for the most thermodynamically stable PAHs commonly identified in flames.<sup>5</sup> These species may be representative of aromatic rings joined by aliphatic-linked or oxygen-containing aromatic hydrocarbons, and their presence provides evidence for additional, yet unexplored, molecular-growth pathways.

We also observed low-molecular-weight radical species, *e.g.*,  $CH_3$ ,  $C_2H_5$ ,  $C_3H_2$ ,  $C_3H_3$ ,  $C_3H_5$ ,  $C_4H_5$ ,  $C_5H_3$ ,  $C_5H_5$ , and  $C_6H_5$ , which only appeared when the target temperature was elevated, suggesting that these radicals are associated with the sampled particles or condensed matter. The PIE curves demonstrate consistency with reference PIE curves for these radicals, at photon energies near their ionization thresholds, indicating that these species are not attributable to photofragmentation. The ion signal intensity of the small radicals increased at higher target temperatures and may be facilitated by thermal processes, but a full understanding of the origin of these radicals (and fragments) will require further investigation.

### III. Future Work

Some of our future work focuses on combustion-generated particles with inorganic and organic coatings representative of particles found in exhaust plumes. In order to simulate exhaust-plume particulates, we have built a flow-tube system to allow controlled deposition of a coating with low volatility on flame-generated soot. The thickness of the coating can be varied, and the particles collected for analysis by TEM or analyzed with an aerosol mass spectrometer that is under construction. Coatings investigated to date have been selected for diagnostic development for diesel exhaust and include sulfuric acid, heptamethylnonane, and oleic acid. We have also developed a model to describe soot detection by laser-induced incandescence. The model is being modified for release as a community-based model in collaboration with Karla Morris, another staff member at Sandia.

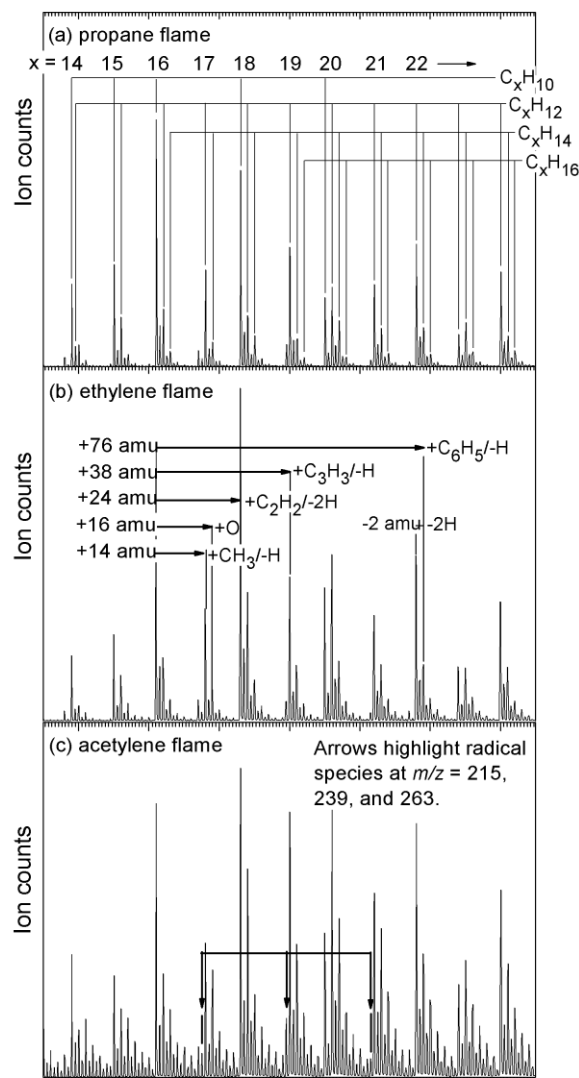


Figure 2. Flame sampled aerosol mass spectra of (a) propane, (b) ethylene, and (c) acetylene flames in the range of 170-310 amu. Samples were collected at a DFFO of 4.5 mm with the heated target at 300 °C, and mass spectra were obtained at a photon energy of 9.0 eV.

#### IV. References

1. (a) Kittelson, D. B., Engines and nanoparticles: A review. *J. Aerosol Sci.* **1998**, *29* (5/6), 575-588; (b) Lighty, J. S.; Veranth, J. M.; Sarofim, A. F., Combustion aerosols: Factors governing their size and composition and implications for human health. *J. Air Waste Manage. Assoc.* **2000**, *50* (9), 1565-1618.
2. Skeen, S. A.; Michelsen, H. A.; Wilson, K. R.; Popolan, D. M.; Violi, A.; Hansen, N., Near-threshold photoionization mass spectra of combustion-generated high-molecular-weight soot precursors. *J. Aerosol Sci.* **2013**, *58*, 86-102.
3. Zhang, X.; Smith, K. A.; Worsnop, D. R.; Jimenez, J.-L.; Jayne, J. T.; Kolb, C. E.; Morris, J.; Davidovits, P., Numerical characterization of particle beam collimation: Part II. Integrated aerodynamic-lens-nozzle system. *Aerosol Sci. Technol.* **2004**, *38* (6), 619-638.
4. (a) Apicella, B.; Carpentieri, A.; Alfè, M.; Barbella, R.; Tregrossi, A.; Pucci, P.; Ciajolo, A., Mass spectrometric analysis of large PAH in a fuel-rich ethylene flame. *Proc. Combust. Inst.* **2007**, *31*, 547-553; (b) Blevins, L. G.; Fletcher, R. A.; Benner, W. H., Jr.; Steele, E. B.; Mulholland, G. W., The existence of young soot in the exhaust of inverse diffusion flames. *Proc. Combust. Inst.* **2002**, *29*, 2325-2333; (c) Bouvier, Y.; Mihehan, C.; Ziskind, M.; Therssen, E.; Focsa, C.; Pauwels, J. F.; Desgroux, P., Molecular species adsorbed on soot particles issued from low sooting methane and acetylene laminar flames: A laser-based experiment. *Proc. Combust. Inst.* **2007**, *31*, 841-849; (d) Dobbins, R. A.; Fletcher, R. A.; Lu, W., Laser microprobe analysis of soot precursor particles and carbonaceous soot. *Combust. Flame* **1995**, *100*, 301-309; (e) Faccinetto, A.; Desgroux, P.; Ziskind, M.; Therssen, E.; Focsa, C., High-sensitivity detection of polycyclic aromatic hydrocarbons adsorbed onto soot particles using laser desorption/laser ionization/time-of-flight mass spectrometry: An approach to studying the soot inception process in low-pressure flames. *Combust. Flame* **2011**, *158*, 227-239; (f) Öktem, B.; Tolocka, M. P.; Zhao, B.; Wang, H.; Johnston, M. V., Chemical species associated with the early stage of soot growth in a laminar premixed ethylene-oxygen-argon flame. *Combust. Flame* **2005**, *142*, 364-373.
5. Stein, S. E.; Fahr, A., High-temperature stabilities of hydrocarbons. *J. Phys. Chem.* **1985**, *89*, 3714-3725.

#### V. Publications and submitted journal articles supported by this project 2011-2013

1. R. P. Bambha, M. A. Dansson, P. E. Schrader, and H. A. Michelsen, "Effects of volatile coatings on the laser-induced incandescence of soot", *Appl. Phys. B* **XX**, submitted (2012).
2. R. P. Bambha, M. A. Dansson, P. E. Schrader, and H. A. Michelsen, "Effects of volatile coatings and coating removal mechanisms on the morphology of graphitic soot", *Carbon* **XX**, submitted (2012).
3. F. Goulay, P. E. Schrader, X. Lopez-Yglesias, and H. A. Michelsen, "A dataset for validation of models of laser-induced incandescence from soot: Temporal profiles of LII signal and particle temperature", *Appl. Phys. B* **XX**, submitted (2012).
4. J. M. Headrick, P. E. Schrader, and H. A. Michelsen, "Radial-profile and divergence measurements of combustion-generated soot focused by an aerodynamic-lens system", *J. Aerosol Sci.* **XXX**, in press (2013).
5. S. A. Skeen, H. A. Michelsen, K. R. Wilson, D. M. Popolan, A. Violi, and N. Hansen, "Near-threshold photoionization mass spectra of combustion-generated high-molecular-weight soot precursors", *J. Aerosol Sci.* **58**, 86-102 (2013).
6. S. A. Skeen, B. Yang, H. A. Michelsen, J. A. Miller, A. Violi, and N. Hansen, "Studies of laminar opposed-flow diffusion flames of acetylene at low pressures with photoionization mass spectrometry", *Proc. Combust. Inst.* **34**, 1067-1075 (2013).
7. F. Goulay, L. Nemes, P. E. Schrader, and H. A. Michelsen, "Spontaneous emission from  $C_2(d^3P_g)$  and  $C_3(A^1P_u)$  during laser irradiation of soot particles", *Mol. Phys.* **108**, 1013-1025 (2010).
8. H. A. Michelsen, P. E. Schrader, and F. Goulay, Erratum to "Wavelength and temperature dependences of the absorption and scattering cross sections of soot" [*Carbon* 48 (2010) 2175-2191], *Carbon* **50**, 740 (2011).
9. J. M. Headrick, F. Goulay, P. E. Schrader, and H. A. Michelsen, "High-vacuum time-resolved laser-induced incandescence of flame-generated soot", *Appl. Phys. B* **104**, 439-450 (2011).

# Detection and Characterization of Free Radicals Relevant to Combustion Processes

Terry A. Miller

Laser Spectroscopy Facility, Department of Chemistry

The Ohio State University, Columbus OH 43210, email: tamiller@chemistry.ohio-state.edu

## 1 Program Scope

Combustion processes have been studied for many years, but the chemistry is very complex and yet to be fully understood. Moreover new fuels have introduced modifications to traditional mechanisms. Modern computer codes for modeling typically employ hundreds of reaction steps with a comparable number of chemical intermediates. The predictions of such models are obviously limited by the dynamical and mechanistic data that are input. Spectroscopic identifications and diagnostics for the chemical intermediates in the reaction mechanisms constitute an important experimental benchmark for the models, as well as providing molecular parameters that are “gold standards” against which quantum chemistry computations of molecular properties may be judged. Our recent work has emphasized the spectroscopy of reactive organic peroxy radicals which are known to be key intermediates in combustion reactions.

## 2 Recent Progress

For several years the technique of cavity ringdown spectroscopy (CRDS) of reactive chemical intermediates has been a mainstay in our laboratory and we have used it to investigate the  $\tilde{A} - \tilde{X}$  absorptions of simple alkyl peroxy radicals. These studies have created a database which allows structural-spectral relationships to be developed. These relationships provide approximate predictions of spectral shifts for structural changes like position (primary, secondary, tertiary) of the peroxy group, length of the hydrocarbon chain, additional substitutions along the chain, etc. For the most part, these relationships have been based on the spectra of small peroxy radicals, often isomer specific. Most combustion fuels contain a mixture of larger hydrocarbons and we have recently concentrated on obtaining the spectroscopy of their combustion intermediates with the goal of determining how well CRDS can characterize complex peroxy radicals and mixtures of such radicals.

A second, and closely related area of work, has been our efforts to develop a practical CRDS apparatus to take advantage of the fact that for any absorption spectroscopy, such as CRDS, in the limit of small absorption, the observed signal intensity is linearly related to the concentration of the molecular species. For that reason we have constructed a dual wavelength CRDS apparatus ( $2\lambda$ -CRDS) capable of pulsed or CW operation to measure absorption cross-sections and rates of reactions for chemical intermediates.

### 2.1 Spectroscopic Investigations of $C_6$ - $C_{10}$ Peroxy Radicals

It is well known that larger chain alkanes ( $>C_4$ ) are important components of gasoline and diesel fuels. Nonetheless our previous CRDS spectroscopy of combustion intermediates has been limited to the  $\tilde{A} - \tilde{X}$  transition of peroxy radicals with  $\leq 5$  carbon atoms. Recently we have extended our observations to larger chain intermediates, e.g. hexyl, heptyl, octyl, nonyl, and decyl peroxy radicals. In these experiments the peroxy radicals were formed from H atom extraction by Cl atom attack on the corresponding hydrocarbon followed by reaction with  $O_2$ . Multiple isomers of peroxy radicals are formed as there are several unique hydrogen atoms that can be abstracted by the Cl atom. Fig. 1 shows that the spectra of all the larger peroxy radicals are dominated by two broad bands. The band

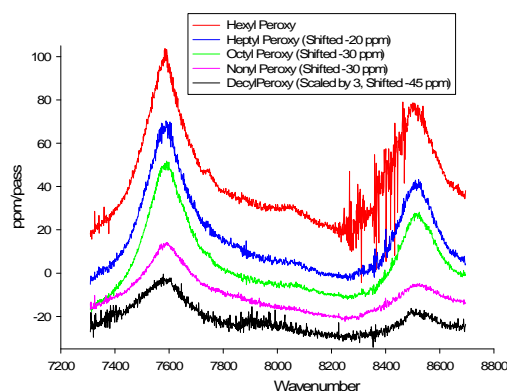


Figure 1:  $\tilde{A} - \tilde{X}$  spectra of the straight chain  $C_6$ - $C_{10}$  peroxy radicals. The sharp lines in the hexyl peroxy trace ( $\approx 8230$ - $8480 \text{ cm}^{-1}$ ) are due to incomplete subtraction of a precursor absorption band.

near  $7585\text{ cm}^{-1}$  is the origin band of the  $\tilde{A} - \tilde{X}$  transition and about  $900\text{ cm}^{-1}$  to the blue, there is another absorption band that results from excitation of the OO stretch vibration.

The chemical formula for the straight chain hydrocarbons is of the form  $\text{CH}_3-(\text{CH}_2)_n-\text{CH}_3$ . Clearly such species will have 6 primary sites for peroxy substitution and  $2n$  sites for secondary substitution. Given that  $n = 4 - 8$  for the hydrocarbons studied and the fact that H atom extraction by Cl is significantly favored at more highly branched sites, one would expect the secondary alkyl peroxy isomers to be predominately produced.

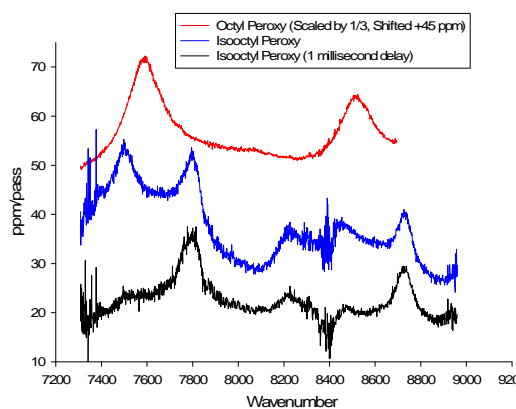


Figure 2:  $\tilde{A} - \tilde{X}$  spectra of octyl and isoctyl peroxy radicals. The sharp lines in the isoctyl peroxy trace ( $\approx 8290\text{--}8420\text{ cm}^{-1}$ ) are from incomplete subtraction of a precursor absorption band. An isoctyl peroxy spectrum taken at a time delay of 1 millisecond (bottom trace) shows the time evolution of the isoctyl peroxy spectrum.

As is well known iso-octane is the standard (100%) for grading gasolines. The peroxy spectra derived from  $n$ -octane and iso-octane are compared in Fig. 2. The spectrum of isoctyl peroxy is easily distinguished from the spectrum of octyl peroxy and the spectra of the other straight-chain peroxy radicals. In the isoctyl peroxy spectrum there are two broad bands appearing at  $7500\text{ cm}^{-1}$  and  $7798\text{ cm}^{-1}$  which we assign to the origin bands of the primary and tertiary peroxy isomers, respectively. This assignment is consistent with our previous argument that secondary peroxy radicals have an origin that is slightly to the blue of primary peroxy radicals. In addition, tertiary peroxy radicals have origin frequencies that are still further to the blue. Moreover, the long lifetime of the band at  $7798\text{ cm}^{-1}$  is consistent with it being the tertiary isomer, as such long lived behavior was previously observed with *tert*-butyl peroxy. The additional bands, COO bend and CO stretch, in the spectrum can also be assigned as belonging to either the primary or tertiary isomer by their temporal behavior and frequency.

## 2.2 Application of the CW $2\lambda$ -CRDS Apparatus to High Precision Reaction Rate Measurements

Our recently developed  $2\lambda$ -CRDS apparatus with optional CW or pulsed operation gives us the capability to measure both absorption cross-sections and rates of reaction for chemical intermediates. The operation of the  $2\lambda$ -CRDS apparatus in the CW mode utilizes a rapid periodic sweep of an external cavity diode laser frequency across a resonance of the cavity to inject light twice per sweep period ( $500\mu\text{s}$ ), whose subsequent ringdown decay time can be measured.

A schematic diagram of the apparatus is shown in Fig. 3. A feedback circuit dynamically “locks” the laser frequency to the cavity mode by compensating for the effects of slow drift of the cavity length or laser frequency. The use of a high repetition rate sweep of the CW laser has two major advantages. It has a duty factor of the order of unity, allowing fast data acquisition. The high duty factor also allows for the near-continuous monitoring of the evolution of the concentration of the same sample of radicals thus eliminating random and/or systematic errors, e.g. the shot-to-shot variation of initial number density of the species of interest, arising from monitoring different samples. This apparatus can be utilized to monitor the absorption of chemically decaying peroxy radicals as a function of time by monitoring the signal strength at the peak of

The position of the origin bands shown in Fig. 1 all lie at  $\sim 7585\text{ cm}^{-1}$ . Primary peroxy radical isomers typically have an origin frequency that is  $\lesssim 7500\text{ cm}^{-1}$ , so we believe that the secondary peroxy radical isomers are responsible for the spectrum. The broad lines in Fig. 1 are likely caused by the strong overlapping of spectral transitions of the different secondary isomers produced. Additionally, upon peroxy radical excitation to the  $\tilde{A}$  state there is a slight lengthening of the O-O bond which gives rise to an OO stretch fundamental, and to which we assign the bands appearing  $\approx 900\text{ cm}^{-1}$  to the blue of the origin bands. The spectrum of hexyl peroxy can be distinguished from that of the other straight chain peroxy radicals by the additional absorption bands around  $7750\text{ cm}^{-1}$  and  $8050\text{ cm}^{-1}$ . While there are differences among the  $\text{C}_7\text{--}\text{C}_{10}$  peroxy radical spectra, they are small and it would be difficult to distinguish among the radicals on the basis of these spectra alone.

As is well known iso-octane is the standard (100%) for

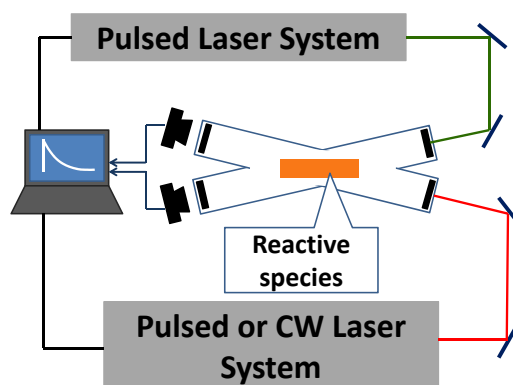
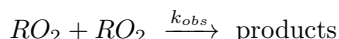


Figure 3: Schematic design of the CW version of the  $2\lambda$ -CRDS spectrometer. See text for details.

the origin band of the  $\tilde{A} \leftarrow \tilde{X}$  transition. The relative width ( $\approx 1 \text{ cm}^{-1}$ ) of the absorption peak at ambient conditions eliminates the need for locking of the midpoint of the frequency sweep to an external reference. If one considers the self-reaction of peroxy radicals,  $RO_2$ ,



monitoring the temporal profile of the absorption allows for the direct determination of the absorption decay rate.

To demonstrate the capabilities of the method and characterize the apparatus, we performed measurements of the self-reaction rate of the ethyl peroxy radical as illustrated in Fig. 4. The rapid periodic sweep of the laser frequency generates a succession of ringdown events which are displayed in panels (a) and (b). Panel (a) shows the succession of decays prior to the photolytic generation of radicals, which determines the ringdown time of the cavity in the absence of ethyl peroxy. Panel (b) shows a succession of more rapid decays shortly after the photolysis pulse and these ringdown curves determine the absorption,  $A(t)$ , with ethyl peroxy sample present. Each ringdown curve in panel (b) determines a single data point for the absorption  $A$  and  $A^{-1}$  vs. time plots shown in panels (c) and (d) respectively.

In the absence of competing removal processes, the number density of radicals and the resulting absorption of a uniform sample of length  $L$ , would decay according to second order kinetics,

$$\frac{L}{2A(t)} = \frac{L}{2A(0)} + \left( \frac{k_{obs}}{\sigma_P} \right) t$$

as is plotted in panel (d). The slope of the straight line in panel (d) is  $k_{obs}/\sigma_P$ , in which  $k_{obs}$  is the effective reaction rate constant for the peroxy radical self-reaction, including secondary chemistry effects. The  $\sigma_P$  is the cross-section at the frequency of the peak absorption, which has been previously obtained by an independent measurement in the same  $2\lambda$ -CRDS apparatus. It can be shown, and is discussed in an upcoming paper, that competing radical removal processes due to macroscopic flow and diffusion, do contribute in a minor way to the observed decay rate, but these effects can be easily accounted for to obtain  $k_{obs}$  for the chemical reaction.

The experimentally observed value for the  $k_{obs}/\sigma_P$  was found to be  $1.827(45) \cdot 10^7 \text{ cm/s}$ , which implies a statistical uncertainty of under 3%. The statistical distribution of the measured values of  $k_{obs}/\sigma_P$  for 1200 individual measurements recorded in under 2 hours of operation time, is shown in Fig. 5. Based on these measurements and the previously obtained value<sup>1</sup> of  $\sigma_P = 5.29(20) \cdot 10^{-21} \text{ cm}^2$ , the effective value for the self-reaction is found to be  $k_{obs} = 9.66(44) \cdot 10^{-14} \text{ cm}^3/\text{s}$  with the error estimate largely due to the uncertainties in  $\sigma_P$ . The newly obtained value is consistent with most of the previously available results but enjoys substantially better precision.

The  $\tilde{A} \leftarrow \tilde{X}$  absorption spectra of peroxy radicals offers two significant advantages for following their chemistry compared to the traditionally used  $\tilde{B} \leftarrow \tilde{X}$  transition. First, despite its weakness, the  $\tilde{A} - \tilde{X}$  transition can be successfully observed and quantified by means of CRDS spectroscopy which allows for accurate measurement of species concentrations, given a known absorption cross-section,  $\sigma_P$ . Second, due to the relatively sharp structure of the transition, one can measure uniquely concentrations of different chemical species and their isomers and conformers, even when several members of the same chemical family are present.

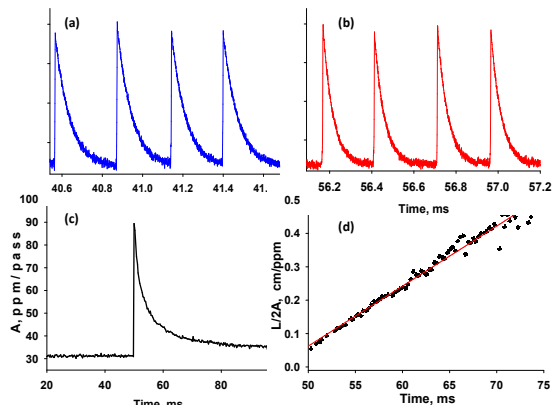


Figure 4: Spectroscopic measurements of the kinetic rate constant. Panels (a) and (b) show decay curves of the probing light without (a) and with (b) radicals present. Each light decay curve produces a single data point on the temporal absorption profile, plotted as absorption (c) and inverse absorption (d) vs. time.

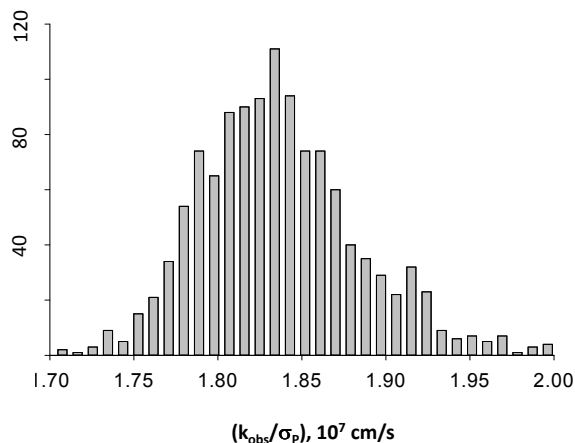


Figure 5: Statistical distribution of the values of  $(k_{obs}/\sigma_P)$  obtained from individual measurements.

### 3 Future Directions

Studies of additional combustion intermediates are planned. A family of molecules closely related to the peroxy radicals is that of the Criegee intermediates, or carbonyl oxides. Criegee intermediates have been implicated in tropospheric oxidation cycles and hydrocarbon autoignition mechanisms. Recently a synthetic pathway to create the Criegee intermediate has been found. The intermediate has been detected by photo-ionization techniques and a structureless  $\tilde{B} - \tilde{X}$  absorption band reported. Our lab is currently preparing to search for the  $\tilde{A} - \tilde{X}$  transition of this molecule which according to electronic structure calculations should be shifted to the visible from the near infrared where alkyl peroxy radicals absorb.

The measurements of the kinetic decay rate of ethyl peroxy radicals showed that the application of the CW CRDS spectroscopy for kinetic studies has substantial potential. We plan to extend these measurements to other peroxy radical species important for combustion and atmospheric chemistry. Additionally, we plan to combine the CW CRDS with the pulsed CRDS system in a  $2\lambda$ -CRDS configuration to measure the absolute absorption cross-sections for a number of peroxy radicals. With the cross-section information available, it should be straight-forward to measure cross-reaction rates between these radical species using the same apparatus.

#### Publications Supported by DOE (2010-2012)

- [1] "Measurement of the Absolute Absorption Cross Sections of the  $\tilde{A} \leftarrow \tilde{X}$  Transition in Organic Peroxy Radicals by Dual Wavelength Cavity-Ringdown Spectroscopy," D. Melnik, R. Chhantyal-Pun, and T. A. Miller, *J. Phys. Chem. A* **114**, 11583 (2010).
- [2] "The  $\tilde{A} - \tilde{X}$  Absorption of Vinyloxy Radical Revisited: Normal and Herzberg-Teller Bands Observed Via Cavity Ringdown Spectroscopy," P. S. Thomas, R. Chhantyal-Pun, N. D. Kline, and T. A. Miller, *J. Chem. Phys.* **132**, 114302 (2010).
- [3] "Cavity Ringdown Spectroscopy of the NIR  $\tilde{A} - \tilde{X}$  Electronic Transition of Allyl Peroxy Radical ( $\text{H}_2\text{C}=\text{CH}-\text{CH}_2\text{OO}\cdot$ )," P. S. Thomas and T. A. Miller, *Chem. Phys. Lett.* **491**, 123 (2010).
- [4] "Observation of the  $\tilde{A} - \tilde{X}$  Electronic Transition of the  $\beta$ -Hydroxyethylperoxy Radical," R. Chhantyal-Pun, N. D. Kline, P. S. Thomas, and T. A. Miller, *J. Phys. Chem. Lett.* **1**, 1846 (2010).
- [5] "Cavity Ringdown Spectroscopy of Peroxy Radicals: The  $\tilde{A} - \tilde{X}$  Absorption of Propargyl Peroxy ( $\text{H}-\text{C}=\text{C}-\text{CH}_2\text{OO}\cdot$ )," P. S. Thomas, N. D. Kline, and T. A. Miller, *J. Phys. Chem. A* **114**, 12437 (2010).
- [6] "The  $\tilde{A} - \tilde{X}$  Absorption of Cyclopentadienyl Peroxy Radical ( $c\text{-C}_5\text{H}_5\text{OO}\cdot$ ): A Cavity Ringdown Spectroscopic and Computational Study," P. S. Thomas and T. A. Miller, *Chem. Phys. Letts.* **514**, 196 (2011).
- [7] "The Electronic Transition Moment for the  $0_0^0$  Band of the  $\tilde{A} - \tilde{X}$  Transition in the Ethyl Peroxy Radical," D. Melnik, P. S. Thomas, and T. A. Miller, *J. Phys. Chem. A* **115**, 13931 (2011).
- [8] "Spectroscopic Studies of the  $\tilde{A} - \tilde{X}$  Electronic Spectrum of the  $\beta$ -Hydroxyethylperoxy Radical: Structure and Dynamics," M.-W. Chen, G. M. P. Just, T. Codd, and T. A. Miller, *J. Chem. Phys.* **135**, 184304 (2011).
- [9] "Analysis of the  $\tilde{A} - \tilde{X}$  Electronic Transition of the 2,1-Hydroxypropylperoxy Radical Using Cavity Ringdown Spectroscopy," N. D. Kline and T. A. Miller, *Chem. Phys. Letts.* **530**, 16 (2012).
- [10] "Detection and Characterization of Reactive Chemical Intermediates Using Cavity Ringdown Spectroscopy," N. Kline and T. A. Miller, in *Cavity Enhanced Spectroscopy and Sensing*, (Springer, New York, accepted).

# Reaction Dynamics in Polyatomic Molecular Systems

William H. Miller

Department of Chemistry, University of California, and  
Chemical Sciences Division, Lawrence Berkeley National Laboratory  
Berkeley, California 94720-1460  
millerwh@berkeley.edu

## I. Program Scope or Definition

The goal of this program is the development of theoretical methods and models for describing the dynamics of chemical reactions, with specific interest for application to polyatomic molecular systems of special interest and relevance. There is interest in developing the most rigorous possible theoretical approaches and also in more approximate treatments that are more readily applicable to complex systems.

## II. Recent Progress

Effort in recent years has focused on finding ways to add quantum mechanical effects to classical molecular dynamics (MD) simulations, which are now so ubiquitously applied to all types of dynamical processes in complex molecular systems, e.g., chemical reactions in clusters, nanostructures, molecules on or in solids, bio-molecular systems, etc. Since quantum effects in *transitions between different electronic states* can obviously be very significant, one of the most important applications of semiclassical (SC) approaches<sup>1-3</sup> is to these non-adiabatic processes. The first approach that allowed both nuclear and electronic degrees of freedom to be treated by SC, or even classical methods, in a unified and completely consistent fashion was the model introduced by Meyer and Miller<sup>4</sup> (MM), in which each electronic state is characterized by a classical degree of freedom (a harmonic oscillator). [Stock and Thoss<sup>5</sup> (ST) later showed this to be an *exact representation* of a vibronic system.] A variety of applications of this approach has demonstrated its usefulness.<sup>6-8</sup>

An even more ambitious classical model for electronic degrees of freedom was introduced later by Miller and White<sup>9</sup> (MW): here the creation/annihilation operators for individual single-particle states in the second-quantized many-electron Hamiltonian operator,

$$\hat{H}_{el} = \sum_{ij} \langle i | j \rangle a_i^\dagger a_j + \frac{1}{2} \sum_{ijkl} \langle ij | kl \rangle a_i^\dagger a_j^\dagger a_l a_k, \quad (1)$$

are replaced by functions of classical action-angle variables ( $n_i, q_i$ ). Since the 1- and 2-electron matrix elements are functions of the nuclear coordinates  $\mathbf{R}$  of the molecular system, the resulting classical electronic Hamiltonian is also a function of nuclear coordinates, and the complete classical vibronic Hamiltonian is obtained by adding the nuclear kinetic energy to it,

$$H(\mathbf{P}, \mathbf{R}, \mathbf{n}, \mathbf{q}) = \sum_k \frac{\mathbf{P}_k^2}{2m_k} H_{el}(\mathbf{n}, \mathbf{q}; \mathbf{R}), \quad (2)$$

where  $\mathbf{P}_k$  are the nuclear momenta and  $\{m_k\}$  their corresponding masses.

This ‘classical second-quantized’ electronic Hamiltonian (with no nuclear degrees of freedom) was recently applied to the resonant level (Landauer) model as a simple example of quantum transport.<sup>10</sup> It consists of a single quantum dot state coupled to two electrodes (left and right) with the following electronic Hamiltonian

$$\hat{H} = \varepsilon_0 \hat{a}_0^\dagger \hat{a}_0 + \sum_{k=1}^N \varepsilon_k \hat{a}_k^\dagger \hat{a}_k + \sum_{k=1}^N t_k (\hat{a}_0^\dagger \hat{a}_k + \hat{a}_k^\dagger \hat{a}_0), \quad (3)$$

where  $\varepsilon_0$  is the energy of the isolated quantum dot (which is used to model a gate voltage),  $\varepsilon_k$  is the energy of level  $k$  of the electrode, and  $t_k$  the coupling between the dot and electrode mode  $k$ ; the classical electronic Hamiltonian corresponding to this is

$$H(n, q) = \varepsilon_0 n_0 + \sum_{k=1}^N \varepsilon_k n_k + \sum_{k=1}^N t_k \sqrt{n_0 - n_0^2 + \frac{1}{2}} \\ \times \sqrt{n_k - n_k^2 + \frac{1}{2}} \cos(q_0 - q_k). \quad (4)$$

Calculations were carried out in this initial application at the primitive ‘quasi-classical’ level, i.e., purely classically, for the flux through the dot, and gave extremely good agreement with the correct quantum results.<sup>10</sup>

Buoyed by this success, a 2-electron term (the Coulomb interaction on the quantum dot) was added to the above Hamiltonian (the Anderson model) to see if this classical theory is capable of describing the effect of Coulomb blockade, i.e., the barrier to electron transmission between the two electrodes when the quantum dot orbital is filled (with two electrons). The original version of the MW Hamiltonian does not capture the Coulomb blockage effect, but a modified version does.<sup>11</sup> Thus the original Coulomb interaction is modified as follows,

$$U d_\uparrow^\dagger d_\uparrow d_\downarrow^\dagger d_\downarrow = U n_\uparrow n_\downarrow \rightarrow U f(n_\uparrow) f(n_\downarrow) \quad (5)$$

where the  $n$ ’s are the classical action variables for the two spin states of the dot’s orbital. The only quantum mechanical restriction on the function  $f(n)$  is that  $f(0) = 0$  and  $f(1) = 1$ . The simplest such function is  $f(n) = n$ , as in the original MW model,<sup>9</sup> but this allows the orbitals on the quantum dot to fill continuously as the bias voltage is increased, not showing the threshold (sigmoid) shape characteristic of Coulomb blockade. We were thus led to try the function

$$f(n) = e^{-(n-1)^2 \lambda^2} \quad (6)$$

which does satisfy  $f(1) = 1$  and  $f(0) \sim 0$  for large values of  $\lambda$ . The Coulomb interaction is thus essentially zero unless both spin states of the dot's orbital are close to 1.

Figure 1 below shows the steady state current versus the bias between the two electrodes: the non-equilibrium Greens function (NEGF) gives the correct quantum result, and small values of  $\lambda$  are essentially the original unmodified Coulomb interaction, not showing the Coulomb blockade effect. One sees, however, that large values of  $\lambda$  do indeed show the correct effect (independent of the precise value of  $\lambda$  once it is large enough), in fact being in excellent agreement with the correct quantum results.

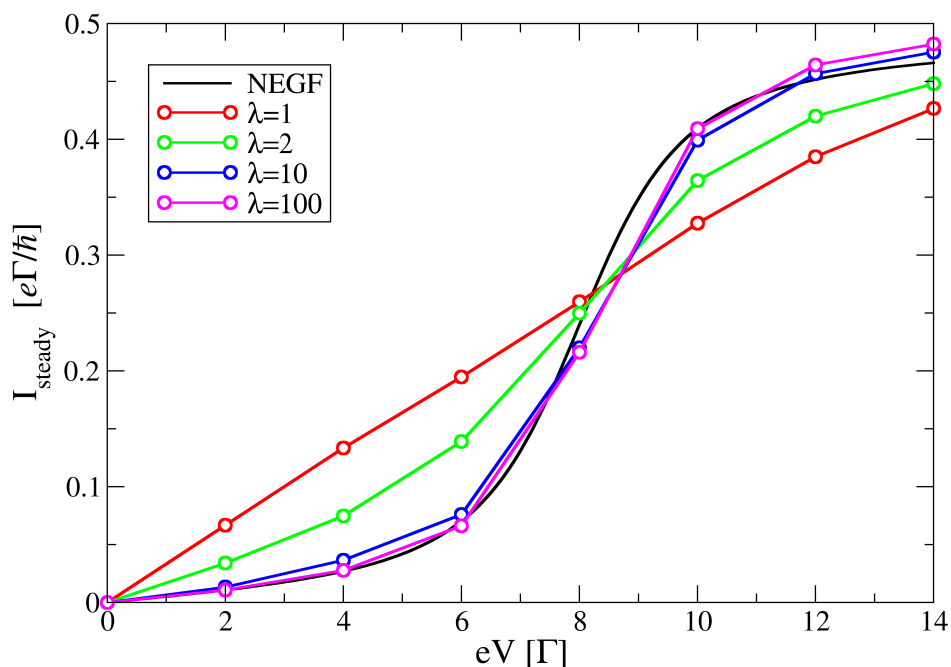


**Figure 1.** Steady-state current versus source-drain bias voltage. NEGF is the correct quantum result. The red curve is essentially the original MW model of the Coulomb interaction, and the others for higher  $\lambda$  values are results with the new modified Coulomb interaction.

### III. Future Plans

This ‘classical second-quantized’ electronic Hamiltonian is thus seen to be capable of describing quite subtle effects in the electronic dynamics and thus clearly bears pursuing to see just how far it can go. The essential attractive feature, of course, is that this classical treatment of the electronic dynamics can be readily combined with a classical treatment of the nuclear dynamics, thus providing for a unified and consistent classical molecular dynamics simulation of the complete vibronic dynamics.

### References

1. For reviews, see W. H. Miller, *Adv. Chem. Phys.* **25**, 69-177 (1974); **30**, 77-136 (1975).
2. W. H. Miller, *J. Chem. Phys.* **53**, 1949-1959 (1970).
3. For reviews, see (a) W. H. Miller, *J. Phys. Chem. A* **105**, 2942-2955 (2001); (b) W. H. Miller, *Proceedings of the National Academy of Sciences*, **102**, 6660-6664 (2005); (c) W. H. Miller, *J. Chem. Phys.* **125**, 132305.1-8 (2006).
4. H. D. Meyer and W. H. Miller, *J. Chem. Phys.* **71**, 2156-2169 (1979).
5. G. Stock and M. Thoss, *Phys. Rev. Lett.* **78**, 578-581 (1997).
6. G. Stock and M. Thoss, *Adv. Chem. Phys.* **134**, 243 (2005).

7. W. H. Miller, *J. Phys. Chem.* **113**, 1405-1415 (2009).
8. D. F. Coker and L. Xiao, *J. Chem. Phys.* **102**, 496-510 (1995).
9. W. H. Miller and K. A. White, *J. Chem. Phys.* **84**, 5059-5066 (1986).
10. See DOE Publication 5 below.
11. See DOE Publication 13 below.

#### IV. 2011 - 2013 (to date) DOE Publications

1. D. Lambrecht, K. Brandhorst, W. H. Miller, C. W. McCurdy, and M. Head-Gordon, A kinetic energy fitting metric for resolution of the identity second-order Möller-Plesset perturbation theory, *J. Phys. Chem. A* **115**, 2794-2801 (2011).
2. J. Liu and W. H. Miller, An approach for generating trajectory-based dynamics which conserves the canonical distribution in the phase space formulation of quantum mechanics. I. Theories, *J. Chem. Phys.* **134**, 104101.1-14 (2011).
3. J. Liu and W. H. Miller, An approach for generating trajectory-based dynamics which conserves the canonical distribution in the phase space formulation of quantum mechanics. II. Thermal Correlation Functions, *J. Chem. Phys.* **134**, 104102.1-19 (2011).
4. J. Liu, Two more approaches for generating trajectory-based dynamics which conserves the canonical distribution in the phase space formulation of quantum mechanics, *J. Chem. Phys.* **134**, 194110.1-9 (2011).
5. D. W. H. Swenson, T. Levy, G. Cohen, E. Rabani and W. H. Miller, Application of a semiclassical model for the second-quantized many-electron Hamiltonian to nonequilibrium quantum transport: The resonant level model, *J. Chem. Phys.* **134**, 164103.1-8 (2011).
6. G. Tao and W. H. Miller, Time-dependent importance sampling in semiclassical initial value representation calculations for time correlation functions, *J. Chem. Phys.* **135**, 024104.1-9 (2011).
7. J. Liu, B. J. Alder and W. H. Miller, A semiclassical study of the thermal conductivity of low temperature liquids, *J. Chem. Phys.* **135**, 114105.1-10 (2011).
8. J. Liu, W. H. Miller, G. S. Fanourgakia, S. S. Xanthas, I. Sho, and S. Saito, Insights in quantum dynamical effects in the infrared spectroscopy of liquid water from a semiclassical study with an ab initio-based force field, *J. Chem. Phys.* **135**, 244503.1-14 (2011).
9. W. H. Miller, Perspective: Quantum or Classical Coherence?, *J. Chem. Phys.* **136**, 210901.1-6 (2012).
10. W. H. Miller, Another Resolution of the Identity for Two-Electron Integrals, *J. Chem. Phys.* **136**, 216101.1-2 (2012).
11. G. Tao and W. H. Miller, Time Dependent Importance Sampling in Semiclassical Initial Value Representation Calculations for Time Correlation Functions. II A Simplified Implementation, *J. Chem. Phys.* **137**, 124105.1-7 (2012).
12. B. Li and W. H. Miller, A Cartesian Classical Second-Quantized Many-Electron Hamiltonian, for Use with the Semiclassical Initial Value Representation, *J. Chem. Phys.* **137**, 154107.1-7 (2012).
13. B. Li, T. J. Levy, W. H. Swenson, E. Rabani and W. H. Miller, A Cartesian Quasi-Classical Model to Nonequilibrium Quantum Transport: The Anderson Impurity Model, *J. Chem. Phys.* **138**, 104110.1-6 (2013).
14. G. Tao and W. H. Miller, Time-Dependent Important Sampling in Semiclassical Initial Value Representation Calculations or Time Correlation Functions. III. A State-Resolved Implementation to Electronically Non-Adiabatic Dynamics, *Mol. Phys.* (accepted).
15. S. J. Cotton and W. H. Miller, Symmetrical Windowing for Quantum States in Quasi-Classical Trajectory Simulations, *J. Phys. Chem. A* (accepted).

# Dynamics of Activated Molecules

Amy S. Mullin

Department of Chemistry and Biochemistry, University of Maryland

College Park, MD 20742

mullin@umd.edu

## I. Program Scope

We investigate the microscopic mechanisms for inelastic collisions of molecules with large amounts of internal energy using high-resolution transient IR absorption probing. Collisional energy transfer is ubiquitous in gas-phase chemistry and impacts overall reaction rates and branching ratios. This is particularly true for high energy molecules that are more likely to undergo chemical transformations. Currently, there are no first-principle theories of collisional energy transfer for high energy molecules and the lack of fundamental knowledge often results in cursory and insufficient treatments in reactive models. A goal of my research program is to gain new insights into the microscopic details of relatively large complex molecules at high energy as they undergo quenching collisions and redistribute their energy. This data provides important benchmarks for the development of new models that account for energy partitioning in molecular collisions.

We use state-resolved transient IR absorption to characterize the energy transfer pathways that are responsible for the collisional cooling of high energy molecules. Direct probing of high energy molecules is challenging due to their transient nature, poorly defined spectral signatures and high state densities. Our approach is to develop a molecular level understanding by focusing instead on the small energy-accepting bath molecules that undergo collisions with high energy molecules. We measure the population changes for individual rotational and vibrational states that are induced by collisions and the nascent translational energies of the scattered molecules. With this technique, we have performed in-depth spectroscopic studies that provide a greater understanding of high energy molecules and their collisional energy transfer. In 2007, we made a major advance in developing the means to characterize the transient behavior for the full range of rotational states for the scattered molecules. Previous measurements had been limited to only the highest energy states, thereby giving information just about the “strongest” collisions. Having eyes also on the so-called “weak” collisions now gives us access to characterize the entire energy transfer distribution with unprecedented detail.

In the current 3-year funding period, we have made major progress expanding our instrumental capabilities, thereby opening exciting new research directions. Just over a year ago, we incorporated a new generation mid-IR optical parametric oscillator (OPO) into one of our transient absorption spectrometers. The OPO offers a number of advantages for high resolution transient IR probing: continuous broad tuning ranges, a high degree of frequency and amplitude stability and high output powers. Our IR tuning range now covers  $\lambda=2.5\text{-}3.9\ \mu\text{m}$  (OPO) and  $4.2\text{-}4.5\ \mu\text{m}$  (diodes). Our first studies using the OPO focused on the collision dynamics of highly vibrationally excited pyrazine ( $\text{C}_4\text{H}_4\text{N}_2$ ,  $E=38000\ \text{cm}^{-1}$ ) with HCl, as described below. The high quality of the OPO light enabled us to complete these measurements, whereas diode laser measurements were stymied by low signal to noise levels.

Our ability to measure the full distribution of scattered molecules allows us to ask even more fundamental questions about the underlying molecular features that are responsible for observed energy transfer behavior. One such question is how the rotational energy structure of the energy-accepting bath molecule affects the energy exchange dynamics in collisions of highly excited molecules. To answer this question, we measured energy gain profiles for HCl following collisions of pyrazine ( $\text{C}_4\text{H}_4\text{N}_2$ ,  $E_{\text{vib}}=38000\ \text{cm}^{-1}$ ) and compared the results to data on DCl collisions with pyrazine.<sup>1</sup> While these experiments were designed to provide information about the importance of energy gaps and angular momentum gaps in collisional energy transfer, the pyrazine-HCl system turns out to be more complex than other collision systems we have studied. Our recent progress in this work is described below.

## II. Recent Progress

### A. Collision dynamics of pyrazine- $h_4$ ( $E=38000\text{ cm}^{-1}$ ) + HCl

**Rotational energy in scattered HCl ( $v=0$ ).** We have completed measurements on the nascent rotational and translational energy profiles for the  $J=2$ -13 states of HCl ( $v=0$ ) following collisions with pyrazine- $h_4(E)$ . We have measured absolute appearance rates for the ( $v=0$ ) and ( $v=1$ ) product channels and find that the appearance rate for ( $v=0$ ) is very close to the Lennard-Jones collision rate. The ( $v=0$ ) channel accounts for more than 99% of pyrazine-HCl collisions. The nascent scattered HCl( $v=0$ ) molecules are rotationally excited and fit to a Boltzmann distribution with  $T_{\text{rot}}=937 \pm 95\text{ K}$ . This result is similar to the rotational distribution measured previously for the ( $v=0$ ) channel from DCl-pyrazine collisions, which fit to  $T_{\text{rot}}=880 \pm 90\text{ K}$ . Thus we find that differences between the rotational energy spacing of HCl and DCl do not influence the amount of rotational energy gained in collisions with highly excited pyrazine. This similarity is likely a result of the large amount of internal energy in pyrazine relative to the rotational energy spacing for the states populated and it may be that differences in rotational energy gain are observed at lower internal energies of pyrazine.

**J-specific translational energies for scattered HCl( $v=0$ ).** The J-dependent translational energy distributions for HCl/pyrazine- $h_4(E)$  collisions are shown in Fig. 1a. Translational energies are shown for appearance of scattered HCl molecules and for depletion of initial HCl states that are thermally populated at 300 K. The depletion measurements show initial temperatures of 230-250 K, indicating that slightly cooler than ambient molecules are favored in the collisions. Similar behavior was observed in DCl depletion measurements. Appearance line widths show that the scattered molecules have translational energy that is greater than the pre-collision value for all HCl J-states observed, indicating that rotational and translational energy are coupled in the relaxation mechanism for pyrazine- $h_4(E)$ -HCl collisions. However, for HCl collisions, the translational energy of the scattered molecules is *inversely* correlated to the final HCl rotational state. Earlier results<sup>1</sup> show that pyrazine-DCl collisions lead the DCl( $v=0$ ) products with the opposite rotation-translational correlation as HCl, as shown in Fig. 1b.

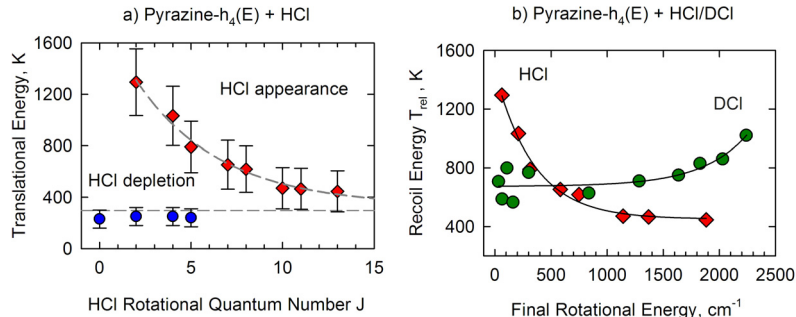


Fig. 1. a) Nascent J-dependent translational energy of HCl( $v=0$ ) products from collisions of pyrazine- $h_4(E)$  and HCl (300 K). b) Comparison with DCl collisions.<sup>1</sup>

Previously we had interpreted the DCl( $v=0$ ) scattering data in terms of an impulsive mechanism for which product rotational and translational energy gains are directly correlated. In this mechanism, we envision that stronger collisions impart large amounts of both rotation and translation while gentler collisions yield more modest amounts of both types of energy. There is ample evidence that the primary pathway for quenching of high energy molecules by  $\text{CO}_2$  involves impulsive collisions, which may be direct single-impact encounters or may be chattering collisions that involve multiple, sequential points of impact. In contrast, the inverted product correlation from HCl collisions suggests that the energy transfer does not occur solely from a random distribution of HCl orientations and this observation has caused us to explore how hydrogen bonding interactions may be influencing the energy transfer mechanisms of HCl. The picture that emerges has HCl molecules experiencing a strong electric field that orients them relative to pyrazine prior to scattering and that the energy transfer occurs in a quasi-complex. The new question

becomes why do HCl and DCI scatter so differently? The following experiments were designed to investigate energy transfer in the presence of strong orienting intermolecular forces.

**Dynamics of the HCl( $v=1$ ) channel.** To sort out the collisional energy transfer of molecules capable of hydrogen bonding, we turned to the body of research on the vibrational predissociation of van der Waals complexes.<sup>2</sup> In the case of acetylene-HCl and -DCI complexes, one study suggests that near-resonant intermolecular vibrational energy transfer causes an anomalously short predissociation lifetime for the HCl complex.<sup>3</sup> Later studies indicate that 1) *intramolecular* vibrational energy transfer is involved instead<sup>4</sup> and 2) the intermolecular vibrational energy transfer is not energetically accessible.<sup>5</sup> To investigate the presence of near-resonant vibrational energy transfer, we have used transient IR absorption to measure product state distributions for the HCl( $v=1$ ) channel in pyrazine-HCl collisions. Rate constant measurements show that this channel represents a minor pathway compared to the ( $v=0$ ) channel and accounts for less than 1% of collisions. The HCl( $v=1$ ) products have a modest amount of rotational energy and a distribution having  $T_{\text{rot}}=614$  K. The translational energy profiles are essentially the same for all final scattered J-states with values near  $T=480$  K. The modest amounts of rotational and translational energy in the products are consistent with a near-resonant intermolecular mechanism.

### B. Isotope Effects: Collision dynamics of pyrazine- $d_4$ ( $E=38000$ $\text{cm}^{-1}$ ) + HCl

A new study is underway to investigate possible hydrogen-bonding effects and the role of near-resonant intermolecular vibrational energy transfer in collisions of pyrazine-HCl. We have turned our attention to collisions of pyrazine- $d_4$ (E) and HCl. Our results so far indicate the HCl( $v=0$ ) channel is again the primary scattering product. Transient Doppler-broadened line profiles have been collected for many states from  $J=2$ -13, as shown in Fig. 2. The thermally populated low-J states show double Gaussian profiles with a negative-going depletion component and a positively-going appearance component. Line profiles for appearance of product molecules have translational temperatures ranging from 1300 K for  $J=2$  to 444 K for  $J=13$ . The depletion of initial states indicates that the initial velocities are 300 K or less.

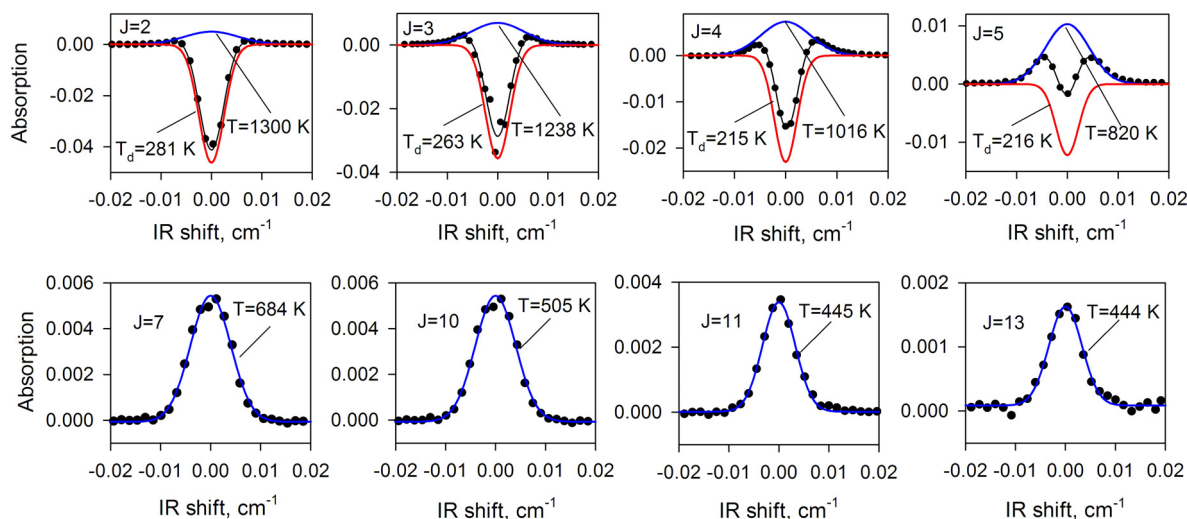


Fig. 2. Nascent Doppler-broadened line profiles for various J states of HCl( $v=0$ ) scattered via collisions with pyrazine- $d_4$ (E). The red curves correspond to depletion of thermally populated states and the blue curves describe the appearance of product states.

The J-dependent recoil velocity distributions for HCl( $v=0$ ) are shown in Fig. 3a. The overall trend for pyrazine- $d_4$  collisions is similar to that for pyrazine- $h_4$ , both for appearance of scattered HCl( $v=0$ ) and depletion of thermally populated HCl low-J states. However, the pyrazine- $d_4$  collisions impart even more translational energy to the HCl( $v=0$ ) products. To understand the meaning of these results we will consider differences in zero point energies and the energy content per mode.

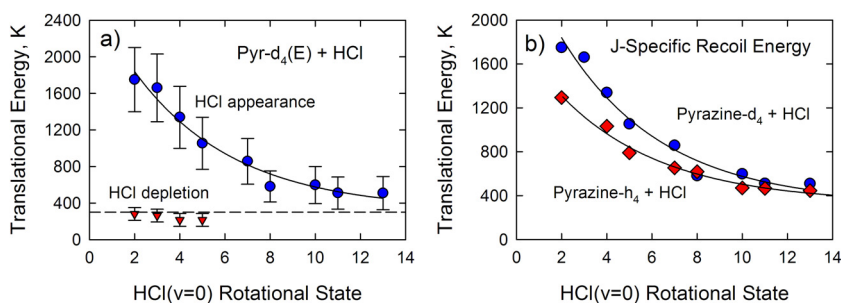


Fig. 3. a) Nascent J-dependent translational energies of HCl( $v=0$ ) products from collisions of pyrazine- $d_4(E)$  and HCl (300 K). b) Comparison of pyrazine- $d_4(E)$  and pyrazine- $h_4(E)$ .

### III. Future Work

In the short term, we will continue our studies on the energy transfer dynamics in collisions of highly excited molecules with HCl. Our immediate goals are to characterize the rotational distribution and rate constants for pyrazine- $d_4$  collisions and then look at the dynamics for ( $v=1$ ) products. We are also gearing up for 2 new studies. In the first we will look at the state-resolved collision dynamics of methane using IR probing at  $\lambda=3.4$   $\mu\text{m}$ . These studies are important for learning how larger molecules accept energy from highly excited donors. The second study will measure state-to-state dynamics and use saturation spectroscopy for labeling an initial collision partner.

### IV. References

1. J. Du, L. Yuan, S. Hsieh, F. Lin and A. S. Mullin, Dynamics of weak and strong collisions: highly vibrationally excited pyrazine ( $E=37900$   $\text{cm}^{-1}$ ) with DCl, *J. Phys. Chem. A* **112**, 9396 (2008)
2. H. Reisler, Photofragment spectroscopy and predissociation dynamics of weakly bound molecules, *Annu. Rev. Phys. Chem.* **60**, 39 (2009)
3. D. C. Dayton, P. A. Block and R. E. Miller, Spectroscopic evidence for near-resonant intermolecular energy transfer in the vibrational predissociation of  $\text{C}_2\text{H}_2\text{-HX}$  and  $\text{C}_2\text{H}_2\text{-DX}$  complexes, *J. Phys. Chem. A* **95**, 2881 (1991).
4. Y. Rudich and R. Naaman, Energy distribution in hydrogen chloride ( $v=1$ ) following vibrational predissociation of acetylene-HCl complex, *J. Chem. Phys.* **96**, 8616 (1992)
5. L. Oudejans and R. E. Miller, State-to-state vibrational predissociation dynamics of the acetylene-HCl complex, *J. Phys. Chem. A* **103**, 4791 (1999)

### V. Publications supported by this project 2010-2012

1. D. K. Havey, J. Du and A. S. Mullin, Full state-resolved energy gain profiles of  $\text{CO}_2$  ( $J=2-80$ ) from collisions with highly vibrationally excited molecules. I. Relaxation of pyrazine ( $E=37900$   $\text{cm}^{-1}$ )” *J. Phys. Chem. A* **114**, 1569-80 (2010)
2. J. Du, N. A. Sassin, D. K. Havey, K. Hsu and A. S. Mullin, “Full energy gain profiles of  $\text{CO}_2$  from collisions with highly vibrationally excited molecules. II. Energy dependent pyrazine ( $E=32700$  and  $37900$   $\text{cm}^{-1}$ ) relaxation” in preparation.
3. J. Du, D. K. Havey, S. W. Teitelbaum and A. S. Mullin, “Full energy gain profiles of  $\text{CO}_2$  from collisions with highly vibrationally excited molecules. III. 2-Methylpyridine, 2,6-dimethylpyridine and 3,5-dimethylpyridine ( $E\sim 38500$   $\text{cm}^{-1}$ ) relaxation” in preparation.
4. G. Echibiri, M. Smarte, W. Walters and A. S. Mullin, “Using a frequency stabilized CW mid-IR OPO for high resolution transient IR absorption spectroscopy,” in preparation for *Optics Express*.
5. M. Smarte, G. Echibiri, W. Walters, J. Cleveland and A. S. Mullin, “Unusual isotope effects in collisions of pyrazine( $E_{\text{vib}}$ ) + HCl and DCl: Evidence of strong interactions”, in preparation for a Letter in the *Journal of Physical Chemistry*.

# Reacting Flow Modeling with Detailed Chemical Kinetics

Habib N. Najm

Sandia National Laboratories  
P.O. Box 969, MS 9051, Livermore, CA 94551  
hnnajm@sandia.gov

## I. Program Scope

The goal of this research program is to improve our fundamental understanding of reacting flow, thereby advancing the state of the art in predictive modeling of combustion. The work involves:

- Developing numerical methods for the efficient solution of reacting flow systems of equations with detailed kinetics and transport, massively parallel codes for computing large scale reacting flow with detailed kinetics, and techniques for analysis of multidimensional reacting flow.
- Using computations to investigate the structure and dynamics of flames using detailed chemical kinetics.
- Developing numerical methods for uncertainty quantification in reacting flow computations.
- Estimation of uncertain chemical model parameters, and calibration/validation of reacting flow models, based on experimental data and computational predictions.
- Uncertainty quantification studies in computations of chemical systems and reacting flow.

In the following, recent progress and future plans in this overall area are discussed.

## II. Recent Progress

### A. Reacting Flow Computations, Analysis, and Model Reduction

**n-Heptane/Air Edge Flame:** We continued our study of the chemical structure of n-heptane/air edge flames using our rectangular-geometry low Mach number reacting flow code. We used a detailed n-heptane/air kinetic model of 560 species and 2538 reversible reactions, with comparisons to simpler models. We relied on computational singular perturbation (CSP) to analyze the flame structure. We identified the dominant chemical pathways contributing to the heat release rate in different edge flame layers. The reactions dominating the heat release rate in the lean premixed branch and the non-premixed central part of this n-heptane edge flame are mostly the same as for methane/air edge flames. Only in the rich premixed branch, do we find a set of dominant reactions specific to the fuel. In this region we find reactions with a negative heat-release rate, being mostly thermal decomposition reactions. The most important one is the decomposition of  $C_2H_5$  to  $C_2H_4$ . We also analyzed fuel consumption pathways, and found that H abstraction by the H radical is the dominating process all along the rich branch and the region around stoichiometric conditions. Only in the lean branch, does H abstraction by OH take over the leading role. Further, thermal decomposition occurs mostly behind the rich branch where the temperature ranges between 1300–1600 K, but has a lower reaction rate than H abstraction. Moreover, using CSP analysis, we derived simplified chemical models in different flame layers. Overall, the analysis confirms the qualitative understanding of an edge/triple flame. We also presented a detailed analysis of CSP explosive modes in different edge flame layers. These findings suggest that there are two different mechanisms responsible for the explosive behavior in the main region inside the premixed branches and in the low-temperature preheat region. In the premixed branches, thermal runaway of the chain-branching  $H_2/O_2$  system seems to be the explosive process while in the preheat region it is the build-up of certain species of the low-temperature ignition chemistry specific to n-heptane. Finally, we compared the flame structure from the detailed 560-species mechanism with that from a 66-species mechanism, which we previously derived using CSP. Significant differences exist, particularly as regards low temperature ignition chemistry of n-heptane. Overall, however, the skeletal 66-species mechanism is found to be accurate in predicting the major flame properties - *e.g.* temperature, propagation speed, mole fractions of major reactants, products, and species of the methane base chemistry - at  $\sim 72\times$  reduced computational cost.

**Sparse Reduced Chemical Models:** On another front, we explored the potential for using  $L_1$ -norm sparsification methods in the context of chemical model reduction with CSP. In general, the goal of such a strategy is to identify the smallest (hence sparse) simplified chemical model that satisfies specified accuracy requirements, relative to the starting detailed mechanism. In this context, we explored means of reformulating our CSP-based chemical model reduction strategy as an optimization problem so that  $L_1$ -norm regularization can be used to impose sparsity. We found, in fact, that this is not feasible nor necessary, unless one discards the requirement of ensuring accurate *dynamical* response. If the measure of model quality were a database-error norm between the computed detailed/reduced solutions, this might have been viable. However, putting the stress on dynamical analysis, which we feel is the best option, it is clear that the present greedy tree-based model reduction strategy based on CSP leads by default to a sparse construction, and deviations from it towards higher sparsity and lower database-error would only be done at the expense of accuracy in dynamical response.

## B. Uncertainty Quantification in Reacting Flow

**Correlations and Rate Rules:** We continued our exploration of the consequences of accounting for correlations among uncertain inputs, whether due to experimental fitting or due to the use of reaction rate rules, in the context of uncertainty quantification (UQ) in chemical ignition. We note that this is important, to begin with, from an accuracy perspective, providing a proper characterization of uncertainty per available information. Beside this, a crucial consequence is the reduction of the effective dimensionality of the UQ problem in chemical kinetics modeling. The uncertainties in rate parameters derived from the same rate rule are perfectly correlated, and therefore can be represented in terms of a single degree of freedom. The potential reduction in the number of degrees of freedom in a large mechanism can be two orders of magnitude. We demonstrated the significant impact of accounting for rate-rule correlations on both accuracy, and dimensionality, with a relatively simple model for the oxidation of a propane/ethane mixture. Specifically, from an accuracy perspective, we found that proper accounting for rate rule induced dependence among rate parameters in this system can lead to large differences in the resulting uncertainty in ignition delay time.

**Estimation of Kinetic Rate Coefficients:** We continued to work on the use of Bayesian methods to infer uncertain chemical rate coefficients for the H-abstraction reaction  $\text{CH}_3\text{CH}(\text{OH})\text{CH}_3 + \text{OH} \rightarrow \text{CH}_3\dot{\text{C}}(\text{OH})\text{CH}_3 + \text{H}_2\text{O}$ , based on data on isopropanol+OH. The results of this analysis provided a rich commentary on the performance of a number of high-level electronic-structure calculations in predicting these rate coefficients. (with J. Zádor)

**Data Free Inference:** We continued to refine the application of our Data Free Inference (DFI) method to chemical systems. We set up a hypothetical scenario where a synthetic data set was used to infer a posterior density on parameters of a single-step global chemistry model for methane-oxidation, and only summaries of this density (nominals/bounds) were reported while the data is discarded. We then used DFI to construct a joint density consistent with this and other presumed-given information, such as *e.g.* the nature of the “instrument” noise model. As part of this study, we improved the robustness of the algorithm by using appropriately normalized density weight functions in the likelihood function on the data space. Results highlighted the convergence of the algorithm, in terms of various accuracy control parameters and the number of data samples. Further, results illustrated the effectiveness of the algorithm in discovering a density that, in fact, approximates the missing density quite well. This last result, while desirable, is not necessarily expected, depending on the amount/nature of given information.

## III. Future Plans

### A. Reacting Flow Computations, Analysis, and Model Reduction

**Reacting Flow Code Development:** We have an ongoing collaboration with MIT, based on our earlier BES-SciDAC developed AMR reacting flow code. A PhD student is presently evolving and using this code. Developments in progress include handling immersed solid bodies, and transitioning the code to a 3D configuration. In this regard, all discretization, interpolation, and filtering stencils are already in 3D. Requisite 3D development will need to target primarily the pressure solver and overall data structures interfacing to the CHOMBO AMR mesh library.

**Analysis of Uncertain Reacting Flow Databases:** Anticipating future flame computations with quantified uncertainty, we will be working on development and optimization of methods for analysis and visualization of uncertain computational reacting flow databases. We have recently made tentative steps in this area, where we have computed a steady-state laminar axisymmetric jet flame with presumed uncertainty in two Arrhenius rate coefficients, and have begun to analyze the resulting uncertain 2D reacting flow. Much further needs to be done in this regard. One necessary part of the strategy, going forward, is to focus on specific flame features, with suitable spatiotemporal shift strategies to provide meaningful analysis of uncertainty in flame-features of interest. At the same time, the correlation structure evident in the computed uncertain reacting flow field is of interest, as it provides useful information on the internal physics of the system. For example, correlation length scales would provide information on the coupling between different flow regions/structures. Moreover, a strong correlation between a specific flame observable at a particular location and another quantity of interest (QoI) would point out specific measurements that can be used to constrain the QoI. Aside from all this, strategies for effective visualization of uncertainty in flames are challenging, and generally lacking. We plan to explore available strategies in this regard.

**Global Sensitivity Analysis in Flames:** For a given detailed chemical model, with typically a large number of parameters, sensitivity analysis can provide information on the impact of any given parameter/reaction onto a given flame QoI. This is of importance for understanding reacting flow physics, and for developing an appreciation of which parameters can be estimated based on measurements of which flame observable. It is also of significant utility in cutting down the dimensionality of the forward UQ problem as pertains to any chosen QoI. However, given uncertainties in parameters, this sensitivity analysis needs to be global, over the range of input uncertainty, and not local at the nominal parameter values. On the other hand, global sensitivity analysis is expensive in high-dimensional spaces, being equivalent to a forward UQ problem. We propose to deal with this challenge using statistical methods for discovering sparsity in high-dimensional models. Specifically, we will make use of Bayesian compressive sensing (BCS) methods, employing Monte Carlo sampling of model parameters over select ranges, in order to identify the sparse dependence of select QoIs on model parameters, thereby providing both associated understanding and feasible paths towards forward UQ and parameter estimation. BCS provides a probabilistic estimation of sparse output dependencies on uncertain inputs, thereby also measuring the quality of the results.

**Application of DFI to an H<sub>2</sub>-O<sub>2</sub> Mechanism:** We will apply the above DFI procedure towards the estimation of a joint density on Arrhenius rate coefficients of a chemical model based on published data. We will do this in the context of a hydrogen-oxygen mechanism, with 9 species and 19 reactions. This work will involve a detailed study of the experimental literature on each of the reactions in this mechanism. For each reaction, we will compile existing information on the parameters in question, and on the measurement strategy and instrument details. Given that fitting to establish rate coefficients of a reaction can rely on previously measured rate constants of other reactions, there will likely be correlation among the rate coefficients of different reactions, beside the expected correlation among the coefficients of any one reaction. We will encompass this picture in the application of the DFI procedure, deriving a pooled joint probability density function (PDF) on all relevant parameters based on available information. To our knowledge, this would be the first such analysis in pursuit of a joint PDF on all parameters of a chemical mechanism. We anticipate challenges with ambiguity in published results, and significant lack of information about the underlying instruments/experiments, particularly for older literature. Where appropriate we will rely on consultations with experts to provide informed judgements in these situations.

## B. Uncertainty Quantification in Reacting Flow

**Forward UQ:** In the forward UQ context, one area of significant challenge has been the use of intrusive *global* Polynomial Chaos (PC) methods for forward propagation of uncertainty in chemical ordinary differential equation (ODE) systems. These methods, if they can be made to work effectively, can lead to significant computational savings, avoiding (sparse) quadrature sampling strategies in high-dimensional spaces. On the other hand, we have experienced first hand their instabilities when applied to chemical ignition computations. It was established in subsequent work that one path towards stability involves the use of *local* PC methods, relying on block decomposition of the parametric space and local, spectral-element type, representations. This path, however, while indeed stable, is not viable for high dimensional spaces because of the challenges with meshing in high-D and large computational cost. Accordingly, there is still a strong need for stabilized intrusive global PC constructions employed in ODEs.

We have recently started a new line of work in this context, focusing on methods for stabilizing global intrusive ODE computations. We have been successful in developing a numerical “filtering” procedure that enforces chosen constraints on the solution PDF in order to minimize the probability of spurious solutions, resulting from aliasing and high-order truncation errors. We have been testing and evaluating this approach in the context of a 2-equation ODE system. Preliminary tests are highly encouraging, leading to stable solutions with acceptable accuracy. Much more needs to be done here going forward. We plan to evaluate and test this filtering approach exhaustively in chemical ODE systems involving both energy and species equations governing hydrocarbon-air mixture ignition. We look forward to demonstrating accurate and efficient filtered intrusive global PC computations in chemical systems.

**Inverse UQ:** In the inverse UQ context, we plan to explore the effectiveness of the DFI algorithm in chemical models with very poor and deficient information, in order to understand the limits of performance of the construction. This includes situations where partial information is available on a subset of the parameters, for example: nominals/bounds on some parameters but only nominals on the rest, no information on instrument errors, and contexts with fitting relying on underlying uncertain information.

**Model Reduction under Uncertainty:** We will also continue to develop both theory and numerical methods pertaining to model reduction under uncertainty. In this context, we need to develop effective means of solving for intrusive Galerkin PC system eigenmodes in the context of chemical models, as we’ve only demonstrated this so far only in simple model ODE systems. We will also formulate means for characterizing uncertain slow manifolds, and estimating probabilistic importance indices for reactions following the CSP method. We will also work on methods for comparison of uncertain models, most likely relying on Kullbeck-Leibler (KL) divergence measures, useful for estimating “distances” between PDFs, in an information-theoretic context. These methods will enable rational comparisons among uncertain simplified and detailed models, and provide means for incorporating uncertainty in the error budget analysis employed in chemical model simplification strategies.

## IV. BES-Supported Published/In-Press Publications [2011-2013]

- [1] Najm, H.N., Berry, R.D., Safta, C., Sargsyan, K., and Debusschere, B.J., Data Free Inference of Uncertain Parameters in Chemical Models, *Int. J. for Uncertainty Quantification* (2013) in press.
- [2] Prager, J., Najm, H.N., Sargsyan, K., Safta, C., and Pitz, W.J., Uncertainty Quantification of Reaction Mechanisms Accounting for Correlations Introduced by Rate Rules and Fitted Arrhenius Parameters, *Combustion and Flame* (2013) in press.
- [3] Prager, J., Najm, H.N., and Zádor, J., Uncertainty Quantification in the *ab initio* Rate-Coefficient Calculation for the  $\text{CH}_3\text{CH}(\text{OH})\text{CH}_3 + \text{OH} \rightarrow \text{CH}_3\text{C}^*(\text{OH})\text{CH}_3 + \text{H}_2\text{O}$  Reaction, *Proc. Comb. Inst.*, 34:583–590 (2013).
- [4] Berry, R.D., Najm, H.N., Debusschere, B.J., Adalsteinsson, H., and Marzouk, Y.M., Data-free inference of the joint distribution of uncertain model parameters, *Journal of Computational Physics*, 231:2180–2198 (2012).
- [5] Alexanderian, A., Maître, O.P. Le, Najm, H.N., Iskandarani, M., and Knio, O.M., Multiscale stochastic preconditioners in non-intrusive spectral projection, *J. Sci. Comp.*, 50:306–340 (2012).
- [6] Salloum, M., Alexanderian, A., Maître, O.P. Le, Najm, H.N., and Knio, O.M., Simplified CSP Analysis of a Stiff Stochastic ODE System, *Computer Methods in Applied Mechanics and Engineering*, 217-220:121–138 (2012).
- [7] Prager, J., Najm, H.N., Valorani, M., and Goussis, D., Structure of n-Heptane/Air Triple Flames in Partially-Premixed Mixing Layers, *Combustion and Flame*, 158:2128–2144 (2011).
- [8] Sondag, B.E., Berry, R.D., Najm, H.N., and Debusschere, B.J., Eigenvalues of the Jacobian of a Galerkin-Projected Uncertain ODE System, *SIAM J. Sci. Comp.*, 33:1212–1233 (2011).
- [9] Najm, H.N., Uncertainty Quantification in Fluid Flow, in *Turbulent Combustion Modeling: Advances, New Trends and Perspectives* (T. Echehki and N. Mastorakos, Eds.), Springer-Verlag, Berlin,, 2011, , pp. 381–407.

# Spectroscopy, Kinetics and Dynamics of Combustion Radicals

David J. Nesbitt

*JILA, University of Colorado and National Institute of Standards and Technology, and  
Department of Chemistry and Biochemistry, University of Colorado, Boulder, Colorado*

Dynamics and spectroscopy of jet cooled hydrocarbon transients relevant to the DOE combustion mission have been explored, utilizing i) high resolution IR lasers, ii) slit discharge sources for formation of jet cooled radicals, and iii) high sensitivity detection with direct laser absorption methods near the quantum shot noise limit. The unique advantage of this powerful experimental combination of tools is that such highly reactive radical transients can be made under pressures/temperatures characteristic of combustion conditions, with the resulting species rapidly cooled to low temperatures ( $T \approx 10\text{-}15\text{K}$ ) in the slit supersonic expansion for spectroscopic simplification. Highlights from work over the last year are summarized below.

## 1. Sub-Doppler Spectroscopy of *trans*-HOCO Radical in the OH Stretching Mode

The chemical reaction,  $\text{OH} + \text{CO} \rightarrow \text{H} + \text{CO}_2$ , has gained significant attention due its critical role in combustion chemistry, and indeed has been labeled the “*second most important combustion reaction*” in a review paper by Miller *et. al*<sup>1</sup>. It is an overall strongly exothermic process and responsible for the final oxidative conversion step of CO to CO<sub>2</sub> which is clearly essential to achieving high efficiency levels of combustion. The unusual nature of this reaction is that it plays a critical and ubiquitous role in oxidative combustion of essentially all hydrocarbons, yet the reaction does not explicitly involve the actual hydrocarbon fuel. Despite its deceptive simplicity, this reaction is clearly far from “elementary” and is known to have multiple barriers, intermediates and pathways along the reaction coordinate. Interestingly, this reaction and its many competing oxidative pathways also strongly impact levels of OH radical concentration in the atmosphere, mainly via oxidation of hydrocarbons to produce the peroxy radical, RO<sub>2</sub>. Indeed, recent laboratory investigations have revealed that current atmospheric models are not able to predict the correct concentration levels of OH radical, which in turn plays a central role in the production of tropospheric ozone.

As one fundamental step toward elucidating these issues, we have investigated the fundamental OH stretching vibrational mode of *trans*-HOCO, investigated herein with supersonic cooling (15 K) and sub-Doppler resolution (60 MHz) in a tunable difference frequency discharge infrared spectrometer. With the combination of slit jet absorption sensitivity and rotational cooling, we are able to observe the predominantly strong *a*-type transitions of the OH stretch band, as well as the much weaker *b*-type transitions undetected in previous studies by Petty and Moore.<sup>2</sup> In addition, the combination of sub-Doppler resolution in the slit jet (~60 MHz) and low jet rotational temperatures enables us to completely resolve electron spin-rotation structure in this radical. From Boltzmann plots for integrated areas of the two band types, the ratio of vibrational transition dipole moments along the A- and B- principal axes can also be determined and compared with quantum theoretical predictions. The *trans*-HOCO

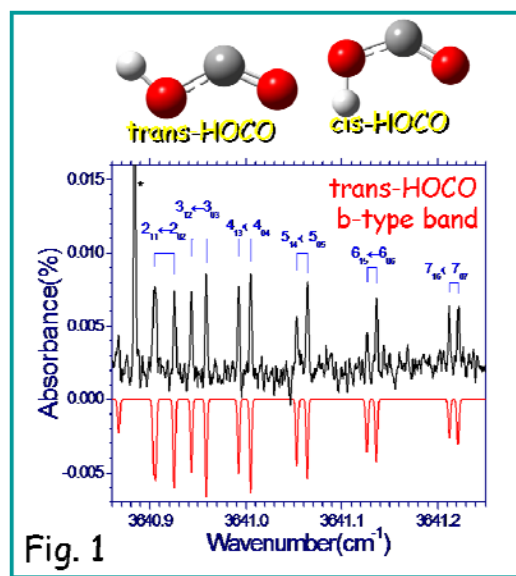


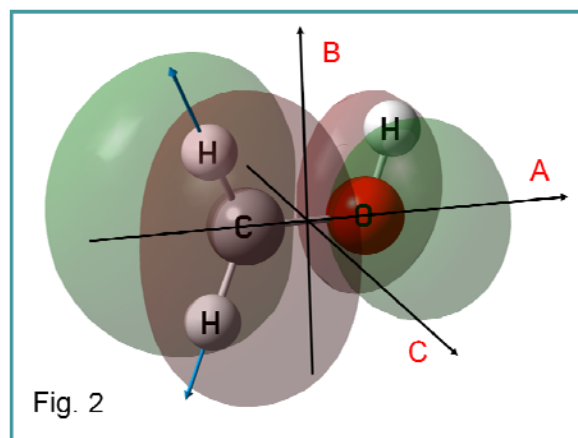
Fig. 1

radical is formed by discharge dissociation of H<sub>2</sub>O to form OH, which then combines with CO and cools in the Ne expansion to a rotational temperature of 16 K. Rigorous assignment of both a-type and b-type spectral transitions is made possible by 2-line combination differences from microwave studies, with full rovibrational analysis of the spectrum based on a Watson asymmetric top Hamiltonian. Additionally, fine structure splittings of each line due to electron spin are completely resolved and thus permitting all three  $\epsilon_{aa}$ ,  $\epsilon_{bb}$ ,  $\epsilon_{cc}$  spin rotation constants to be experimentally determined in the vibrationally excited state. Furthermore, as both a- and b-type transitions for trans-HOCO are observed for the first time, the ratio of transition dipole moment projections along the A, B principal axes is determined to be  $\mu_a/\mu_b = 1.72(5)$ , which is in very close agreement with density functional quantum theoretical predictions (B3LYP/6-311++g(3df,3pd),  $\mu_a/\mu_b = 1.85$ ). Most importantly, these studies lay the essential groundwork for establishing necessary confidence in the trans-HOCO discharge chemistry, which will be the basis for future search in the OH stretching region for the IR spectrum of the surprisingly elusive *cis*-HOCO radical.

## 2. High-Resolution Spectroscopy of Jet-cooled Hydroxymethyl Radical

Hydroxymethyl radical, CH<sub>2</sub>OH, has been the subject of over 100 experimental and theoretical papers in the last 40 years, in large measure due to the important role it plays as a reactive intermediate in combustion and environmental chemistry. As one example, the combustion initiation step for oxygenated hydrocarbon fuels such as methanol is thought to be hydrogen abstraction by O<sub>2</sub> to produce hydroxymethyl radical, i.e., CH<sub>3</sub>OH + O<sub>2</sub> → CH<sub>2</sub>OH + HO<sub>2</sub>. There is also central involvement of hydroxymethyl radical in many of the subsequent chain reaction kinetics, for example, a fundamental chain propagation step in the oxidative combustion of methanol is CH<sub>3</sub>OH + HO<sub>2</sub> → CH<sub>2</sub>OH + H<sub>2</sub>O<sub>2</sub>. Indeed, real time monitoring capabilities for CH<sub>2</sub>OH radical in methanol combustion, as well as a detailed understanding of the underlying kinetics would be very desirable in optimizing combustion processes. Significantly complicating this task is the ubiquitous presence of methoxy radical (CH<sub>3</sub>O) in many combustion systems, which has the same chemical composition as hydroxymethyl radical. This makes mass spectrometry a less versatile method for monitoring the underlying radical kinetics, although the recent combination of synchrotron VUV photoionization and mass spectroscopy looks especially promising.<sup>3</sup> In addition to fundamental combustion processes, hydroxymethyl radical is an important intermediate for oxidative reactions occurring in the troposphere. Indeed, atmospheric scrubbing reactions of alkanes, alkenes, and alcohols all involve hydroxymethyl radical as a reactive intermediate. Alkenes account for about 10% of the non-methane organic compound concentration in many urban areas as a result of gasoline-based fuels and motor vehicle exhaust emissions. The initial oxidative scrubbing reactions of simple alkenes such as ethene are initiated by hydroxyl (OH) radical attack, which features several steps involving CH<sub>2</sub>OH as an intermediate. Furthermore, methanol itself has a non-trivial concentration in the troposphere, ranging from 400-700 ppt depending upon the latitude, with about 85% of atmospheric oxidative scrubbing reactions producing hydroxymethyl radical as a transient intermediate.

In this past year, we have built on the pioneering work of Reisler and coworkers<sup>4</sup> to help



guide a near IR search for hydroxymethyl radical with sub-Doppler, fully rovibrationally resolved spectral resolution. Although we have very good estimates from the previous studies for all three H-stretching bands, we have chosen first to focus on the symmetric CH stretch spectral region near  $3043\text{ cm}^{-1}$ , which is predicted to have the highest integrated CH band intensity. Indeed, we have observed a surprisingly rich spectrum in this region, partially congested by discharge induced hot band transitions in methanol and which is still under further analysis. However, as first high resolution data on this critical combustion radical, we have been able to unambiguously identify and assign the  $K_a = 0 \leftarrow 0$  progression of symmetric stretch excited  $\text{CH}_2\text{OH}$ , which serves as the primary focus of this report. Specifically, high resolution, fully rotationally resolved direct absorption spectra of hydroxymethyl radical,  $\text{CH}_2\text{OH}$ , are presented in the infrared CH stretching region. As a result of low rotational temperatures and sub-Doppler linewidths obtained in the slit supersonic expansion, the  $K_a = 0 \leftarrow 0$  band of the symmetric CH stretch for  $\text{CH}_2\text{OH}$  has been unambiguously identified and analyzed. By way of chemical confirmation, hydroxymethyl radical is generated via two different slit jet discharge “syntheses”: i) direct dissociation of  $\text{CH}_3\text{OH}$  to form  $\text{CH}_2\text{OH}$  and ii) dissociation of  $\text{Cl}_2$  followed by the radical H atom extraction reaction  $\text{Cl} + \text{CH}_3\text{OH} \rightarrow \text{HCl} + \text{CH}_2\text{OH}$ . The identified transitions are fit to a Watson A-reduced symmetric top Hamiltonian to yield first precision experimental values for the ground state rotational constants as well as improved values for the symmetric stretch rotational constants and vibrational band origin. The results both complement and substantially improve upon spectral efforts via previous double resonance ionization detected IR methods by Reisler and coworkers<sup>4</sup> as well as offer high resolution predictions for laboratory and astronomical detection of hydroxymethyl radical in the mm-wave region.

### 3. Spectroscopy and Spin–Rotation Dynamics of Jet-Cooled Propargyl Radical

Propargyl radical is one of the most abundant conjugated linear radicals produced as a reactive intermediate in the combustion of complex hydrocarbon fuels. Of special importance, propargyl radical is also postulated to be the raw material for “head to tail” bimolecular formation of the simplest aromatic ring product species (e.g., phenyl + H). This is exceptionally important, since the formation of even these simplest aromatic species from combustion of non-aromatic fuels is still poorly understood. The chemical stability of propargyl radical arises from delocalization of the unpaired electron, which yields resonance structures corresponding to both propargyl-like ( $\text{H}_2\text{C}-\text{C}\equiv\text{CH}$ ) or an allenyl-like ( $\text{H}_2\text{C}=\text{C}=\text{CH}$ ) forms, with some suggestions that a balanced intermediate resonance structure  $[\text{H}_2\text{C}-\text{C}\equiv\text{CH} \leftrightarrow \text{H}_2\text{C}=\text{C}=\text{CH}]$ , which may be an more appropriate description for this system. To help contribute to the knowledge base on this crucial combustion radical, we have utilized slit supersonic discharges of 0.1% propargyl bromide/Ne in the slit jet spectrometer to obtain high sensitivity ( $S/N > 100:1$ ) sub-Doppler resolution ( $\sim 60\text{ MHz}$ ) spectra on the C–H stretching mode. This permits complete rovibrational analysis of the propargyl spectrum under jet cooled conditions ( $T \approx 17\text{ K}$ ) that nicely complements the elegant flash kinetic

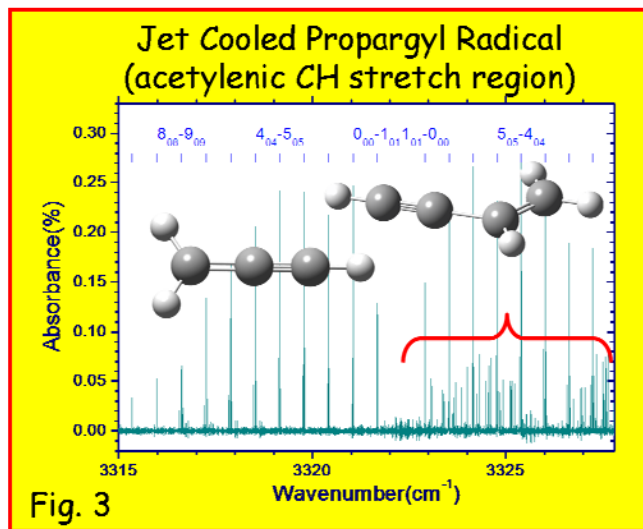
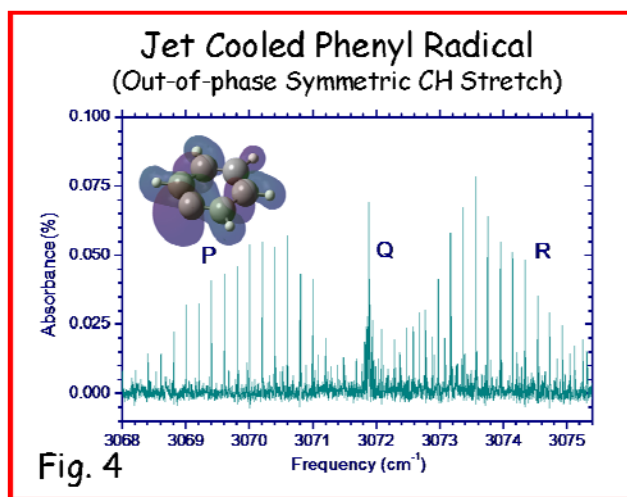


Fig. 3

spectroscopy of Curl *et al.*<sup>5</sup> Furthermore, the sub-Doppler capabilities of the slit jet expansion permit spin rotation and structure and even partial Fermi contact hyperfine interactions to be observed as a function of total rotational angular momentum and projection quantum state. As a result, the spin-rotation and Fermi contact interactions in the upper state are analyzed for the first time, which help provide insight into electron spin density contributions for the various resonance structure contributions.

#### 4. High Resolution IR Spectroscopy of Open Shell Aromatics: Phenyl Radical

We have quite recently refocused our efforts in exploring IR spectroscopy of jet cooled phenyl radical ( $C_6H_5$ ) in the CH stretching region, building on and extending our earlier efforts with considerably improved S/N. Phenyl is a highly reactive 6-membered organic hydrocarbon ring intermediate formed from homolytic cleavage of a CH bond in benzene. By virtue of its overall reactivity, this radical plays a central role in combustion, especially for fossil fuels typically rich in aromatics. It is the classic prototype of an open shell aromatic species, achieving partial stabilization of the radical due to resonance structures arising from electron delocalization around the ring. This radical stabilization also makes it a prime target



intermediate for ring formation in complex combustion processes, which identifies phenyl as a crucial species in mediating the early stages of soot formation. Fig. 4 displays a rotationally resolved spectrum of the in-phase asymmetric CH stretch band ( $\nu_{19}$ ) in phenyl radical obtained with significantly improved S/N, which is just one of 3 bands currently being explored with sufficient IR intensity to observe and analyze. Indeed, we have also now observed the  $\nu_1$  (*in-phase*, symmetric stretch of all 5 CH bonds) and  $\nu_2$  (*out-of-phase*, symmetric stretch of the ortho and para CH bonds) vibrational modes of  $a_1$  symmetry, with band origins at  $3073.96850(8) \text{ cm}^{-1}$  and  $3062.26480(7) \text{ cm}^{-1}$ , respectively. Interestingly, the  $\nu_{19}$ ,  $\nu_1$  and  $\nu_2$  features each agree well with anharmonic scaling predictions based on B3LYP/6-311g++(3df,3dp) calculations, but differ dramatically ( $\approx 11 \text{ cm}^{-1}$  vs.  $< 1 \text{ cm}^{-1}$ ) in terms of red shift from experimental Ar-matrix results. It is worth stressing that the ability to obtain rovibrationally resolved spectra for such a large but fundamental aromatic species represents a critical milestone for spectroscopic study, detection and analysis of even more complex aromatic combustion radical intermediates implicated in the soot formation process.

- <sup>1</sup> J. A. Miller, R. J. Kee, and C. K. Westbrook, *Annu. Rev. Phys. Chem.* **1990**, *41* (1), 345.
- <sup>2</sup> J. T. Petty and C. B. Moore, *J. Mol. Spectrosc.* **1993**, *161* (1), 149.
- <sup>3</sup> C. A. Taatjes, N. Hansen, D. L. Osborn, K. Kohse-Hoinghaus, T. A. Cool, and P. R. Westmoreland, *Phys. Chem. Chem. Phys.* **2008**, *10* (1), 20.
- <sup>4</sup> L. Feng, J. Wei, and H. Reisler, *J. Phys. Chem. A* **2004**, *108* (39), 7903.
- <sup>5</sup> C. L. Morter, C. Domingo, S. K. Farhat, E. Cartwright, G. P. Glass, and R. F. Curl, *Chem. Phys. Lett.* **1992**, *195* (4), 316.

## Radical Photophysics and Photochemistry

Daniel Neumark  
Chemical Sciences Division  
Lawrence Berkeley National Laboratory  
Berkeley, CA 94720

This project applies complementary experimental techniques to study the spectroscopy and photodissociation of free radicals, with a particular focus on species that play a key role in combustion chemistry. These experiments also provide fundamental new insights into the chemical dynamics of free radicals. These species, owing to their high reactivity, present unique experimental challenges that are absent for closed shell molecules. The experiments are carried out on two instruments: a fast radical beam instrument (FRBM) and a molecular beam apparatus. In the FRBM instrument, free radicals are formed by photodetaching a fast beam of mass-selected negative ions. The resulting radicals are photodissociated by a second laser. Photofragments are detected in coincidence using a time-and-position sensitive (TPS) detector. In the molecular beam apparatus, radicals are generated by flash photolysis of a suitable precursor and photodissociated. Photofragments are detected with a rotating mass spectrometer. Both experiments yield primary photochemistry along with translational energy and angular distributions for each product channel.

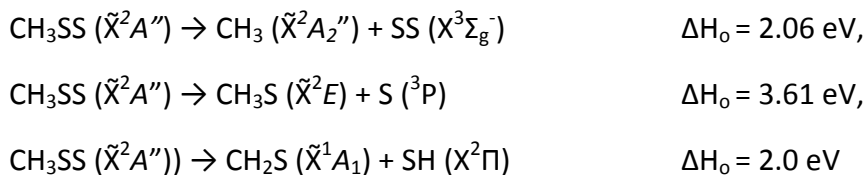
To measure the relative position and arrival time of coincident photofragments in the FRBM experiment, we have recently upgraded our previous TPS detection scheme to a Roentdek Hex80 delay line anode detector. Our previous detector involved a microchannel plate (MCP) assembly with phosphor screen and CCD camera for accurate position measurement and 4x4 multianode PMT array for accurate timing and rough position information. The delay-line anode has the advantage of much simpler data acquisition and read out while requiring fewer detection components and less alignment for operation. The previous setup also has some limitations on timing recognition of neighboring particle hits that are encoded by the same PMT anode. While uncommon with traditional 2-body dissociation, multi-fragment dissociation can result in two fragments read by the same PMT anode, resulting in a discarded data point. However, the delay line anode allows more efficient collection of events with small inter-fragment separation.

Research during the last year has focused on the sulfur-containing radicals methyl perthiyl ( $\text{CH}_3\text{SS}$ ) and thiophenoxy ( $\text{C}_6\text{H}_5\text{S}$ ). Sulfur-containing molecules are a major constituent of both fossil fuels and biomass, and the combustion of these materials results in the emission of many sulfur oxide ( $\text{SO}_x$ ) pollutants. Gas phase reactions of sulfur containing radicals are of particular importance as these highly reactive species can act as key intermediates in these hydrocarbon combustion processes and have a major influence on the ultimate reaction products. With molecular beam photodissociation experiments, the kinetics and energetics of the decomposition of these molecules can be probed in detail to provide a deeper understanding of these species and their reactivity. Moreover, it is of interest to compare these species to the oxygen-containing analogs,  $\text{CH}_3\text{OO}$  and  $\text{C}_6\text{H}_5\text{O}$ ,

Herein, we report the photodissociation dynamics of the thiophenoxy radical ( $C_6H_5S\cdot$ ) studied by fast beam coincidence translational spectroscopy at 248 and 193 nm.

Photofragment translational spectroscopy was used to study the photodissociation of the methyl perthiyl radical  $CH_3SS$  at 248 nm. The radical was produced by flash pyrolysis of dimethyl disulfide ( $CH_3SSCH_3$ ). The primary objectives of this study were (a) to probe the primary photochemistry of the methyl perthiyl radical and (b) to gain insight into the photodissociation mechanism at 248 nm. A key question is whether photodissociation occurs on an excited state surface or if the excited radical undergoes internal conversion to the ground state followed by statistical dissociation. This issue can be addressed by examining the translational energy distributions for the observed channels to see if they are consistent with statistical decay on the ground state surface.

At 248 nm, corresponding to a photon energy of 5.0 eV, there are several energetically allowed products from the photodissociation of the methyl perthiyl radical:



Two channels were observed:  $CH_3 + S_2$  and  $CH_2S + SH$ . Photofragment translational energy ( $E_T$ ) distributions for the  $CH_3 + S_2$  channel peaked near zero translational energy and were well-fit by a prior distribution, indicating that  $CH_3 + S_2$  results from C-S bond fission on the ground state surface. The  $P(E_T)$  distribution for the  $CH_2S + SH$  channel peaked further from zero. This distribution suggests isomerization to  $CH_2SSH$  on the ground state surface followed by dissociation over a small exit barrier, but the energetics are also consistent with production of electronically excited  $CH_2S$ .

The photodissociation dynamics of the thiophenoxy radical ( $C_6H_5S\cdot$ ) at 248 and 193 nm were investigated using fast beam coincidence translational spectroscopy. Thiophenoxy radicals were produced by photodetachment of the thiophenoxide anion followed by photodissociation at 248nm (5.0 eV) and 193nm (6.4eV). Experimental results show two competing dissociation channels leading to  $S + C_6H_5\cdot$  (phenyl) and  $CS + C_5H_5\cdot$  (cyclopentadienyl). The bond dissociation energies for these channels are 3.90 and 3.10 eV, respectively.

The S:CS branching ratio was found to be 0.5 at 248 nm and 1.2 at 193 nm. Translational energy distributions were measured for both channels at each wavelength. Zero-point energy corrected potential energy surfaces were calculated using DFT to aid the experimental interpretation. The proposed dissociation mechanism involves internal conversion from an excited state prior to statistical dissociation on the ground state surface. Calculations (see Figure 1) show that the S loss channel is simple bond fission whereas the CS loss pathway entails multiple transition states as it undergoes bicyclic isomerization followed by five membered ring formation. The potential energy surface in Fig. 1 is consistent with the

experimental translational energy distributions where CS loss is broader and peaks farther away from zero than the corresponding distribution for S loss. It also explains the photon energy dependence of the product branching ratio, because the more endothermic channel (S atom loss) proceeds via a loose transition state and thus becomes more favored at higher excitation energy.

While the reaction pathway for CS loss in Fig.1 is similar to that for CO loss from phenoxy, the energetics of the phenoxy radical are very different. The CO loss channel is considerably lower in energy than O atom loss and thus dominates the unimolecular decay of phenoxy. Moreover, the analog of TS2 is the highest barrier along the pathway for CO loss owing to the asymptotic energetics.

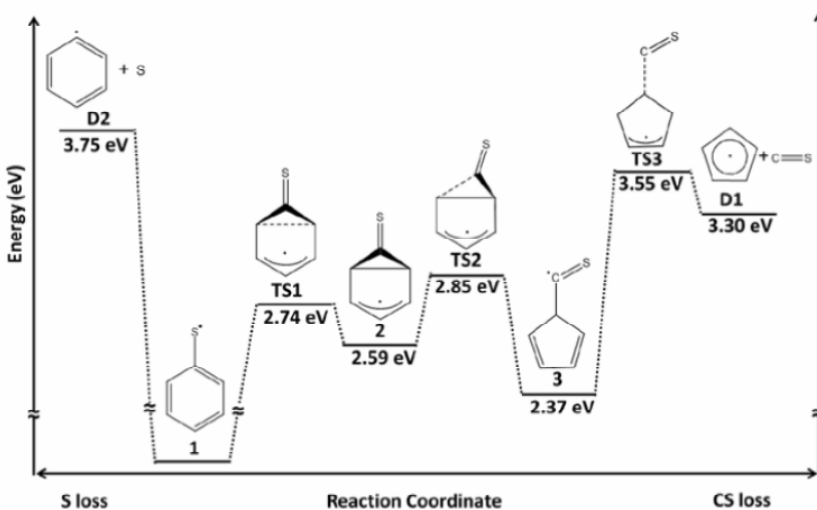


Fig. 1. Calculated potential energy surface for the ground state dissociation of the thiophenoxy radical

In the future, the two radical photodissociation experiments along with anion slow electron velocity map imaging will be used to study the spectroscopy and photodissociation of free radicals, with a particular focus on species that play a key role in combustion chemistry. Specific target systems include radicals with relative low bond dissociation energies that take part in low-temperature (<1000 K) autoignition chemistry, particularly peroxy ( $\text{RO}_2$ ) radicals, their as-yet unobserved QOOH isomers, and the radicals resulting from the subsequent reactions of these species. Radicals such as benzyl and benzoyl are of interest as intermediates in the oxidation of aromatic hydrocarbons. Finally, resonance-stabilized radicals, including open chains (pentadienyl, heptadienyl,  $\text{C}_4\text{H}_3$ ,  $\text{C}_5\text{H}_3$ ) and radicals comprising an intact aromatic ring (phenoxy, indenyl, phenalenyl), are of interest owing to their role in the growth of complex hydrocarbons such as PAH's in combustion.

Recent Publications:

W. A. Donald, R. D. Leib, M. Demireva, B. Negru, D. M. Neumark, and E. R. Williams, "Weighing' Photons with Mass Spectrometry: Effects of Water on Ion Fluorescence," J. Am. Chem. Soc. **132**, 6904, (2010).

B. Negru, S. J. Goncher, A. L. Brunsvold, G. M. P. Just, D. Park, and D. M. Neumark, "Photodissociation Dynamics of the Phenyl Radical via Photofragment Translational Spectroscopy," J. Chem. Phys. **133**, 074302, (2010).

L. Castiglioni, S. Vukovic, P. E. Crider, W. A. Lester, and D. M. Neumark, "Intramolecular Competition in the Photodissociation of C<sub>3</sub>D<sub>3</sub> Radicals at 248 and 193 nm," Phys. Chem. Chem. Phys. **12**, 10714, (2010).

W. A. Donald, R. D. Leib, M. Demireva, B. Negru, D. M. Neumark, and E. R. Williams, "Average Sequential Water Molecule Binding Enthalpies of M(H<sub>2</sub>O)<sub>19-24</sub><sup>2+</sup> (M=Co, Fe, Mn, and Cu) Measured with Ultraviolet Photodissociation at 193 and 248nm," J. Phys. Chem. A. **115**, 2, (2011).

P. E. Crider, A. W. Harrison, D. M. Neumark, "Two-and Three-body Photodissociation Dynamics of the Diiodobromide (I<sub>2</sub>Br<sup>-</sup>) Anion," J. Chem. Phys. **134**, 134306, (2011).

B. Negru, G. M. P. Just, D. Park, and D. M. Neumark, "Photodissociation Dynamics of the t-butyl Radical via Photofragment Translational Spectroscopy at 248 nm," Phys. Chem. Chem. Phys. **13**, 8180, (2011).

A. W. Harrison, J. S. Lim, P. E. Crider, D. M. Neumark, "Three-body Photodissociation Dynamics of I<sub>2</sub><sup>-</sup>(CO<sub>2</sub>)," Chem. Phys. Lett. **512**, 30, (2011).

G. M. P. Just, B. Negru, D. Park, and D. M. Neumark, "Photodissociation of Isobutene at 193 nm," Phys. Chem. Chem. Phys. **14**, 675 (2012).

N. C. Cole-Filipiak, B. Negru, G. M. P. Just, D. Park, D. M. Neumark, "Photodissociation dynamics of the methyl perthiyl radical at 248 nm via photofragment translational spectroscopy," J. Chem. Phys. **138**, 054301 (2013).

# Determination of Accurate Energetic Database for Combustion Chemistry by High-Resolution Photoionization and Photoelectron Methods

C. Y. Ng

Department of Chemistry, University of California, Davis, California 95616

E-mail Address: [c yng@ucdavis.edu](mailto:c yng@ucdavis.edu)

## I. Program Scope:

The main goal of this research program is to obtain accurate thermochemical data, such as ionization energies (IEs), 0 K dissociative photoionization thresholds or appearance energies (AEs), 0 K bond dissociation energies ( $D_0$ 's), and 0 K heats of formation ( $\Delta H^\circ_{f,0}$ 's) for small and medium sizes molecular species and their ions of relevance to combustion chemistry. Accurate thermochemical data determined by high-resolution photoionization and photoelectron studies for selected polyatomic neutrals and their ions are also useful for benchmarking the next generation of *ab initio* quantum computational procedures.

## II. Recent Progress:

The propargyl radical ( $C_3H_3$ ) and its cation ( $C_3H_3^+$ ) play an important role in the chemistry occurring in combustion and planetary atmospheres. The primary motivation for spectroscopic studies of  $C_3H_3/C_3H_3^+$  in the fields of combustion and astrochemistry is concerned with finding the appropriate spectroscopic signatures for the detection of these species. Being the smallest  $\pi$ -conjugated hydrocarbon system, the  $C_3H_3/C_3H_3^+$  system has been the subject of many experimental and theoretical investigations, aiming to obtain fundamental insight into the electronic and bonding structures of  $\pi$ -conjugated hydrocarbon species. The recent efforts in accurate determinations of the ionization energy (IE) and vacuum ultraviolet (VUV) photoionization cross sections of  $C_3H_3$  radical have made possible the quantitative detection of  $C_3H_3$  in combustion flames using the VUV photoionization mass spectrometric method.

Due to the space charge effect, ions cannot be prepared with high intensities, and thus high-resolution spectroscopic data for ions are more difficult to obtain compared to those for neutral species. Although all the twelve vibrational frequencies for  $C_3H_3$  have been well determined with selected vibrational bands measured to the rotational detail, the vibrational frequencies for gaseous  $C_3H_3^+$  were not known until about ten years ago. To our knowledge, well resolved vibrational spectra of neat gaseous  $C_3H_3^+$  have not yet been reported previously. The current most precise vibrational frequencies for the C-H, C-C, and C $\equiv$ C stretching modes of these ion species were obtained indirectly by IR-photodissociation (IRPD) of weakly bound Ar-tagged complex Ar- $C_3H_3^+$ .<sup>1</sup> Since the IR absorption frequencies of the Ar-tagged complex are different from the gaseous  $C_3H_3^+$ , it is not surprising that discrepancies were observed between the IRPD determinations and theoretical predictions. A notable example is that the  $\nu_5^+(a_1)$  C-C stretching frequency of  $C_3H_3^+$  determined by the recent Ar-tagged IRPD method was found to be  $\approx 100$   $cm^{-1}$  lower than the predictions based on the current state-of-the-art *ab initio* quantum calculations. Furthermore, due to the restricted tuning range of commercial IR laser sources, the vibrational frequencies observed in the IRPD studies were limited to frequencies above 1000  $cm^{-1}$ . Photoelectron spectroscopy is a reliable method for vibrational spectroscopy measurements of neat gaseous ions.

Motivated by the discrepancy observed between the  $\nu_5^+(a_1)$  C-C stretching frequency of  $C_3H_3^+$  measured by Ar-tagged IRPD and those obtained by state-of-the-art theoretical calculations, we have performed a velocity-map imaging (VMI) of photoelectrons produced by tunable VUV laser PD of  $C_3H_3$  radicals<sup>2</sup> prepared by a supersonically cooled radical beam source. The VMI-photoelectron (VMI-PE) technique has been shown to achieve similar resolution and higher collection efficiency compared to the pulsed field ionization-photoelectron method. This experiment represents the first application of the VMI-PE method for the photoelectron study of neutral free radicals, particularly using tunable VUV laser as the photoionization source. The ability for the identification of weak vibrational bands for  $C_3H_3^+$  in the range of

0-4,600  $\text{cm}^{-1}$  above the  $\text{IE}(\text{C}_3\text{H}_3)$  in this experiment can be attributed to the high detection sensitivity achieved in the VMI-PE measurement.

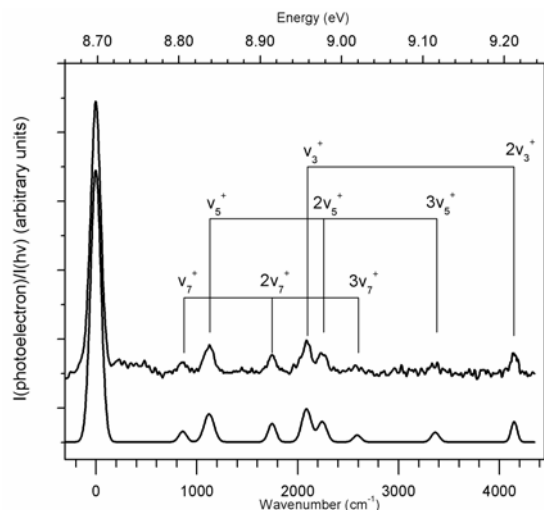
The VUV laser VMI-PE apparatus used consists of a tunable VUV laser, a supersonically cooled  $\text{C}_3\text{H}_3$  radical beam source, and a VMI-PE detection system. Tunable VUV laser radiation was generated by four-wave difference-frequency mixing using a Xe jet as the nonlinear medium. The cold  $\text{C}_3\text{H}_3$  sample was produced by a supersonically cooled excimer laser PD radical beam source. We have measured the VMI-PE images of  $\text{C}_3\text{H}_3$  at the VUV photoionization energies of 8.927, 8.966, 9.109, 9.157, 9.219, and 9.277 eV. The VMI-PE images thus obtained reveal rings of photoelectron images with quite homogeneous angular intensities, allowing the observation of the photoelectron bands for  $\text{C}_3\text{H}_3^+(X^1A_1)$  formed in the energy region of 0-4600  $\text{cm}^{-1}$  above the  $\text{IE}(\text{C}_3\text{H}_3) = 8.6982 \pm 0.0005$  eV.

Figure 1 depicts the VMI-PE spectrum derived from the VMI-PE images, which was found to exhibit an overwhelmingly strong origin band along with several weak vibrational peaks. The energy calibration of the VMI-PE spectrum was achieved by setting the peak position of the VMI-PE origin band to be the  $\text{IE}(\text{C}_3\text{H}_3)$ . The VMI-PE bands at 71014, 71276, 71900, 72242, 72403, and 74300  $\text{cm}^{-1}$  are discernible in individual VMI-PE spectra. Two very weak vibrational bands at 72728 and 73513  $\text{cm}^{-1}$  are also evident in the spectrum. The observed vibrational frequencies 858, 1120, 1744, 2086, 2247, 2572, 3357, and 4152  $\text{cm}^{-1}$  determined for the VMI-PE vibrational bands of  $\text{C}_3\text{H}_3^+(X^1A_1)$  are given in Table I for comparison with the IRPD measurements and theoretical predictions.

In order to deduce the peak heights and widths of the observed vibrational bands, we have obtained a simulated spectrum (shown as the lower spectrum of Fig. 1) for the VMI-PE spectrum assuming a Gaussian instrumental peak profile for the VMI-PE bands. While the peak width for the origin band is found to be 116  $\text{cm}^{-1}$ , the widths of other excited vibrational bands are generally become narrower as their positions are closer to VUV photoionization energy. For the vibrational band at 74300  $\text{cm}^{-1}$  (9.2120 eV), the width is found to be 87  $\text{cm}^{-1}$ . This observation is consistent with the trend for the achievable energy resolution in near threshold VMI-PE measurements.

The electronic configuration for the ground state of  $\text{C}_3\text{H}_3$  is  $\dots 7a_1^2 1b_2^2 1b_1^2 2b_2^2 2b_1^1$ , giving rise to a ground state of  $^2B_1$  symmetry in the  $C_{2v}$  point group. The highest occupied  $2b_1$

orbital is essentially a delocalized  $\pi$ -type orbital covering the linear CCC structure of  $\text{C}_3\text{H}_3$ . Thus, the ejection of the unpaired  $2b_1$  electron by photoionization is expected to affect the bonding of the CCC structure, inducing the excitations of the C–C and C $\equiv$ C stretching and CCC and CCH bending modes of  $\text{C}_3\text{H}_3^+(X^1A_1)$ . Guided by the calculated anharmonic vibrational frequencies, the theoretical normalized FCFs, and the IRPD measurements, we have assigned the vibrational bands observed in the VMI-PE spectrum as shown in Table I and marked in Fig. 1 by drop lines. The assignments of the vibration band,  $2\nu_7^+(a_1) = 1744$   $\text{cm}^{-1}$  and the vibration progressions:  $\nu_5^+(a_1, \text{C–C stretch}) = 1120$   $\text{cm}^{-1}$ ,  $2\nu_5^+ = 2247$   $\text{cm}^{-1}$ , and



**Fig. 1.** The VMI-PE spectrum for  $\text{C}_3\text{H}_3$  derived from the VMI-PE images. The vibrational assignments are marked on top of the averaged VMI-PE spectrum by drop lines.<sup>2</sup>

**Table I.** Assignment of near threshold VMI-PE bands for  $\text{C}_3\text{H}_3^+$  in the 0-4436  $\text{cm}^{-1}$  above the  $\text{IE}(\text{C}_3\text{H}_3)$ .<sup>2</sup>

Vibrational assignment	Experiment ( $\text{cm}^{-1}$ )		Ab initio Calculations ( $\text{cm}^{-1}$ )	
	This work <sup>2</sup>	Rick et al. <sup>1</sup>	Huang et al. <sup>3</sup>	Botschwina et al. <sup>4</sup>
$\nu_7(b_1)$	858	---	862	872
$\nu_5(a_1)$	1120	1222	1132	1123
$2\nu_7(a_1)$	1744	---	1724	1744
$\nu_3(a_1)$	2086	2077	2082	2080
$2\nu_5(a_1)$	2247	---	2264	2245
$3\nu_7^+(b_1)$	2572	---	2586	2616
$3\nu_5(a_1)$	3357	---	3395	3369
$2\nu_3(a_1)$	4144	---	4164	4160

$3\nu_5^+ = 3357\text{ cm}^{-1}$ , and  $\nu_3^+(\text{a}_1, \text{C}\equiv\text{C stretch}) = 2086\text{ cm}^{-1}$  and  $2\nu_3^+ = 4144\text{ cm}^{-1}$  are Franck-Condon allowed photoionization transitions. An important result of this study is that the  $\nu_5^+(\text{a}_1)$  frequency of  $1120\text{ cm}^{-1}$  determined by the VMI-PE study is found to be smaller than the IRPD value of  $1222\text{ cm}^{-1}$  by  $102\text{ cm}^{-1}$ , confirming the result high-level theoretical predictions of  $1123\text{--}1132\text{ cm}^{-1}$ . The observation of the weaker bands  $\nu_7^+(\text{b}_1)$  and  $3\nu_7^+(\text{b}_1)$  is interesting, as the excitation of these vibration bands may involve vibronic interactions. We note that the  $3\nu_7^+(\text{b}_1)$  band can be assigned to the  $\nu_4^+ + \nu_5^+$  combination band as they are predicted to have similar vibrational frequencies. As shown in Table I, the vibrational frequencies of  $\text{C}_3\text{H}_3^+(\text{X}^1\text{A}_1)$  determined here, i.e.,  $\nu_7^+(\text{b}_1) = 858\text{ cm}^{-1}$ ,  $\nu_5^+ = 1120\text{ cm}^{-1}$ ,  $2\nu_7^+ = 1744\text{ cm}^{-1}$ ,  $\nu_3^+ = 2086\text{ cm}^{-1}$ ,  $2\nu_5^+ = 2247\text{ cm}^{-1}$ ,  $3\nu_7^+(\text{b}_1) = 2572\text{ cm}^{-1}$ ,  $3\nu_5^+ = 3357\text{ cm}^{-1}$ , and  $2\nu_3^+ = 4144\text{ cm}^{-1}$ , are in excellent accord with the predictions of the high-level *ab initio* quantum theoretical calculations.

The relative peak heights for the VMI-PE vibrational bands observed in Fig. 1 can be considered as relative Franck-Condon factors (FCFs) for the photoionization process. A high-level theoretical investigation of the FCFs for the  $\text{C}_3\text{H}_3/\text{C}_3\text{H}_3^+$  photoionization system has been reported previously by Botschwina and Oswald.<sup>5</sup> The FCFs calculated by Botschwina and Oswald predicted the excitations of the vibrational bands, in the order of increasing vibrational frequency,  $\nu_5^+$ ,  $\nu_4^+$ ,  $\nu_3^+$ ,  $2\nu_5^+$ ,  $\nu_4^+ + \nu_5^+$ ,  $2\nu_4^+$ ,  $\nu_2^+$ ,  $\nu_3^+ + \nu_5^+$ , and  $\nu_1^+$ . Nevertheless, among these predictions, only the  $\nu_5^+$ ,  $\nu_3^+$ , and  $2\nu_5^+$  bands are observed in the present study. Furthermore, the calculated FCFs for the  $\nu_3^+$  and  $2\nu_5^+$  bands are found to be significantly smaller than the experimental observation. In addition, the observation of the  $\nu_7^+(\text{b}_1)$ ,  $2\nu_7^+$ ,  $3\nu_7^+(\text{b}_1)$ ,  $3\nu_5^+$ , and  $2\nu_3^+$  bands in the present experiment was not predicted by the theoretical calculation of Botschwina and Oswald. These discrepancies observed between the experiment and theoretical results indicate that the potential energy surfaces governing the photoionization of  $\text{C}_3\text{H}_3$  near its IE are in need of further improvement in order to provide a reliable FCF prediction for the  $\text{C}_3\text{H}_3/\text{C}_3\text{H}_3^+$  photoionization system. We note that the observation of the  $\nu_7^+(\text{b}_1)$  and  $3\nu_7^+(\text{b}_1)$  bands is indicative of vibronic interactions, which were not taken into account in the theoretical calculation. Furthermore, the relative intensities for the vibrational bands observed can also be affected by near resonance autoionizing Rydberg states in the present study.

### III. VUV laser PIE, PFI-PE and VMI-PE and VMI-TPE studies of radicals

We are making excellent progress in VUV-PIE and VUV-PFI-PE measurements of small radicals using the VUV laser photoion-photoelectron apparatuses established in our laboratory. In collaboration with Xu Zhang (Jet propulsion Laboratory, NASA), Barney Eillison (Univ. of Colorado, Boulder), we also plan to study of the IR spectroscopy of hydrocarbon radicals and their ions using the two-color IR-VUV PI, and IR-VUV-PFI-PE methods, which have recently developed in our laboratory. We have also been successful in performing high-resolution VUV laser VMI-PE and VMI-TPE imaging measurements on selected radicals, such as propargyl ( $\text{C}_3\text{H}_3$ ), allyl ( $\text{C}_3\text{H}_5$ ), and halogenated hydrocarbon methyl radicals  $\text{CH}_2\text{X}$ ,  $\text{X} = \text{Cl}$  and  $\text{Br}$ .

#### References:

1. A. M. Ricks, G. E. Douberly, P. v. R. Schleyer, and M. A. Duncan, *J. Chem. Phys.* **132** (5), 051101 (2010).
2. Hong Gao, Zhou Lu, Lei Yang, Jingang Zhou, and C. Y. Ng, *J. Chem. Phys.* **137**, 161101 (2012).
3. X. Huang, P. R. Taylor, and T. J. Lee, *J. Phys. Chem. A* **115** (19), 5005 (2011).
4. P. Botschwina, R. Oswald, and G. Rauhut, *Phys. Chem. Chem. Phys.* **13** (17), 7921 (2011).
5. P. Botschwina and R. Oswald, *Chem. Phys.* **378** (1–3), 4 (2010).

### IV. Publications acknowledged the support of DOE (2011-present)

1. C.-S. Lam, H. Wang, Y. Xu, “A Vacuum-Ultraviolet Laser Pulsed Field Ionization-Photoelectron Study of Sulfur Monoxide (SO) and its Cation ( $\text{SO}^+$ )”, *J. Chem. Phys.* **134**, 144304 (2011).
2. Y. C. Chang, H. Xu, Y. Xu, Zhou Lu, Y.-H. Chiu, D. J. Levandier and C. Y. Ng. “*Communcation*: Rovibrationally selected study of the  $\text{N}_2^+(\text{X}; \nu^+ = 1, N^+ = 0\text{--}8) + \text{Ar}$  charge transfer reaction using the vacuum ultraviolet laser pulsed field ionization-photoion method”, *J. Chem. Phys.* **134**, 201105 (2011).

3. Yan Pan, Hong Gao, Lei Yang, Jingang Zhou, C. Y. Ng, and W. M. Jackson, “*Communication: VUV laser photodissociation studies of small molecules by the VUV laser photoionization time-sliced velocity-mapped ion imaging method*”, *J. Chem. Phys.* **135**, 071101 (2011). Among the top 20 most download JCP articles in Aug., 2011.
4. Hong Gao, Lei Yang, Yan Pan, Jingang Zhou, C. Y. Ng, and W. M. Jackson, “Time-sliced velocity-mapped imaging studies of the predissociation of single rovibronic energy levels of N<sub>2</sub> in the extreme ultraviolet region using VUV photoionization”, *J. Chem. Phys.* **135**, 134319 (2011).
5. Hong Gao, Yuntao Xu, Lei Yang, Chow-Shing Lam, Hailing Wang, Jingang Zhou, and C. Y. Ng, “High-resolution threshold photoelectron study of the propargyl radical by the vacuum ultraviolet laser velocity-map imaging method”, *J. Chem. Phys.* **135**, 224304 (2011).
6. Hong Gao, Yu Song, Lei Yang, Xiaoyu Shi, Qingzhu Yin, C. Y. Ng, and W. M. Jackson, “*Communication: Branching ratio measurement in the predissociation of <sup>12</sup>C<sup>16</sup>O by time-slice velocity-map ion imaging in the vacuum ultraviolet region*”, *J. Chem. Phys.* **135**, 221101 (2011).
7. Kai-Chung Lau and C. Y. Ng, “Accurate *ab initio* predictions of ionization energies of propargyl radical: revisited”, *J. Chem. Phys.* **135**, 246101 (2011).
8. Hong Gao, Yang Pan, Lei Yang, Jingang Zhou, C. Y. Ng, and W. M. Jackson, “Time-sliced velocity-map ion imaging studies of the photodissociation of NO in the extreme vacuum ultraviolet (EUV) region”, *J. Chem. Phys.* **136**, 134302 (2012).
9. X. Shi, H. Huang, B. Jacobson, Y.-C. Chang, Q.-Z. Yin, and C. Y. Ng, “A high-resolution photoionization and photoelectron study of <sup>58</sup>Ni using a vacuum ultraviolet laser”, *Astrophys. J.* **747**, 20 (2012).
10. Hong Gao, Yu Song, Lei Yang, Xiaoyu Shi, Qing-Zhu Yin, Cheuk-Yiu Ng, and William M. Jackson, “Branching ratio measurements of the predissociation of <sup>12</sup>C<sup>16</sup>O by time-slice velocity imaging in the energy region from 108,000 to 110,500 cm<sup>-1</sup>”, *J. Chem. Phys.* **137**, 034305 (2012).
11. Y.-C. Chang, Y. Xu, Z. Lu, H. Xu, and C. Y. Ng, “Rovibrationally selected ion-molecule collision study using the molecular beam vacuum ultraviolet laser pulsed field ionization-photoion method: charge transfer reaction of N<sub>2</sub><sup>+</sup>(X; v<sup>+</sup> = 0-2, N<sup>+</sup> = 0-9) + Ar”, *J. Chem. Phys.* **137**, 104202 (2012).
12. Hong Gao, Zhou Lu, Lei Yang, Jingang Zhou, and C. Y. Ng, “*Communication: A vibrational study of propargyl cation using the vacuum ultraviolet laser velocity-map imaging photoelectron method*”, *J. Chem. Phys.* **137**, 161101 (2012).
13. Yuntao Xu, Bo Xiong, Yih Chung Chang, and C. Y. Ng, “*Communication: Rovibrationally selected absolute total cross sections for the reaction H<sub>2</sub>O<sup>+</sup>(X<sup>2</sup>B<sub>1</sub>; v<sub>1</sub><sup>+</sup>v<sub>2</sub><sup>+</sup>v<sub>3</sub><sup>+</sup> = 000; N<sup>+</sup><sub>Ka+Kc+</sub>) + D<sub>2</sub>: Observation of the rotational enhancement effect*”, *J. Chem. Phys.* **137**, 241101 (2012).
14. Yih-Chung Chang, Huang Huang, Zhihong Luo, and C. Y. Ng, “*Communication: A vibrational study of titanium dioxide cation using the vacuum ultraviolet laser pulsed field ionization-photoelectron method*”, *J. Chem. Phys.* **138**, 041101 (2013).
15. H. Huang, Y. C. Chang, Z. Luo, X. Shi, C.-S. Lam, K.-C. Lau, and C. Y. Ng, “Rovibronically selected and resolved two-color laser photoionization and photoelectron study of cobalt carbide cation”, *J. Chem. Phys.*, **138**, 094301 (2013).
16. H. Gao, Y. Song, Y.-C. Chang, X. Shi, Q.-Z. Yin, R. C. Wiens, W. M. Jackson, and C. Y. Ng, “Branching ratio measurements of the photodissociation of <sup>12</sup>C<sup>16</sup>O by time-slice velocity-map imaging photoion method in the vacuum ultraviolet region from 102,500 to 106,300 cm<sup>-1</sup>”, *J. Phys. Chem. A* (invited), to be revised.
17. Y. Xu, Y. C. Chang, Z. Lu, and C. Y. Ng, “Absolute total cross sections and product branching ratios for the vibrationally selected ion-molecule reactions: N<sub>2</sub><sup>+</sup>(X<sup>2</sup>Σ<sub>g</sub><sup>+</sup>; v<sup>+</sup> = 0-2) + CH<sub>4</sub>”, *Astrophys. J.*, submitted.
18. H. Huang, Z. Luo, Y. C. Chang, K.-C. Lau, and C. Y. Ng, “Rovibronically selected and resolved two-color laser photoionization and photoelectron study of titanium oxide cation”, *J. Chem. Phys.*, submitted.

# LES of Turbulence-Chemistry Interactions in Reacting Multiphase Flows

Joseph C. Oefelein

Combustion Research Facility, Sandia National Laboratories

Livermore, CA 94551-0969

oefelei@sandia.gov

## I. Program Scope

Application of the Large Eddy Simulation (LES) technique within the Diagnostics and Reacting Flows program at the CRF is based on two primary objectives. The first is to establish a set of high-fidelity “first-principles” computational benchmarks that identically match the geometry (i.e., experimental test section and burner) and operating conditions of selected experimental target flames. The second is to establish a scientific foundation for advanced model development that effectively bridges the gap between the idealized jet flame processes studied under this program and application relevant processes exhibited at the device scale. The goal is to provide direct one-to-one correspondence between measured and modeled results at conditions unattainable using Direct Numerical Simulation (DNS) by performing a series of detailed simulations that progressively incorporate the fully coupled dynamic behavior of reacting flows with detailed thermodynamics, transport, chemistry, and realistic levels of turbulence. Our primary focal point is the series of flames that have been studied as part of the Experimental Reacting Flow Research program in collaboration with Rob Barlow and Jonathan Frank. This represents a direct extension of joint activities being pursued as part of the *International Workshop on Measurement and Computation of Turbulent (Non)premixed Flames*<sup>1</sup> (i.e., the “TNF Workshop”). Complementary information from highly specialized LES calculations, combined with detailed laser-based measurements, provide new opportunities to understand the central physics of turbulence-chemistry interactions in realistic parameter spaces and for the development of accurate predictive models for turbulent combustion. After achieving an adequate level of validation, results from high-fidelity LES provide fundamental information that cannot be measured and a strong link between theory, experiments, and relevant applications. The insights gained provide a basic science foundation for development of models and simulation techniques for state-of-the-art transportation, propulsion, and power devices such as internal combustion engines (e.g., reciprocating, gas turbine, liquid rockets).

## II. Recent Progress

The need for improved quality metrics for LES has been recognized now for many years. Activities associated with the TNF Workshop, for example, has identified many issues. In TNF8 (Heidelberg Germany, 2006), attempts to model simple bluff-body flames (the HM1 case for example) by several different research groups around the world illustrated many ambiguities. Two issues arose from initial comparisons with available experimental data: 1) uncertainty with respect to boundary conditions, and 2) uncertainty with respect to code and simulation parameters (i.e., numerics, grid resolution, time-step, integration time, etc.). Codes with a variety of different numerical schemes and capabilities (e.g., with and without artificial dissipation added for stability) were used. Geometric details of the burner were not resolved. Limited computational resources imposed significant constraints on the levels spatial and temporal resolution applied. The combined uncertainties made it impossible to draw any conclusions regarding model accuracy. The reason for these ambiguities is due to the fact that all Computational Fluid Dynamics (CFD) calculations are composed of different mathematical elements: 1) numerical methods, 2) physical models, 3) a discretized physical domain, and 4) boundary conditions. Each of these elements introduces uncertainties, and the competing errors interact in a highly nonlinear manner due to the coupled nature of the mathematical systems (see Geurts *et al.*<sup>7</sup>). The broadband multi-scale nature of LES makes it particularly sensitive to these errors. In addition, the integral-scale Reynolds number for the flames studied under this program (e.g., TNF flames) are of  $\mathcal{O}(10^4)$  whereas those associated with most transportation, propulsion, and power devices are of  $\mathcal{O}(10^5)$  or greater. Thus, there is a related need to quantify the effects of increasing Reynolds number and other key quantities on turbulent flame dynamics and understand how to scale validated LES to conditions exhibited at the application level. Accomplishing this hinges on understanding the ranges of scales that a given system of subgrid models accurately operates over.

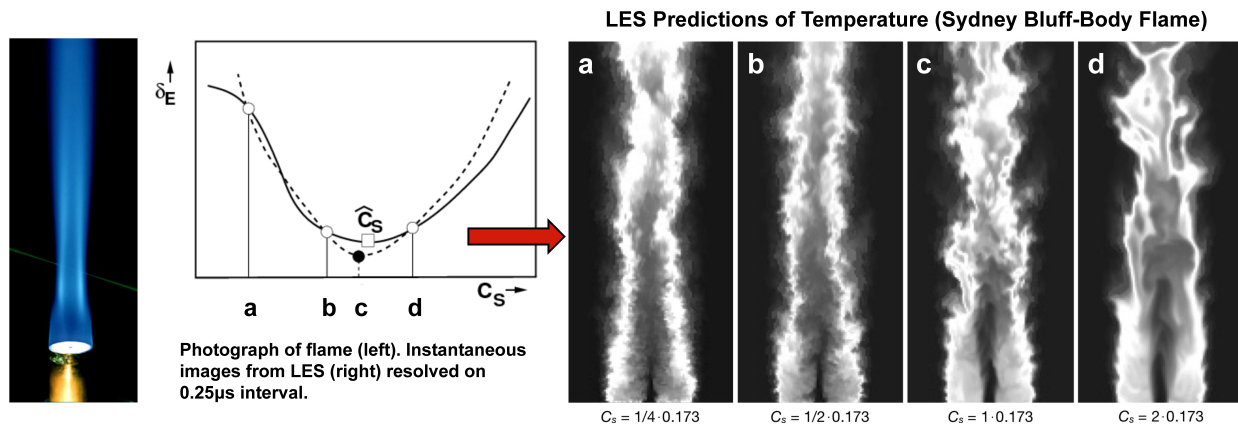


Figure 1: The Sydney bluff-body flame shown at left is used to demonstrate the error-landscape method (see Kempf, Geurts, and Oefelein<sup>11</sup>). Figures a-d show the instantaneous temperature from LES and illustrate the effects of different values of the Smagorinsky constant  $C_s$ . Small values of  $C_s$  (a) allow structures on order of the grid spacing where numerical errors dominate. Large values (d) suppress structures. The optimal value is found at  $C_s = 0.173$ . (c)

Development of predictive LES is complicated by the interdependence of different subgrid models, competition between modeling and numerical errors, model variability, and numerical implementation. Errors and ambiguities are multiplying, and control of accuracy has become a critical aspect in the development of predictive LES for design. When accuracy is not sufficient, results can be misleading and intractably erroneous due to factors such as poor numerics, poor grid quality, lack of appropriate spatial or temporal resolution, ill-posed boundary conditions, and inaccurate models. Given the myriad of competing interdependencies that affect solution accuracy, time to solution, and the overall confidence in the predictive quality of LES, we have devoted significant time recently to begin to establish robust performance metrics to assess the “quality” of a given simulation in a manner that minimizes potential sources of error and provides a clear set of quantitative implementation requirements for different classes of subgrid models. Collaborative efforts were coordinated as part of recent TNF workshops.<sup>1</sup>

Initial studies aimed at understanding and improving the accuracy of LES focused on the impact of grid resolution on numerical errors and/or model errors. Past criteria have been developed to assess LES quality in simple geometries, under simple conditions (single phase, low turbulence intensity, non-reacting). Similarly, various algebraic error indicators (such as Popes 80 % criterion<sup>2</sup>) have been developed in an attempt to provide some guiding metrics (see for example Gant<sup>3</sup> and Celik *et al.*<sup>4</sup>). In TNF9 (Montreal Canada, 2009), algebraic error indicators were applied to the Sydney bluff-body flame (HM1) to explore their utility in the context of the observations above. It was shown that these indicators produce anomalous results. In dissipative schemes, for example, measures of the resolved turbulent kinetic energy in an LES can be misleadingly high since dissipative errors incorrectly damp the velocity fluctuations and thus the total level of turbulent kinetic energy in the system. As a consequence, low values of turbulent viscosity suggest good resolution, when in reality artificial dissipation introduced non-physical damping of the turbulence.

A second focal point in TNF9, followed by TNF10 (Beijing China, 2010), was application of more advanced techniques based on multi-objective optimizations to reach an ideal set of simulation parameters (see for example the pioneering work of Meyers *et al.*<sup>5,6</sup>). One such technique known as the error-landscape method was applied to the Sydney bluff-body flame (HM1) by Kempf, Geurts, and Oefelein.<sup>11</sup> Figure 1 shows representative results that demonstrate how to optimize the widely used Smagorinsky model on a given grid. Small values of the Smagorinsky constant  $C_s$  (a) allow structures on order of grid spacing where numerical errors dominate. Large values (d) suppress structures. The optimal value is found in between at  $C_s = 0.173$  (c). The error-landscape method is used to systematically assess the total simulation error that results from the combination of specific models and numerical methods. The novel feature of this method is that it makes use of available experimental data to quantify the error in corresponding simulations. This is in contrast to more sophisticated uncertainty quantification methods that require significantly more input than is typically available from an experiment. The primary advantage the technique is that it identifies combinations of grid, filter, and model parameters that introduce incorrect flow physics. This allows one to simultaneously minimize the competing effects of these errors. The disadvantage, however, is that combined errors are lumped together and the total error cannot be reduced to any arbitrary level.

A major deficiency with the quality indicators used to date is that none of them account for the various sources of error rigorously. Only the bulk error from multiple competing sources has been considered instead of the distinct sources of error. Discretization and modeling associated with LES introduces three distinct forms of error: 1) discretization errors associated with the numerical techniques; i.e., temporal integration, spatial differencing, and related stabilization schemes, which can induce damping and dispersion of broadband flow processes; 2) the total model residual error, which is caused by discretization of the sub-models themselves; and 3) the error associated with the model approximation itself due to both the basic assumptions and the related range of subgrid- or subfilter-scales it is specified to work over. Ongoing work is focused on understanding and minimizing these three distinct sources of error and the interactions between them.

Quality metrics that relate local grid resolution, the spatial filter size, and corresponding integration time-step to key physical scales such as the Kolmogorov time and length scales, scalar thickness, flame thickness, reaction zone thickness (depending on the flow system of interest) are being developed that can be used to quantify each of the sources of error individually. Once the errors are quantified, implementation requirements aimed at simultaneously minimizing respective errors and the compounding interactions between them will be developed. To accomplish this goal, we use a framework similar to that developed by Vervisch *et al.*<sup>8</sup> as the initial starting point. In contrast to Vervisch *et al.*, who focused on developing mesh quality criterion aimed exclusively at minimizing the total model residual error for accurate treatment and analysis of DNS data, our effort will extend these ideas with emphasis on treating all three forms of error in the context of LES. Development of the quality assessment techniques and corresponding implementation requirements for accurate LES will be directly linked to the hierarchy of experiments that Barlow and Frank have proposed.

### III. Future Work

We will continue to use the foundational approach and framework described above with emphasis placed on three interrelated areas of research: 1) Maintain close coordination between LES and the experimental reacting flow research program with emphasis on the collaborative activities of the TNF Workshop to advance our fundamental understanding of turbulent reacting flows. 2) Initiate a significant effort in the development of quality assessment techniques for LES aimed at understanding and controlling the myriad of errors that complicate the development and validation of predictive models. 3) Continue to develop advanced models and simulation techniques aimed at accurate prediction of flame behavior across a broad range of combustion modes, regimes, and fuels. Tasks related to research area 1 will be pursued through close collaborations with R. Barlow and J. Frank following the proposed series of experiments outlined in their respective abstracts. Tasks related to research area 2 will be pursued through close collaborations with R. Dahms and H. Najm (e.g., see Najm's abstract). Calculations will be performed in a manner that leverages our combined expertise in LES, high performance computing, and access to unique massively parallel computational facilities. Emphasis will be placed on establishing high-fidelity computational benchmarks that identically match the geometry and operating conditions of the selected experimental target flames. The goal is to establish a scientific foundation for advanced model development that bridges the gap between the idealized jet flame processes studied under this program and application relevant processes exhibited at the device scale.

### IV. Literature Cited

1. R. S. Barlow. International workshop on measurement and computation of turbulent (non)premixed flames. [www.sandia.gov/TNF](http://www.sandia.gov/TNF), 1996-2013. Sandia National Laboratories, Combustion Research Facility, Livermore, California.
2. S. B. Pope. *Turbulent Flows*. Cambridge University Press, Cambridge, United Kingdom, 2000.
3. S. E. Gant. Reliability issues of LES-related approaches in an industrial context. *Flow, Turbulence and Combustion*, 84(2): 325–335, 2010. doi: 10.1007/s10494-009-9237-8.
4. I. B. Celik, Z. N. Cehreli, and I. Yavuz. Index of resolution quality for large eddy simulations. *Journal of Fluids Engineering*, 127:949–958, 2005.
5. J. Meyers, B. J. Geurts, and M. Baelmans. Database analysis of errors in large-eddy simulation. *Physics of Fluids*, 15(9): 2740–2755, 2003. doi: 10.1063/1.1597683.
6. J. Meyers, P. Sagaut, and B. J. Geurts. Optimal model parameters for multi-objective large-eddy simulations. *Physics of Fluids*, 18(095103):1–12, 2006. doi: 10.1063/1.2353402.

7. B. J. Geurts and J. Fröhlich. A framework for predicting accuracy limitations in large-eddy simulation. *Physics of Fluids*, 14(6):41–44, 2002. doi: 10.1063/1.1480830.
8. L. Vervisch, P. Domingo, G. Lodato, and D. Veynante. Scalar energy fluctuations in large-eddy simulation of turbulent flames. *Combustion and Flame*, 157:778–789, 2010. doi: 10.1016/j.combustflame.2009.12.017.

## V. BES Sponsored Publications (2011–2013)

1. R. N. Dahms and J. C. Oefelein. Regimes of supercritical injection phenomena in advanced propulsion and power systems. *Combustion and Flame*, 2013. Submitted.
2. R. N. Dahms and J. C. Oefelein. On the transition between two-phase and single-phase interface dynamics in multicomponent fluids at supercritical pressures. *Combustion and Flame*, 2013. Submitted.
3. R. N. Dahms, J. Manin, L. M. Pickett, and J. C. Oefelein. Understanding high-pressure gas-liquid interface phenomena in diesel engines. *Proceedings of the Combustion Institute*, 34:1667–1675, 2013. doi: 10.1016/j.proci.2012.06.169.
4. L. Lu, P. M. Najt, T.-W. Kuo, V. Sankaran, and J. C. Oefelein. A fully integrated linear eddy and chemistry agglomeration method with detailed chemical kinetics for studying the effect of stratification on HCCI combustion. *Fuel*, 105:653–663, 2013. doi: 10.1016/j.fuel.2012.09.031.
5. J. Manin, M. Bardi, L. M. Pickett, R. N. Dahms, and J. C. Oefelein. Development and mixing of diesel sprays at the microscopic level from low to high temperature and pressure conditions. *Proceedings of the 7th THIESEL Conference on Thermo- and Fluid-Dynamic Processes in Direct Injection Engines*, September 11-14 2012. Valencia, Spain.
6. J. C. Oefelein, R. N. Dahms, G. Lacaze, J. L. Manin, and L. M. Pickett. Effects of pressure on the fundamental physics of fuel injection in diesel engines. *Proceedings of the 12th International Conference on Liquid Atomization and Spray Systems*, September 2-6 2012. Heidelberg, Germany. ISBN 978-88-903712-1-9.
7. J. C. Oefelein, R. N. Dahms, and G. Lacaze. Detailed modeling and simulation of high-pressure fuel injection processes in diesel engines. *SAE International Journal of Engines*, 5(3):1–10, 2012. doi: 10.4271/2012-10-1258.
8. R. Knaus, J. Oefelein, and C. Pantano. On the relationship between the statistics of the resolved and true rate of dissipation of mixture fraction. *Flow, Turbulence and Combustion*, 89(1):37–71, 2012. doi: 10.1007/s10494-012-9391-2.
9. G. Lacaze and J. C. Oefelein. A non-premixed combustion model based on flame structure analysis at supercritical pressures. *Combustion and Flame*, 159:2087–2103, 2012. doi: 10.1016/j.combustflame.2012.02.003.
10. B. Hu, M. P. Musculus, and J. C. Oefelein. The influence of large-scale structures on entrainment in a decelerating transient turbulent jet revealed by large eddy simulation. *Physics of Fluids*, 24(045106):1–17, 2012. doi: 10.1063/1.3702901.
11. A. M. Kempf, B. J. Geurts, and J. C. Oefelein. Error analysis of large eddy simulation of the turbulent non-premixed Sydney bluff-body flame. *Combustion and Flame*, 158:2408–2419, 2011. doi: 10.1016/j.combustflame.2011.04.012.
12. J. C. Oefelein and G. Lacaze. Low-temperature injection dynamics and turbulent flame structure in high-pressure supercritical flows. *Proceedings of the 23rd International Colloquium on the Dynamics of Explosions and Reactive Systems*, July 24-29 2011. Irvine, California.
13. R. N. Dahms, L. M. Pickett, and J. C. Oefelein. A dense fluid approximation for the simulation of Diesel engine fuel injection processes. *Proceedings of the 23rd Annual Conference on Liquid Atomization and Spray Systems*, May 15-18 2011. Ventura, California.
14. J. H. Frank, S. A. Kaiser, and J. C. Oefelein. Analysis of scalar mixing dynamics in LES using high-resolution imaging of laser Rayleigh scattering in turbulent non-reacting jets and non-premixed jet flames. *Proceedings of the Combustion Institute*, 33:1373–1381, 2011.

# KINETICS AND DYNAMICS OF COMBUSTION CHEMISTRY

David L. Osborn

Combustion Research Facility, Mail Stop 9055

Sandia National Laboratories

Livermore, CA 94551-0969

Telephone: (925) 294-4622

Email: dlosbor@sandia.gov

## PROGRAM SCOPE

The goal of this program is to elucidate mechanisms of elementary combustion reactions through the use of multiplexed optical spectroscopy and mass spectrometry. We developed a technique known as time-resolved multiplexed photoionization mass spectrometry (MPIMS), which is used to sensitively and selectively probe unimolecular and bimolecular reactions. This work is in collaboration with Craig Taatjes and many scientists from other institutions in the US and abroad. The Sandia-designed MPIMS instrument utilizes tunable vacuum ultraviolet light from the Advanced Light Source synchrotron at Lawrence Berkeley National Laboratory for sensitive, isomer-specific ionization of reactant and product molecules in chemical reactions.

As a complementary approach, we utilize time-resolved Fourier transform spectroscopy (TR-FTS) to probe multiple reactants and products with broad spectral coverage ( $> 1000 \text{ cm}^{-1}$ ), moderate spectral resolution ( $0.1 \text{ cm}^{-1}$ ), and a wide range of temporal resolution (ns – ms). The inherently multiplexed nature of TR-FTS makes it possible to simultaneously measure product branching ratios, internal energy distributions, energy transfer, and spectroscopy of radical intermediates. Together with total rate coefficients, this additional information provides further constraints upon and insights into the potential energy surfaces that control chemical reactivity. Because of its broadband nature, the TR-FTS technique provides a global view of chemical reactions and energy transfer processes that would be difficult to achieve with narrow-band, laser-based detection techniques.

## RECENT PROGRESS

### Isomer-resolved mass spectrometry

The multiplexed chemical kinetics photoionization mass spectrometer operates both at Sandia National Laboratories (using a discharge lamp to create VUV radiation), and at the Chemical Dynamics Beamline of the Advanced Light Source (ALS) synchrotron of LBNL. The chemical reactor is based on the Gutman design,<sup>1</sup> which allows the study of photodissociation and bimolecular reactions at pressures of 1 – 10 Torr and temperatures of 300 – 1000 K.

While the study of chemical kinetics using PIMS is well-established, this apparatus has two unique features that make it especially powerful for chemical kinetics. First, the widely tunable, intense VUV radiation from the ALS enables isomer-specific ionization of product species. Second, the high repetition rate of the mass spectrometer allows us to take snapshots of the complete chemical composition in our reactor as a function of time at a repetition rate of 50 kHz. Mass resolution of  $m/\Delta m \sim 1600$  has been achieved using a simple linear (i.e., not reflectron) approach. This mass resolution has already been used to separate  $\text{HCCO}^+$  from  $\text{C}_3\text{H}_5^+$  (both nominally mass 41),  $\text{CH}_2\text{OO}$  vs.  $\text{CH}_2\text{S}$ , and will be increasingly valuable in separating other  $\text{O} \leftrightarrow \text{CH}_4$  substitutions in larger hydrocarbons (e.g., acetone vs. butane, ketene vs. propene) in the chemistry of hydrocarbon oxidation.

### **The absolute photoionization cross section of the vinyl ( $\text{H}_2\text{CCH}$ ) radical**

The vinyl radical ( $\text{H}_2\text{CCH}$ ) is a combustion intermediate that has long been implicated in molecular weight growth chemistry. As more experiments attempt to measure concentrations of transient intermediates via photoionization, the need for accurate photoionization cross sections grows. However, the absolute number density of a free radical sample is time dependent due to loss via chemical reactions, making it challenging to obtain absolute photoionization cross sections. Our approach follows closely a method developed by Neumark and co-workers,<sup>2</sup> in which a stable, closed-shell precursor molecule is photodissociated, yielding two free radical fragments in a 1:1 ratio, both of which are detected via photoionization. If the absolute photoionization cross section of one radical is known, the cross section of the partner radical may be determined from the ratio of signal strengths, properly corrected for instrumental factors.

For the vinyl radical, we chose two precursors: methyl vinyl ketone (MVK) and vinyl iodide (VI). In the former case we measure the cross section of the vinyl radical by comparison with its cofragment, the methyl radical, following 193 nm photodissociation of MVK. Fahr and coworkers<sup>3</sup> have measured the quantum yield ( $\Phi_{\text{methyl}}/\Phi_{\text{vinyl}} = (1.11 \pm 0.04)$ ) from MVK photodissociation, which is used to scale our signals. We utilize the absolute photoionization cross section of the  $\text{CH}_3$  radical, which has been measured with good agreement by three independent scientific teams.<sup>4</sup> For vinyl iodide photodissociation at 248 nm, the quantum yield of the  $\text{I} + \text{C}_2\text{H}_3$  channel is close to unity ( $> 0.91$ ). With this system we can measure the vinyl cross section from the number density and absolute cross section of  $\text{C}_2\text{H}_3\text{I}$  combined with its fractional depletion due to photodissociation. Using the MPIMS spectrometer for this measurement has two important advantages. First, the nascent radicals are thermalized rapidly to 300K via collisions with helium, ensuring that the thermal energy in each radical is small and well-determined. Second, the time-resolved signals of each radical can be used to extrapolate to signals that would be observed immediately following dissociation at  $t \sim 0$ . We are finalizing our analysis of this data at present, but the preliminary results point to a smaller value than that obtained by Robinson et al.<sup>5</sup> In our measurements, both the reference and the unknown radical can be measured at the same photoionization energy, eliminating the need to measure the VUV photon flux, thereby cancelling any systematic errors that may accompany such measurements.

### **The $\text{O}({}^3\text{P})$ + methylacetylene reaction: Intersystem crossing plays a key role**

Reactions of ground state oxygen atoms with unsaturated hydrocarbons are important reactions in some regions of flames. The primary loss channel for acetylene ( $\text{HCCH}$ ) is reaction with  $\text{O}({}^3\text{P})$ , yielding the major product channel  $\text{H} + \text{HCCO}$  and the minor channel  ${}^3\text{CH}_2 + \text{CO}$ . All evidence (experimental and theoretical) argues that this reaction takes place entirely on the triplet  $\text{C}_2\text{H}_2\text{O}$  surface. By contrast, there is significant evidence that the reaction of  $\text{O}({}^3\text{P})$  with ethene ( $\text{C}_2\text{H}_4$ ) occurs on both the initial triplet and the singlet surface, despite the fact that all the atoms are light. The nonadiabatic interactions leading to the surprisingly facile intersystem crossing (ISC) are reasonably well documented for the case of  $\text{O}({}^3\text{P}) + \text{C}_2\text{H}_4$ , notably in a recent study by the groups of Bowman and Casavecchia.<sup>6</sup>

We recently completed a study of the  $\text{O}({}^3\text{P}) + \text{propene}$  ( $\text{C}_3\text{H}_6$ ) reaction as a gateway to the richer chemical pathways available in larger alkenes. For example, in the propene reaction the oxygen atom may add to the central or the terminal carbon. These distinct entrance channels lead to different reaction pathways, and offer clues to the mechanism of ISC. More recently we have studied the reaction of  $\text{O}({}^3\text{P}) + \text{methylacetylene}$  ( $\text{HC}\equiv\text{CCH}_3$ ) to compare with the analogous reaction with acetylene.

We have studied this reaction at a pressure of 4 torr and temperature of 300K, and with both  $d_0$ - and  $d_1$ -methylacetylene for additional mechanistic insight. Under these low pressure conditions, stabilization of the  $C_3H_4O$  adduct is disfavored, and bimolecular reaction channels dominate. We observe evidence for 7 different product channels of this reaction, including the two simple bond fission channels characterized by methyl and H atom loss. The major species we identify are vinyl ( $C_2H_3$ ), formyl (HCO), methylketenyl  $CH_3CCO$ , methyl ( $CH_3$ ), ethene ( $C_2H_4$ ), and acetylene (HCCH). A very small amount of propadienal ( $CH_2CCO$ ) is detected, evidence for a  $H_2$  loss channel.

Our preliminary analysis leads to two (preliminary) conclusions. First, that  $O(^3P)$  addition to the central carbon is quite minor ( $< 10\%$ ), and second, that  $\sim 70\%$  of the products arise from intersystem crossing to the singlet surface. The second finding is in stark contrast to the electronically similar reaction with acetylene.

### **Photochemical conversion of acetaldehyde to vinyl alcohol**

In collaboration with Scott Kable and Meredith Jordon of the University of Sydney, we have investigated the photolysis of acetaldehyde in a bath gas of nitrogen at total pressure  $P = 20 - 760$  torr, over the wavelength range  $\lambda = 330 - 295$  nm. In this region acetaldehyde absorbs to the  $S_1$  state followed by intersystem crossing and/or internal conversion to highly vibrationally excited states on  $S_0$ . At moderate pressure, collisional stabilization competes with decay to bimolecular products. We have observed for the first time that part of the collisional stabilization channel includes isomerization to vinyl alcohol. Because this species does not absorb in the in this wavelength region, photoisomerization is a one-way street leading to a buildup of vinyl alcohol. This result has clear implications for tropospheric chemistry, but also points out how this system is an ideal one for tuning a master equation analysis in a system where the total energy is well controlled.

### **Future Directions**

Using TR-FTS, we will continue to investigate photodissociation reactions that show evidence for roaming dynamics. Following on the recent work of Suits and coworkers<sup>7</sup> on acetone photodissociation, we plan to study production of  $C_2H_6$  in this system. Using MPIMS, we will continue studies of  $O(^3P) +$  unsaturated molecules to explore more deeply the factors governing intersystem crossing rates in these systems.

### **BES-sponsored publications, 2011 – present**

- 1) Phototautomerization of Acetaldehyde to Vinyl Alcohol: A Primary Process in UV-Irradiated Acetaldehyde from 295 to 335 nm, A. E. Clubb, M. J. T. Jordan, S. H. Kable, and D. L. Osborn, *Journal of Physical Chemistry Letters* **3**, 3522 (2012).
- 2) Thermal decomposition of  $CH_3CHO$  studied by matrix infrared spectroscopy and photoionization mass spectroscopy, A. K. Vasiliou, K. M. Piech, B. Reed, X. Zhang, M. R. Nimlos, M. Ahmed, A. Golan, O. Kostko, D. L. Osborn, D. E. David, K. N. Urness, J. W. Daily, J. W. Stanton, and G. B. Ellison, *Journal of Chemical Physics* **137**, 164308 (2012).
- 3) Synchrotron photoionization measurements of fundamental autoignition reactions: Product formation in low-temperature isobutane oxidation, A. J. Eskola, O. Welz, J. D. Savee, D. L. Osborn, and C. A. Taatjes, *Proc. Combust. Inst.*, <http://dx.doi.org/10.1016/j.proci.2012.06.0116> (2012).
- 4) Low-temperature combustion chemistry of biofuels: Pathways in the low-temperature (550 – 700 K) oxidation chemistry of isobutanol and tert-butanol, O. Welz, J. D. Savee, A. J. Eskola, L. Sheps, D. L. Osborn, and C. A. Taatjes, *Proc. Combust. Inst.* <http://dx.doi.org/10.1016/j.proci.2012.05.058> (2012).
- 5) Product Detection of the CH Radical Reaction with Acetaldehyde, F. Goulay, A. J. Trevitt, J. D. Savee, J. Bouwman, D. L. Osborn, C. A. Taatjes, K. R. Wilson, and S. R. Leone, *Journal of Physical Chemistry A* **116**, 6091 (2012).
- 6) Synchrotron photoionization measurements of OH-initiated cyclohexene oxidation: ring-preserving products in the OH + cyclohexene and hydroxycyclohexyl +  $O_2$  reactions, A. W. Ray, C. A. Taatjes, O. Welz, D. L. Osborn, and G. Meloni, *Journal of Physical Chemistry A* **116**, 6720 (2012).

- 7) New mechanistic insights to the  $O(^3P) + \text{propene}$  reaction from multiplexed photoionization mass spectrometry, J. D. Savee, O. Welz, C. A. Taatjes, and D. L. Osborn, *Physical Chemistry Chemical Physics* **14**, 10410 (2012).
- 8) Spectroscopy of the simplest Criegee intermediate  $\text{CH}_2\text{OO}$ : simulation of the first bands in its electronic and photoelectron spectra, E. P. F. Lee, D. K. W. Mol, D. E. Shallcross, C. J. Percival, D. L. Osborn, C. A. Taatjes, and J. M. Dyke, *Chemistry – A European Journal* **18**, 12411 (2012).
- 9) Direct measurement of Criegee intermediate ( $\text{CH}_2\text{OO}$ ) reactions with acetone, acetaldehyde, and hexafluoroacetone, C. A. Taatjes, O. Welz, A. J. Eskola, J. D. Savee, D. L. Osborn, E. P. F. Lee, J. M. Dyke, D. W. K. Mok, D. E. Shallcross, and C. J. Percival, *Physical Chemistry Chemical Physics* **14**, 10391 (2012).
- 10) Absolute photoionization cross-section of the propargyl radical, J. D. Savee, S. Soorkia, O. Welz, T. M. Selby, C. A. Taatjes, and D. L. Osborn, *Journal of Chemical Physics* **136**, 134307 (2012).
- 11) Ground and low-lying excited states of propadienyliene ( $\text{H}_2\text{C}=\text{C}=\text{C}:$ ) obtained by negative ion photoelectron spectroscopy, J. F. Stanton, E. Garand, J. Kim, T. I. Yacovitch, C. Hock, A. S. Case, E. M. Miller, Y. J. Lu, K. M. Vogelhuber, S. W. Wren, T. Ichino, J. P. Maier, R. J. McMahon, D. L. Osborn, D. M. Neumark, and W. C. Lineberger, *Journal of Chemical Physics* **136**, 134312 (2012).
- 12) Low-temperature combustion chemistry of biofuels: pathways in the initial low-temperature (550 – 750K) oxidation chemistry of isopentanol, O. Welz, J. Zador, J. D. Savee, M. Y. Ng, G. Meloni, R. X. Fernandes, L. Sheps, B. A. Simmons, T. S. Lee, D. L. Osborn, and C. A. Taatjes, *Physical Chemistry Chemical Physics* **14**, 3112 (2012).
- 13) “Direct kinetic measurements of the Criegee intermediate ( $\text{CH}_2\text{OO}$ ) formed by reaction of  $\text{CH}_2\text{I}$  with  $\text{O}_2$ ” O. Welz, J. D. Savee, D. L. Osborn, S. S. Vasu, C. J. Percival, D. E. Shallcross, and C. A. Taatjes, *Science* **335**, 204 (2012).
- 14) “Absolute photoionization cross-sections of some combustion intermediates” B. Yang, J. Wang, T. A. Cool, N. Hansen, S. Skeen, and D. L. Osborn, *International Journal of Mass Spectrometry* **309**, 118 (2012).
- 15) “Branching fractions of the  $\text{CN} + \text{C}_3\text{H}_6$  reaction using synchrotron photoionization mass spectrometry: evidence for the 3-cyanopropene product” A. J. Trevitt, S. Soorkia, J. D. Savee, T. S. Selby, D. L. Osborn, C. A. Taatjes, S. R. Leone, *Journal of Physical Chemistry A* **115**, 13467 (2011).
- 16) “Detection of pentatetraene by reaction of the ethynyl radical ( $\text{C}_2\text{H}$ ) with allene ( $\text{CH}_2=\text{C}=\text{CH}_2$ ) at room temperature” F. Goulay, S. Soorkia, G. Meloni, D. L. Osborn, C. A. Taatjes, and S. R. Leone, *Physical Chemistry Chemical Physics* **13**, 20820 (2011).
- 17) “The products of the thermal decomposition of  $\text{CH}_3\text{CHO}$ ” A. Vasiliou, K. M. Piech, X. Zhang, M. R. Nimlos, M. Ahmed, A. Golan, O. Kostko, D. L. Osborn, J. W. Daily, J. F. Stanton, and G. B. Ellison, *Journal of Chemical Physics* **135**, 014306 (2011).
- 18) “Near-threshold H/D exchange in  $\text{CD}_3\text{CHO}$  photodissociation,” B. R. Heazlewood, A. T. Maccarone, D. U. Andrews, D. L. Osborn, L. B. Harding, S. J. Klippenstein, M. J. T. Jordan, and S. H. Kable, *Nature Chemistry* **3**, 443 (2011).
- 19) “Infrared emission following photolysis of methylisothiocyanate and methylthiocyanate,” E. A. Wade, J. L. Pore, and D. L. Osborn, *J. Phys. Chem. A* **115**, 014306 (2011).

## References

- <sup>1</sup> I. R. Slagle and D. Gutman, *J. Am. Chem. Soc.* **107**, 5342 (1985).
- <sup>2</sup> J. C. Robinson, N. E. Sveum, and D. M. Neumark, *Chem. Phys. Lett.* **383**, 601 (2004).
- <sup>3</sup> A. Fahr, W. Braun, and A. H. Laufer, *J. Phys. Chem.* **97**, 1502 (1993).
- <sup>4</sup> C. A. Taatjes, D. L. Osborn, T. M. Selby, G. Meloni, H. Y. Fan, and S. T. Pratt, *J. Phys. Chem. A* **111**, 12417 (2008); B. Gans et al., *J. Phys. Chem. A* **114**, 3237 (2010); J. C. Loison, *J. Phys. Chem. A* **114**, 65151 (2010).
- <sup>5</sup> J. C. Robinson, N. E. Sveum, and D. M. Neumark, *J. Chem. Phys.* **119**, 5311 (2003).
- <sup>6</sup> B. N. Fu, Y. C. Han, J. M. Bowman, F. Leonori, N. Balucani, L. Angelucci, A. Occhiogrosso, R. Petrucci, and P. Casavecchia, *J. Chem. Phys.* **137**, 22A532 (2012).
- <sup>7</sup> V. Goncharov, N. Herath, and A. G. Suits, *J. Phys. Chem. A* **112**, 9423 (2008).

**Program Title:** A Theoretical Investigation of the Structure and Reactivity of the Molecular Constituents of Oil Sand and Oil Shale

**Principle Investigator:** Carol Parish

Address: Department of Chemistry, University of Richmond, Richmond, VA 23227  
cparish@richmond.edu

## **PROGRAM SCOPE**

Our work focuses on the theoretical characterization of the gas phase structures, energies and reactivities of the molecular constituents of asphaltenes contained in oil sand and oil shale. Asphaltenes represent an untapped source of hydrocarbon fuel in North America; however, information about the molecular nature of these deposits has only recently become available. Theoretical and experimental evidence suggests that asphaltenes are composed of aromatic molecules that contain 4-10 fused ring cores, with alkyl chain arms extending from the core. Sulfur and nitrogen are also present. Very little is known about the reaction pathways, combustion efficiency and reactivity of these heteroaromatic species. We are currently characterizing the combustion and pyrolysis reaction channels available to asphaltene constituents such as thiophene and methyl thiophene.

## **RECENT PROGRESS - FY 2012 HIGHLIGHTS**

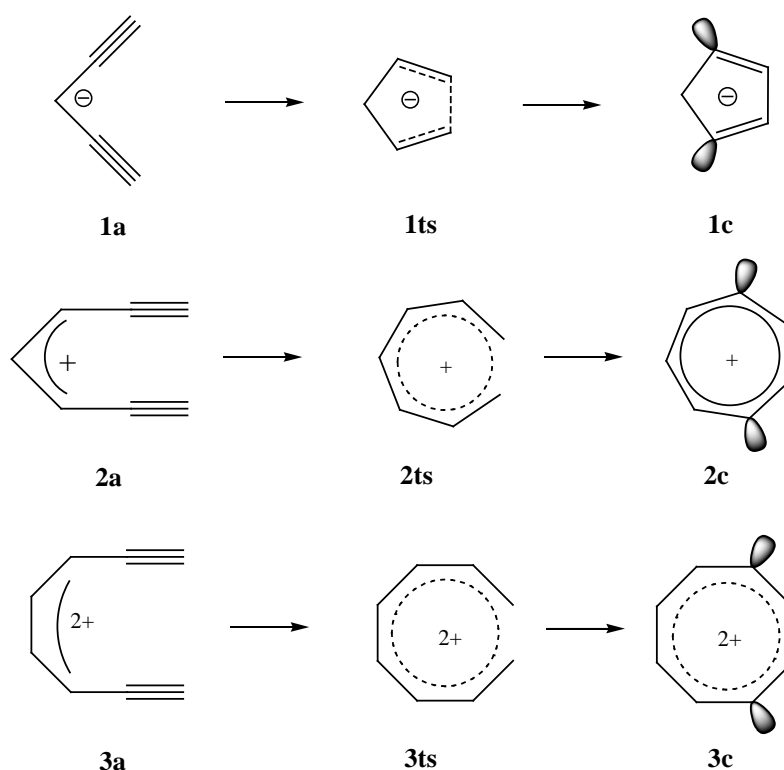
### **Singlet Oxygen (2+4) Cycloaddition to Heteroaromatic Compounds**

The 2+4 cycloaddition reactions of singlet molecular oxygen ( $^1\Delta_g$ ) with a series of aromatic heterocyclic compounds were investigated at both the MP2/6-311++G(d, p) and B3LYP/6-311++G(d, p) levels of theory. Several factors related to heteroaromatic ring structure were determined to affect the activation energy of the cycloaddition and the stability of the corresponding endoperoxide products. Such factors include: (1) the position of methyl substitution; (2) the number of methyl substituents; (3) the alkyl chain length of substituents; (4) the electronic structure of substituents and; (5) the type of heteroatom in the ring. In total, fourteen 2+4 cycloaddition routes were examined and in each case the mechanism is concerted. The order of reactivity toward  $O_2$  ( $^1\Delta_g$ ) was determined to be: 2,3,4,5-tetramethylthiophene > 2,3,5-trimethylthiophene > 2,5-dimethylthiophene > 2-methylthiophene > 2-ethylthiophene > 2-propylthiophene > 3-methylthiophene > thiophene > benzothiophene > dibenzothiophene; and furan > pyrrole > thiophene > benzene. The stability of the endoperoxide products follows a similar trend. Each of the reaction pathways is initiated by the formation of a pre-reactive complex, formed by a van der Waals interaction between a C atom on the ring and an O atom on  $O_2$ . To the best of our knowledge, this type of VDW pre-

reactive complex has not been identified in previous studies of cycloaddition reactions of singlet oxygen with arenes.

### Minding the Gap: Variations on the Bergman Theme. Electrocyclizations of Penta-, Hepta- and Octa-diyne

The electrocyclization reactions of the penta-1,4-diyne anion, the hepta-1,6-diyne cation and the octa-1,7-diyne dication, to form the corresponding aromatic diradicals, were investigated using the BLYP and B3LYP functionals with different basis sets.



The energetics of these cyclization reactions shed light on the structural factors underlying these important processes. The resultant diradicals provide information regarding through-bond and through-space electron coupling and the role of aromaticity in the energetics of the cyclizations. The geometries obtained at different levels of DFT are quite similar; however, the relative energies depend upon the methodological approach. Therefore, energies were also calculated using the BCCD(T)/cc-pVDZ treatment using BLYP/6-31G\* geometries, and compared with the results obtained at DFT levels. The cyclization barrier for the 1,6-heptadiyne cation (25 kcal mol<sup>-1</sup>) is energetically comparable to that of the Bergman cyclization of (Z)-hexa-3-ene-1,5-diyne (28 kcal mol<sup>-1</sup>), while the cyclization barrier for the 1,7-octadiyne dication (15 kcal mol<sup>-1</sup>)

is significantly lower. All three diradicals display aromatic behavior as measured by nucleus independent chemical shifts.

## FUTURE WORK

Work is currently underway to characterize ground and excited states of heteroaromatic diradicals such as thiophene, fulvene and pyrrole. We are also pursuing a complete characterization of the singlet and triplet surfaces of the electrocyclization reaction of (Z)-hexa-1,3,5-triene leading to *p*-benzyne as well as a characterization of the endo and exo-dig radical cyclization reactions.

## PUBLICATIONS

1. "Mechanisms for the reaction of thiophene and methylthiophene with singlet and triplet molecular oxygen," Xinli Song, Matthew G. Fanelli, Justin M. Cook, Furong Bai and Carol A. Parish\*, *Journal of Physical Chemistry A*, **2012**, *116*, 4934-4946.
2. "A Mechanistic Study of the 2-Thienylmethyl + HO<sub>2</sub> Radical Recombination Reaction," Xinli Song and Carol Parish\*, *Journal of Physical Chemistry A*, **2011**, *115*, 14546-14557
3. "Pyrolysis Mechanisms of Thiophene and Methylthiophene in Asphaltenes," Xinli Song and Carol Parish\*, *Journal of Physical Chemistry A* **2011**, *115*, 2882-2891.

## PUBLICATIONS - NOT RELATED TO THE PROJECT

1. "Halogen bonding in DNA base pairs," Anna J. Parker, John Stewart, Kelling Donald\* and Carol Parish\*, *Journal of the American Chemical Society*, **2012**, *134*, 5165-5172.
2. "Evidence that the kinesin light chain contains tetratricopeptide repeat units." Sally Q. Fisher, Meredith Weck, Jenna E. Landers, Jeffrey Emrich, Shana A. Middleton, Jordan Cox, Lisa N. Gentile and Carol A. Parish\*, *Journal of Structural Biology*, **2012**, *177*, 602-612.
3. "Challenging Disciplinary Boundaries in the First-Year: A New Introductory Integrated Science Course for STEM Majors", Gentile, L.\*; Caudhill, L.; Fetea, M.; Hill, A.; Hoke, K.; Lawson, B.; Lipan, O.; Kerckhove, M.; Parish, C.; Stenger, K.; Szajda, D., *Journal of College Science Teaching*, **2012**, *41(5)*, 24-30.
4. "(*rac*)- 1,1'-Binaphthyl-based simple receptors designed for fluorometric discrimination of maleic and fumaric acids," Kumares Ghosh\*, Tanushree Sen, Amarnedra Patra, John S. Mancini, Justin M. Cook and Carol A. Parish\*, *Journal of Physical Chemistry B*, **2011**, *115*, 8597-8608.
5. "Oligonucleotide Incorporation and Base Pair Stability of 9-deaza-2'-deoxyguanosine," Michelle L. Hamm\*, Anna J. Parker, Jennifer L. Carman, Tyler W. E. Steele, and Carol A. Parish\*, *Journal of Organic Chemistry* **2010**, *75*, 5661-5669.
6. "Conformational Analysis of a Model for the trans-fused FGH Ether Rings in Brevetoxin A," Evan B. Wang and Carol A. Parish\*, *Journal of Organic Chemistry*, **2010**, *75*, 1582-1588.

7. "Triphenylamine-Based Receptors for Selective Recognition of Dicarboxylates,"  
Kumaresh Ghosh\*, Indrajit Saha, Goutam Masanta, Evan B. Wang and Carol A. Parish,\*  
*Tetrahedron Letters*, **2010** *51*, 343-347.

# The Dynamics of Large-Amplitude Motion in Energized Molecules

David S. Perry, Principal Investigator  
Department of Chemistry, The University of Akron  
Akron OH 44325-3601  
DPerry@UAkron.edu

## I. Program Scope

Chemical reactions, by definition, involve large-amplitude nuclear motion along the reaction coordinate that serves to distinguish reactants from products. Some reactions, such as roaming reactions and reactions proceeding through a loose transition state, involve more than one large amplitude degree of freedom. In principle, the exact quantum nuclear dynamics may be calculated, but such calculations are limited by practical considerations to a few degrees of freedom. Thus in systems larger than 3 or 4 atoms, one must define the active degrees of freedom and separate them in some way from the other degrees of freedom. In this project, we use large-amplitude motion in bound model systems to investigate the coupling of large-amplitude degrees of freedom to other nuclear degrees of freedom. This approach allows us to use the precision and power of high-resolution molecular spectroscopy to probe the specific coupling mechanisms involved, and to apply the associated theoretical tools. In addition to cavity ringdown experiments and calculations at the University of Akron, work on this project involves collaboration with Brooks Pate's group at the University of Virginia (CD-FTMW-IR spectroscopy of methanol and methylamine), with Michel Herman of the Université Libre de Bruxelles (rotationally dependent vibrational dynamics of acetylene), and with Brant Billinghurst at the Canadian Light Source (torsion-vibration coupling in nitromethane). The concepts developed in this project are finding application to the coupled torsional motions in 3-hexylthiophene oligomers.

## II. Recent Progress

### A. Two-Dimensional Large-Amplitude Motion

In molecules with two large-amplitude vibrations (LAV), the LAV's are coupled both to each other and to the other small-amplitude vibrations (SAV) such as CH stretches. This part of the work is focused on molecules where one LAV is a methyl internal rotation (angle,  $\alpha$ ), and the other is either an inversion motion such as at an amine nitrogen or a proton transfer (coordinate,  $\tau$ ). These molecules of  $G_{12}$  symmetry have 6 equivalent minima connected by quantum mechanical tunneling.

Our *ab initio* calculations on  $\text{CH}_3\text{NH}_2$ ,  $\text{CH}_3\text{OH}_2^+$ , and  $\text{CH}_3\text{CH}_2\cdot$  have shown that the couplings connecting the torsion and inversion LAV's are very similar across these systems despite the wide variation in the tunneling barriers - 704, 400, and 21  $\text{cm}^{-1}$  respectively for torsional barriers, and 1950, 875, and 0  $\text{cm}^{-1}$  respectively for the barriers to inversion. The dominant torsion-inversion coupling term in all three cases has the form,  $V_{1,3}\tau \cos 3\alpha$ , with  $V_{1,3}$  in the range

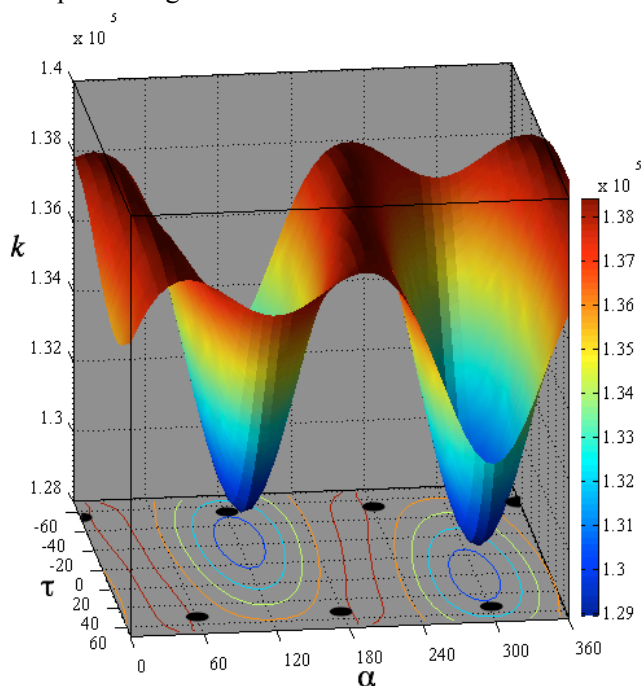


Fig. 1. The computed CH stretch force constant in  $\text{CH}_3\text{NH}_2$  as a function of the torsion ( $\alpha$ ) and inversion ( $\tau$ ) angles. The black ovals on the base plane indicate the locations of the six equivalent equilibrium geometries of  $\text{CH}_3\text{NH}_2$ .

280 to 450  $\text{cm}^{-1}$ .

The work on these systems has now been extended to the coupling of the two LAV's to the SAV's, specifically the CH stretches. Such coupling can occur via the variation force constant of one CH bond across the 2-D space of the LAV coordinates,  $\alpha$  and  $\tau$  (Fig. 1). Additional coupling results from the variation of the coupling between two of the CH bonds in this 2-D space. These couplings are responsible for resolution of the E-type degenerate asymmetric CH stretch in a symmetric rotor into two nondegenerate stretches  $\nu_2$  and  $\nu_{11}$  in methylamine and they also impact the torsion-inversion level structure in the CH stretch excited states. The magnitude of the couplings is a few tens of  $\text{cm}^{-1}$  in the CH stretch fundamental region, and they scale with the quantum numbers to become much larger at higher energies.

Although the torsional barriers for  $\text{CH}_3\text{NH}_2$  and  $\text{CH}_3\text{CH}_2\cdot$  differ by more than a factor of 20, we find that the torsion-inversion-vibration coupling patterns, such as illustrated in Fig. 1, are very similar. On the other hand, the torsion-inversion-vibration coupling in the charged species  $\text{CH}_3\text{OH}_2^+$  is much weaker. Ongoing work is directed at determining the extent to which the SAV-LAV coupling is transferable between molecular systems.

Methylamine is our experimental prototype for these six-well  $G_{12}$  systems. Results to date include high-resolution slit-jet spectra of the  $\nu_{11}$  asymmetric CH stretch (2965-3005  $\text{cm}^{-1}$ ) [6] and the first FTMW-IR spectra in the  $\nu_3$  symmetric CH stretch region. Whereas there is a single multiply perturbed vibrational band in the  $\nu_{11}$  region, four distinct vibrational bands appear in the  $\nu_3$  region. The extra bands in the  $\nu_3$  region likely result, as in methanol [3,4], from interactions with bending combinations that serve as “doorway” states for intramolecular vibrational redistribution (IVR). The torsion and inversion tunneling patterns involve four distinct symmetry species in the  $G_{12}$  group. Our high-resolution spectra for  $\nu_{11}$  yield a pattern ( $E_2 < A < B < E_1$ ) qualitatively different from the allowed range of patterns for the ground state. The observed  $\nu_{11}$  tunneling patterns result from the combination of accidental perturbations and systematic effects attributable to torsion-inversion-vibration coupling.

To investigate the tunneling patterns attributable to systematic torsion-inversion-vibration coupling, we have developed two different models (Fig. 2). The present models incorporate torsion-inversion tunneling parameters  $h_{2v}$  and  $h_{3v}$ , respectively and a number of low-order terms couplings to the CH-stretch vibrations. Of the three methyl CH stretch vibrations, Model I includes only the two asymmetric stretches that correlate to the E-type degenerate CH stretch in a symmetric rotor; Model II includes all three. The models yield the torsion-inversion tunneling patterns of the four symmetry species, A, B,  $E_1$  and  $E_2$ , in the CH-stretch excited states (Fig. 2). The principal results are as follows. (i) Both models and each of the coupling terms considered yield the same tunneling patterns, which are different in the asymmetric CH stretch excited states as compared to those in the ground state. (ii) In Model I, the magnitude of the tunneling splittings in the two asymmetric CH stretch excited states is exactly half of that in the ground state. (iii) In Model II, the relative magnitude of

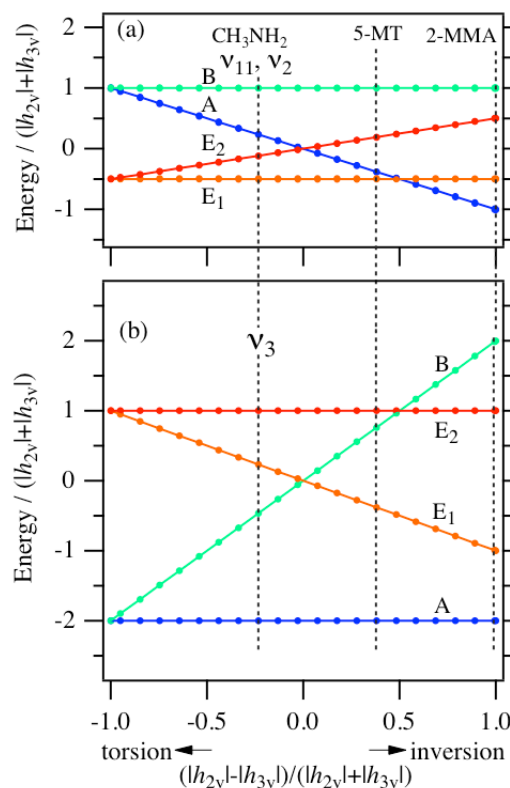


Fig. 2. The range of possible torsion-inversion tunneling patterns according to Model I (lines) and Model II (points).

these splittings depends on the ratio  $|\mu|/(|h_{2v}| + |h_{3v}|)$  where  $\mu$  is the torsion-inversion-vibration coupling parameter. This ratio varies from 3 to 308 across the series methanol, methylamine, 2-methylmalonaldehyde and 5-methyltropolone, with a consequent variation in the magnitude of the tunneling splittings.

### B. Six-Fold Internal Rotation

As slightly oblate asymmetric top molecule ( $\kappa = 0.25$ ) with both a free internal rotor and a methyl group,  $\text{CH}_3\text{NO}_2$  is a benchmark system for studies of torsional motion in a 6-fold potential and of the coupling between a large amplitude vibration and other small-amplitude vibrations. Like the molecules in the sections above,  $\text{CH}_3\text{NO}_2$  has six equivalent minima and  $G_{12}$  symmetry, but the heavy atoms are coplanar in the equilibrium geometry. The result is a 6-fold internal rotation potential with a very low barrier ( $2 \text{ cm}^{-1}$ ). Rotationally resolved infrared spectra of  $\text{CH}_3\text{NO}_2$  have been recorded using far-infrared beamline at Canadian Light Source on a high resolution Bruker IFS 125HR spectrometer. The observed infrared spectra, in the range  $550\text{-}1000 \text{ cm}^{-1}$ , are recorded at a nominal resolution of  $0.00096 \text{ cm}^{-1}$ . Two  $a$ -type bands, centered at  $657.08 \text{ cm}^{-1}$  for NO symmetric bend and at  $917.99 \text{ cm}^{-1}$  for CN-stretch, have been measured. The analysis of these vibrational bands is currently underway.

### C. Rotational Dependence of the Intramolecular Dynamics in Acetylene

Acetylene high-resolution infrared spectra ( $17,625$  lines) have been analyzed and fit with precision up to  $8900 \text{ cm}^{-1}$  including high rotational levels [Amyay, B.; Herman, M.; Fayt, A.; Campargue, A.; Kass, S. *J. Mol. Spectrosc.* 2011, 267, 80]. As part of this collaboration, the Herman group has extended the fit (882 additional lines) up to  $13,000 \text{ cm}^{-1}$ . The resulting spectroscopic Hamiltonian in the normal mode basis contains 155 off-diagonal terms representing four different coupling types (Fig. 3): (i) anharmonic, including Darling-Dennison (DD),

(ii) vibrational  $l$ -resonance, (iii) rotational  $l$ -resonance, and (iv) Coriolis [1, 5]. All of these couplings conserve the polyad quantum number,  $N_r \equiv 5v_1 + 3v_2 + 5v_3 + v_4 + v_5$ , and the  $ef$  and  $g/u$  symmetries. Only the Coriolis coupling mixes states with different numbers of stretching quanta,  $N_s \equiv v_1 + v_2 + v_3$ .

This detailed Hamiltonian provides an unprecedented opportunity to study the vibration-rotation dynamics up into the energy range above the onset of new kinds of vibrational motion, such as the local CH stretch, the local bender, and the counter rotator [work in this program by the Kellman and Field groups]. By computing time-dependent wavefunctions following different kinds of coherent excitations, we find hierarchies of sequentially coupled states that are populated on timescales ranging from 20 fs to 20 ps. The dynamics are strongly

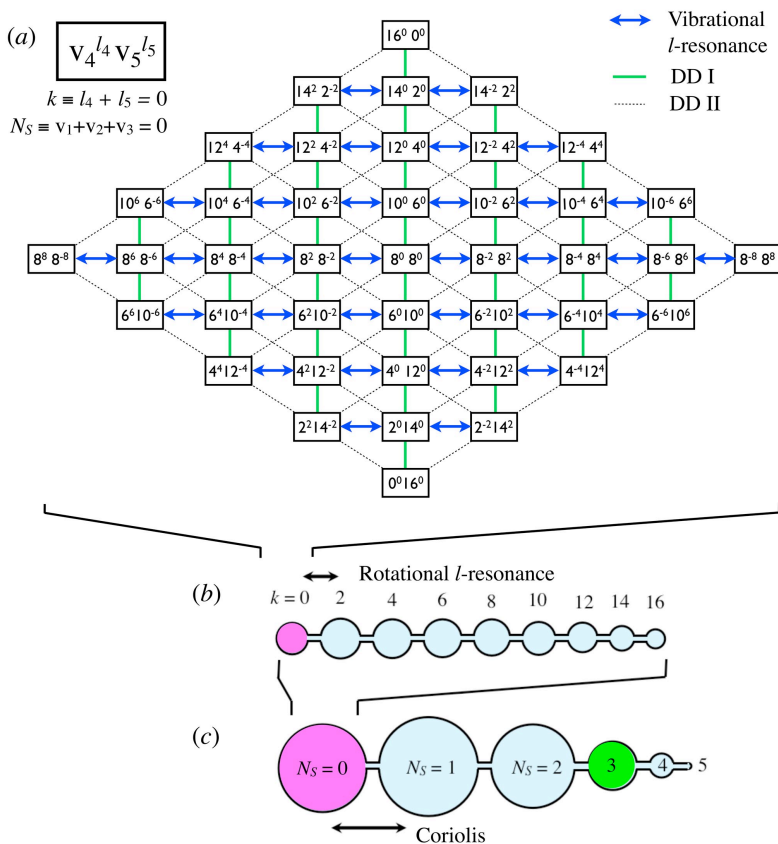


Fig. 3. A schematic representation of the hierarchical coupling pathways in the acetylene  $\{N_r=16, e g\}$  polyad.

mode-dependent with interior states relaxing faster than edge states, and the local bender relaxing faster than the counter-rotator. The highest polyad investigated,  $\{N_r = 18, e, g\}$  includes more than 1,400 coupled states. The time-dependent volume of phase space explored is measured both by the participation number and by the Shannon entropy. Since the Coriolis coupling is relatively weak, there are bottlenecks (Fig. 3) that result in slower and less complete exploration of parts of phase space that have different total vibrational angular momenta ( $k$ ) and different numbers of stretching quanta ( $N_s$ ).

### III. Future Work

The computational work on the  $\text{CH}_3\text{XH}_2$  systems will be directed at determining the similarities and differences in the SAV-LAV coupling across the range of  $G_{12}$  systems and at understanding how these coupling impact the LAV level structure in the excited states of SAV's. Additional  $\text{CH}_3\text{NO}_2$  spectra will be recorded and the analysis of those spectra will continue. The work on vibration-rotation dynamics of acetylene will be directed at understanding phase space exploration and its impact on experiments such as the chirped-pulse mm-wave-detected photodissociation work in the Field group.

### IV. Publications supported by this project, 2010-2013

- [1] David Perry, Anthony Miller, B. Amyay, A. Fayt and M. Herman, Vibration-rotation alchemy in acetylene ( $^{12}\text{C}_2\text{H}_2$ ),  $X^1\Sigma_g^+$  at low vibrational excitation: From high resolution spectroscopy to fast intramolecular dynamics (invited article), *Mol. Phys.* **108**, 1115-1132, 2010, <http://dx.doi.org/10.1080/00268971003660874>.
- [2] Sylvestre Twagirayezu, David S. Perry, Justin L Neill and Matt T Muckle, Coherence-converted population transfer FTMW-IR double resonance spectroscopy of  $\text{CH}_3\text{OD}$  in the OD -stretch region, *J. Mol. Spectrosc.* **262**, 65-68 (2010), <http://dx.doi.org/10.1016/j.jms.2010.05.003>.
- [3] Sylvestre Twagirayezu, Trocia N. Clasp, David S. Perry, Justin L. Neill, Matt T. Muckle, Brooks H. Pate, Vibrational coupling pathways in methanol as revealed by coherence-converted population transfer FTMW-IR double resonance spectroscopy, *J. Phys. Chem. A* **114**, 6818-6828 (2010), <http://dx.doi.org/10.1021/jp1019735>.
- [4] Sylvestre Twagirayezu, Xiaoliang Wang, David S. Perry, Justin L. Neill, Matt T. Muckle, Brooks H. Pate, Li-Hong Xu, IR and FTMW-IR Spectroscopy and Vibrational Relaxation Pathways in the CH Stretch Region of  $\text{CH}_3\text{OH}$  and  $\text{CH}_3\text{OD}$ , *J. Phys. Chem. A* **115**, 9748-9763 (2011), <http://dx.doi.org/10.1021/jp202020u>.
- [5] David S. Perry, Jonathan Martens, Badr Amyay, and Michel Herman, Hierarchies of Intramolecular Vibration-Rotation Dynamical Processes in Acetylene up to  $13,000\text{ cm}^{-1}$ , *Mol. Phys.* **110**, 2687-2705 (2012), <http://dx.doi.org/10.1080/00268976.2012.711493>.
- [6] Mahesh B Dawadi, C. Michael Lindsay, Andrei Chirokolava, David S. Perry and Li-Hong Xu, Novel patterns of torsion-inversion-rotation energy levels in the  $\nu_{11}$  asymmetric CH-stretch spectrum of methylamine, *J. Chem. Phys.* **138**, XXXX (2013), in press, <http://dx.doi.org/10.1063/1.4794157>.

# New Single- and Multi-Reference Coupled-Cluster Methods for High Accuracy Calculations of Ground and Excited States

Piotr Piecuch

Department of Chemistry, Michigan State University, East Lansing, MI 48824

piecuch@chemistry.msu.edu

## I. Program Scope

This project focuses on the development and applications of new generations of *ab initio* electronic structure methods and computer codes, exploiting the coupled-cluster (CC) wave function ansatz, which can provide an accurate description of chemical reaction pathways and potential energy surfaces (PESs), radicals, biradicals, and other open-shell species, properties other than energy, and molecular electronic excitations. The goal is to design and apply affordable computational approaches that enable precise modeling of molecular systems relevant to combustion, catalysis, and photochemistry. Among the most successful methods developed in this program to date are (i) the completely renormalized (CR) CC and equation-of-motion CC (EOMCC) approaches, (ii) the local correlation, low-order scaling extensions of the conventional and CR CC methods to larger systems involving hundreds of correlated electrons, (iii) the active-space CC/EOMCC approaches, and (iv) the genuine multi-reference CC (MRCC) theories. The focus is on methods that are predictive and systematically improvable, and methods that offer high accuracy, ease of use, and relatively low computer costs compared to other approaches that aim at similar accuracies, so that one can apply them to complex molecular problems with dozens or hundreds of non-hydrogen atoms, in addition to smaller systems. The CR-CC methods and their open-shell, local correlation, and excited-state generalizations extend the conventional single-reference theories to multi-reference situations created by radicals, biradicals, bond breaking, and two-electron excitations with an ease of a black-box calculation that can be performed by non-experts. The active-space CC and EOMCC approaches, and their open-shell generalizations via the electron attached (EA) and ionized (IP) theories as well as the genuine MRCC methods have the flexibility that enables high-accuracy *ab initio* calculations for a wide variety of closed- and open-shell electronic states, with manageable computer costs, including challenging systems characterized by strong electronic quasi-degeneracies that cannot be handled by single-reference approaches. All methods pursued in this program can utilize modern multi-node, multi-core computer architectures and are well suited for automated and parallel implementations. They address two main challenges of electronic structure theory, which are (i) the development of practical and systematically improvable computational schemes that can provide an accurate description of closed-shell, open-shell, and strongly correlated complex systems, and the rapidly changing electron correlation effects along reaction coordinates and in electronic excitations, and (ii) the development of algorithms that can reduce prohibitive costs of traditional high-accuracy *ab initio* calculations by orders of magnitude by directly attacking the intrinsic scaling laws that define the dependence of computer costs on the system size. Methods developed in this project are shared with the community through the GAMESS package. Some of them have also been incorporated in NWChem.

## II. Recent Progress (1/1/2010 – 3/6/2013)

We introduced the generalization of the previously developed biorthogonal method of moments of CC equations, which in the past had resulted in the left-eigenstate CR-CC and CR-EOMCC approaches, such as CR-CC(2,3) and CR-EOMCC(2,3) [4,6,8,11,17], that enables one to correct the CC/EOMCC energies obtained with the arbitrary, conventional as well as unconventional, truncations in the cluster operator  $T$  and the EOM excitation operator  $R_{\mu}$  for the missing many-electron correlation effects of interest [11,12,15]. The resulting moment energy expansions, defining the  $CC(P;Q)$  formalism [11,12,15], enable one to contemplate a variety of novel *ab initio* schemes for practical, systematically improvable, high accuracy calculations of ground- and excited-state PESs. Among them is the  $CC(t;3)$ ,  $CC(t,q;3)$ ,  $CC(t,q;3,4)$ , etc. hierarchy, in which energies obtained in the active-space CC/EOMCC calculations [5], such as CCSDt/EOMCCSDt or CCSDtq/EOMCCSDtq, which recover much of the non-dynamical and some dynamical electron correlation effects, are corrected for the higher-order, primarily dynamical, correlations, such as triples (3) or triples and quadruples (3,4) missing in the active-space

CC/EOMCC considerations, using the non-iterative corrections which are operationally similar to those of CR-CC/CR-EOMCC [11,12,15]. The potential advantages of the  $CC(P;Q)$  formalism were illustrated by the numerical tests of the new  $CC(t;3)$  scheme, in which one corrects the results of the CC calculations with singles, doubles, and active-space triples, termed CCSDt, for the remaining effects due to connected triple excitations missing in CCSDt [11,12,15]. By examining bond breaking in the HF,  $F_2$ , and  $F_2^+$  molecules [11,12], the challenging multi-reference problems of the automerization of cyclobutadiene and isomerization of bicyclo[1.1.0]butane to trans-but-1,3-diene involving strongly biradical transition states [12], and the similarly challenging singlet-triplet gaps in the methylene, (HFH) $^\cdot$ , and trimethylenemethane (TMM) biradicals [15], we showed that  $CC(t;3)$  greatly improves the CCSD(T), CCSD(2) $_T$ ,  $\Lambda$ -CCSD(T), CR-CC(2,3), CCSDt, and CCSD(T)-h results, providing PESs that agree with those obtained with full CCSDT to within, typically,  $\sim 0.1$  millihartree for total energies and  $\sim 0.1$  kcal/mol for relative energies at the small fraction of the computer costs of the CCSDT calculations, which are competitive with the sophisticated MRCC and Quantum Monte Carlo (QMC) computations.

We implemented the size-intensive modification of the previously developed (see [11,17] for reviews) CR-EOMCC(2,3) approach, termed  $\delta$ -CR-EOMCC(2,3) [6,8], which corrects the EOMCCSD energies for triple excitations using the non-iterative  $N^7$  steps similar to CCSD(T) or CR-CC(2,3), offering great improvements in the EOMCCSD results. The  $\delta$ -CR-EOMCC(2,3) codes, along with the extension of the EOMCCSD routines to open shells, were incorporated in GAMESS as additions to a variety of the CC/EOMCC options that we developed for GAMESS in the past. In our continuing effort to examine the CR-CC and CR-EOMCC methodologies, we showed that the CR-CC(2,3) and CR-EOMCC(2,3) approaches provide excellent results for the low-lying singlet and triplet states of biradical species, such as methylene, where the CR-CC(2,3)/CR-EOMCC(2,3) results for the adiabatic excitation and total energies extrapolated to the complete basis set limit, including states dominated by two-electron transitions, are in perfect agreement with the converged QMC and the available experimental data, eliminating, in particular, large errors in the CCSD/EOMCCSD results [4]. We used the  $\delta$ -CR-EOMCC(2,3) method to examine shifts in the  $\pi \rightarrow \pi^*$  excitation energy in cis-7-hydroxyquinoline (cis-7HQ) induced by hydrogen bonding, on the order of  $500\text{-}2000\text{ cm}^{-1}$ , along with the corresponding excitation energies, on the order of  $30,000\text{ cm}^{-1}$ , obtained in the frozen-density embedding theory (FDET) and supermolecular time-dependent density functional theory (TDDFT) calculations, and in experiment [6,8]. By considering eight complexes of cis-7HQ with up to three hydrogen-bonded molecules, including water, ammonia, methanol, formic acid, and their combinations, we demonstrated that the spectral shifts resulting from the FDET and  $\delta$ -CR-EOMCC(2,3) calculations are in excellent agreement with one another and experiment (to within  $100\text{ cm}^{-1}$  or 15 % on average), whereas the analogous shifts obtained in the supermolecular TDDFT calculations do not agree with the  $\delta$ -CR-EOMCC(2,3) data, producing large errors (39% on average). The  $\delta$ -CR-EOMCC(2,3) excitation energies match the experimental ones to within  $\sim 500\text{ cm}^{-1}$  in each case examined, as compared to  $4,000\text{-}5,000\text{ cm}^{-1}$  errors in the EOMCCSD calculations. We continued applying the CR-CC/CR-EOMCC methods to important chemical problems, including accurate modeling of JP-10 (*exo*-tetrahydrodicyclopentadiene) high temperature oxidation [10], and incorporated CR-CC(2,3) into a correlation consistent composite approach (ccCA) for thermodynamic properties and reaction paths [13]. We demonstrated that the resulting ccCA-CC(2,3) method, interfaced with GAMESS, produces a mean absolute deviation of 1.7 kcal/mol for predicted heats of formation at 298 K, based on calibration with the G2/97 set of 148 molecules, while improving the performance of the CCSD(T)-based ccCA approaches in calculations involving more demanding radicals and biradicals [13]. We also used the EOMCC methodology, along with the multi-reference perturbation theory and TD-DFT approaches, to provide insights into the low-lying excitations in methylcobalamin, showing that its  $S_1$  state is a metal-to-ligand charge transfer transition, in agreement with transient absorption spectroscopy measurements [16]. We used the  $\delta$ -CR-EOMCC(2,3) approach to reveal the existence of the previously unknown doubly excited state of azulene, located below the ionization threshold, which can mediate the 1+2' multi-photon ionization that leads to a Rydberg fingerprint [18], explaining why the Rydberg fingerprints observed in the 1+2' photo-electron spectrum of

azulene do not change with the wavelength of the pump laser or the pump-probe delay time [18]. This doubly excited state of azulene would not be discovered if we relied on the conventional EOMCC approaches, such as EOMCCSD, and did not use our  $\delta$ -CR-EOMCC(2,3) approach.

We continued our work on extending the active-space CC and EOMCC theories, reviewed in [5], to ground and excited states of radicals and other valence systems by combining them with the EA/IP EOMCC methodology [5,7,9]. We demonstrated an excellent performance, in terms of accuracy and computational efficiency, of the active-space EA-EOMCCSD(3p2h) and IP-EOMCCSD(3h2p) approaches in calculations of the excitation energies in CNC, C<sub>2</sub>N, N<sub>3</sub>, and NCO, where some of the low-lying excited states have a significant multi-reference character, particularly in CNC and C<sub>2</sub>N, causing problems to EOMCCSD and EA-EOMCCSD(2p1h). We showed that the active-space EA/IP EOMCC schemes, which use small subsets of higher-than-2p1h and 2h1p excitations, reproduce the results of their parent methods, while requiring a computational effort similar to CCSD. This applies to excitation energies and ground- and excited-state geometries [7]. We completed our work on incorporating the EA-EOMCCSD(2p1h), IP-EOMCCSD(2h1p), and full and active-space EA-EOMCCSD(3p2h) and IP-EOMCCSD(3h2p) codes into the official GAMESS distribution. This allowed us to perform the scalar relativistic IP- and EA-EOMCC calculations with up to 3h2p and 3p2h excitations, using the spin-free part of the second-order Douglass-Kroll-Hess (DKH2) Hamiltonian, along with the corresponding SAC-CI calculations, for the valence excitation spectra of the CuCl<sub>4</sub><sup>2-</sup> and CuBr<sub>4</sub><sup>2-</sup> complexes [9]. We demonstrated that the DKH2-based IP-EOMCC and SAC-CI methods reproduce the observed UV-vis photoabsorption spectra of CuCl<sub>4</sub><sup>2-</sup> and CuBr<sub>4</sub><sup>2-</sup> in both peak positions and intensities, allowing us to provide a rigorous assignment of the observed strong bands and weaker shoulder transitions, and showing that relativity affects excitation energies and geometries. We also developed initial versions of the doubly electron-attached (DEA) and doubly ionized (DIP) EOMCC methods with up to 4p2h and 4h2p excitations, and their practical active-space variants, which provide a highly accurate and spin-adapted description of multi-reference systems having two electrons outside the closed-shell core, such as biradicals [19]. By examining bond breaking in F<sub>2</sub> and low-lying singlet and triplet states in the methylene, (HFH)<sup>-</sup>, and TMM biradicals, we demonstrated that the DEA- and DIP-EOMCC methods with an active-space treatment of 4p2h and 4h2p excitations reproduce the results of the analogous full calculations, which themselves are nearly exact in the above cases, at the small fraction of the computer effort, while improving the existing DEA/DIP-EOMCC theories truncated at 3p1h/3h1p excitations [19].

We continued developing the local correlation CC approaches, and their multi-level extensions, called ‘cluster-in-molecule’ (CIM) methods [1-3,14]. The resulting CIM-CCSD, CIM-CCSD(T), and CIM-CR-CC(2,3) schemes, and their CIM-MP<sub>n</sub> analogs use orthonormal localized orbitals and enable high-accuracy calculations for systems with hundreds of correlated electrons. Our CIM-CC and CIM-MP2 codes, which we incorporated in GAMESS (the official release in the near future), are characterized by the linear scaling of the CPU time with the system size when a single-level CIM-CC or CIM-MP2 approach is used, memory requirements that do not grow with the system size, coarse-grain parallelism, which can be further enhanced by the fine-grain parallelism of each CIM subsystem calculation, and the purely non-iterative character of the local triples and other perturbative energy corrections. They enable one to combine affordable canonical calculations, such as MP2 or CCSD, with a local CIM approach to handle higher-order correlation effects, such as the triples corrections of CR-CC(2,3) [14]. Another possibility is represented by the purely local multi-level theories exploiting the CIM framework that combine high-level CC methods, such as CR-CC(2,3), to treat the reactive part of the large molecular system with the lower-order (e.g., MP2) scheme(s) to handle the chemically inactive regions without splitting it into *ad hoc* fragments and saturating dangling bonds [1]. We applied CIM-CR-CC(2,3), combined with the embedded cluster SIMOMM model, to the etching and diffusion of atomic oxygen on the Si(100) surface, obtaining precise information about the activation barriers and energetics characterizing these processes [3]. The multi-level CIM-CC/MP2 results for bond breaking in large alkanes and the reactions between the bis(2,4,4-trimethylpentyl)dithiophosphinic acid and water or water dimer are outstanding [1]. We also performed the unprecedented calculations for the Co-methyl bond dissociation in methylcobalamin [14]. Local CIM-CR-CC(2,3) combined with canonical CCSD allowed

us to produce the entire Co-methyl bond breaking curve and the dissociation energy in the 37-38 kcal/mol range. Experiment gives  $37\pm 3$  or  $36\pm 4$  kcal/mol, and DFT all kinds of values between -2 and 41 kcal/mol. Thanks to the availability of the CR-CC(2,3)-level results, obtained with the help of CIM, we were able to provide recommendations regarding the proper way of performing DFT calculations for cobalamins and information about suitable choices of active orbitals for multi-reference calculations [14]. We developed the improved CIM orbital subsystem design, which is particularly relevant for large weakly bound molecular clusters, while helping the description of covalently bound systems [2].

### III. Immediate Future Plans (2013/2014)

We will work on the hybrid CC and EOMCC schemes based on the CC( $P;Q$ ) formalism, with a focus on extensions to quadruple excitations and excited states, and the active-space DEA- and DIP-EOMCC methods. We also plan new studies of radical and biradical reactions, and molecular electronic spectra.

### IV. Publications and submitted journal articles supported by this project (1/1/2010 – 3/6/2013)

1. W. Li and P. Piecuch, "Multi-level Extension of the Cluster-in-Molecule Local Correlation Methodology: Merging Coupled-Cluster and Møller-Plesset Perturbation Theories," *J. Phys. Chem. A* **114**, 6721-6727 (2010).
2. W. Li and P. Piecuch, "Improved Design of Orbital Domains within the Cluster-in-Molecule Local Correlation Framework: Single-Environment Cluster-in-Molecule Ansatz and its Application to Local Coupled-Cluster Approach with Singles and Doubles," *J. Phys. Chem. A* **114**, 8644-8657 (2010).
3. P. Arora, W. Li, P. Piecuch, J.W. Evans, M. Albao, and M.S. Gordon, "Diffusion of Atomic Oxygen on the Si(100) Surface," *J. Phys. Chem. C* **114**, 12649-12658 (2010).
4. J.R. Gour, P. Piecuch, and M. Włoch, "Comparison of the Completely Renormalized Equation-of-Motion Coupled-Cluster and Quantum Monte Carlo Results for the Low-Lying Electronic States of Methylene," *Mol. Phys.* **108**, 2633-2646 (2010).
5. P. Piecuch, "Active-space coupled-cluster methods," *Mol. Phys.* **108**, 2987-3015 (2010).
6. G. Fradelos, J.J. Lutz, T.A. Wesolowski, P. Piecuch, and M. Włoch, "Embedding vs Supermolecular Strategies in Evaluating the Hydrogen-Bonding-Induced Shifts of Excitation Energies," *J. Chem. Theory Comput.* **7**, 1647-1666 (2011).
7. J.A. Hansen, P. Piecuch, J.J. Lutz, and J.R. Gour, "Geometries and Adiabatic Excitation Energies of the Low-Lying Valence States of CNC, C<sub>2</sub>N, N<sub>3</sub>, and NCO Studied with the Electron-Attached and Ionized Equation-of-Motion Coupled-Cluster Methodologies," *Phys. Scr.* **84**, 028110 (2011) (17 pp).
8. G. Fradelos, J.J. Lutz, T.A. Wesolowski, P. Piecuch, and M. Włoch, "Shifts in Excitation Energies Induced by Hydrogen Bonding: A Comparison of the Embedding and Supermolecular Time-Dependent Density Functional Theory Calculations with the Equation-of-Motion Coupled-Cluster Results," *Prog. Theor. Chem. Phys.* **22**, 219-248 (2012).
9. M. Ehara, P. Piecuch, J.J. Lutz, and J.R. Gour, "Symmetry-Adapted-Cluster Configuration-Interaction and Equation-of-Motion Coupled-Cluster Studies of Electronically Excited States of Copper Tetrachloride and Copper Tetrabromide Dianions," *Chem. Phys.* **399**, 94-110 (2012).
10. G.R. Magoon, J. Aguilera-Iparraguirre, W.H. Green, J.J. Lutz, P. Piecuch, O.O. Oluwole, and H.-W. Wong, "Detailed Chemical Modeling of JP-10 (*exo*-tetrahydrodicyclopentadiene) High Temperature Oxidation: Exploring the Role of Biradical Species in Initial Decomposition Steps," *Int. J. Chem. Kin.* **44**, 179-193 (2012).
11. J. Shen and P. Piecuch, "Biorthogonal Moment Expansions in Coupled-Cluster Theory: Review of Key Concepts and Merging the Renormalized and Active-Space Coupled-Cluster Methods," *Chem. Phys.* **401**, 180-202 (2012).
12. J. Shen and P. Piecuch, "Combining Active-Space Coupled-Cluster Methods with Moment Energy Corrections via the CC( $P;Q$ ) Methodology, with Benchmark Calculations for Biradical Transition States," *J. Chem. Phys.* **136**, 144104-1 - 144104-16 (2012).
13. S.A. Nedd, N.J. De Yonker, A.K. Wilson, P. Piecuch, and M.S. Gordon, "Incorporating a Completely Renormalized Coupled Cluster Approach into a Composite Method for Thermodynamic Properties and Reaction Paths," *J. Chem. Phys.* **136**, 144109-1 - 144109-13 (2012).
14. P.M. Kozłowski, M. Kumar, P. Piecuch, W. Li, N.P. Bauman, J.A. Hansen, P. Lodowski, and M. Jaworska, "The Cobalt-Methyl Bond Dissociation in Methylcobalamin: New Benchmark Analysis Based on Density Functional Theory and Completely Renormalized Coupled-Cluster Calculations," *J. Chem. Theory Comput.* **8**, 1870-1894 (2012).
15. J. Shen and P. Piecuch, "Merging Active-Space and Renormalized Coupled-Cluster Methods via the CC( $P;Q$ ) Formalism, with Benchmark Calculations for Singlet-Triplet Gaps in Biradical Systems," *J. Chem. Theory Comput.* **8**, 4968-4988 (2012).
16. K. Kornobis, N. Kumar, P. Lodowski, M. Jaworska, P. Piecuch, J.J. Lutz, B.M. Wong, and P.M. Kozłowski, "Electronic Structure of the S<sub>1</sub> State in Methylcobalamin: Insight from CASSCF/MC-XQDPT2, EOM-CCSD, and TD-DFT Calculations," *J. Comp. Chem.*, in press; published online: 19 Jan. 2013; doi: 10.1002/jcc.23204.
17. P. Piecuch, M. Włoch, J.R. Gour, W. Li, and J.J. Lutz, "Dealing with Chemical Reaction Pathways and Electronic Excitations in Molecular Systems via Renormalized and Active-Space Coupled-Cluster Methods," in: AIP Conference Proceedings, Vol. XXX, edited by T.E. Simos and G. Maroulis (American Institute of Physics, Melville, NY, 201X), in press.
18. P. Piecuch, J.A. Hansen, D. Staedter, S. Faure, and V. Blanchet, "The Existence of the Doubly Excited State that Mediates the Photoionization of Azulene," *Phys. Rev. Lett.*, submitted.
19. J. Shen and P. Piecuch, "Doubly Electron-Attached and Doubly Ionized Equation-of-Motion Coupled-Cluster Methods with 4-particle–2-hole and 4-hole–2-particle Excitations and their Active-Space Extensions," *J. Chem. Phys.*, submitted.

# Kinetic Modeling of Combustion Chemistry

W.J. Pitz and C. K. Westbrook  
Physical and Life Sciences Directorate  
Lawrence Livermore National Laboratory  
Livermore, CA 94550  
pitz1@llnl.gov

## I. Program Scope

We develop chemical kinetic reaction mechanisms to describe the combustion of hydrocarbons and biofuels. These mechanisms are validated through comparisons between computations and experiments in carefully-controlled laboratory-scale facilities including laminar flames, shock tubes, stirred reactors and rapid compression machines, and then are used to understand more complex combustion phenomena in practical engines and other combustion systems. Chemical systems and fuels are chosen for analysis because they represent practical fuels used in transportation and other energy devices. We strive to identify key reactions that need further study by DOE BES researchers. We do attempt to anticipate kinetic modeling needs of the DOE combustion community, so other researchers can have useful reaction mechanisms to use in their programs. Our resulting kinetic mechanisms are routinely available on the LLNL web page at [https://www-pls.llnl.gov/?url=science\\_and\\_technology-chemistry-combustion](https://www-pls.llnl.gov/?url=science_and_technology-chemistry-combustion) and provide a valuable service to the combustion community.

## II. Recent Progress

### A. Low temperature chemistry of n-heptane and its mixtures with n-butanol

The next generation of internal combustion engines relies critically on the use of low temperature combustion. The ability to accurately predict low temperature chemistry is needed to simulate combustion in these engines. Responding to this challenge, we have been improving the accuracy of low temperature models by including more fundamentally-based rate constants and product channels using recent theoretical values<sup>1,2</sup>. Additionally, the necessity to improve our low temperature mechanisms was also highlighted by recent rapid compression facility experiments by Wooldridge and coworkers on n-heptane/n-butanol mixtures<sup>3</sup>. We found that our n-heptane/n-butanol mechanism overpredicted the amount of heptenes sampled from their rapid compression facility during the ignition of these mixtures. This issue was resolved by adopting more fundamentally-based rate constants for the heptyl + O<sub>2</sub> system<sup>1,2</sup> than present in our previous n-heptane mechanism.

### B. Modeling of low pressure methyl cyclohexane flames

Methyl cyclohexane (MCH) is the simplest alkyl cyclohexane, and is a component used to represent alkyl cyclohexanes in gasoline and jet fuels. It is important to be able to accurately predict the chemical behavior of MCH. Skeen and Hansen et al.<sup>4</sup> found that literature MCH chemical kinetic mechanisms were unable to satisfactorily predict many of the intermediate species measured in their low-pressure flames. Consequently, we have made improvements to our MCH model, including updated submodels for C1-C4, aromatics and cyclohexane. Also, other updates were made. The rate constants for abstraction reactions from MCH were improved using recent experimentally measured values from ANL<sup>5</sup>. The previous 2007 MCH model lumped many of unsaturated ring products of MCH that lead to soot precursors. This led to an inadequate description of many of the unsaturated cyclic products in low pressure MCH flames<sup>4</sup>. These lumped species have been replaced by including all relevant isomers and their associated reactions. The greater fidelity in the treatment of the unsaturated cyclic species leads to much better agreement with the measured intermediates in the low-pressure MCH flames (e.g. Fig. 1).

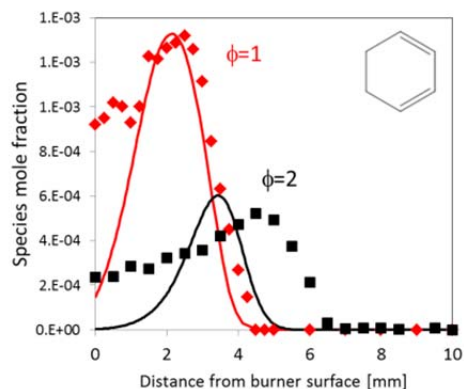


Figure 1: Experimental measurements (symbols)<sup>4</sup> and predictions (curves) for 1,3-cyclohexadiene using an updated MCH mechanism.

### C. Reactions involving addition of OH to alkenes

The low temperature chemistry of alkenes has a key feature not found in alkanes that needs to be properly treated: the addition of radicals to double bonds. In collaboration KAUST, Saudi Arabia, we systematically investigated the potential energy surfaces for the addition reaction of OH to the double bond of all the acyclic isomers of C<sub>5</sub>H<sub>10</sub>, followed by O<sub>2</sub> addition and internal H

transfers. These reactions include the Waddington mechanism that causes the overall reactivity of alkenes to be different than that of alkanes. Using different theories and methods (e.g. B3LYP, CBSQB3, G3 and G4), important reaction pathways resulting from the addition of OH to different alkene molecular structures were calculated. These results will be used to develop reaction rate rules needed to build detailed kinetic mechanisms for fuel components containing alkene moieties relevant to conventional and bio-derived fuels.

### D. New mechanism for aromatics and alkyl-benzenes

Aromatics and alkyl-aromatics are an important chemical class in gasoline, jet and diesel fuels. When present in real fuels, they play a key role in controlling ignition behavior in internal combustion engines. In collaboration with National University of Ireland, Galway (NUIG), a new detailed chemical kinetic mechanism for aromatics and alkyl-benzenes was developed and validated by comparison of predicted results to ignition measurements from shock tubes and rapid compression machines. This validated mechanism is able to predict the oxidation of cyclopentadiene, benzene, toluene, n-propyl benzene, and n-butyl benzene over a wide range of temperature, pressure and equivalence ratios.

### E. New mechanism for syngas (CO/H<sub>2</sub>) mixtures

Syngas (hydrogen and carbon monoxide) is an attractive fuel that can be derived from biomass. In an effort led by NUIG, we have collaborated in the development of a new mechanism for hydrogen and carbon monoxide (syngas)<sup>6</sup>. This updated mechanism simulates a wide variety of experimental targets including fundamental combustion experiments in flames, shock tubes, stirred reactors, and flow reactors. The mechanism was validated over a wide range of pressure, temperature, and equivalence ratio, and for a variety of diluents.

### F. New mechanism for n-pentanol

In collaboration with NUIG and KAUST, we assisted in the development and validation of a new chemical kinetic mechanism for n-pentanol, a potential biofuel<sup>7</sup>. The new chemical kinetic mechanism was based on our previously developed mechanism for n-butanol<sup>8</sup>. The mechanism was validated by comparing computed results to experimental results from fundamental experiments in a shock tube, rapid compression machine, jet stirred reactor and laminar flame. Although n-butanol shows little low temperature reactivity, n-pentanol was found to exhibit a negative temperature coefficient regime. This was attributed to the fact that n-pentanol has an additional CH<sub>2</sub> group in its carbon chain that enables facile RO<sub>2</sub> isomerizations involving a six-membered transition states that lead to chain branching, a feature that is lacking in n-butanol.

### G. Uncertainty quantification of the use of reaction rate rules in a mechanism

For large chemical kinetic mechanisms, the use of reaction rate rules for different reaction classes is necessary because all the needed reaction rate constants have not been measured or computed. We

collaborated with Jens Prager and Habib Najm on uncertainty quantification of the use of reaction rate rules in a reaction mechanism<sup>9</sup>. As a test case, the high-pressure ignition of a mixture of propane, ethane and air was used. In this example, it was found that the use of reaction rate rules can have a significant impact on the magnitude of the uncertainty in the computed ignition delay time.

### Future Work

We will continue to incorporate into our mechanisms more accurate reaction rate constants and product paths becoming available from fundamental theoretical and experimental studies. These changes will be validated by comparing predictions from the updated mechanisms with fundamental combustion data from shock tubes, laminar flames, rapid compression machines, stirred reactors and flow reactors.

Acknowledgements: This work was performed under the auspices of the U.S. Department of Energy by Lawrence Livermore National Laboratory under Contract DE-AC52-07NA27344.

### III. References

- (1) Villano, S. M.; Huynh, L. K.; Carstensen, H.-H.; Dean, A. M. *The Journal of Physical Chemistry A* 2012, 116, 5068.
- (2) Villano, S. M.; Huynh, L. K.; Carstensen, H.-H.; Dean, A. M. *The Journal of Physical Chemistry A* 2011, 115, 13425.
- (3) Karwat, D. M. A.; Wagnon, S. W.; Wooldridge, M. S.; Westbrook, C. K. *J. Phys. Chem. A* 2012, 116, 12406.
- (4) Skeen, S. A.; Yang, B.; Jasper, A. W.; Pitz, W. J.; Hansen, N. *Energy & Fuels* 2011, 25, 5611.
- (5) Sivaramakrishnan, R.; Michael, J. V. *Combust. Flame* 2009, 156, 1126.
- (6) Keromnes, A.; Metcalfe, W. K.; Heufer, K. A.; Donohoe, N.; Das, A. K.; Sung, C. J.; Herzler, J.; Naumann, C.; Griebeld, P.; O. Mathieue; Krejci, M. C.; Petersen, E. L.; Pitz, W. J.; Curran, H. J. *Combust. Flame* 2012.
- (7) Heufer, K. A.; Sarathy, S. M.; Curran, H. J.; Davis, A. C.; Westbrook, C. K.; Pitz, W. J. *Energy & Fuels* 2012, 26, 6678.
- (8) Sarathy, S. M.; Vranckx, S.; Yasunaga, K.; Mehl, M.; Oßwald, P.; Metcalfe, W. K.; Westbrook, C. K.; Pitz, W. J.; Kohse-Höinghaus, K.; Fernandes, R. X.; Curran, H. J. *Combust. Flame* 2012, 159, 2028.
- (9) Prager, J.; Najm, H. N.; Sargsyan, K.; Safta, C.; Pitz, W. J. *Combust. Flame* 2013, <http://dx.doi.org/10.1016/j.combustflame.2013.01.008>.

### IV. References and Journal articles supported by this project 2011-2013

1. Westbrook, C. K., Pitz, W. J., Sarathy, S. M. and Mehl, M., "Detailed Chemical Kinetic Modeling of the Effects of C-C Double Bonds on the Ignition of Biodiesel Fuels," *Proceedings of The Combustion Institute*, 34 (2) (2013) 3049-3056.
2. B. Yang, C. K. Westbrook, T. A. Cool, N. Hansen and K. Kohse-Höinghaus, "Photoionization mass spectrometry and modeling study of premixed flames of three unsaturated C<sub>5</sub>H<sub>8</sub>O<sub>2</sub> esters," *Proc. Combust. Inst.* 34 (1) (2013) 443-451.
3. M. F. Campbell, D. F. Davidson, R. K. Hanson and C. K. Westbrook, "Ignition delay times of methyl oleate and methyl linoleate behind reflected shock waves," 34 (1) (2013) 419-425.
4. W. Wang, Z. Li, M. A. Oehlschlaeger, D. Healy, H. J. Curran, S. M. Sarathy, M. Mehl, W. J. Pitz and C. K. Westbrook, "An experimental and modeling study of the autoignition of 3-methylheptane," *Proc. Combust. Inst.* 34 (1) (2013) 335-343.
5. MacDonald, M.E., Davidson, D.F., Hanson, R.K., Pitz, W.J., Mehl, M., and Westbrook, C.K., "Formulation of an RP-1 pyrolysis surrogate from shock tube measurements of fuel and ethylene time histories", *Fuel* 103 (2013) 1051-1509.
6. Prager, J., Najm, H. N., Sargsyan, K., Safta, C. and Pitz, W. J., "Uncertainty Quantification of Reaction Mechanisms Accounting for Correlations Introduced by Rate Rules and Fitted Arrhenius Parameters," *Combustion and Flame* (2013), In Press.

7. Keromnes, A., Metcalfe, W. K., Heufer, K. A., Donohoe, N., Das, A. K., Sung, C. J., Herzler, J., Naumann, C., Griebeld, P., O. Mathieue, Krejci, M. C., Petersen, E. L., Pitz, W. J. and Curran, H. J., "An Experimental and Detailed Chemical Kinetic Modelling Study of Hydrogen and Syngas Mixtures at Elevated Pressures," *Combustion and Flame* (2013), In press.
8. Darcy, D., Mehl, M., Simmie, J. M., Wurmel, J., Metcalfe, W. K., C. K., W., Pitz, W. J. and Curran, H. J., "An Experimental and Modeling Study of the Shock Tube Ignition of a Mixture of N-Heptane and N-Propylbenzene as a Surrogate for a Large Alkyl Benzene," *Proceedings of the Combustion Institute* 34 (1) (2013) 411-418.
9. S.M. Sarathy, S. Vranckx, K. Yasunaga, M. Mehl, P. Oßwald, C. K. Westbrook, W.J. Pitz, K. Kohse-Höinghaus, R.X. Fernandes, H.J Curran, "A comprehensive chemical kinetic combustion model for the four butanol isomers", *Combust. Flame*, 159 (6) (2012) 2028–2055.
10. Scott A. Skeen, Bin Yang, Ahren W. Jasper, William J. Pitz and Nils Hansen, "The Chemical Structure of Low-Pressure Premixed Methylcyclohexane Flames as Benchmarks for the Development of a Predictive Combustion Chemistry Model", *Energy and Fuels*, 25 (12) (2012) 5611–5625.
11. Heufer, K. A., Sarathy, S. M., Curran, H. J., Davis, A. C., Westbrook, C. K. and Pitz, W. J., "A Detailed Kinetic Modeling Study of n-Pentanol Oxidation," *Energy and Fuels* 26 (11) (2012) 6678-6685.
12. Karsenty, F., Sarathy, S.M., Togbe, C., Westbrook, C.K., Dayma, G., Dagaut, P., Mehl, M., and Pitz, W.J., "Experimental and kinetic modeling study of 3-methyl heptane in a jet stirred reactor", *Energy Fuels* 26 (8), 4680-4689 (2012).
13. Westbrook, C.K., "Biofuels Combustion", *Ann. Rev. Phys. Chem.* 64, 201-219 (2013).
14. Karwat, D.M.A., Wagnon, S.W., Wooldridge, M.S., and Westbrook, C.K., "On the combustion chemistry of n-heptane and n-butanol blends", *J. Phys. Chem. A* 116, 12406-12421 (2012).
15. Veloo, P.S., Dagaut, P., Togbe, C., Dayma, G., Sarathy, S.M., Westbrook, C.K., and Egolfopoulos, F.N., "Jet-stirred reactor and flame studies of propanal oxidation", *Proc. Combust. Inst.* 34, 599-606 (2013).
16. S. M. Sarathy, C. K. Westbrook, M. Mehl, W. J. Pitz, C. Togbe, P. Dagaut, H. Wang, M. A. Oehlschlaeger, U. Niemann, K. Seshadri, P. S. Veloo, C. Ji, F. Egolfopoulos and T. Lu, "Comprehensive chemical kinetic modeling of the oxidation of 2-methylalkanes from C7 to C20," *Combust. Flame* 158 (12) (2011) 2338-2357.
17. C. Ji, S. M. Sarathy, P. S. Veloo, C. K. Westbrook and F. N. Egolfopoulos, "Effects of fuel branching on the propagation of octane isomers flames," *Combust. Flame* 159 (4) (2012) 1426-1436.
18. M. Mehl, W. J. Pitz, S. M. Sarathy, C. K. Westbrook, H. J. Curran, "Modeling the combustion of high molecular weight fuels by a functional group approach", *Int. J. Chem. Kinet.*, 44 (4) (2012) 257-276.
19. C. K. Westbrook and W. J. Pitz, "Fundamental Chemical Kinetics," *Encyclopedia of Automotive Engineering* (2012).
20. C.K. Westbrook, C.V. Naik, O. Herbinet, W.J. Pitz, M. Mehl, S.M. Sarathy and H.J. Curran, "Detailed chemical kinetic reaction mechanisms for soy and rapeseed biodiesel fuels", *Combust. Flame* 158 (4) (2011) 742-755.

# INVESTIGATION OF NON-PREMIXED TURBULENT COMBUSTION

Grant: DE-FG02-90ER14128

Stephen B. Pope & Perrine Pepiot  
Sibley School of Mechanical & Aerospace Engineering  
Cornell University  
Ithaca, NY 14853  
s.b.pope@cornell.edu, pp427@cornell.edu

## 1 Scope of the Research Program

The focus of the current work is on the development of computational approaches which allow our detailed knowledge of the chemical kinetics of combustion to be applied to the modeling and simulation of combustion devices. The principal modeling approaches used are large-eddy simulation (LES) to describe the flow and turbulence, and probability density function (PDF) methods to treat the turbulence-chemistry interactions. The chemistry is handled efficiently using different combinations of *in situ* adaptive tabulation (ISAT), rate-controlled constrained equilibrium (RCCE), and directed relation graphs with error propagation (DRG-EP). In the past year, the research has focused on the following three topics: (1) LES/PDF modeling of bluff-body stabilized flames; (2) investigation of different implementations of RCCE; and (3) the development of a methodology for adaptive chemistry.

## 2 Recent Progress

The principal research results from this program are described in the publications listed in Section 4. The following subsections detail the progress made on the three focused topics mentioned above.

### 2.1 LES/PDF Studies of Bluff-Body Stabilized Turbulent Flames

In the work of Popov & Pope (2012), a state of the art LES/PDF algorithm is applied to the Sandia/Sydney series of CH<sub>4</sub>/H<sub>2</sub> bluff body stabilized flames[1], in particular the flames HM1, HM2 and HM3. These flames feature a hydrodynamically complex flow with a recirculation region attached to the bluff body face – a stabilization mechanism used in many technical applications – and local extinction occurs for the cases HM2 and HM3. These features make the Sandia/Sydney bluff body flames both physically relevant and a natural application for an LES-based simulation, as opposed to Reynolds-averaged Navier-Stokes (RANS) modeling.

These LES/PDF simulations employ reduced chemistry, using the ARM2 chemical mechanism, and the results are compared with the RANS/PDF results of Liu *et al.*[2] and Merci *et al.*[3], as well as with the LES/PDF results of Raman *et al.*[4], which for the HM1 case yield the best agreement with the experimental data.

Overall, the present calculations are a substantial improvement on previous computational studies of the same flame, with better prediction of the local extinction in flames HM2 and HM3.

For example, Fig. 1 shows radial profiles of the mean mass fraction of OH at successive downstream locations. As may be seen, the LES/PDF calculations are in good agreement with the experimental data, whereas the earlier RANS/PDF calculations show significant discrepancies.

It is found that the simulations are sensitive to the treatment of heat transfer to the bluff body face, and better agreement of the temperature profiles with experiment is obtained with the implementation of a Dirichlet temperature boundary condition, which enforces the experimentally-observed mean temperature on the bluff-body face.

## 2.2 A Study of Different Implementations of RCCE

Rate-Controlled Constrained-Equilibrium (RCCE) is a thermodynamic-based dimension reduction method which enables the representation of chemistry involving  $n_s$  species in terms of fewer  $n_r$  constraints. We focus on the application of the RCCE method to Lagrangian particle Probability Density Function based computations. In Hiremath & Pope (2012), three different implementations of RCCE for computing this reaction mapping are studied, and compared in their relative accuracy and efficiency.

The reduced representation of chemistry using the RCCE dimension reduction method is denoted by an  $n_r$ -vector  $\mathbf{r}$ . In PDF based simulations of reacting flows using the RCCE method, given the initial reduced composition of a particle at the beginning of a reaction time step,  $\mathbf{r}(0)$ , the task is to compute the reaction mapping,  $\mathbf{r}(t)$ , at the end of the reaction time step  $t$ . There are different ways of implementing the RCCE dimension reduction method to obtain this reaction mapping. Our implementation of RCCE is different from the classical RCCE approach first introduced by Keck & Gillespie[5]. The Close Parallel Inertial Manifold (CPIM) method[6] describes yet another way of implementing RCCE. The three implementations of RCCE considered are: (1) RCCE/TIFS (Trajectory In Full Space): this is the implementation used in our previous work[7]; (2) RCCE: this is the classical implementation introduced in[5]; and (3) RCCE/RAMP (Reaction-mixing Attracting Manifold Projector): this is a new implementation (based on the CPIM method).

To compute the reaction mapping, the RCCE/TIFS implementation solves a system of  $n_s$  ODEs in the full composition space for all the species. In contrast, the RCCE and RCCE/RAMP implementations solve a reduced system of  $n_r$  ODEs for the constraints by projecting the full system of ODEs onto the constrained subspace. It is found that for small reaction time steps, all three implementations yield similar levels of error. However, as the reaction time step increases, the RCCE/RAMP and RCCE/TIFS implementations yield orders of magnitude smaller error than the RCCE implementation. The principal conclusions from the work are:

- the RCCE/TIFS implementation is the most accurate, robust and efficient among the three implementations of RCCE;

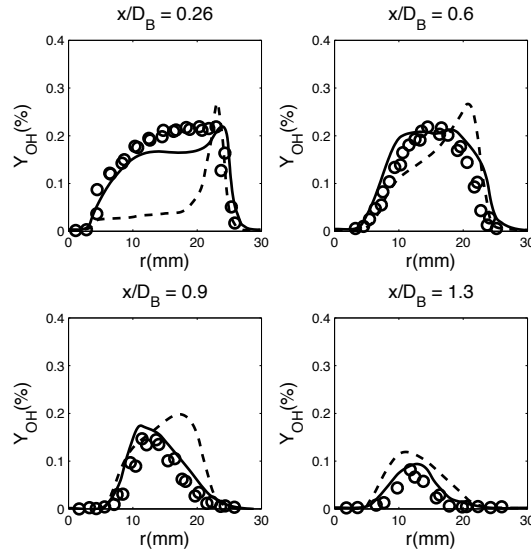


Figure 1: For flame HM3, radial profiles of the mean mass fraction of OH at successive downstream measurement locations. Symbols, experimental data[1]; solid lines, LES/PDF; dashed lines, RANS/PDF[2].

- the RCCE implementation is based on an inaccurate projection of the chemical source term onto the represented subspace, which does not take into account the non-invariance of the constrained-equilibrium manifold and thus yields large errors;
- the RAMP approach provides a more accurate projection for the source vector evaluation (based on the CPIM method) which significantly reduces the error;
- for the methane/air test case considered in this work, both RCCE/TIFS and RCCE/RAMP implementations yield less than 2% error in the reaction mapping compared to over 50% using the RCCE implementation;
- computationally, however, the RCCE/RAMP is an order of magnitude more expensive than the RCCE/TIFS and RCCE implementations due to the need for expensive Jacobian evaluations in the RAMP approach.

### 2.3 An Adaptive Methodology to Implement Detailed Chemistry in LES/PDF

The basic observation motivating adaptive chemistry is that, in any small region of the composition space, many species have negligible concentration, and only a few are chemically active. Hence, the chemistry in the small region can be described by a kinetic model involving many fewer species and reactions than a more detailed model applicable over the entire composition space. Our adaptive chemistry methodology is tailored to particle PDF methods, and consists of the following ingredients:

- a suitable partition of the composition space into regions, each of them linked to a locally valid reduced chemical model much smaller than the detailed kinetic mechanism, and a corresponding reduced representation for the particle composition.
- a classification algorithm that identifies the region in composition space a given composition, detailed or reduced, belongs to.
- a conversion algorithm to adapt the reduced representation of a particle composition as it moves from region to region.
- a method to perform mixing between particles with different reduced representations.

In the current implementation, the partition of the composition space is obtained prior to the turbulent flame calculation of interest using a representative Partially Stirred Reactor (PaSR) configuration. The partition is stored as a binary tree, a set of reduced models, one for each leaf of the tree, and a set of cutting planes, one for each node of the tree. The feasibility of the adaptive approach has been demonstrated for propane/air non-premixed flame in a PaSR using straight-forward implementations of each component of the algorithm. Preliminary results show a computational gain of up to an order of magnitude compared to the single reduced model approach.

## 3 Future Plans

The work in the next year will focus on the further development of adaptive chemistry, and on the further development and application of the shadow-position mixing model.

## 4 Publications from DOE Research 2010-2012

1. V. Hiremath, Z. Ren and S.B. Pope (2010) “A Greedy Algorithm for Species Selection in Dimension Reduction of Combustion Chemistry,” *Combustion Theory and Modelling*, **14**, 619–652.
2. D.C. Haworth and S.B. Pope (2011) “Transported Probability Density Function and Filtered Density Function Methods,” in *Turbulent Combustion Modeling: Advances, New Trends and Perspectives*, eds. T. Echekki, E. Mastorakos, Springer.
3. V. Hiremath, Z. Ren and S.B. Pope (2011) “Combined Dimension Reduction and Tabulation Strategy using ISAT-RCCE-GALI for the Efficient Implementation of Combustion Chemistry”, *Combustion and Flame*, **158**, 2113–2127.
4. S.B. Pope (2011) “Simple Models of Turbulent Flows”, *Physics of Fluids* **23**, 011301.
5. Z. Ren, G.M. Goldin, V. Hiremath and S.B. Pope (2011) “Reduced Description of Reactive Flows with Tabulated Chemistry”, *Combustion Theory and Modelling*, **15**, 827–848.
6. S. Viswanathan, H. Wang and S.B. Pope (2011) “Numerical Implementation of Mixing and Molecular Transport in LES/PDF Studies of Turbulent Reacting Flows”, *Journal of Computational Physics*, **230** 6916–6957.
7. V. Hiremath, S.R. Lantz, H. Wang and S.B. Pope (2012) “Computationally-Efficient and Scalable Parallel Implementation of Chemistry in Simulations of Turbulent Combustion”, *Combustion and Flame*, **159**, 3096–3109.
8. V. Hiremath and S.B. Pope (2012) “A Study of the Rate-Controlled Constrained-Equilibrium Dimension Reduction Method and its Different Implementations, *Combustion Theory and Modelling* (to be published).
9. A.Y. Klimenko and S.B. Pope (2012) “Propagation Speed of Combustion and Invasion Waves in Stochastic Simulations with Competitive Mixing, *Combustion Theory and Modelling*, **16**, 679–714.
10. S.B. Pope (2012) “A Model for Turbulent Mixing Based on Shadow-Position Conditioning, *Physics of Fluids* (submitted).
11. P.P. Popov and S.B. Pope (2012) “Large Eddy Simulation/Probability Density Function Simulations of Bluff Body Stabilized Flames, *Combustion & Flame* (submitted).
12. V. Hiremath, S.R. Lantz, H. Wang and S.B. Pope (2013) “Large-Scale Parallel Simulations of Turbulent Combustion using Combined Dimension Reduction and Tabulation of Chemistry, *Proceedings of the Combustion Institute*, **34**, 205–215.
13. S.B. Pope (2013) “Small Scales, Many Species and the Manifold Challenges of Turbulent Combustion, *Proceedings of the Combustion Institute*, **34**, 1–31.
14. Z. Ren, G. M. Goldin, V. Hiremath, S. B. Pope (2013) “Simulations of a Turbulent non-Premixed Flame Using Combined Dimension Reduction and Tabulation for Combustion Chemistry, *Fuel*, **105**, 636–644.

## References

- [1] A. R. Masri, and R. W. Bilger, *Proc. Comb. Inst.*, **20**, (1985) 319–326.
- [2] K. Liu, S. B. Pope, and D. A. Caughey, *Comb. Flame*, **141**, (2005) 89–117.
- [3] B. Merci, D. Roekaerts, B. Naud, and S.B. Pope, *Comb. Flame*, **146**, (2006) 109–130.
- [4] V. Raman, H. Pitsch, and R. O. Fox, *Comb. Flame*, **143**, (2005) 56–78
- [5] J.C. Keck and D. Gillespie, *Combust. Flame* **17** (1971) 237-241.
- [6] Q. Tang and S.B. Pope, *Combust. Theory Modelling* **8** (2004) 255-279.
- [7] V. Hiremath, Z. Ren, and S.B. Pope, *Combust. Flame* **158** (2011) 2113-2127.

## OPTICAL PROBES OF ATOMIC AND MOLECULAR DECAY PROCESSES

S.T. Pratt  
Building 200, B-125  
Argonne National Laboratory  
9700 South Cass Avenue  
Argonne, Illinois 60439  
E-mail: [stpratt@anl.gov](mailto:stpratt@anl.gov)

### PROJECT SCOPE

Molecular photoionization and photodissociation dynamics can provide considerable insight into how energy and angular momentum flow among the electronic, vibrational, and rotational degrees of freedom in isolated, highly energized molecules. This project involves the study of these dynamics in small polyatomic molecules, with an emphasis on understanding the mechanisms of intramolecular energy flow and determining how these mechanisms influence decay rates and product branching ratios. Such studies also provide insight into related collision processes such as the dissociative recombination of electrons and ions. One goal of the project is to understand how internal energy can influence photoionization cross sections and dissociative ionization processes, and recent work has involved the determination of absolute photoionization cross sections for a number of radicals. The experimental approach combines a variety of laser-based techniques, including nonlinear methods to generate tunable vacuum ultraviolet light, and double-resonance methods to prepare selected excited states of the species of interest. The detection methods include mass spectrometry, photoion- and photoelectron-imaging, and high-resolution photoelectron spectroscopy, which are used to characterize the decay processes of the selected excited states.

### RECENT PROGRESS

#### *Photoionization studies and absolute photoionization cross sections*

We are continuing to use photoion and photoelectron imaging, vacuum-ultraviolet (vuv) single-photon ionization, and resonant multiphoton ionization to probe the photodissociation dynamics of small polyatomic molecules, and to characterize the photoionization dynamics of combustion-relevant species. One aspect of this work is to determine the absolute photoionization cross sections of radicals and other reactive species. In these experiments, an appropriate precursor is chosen that can be photodissociated to give the radical of interest and a second species with a known photoionization cross section. Velocity map ion imaging of the fragments is used to show that the two species are momentum matched, and thus produced in equal numbers by the same process. The determination of the ratio of the photoionization cross sections for the two fragments, combined with the known absolute photoionization cross section of one of the species, then allows the determination of the absolute cross section for the other. We have previously reported absolute photoionization cross sections for CH<sub>3</sub> and HCO.

The absolute photoionization cross section of the propargyl radical was first determined by Robinson et al. [*J. Chem. Phys.* **2003**, *119*, 5311-5314]. In these groundbreaking experiments, they used a scheme similar to ours, but with the laser source replaced by a synchrotron light source, and the imaging apparatus replaced by a photofragment translational spectrometer. They photodissociated propargyl chloride for a precursor, and measured the cross section of propargyl relative to the known cross section of the chlorine atom. Recently, Savee et al. [*J. Chem. Phys.* **2012**, *136*, 134307] performed a new measurement of the photoionization cross section of the propargyl radical by using a very different method based on a flow tube experiment. Their value was almost a factor of three greater than the value determined by Robinson et al. One of the differences between the two experiments is that the propargyl radicals in the earlier experiments had significant internal energy, while those in the more recent experiment were vibrationally relaxed. To shed some light on this discrepancy, we have recently performed a new measurement of the absolute photoionization cross section of the propargyl radical near 118.2 nm by using the photodissociation of 2-butyne and 1,2-butadiene. A significant dissociation channel for both species produces CH<sub>3</sub> + C<sub>3</sub>H<sub>3</sub>, and the latter has been determined to correspond to the

propargyl radical. The known photoionization cross section for the methyl radical can then be used to determine the cross section of the propargyl radical. As in the experiments of Robinson et al., the propargyl radicals in our experiment have considerable internal energy. Nevertheless, the cross section we derive is in good agreement with the determination of Savee et al. [*J. Chem. Phys.* **2012**, *136*, 134307]. Thus, it does not appear that vibrational excitation of the radicals is responsible for the discrepancy.

Photoionization cross sections are difficult to calculate, especially if processes like autoionization and predissociation are considered. Approximate schemes to estimate photoionization cross sections have been developed, and those of Bobeldijk et al. [*Chem. Phys.* **179**, 125-130 (1994)] and Koizumi [*J. Chem. Phys.* **95**, 5846-5852 (1991)], have proven to be quite valuable. We have tried to understand the results for the propargyl radical by considering the photoionization cross sections of closed shell species with similar molecular orbitals. A variety of experiments on related closed-shell molecules with similar molecular orbitals can be used to rationalize the present observations for propargyl. These data include photoabsorption cross sections, photoionization quantum yields, and photoelectron spectra. We have shown that the observed large cross sections are consistent with the corresponding cross sections for allene and propyne, particularly when one considers the possibility of photoionization into excited states of the propargyl cation. We also showed how analogous data can be used to estimate photoionization cross sections of other radicals, including methyl, allyl, 2-propenyl, and vinyl. For the most part, these estimates are in reasonable agreement with existing experimental data.

We are currently using the same experimental approach to determine the absolute photoionization cross sections of the phenyl, phenoxy, and benzyl radicals by using the photodissociation of iodobenzene, anisole, and ethyl benzene, respectively. In iodobenzene, the co-fragment is of course I, while in the latter two samples, the co-fragment is CH<sub>3</sub>. In contrast to our earlier experiments, each of these samples presents a different kind of problem. For example, in iodobenzene, the branching ratio between the I <sup>2</sup>P<sub>3/2</sub> and I <sup>2</sup>P<sub>1/2</sub> must be characterized. In anisole, the phenoxy radical is produced with substantial internal energy, and while we see no evidence for neutral (secondary) dissociation of the phenoxy, photoionization near 10.5 eV is essentially pure dissociative ionization. Finally, for ethylbenzene, the dissociation is relative slow, so that we must take into account dissociative ionization of hot (not-yet-dissociated) ethylbenzene, which provides another source of benzyl cations, as well as the finite rise-time of the methyl fragments. In spite of these issues, we expect to have new values for the radical cross sections in the near future.

#### *Dissociative recombination of small polyatomic ions*

In collaboration with Christian Jungen, I have continued to work on theoretical models of vibrational autoionization and, most recently, on dissociative recombination. In one project of the past year [Reference 7], the existing experimental and theoretical data on the low-lying npe' Rydberg states were reviewed, and new fits to the data allowed the determination of more accurate Jahn-Teller interaction parameters. In particular, for the 3pe' state, both the linear and quadratic Jahn-Teller parameters were determined. In the framework of multichannel quantum defect theory, these parameters can be used to predict the behavior of higher Rydberg states in the npe' series, as well as the behavior of the corresponding ionization continuum. Earlier work [see, for example, S. F. dos Santos, V. Kokoouline, and C. H. Greene, *J. Chem. Phys.* **127**, 124309 (2007)] has shown that, at low collision energies, electron capture by H<sub>3</sub><sup>+</sup> into this npe' series is enhanced by the Jahn-Teller interaction, and is the principal reason that the dissociative recombination cross section of H<sub>3</sub><sup>+</sup> + e<sup>-</sup> is so large at low energies. The improved analysis reaffirms this conclusion, and demonstrates the consistency of the data obtained from experiment and from ab initio calculations. The analysis also shows that the quadratic Jahn-Teller interaction parameter is quite small, and thus capture processes involving this interaction are not likely to contribute significantly to the dissociative recombination cross section.

In a second project [Reference 8], we showed that our analytic formula for the cross section for low-energy dissociative recombination of molecular ions and electrons involving capture into vibrationally excited Rydberg states also provides a simple expression for the isotope dependence of the process. This expression depends only on the ratio of the relevant vibrational frequencies of the two isotopomers of interest, and can therefore be evaluated even without a knowledge of the dynamical parameters required to determine the recombination cross sections. The expression was used to predict the isotope dependence for a number of molecular ions, and the results were compared with available experimental data for a number of small molecular ions. While the agreement with experiment was generally quite reasonable, discrepancies indicate a breakdown of the assumptions used to derive the cross section formula or potential inaccuracies in the experiments. This formula should provide a useful tool for assessing new experimental data and for estimating isotope dependences when data is unavailable.

## FUTURE PLANS

We plan on continuing our studies of the photodissociation and photoionization of combustion-relevant radicals by using ion-imaging techniques, vacuum-ultraviolet single-photon ionization, and resonant multiphoton ionization techniques. We will complete our studies of the absolute photoionization cross sections for the phenyl, phenoxy, and benzyl radicals, and extend these studies to other systems. Potential targets include the  $\text{CH}_2\text{CH}_2\text{OH}$  radical, which can be prepared by the photodissociation of 2-iodoethanol, and the vinoxy radical,  $\text{CH}_2\text{CH}$ , which can be produced in conjunction with  $\text{CH}_2\text{CH}_2\text{OH}$  by the photodissociation of ethylene glycol vinyl ether. Potential schemes to determine the absolute photoionization cross section of the methoxy radical,  $\text{CH}_3\text{O}$ , will also be investigated.

We are in the process of developing a pulsed discharge source for our velocity map imaging machine to allow the direct production of cold radicals and other reactive species. This new source will be tested in the coming year. Our initial efforts will focus on the study of OH radicals by using the excitation scheme developed by Marsha Lester's group [J. M. Beames, F. Liu, M. I. Lester, and C. Murray, *J. Chem. Phys.* **134**, 241102 (2011)]. In this scheme, the uv light excites the  $A \leftarrow X$  transition, and vuv light at 118 nm drives transitions from the A state to the region above the lowest ionization threshold. Our goal is to use tunable vuv light for the second step, as well as photoelectron imaging, to allow a more thorough characterization of autoionizing resonances accessed via this excitation scheme. The discharge source should also allow the production of a wide variety of other radicals and metastable species.

I will continue to collaborate with Christian Jungen on theoretical models of vibrational autoionization and dissociative recombination in polyatomic molecules. Our efforts are expected to focus on two problems. First, we will attempt to identify the resonances observed in the low-energy dissociative recombination of  $\text{H}_3^+ + e^-$ . Specifically, the experimental cross sections show a number of strong resonances at low energy that almost certainly must be associated with capture into specific Rydberg states based on rovibrationally excited  $\text{H}_3^+$  in its electronic ground state. Although this is the simplest triatomic molecule, no convincing assignments have been made to date. Second, we will re-examine the low-energy dissociative recombination of  $\text{HCO}^+ + e^-$ . Although significant progress has been made on this system, there is still a factor of approximately two discrepancy in the theoretical and experimental cross sections. We will try to assess the relative importance of reaction pathways missing in the theoretical descriptions, and attempt to determine if these could account for the discrepancy.

I have successfully applied for beamtime to use the very high-resolution, Fourier-transform vacuum ultraviolet spectrometer at the Soleil Synchrotron in France [N. de Oliveira et al., *Rev. Sci. Instrum.* **80**, 043101 (2009)], and I will perform my first experiments there in April 2013 on the photoabsorption spectrum of acetylene, propyne, 1-butyne, and 2-butyne. The apparatus allows the recording of absorption spectra of both room-temperature and jet-cooled samples. The proposed work builds on my previous work on an intense near-threshold shape resonance in 2-butyne, with the goal of observing the effect of this shape resonance on the Rydberg series converging to the first ionization potential of the molecule. Because the shape resonance has  $\ell = 4$ ,  $\pi$  character, a significant enhancement is expected in the intensity of the  $g\pi$  Rydberg series near threshold. The combination of a jet-cooled sample and the

very high resolution of the instrument will provide a unique window onto this portion of the absorption spectrum, and improve the understanding of the photoionization dynamics. The corresponding portions of the jet-cooled spectra of acetylene, propyne, and 1-butyne have not been recorded previously, and these are expected to reveal significant new information as well.

This work was supported by the U.S. Department of Energy, Office of Science, Office of Basic Energy Sciences, Division of Chemical Sciences, Geosciences, and Biological Sciences under contract No. DE-AC02-06CH11357.

#### DOE-SPONSORED PUBLICATIONS SINCE 2011

1. S. T. Pratt  
HIGH-RESOLUTION VALENCE-SHELL PHOTOIONIZATION  
in *Handbook of High-Resolution Spectroscopies*, edited by M. Quack and F. Merkt (Wiley, New York, 2011), pp 1595-1616. (October 18, 2011).
2. S. T. Pratt and Ch. Jungen  
DISSOCIATIVE RECOMBINATION OF SMALL POLYATOMIC MOLECULES  
J. Phys. Conf. Ser. **300**, 012109 (8 pages) (2011).
3. V. A. Shubert and S. T. Pratt  
PHOTOELECTRON IMAGING OF SEVERAL 5d AND 6p RYDBERG STATES Xe<sub>2</sub> AND IMPROVING THE Xe<sub>2</sub><sup>+</sup> I(1/2g) POTENTIAL  
J. Chem. Phys. **134**, 044315 (12 pages) (2011).
4. N. Thiré, R. Cireasa, D. Staedter, V. Blanchet, and S. T. Pratt  
TIME-RESOLVED PREDISSOCIATION OF THE VIBRATIONLESS LEVEL OF THE B STATE OF CH<sub>3</sub>I  
Phys. Chem. Chem. Phys. **13**, 18485-18496 (2011).
5. V. Alvin Shubert and S. T. Pratt  
PHOTOELECTRON IMAGING OF AUTOIONIZING STATES OF XENON: THE EFFECT OF EXTERNAL ELECTRIC FIELDS  
Phys. Rev. A, **84**, 053413 (10 pages) (2011).
6. H. Xu, U. Jacovella, B. Ruscic, S. T. Pratt, and R. R. Lucchese  
NEAR-THRESHOLD SHAPE RESONANCE IN THE PHOTOIONIZATION OF 2-BUTYNE  
J. Chem. Phys., **136**, 154303 (10 pages) (2012).
7. Ch. Jungen, M. Jungen, and S. T. Pratt  
THE JAHN-TELLER EFFECT IN THE 3pe' RYDBERG STATE OF H<sub>3</sub>. REVIEW OF EXPERIMENTAL AND AB INITIO DETERMINATIONS  
Phil. Trans. Roy. Soc. London, **370**, 5074-5087 (2012).
8. S. T. Pratt and Ch. Jungen  
THE ISOTOPE DEPENDENCE OF DISSOCIATIVE RECOMBINATION VIA THE INDIRECT MECHANISM  
J. Chem. Phys. **137**, 174306 (6 pages) (2012).
9. H. Xu and S. T. Pratt  
THE PHOTOIONIZATION CROSS SECTION OF PROPARGYL RADICAL AND SOME GENERAL IDEAS FOR ESTIMATING RADICAL CROSS SECTIONS  
J. Phys. Chem. A (in press).

## Photoinitiated Reactions of Radicals and Diradicals in Molecular Beams

Hanna Reisler

Department of Chemistry, University of Southern California

Los Angeles, CA 90089-0482

reisler@usc.edu

### Program Scope

Open shell species such as radicals and diradicals are central to reactive processes in combustion and environmental chemistry. Our program is concerned with photoinitiated reactions of hydroxyalkyl radicals and carbenes. The goal is to investigate the detailed dynamics of dissociation of free radicals and diradicals for which multiple pathways including molecular rearrangements compete, and compare them with high level calculations. Studies include unimolecular reactions on the ground state as well as photodissociation dynamics on excited Rydberg and valence states that involve multiple potential energy surfaces. The photodissociation of these species can exhibit several conical intersections and the experiments will be compared with high-level electronic structure calculations. The detailed measurements on simple systems will serve as benchmarks for homologous series.

### Recent Progress

#### **An improved sliced velocity map imaging (SVMI) apparatus optimized for hydrogen products**

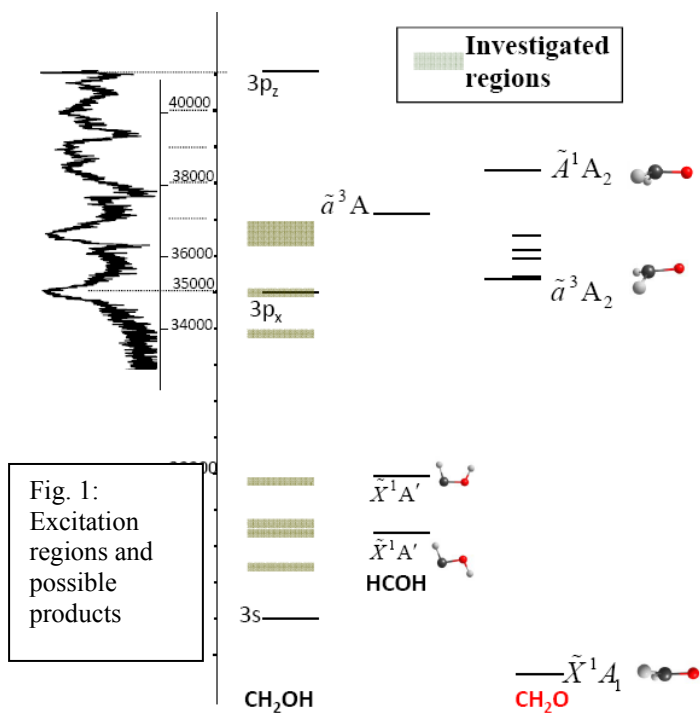
In order to determine product state distributions in photoinitiated dissociation of combustion-relevant radicals with vibrational resolution and infer mechanisms, the time-of-flight detection system in our experimental arrangement was replaced with an imaging arrangement designed specifically to achieve SVMI of H-photofragments with comparable resolution to that obtained in full projection VMI. To this end, we designed and constructed a high-voltage pulser with pulses of  $< 5$  ns duration, and completely redesigned the ion optics to achieve a large dynamic range of translational energies with minimal aberrations and distortions.

The ion optics design enables SVMI of H fragments in a broad range of kinetic energies (KE), from a fraction of an electronvolt to a few electronvolts. In order to enable consistently thin slicing for any imaged KE range, an additional electrostatic lens is introduced in the drift region for radial magnification control without affecting temporal stretching of the ion cloud. Time slices of  $\sim 5$  ns out of a cloud stretched to  $\sim 50$  ns are used. An accelerator region with variable dimensions (using multiple electrodes) is employed for better optimization of radial and temporal space focusing characteristics at each magnification level. The performance of the design was tested by recording images of H fragments from the photodissociation of HBr, H<sub>2</sub>S, and the CH<sub>2</sub>OH radical, with kinetic energies ranging from  $< 0.4$  eV to  $> 3$  eV. It demonstrated KE resolution of 1–2 %, similar to that obtained in traditional velocity map imaging followed by reconstruction, and to KE resolution achieved previously in SVMI of heavier products. We expect it to perform just as well up to at least 6 eV of kinetic energy. The tests showed that numerical simulations of the electric fields and ion trajectories in the system, used for optimization of the design and operating parameters, provide an accurate and reliable description of all aspects of system performance. This offers the advantage of selecting the best operating conditions in each measurement without the need for additional calibration experiments. This arrangement is cost effective because it uses a small MCP detector (40 mm dia.) and an inexpensive CCD camera.

A full description of the apparatus is posted on our website and includes drawings and SIMION simulation scripts (<http://www-bcf.usc.edu/~reisler/assets/pdf/SVMI.pdf>). A manuscript was submitted to J. Chem. Phys. in January 2013.

## Photodissociation of the hydroxymethyl radical via conical intersections: Formaldehyde and hydroxymethylene products

The first implementation of our new SVMI arrangement was to examine the overtone-induced vibrational predissociation of the hydroxymethyl radical with special emphasis on the relative roles of direct dissociation,  $\text{CH}_2\text{OH} \rightarrow \text{CH}_2\text{O} + \text{H}$ , and dissociation following  $\text{CH}_2\text{OH} \leftrightarrow \text{CH}_3\text{O}$  isomerization. These studies were published last year, demonstrating our capability to obtain vibrational energy distributions in  $\text{CH}_2\text{O}$  co-fragments from sliced images of H photofragments. Our work benefited greatly from the collaboration with the theory groups of Anna Krylov and Joel Bowman.



Our current experiments focus on photodissociation dynamics of the hydroxymethyl radical following excitation to the 3s and 3p<sub>x</sub> Rydberg states. We were inspired to return to these experiments by the high level conical intersection calculations of David Yarkony and coworkers.[1] It was clear that in order to check some of his predictions, greater velocity resolution of products was necessary. In our previous experiments we characterized the lowest excited states of the radicals (3s, 3p<sub>x</sub> and 3p<sub>z</sub> Rydberg states) and identified formaldehyde and its isomer, hydroxymethylene, as the two main product channels.[2,3] No evidence of isomerization was obtained. However, the translational energy resolution achieved with time-of-flight detection was insufficient to characterize the vibrational distribution in the molecular products.

One of the advantages of studying the hydroxyalkyl radicals is that they have continuous absorption from the visible to the ultraviolet, and thus the excitation energy can be tuned continuously to regions of interest. Figure 1 shows the excitation energies that were interrogated so far. These include 3s and 3p<sub>x</sub> excitations. Absorption to 3s is structureless, whereas absorption to 3p<sub>x</sub> exhibits broad vibronic bands above a background of 3s absorption (see Fig. 1, left panel). From images of H photofragments at excitation energies where the C-H bond cannot be broken (see an example in Fig. 2), we conclude that most of the formaldehyde products are born with high kinetic energies but some excitation is deposited in the CO stretch. The recoil anisotropy parameter at high KE is close to the maximum for a perpendicular transition:  $\beta = -0.7$ . We also note that a minor fraction of the products have lower translational energies (i.e. higher internal excitation in the formaldehyde fragment), and a more isotropic angular distribution. This results agree with the predictions of Yarkony, who analyzed the the g-h branching plane and concluded that the majority of products would form promptly following conical intersection with the ground state, and they would have CO stretch excitation. He also predicted that a minor component, which he called “statistical”, would arise from dissociation processes that sample the bound region of the ground state potential energy surface following the same conical intersection. Because the radical is a minor constituent in the molecular beam, we are now using different isotopologs to confirm that the observed slow component is indeed correlated with the hydroxymethyl radical.

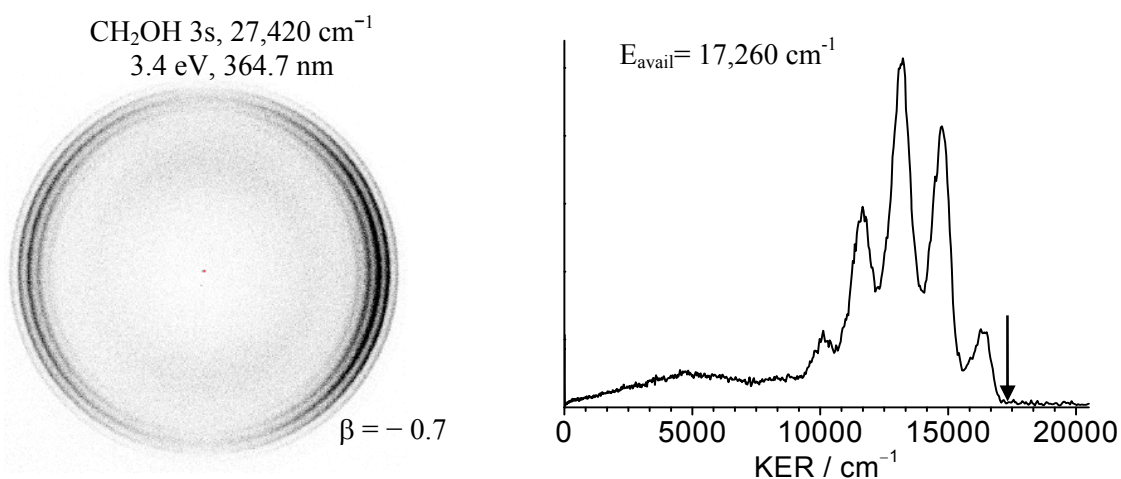


Fig. 2. An image and corresponding kinetic energy release (KER) obtained by SVMI of H fragments from CH<sub>2</sub>OH

Near the threshold of breaking the C-H bond of CH<sub>2</sub>OH(D), we observe a small signal in the low KER region, which is correlated with formation of HCOH(D) radicals. The lowest energy isomer is *trans*-HCOH and it appears first but at low yield. The yields of both *trans*-HCOH and *cis*-HCOH remain relatively low until the origin band of the 3p<sub>x</sub> state is reached. At this energy, which is above the calculated barrier for the conical intersection leading to C-H bond breaking,[1] the yield increases and the *cis* isomer becomes dominant (see Fig. 3). This is again in agreement with the conical-intersection calculations of Yarkony, who predicted that the higher lying *cis* isomer would be preferred. The HCOH radical is born with much rotational and vibrational excitation. We extended these studies to the CH<sub>2</sub>OD isotopolog, which allowed us to distinguish better between O-D and C-H bond breaking. The H product is pair-correlated with HCOD and the peak in the velocity distribution corresponds to the threshold of formation of *cis*-HCOD (Fig. 3). This is the first time that the *cis* isomer of hydroxymethylene has been observed. We do not see evidence of isomerization in any isotopolog. These results are being prepared for publication in the J. Phys. Chem. A issue honoring Curt Wittig.

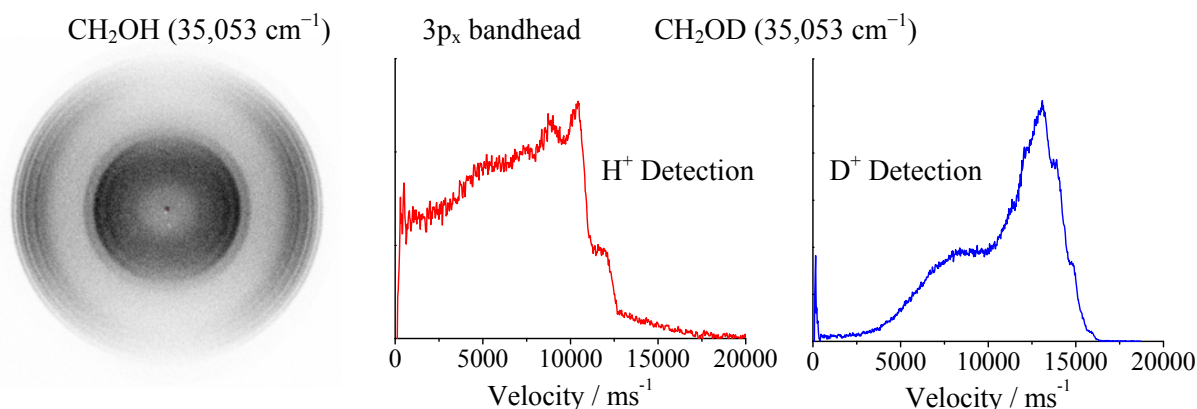


Fig. 3. On the left is an SVMI image of H fragments from CH<sub>2</sub>OH showing production of CH<sub>2</sub>O and HCOH (outer and inner rings, respectively). The right panels show velocity distributions obtained by monitoring H and D products from CH<sub>2</sub>OD.

### Future Work

Our immediate goal is to extend the hydroxymethyl studies to higher energies, where the  $3p_z$  state of  $\text{CH}_2\text{OH}$  is reached and excited electronic states of the  $\text{CH}_2\text{O}$  and  $\text{HCOH}$  can be produced. Our preliminary SVMI results show formation of triplet formaldehyde at its threshold. Its vibrational excitation increases with increasing excitation energy. We hope to identify the triplet state of  $\text{HCOH}$  as well. Following  $3p_z$  excitation we also observe secondary dissociation of “hot”  $\text{CH}_2\text{O}$  and  $\text{HCOH}$ . We hope that these detailed results would serve as benchmarks for dynamical calculations. Our next goal is to study the photodissociation dynamics of the hydroxyethyl radical, especially near the threshold of the  $3p_x$  absorption, and compare them with the calculations of Yarkony and coworkers.

### References

1. B. C. Hoffman and D. R. Yarkony, *J. Chem. Phys.* **116**:8300 (2002); D. R. Yarkony, *J. Chem. Phys.* **122**, 084316 (2005).
2. L. Feng, X. Huang and H. Reisler, *J. Chem. Phys.* **117**, 4820-4824 (2002).
3. L. Feng, A.V. Demyanenko, and H. Reisler, *J. Chem. Phys.* **118**(21), 9623 (2003); *ibid*, **120**, 6524 (2004).

### Publications, 2010-2013

1. B. Karpichev, L. Koziol, K. Diri, H. Reisler and A. I. Krylov, “Electronically excited and ionized states of the  $\text{CH}_2\text{CH}_2\text{OH}$  radical: A theoretical study”, *J. Chem. Phys.*, **132**, 114308 (2010).
2. L.W. Edwards, M. Ryazanov, H. Reisler and S. J. Klippenstein, “D-atom products in predissociation of  $\text{CD}_2\text{CD}_2\text{OH}$  from the 202-215 nm photodissociation of 2-bromoethanol”, *J. Phys. Chem. A*, **114** (17), 5453–5461 (2010).
3. E. Kamarchik, L. Koziol, H. Reisler, J. M. Bowman, and A. I. Krylov, “Unexpected roaming pathway leading to water plus vinyl products in  $\text{C}_2\text{H}_4\text{OH}$  dissociation.” *J. Phys. Chem. Lett.* **1**, 3058-3065 (2010).
4. E. Kamarchik, C. Rodrigo, J.M. Bowman, H. Reisler, and A. I. Krylov, “Overtone-induced dissociation and isomerization dynamics of the hydroxymethyl radical ( $\text{CH}_2\text{OH}$  and  $\text{CD}_2\text{OH}$ ). I. A theoretical study”, *J. Chem. Phys.* **136**, 084304 (2012).
5. M. Ryazanov, C. Rodrigo and H. Reisler, “Overtone-induced dissociation and isomerization dynamics of the hydroxymethyl radical ( $\text{CH}_2\text{OH}$  and  $\text{CD}_2\text{OH}$ ). II. Velocity map imaging studies”, *J. Chem. Phys.* **136**, 084305 (2012).
6. M. Ryazanov and H. Reisler, “Improved sliced velocity map imaging apparatus optimized for H photofragments”, *J. Chem. Phys.* (in press, 2013).

# Accurate Calculations and Analyses of Electronic Structure, Molecular Bonding and Potential Energy Surfaces

Klaus Ruedenberg

Ames Laboratory USDOE, Iowa State University, Ames, Iowa, 50011

ruedenberg@iastate.edu

## Scope

Theoretical treatments of molecular reactions and their kinetics require accurate potential energy surfaces in non-equilibrium regions of coordinate space. A major challenge is the accurate description of the non-relativistic electron correlations in the presence of a multi-configurational dominant zeroth-order component in the electronic wave function, as is the case along most reaction paths. A substantial advance towards this goal has been made through the correlation energy extrapolation by intrinsic scaling (CEEIS) method, developed in this group. By combining it with the extrapolation to the complete basis limit, potential energy curves were obtained within about 0.1 kcal/mol for ground and excited states of diatomic molecules.

## Recent Work

CEEIS strategies were developed with respect to the spatial distribution of correlation contributions by resolutions in terms of interactions between localized orbitals in polyatomic molecules. CEEIS-type proportionalities between partial geometric summations and exact correlation energies were identified.

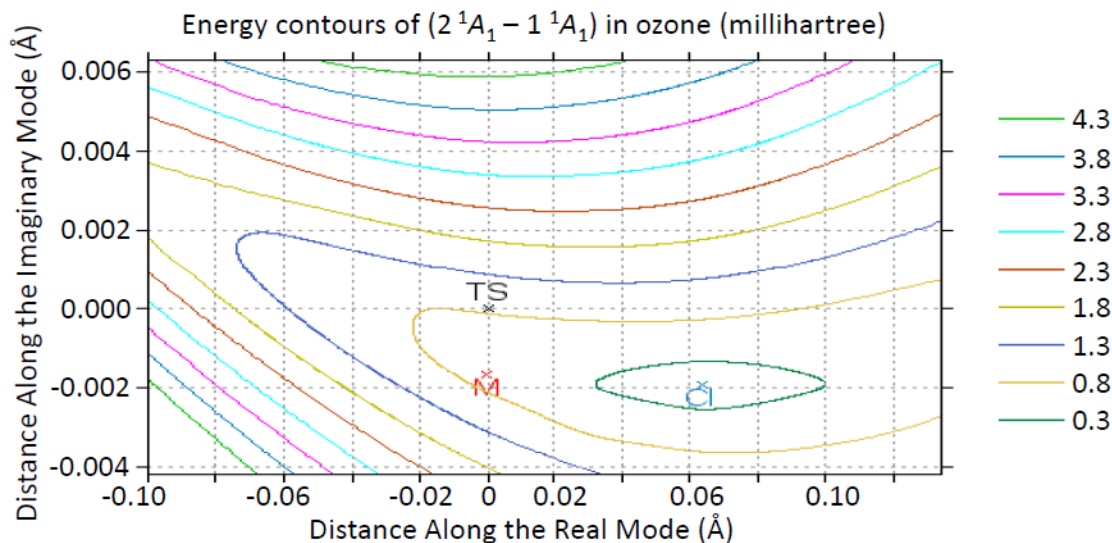
CEEIS strategies based on state averaged reference functions were also developed for the simultaneous treatment of several electronic states to high accuracy. In contrast to conventional state averaged calculations, the high-accuracy CEEIS results were shown to be independent of the weighting used in the state averaging.

The unique features of the lowest two  $^1A_1$  potential energy surfaces of ozone are being determined with very high accuracy, viz: the known open structure, the equilateral ring structure and the transition state between them, as well as the minimum on the lowest excited  $^1A_1$  state surface and the conical intersection between the ground state and the excited state. With the exception of the open ground state minimum, all these features still await experimental discovery so that hard targets of geometries, energies and vibrational spectra, predicted with very high accuracy, will be valuable for the experimental search. The MCSCF reference wave functions of high accuracy, on which the CEEIS correlation recovery is based, have been determined. Contours of the energy difference ( $2^1A_1 - 1^1A_1$ ) are displayed in the Figure below, which also shows the mutually close locations of the ground-state transition-state, the excited state minimum and the conical intersection. The CEEIS recovery of the dynamic correlation at these critical points is in progress. The determination of the conical intersection will represent the first high-accuracy determination of any such potential energy surface crossing.

It was shown that biradical character can play a marked role in molecules that are valence-iso-electronic with ozone. The relation of this theoretical characteristic to the variation of experimental properties was documented for the series  $(CX_2)^{2-}$ ,  $(NX_2)^-$ ,  $X_3$ ,  $OX_2$ ,  $(FX_2)^+$ , where  $X = O, S, Se, Te, Po$ .

In an invited lead chapter of a forthcoming book on the chemical bond, all physical agents involved in the synergism that leads to the formation of covalent bonding

were identified and their interactions analyzed through in-depth ab-initio studies of the diatomic molecules  $\text{H}_2^+$ ,  $\text{H}_2$ ,  $\text{B}_2$ ,  $\text{C}_2$ ,  $\text{N}_2$ ,  $\text{O}_2$ ,  $\text{F}_2$ .



TS = transition state of  $1^1A_1$  , M = minimum of  $2^1A_1$   
 CI = conical intersection between  $1^1A_1$  and  $2^1A_1$

### Future Work

The above mentioned high-accuracy CEEIS determination of the ozone potential energy surfaces will be completed.

The basis of the CEEIS approach, viz. the proportionality of the correlation energy to systematic enlargements of the correlating virtual orbital space, represents a targeted use of the posited *randomness* of large correlating configuration spaces that generate very large numbers of small individual contributions of similar magnitudes. This conjecture of randomness has recently been confirmed from a different angle by the success of *Monte-Carlo treatments in configuration interaction spaces* of large systems by A. Alevi at Cambridge University, UK. In view of this corroboration, a wider scope of application of the CEEIS concept will be developed, in particular regarding applications to larger molecules..

### Publications in 2010, 2011, 2012

*The range of electron correlation between localized molecular orbitals. A full configuration interaction analysis for the NCCN molecule*

L. Bytautas and K. Ruedenberg, J. Phys. Chem. A 114, 8601–8612 (2010)

*Toward a Physical Understanding of Electron-Sharing Two-Center Bonds. II. A Pseudo-Potential Based Approach*

T. Bitter, S.G. Wang, K. Ruedenberg, W.H.E. Schwarz, Theor. Chem Acc. 127, 237–257 (2010)

*Electronic structure analysis of the ground state potential energy curve of Be<sub>2</sub>*

M.W. Schmidt, J. Ivanic, K. Ruedenberg, J. Phys. Chem. A 114, 8687-8696 (2010)

*Analysis of the bonding patterns in the valence isoelectronic series O<sub>3</sub>, S<sub>3</sub>, SO<sub>2</sub> and OS<sub>2</sub> in terms of oriented quasi-atomic molecular orbitals*

V.A. Glezakou, S.T. Elbert, S. S. Xantheas, K. Ruedenberg, J. Phys. Chem. A 114, 8923–8931 (2010)

*Accurate potential energy curve for B<sub>2</sub>. Ab initio elucidation of the experimentally elusive ground state rotation-vibration spectrum*

L. Bytautas, N.Matsunaga, G. Scuseria, K. Ruedenberg, J. Phys. Chem. A., 116, 1717-1729 (2012)

*The dispersion interaction between quantum mechanics and effective fragment potential molecules*

Q.A. Smith, K. Ruedenberg, M.S. Gordon, L.V. Slipchenko, J. Chem. Phys. 136, 244107 (2012)

*Three Millennia of Atoms and Molecules*

K. Ruedenberg and W.H.E. Schwarz, Invited Chapter 1, pages 1-45, in the book "Pioneers of Quantum Chemistry" (T. Strom and A. Wilson Editors, American Chemical Society, ACS Symposium Series 1122, 2013)

*Unusual Inorganic Biradicals*

E. Miliordos, K. Ruedenberg, S. S. Xantheas, Angewandte Chemie, accepted

*The Physical Origin of Covalent Binding*

K. Ruedenberg, M. W. Schmidt, J. Ivanic, Invited Chapter 1 (50 pages) in the book "The Nature of the Chemical Bond Revisited" (G. Frenking and S. Shaik Editors, Wiley-VCH, 2013), accepted



## Active Thermochemical Tables – Progress Report

Branko Ruscic

Chemical Sciences and Engineering Division, Argonne National Laboratory,  
9700 South Cass Avenue, Argonne, IL 60439  
ruscic@anl.gov

### Program Scope

The *spiritus movens* of this program is the need to provide the scientific community with accurate and reliable thermochemical information on chemical species that are relevant in combustion, or play prominent roles in the related post-combustion environmental chemistry, thus contributing to the comprehension of the underlying chemical reactions, providing the necessary thermochemical base for their quantitative modeling, as well as furnishing reliable benchmark values that act as an impetus for further development, improvement, and testing of state-of-the-art theoretical electronic structure approaches. Thermochemistry is, in fact, one of the essential underpinning scientific domains that is enabling DOE to successfully interpret, analyze, model, and optimize energy-producing chemical reactions and thus fulfill its mission, and has, as such, established itself as a long-term component of the DOE BES research program. The current focus of this program is on bringing substantial innovations to the field of thermochemistry through the development of new tools and methodologies, and utilizing these new approaches to systematically advance both the quality and quantity of available thermochemical data relevant to energy-producing processes. In order to accomplish the stated goals, this program has undertaken the development of a novel approach that is centered on the idea of analyzing and optimally utilizing the information content of all available thermochemically relevant measurements. The aim of these developments is not only to dynamically produce *the best currently possible* thermochemical parameters for the targeted chemical species, but also to allow *efficient updates with new knowledge*, properly propagating its consequences through all affected chemical species, as well as to provide *critical tests of new experimental or theoretical data*, and, when possible, to develop *pointers to future determinations that are likely to most efficiently improve the overall thermochemical knowledge base*. In order to provide a broad perspective of this area of science, the effort of this program is synergistically coordinated with related experimental and theoretical efforts within the Gas-phase Chemical Dynamics Group at Argonne.

### Recent Progress

#### Development of Active Thermochemical Tables and the Core Thermochemical Network

Over the past year we have continued the development of various aspects of Active Thermochemical Tables (ATcT) together with improving both the quantity and quality of the resulting thermochemical values. ATcT are a novel paradigm of how to develop accurate, reliable, and internally consistent thermochemical quantities for stable, reactive, and transient chemical species by utilizing to the fullest all available experimental measurements as well as high-accuracy state-of-the-art theoretical results. Traditional sequential thermochemistry develops thermochemical values in discrete steps that focus on a single target species at the time, and produces sets of values that are plagued by hidden progenitor-progeny relationships and thus are impossible to update with new knowledge without introducing serious inconsistencies. In contrast to the sequential approach, ATcT is based on analyzing and simultaneously solving a Thermochemical Network (TN) that (typically) involves a large number of species. Even at the dawn of quantitative thermochemistry it must have been clear that crucial thermodynamical properties of various chemical species are underpinned by massive interdependencies, which should be simultaneously satisfied by the ‘proper’ thermochemical values.

Multiple interdependencies were historically considered as a generally intractable complication (at least partly because of the absence of adequate computational hardware), leading to the adoption of a simplified sequential approach to thermochemistry (A begets B, B begets C, etc). In spite of the fact that this results in discarding most of the information embedded in the simultaneous interdependences, the sequential approach has persisted as the prevailing state of affairs even as speed and bandwidth of modern information-processing capabilities grew exponentially with time. The quantum leap in quality and reliability of the thermochemical values resulting from the ATcT approach is rooted in readdressing the original problem and organizing the underlying interdependencies in a Thermochemical Network amenable to explicit mathematical and statistical manipulation that leverage the inherent information content to its fullest.

The ATcT effort has two essential fronts: the development of the ATcT methodology and the development of the underlying Thermochemical Network and other thermochemically-relevant data on which ATcT operates. On the methodology front, we have now fully developed a variance/covariance decomposition approach that further enhances the ATcT capabilities. Namely, if the Thermochemical Network includes  $m$  thermochemically-relevant determinations that describe  $n$  chemical species (currently,  $n \approx 1000$  and  $m \approx 15000$ ), then the essential final product of the ATcT analysis is a vector of size  $n$  containing the desired enthalpies of formation of the targeted species and a symmetric covariance matrix of size  $n \times n$  that provides  $n$  uncertainties for the optimized enthalpies of formation and  $n \times (n-1)/2$  covariances that indicate how tightly the resulting enthalpies are correlated (or anticorrelated). While condensing the initial  $m \times n$  problem contained in the Thermochemical Network to an  $n \times n$  problem significantly speeds up the ATcT numerical processing, detailed information on how exactly each of the  $m$  thermochemically-relevant determinations influences the  $n$  resulting enthalpies is lost. By carefully analyzing and dissecting the underlying matrix operations, we have now devised an expanded approach that, without adding a significant computational burden, produces an additional  $n \times n \times m$  covariance cube, i.e. it decomposes the overall  $n \times n$  covariance matrix into  $m$  discrete layers, where each layer corresponds to an  $n \times n$  matrix that quantifies the contribution of a single TN determination to the final result. The sum over all  $m$  layers corresponds exactly to the overall  $n \times n$  covariance matrix. This development opens up the possibilities for a number of additional ATcT analyses, many of which we are still exploring. We are, for example, exploring the possibility of using the variance/covariance decomposition as a tool that allows us to prune down the Thermochemical Network, i.e. further alleviate the computational burden by identifying and eliminating determinations that do not significantly contribute to the knowledge content of the Thermochemical Network. We hope that in future developments this variance/covariance decomposition approach may also enable us to partially automate the search for 'weak links' and/or pointers to desired determinations. The immediately obvious ramification of the variance/covariance decomposition is that now we can entirely quantitatively determine the full provenance of each ATcT enthalpy of formation. In general, while the enthalpies of formation obtained in a traditional sequential approach are extremely highly mutually correlated and are exceedingly dependent on a small set of select determinations, the ATcT enthalpies of formation are substantially less mutually correlated and their provenance is typically much more delocalized. Inspection of recent ATcT runs strongly suggests that provenance delocalization reduces both the variance and covariance of the involved species, and is thus the inherent advantage that provides ATcT the capability of producing results that are significantly more accurate and reliable than those obtained by sequential thermochemistry, even in extreme situations when there are no new substantial determinations involving a particular target species.

We have previously reported on the development of a number of additional software tools that enable us to gradually replace the respective RRHO (rigid rotator, harmonic oscillator) partition functions with NRRAO (nonrigid rotator, anharmonic oscillator) partition functions, either by including

various additional corrections that influence the thermochemistry at temperatures relevant in combustion processes (such as, for example, anharmonicity, centrifugal stretching, internal rotation) or by replacing the related RRHO contribution with contributions obtained by level counting. Note that as opposed to bond dissociation energies, reaction enthalpies, etc. that are contained in the Thermochemical Network, partition function related properties, such as heat capacity, entropy, and enthalpy increments are species-specific data and generally does not lend itself particularly well to the ATcT analysis that exploits inter-species dependencies. We have originally hoped to simply import these species-specific properties from traditional compilations, but have time and again concluded that the imported data leaves a lot to be desired, effectively not only limiting the accuracy of the final ATcT results, but also severely confining their accuracy and reliability in combustion applications. We have now completed a lengthy process of replacing the RRHO partition functions and the imported NRRAO partition functions that were based on outdated data with newly calculated and fully corrected partition functions for all  $H_nO_m$  species relevant in combustion and in atmospheric chemistry. The new set of partition functions allowed us to produce definitive ATcT thermochemistry for this group of species, and we are currently in the process of writing up the results for formal publication. These results are highly relevant to the thermochemistry involved in  $C_0$  combustion mechanisms and involve, *inter alia*, no less than 80 JANAF-style tables (replacing, for example, two entire chapters in the thermochemical tables of Gurvich et al.).

While the primary focus was on improving the existing ATcT data by producing NRRAO partition functions for  $H_nO_m$  species, we have also invested a significant effort into expanding the Thermochemical Network to include  $C_3H_n$  species relevant in combustion. We have now completed the first phase of this expansion and believe to have very reasonable 0 K enthalpies of formation for this group. The expansion with  $C_3H_n$  species started as a partial collaboration with R. Sivaramakrishnan and J. V. Michael (ANL) that targeted a few select species, but subsequently expanded into a separate effort attempting to cover nearly all species from this group. In a somewhat related effort, we are collaborating with S. Klippenstein to systematically produce reliable thermochemistry for all chemical species involved in the  $C_0$  through  $C_3$  hierarchy of combustion chemical mechanisms. For this effort we are synergistically combining the best aspects of highly accurate theoretical approaches (with the aim to provide values for species not currently covered by ATcT) and ATcT (currently supplying values that benchmark the theoretical approach, but will in a second step result in an expansion of the Thermochemical Network by including these new theoretical determinations).

We also have an ongoing collaborative effort (E. Goos, DLR) that addresses the species involved in  $NO_x$  formation mechanisms, which recently resulted in showing the importance of the NCN species and the reevaluation of its thermochemistry. We are also currently intensely working with A. Burcat (Technion) and E. Goos (DLR) on continuously updating the widely used Goos/Burcat/Ruscic database with available ATcT results.

### Future Plans

Future plans of this program pivot around further developments and expansive use of Active Thermochemical Tables, providing accurate thermochemistry, and driving targeted theoretical and laboratory experimental investigation of radicals and transient species that are intimately related to combustion processes as well as post-combustion atmospheric processes. A significant part of the effort during the forthcoming period will be devoted to continued ‘finalization’ and dissemination of the resulting ATcT thermochemistry. A necessary component of the ‘finalization’ of results for groups of related chemical species consists of testing and analyzing in detail their TN dependencies (in part using the newly developed variance/covariance decomposition approach) as well as enhancing the accuracy of their partition functions (by gradually replacing them with new NRRAO

partition functions), and, when suggested by ATcT analyses, adding new high-quality results (either virtual, i.e. computational, or actual, i.e. experimental) to coerce the resulting thermochemistry toward stable, ‘release quality’ values. This iterative process will also result in an expansion of the number of species that belong to the ‘release quality’ category. Another important component in the dissemination of ATcT results is the continuation of the current effort of designing and producing an entirely computer-generated ATcT web site that will be populated by ‘release quality’ results automatically by a suitable post-processing step of ATcT. Besides full automation with archival capability, an additional desideratum for an improved ATcT website is the automatic inclusion of sufficient background information that will document the pedigree for every recommended thermochemical value, providing proper credit to the actual original (experimental and/or theoretical) determination(s) that are responsible for the final ATcT value. Finally, a significant long-term component of future progress in this area will consist of building a second generation of ATcT software. This will be based on a thorough redesign of the current ATcT software, with the aim of making the software not only significantly more streamlined and efficient, but also allowing sufficient flexibility that will enable the adoption and utilization of emerging computing technologies as they become available.

*This work is supported by the U.S. Department of Energy, Office of Basic Energy Sciences, Division of Chemical Sciences, Geosciences, and Biosciences, under Contract No. DE-AC02-06CH11357.*

#### **Publications resulting from DOE sponsored research (2010 – present)**

- *Rate Constants for the Thermal Decomposition of Ethanol and Its Bimolecular Reactions with OH and D: Reflected Shock Tube and Theoretical Studies*, R. Sivaramakrishnan, M.-C. Su, J. V. Michael, S. J. Klippenstein, L. B. Harding, and B. Ruscic, *J. Phys. Chem. A* **114**, 9425-9439 (2010).
- *The Heats of Formation of C<sub>6</sub>H<sub>5</sub>, C<sub>6</sub>H<sub>5</sub><sup>+</sup>, and C<sub>6</sub>H<sub>5</sub>NO by TPEPICO and Active Thermochemical Tables Analysis*, W. R. Stevens, B. Ruscic, and T. Baer, *J. Phys. Chem. A* **114**, 13134–13145 (2010).
- *Shock Tube and Theoretical Studies on the Thermal Decomposition of Propane: Evidence for a Roaming Radical Channel*, R. Sivaramakrishnan, M.-C. Su, J. V. Michael, S. J. Klippenstein, L. B. Harding, and B. Ruscic, *J. Phys. Chem. A* **115**, 3366-3379 (2011).
- *Extended Third Millennium Ideal Gas and Condensed Phase Thermochemical Database for Combustion with updates from Active Thermochemical Tables*, E. Goos, A. Burcat and B. Ruscic, *progressive updates of thermochemical polynomials available at <ftp://ftp.technion.ac.il/pub/supported/aetdd/thermodynamics/> (also mirrored at <http://garfield.chem.elte.hu/Burcat/burcat.html>), and available from DLR webpage <http://www.dlr.de/vt/> (2012-2013).*
- *Inhibition of Hydrogen Oxidation by HBr and Br<sub>2</sub>*, G. Dixon-Lewis, P. Marshall, B. Ruscic, A. Burcat, E. Goos, A. Cuoci, A. Frassoldati, T. Faravelli, and P. Glarborg, *Combust. Flame* **159**, 528-540 (2012).
- *High-Temperature Rate Constants for H/D + C<sub>2</sub>H<sub>6</sub> and C<sub>3</sub>H<sub>8</sub>*, R. Sivaramakrishnan, J. V. Michael, and B. Ruscic, *Int. J. Chem. Kin.* **44**, 194-205 (2012).
- *Near-threshold shape resonance in the photoionization of 2-butyne*, H. Xu, U. Jacovella, B. Ruscic, S. T. Pratt, and R. R. Lucchese, *J. Chem. Phys.* **136**, 154303/1-10 (2012).
- *Prompt NO formation in flames: The influence of NCN thermochemistry*, E. Goos, C. Sickfeld, F. Mauss, L. Seidel, B. Ruscic, A. Burcat, and T. Zeuch, *Proc. Comb. Inst.* **34**, 657-666 (2013).

# Gas-Phase Molecular Dynamics: High Resolution Spectroscopy and Collision Dynamics of Transient Species

Trevor J. Sears

Department of Chemistry, Brookhaven National Laboratory

Upton, NY 11973-5000

[sears@bnl.gov](mailto:sears@bnl.gov)

## Program Scope

This research is carried out as part of the Gas-Phase Molecular Dynamics program in the Chemistry Department at Brookhaven National Laboratory. High-resolution spectroscopic methods, augmented by theoretical and computational work, are used to investigate the structure, collision dynamics and chemical behavior of intermediates in the elementary gas-phase reactions involved in combustion chemistry. There is an emphasis on new technique development with the aim of improving both the sensitivity and resolution of spectroscopic measurements.

## I. Recent Progress

### A. Spectroscopy with comb-stabilized extended cavity diode lasers

Recently designed frequency comb-referenced spectrometers are now permitting spectroscopic measurements with previously unprecedented precision and accuracy. Using the newly developed instruments we are developing new insights and can attack new problems in molecular structure and dynamical processes.

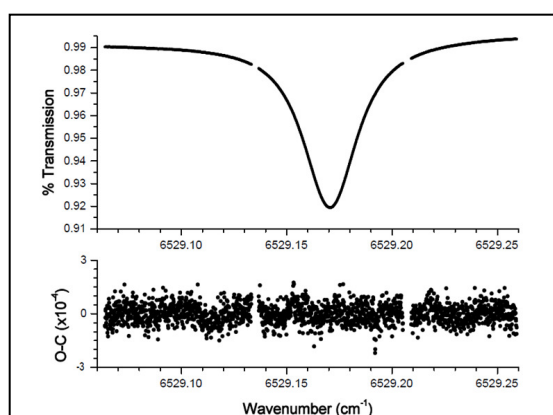


Fig. 1: Transmission spectrum of the acetylene P(11) line at 160 K, 74.3 Torr 0.3% C<sub>2</sub>H<sub>2</sub> in N<sub>2</sub>. Bottom panel show residuals (O-C) resulting from least squares multispectrum fitting of experimental data to a speed-dependent Voigt line profile model.

For example, precision line-shape measurements are leading to a greater understanding of the relative importance of different collision-induced processes in molecular systems as detailed in G. Hall's abstract elsewhere in this collection. The measurement of line shapes is also important for the spectroscopic and analytical communities because precise characterization is needed for accurate determinations of species concentrations. We have continued our measurements of acetylene perturbed by both self- and nitrogen molecule-collisions as a function of temperature. An example of some recent measurements is shown in Figure 1. The obvious gaps in the scan are the result of concatenating several separate scans and illustrate the reproducible accuracy of the spectrometer. Several general conclusions have been reached as a result of the analysis of an

extensive set of temperature and concentration dependent measurements. The first is that the observed line profiles cannot be satisfactorily fit to empirical models that do not include a speed-dependent contribution to the collisional relaxation processes. Secondly, the accuracy of the new measurements has highlighted the importance of the pressure-induced shift in the line center and its temperature dependence. Theory connects the observed broadening and shifts and their temperature dependence and the measurements permit accurate tests of different models for the collisional processes that lead to the observed line-shape changes. Precisely known spectral line shapes are also needed for the determination of species concentrations from

remote sensing measurements, for example. Our understanding of the properties and behavior of laser frequency comb sources continues to evolve and changes made to the spectrometer over the past year have led to more precise control of the laser scanning, faster data acquisition and improved data.

Sub-Doppler measurements allow the determination of accurate line positions as well as permitting otherwise unresolvable spectral lines to be separated. We have continued to develop methods to improve our sensitivity in various saturation dip experiments. Figure 2 shows an example of a recent measurement

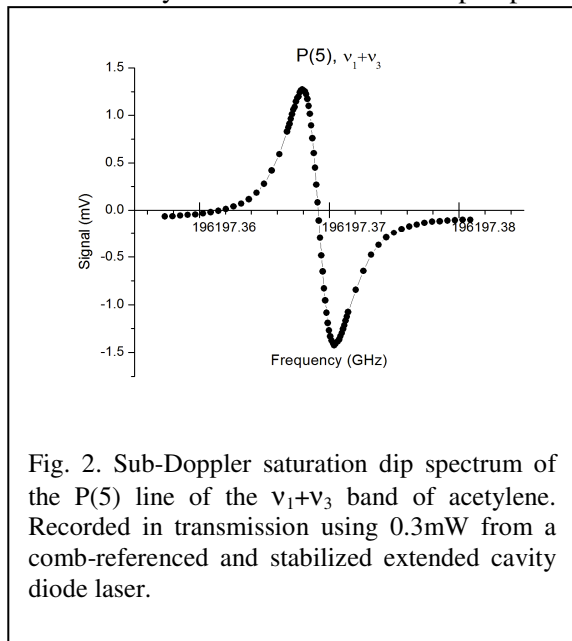


Fig. 2. Sub-Doppler saturation dip spectrum of the P(5) line of the  $\nu_1+\nu_3$  band of acetylene. Recorded in transmission using 0.3mW from a comb-referenced and stabilized extended cavity diode laser.

made in a Fabry-Perot cavity using a low power ECDL locked to the both the cavity and the frequency comb. Careful inspection of the line shape shows that it is very slightly asymmetric and we find this effect increases with higher optical powers. We believe this is due to the second order Doppler effect due to molecules moving transversely to the laser beam in the cavity. This effect, including a contribution from molecules traversing a non-planar optical wave front at the focus of the cavity, has been studied in the optical physics community and is well-understood. For our purposes, accurate line position determinations will have to take into account the precise line shape function. The degree of distortion measured in high signal-to-noise spectra such as shown in the figure may also permit an indirect determination of the squared transition moment integral.

## B. Hyperfine structure in the $B^3\Pi_g-A^3\Sigma_u^+$ band of $N_2$

Continuing the theme of precise spectroscopic line measurements, we have measured hyperfine splittings in selected rotational lines of the (1-0) vibrational band of the  $B^3\Pi_g - A^3\Sigma_u$  transition of  $^{14}N_2$  in a low pressure discharge. Frequency modulated saturation dip spectroscopy produced hyperfine resolved, sub-Doppler lines with typical full-width at half-maximum line widths of 7 MHz. Hyperfine transitions within 27 rotational lines in the R33, Q33, Q21, Q22, R11, and Q11 branches were recorded for J between 2 and 12, and fit with the same Hamiltonian used previously by Geisen, Neuschafer and Ottinger [Z. Phys. D **4**, 263 (1987)]. The resulting parameters are related to the distribution of the unpaired electron density around the nuclei as probed by the expectation of the electron spin and orbital angular momenta. In combination with the results of the reference above, we were able to characterize the vibrational level dependence of the hyperfine parameters. Only the Fermi contact interaction showed significant changes with vibrational level and it was found to have a significant quadratic component to its vibrational dependence

## II. Future Work

### A. Spectroscopy and dynamics of transient species

We have made some preliminary efforts to detect the spectrum of triplet  $C_3$  in a discharge source similar to that used to study metastable nitrogen above. These have so far been unsuccessful, although in published reports the radical has been detected in similar sources. We plan to improve the discharge power

supply to permit operation at higher frequencies where the system noise will be lower. In addition, we plan to search for the expected near-infrared spectra of some small hydrocarbon radicals. In collaboration with Hua-Gen Yu in the group, we have begun a program to calculate the near-infrared spectra of such species, beginning with propargyl,  $C_3H_3$ , which is the main precursor to aromatic radicals and soot production in flames. These species have significant anharmonicity in their vibrational potentials and, by analogy to acetylene, one would expect significant intensity in their overtone and combination vibrational bands in the near-infrared. A sensitive spectroscopic method for detection at these wavelengths would be very convenient because the necessarily smaller transition moments can be more than overcome by better laser and detector technology than in the mid-infrared and electronic spectra of many species are complicated, lie at inconveniently short wavelengths or are predissociative.

Initial calculations on propargyl show that the combination band calculated at  $6334.8\text{ cm}^{-1}$  assigned to  $\nu_1+\nu_9$ , has an intensity of 0.022 relative to the strongest infrared band,  $\nu_1$  at  $3326.9\text{ cm}^{-1}$ . By comparison, the ratio for  $\nu_3$  and  $\nu_1+\nu_3$  combination in acetylene is 0.064 from experiment, showing that the strongest near infrared band in propargyl is broadly comparable to that of acetylene in its strength. The propargyl  $\nu_1$  infrared spectrum was detected and assigned by Curl and co-workers [L. Yuan, J. DeSain and R. F. Curl, *J. Molec. Spectrosc.* **187**, 102 (1998)]. Using the same photolytic route for production, we anticipate that the predicted near infrared band should be easily detectable in our spectrometers. By analogy, other important combustion radicals such as methyl and vinyl should also be detectable this way.  $C_2H$  has a low-lying electronic excited state which makes its infrared and near-infrared spectra anomalously strong. [W.B. Yan et al. *J. Molec. Spectrosc.* **123**, 986, (1987)].

## B. Line shape and sub-Doppler measurements

Line shape measurements using the comb referenced spectrometer are producing data resulting in pressure broadening and shift parameters that are some two to three orders of magnitude more precise than any previously published. This means that effects such as the rotational level dependence of the collisionally perturbed line shapes can now be determined far more precisely than before and provides a window into the rotational dependence of collisional processes not previously available. Some initial work on CN radical along these lines is described in G. Hall's abstract. We will extend these measurements to the acetylene  $\nu_1+\nu_3$  spectrum which is a prototype for high resolution line shape studies. While comparatively simple, this spectrum also contains examples of overlapped lines at Doppler resolution and thus is also useful for the characterization of line mixing effects whereby collisional coupling between overlapped lines causes non-linear effects on the observed line shape.

Following the precise characterization of the sub-Doppler line shapes observed in a Fabry-Perot cavity we will measure rest frequencies for a series of hot band lines in the acetylene spectrum. Many of these overlap the stronger fundamental lines and the relatively poor knowledge of the hot band line frequencies affects the accuracy of line profile extractions. Experience gained in this work will carry over to future measurements of free radical spectra.

### III. Publications supported by this project since 2011

- The CH<sub>2</sub>  $\tilde{b}^1B_1 - \tilde{a}^1A_1$  band origin at 1.20 $\mu$ m, C.-H. Chang, J. Xin, T. Latsha, E. Otruba, Z. Wang, G. E. Hall and T. J. Sears, *J. Phys. Chem. A*, **115**, 9440-9446 (2011).
- Transient laser absorption spectroscopy of CH<sub>2</sub> near 780 nm, C.-H. Chang, Z. Wang, G. E. Hall, T. J. Sears and J. Xin, *J. Molec. Spectrosc.* **267**, 50-57 (2011).
- Frequency comb-referenced measurements of self- and nitrogen-broadening in the  $\nu_1 + \nu_3$  band of acetylene, C. P. McRaven, M. J. Cich, G. V. Lopez, T. J. Sears, D. Hurtmans and A. W. Mantz, *J. Molec. Spectrosc.* **266**, 43-51 (2011).
- Precision spectroscopy of the  $^{207}\text{Pb}^{19}\text{F}$  molecule: implications for measurement of P-odd and T-odd effects, L. D. Alpei, J.-U Grabow, A. N. Petrov, R. Mawhorter, B. Murphy, A. Baum, T. J. Sears, T. Zh. Yang, P. M. Rupasinghe, C. P. McRaven and N. E. Shafer-Ray, *Phys. Rev. A* **83** 040501 (2011).
- Precise characterization of the ground X<sub>1</sub> state of  $^{206}\text{Pb}^{19}\text{F}$ ,  $^{207}\text{Pb}^{19}\text{F}$  and  $^{208}\text{Pb}^{19}\text{F}$ , R. Mawhorter, B. Murphy, A. Baum, T. J. Sears, T. Zh. Yang, P. M. Rupasinghe, C. P. McRaven, N. E. Shafer-Ray, L. D. Alpei and J.-U. Grabow, *Phys. Rev. A* **84** 022508(12) (2011).
- Temperature-dependent pressure broadened line shape measurements of self- and nitrogen-broadening in the  $\nu_1 + \nu_3$  band of acetylene, M. J. Cich, C. P. McRaven, G. V. Lopez, T. J. Sears, D. Hurtmans and A. W. Mantz, *Appl. Phys. B*, **109**, 373-384 (2012).
- What is the best DFT function for vibronic calculations? A comparison of the calculated vibronic structure of the S<sub>1</sub> – S<sub>0</sub> transition of phenylacetylene with accurate experimental band intensities, G. V. Lopez, C.-H. Chang, P. M. Johnson, G. E. Hall, T. J. Sears, B. Markiewicz, M. Milan and A. Teslja, *J. Phys. Chem. A* **116**, 6750-6758 (2012).
- Hyperfine structures in the  $\nu=1-0$  vibrational band of the B<sup>3</sup> $\Pi_u - A^3\Sigma^+_u$  of N<sub>2</sub>, D. Forthomme, C. P. McRaven, G. E. Hall, and T. J. Sears. *J. Molec. Spectrosc.* **282**, 50-55 (2012).
- Argon-induced pressure broadening, shifting and narrowing in the CN A<sup>2</sup> $\Pi - X^2\Sigma^+$  (1-0) band, D. Forthomme, C. P. McRaven, T. J. Sears, and G. E. Hall. (submitted).

# Theoretical Studies of Potential Energy Surfaces and Computational Methods

Ron Shepard

Chemical Sciences and Engineering Division,  
Argonne National Laboratory, Argonne, IL 60439  
[email: shepard@tcg.anl.gov]

**Program Scope:** This project involves the development, implementation, and application of theoretical methods for the calculation and characterization of potential energy surfaces (PES) involving molecular species that occur in hydrocarbon combustion. These potential energy surfaces require an accurate and balanced treatment of reactants, intermediates, and products. This difficult challenge is met with general multiconfiguration self-consistent field (MCSCF) and multireference single- and double-excitation configuration interaction (MR-SDCI) methods. In contrast to the more common single-reference electronic structure methods, this approach is capable of describing accurately molecular systems that are highly distorted away from their equilibrium geometries, including reactant, fragment, and transition-state geometries, and of describing regions of the potential surface that are associated with electronic wave functions of widely varying nature. The MCSCF reference wave functions are designed to be sufficiently flexible to describe qualitatively the changes in the electronic structure over the broad range of molecular geometries of interest. The necessary mixing of ionic, covalent, and Rydberg contributions, along with the appropriate treatment of the different electron-spin components (e.g. closed shell, high-spin open-shell, low-spin open shell, radical, diradical, etc.) of the wave functions are treated correctly at this level. Further treatment of electron correlation effects is included using large-scale multireference CI wave functions, particularly including the single and double excitations relative to the MCSCF reference space. This leads to the most flexible and accurate large-scale MR-SDCI wave functions that have been used to date in global PES studies.

**Recent Progress:** ELECTRONIC STRUCTURE CODE MAINTENANCE, DEVELOPMENT, AND APPLICATIONS: A major component of this project is the development and maintenance of the COLUMBUS Program System. The COLUMBUS Program System computes MCSCF and MR-SDCI wave functions, MR-ACPF (averaged coupled-pair functional) energies, MR-AQCC (averaged quadratic coupled cluster) energies, spin-orbit CI energies, analytic energy gradients, and nonadiabatic coupling. Geometry optimizations to equilibrium and saddle-point structures can be done automatically for both ground and excited electronic states. The COLUMBUS Program System is maintained and developed collaboratively with several researchers including Isaiah Shavitt (University of Illinois, deceased December 2012), Russell M. Pitzer (Ohio State University), Thomas Mueller (Jülich Supercomputer Center, Germany), and Hans Lischka (University of Vienna, Austria, and Texas Tech University). The nonadiabatic coupling and geometry optimizations for conical intersections is done in collaboration with David R. Yarkony (Johns Hopkins University). The distributed development effort and software coordination uses an svn repository of source code. The parallel sections of the code are based on the single-program multiple-data (SPMD) programming model

This work was performed under the auspices of the Office of Basic Energy Sciences, Division of Chemical Sciences, Geosciences, and Biosciences, U.S. Department of Energy, under contract number DE-AC02-06CH11357.

with explicit message passing using the portable MPI library, and the portable Global Array Library (distributed from PNNL) is used for data distribution. The COLUMBUS codes incorporate several of the newer language features of F90 and later in order to facilitate future development and maintenance efforts.

**REVIEW OF MULTIREFERENCE METHODS:** In the past year we have published two major invited review articles on multireference methods. The first [*Advanced Series in Physical Chemistry*, **17** pp. 415-462 (World Scientific, Singapore, 2011)] is an overview of applications and methodology of nonadiabatic coupling and nonadiabatic direct dynamics using multireference methods. The second [*Chem. Rev.* **112**, 108-181 (2012)] is a general review with 860 references of the MCSCF, MRCI, MR-ACPF, MR-AQCC, and related methods and applications over the past decade.

**GRAPHICALLY CONTRACTED FUNCTION METHOD:** We have recently developed a novel expansion basis for electronic wave functions [see *Mol. Phys.* **108**, 2717 (2010) and references therein]. In this approach, the wave function is written as a linear combination of *graphically contracted functions* (GCFs), and each GCF in turn is formally equivalent to a linear combination of configuration state functions (CSFs) that comprise an underlying linear expansion space of dimension  $N_{\text{csf}}$ . The CSF coefficients that define the GCFs are nonlinear functions of a smaller number of variables  $N_{\phi} \ll N_{\text{csf}}$ . GCF expansions with 10 to 20 basis functions can approach the full-CI PES to within chemical accuracy (1 kcal/mole or better) [*Int. J. Quantum Chem.* **107**, 3203 (2007)]. The method is formulated in terms of spin-eigenfunctions using the Graphical Unitary Group Approach (GUGA) of Shavitt, and consequently it does not suffer from spin contamination or spin instability.

This new method is characterized by several important features. First, open-shell spin-eigenfunctions are included in the wave function expansions. This allows our new method to be used for the chemical reactions that are important to combustion chemistry (e.g. involving radicals and other open-shell electronic states) without introducing artificial spin contamination. Second, no intrinsic restrictions are imposed on the orbital occupations, so the GCFs are not restricted to only geminals or to other preselected molecular fragments, and there are no artificial excitation-level or occupation restrictions with respect to a reference function or reference space; in this sense, the method is more correctly characterized as a multiconfigurational method rather than a multireference method. Third, we use linear combinations of  $N_{\text{GCF}}$  basis functions rather than a single expansion term. This allows our method to be used for both ground and excited electronic states, the increased wave function flexibility leads to more accurate wave functions, and it will allow the computation of transition moments, nonadiabatic coupling, and other properties that at present can only be computed reliably with MCSCF and MRCI approaches.

In the past year our focus has been on the development and implementation of a *multifacet* generalization of the GCF method. In the previous implementations, a single lower- or upper-walk, recursively contracted, wave function is associated with each node of the Shavitt graph within a GCF basis function; we now term this the *single-facet* GCF approach. With the multifacet approach, each MFGCF basis function has more flexibility than a SFGCF function. This increased flexibility allows accurate wave functions to be represented with smaller  $N_{\text{GCF}}$  expansion dimensions. This reduces the  $N_{\text{GCF}}^2$  factor in the effort required for Hamiltonian matrix element, reduced density matrix (RDM) elements,

and other computational tasks. A general feature of the new method is that arithmetic operations that previously involved scalars are replaced with matrix-vector and matrix-matrix products where the matrix dimensions depend on the number of facets associated with the nodes;  $f_k^P$  denotes the number of facets for node  $k$  in the GCF  $|P\rangle$ . Thus the computational effort associated with more flexible wave functions increases with larger  $f_k$  values rather than with larger  $N_{\text{GCF}}$  values alone. The efficient recursive algorithms developed previously for the SFGCF approach carry over in a straightforward way for MFGCF expansions. For the new MFGCF method, we have fully implemented the computation of Hamiltonian matrix elements, 1-RDM, 2-RDM [*J. Phys. Chem. A* **110**, 8880 (2006)], spin-Density matrices [*Int. J. Quantum Chem.* **109**, 3552 (2009)], CSF overlaps [*J. Phys. Chem. A* **109**, 11629 (2005)], Slater determinant overlaps [*J. Comp. Chem.* **30**, 2414 (2009)], and the computation of the optimization gradient for the optimization of the nonlinear arc factor parameters [*Int. J. Quantum Chem.* **110**, 2938 (2010)]. We have succeeded in optimizing some wave functions for a few particular cases with the multifacet expansion. From this limited set of initial calculations we can report that for a given wave function accuracy, the maximum number of facets  $f_{\text{max}}$  in the MFGCF basis is usually smaller than the number of basis functions  $N_{\text{GCF}}$  with the corresponding SFGCF basis. In principle, there is an exponential bound relationship between these two parameters,  $N_{\text{GCF}} \leq (f_{\text{max}})^n$  where  $n$  is the number of molecular orbitals, but the observed relation between these quantities is milder. A comparison of these two expansions is shown in Fig. 1 for the ground state  $\text{N}_2(^1\Sigma_g^+) \rightarrow 2\text{N}(^4\text{S})$  dissociation curve. We expect to extend the range of applications over the next year as this new implementation matures and as we formulate more robust optimization approaches.

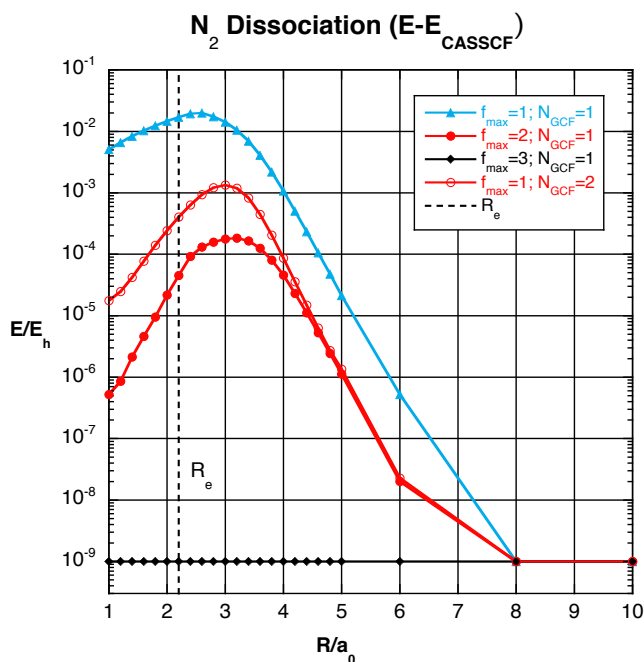


**Fig. 1.** Errors for the ground state  $\text{N}_2(^1\Sigma_g^+) \rightarrow 2\text{N}(^4\text{S})$  dissociation curve for the  $6^6$  Shavitt graph SFGCF and MFGCF wave function expansions relative to the (exact) CASSCF linear expansion. The important differences are seen for the  $N_{\text{GCF}}=2$  SFGCF and the  $f_{\text{max}}=2$  MFGCF curves, for which the MFGCF maximum error is about an order of magnitude smaller than the SFGCF maximum error. Both expansions reproduce the CASSCF curve exactly when  $N_{\text{GCF}}=f_{\text{max}}=3$ .

**Future Plans:** GCF METHOD: Our MFGCF implementation has so far used single-headed Shavitt graphs appropriate for describing individual molecular states with a given number of electrons, with a particular spin state, and that belong to a particular point

group irreducible representation (irrep). We will generalize this in several respects. First, we will introduce state averaging over individual irreps and state averaging over multiple irreps. This will allow the nonlinear arc factor parameters to be optimized for several electronic states simultaneously rather than for individual electronic states. For the multiple-irrep case, this will allow the computation of several molecular states with essentially no additional effort over single-irrep calculations. Next, we will employ multiheaded Shavitt graphs in the state-averaging procedure. This will allow the computation of Hamiltonian matrix elements corresponding to states with different numbers of electrons, different spin values, and different irreps simultaneously with only a relatively small increase in effort over the current single-state approach.

The GCF code has now been placed in a development branch of the COLUMBUS svn repository. In this way the code is now available for a wider range of inspection and scrutiny by COLUMBUS developers. We hope to develop a robust implementation and incorporate the GCF method into the standard distribution version of COLUMBUS for even wider use by the broader user community for general chemical applications in the near future.

### **Publications:**

“COLUMBUS—A Program System for Advanced Multireference Theory Calculations,” H. Lischka, T. Müller, P. G. Szalay, I. Shavitt, R. M. Pitzer, R. Shepard, *WIREs Comput. Mol. Sci.* **1**, 191 (2011).

“Computational and Methodological Elements for Nonadiabatic Trajectory Dynamics Simulations of Molecules,” M. Barbatti, R. Shepard, and H. Lischka, in “Conical Intersections: Theory, Computation and Experiment”, W. Domcke, D.R. Yarkony and H. Köppel, Eds., *Advanced Series in Physical Chemistry*, **17** (World Scientific, Singapore, 2011) pp. 415-462.

“Reduced Density Matrices Within the Graphically Contracted Function Method,” R. L. Shepard, *Abstracts of Papers of the American Chemical Society* **242**, 278-PHYS (2011).

“Multiconfiguration Self-Consistent Field and Multireference Configuration Interaction Methods and Applications,” P. G. Szalay, T. Mueller, G. Gidofalvi, H. Lischka, R. Shepard, *Chem. Rev.* **112**, 108-181 (2012).

“The Multiradical Character of One- and Two-Dimensional Graphene Nanoribbons,” F. Plasser, H. Pašalić, M. H. Gerzabek, F. Libisch, R. Reiter, J. Burgdörfer, T. Müller, R. Shepard, and H. Lischka, *Angewandte Chemie International Edition* **52**, (2013).

“Der Multiradikalcharakter ein- und zweidimensionaler Graphen-Nanobänder,” F. Plasser, H. Pašalić, M. H. Gerzabek, F. Libisch, R. Reiter, J. Burgdörfer, T. Müller, R. Shepard, and H. Lischka, *Angewandte Chemie* **125**, (2013).

# Mechanisms and Models for Combustion Simulations

Raghu Sivaramakrishnan

Chemical Dynamics Group, Chemical Sciences & Engineering Division

Argonne National Laboratory, Argonne, IL 60439

[raghu@anl.gov](mailto:raghu@anl.gov)

## I. Program Scope

Mechanisms describing the combustion chemistry of even simple fuels can be complex involving a myriad of unimolecular and bimolecular elementary steps. The primary scope of this program is to develop and validate detailed chemical kinetics mechanisms and models for use in simulations for combustion.

The kinetics models will be developed on the basis of a consistent framework incorporating theoretical predictions, experimental measurements, and evaluations of elementary reaction rate coefficients, with feedback loops between them. The detailed models will subsequently be used for simulations of data from reactors, shock-tubes, rapid compression machines, and flames with the aim of validating the mechanistic and kinetic aspects of these models over practical combustion regimes.

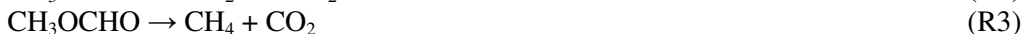
## II. Recent Progress

### A. The High Temperature Thermal Decomposition Mechanism of Methylformate

Biodiesel is a prevalent alternative that can be used as a neat fuel or in blends with conventional fuels. In either case, it offers substantial emissions advantages in compression ignition engines [1, 2]. Typically, biodiesel derived from soybean oil (primary source in US) or rapeseed oil (major source in Europe) consists of varying amounts of C<sub>16</sub>-C<sub>18</sub> saturated and unsaturated methyl esters. Methyl ester combustion chemistry has therefore been the subject of numerous experimental and modeling studies over the past few years [3, 4]. Unlike alkane combustion, where detailed chemistry modeling relied on an extensive database of elementary kinetics information, methylester kinetics is still in an age of infancy with studies largely spurred by analogy based modeling efforts. This is particularly evident even in the chemical kinetics of the thermal decomposition of the simplest methylester, methylformate (MF). Despite being the subject of numerous early gas phase and photolysis studies [5-7], there is surprisingly not a single report of measured rate constants in MF. The later studies agree with Steacie's [5] mechanistic predictions that the favored decomposition channel is CO elimination through (R1),



While reaction (R1) is well established as the dominant decomposition channel in MF, recent modeling and experimental studies [8,9] appear to differ from theoretical predictions [10,11] on the magnitude of the activation energies and rate constants for the minor decomposition channels (R2) and (R3),



The experimental and modeling studies [8,9] indicate that the activation energies for all three processes, (R1)-(R3) are ~ 60 kcal/mol. This is in stark contrast to the predictions from the two recent theoretical studies [10,11] that suggest barrier heights ~ 68, 76 and 83 kcal/mol for (R1) – (R3) respectively.

The present modeling study in collaboration with M. J. Davis (Argonne) was primarily driven by the need to understand the source of these substantial discrepancies between experiments and theory. Our preliminary model for MF pyrolysis relies on our recent a-priori theoretical kinetics estimates [11] for all the important molecular and bond fission processes (see Fig 1. for CH<sub>3</sub>OCHO PES at CCSD(T)/CBS(tz-qz)//B3LYP/6-311++G(d,p) level of theory). Comparisons made by Ren et al. [9] for k<sub>1</sub> indicated that our theoretical predictions [11] were ~ a factor of two lower than the experimental measurements. A reanalysis of our theoretical kinetics with a downward adjustment in barrier height by ~ 0.5 kcal/mol for (R1) gives near perfect agreement with the experimental k<sub>1</sub> and temporal CO profiles measured by Ren et al. [9]. For channel (R2), the Ren et al. [9] k<sub>2</sub> estimates are ~ a factor of 100 larger than our recent

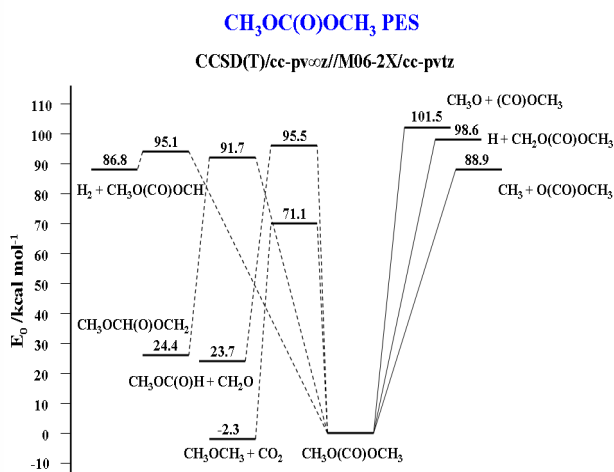
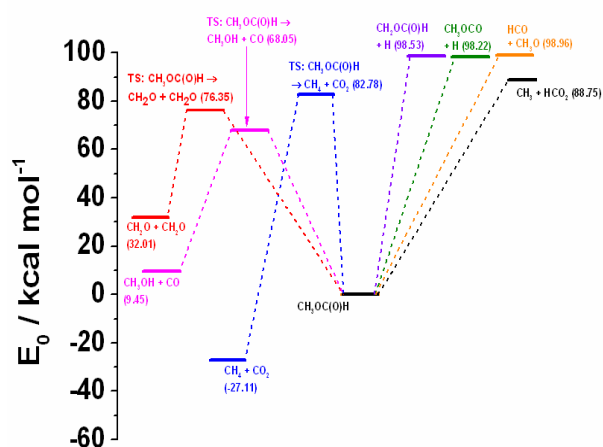


Fig. 1: Potential Energy Surface for Methyl Formate

Fig. 2: Potential Energy Surface for DMC

theoretical estimates [11]. Such a large discrepancy between theory and experiment cannot be merely reconciled by the uncertainties ( $\sim 1$ -2 kcal/mol) in the theoretical barrier heights for (R2). The study by Ren et al. [9] measured  $\text{CH}_2\text{O}$  behind reflected shock waves and assumed that the source of  $\text{CH}_2\text{O}$  was primarily due to (R2). Simulations with our a-priori model for MF pyrolysis indicate that  $\text{CH}_2\text{O}$  in the Ren et al. [9] experiments is produced primarily due to the bimolecular reaction of H-atoms with MF and the subsequent decomposition of the radical through (R4) and (R5),



The Dooley et al. [8] model that was used by Ren et al. to simulate the  $\text{CH}_2\text{O}$  profiles assumed a lower ( $\sim 60$  kcal/mol) activation energy for (R2) than theoretically predicted. This when coupled with substantially lower (by factors of 6-8 at 1 atm in the 1000-2000 K T-range) rate constants in this model [8] for the dominant radical channel in MF pyrolysis (R6),



then leads to the molecular process (R2) being favored and radical processes suppressed. This is also the cause for the presumed discrepancies between theory and experiment for  $k_3$  based on the Ren et al. [9]  $\text{CH}_4$  measurements. As part of this study, we have also reanalyzed the  $\text{C}_2\text{H}_5\text{O}_2$  ( $\text{H} + \text{MF}$ ) [12], and the  $\text{C}_2\text{H}_3\text{O}_2$  ( $\text{CH}_3\text{OCO}$  and  $\text{CH}_2\text{OCHO}$ ) PES's and utilized these to obtain theoretical rate constants for the major propagation reactions in our MF pyrolysis model. The present pyrolysis model for MF will also be extended to describe its high temperature oxidation.

### B. Thermal Decomposition and Abstraction Reactions in Dimethyl Carbonate

In collaboration with J. V. Michael (Argonne) we have initiated a joint experiment/theory study [13] on the thermal decomposition of dimethyl carbonate (DMC),  $\text{CH}_3\text{OC}(\text{O})\text{OCH}_3$ , an highly oxygenated fuel additive. A master equation analysis was performed with a potential energy surface (Fig. 2) calculated at the CCSD(T)/CBS(tz-qz)//M062X/cc-pvtz level of theory for thermal decomposition processes of relevance in DMC. The theoretical predictions were found to be in good agreement with the present experimentally derived rate constants for the energetically lowest-lying bond fission channel (R7),



The present study suggests that the thermal decomposition mechanism in DMC is essentially a two-channel process with the dominant channel being the molecular elimination (R8),



to form dimethyl ether and carbon di-oxide. Channel (R7) is a minor contributor (1-10%) to the thermal kinetics at high temperatures (1000-2000 K).

Joint experiment/theory studies [13,14] on the bimolecular reactions of H and O-atoms with DMC were also performed. At high temperatures, abstraction via channels (R9) and (R10) is the only



kinetically dominant channel in either of these bimolecular reactions. TST calculations using CCSD(T)/CBS(tz-qz)//M062X/cc-pvtz energies and molecular properties for these abstraction reactions are in good agreement with the experimentally measured rate constants.

### *C. Developing detailed and reduced chemical kinetics models for engine simulations*

We continue our collaborations with Michael Davis (Argonne), Sibendu Som and Douglas Longman (Engines & Emissions group at Argonne) and T. F. Lu (Univ. of Connecticut) on developing reduced and detailed kinetics models for realistic engine modeling studies of biodiesel surrogates [15]. We propose to test effects of varying the reactivity for a 1<sup>st</sup> generation biodiesel surrogate (a blend of methyl butanoate and n-heptane) by doping cetane enhancers and inhibitors. We also propose to initiate kinetics modeling studies on dimethylether, DME, as a simple real fuel. A chemical kinetic model for DME can be directly applied in engine simulations without any model reduction thereby allowing for a direct probe of a detailed chemistry model under practical conditions.

### **III. Future work**

We plan to complete our small alcohol (C<sub>1</sub>-C<sub>2</sub>) combustion modeling and theoretical studies and use this experience to focus on developing models in a systematic approach for selected C<sub>3</sub>-C<sub>4</sub> alcohols. We have initiated joint theory and experiment studies on iso-propanol to further our understanding of high temperature alcohol decompositions. Our current efforts on modeling methylformate combustion are expected to lead into systematic modeling studies of larger C<sub>2</sub>-C<sub>4</sub> methylesters. We also propose to continue our modeling efforts on small aromatics such as toluene and xylenes.

### **IV. References**

1. M. S. Graboski, R. L. McCormick, Prog. Energy Combust. Sci. **1998**, 24, 125-164.
2. A. K. Agarwal, Prog. Energy Combust. Sci. **2007**, 33, 233-271.
3. K. Kohse-Hoeinghaus, P. Osswald, T. A. Cool, T. Kasper, N. Hansen, F. Qi, C. K. Westbrook, P. R. Westmoreland, Angew. Chem. Int. Ed. **2010**, 49, 3572- 3597.
4. J. Y. W. Lai, K. C. Lin, A. Violi, Prog. Energy Combust. Sci. **2011**, 37, 1-14 and references within.
5. E. W. R. Steacie, Proc. Roy. Soc. London A **1930**, 127, 314-330.
6. J. K. Royal, G. K. Rollefson, J. Amer. Chem. Soc. **1941**, 63, 1521-1525.
7. D. H. Volman, J. Amer. Chem. Soc. **1942**, 64, 1820-1821.
8. S. Dooley, M. P. Burke, M. Chaos, Y. Stein, F. L. Dryer, V. Pl. Zhukov, O. Finch, J. M. Simmie, H. J. Curran, Int. J. Chem. Kinet. **2010**, 42, 527-549.
9. W. Ren, K.-Y. Lam, S.H. Pyun, A. Farooq, D.F. Davidson, R.K. Hanson, Proc. Combust. Inst. **2013**, 34, 453-461.
10. W. K. Metcalfe, J. M. Simmie, H. J. Curran, J. Phys. Chem. A **2010**, 114, 5478-5484.
11. S. L. Peukert, R. Sivaramakrishnan, M.-C. Su, J. V. Michael, Comb and Flame **2012**, 159, 2312-2323.
12. S. L. Peukert, R. Sivaramakrishnan, M.-C. Su, J. V. Michael, Proc. Combust. Inst. **2013**, 34, 463-471.
13. S. L. Peukert, R. Sivaramakrishnan, and J. V. Michael, In Review (Submitted Dec 2012), J. Phys. Chem. A **2013**.
14. S. L. Peukert, R. Sivaramakrishnan, and J. V. Michael, In Review (Submitted Jan 2013), J. Phys. Chem. A **2013**.
15. R. Sivaramakrishnan, W. Liu, M. J. Davis, S. Som, D. E. Longman, T. F. Lu, Proc. Combust. Inst. **2013**, 34, 401-409.

## V. Journal articles supported by this project 2011-2013

1. R. Sivaramakrishnan, M.-C. Su, and J. V. Michael, "H- and D-atom formation from the pyrolysis of  $C_6H_5CH_2Br$  and  $C_6H_5CD_2Br$ : Implications for high-temperature benzyl decomposition", *Proc. Combust. Inst.* **33**, 243-250 (2011).
2. R. Sivaramakrishnan and J. V. Michael, "Pyrolysis of  $C_6D_5CH_3$ : Rate constants and branching ratios in the high temperature thermal decomposition of toluene", *Proc. Combust. Inst.* **33**, 225-232 (2011).
3. R. Sivaramakrishnan, J. V. Michael, A. F. Wagner, R. Dawes, A. W. Jasper, L. B. Harding, Y. Georgievskii and S. J. Klippenstein, "Roaming radicals in the thermal decomposition of dimethyl ether: Experiment and theory", *Combust. and Flame* **158**, 618-632 (2011).
4. S. L. Peukert, R. Sivaramakrishnan, M.-C. Su, and J. V. Michael, "Experiment and theory on methylformate and methylacetate kinetics at high temperatures: Rate constants for H-atom abstraction and thermal decomposition, *Comb. and Flame* **159**, 2312-2323 (2012).
5. S. L. Peukert, R. Sivaramakrishnan, M.-C. Su, and J. V. Michael, "High temperature rate constants for H/D + methylformate and methylacetate", *Proc. Combust. Inst.* **34**, 463-471 (2013).
6. R. Sivaramakrishnan, W. Liu, M. J. Davis, S. Som, D. E. Longman, and T. F. Lu, "Development of a reduced biodiesel surrogate model for compression ignition engine modeling", *Proc. Combust. Inst.* **34**, 401-409 (2013).
7. S. L. Peukert, R. Sivaramakrishnan, and J. V. Michael, "High temperature shock tube and theoretical studies on the thermal decomposition of dimethylcarbonate and its bimolecular reactions with H and D-Atoms", In Review, *J. Phys. Chem. A* (2013).
8. S. L. Peukert, R. Sivaramakrishnan, and J. V. Michael, "High temperature shock tube studies on the thermal dissociation of  $O_3$  and the reaction of dimethyl carbonate with O-atoms", In Review, *J. Phys. Chem. A* (2013).
9. R. Sivaramakrishnan, J. V. Michael, L. B. Harding and S. J. Klippenstein, "Revisiting the thermal decomposition mechanism of  $CH_3CHO$ ", In Preparation, *J. Phys. Chem. A*, 2013.
10. R. Sivaramakrishnan, N. J. Labbe, W. Liu and M. J. Davis, "A high temperature mechanism for methylformate combustion", In Preparation, *Comb. and Flame*, 2013.
11. D. Polino, C. Cavallotti, R. Sivaramakrishnan, S. J. Klippenstein, J. V. Michael, "The thermal decomposition kinetics of o-xylylbromide and o-xylyl radicals", In Preparation, *J. Phys. Chem. A*, 2013.

### Other Publications and Presentations supported by this project 2011-2013

1. R. Sivaramakrishnan, D. Y. Zhou, R. T. Skodje and M. J. Davis, "A comprehensive mechanism for ethanol combustion" Paper 3A03, 7<sup>th</sup> National Technical Meeting of the Combustion Institute, Atlanta, GA, Mar 20-23, 2011.
2. R. Sivaramakrishnan and J. V. Michael, "The thermal decomposition of o-xylyl radicals," Paper 2B03, 7<sup>th</sup> National Technical Meeting of the Combustion Institute, Atlanta, GA, Mar 20-23, 2011.
3. R. Sivaramakrishnan, W. Liu, M. J. Davis, S. Som, D. E. Longman, "A high-temperature model for methylbutanoate combustion," Fall Technical Meeting of Eastern States Section of the Combustion Institute, Storrs, CT, Oct 09-12, 2011.
4. R. Sivaramakrishnan, W. Liu, M. J. Davis, S. Som, D. E. Longman, "Development of a Reduced Biodiesel Surrogate Model for Compression Ignition Engine Modeling", Spring Technical Meeting of the Central States Section of the Combustion Institute, Dayton, OH, Apr 22-24, 2012.
5. R. Sivaramakrishnan, J. V. Michael, L. B. Harding and S. J. Klippenstein, "Revisiting the Thermal Decomposition of  $CH_3CHO$ ", 22<sup>nd</sup> International Symposium on Gas Kinetics, Boulder, CO, 2012.
6. S. L. Peukert, R. Sivaramakrishnan, M.-C. Su, and J. V. Michael, "Experiment and Theory on methylformate and methylacetate kinetics at high temperatures: Rate constants for H-atom abstraction and thermal decomposition", 22<sup>nd</sup> International Symposium on Gas Kinetics, Boulder, CO, 2012.

## COMPUTATIONAL AND EXPERIMENTAL STUDY OF LAMINAR FLAMES

M. D. Smooke and M. B. Long  
Department of Mechanical Engineering  
Yale University  
New Haven, CT 06520  
[mitchell.smooke@yale.edu](mailto:mitchell.smooke@yale.edu)

### Program Scope

Our research has centered on an investigation of the effects of complex chemistry and detailed transport on the structure and extinction of hydrocarbon flames in coflowing axisymmetric configurations. We have pursued both computational and experimental aspects of the research in parallel. The computational work has focused on the application of accurate and efficient numerical methods for the solution of the boundary value problems describing the various reacting systems. Detailed experimental measurements were performed on axisymmetric coflow flames using two-dimensional imaging techniques. Spontaneous Raman scattering and laser-induced fluorescence were used to measure the temperature, and major and minor species profiles. Laser-induced incandescence (LII) has been used to measure soot volume fractions and particle sizes. A new approach to optical pyrometry has been developed to measure temperatures where the other techniques fail due to the presence of soot. Our goal has been to obtain a more fundamental understanding of the important fluid dynamic and chemical interactions in these flames so that this information can be used effectively in combustion modeling.

### Recent Progress

#### *Improving Velocity-Vorticity Flame Computations*

The computation of laminar flames in two-dimensional coflow geometries requires the solution of the fluid dynamic conservation equations along with the thermochemistry. The fluid portion of the problem is often solved by employing a stream function-vorticity, primitive variables or velocity-vorticity approach. Our work in recent years has focused on the hybrid velocity-vorticity methodology as it does not require the solution of the pressure field and it enables velocity boundary conditions to be employed directly. One of the shortcomings of the method is that it can only guarantee that the gradient of the continuity equation is solved to machine zero. As a result, there are times when small amounts of mass can be either gained or lost in the computational domain. While the temperature and major species are affected only marginally, we have noticed that the axial velocity and some minor species have small perturbations in the regions of the domain where the mass loss/gain occurs. To alleviate this situation, we have focused our efforts on modifying the discretizations of the axial velocity equation so that terms involving vorticity gradients are represented more accurately. As a means of comparison, we are also investigating replacing one of the Navier-Stokes equations by the continuity equation directly.

#### *Radiation Models in Sooting Flames*

Power loss in diffusion flames results from both gas phase species ( $\text{CO}_2$ ,  $\text{H}_2\text{O}$ , and  $\text{CO}$ ) and soot radiation. To model these processes in our previous computations, we have typically employed an optically thin approximation that uses an exponential wideband model [1]. A more sophisticated analysis to assess the importance of optical thickness or radiative re-absorption effects is being developed. We are utilizing a discrete ordinates method [1,2] to account for such optical thickness effects. While we do not expect a significant difference between the optically thin approximation

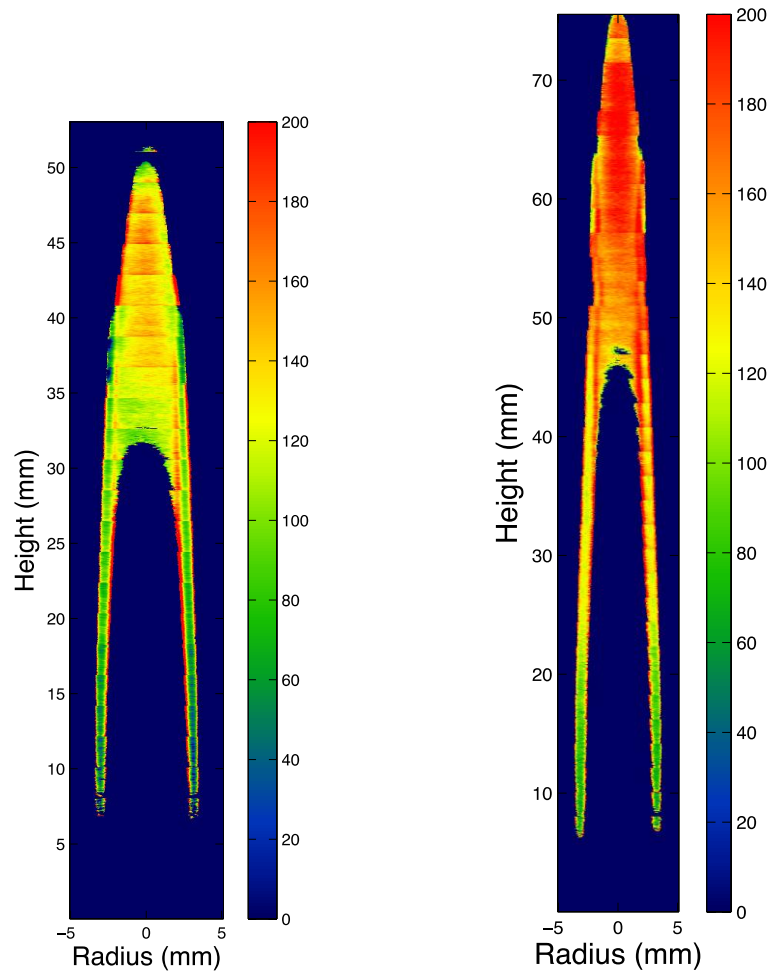
and the re-absorption model for low sooting flames, we anticipate that there could be differences as the peak volume fraction increases above several ppm. This could produce local temperature increases on the wings or near the centerline of the flames. This would in turn affect temperature dependent processes such as NO formation.

### *High-Order Discretizations*

We continue to apply high-order compact spatial discretizations in a fully implicit framework for time-dependent flames. Such methods offer many advantages over other current approaches to solving time-dependent reacting flow problems. Compact schemes are well suited to the simulation of time-dependent flows with complicated structures due to their excellent resolution characteristics [3,4]. Their integration into an efficient Newton-based flame code requires modern iterative linear algebra solvers and preconditioning, novel storage/retrieval methodologies, fast Jacobian matrix algorithms, and domain decomposition methods. The necessity of implementing all these numerical techniques on message-passing parallel architectures only compounds the difficulty. However, efficiency arguments indicate that the use of compact spatial discretizations with implicit time stepping may be able to reduce overall computation times dramatically compared to other numerical methods commonly employed in detailed-chemistry combustion simulations [5].

### *Two-dimensional Soot Aggregate Sizing by Multi-angle Light Scattering*

As we continue to develop our soot modeling capabilities, there is an increased need to determine more information on the soot morphology. Multi-angle light scattering has been shown to be a powerful in-situ means to determine the radius of gyration of fractal aggregates. The approach involves detecting the elastically-scattered signal from aerosols being illuminated by a laser beam at a set of angles, and applying Guinier analysis to determine the aggregate sizes. Most multi-angle light scattering experiments are limited to point measurements, where the soot radius of gyration is often reported as a function of flame downstream location. Recent work in our lab has demonstrated two-dimensional soot aggregate size measurement in sooting coflow laminar diffusion flames using multi-angle light scattering. The experiment employed a pulsed laser at 532 nm that was focused into a sheet 4 mm high. The scattered light was imaged onto a cooled EMCCD camera with optics set to maximize spatial resolution while maintaining sufficient depth of field. The detection angle was varied from 10 to 70 degrees with respect to the laser beam at intervals of 10 degrees. The distance between the camera and flame was kept constant to ensure the same collection efficiency. The Guinier analysis involves normalizing signals at all angles over the signal at near-zero angle. In order to obtain information in two dimensions, the images at different angles were geometrically warped to ensure spatial coincidence. The spatially transformed images at all angles were then normalized to that at 10 degrees. A set of seven ratio images was obtained and Guinier analysis was applied for each set of corresponding pixels. The normalized ratios at the seven angles were found to have good linear relations with respect to the square of the wave vectors,  $q$ , at these angles. The radius of gyration was then determined on a pixel-by-pixel basis from the slope of the ratio vs.  $q^2$  plot. A full two-dimensional map of soot radius of gyration was obtained by sequential measurements at different flame heights as shown in the Figure below. Measurements were performed on  $C_2H_4/N_2$  coflow laminar diffusion flames at a set of dilution levels and, hence, soot loadings.



Radius of gyration (color coded in nm) in 60% and 80%  $C_2H_4/N_2$  flames.

### Future Plans

During the next year we will continue our study of velocity-vorticity discretizations to minimize errors in mass conservation and to reduce variations in velocity and minor species profiles. In addition, we will continue our analysis of optically thin versus radiation re-absorption approaches in sooting coflow flames. Experimentally, we will continue our efforts to provide more complete information on soot particle morphology and optical properties, each of which is important for further developing the soot model. We will also perform minor species measurements ( $OH$ ,  $CH$  and  $NO$ ) with laser-induced fluorescence to complete the characterization of species in time-varying flames that will be compared to simulations with high-order spatial discretizations. Further, we will perform phase-resolved PIV measurements of the velocity profiles within the flames and, using the same techniques that we have developed for the steady sooting flames, we will perform phase-averaged measurements to characterize the soot in the time-varying flames.

### References

1. Hyde, D.J. and Truelove, J.S., "The Discrete Ordinates Approximation for Multidimensional Radiant Heat Transfer in Furnaces", AERE Harwell Report HTFS RS 189, February, 1977.
2. Raithby, G.D. and Chui, E.H., J Heat Transfer, 112:415 (1990).

3. S.K. Lele, "Compact Finite Difference Schemes with Spectral-Like Resolution," *J. Comput. Phys.*, **103**, (1992).
4. R.V. Wilson, A.O. Demuren, and M. Carpenter, "Higher-Order Compact Schemes for Numerical Simulation of Incompressible Flows, Part II: Applications," *Numer. Heat Transfer, Part B*, **39**, (2001).
5. M. Noskov, Ph.D. Thesis, Yale University, 2004.

### **DOE Sponsored Publications since 2011**

1. P. B. Kuhn, B. Ma, B. C. Connelly, M. D. Smooke, and M. B. Long, "Soot and Thin-filament Pyrometry Using a Color Digital Camera," *Proceedings of the Combustion Institute*, 33, 2011.
2. B. Coriton, J. H. Frank, A. G. Hsu, M. D. Smooke and A. Gomez, "Effect of Quenching of the Oxidation Layer in Highly Turbulent Counterflow Premixed Flames," *Proceedings of the Combustion Institute*, 33, 2011.
3. L. Tosatto, B. A. V. Bennett and M. D. Smooke, "Parallelization Strategies for an Implicit Newton-based Reactive Flow Solver," *Comb. Theory and Modelling*, 15, (2011).
4. L. Tosatto, T. Lu, B. A. V. Bennett and M. D. Smooke, "A Flux-Based Directed Relation Graph Method for the Adaptive On-the-Fly Reduction of Chemical Mechanisms," *Comb. and Flame*, 158, (2011).
5. J. D. Herdman, B. C. Connelly, M. D. Smooke, M. B. Long, and J. H. Miller, "A Comparison of Raman Signatures and Laser-Induced Incandescence with Direct Numerical Simulation of Soot Growth in Non-Premixed Ethylene/Air Flames," *Carbon*, 49, (2011).
6. M. B. Colket, S. P. Zeppieri, M. D. Smooke and W. W. Kim, "Laminar Flame Speeds, Flammability Limits, and Flame/Reaction Zone Thicknesses for a Surrogate Kerosene Fuel at Engine Operating Conditions," *AIAA Paper* 2011.
7. M. B. Long, "Imaging Flames: From advanced laser diagnostics to snapshots," in *Optical Processes in Microparticles and Nanostructures*, A. Serpengüzel and A.W. Poon, Editors. 2011, World Scientific.
8. L. Tosatto, F. Mella, M. B. Long, and M. D. Smooke, "A Study of JP-8 Scoflow Flame Structure by Combined Use of Laser Diagnostics and Numerical Simulation," *Comb. and Flame*, 159, (2012).
9. J. Cancian, B. A. V. Bennett, M. B. Colket, and M. D. Smooke, "Prediction of Electron and Ion Concentrations in Low-Pressure Premixed Acetylene and Ethylene Flames," accepted for Publication, *Comb. Theory and Modelling*, (2012).
10. L. Tosatto, B. A. V. Bennett, and M. D. Smooke, "Comparison of Different DRG-Based Methods for the Skeletal Reduction of JP-8 Surrogate Mechanisms," to be published, *Comb. and Flame*, (2013).
11. S. Cao, B. A. V. Bennett, B. Ma, M. B. Long, and M. D. Smooke, "Effects of Pressure and Dilution Level on the Structure of Coflow Laminar Methane-Air Diffusion Flames: Computational and Experimental Study," to be submitted, *Comb. and Flame*, 2013.
12. M. D. Smooke, "The Computation of Laminar Flames," *Proceedings of the Combustion Institute*, 34, 2013.

# Quantum Chemistry of Radicals and Reactive Intermediates

John F. Stanton  
Institute for Theoretical Chemistry  
University of Texas  
Austin, TX 78712

## Scope of Research

My research group works in the area of theoretical chemical physics, especially on the thermodynamic properties, spectra, and reactions of organic radicals and other transient intermediates. This research follows a number of paths, including first-principles calculations of bond energies and other thermochemical information (as well as development of methodology for such calculations), methods for the simulation and analysis of molecular spectroscopy, especially those relevant to experiments that can be used to glean thermochemical information, and the development of *ab initio* methods needed for the accurate treatment of transient organic molecules.

## Summary of Selected Recent Accomplishments

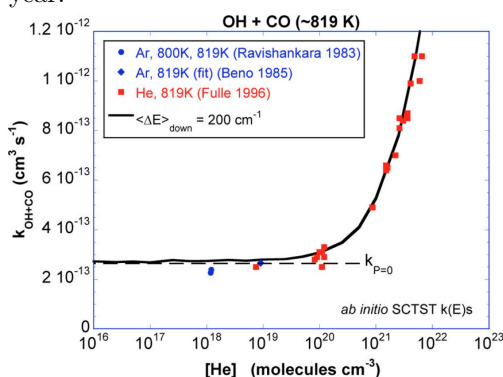
We have continued our work using the HEAT protocol<sup>1</sup> for the study of transition states, research that was part of our most recent renewal proposal. To summarize, the HEAT protocol is a strategy for the computation of molecular energies (both adiabatic electronic energies and zero-point corrections) that is designed to be as accurate as possible, and to involve – apart from basis set extrapolation methods – no “empirical” corrections or assumptions. A number of calibration studies established HEAT to be accurate to within 1 kJ mol<sup>-1</sup> (*ca.* 80 cm<sup>-1</sup>) in the calculation of enthalpies of formation for molecules containing four and fewer atoms (a necessary restriction in the scope of applicability of the method at the time of the studies); more recent work has suggested that a high level of accuracy is maintained for larger molecules that are now accessible due to advances in both algorithmic development and available computational resources. In thermochemistry, the quantities of interest are well-defined quantum mechanically, but the relevant quantity in reaction dynamics – the activation energy – is not similarly well-defined and therefore not amenable to comparable calibration studies. However, for those cases in which the electronic structure of the activated complex is similarly “complicated” to those molecules in the calibration set, a similar level of accuracy can be expected for the corresponding electronic energies and zero-point corrections. We have now applied HEAT to a number of different reaction systems: the abstraction of a hydrogen atom from H<sub>2</sub> by the hydroxyl radical; the abstraction of a hydrogen atom in methane by chlorine atoms, and the reaction of OH with CO to form CO<sub>2</sub> and hydrogen atoms, the self-reaction of OH radicals (producing H<sub>2</sub>O and O atoms), the hydration of ketene (still unpublished), and the water-catalyzed hydration of ketene. The reactions of hydroxy with itself and with carbon monoxide are both important in combustion. For all reactions where appropriate data is available, the calculated barriers and rates are in good agreement with experimental data, which attests to both the accuracy of the quantum chemistry part – HEAT – and the dynamical treatment (see below).

We have continued our work on the applications of semiclassical transition state theory (SCTST) to chemical reactions and the algorithmic improvement of SCTST. SCTST is a method that was conceived of some time ago<sup>2</sup> and provides rate constants that incorporate effects of both quantum-mechanical tunneling and reaction path curvature. However, unlike formally exact quantum calculations that require extensive

<sup>1</sup>A. Tajti *et al.* *J. Chem. Phys.* 121, 11599 (2004).

<sup>2</sup>W.H. Miller *Faraday Transactions* 62, 40 (1977).

information about the potential energy surface, efficient realizations of SCTST can be formulated which use only local information (derivatives through fourth-order in displacement) in regions of the potential surface around the transition state. With advances in quantum chemical methodology – particularly the calculation of analytic derivatives of the potential surface – the ability of SCTST to calculate reaction rates for *real* reactive systems was first realized some time ago<sup>3</sup>, but only recently has the quantum chemistry become available to make truly accurate calibration of SCTST feasible. Our major research effort in the use of SCTST in the past year has been a detailed study of the kinetics, H/D isotope effects and pressure dependence of the OH + CO reaction, done in collaboration with J.R. Barker (Michigan) and R.E. Weston (Brookhaven National Laboratory). In this study, the kinetics of the reaction were studied over a temperature range from 75 K to 2500 K and  $0 \leq [\text{He}] \leq 10^{23} \text{ cm}^{-3}$ . At all pressures and temperatures relevant to combustion (as well as to the atmosphere), agreement of the rate constants with experiment is good, although some problems were found at extremely low (below 200 K) temperatures that are believed to be due to dimers and some prereactive complexes that were not considered in the stochastic simulations. The agreement between calculated and observed H/D isotope effects was in good agreement with experiment and much better than previously theoretical determinations. This work used SCTST, our recent high-level calculated stationary points for this reaction<sup>4</sup> and master equation methods, the latter using some new methods developed in the past year.



Rates of the reaction  $\text{OH} + \text{CO} \rightarrow \text{HOCO}$ , calculated at various pressures (solid black line) and in the low-pressure limit (dashed black line). High- and low-pressure limit calculations were done with SCTST and the two-dimensional master equation; finite-pressure simulations used the one-dimensional master equation with an empirical energy transfer parameter (see inset). Experimental data is shown with red, blue and green points.

In the area of traditional computational thermochemistry, we have published a HEAT study of the enthalpies of formation for three important small hydrocarbon radicals - vinyl, allyl and vinoxy ( $\text{HCCH}_2$ ,  $\text{H}_2\text{CCHCH}_2$  and  $\text{OCHCH}_2$ , respectively) - that are important combustion intermediates. In addition, we have completed the most high-level calculation of the vinylidene/acetylene isomerization energy yet done<sup>5</sup> ( $45.53 \pm 0.13 \text{ kcal mol}^{-1}$ ) that, as a by-product, also allows the H-CCH<sub>2</sub> bond energy in vinyl to be determined with unprecedented accuracy ( $77.7 \pm 0.3 \text{ kcal mol}^{-1}$ ). Finally, we are in the process of determining the thermodynamic stabilities of all species that can in principle be generated by 193 nm UV photolysis of vinyl cyanide, a project that is being done in collaboration with the Field group at MIT.

Another project that has been completed is an in-depth study of the negative-ion electron photodetachment spectrum of the nitrate anion ( $\text{NO}_3^-$ ). In addition to calculating the energy levels of the final states of the nitrate radical, this work represents our first application of methods for calculating cross-sections for electron photodetachment, an area of research proposed in our last funding request. The latter work, which remains unpublished, has used two methods – Stieltjes imaging<sup>6</sup> and Dyson orbitals, in connection with equation-of-motion coupled-cluster methods<sup>7</sup>. The two approaches are in good agreement with both one another and experiment for atomic systems, but the Dyson orbital method is better suited to polyatomic molecules. Using the latter approach for the  $\text{NO}_3^-$  photoelectron spectrum, analysis of which is greatly

<sup>3</sup>M.J. Cohen, N.C. Handy, R. Hernandez and W.H. Miller *Chem. Phys. Lett.* 192, 407 (1992).

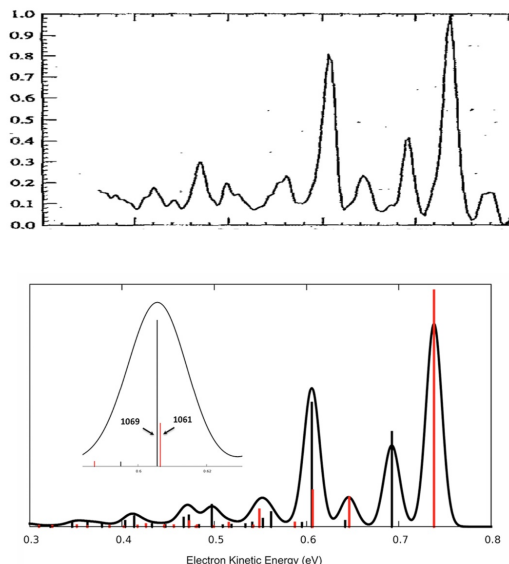
<sup>4</sup>L.T. Nguyen, R. Weston, J.R. Barker and J.F. Stanton *J. Phys. Chem. Lett.* 3, 1549 (2012).

<sup>5</sup>H. Lee, J.H. Baraban, R.W. Field and J.F. Stanton *J. Phys. Chem. A*, in press.

<sup>6</sup>P.W. Langhoff and C.T. Corcoran *J. Chem. Phys.* 61, 146 (1974).

<sup>7</sup>The Dyson-orbital-based approach built upon EOM-CC methods was first reported by: C.M. Oana and A.I. Krylov *J. Chem. Phys.* 131, 124114 (2009).

facilitated by knowing the relative intensities of the Franck-Condon ( $a_1'$  vibrational symmetry) and vibronic ( $e'$ ) bands, a nearly perfect agreement with the experimental profile is obtained. Consequently, confident assignments can be made for a number of vibrational levels within  $2000\text{ cm}^{-1}$  of the ground state. Most significantly, the band originally assigned to the  $\nu_1$  vibrational band can be seen to comprise two transitions:  $\nu_1$  and the  $\nu_3$  level originally assigned to an infrared feature at  $1492\text{ cm}^{-1}$  but which has been questioned in recent years.



Experimental photoelectron spectrum of the nitrate anion (top) and simulated spectrum (bottom). The simulation used a diabatic three-state Hamiltonian parametrized by equation-of-motion coupled-cluster theory (EOMIP-CCSDT) using a large atomic natural orbital basis set. Intensities are based on photodetachment cross sections to the ground  $X^2A_2'$  and excited  $\tilde{B}^2E'$  excited electronic states of the neutral, using Krylov's Dyson orbital approach. The prominent band at *ca.* 0.6 eV electron kinetic energy was originally assigned to the  $\nu_1$  fundamental of the electronic ground state. However, note that there are two principal contributors to this state; the stronger of the two (black) is actually the  $\nu_3$  level.

### Ongoing Research and Future Plans

Our efforts to implement very high-level coupled cluster methods in an efficient computational manner has begun to bear its first fruit. We have started work on a new coupled cluster module (NCC), which will eventually become a module in the freely-available CFOUR program system that is developed and maintained by my group and those of Jürgen Gauss in Mainz (Germany) and Peter Szalay in Budapest (Hungary). NCC, which is written in C++ and is suited to parallel computing environments, now has the capability to do full CCSDT and CCSDTQ calculations, developments that have taken place in the early months of 2013. The CCSDT code is already considerably faster than the standard module for this purpose in CFOUR, and the CCSDTQ code is expected, after optimization and refinement, to be roughly twenty times faster than the MRCC code of Kallay, which is currently the best available code for such calculations. The NCC codes – currently limited to closed-shell reference functions – exploit a very efficient scheme for spin-adaptation that has also recent been submitted for publication<sup>8</sup>. In the future, NCC will be extended to open-shell references, analytic derivatives and excited states with the EOM-CCSDT and EOM-CCSDTQ methods, developments that should play out in the years ahead and significantly expand the range of applicability of these high-accuracy methods in quantum chemistry.

### Students and Postdoctoral Supported:

T.L. Nguyen (postdoc)

### References supported by DE-FG02-07ER15884 (2012-)

J.F. Stanton, E. Garand, J. Kim, T.I. Yacovitch, A.S. Case, E.M. Miller, J.-Y. Lu, K.M. Vogelhuber, S.W. Wren, T. Ichino, J.P. Maier, R.J. McMahon, D.L. Osborn, D.M. Neumark and W.C. Lineberger  
 “Ground and Low-Lying Excited States of Propadienylidene Obtained by Negative-Ion Photoelectron

<sup>8</sup>D.A. Matthews, J. Gauss and J.F. Stanton *Theo. Chem. Acc.*, submitted.

Spectroscopy *J. Chem. Phys.* 136, 134312 (2012).

M.E. Harding, J. Vazquez, J. Gauss, J.F. Stanton and M. Kallay "Towards Highly Accurate Ab Initio Thermochemistry of Larger Systems: Benzene *J. Chem. Phys.* 135, 044513 (2011).

C. S. Simmons, T. Ichino and J.F. Stanton "The  $\nu_3$  Fundamental of NO<sub>3</sub> Has Been Seen Near 1060 cm<sup>-1</sup>, Albeit Some Time Ago *J. Phys. Chem. Letters* 3, 1946 (2012).

S.W. Wren, K.M. Vogelhuber, T. Ichino, J.F. Stanton and W.C. Lineberger "Photoelectron Spectroscopy of Anilide and Acidity of Aniline *J. Phys. Chem. A* 116, 3118 (2012).

D.P. Tabor, M.E. Harding, T. Ichino and J.F. Stanton "High Accuracy Extrapolated Ab Initio Thermochemistry of the Vinyl, Allyl and Vinyloxy Radicals *J. Phys. Chem. A* 116, 7668 (2012).

A. Vasiliou, K.M. Piech, B. Reed, X. Zhang, M.R. Nimlos, M. Ahmed, A. Golan, O. Kostko, D.L. Osborn, J.W. Daily, J.F. Stanton and G.B. Ellison "Thermal Decomposition of CH<sub>3</sub>CHO Studied by Matrix Infrared Spectroscopy and Photoionization Mass Spectroscopy *J. Chem. Phys.* 137, 164308 (2012).

X. Zhang, S.R. Sander and J.F. Stanton "Detection of the Far IR 12 Bending Level in Propargyl: A Complete Set of Fundamentals for an Important Molecule *J. Phys. Chem. A* 116, 10338 (2012).

T.L. Nguyen, B.C. Xue, R.E. Weston, J.R. Barker and J.F. Stanton "Reaction of HO with CO: Tunneling is Indeed Important *J. Phys. Chem. Lett.* 3, 1549 (2012).

J.H. Baraban, J.F. Stanton, A.J. Merer and R.W. Field "Anharmonic Force Fields of cis- and trans-S<sub>1</sub> C<sub>2</sub>H<sub>2</sub> *Mol. Phys.* 110, 2725 (2012).

A.M. Nolan, B.K. Amberger, B.J. Esselman, V.S. Thimmakonda, J.F. Stanton, R.C. Woods and R.J. McMahon "Carbonyl Diazide, OC(N<sub>3</sub>)<sub>2</sub>: Synthesis, Purification, and IR Spectrum *Inorg. Chem.* 51, 9846 (2012).

R.E. Weston, T.L. Nguyen, J.R. Barker and J.F. Stanton "HO + CO Reaction Rates and H/D Kinetic Isotope Effects: Master Equation Models using ab initio SCTST Rate Constants *J. Phys. Chem. A* 117, 821 (2013).

# Universal and State-Resolved Imaging Studies of Chemical Dynamics

Arthur G. Suits

Department of Chemistry, Wayne State University  
5101 Cass Ave, Detroit, MI 48202  
asuits@chem.wayne.edu

## I. Program Scope

The focus of this program is on combining universal ion imaging probes providing global insight, with high-resolution state-resolved probes providing quantum mechanical detail, to develop a molecular-level understanding of chemical phenomena. Particular emphasis is placed upon elementary reactions important in understanding and predicting combustion chemistry. This research is conducted using state-of-the-art molecular beam machines, photodissociation, reactive scattering, and vacuum ultraviolet lasers in conjunction with ion imaging techniques. An ongoing parallel effort is made to develop new tools and experimental methods directed to these goals.

## II. Recent Progress

Ablation radical source. In the past year we have devoted considerable effort to developing a more intense atomic radical source for crossed-beams studies. We examined discharge sources and photolytic sources with various precursors. We found that a simple ablation plasma formed when a 10 mJ focused 355nm YAG beam strikes an aluminum channel at the nozzle opening gives us an order of magnitude increase in Cl atoms and a significantly improved speed ratio ( $v/\delta v \sim 10$ ) compared to our previous approach or to a pulsed discharge (Fig. 1). This allows us to examine systems whose detection efficiency at 157 nm is lower than the larger hydrocarbons we have previously employed, providing more detailed insight into the dynamics as these systems are of intermediate complexity.

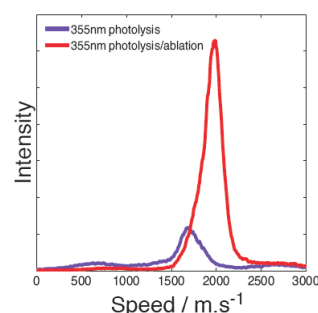


Figure 1. Ablation and open photolysis Cl sources.

Systematic studies of polyatomic reaction dynamics. In the last abstract we reported our initial study of Cl + alkene reactions. In these crossed-beam studies of Cl with pentene and hexene, we saw evidence both for addition/elimination and direct H abstraction from the alkyl side chain. More recently we have studied Cl atom reactions with a range of butene isomers. The addition and abstraction energetics have been calculated at the CBS-QB3 level of theory, and are shown in Fig. 2. We have not yet determined barriers separating these adducts and the anticipated product branching but plan to do so in the future in collaboration with Alex Mebel. In all cases, Cl addition to the double bond contributes about 20 kcal/mol stabilization energy, with reaction at remote alkylic sites exoergic by 3-4 kcal/mol/ reaction at vinylic sites endoergic by 3-5 kcal/mol, and reaction at allylic sites exoergic by 15-20 kcal/mol. These are largely consistent with those we reported earlier for 1-pentene. The DC sliced imaging results and derived angular and translational energy distributions are shown in Fig. 3 for the four principal isomers studied. The results show a fascinating variation across the series of isomers studied, something we have not seen clearly with the former Cl atom source and the larger hydrocarbons. The signature of addition/elimination is in low translational energy, forward-backward symmetric distributions.

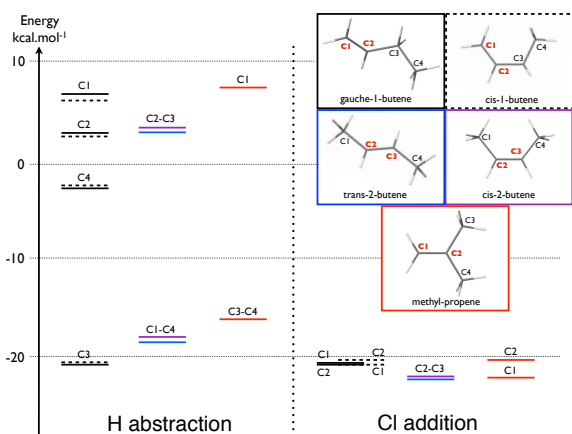


Figure 3. Energetics for Cl-butene isomers at the CBS-QB3 level of theory. cis-1-butene is not believed to be present in beam conditions.

The addition/elimination is seen to dominate only for isobutene. This is the system that shows the lowest exoergicity for the allylic site, but also the deepest well for the C1 addition to the double bond. For 1-butene, addition and abstraction are equi-energetic and the abstraction exoergicity is the greatest. Little indication of the addition/elimination channel is seen in this case.

*Reaction of selectively deuterated propane.* Previously we reported the first crossed-beam imaging study directly probing primary vs. secondary H abstraction in the reaction of Cl with butane-1,1,1,4,4,4- $d_6$ . The H- and D-atom abstraction channels were studied over a range of collision energies using crossed molecular beam dc slice ion imaging techniques. These two channels manifest modestly distinct dynamics principally in the translational energy distributions, while the angular distributions are remarkably similar. At the collision energies studied, no strong correlation between abstraction site and differential cross section was seen, perhaps accounting for inconsistent conclusions on this point arising from more indirect approaches over the years. In the past year we have extended this using our intense Cl atom source to study DC slice imaging of Cl atom reaction with normal and selectively deuterated propane. In this case our 157nm probe is not sensitive to the primary radical, whose ionization energy is above the energy of the probe photon. This gives us the unique opportunity to study reaction at a particular site (the central, secondary C atom) with no deuteration or with deuteration on the primary or secondary sites. The results for the undeuterated species closely reproduce the results of Blank et al. performed using tunable synchrotron radiation on the Chemical Dynamics Beamline, suggesting either that the secondary abstraction is dominant even at high collision energies, or that the primary and secondary abstraction distributions are remarkably similar. However, we see significant differences in the translational energy and angular distributions for both partially deuterated species.

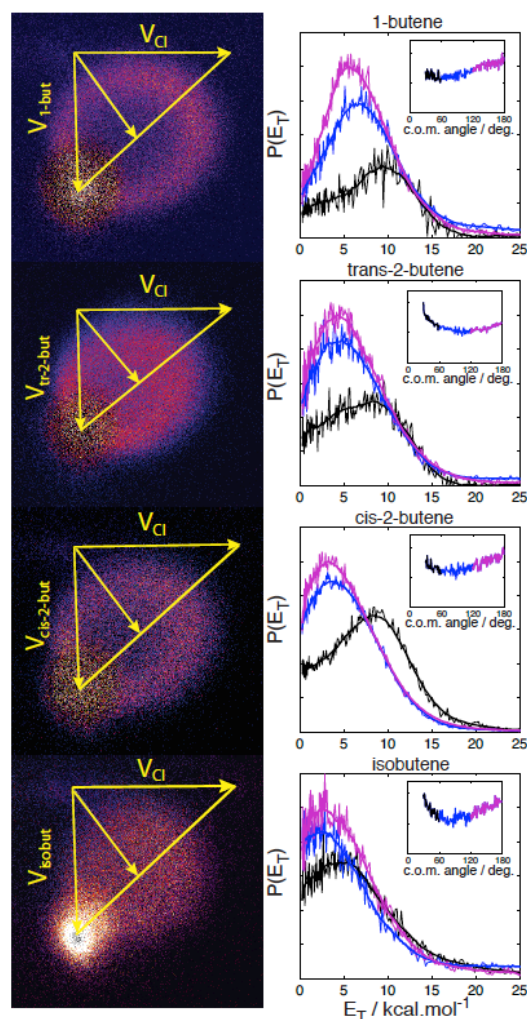


Figure 2. DC sliced images (left) and derived translational energy and angular distributions (right) for  $C_4H_7$  product of Cl reaction with indicated butene isomer at  $\sim 13.5$  kcal/mol. The forward scattered are shown in black; sideways in blue and backward in purple. Center-of-mass angular distributions are shown inset in each figure.

*Isomer-specific detection and imaging via “semi-soft” ionization.* The use of “soft” vacuum ultraviolet photoionization to achieve universal but selective detection of reaction products and photofragments was pioneered in dynamics studies at the Chemical Dynamics Beamline at the Advanced Light Source (ALS) in the mid nineties. However, it was in flame studies by T. Cool and coworkers exploiting the overall shape of the photoionization efficiency (PIE) curves that the full power of this approach became clear. This technique has since been widely exploited in flame characterization and kinetics studies both at the ALS and at the National Synchrotron Radiation Laboratory in Hefei, China with extraordinary success. The origin of the characteristic shapes of these PIE curves is less important than that they be consistent and relatively insensitive to internal energy in the products. Traditional universal ionization techniques relying on electron impact ionization generate extensive fragmentation, and cannot so readily be adapted to these approaches.

Non-resonant ionization by relatively high peak power femtosecond lasers has clear parallels to tunable VUV photoionization, in that the power needed to induce ionization closely tracks the ionization energy of the subject molecule. Tuning the power of a nonresonant femtosecond pulse, without changing any other characteristics, is quite like tuning the ionizing photon energy, both through the ionization onset and beyond. This is because the photons come sufficiently quickly that they are not registered as distinct entities by virtue of the uncertainty principle. However, little variation in the shape of the photoion yield spectra is seen beyond the fact that the saturation intensity closely parallels the ionization energy. But an important aspect of strong-field ionization by short-pulse lasers is that some molecules undergo fragmentation upon ionization in the laser field, while others do not. For short pulses, this fragmentation is modest and it has been attributed to the presence of resonances in the cation that are overlapped by the femtosecond laser wavelength. It has also been shown that longer pulses induce greater fragmentation, so to minimize fragmentation, Fourier transform-limited pulses are optimal. Finally, the variability in this limited fragmentation is strongly system-dependent. These observations suggest that, as has been demonstrated to great effect in the kinetics and flame studies at the ALS and Hefei, “basis functions” provided by known samples under well-defined conditions may be used to identify and quantify the chemical and even isomeric composition of unknown mixtures or reaction products in a variety of experiments in a manner analogous to that employed in the synchrotron studies. In our work the “basis functions” are time-of-flight (TOF) spectra obtained under well-defined conditions and a given laser pulse energy or range of pulse energies, rather than PIE curves, but the strategy is much the same as in the flame studies. We have applied this approach to many trial systems, and examples are shown in Fig. 4. Mixture compositions are reproduced from basis spectra within 1% or so at number densities comparable to the flame or kinetics experiments at the ALS.

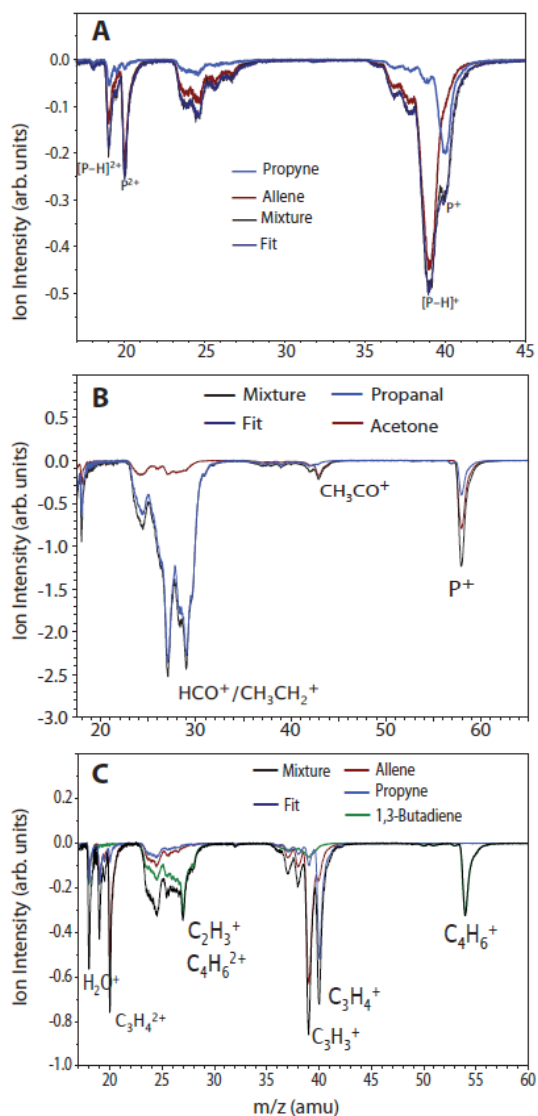


Figure 4. TOF mass spectra from strong-field ionization for various pure isomers and mixtures.

### III. Selected Future Plans

*State-resolved and universal crossed-beam DC slice imaging.* We plan to continue exploring a range of systems using our crossed-beam sliced imaging approach. We have increased the radical beam intensity so our background problems are greatly reduced. We can go to lower collision energy and revisit a number of systems mentioned above. We also plan to extend the DC slice crossed beam imaging to study radical-radical reactions. Our first target will be the  $O+CH_3$  reaction, a fascinating system that showed a novel  $H_2$  elimination pathway which anticipated the roaming dynamics seen in formaldehyde. For this system we can use REMPI detection of H,  $H_2$  and CO products. We will prepare the O atoms photolytically, and the methyl radicals using flash pyrolysis. Another fascinating system on the agenda is  $N(^2D)+H_2O$ . Casavecchia and coworkers have seen NO product from this reaction which would be a "roaming" reaction analogous to formaldehyde, but strictly bimolecular. We also have plans to use CH and  $CH_2$  radicals to implement a "chemical activation" investigation of roaming systems. These radicals can insert directly into bonds, forming highly energetic ground state systems at a well-defined total energy. This is ideal for probing roaming reactions quite generally. We will employ both universal and state-resolved detection, and complement these studies using a TEA-CO<sub>2</sub> laser and the CP-mm approach described in the following paragraph.

*Chirped-pulse mm-wave detection in uniform supersonic flows.* In collaboration with Bob Field, we are developing a unique and powerful new instrument that will combine two uniquely well-matched, emerging technologies: chirped-pulse Fourier-transform micro/mm-wave spectroscopy developed by Brooks Pate and pulsed uniform supersonic flows. This combination promises a nearly *universal detection method that can deliver isomer and conformer specific, quantitative detection and spectroscopic characterization* of unstable reaction products and intermediates, product vibrational distributions, and molecular excited states. The proposed technique will be suitable for application in diverse fields including fundamental studies in spectroscopy and reaction dynamics, kinetics, and combustion. Among the first targets for this system, which is almost completed, will be roaming dynamics in ethyl hydroperoxide. Here we can *quantitatively* determine the branching between roaming production of acetaldehyde and water or bond fission giving ethoxy and OH, This will be the first of countless systems we will pursue using this powerful new technology.

### V. DOE Publications 2010-present

A. D. Estillore, L. M. Visger, and A. G. Suits, "Imaging the dynamics of chlorine atom reactions with alkenes," *J. Chem. Phys.* **133**, 7 (2010).

M. P. Grubb, M. L. Warter, A. G. Suits, S. W. North, "Evidence of roaming dynamics and multiple channels for molecular elimination in  $NO_3$  photolysis," *J. Phys. Chem. Lett.* **1**, 2455 (2010).

A. D. Estillore, L. Visger and A. G. Suits, "Crossed-beam DC slice imaging of chlorine atom reactions with pentane isomers," *J. Chem. Phys.* **132** 164313 (2010).

A. D. Estillore, L. M. Visger-Kiefer, T. A. Ghani, A. G. Suits, "Dynamics of H and D abstraction in the reaction of Cl atom with butane-1,1,1,4,4,4-d6," *Phys. Chem. Chem. Phys.* DOI:10.1039/c1cp20137a (2011).

N. Herath and A. G. Suits, "Roaming radical reactions," *J. Phys. Chem. Lett.*, **2** 642 (2011).

J.M. Bowman and A. G. Suits, "Roaming reactions: The Third Way," *Phys. Today*, **64** 33 (2011).

A. M. Estillore, L. M. Visger-Kiefer and A. G. Suits, "Reaction dynamics of Cl + butanol isomers by crossed-beam sliced ion imaging," *Faraday Discussion* **157** 181 (2012).

# A Novel Multiscale Simulation Strategy for Turbulent Reacting Flows

PI: James C. Sutherland

Department of Chemical Engineering, The University of Utah

Salt Lake City, UT 84112-9203

James.Sutherland@utah.edu

Project start date: October, 2012

## I. Lattice Based Multiscale Simulation

### A. Introduction

We propose to new methodology to address the large range of length and time scales associated with turbulent combustion simulation. Currently, the only approach that directly captures all nonlinear interactions between these scales is Direct Numerical Simulation (DNS). However, the exceptional computational cost associated with DNS limits it to all but the simplest of problems. Large Eddy Simulation (LES) requires models to obtain appropriate closure, and this is particularly challenging in the context of reacting flows where source term closure is difficult. We have proposed a new methodology, named Lattice-Based Multiscale Simulation (LBMS), that utilizes intersecting bundles of One-Dimensional Turbulence (ODT) models [1]. ODT has been shown to be effective at capturing phenomena associated with turbulent combustion [1, 2]. Because the length scales are fully resolved on an ODT line, the model will reduce to DNS as the distance between each line approaches the limit of the fully resolved length scale. The LBMS model overcomes many of the limitations inherent in the ODT model and should provide higher fidelity than LES for a given computational cost.

### B. Motivation

The ODT model fully resolves length and time scales but only in one spatial dimension. Three-dimensional turbulent mixing is represented by an instantaneous, stochastic event which rearranges the fields associated with the problem. The triplet maps that defines these events ensure conservation, preserve scale locality and have been successful in modeling a wide variety of flows [1]. This one-dimensional model has been able to reproduce statistics from DNS datasets with accuracy comparable to high-fidelity LES simulations [2]. However, due to the inherent limitations of a one-dimensional model, ODT cannot capture multidimensional phenomena such as recirculation or vortex pairing. We have proposed to create a lattice structure of ODT models, as represented by Figure 1. Each direction will contain a bundle of ODT models. The resolution associated with a given bundle oriented in the  $x_1$  direction, for example, will be  $\delta x_1 \Delta x_2 \Delta x_3$ , where  $\delta x$  represents the fully resolved “fine” spacing and  $\Delta x$  represents the “coarse” spacing, or the distance between lines on the bundle. With this formation, each line will solve all length and time scales but only in one spatial dimension.

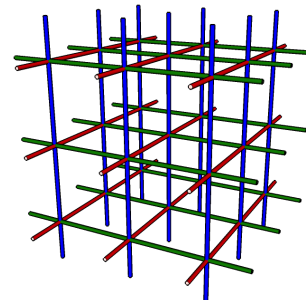


Figure 1: 3D representation of LBMS. Each color represents a bundle of ODT models in a given direction.

## C. Governing Equations

Our generalized balance equations, using an Eulerian formulation necessary for bundle interaction, are written in finite-volume form as

$$\int_{V(t)} \frac{\partial \rho \psi}{\partial t} dV = - \int_{S(t)} \Theta_\psi \cdot \mathbf{n} dS + \int_{V(t)} \sigma_\psi dV, \quad (1)$$

where  $\psi$  is the transported variable,  $\Theta_\psi$  is the total flux of  $\psi$  and  $\sigma_\psi$  is the volumetric source term. Note that this formulation implies that the control volumes are temporally fixed. This is necessary to ensure that the bundles can communicate with each other.  $\psi$  and the associated terms are given by Table 1.

Table 1: Quantities in (1) for each governing equation.  $\mathbf{u}$  represents the velocity,  $\rho$  the density,  $\boldsymbol{\tau}$  is the stress tensor,  $p$  represents the pressure,  $\mathbf{g}$  the gravitational acceleration,  $e_0$  the total internal energy,  $\mathbf{q}$  the energy diffusive flux,  $Y_i$  the mass fraction of species  $i$ ,  $\mathbf{j}_i$  the diffusive flux of species  $i$  and  $\sigma_i$  the reaction rate of species  $i$ .

Equation	$\psi$	Total Flux, $\Theta_\psi$	Source Term, $\sigma_\psi$
Mass	1	$\rho \mathbf{u}$	0
Momentum	$\mathbf{v}$	$p \mathbf{I} + \boldsymbol{\tau} + \rho \mathbf{u} \mathbf{u}$	$\rho \mathbf{g}$
Species	$Y_i$	$\rho Y_i \mathbf{u} + \mathbf{j}_i$	$\sigma_i$
Total Internal Energy	$e_0$	$e_0 \mathbf{u} - p \mathbf{u} - \boldsymbol{\tau} \cdot \mathbf{u} + \mathbf{q}$	$\rho \mathbf{g} \cdot \mathbf{u}$

Figure 2 depicts the project timeline that was provided in the original project proposal.

## II. Recent Progress

### A. Triplet Mapping

Currently, the triplet-map permutation associated with previous work [3] has been integrated into the LBMS infrastructure and expanded to apply to ODT lines in all three spatial directions. Additionally, verification tests have been performed by implementing test fields and integrating over a mapping to ensure that conserved variables are, in fact, conserved, an important trait of the triplet mapping.

### B. Conserved Variables in Coarse Control Volumes after Triplet Mapping

Since each line bundle will solve a full set of governing equations, the system will be over-specified. However, by applying the constraint that, in the limit of fully resolved length scales, we recover three identical models, the system will be fully consistent. This will help ensure that the LBMS model reduces to DNS in that limit. If a conserved variable is transported, via a triplet-map, across large-scale control volumes, the orthogonal lines associated with the control volume must be affected. At the time of writing, this functionality been implemented into the LBMS framework.

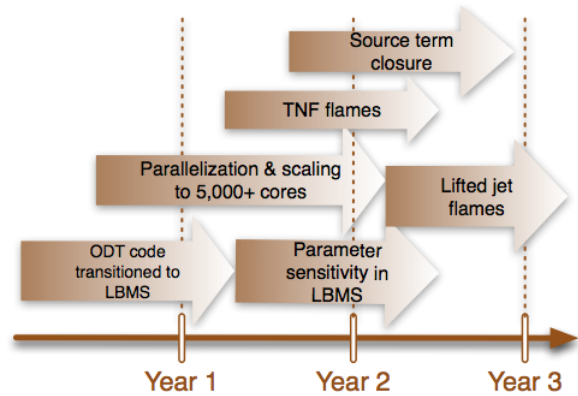


Figure 2: Project timeline.

### C. Cross Line Flux Resolution

A line oriented in the  $x$ -direction will not contain fully resolved fluxes in the  $y$  and  $z$ -directions. We can break the total flux into its components, as shown in (2). Three sets of governing equations will need to be solved, one associated with each bundle direction. However, only the flux in the direction of the bundle is fully resolved. Taking the flux term from (1) and expanding,

$$-\int_S (\Theta_\psi \cdot \mathbf{n}) \, dS = -\int_S (\Theta_{\psi,1} \cdot \mathbf{n}_1 + \Theta_{\psi,2} \cdot \mathbf{n}_2 + \Theta_{\psi,3} \cdot \mathbf{n}_3) \, dS, \quad (2)$$

we see that solving the governing equations on a specific bundle will require resolution of fluxes perpendicular to the bundle direction. These fluxes can be obtained from nearby orthogonal lines within a coarse control volume. However, the limitation of this approach is that these will be low-wavenumber fluxes. Instead, we can construct high-wavenumber fluxes by decomposing a flux into  $\mathbf{n}_\psi = \bar{\mathbf{n}}_\psi + \mathbf{n}'_\psi$ , where  $\mathbf{n}_\psi$  is the total flux of  $\psi$ .  $\bar{\mathbf{n}}_{\psi,1}$  is the fully resolved, but spatially filtered, flux obtained from the  $x_1$ -bundle line. Nearby orthogonal lines will provide  $\mathbf{n}'_\psi$ , which is the high-wavenumber flux, with a mean of zero. In this way, we will construct fluxes that are fully resolved across coarse volumes but still capture high-wavenumber fluctuations. This is analogous to a synthetic field approach. For example, the  $x$ -direction flux on the  $x$ -bundle,  $\Theta_{\psi,1}$ , as shown

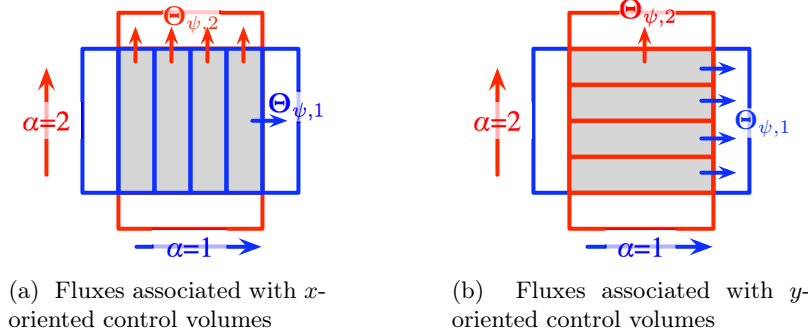


Figure 3: Fully resolved and high wave-number fluxes in the  $x$  and  $y$  direction

in Figure 3a, is fully resolved but only contains low-wavenumber information. By subtracting the high-wavenumber flux,  $\Theta_{\psi,1}$ , obtained from the  $y$ -bundle shown in Figure 3b, from the fully resolved flux, a synthetic field is constructed.

All of the software developed to implement the above-mentioned functionality is under regression testing to maintain reliability as further capabilities are added to the code base.

## III. Future Plans

### A. Implementation of Physics and Source Term Closure

As the ODT elements become integrated into the LBMS structure, the next step is the implementation of the full set of governing equations for turbulent combustion flow. Any given ODT line will be fully resolved in its direction. However, chemical source terms associated with that line will only be coarsely resolved in the directions orthogonal to any given line. That is, a control volume on an  $x$ -direction line will have a volume of  $\delta x \Delta y \Delta z$ . However, because each bundle will be fully resolved in its direction, a synthetic source term field can be constructed to contain high wave-number information by using information from the intersecting lines. Currently, methods to construct this field

are being investigated. Interpolating source term information between lines will need particular consideration due to the uniqueness of the LBMS geometry. However, the ODT model implicitly assumes spatial homogeneity in orthogonal directions. In a flow with a dominant direction, accurate source term closure will not be necessary. Thus, both computationally inexpensive and expensive methods, *e.g.* interpolating source terms versus interpolating temperature and species, are being considered.

## B. Parallelization and Scaling

Turbulent Combustion simulation will require high performance computing. Thus, we plan to use parallelization techniques that allow us to scale the LBMS methodology to utilize high performance platforms. Each line will be maintained on a single processor. This leads to several advantages. First, eddy events are random in location and size. Additional thread-level parallelization will be implemented through a novel graph-theory approach [4].

## C. Verification and Validation

Validation against experimental data will begin in year 2, as shown in Figure 2. However, formal verification [5] has and will continue to be utilized. The LBMS software is version-controlled and the implementation of the code includes regression tests automatically performed after updates, ensuring integrity. As the software reaches later stages of development, validation studies will be performed, with simulations run against both experimental and DNS data sets, with one goal being the recovery of DNS in the limit of  $\Delta x_i \rightarrow \delta x_i$  for every direction  $i$ . Additionally, fidelity of closure, particularly as  $\Delta/\delta$  increases, will be addressed.

## References

- [1] Alan R. Kerstein. One-dimensional turbulence: model formulation and application to homogeneous turbulence, shear flows, and buoyant stratified flows. *Journal of Fluid Mechanics*, 392:277–334, August 1999.
- [2] Naveen Punati, James C Sutherland, Alan R Kerstein, Evatt R Hawkes, and Jacqueline H Chen. An evaluation of the one-dimensional turbulence model: Comparison with direct numerical simulations of CO/H<sub>2</sub> jets with extinction and reignition. *Proceedings of the Combustion Institute*, 33(1):1515–1522, 2011.
- [3] J. C. Sutherland, N. Punati, and A. R. Kerstein. A Unified Approach to the Various Formulations of the One-Dimensional Turbulence Model. Technical Report ICSE091201, Institute for Clean and Secure Energy, The University of Utah, Salt Lake City, UT, 2010.
- [4] Patrick K Notz, Roger P Pawlowski, and James C. Sutherland. Graph-based software design for managing complexity and enabling concurrency in multiphysics PDE software. *ACM Transactions on Mathematical Software*.
- [5] William L Oberkampf and Timothy G Trucano. Verification and validation in computational fluid dynamics. *Progress in Aerospace Sciences*, 38(3):209–272, 2002.

# Elementary Reaction Kinetics of Combustion Species

Craig A. Taatjes

*Combustion Research Facility, Mail Stop 9055, Sandia National Laboratories,  
Livermore, CA 94551-0969  
cataatj@sandia.gov*

## SCOPE OF THE PROGRAM

This program aims to develop new methods for studying chemical kinetics and to apply these methods to the investigation of fundamental chemistry relevant to combustion science. One central goal is to perform accurate measurements of the rates at which important free radicals react with each other and with stable molecules. Another goal is to characterize complex reactions that occur via multiple potential wells by investigating the formation of products. Increasingly, these investigations are moving towards simultaneous time-resolved detection of multiple species in well-characterized photolytically-initiated reaction systems where multiple consecutive and competing reactions may occur. Understanding the reactions in as much detail as possible under accessible experimental conditions increases the confidence with which modelers can treat the inevitable extrapolation to the conditions of real-world devices. This research often requires the development and application of new detection methods for precise and accurate kinetics measurements. Absorption-based techniques and mass-spectrometric methods have been emphasized, because many radicals critical to combustion are not amenable to fluorescence detection.

An important part of our strategy, especially for complex reaction systems, is using experimental data to test and refine detailed calculations (working in close cooperation with Stephen Klippenstein at Argonne and Ahren Jasper and Judit Zádor at Sandia), where the theory offers insight into the interpretation of experimental results and guides new measurements that will probe key aspects of potential energy surfaces. This methodology has been applied in our investigations of the reactions of alkyl radicals with O<sub>2</sub>, where the combination of rigorous theory and validation by detailed experiments has made great strides toward a general quantitative model for alkyl oxidation. The focus of our laboratory is shifting to include investigations of the reactions of oxygenated molecules relevant to biofuel combustion as well as studies of the effects of unsaturation on the chemistry leading to autoignition. Moreover, we have increasingly aimed at producing species that are intermediates in oxidation systems (e.g., Criegee intermediates, hydroperoxyalkyl radicals) and directly probing their reaction kinetics.

## RECENT PROGRESS

We continue to apply frequency-modulation and direct absorption spectroscopy to measurements of product formation in reactions of alkyl radicals with O<sub>2</sub> and kinetics of unsaturated hydrocarbon radicals. In addition, the multiplexed photoionization mass spectrometric reactor at the Advanced Light Source (ALS), an experimental effort led by David Osborn (see his abstract), has become a major part of our investigations of low-temperature hydrocarbon oxidation chemistry. Several highlights of the recent work are described briefly below.

**Autoignition chemistry of *n*-butanol.** Reactions of hydroxybutyl radicals with O<sub>2</sub> were investigated by experimental measurements of product formation in pulsed-photolytic Cl-initiated oxidation of *n*-butanol. The time-resolved and isomer-specific product concentrations were probed by using multiplexed tunable synchrotron photoionization mass spectrometry (MPIMS). The product yields display substantial temperature dependence, arising from a competition among three fundamental pathways: (1) stabilization of hydroxybutylperoxy radicals, (2) bimolecular product formation in the hydroxybutyl + O<sub>2</sub> reactions, and (3) decomposition of hydroxybutyl radicals. The chemistry of the hydroxybutylperoxy radicals is governed by alcohol-specific internal H-atom abstractions involving the H atom from either the –OH group or from the carbon attached to the –OH group. We observe evidence of the recently reported water elimination pathway<sup>(d)</sup> (see Judit Zádor’s abstract) from the 4-hydroxy-2-butyl + O<sub>2</sub> reaction, supporting its importance in  $\gamma$ -hydroxyalkyl + O<sub>2</sub> reactions. Experiments using the 1,1-d<sub>2</sub> and 4,4,4-d<sub>3</sub> isotopologs of 1-butanol suggest the presence of still unexplored pathways leading to acetaldehyde. These low-pressure experimental measurements are coordinated with kinetics calculations and pressure-dependence measurements supported under the Argonne-Sandia Consortium on High-Pressure Combustion Chemistry.

**Chemistry of QOOH radicals.** As detailed in Judit Zádor’s abstract, we have experimentally characterized both the decomposition and the reaction with O<sub>2</sub> of a QOOH radical, 2-hydroperoxy-2-methylpropan-1-yl, (CH<sub>3</sub>)<sub>2</sub>C(CH<sub>2</sub>)OOH. In the past year, new measurements of OH radical formation (with oxalyl chloride as the photolyte) were implemented to improve the experimental constraints on the rate coefficients. Moreover, the O<sub>2</sub>QOOH product of the QOOH + O<sub>2</sub> reaction was detected by photoionization.

**Chemistry of carbonyl oxides.** Carbonyl oxides (often known as “Criegee intermediates” after Rudolf Criegee) are principally produced as intermediates in ozonolysis, and are hence important intermediates in tropospheric hydrocarbon oxidation. They are the intermediates in combustion reactions of carbenes with O<sub>2</sub>, and calculations suggest that they may also be products of QOOH + O<sub>2</sub> reactions [1]. The carbonyl oxides are singlet biradicals, and their reactivity is of considerable fundamental interest. However, they have been difficult to detect and study in the gas phase, before our detection of CH<sub>2</sub>OO [2] and measurement of its reaction kinetics<sup>(i,1)</sup> by photoionization mass spectrometry. We have continued to measure reactions of CH<sub>2</sub>OO, determining upper limits for reactions with alkenes, for example.

**Pressure Dependence and Chemical Activation.**<sup>(e)</sup> The stabilization of chemically activated intermediates is important in many oxidation systems, for example in the reactions of hydroxyl radicals with unsaturated organic compounds. In combustion or atmospheric oxidation, stabilization competes with further reaction with the O<sub>2</sub> that is typically present in great excess, and bimolecular reactions of chemically activated radical adducts can occur [3]. However in these systems O<sub>2</sub> can also act as a simple “third body” and collisionally thermalize the excited adduct. Typical models of pressure-dependent reactions in combustion treat stabilization by O<sub>2</sub> as roughly equivalent to, or slightly less effective than, stabilization by N<sub>2</sub>. In the process of investigating formation of Criegee intermediate (CH<sub>2</sub>OO) in the reaction of CH<sub>2</sub>I with O<sub>2</sub>, we measured the absolute yield of I atom as a function of pressure for N<sub>2</sub>, He, and O<sub>2</sub> buffer at 298 K, and

discovered a surprising anomaly. The apparent collision efficiency of O<sub>2</sub> in stabilizing CH<sub>2</sub>IOO is a remarkable factor of 13 larger than that of N<sub>2</sub>, which suggests either an unusually strong interaction or a reaction between the chemically activated CH<sub>2</sub>IOO<sup>#</sup> and O<sub>2</sub>. These two possible explanations have different potential implications. Reaction of chemically activated molecules with O<sub>2</sub> has been discussed by Glowacki et al. in the context of tropospheric chemistry [3]. The effects in combustion chemistry would be similarly governed by the relationship between the lifetime of the activated intermediate and the rate coefficient for reaction. On the other hand, if the higher apparent collision efficiency for O<sub>2</sub> in the CH<sub>2</sub>I + O<sub>2</sub> reaction reflects stabilization rather than reaction, additional investigation may be required to understand its mechanism, and whether other systems may exhibit similar effects for collisions with O<sub>2</sub>.

### FUTURE DIRECTIONS

We will continue to expand our exceptionally productive collaboration with David Osborn, using the photoionization mass spectrometry machine at the Advanced Light Source. The effects of unsaturation and oxygenation on low-temperature oxidation chemistry will be further explored. Measurements of elementary oxidation reactions of representative biofuel molecules in the temperature region 500 K – 800 K will continue, with a continuing goal of developing a more general understanding of the ignition chemistry of alternative fuels. We have begun to measure the fundamental chemistry of some esters in collaboration with former postdoc Giovanni Meloni (now at University of San Francisco) and will extend those efforts in the near future.

The <sup>3</sup>CH<sub>2</sub> + O<sub>2</sub> reaction takes place on both singlet and triplet surfaces. Reaction on the singlet surface proceeds through the Criegee intermediate, CH<sub>2</sub>OO [4], the decomposition of which can lead to several exothermic channels: HCO + OH, CO<sub>2</sub> + H<sub>2</sub> (or 2 H), or CO + H<sub>2</sub>O (or OH + H). The ability to directly produce the Criegee intermediate allows investigations of its thermal dissociation, which will characterize the transition state out of that initial singlet intermediate. The ultraviolet absorption spectrum of CH<sub>2</sub>OO<sup>(f)</sup> has been determined by Marsha Lester and coworkers [5]; although it partially overlaps with the expected spectrum for other species in the CH<sub>2</sub>I + O<sub>2</sub> reaction system, it may be possible to choose a wavelength that will probe the kinetics of CH<sub>2</sub>OO. We will also pursue methods to produce larger Criegee intermediates, first by simply extending our method of reacting α-iodoalkyl radicals with O<sub>2</sub>. Measurement of the kinetics of larger Criegee species will probe how substitution affects their reactivity and stability.

The study of QOOH reactions will continue the longstanding quest to directly detect QOOH. One key difficulty has been simply making a high enough concentration of QOOH, and the reactions of Cl with alkyl hydroperoxides offer a path to overcome this difficulty. Reactions of QOOH with molecular oxygen remain the most important unmapped area in autoignition chemistry. As advanced theoretical kinetics develops rigorous predictions for these reactions, experiment must be able to detect products of these reactions for validation of theory.

### References

1. A. Andersen; E. A. Carter, *J. Phys. Chem. A* 107 (44) (2003) 9463-9478
2. C. A. Taatjes; G. Meloni; T. M. Selby; A. J. Trevitt; D. L. Osborn; C. J. Percival; D. E. Shallcross, *J. Am. Chem. Soc.* 130 (2008) 11883-11885

3. D. R. Glowacki; J. Lockhart; M. A. Blitz; S. J. Klippenstein; M. J. Pilling; S. H. Robertson; P. W. Seakins, *Science* **337** (2012) 1066-1069
4. B.-Z. Chen; J. M. Anglada; M.-B. Huang; F. Kong, *J. Phys. Chem. A* **106** (2002) 1877-1884
5. J. M. Beames; F. Liu; L. Lu; M. I. Lester, *J. Am. Chem. Soc.* **134** (2012) 20045-20048 doi:10.1021/ja310603j.

#### Publications acknowledging BES support, 2011 –

- a. Xia Zhang, Chris J. Eyles, Craig A. Taatjes, Dajun Ding and Steven Stolte, “A general scaling rule for the collision energy dependence of a rotationally inelastic differential cross-section and its application to NO(X) + He,” *Phys. Chem. Chem. Phys.* in press, doi: 10.1039/C3CP50558H (2013).
- b. Fabien Goulay, Adeeb Derakhshan, Eamonn Maher, Adam J. Trevitt, John D. Savee, Adam M. Scheer, David L. Osborn, and Craig A. Taatjes, “Formation of dimethylketene and methacrolein by reaction of the CH radical with acetone,” *Phys. Chem. Chem. Phys.* **15**, 4049–4058 doi:10.1039/c3cp43829e (2013).
- c. Oliver Welz, Stephen J. Klippenstein, Lawrence B. Harding, Craig A. Taatjes and Judit Zádor “Unconventional Peroxy Chemistry in Alcohol Oxidation – The Water Elimination Pathway,” *J. Phys. Chem. Lett.* **4**, 350–354 doi:10.1021/jz302004w (2013).
- d. Oliver Welz, John D. Savee, Arkke J. Eskola, Leonid Sheps, David L. Osborn, and Craig A. Taatjes, “Low-Temperature Combustion Chemistry of Biofuels: Pathways in the Low-Temperature (550-700 K) Oxidation Chemistry of Isobutanol and *tert*-Butanol,” *Proc. Combust. Inst.* **34**, 493-500 doi:10.1016/j.proci.2012.05.058 (2013).
- e. Haifeng Huang, Arkke J. Eskola, and Craig A. Taatjes, “Pressure-dependent I atom yield in the reaction of CH<sub>2</sub>I with O<sub>2</sub> shows a remarkable apparent third-body efficiency for O<sub>2</sub>,” *J. Phys. Chem. Lett.* **3**, 3399–3403 doi:10.1021/jz301585c (2012).
- f. Edmond P. F. Lee, Daniel K. W. Mok, Dudley E. Shallcross, Carl J. Percival, David L. Osborn, Craig A. Taatjes, and John M. Dyke, “Spectroscopy of the simplest Criegee intermediate CH<sub>2</sub>OO: Simulation of the first bands in its electronic and photoelectron spectra,” *Chem.–Eur. J.* **18**, 12411–12423 doi:10.1002/chem.201200848 (2012).
- g. Amelia W. Ray, Craig A. Taatjes, Oliver Welz, David L. Osborn, and Giovanni Meloni, “Synchrotron Photoionization Measurements of OH-initiated Cyclohexene Oxidation: Ring-Preserving Products in OH + Cyclohexene and 2-Hydroxycyclohexyl + O<sub>2</sub> Reactions,” *J. Phys. Chem. A* **116**, 6720–6730 doi: 10.1021/jp3022437 (2012).
- h. Fabien Goulay, Adam J. Trevitt, John D. Savee, Jordy Bouwman, David L. Osborn, Craig A. Taatjes, Kevin R. Wilson, and Stephen R. Leone, “Product detection of the CH radical reaction with acetaldehyde,” *J. Phys. Chem. A* **116**, 6091–6106 doi:10.1021/jp2113126 (A. R. Ravishankara festschrift) (2012).
- i. Craig A. Taatjes, Oliver Welz, Arkke J. Eskola, John D. Savee, David L. Osborn, Edmond P.F. Lee, John M. Dyke, Daniel W. K. Mok, Dudley E. Shallcross, and Carl J. Percival, “Direct Measurement of Criegee Intermediate (CH<sub>2</sub>OO) Reactions with Acetone, Acetaldehyde, and Hexafluoroacetone,” *Phys. Chem. Chem. Phys.* **14**, 10391–10400, doi:10.1039/C2CP40294G (2012).
- j. John D. Savee, Oliver Welz, Craig A. Taatjes, and David L. Osborn, “New Mechanistic Insights to the O(<sup>3</sup>P) + Propene Reaction from Multiplexed Photoionization Mass Spectrometry,” *Phys. Chem. Chem. Phys.* **14**, 10410–10423 DOI: 10.1039/c2cp41200d (2012).
- k. John D. Savee, Satchin Soorkia, Oliver Welz, Talitha M. Selby, Craig A. Taatjes, and David L. Osborn, “Absolute Photoionization Cross-Section of the Propargyl Radical,” *J. Chem. Phys.* **136**, 134307 (2012).
- l. Oliver Welz, John D. Savee, David L. Osborn, Subith S. Vasu, Carl J. Percival, Dudley E. Shallcross, and Craig A. Taatjes, “Direct Kinetic Measurements of Criegee Intermediate (CH<sub>2</sub>OO) Formed by Reaction of CH<sub>2</sub>I with O<sub>2</sub>,” *Science*, **335**, 204–207 doi:10.1126/science.1213229 (2012).
- m. Fabien Goulay, Satchin Soorkia, Giovanni Meloni, David L. Osborn, Craig A. Taatjes, and Stephen R. Leone, “Detection of pentatetraene by reaction of the ethynyl radical (C<sub>2</sub>H) with allene (CH<sub>2</sub>=C=CH<sub>2</sub>) at room temperature,” *Phys. Chem. Chem. Phys.* **13**, 20820-20827 doi:10.1039/C1CP22609F (2011).
- n. Adam J. Trevitt, Satchin Soorkia, John D. Savee, Talitha M. Selby, David L. Osborn, Craig A. Taatjes, and Stephen R. Leone, “Revisiting the Branching Fractions of the CN + C<sub>3</sub>H<sub>6</sub> Reaction Using Synchrotron Photoionization Mass Spectrometry: Evidence for the 3-Cyanopropene Product,” *J. Phys. Chem. A* **115**, 13467–13473 doi:10.1021/jp208496r (2011).
- o. Judit Zádor, Craig A. Taatjes, Ravi X. Fernandes, “Kinetics of Elementary Reactions in Low-Temperature Autoignition Chemistry,” *Prog. Energy Combust. Sci.* **37**, 371-421 doi:10.1016/j.pecs.2010.06.006 (2011).
- p. Haifeng Huang, Daniel J. Merthe, Judit Zádor, Leonard E. Jusinski, and Craig A. Taatjes, “New experiments and validated master-equation modeling for OH production in propyl + O<sub>2</sub> reactions,” *Proc. Combust. Inst.* **33**, 293–299 doi:10.1016/j.proci.2010.06.039 (2011).

# Elementary Reactions of PAH Formation

Robert S. Tranter

Chemical Sciences and Engineering Division, Argonne National Laboratory

Argonne, IL-60439

tranter@anl.gov

## I. Program Scope

This program is focused on the experimental determination of kinetic and mechanistic parameters of elementary reactions, in particular those involved in the formation and destruction of the building blocks for aromatic species. Recently, the program has also encompassed the study of ethers and cyclic species and their dissociation products that are representative of oxygenated intermediates in combustion mechanisms. In addition, thermal sources of radicals are investigated and characterized for use in more complex reaction systems where secondary chemistry can be significant. The approach involves a diaphragmless shock tube (DFST) equipped with laser schlieren (LS) and a time-of-flight mass spectrometer (TOF-MS) and low pressure, fast flow, reactor equipped with a quadrupole MS. The combination of these techniques accesses a wide range of reaction temperatures and pressures.

## II. Recent Progress

### A. Fluorobenzene, chlorobenzene and *o*-benzyne

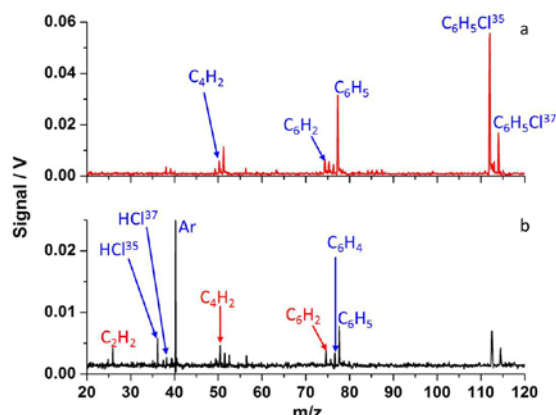


**Figure 1:** TOF-MS of  $C_6H_5Cl$ . a) Pure  $C_6H_5Cl$ . b) 2%  $C_6H_5Cl$ /3% Ar/ 95% Neon.  $T_5 = 1844$  K,  $P_5 = 195$  Torr,  $t \sim 150$   $\mu$ s after reflected shock wave.

Previous studies<sup>i</sup> demonstrated that the role of *o*-benzyne in the formation of polyaromatic hydrocarbons and soot is much more significant than previously thought. Consequently, a series of experiments were started to develop well characterized sources of *o*-benzyne for DFST/LS and TOF-MS studies and to study the dissociation of the diradical. In an earlier abstract results from experiments with thermal dissociation of fluorobenzene, reaction (1), as the source of *o*- $C_6H_4$  were reported as were initial studies at lower but overlapping temperatures with chlorobenzene as the radical source. Chlorobenzene is not as clean a source because dissociation proceeds by both HCl elimination, reaction (2a) and C-Cl scission, reaction (2b). The barrier to HCl

elimination was calculated as 87.8 kcal/mol (B3LYP/6-311+G(d,p)) and at the conditions of the current work  $k_{2a}/k_{2b} \sim 0.5$ . Reaction (2b) produces phenyl radicals rather than the desired *o*-benzyne radicals. However, dissociation of phenyl generates *o*-benzyne and recombination of phenyl radicals have been previously studied in the DFST/LS<sup>i</sup> and thus provide little complication to interpretation of the  $C_6H_5Cl$  experiments.



The literature on chlorobenzene dissociation is sparse but the HCl elimination channel appears to have been neglected in prior shock tube studies.<sup>ii,iii</sup> The LS experiments were complemented by DFST/TOF-MS experiments to examine the reaction products and help unravel the reaction mechanism. A sample mass spectrum is shown in Fig. 1. The presence of acetylene and diacetylene in Fig. 1b are consistent with those expected with dissociation of *o*-benzyne by a reverse Diels-Alder reaction.<sup>iv,v</sup>

Triacetylene is consistent with the minor path for dissociation of *o*-C<sub>6</sub>H<sub>4</sub>, proposed by Xu et al.,<sup>iv</sup> through loss of an H-atom followed by dissociation of the resulting C<sub>6</sub>H<sub>3</sub> radical. An unexpected result from the LS experiments with both chloro and fluorobenzene is that *o*-benzyne reacts readily with the parent molecule abstracting a hydrogen atom and the resulting halophenyl radical eliminates HF/Cl to form C<sub>6</sub>H<sub>3</sub> and hence enhances early production of C<sub>6</sub>H<sub>2</sub>. It is likely that this route is responsible for the relatively large amount of triacetylene found early in DFST/TOF-MS experiments with both precursors, although more work is required to fully understand the production of triacetylene.

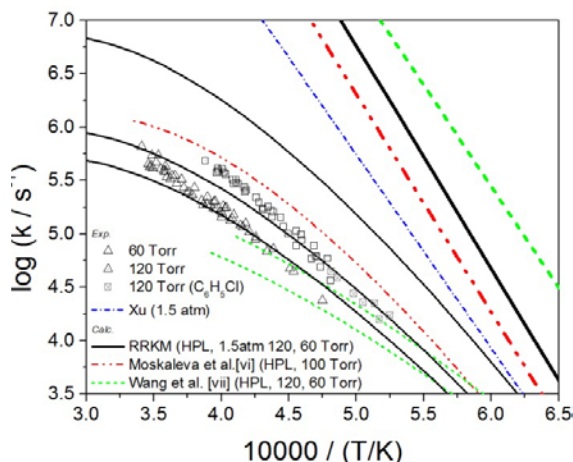
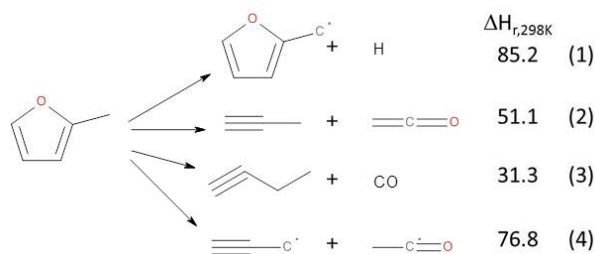


**Figure 2** First order rate coefficients for *o*-C<sub>6</sub>H<sub>4</sub> → C<sub>2</sub>H<sub>2</sub> + C<sub>4</sub>H<sub>2</sub>. RRKM model: E<sub>0</sub> = 89.3 kcal/mol, ΔE<sub><down></sub> = 700 cm<sup>-1</sup>.

Diels Alder dissociation of *o*-C<sub>6</sub>H<sub>4</sub> were derived by simulating the LS profiles and are shown in Fig. 2 along with results from RRKM calculations and literature values. In the RRKM model E<sub>0</sub> = 89.3 kcal/mol and ΔE<sub><down></sub> = 700 cm<sup>-1</sup> and were treated as adjustable. E<sub>0</sub> is a little larger than the most recent theoretical estimate of 88 ± 0.5 kcal/mol.<sup>v</sup> The RRKM agrees well with the lower temperature values from the only other experimental measurement of *o*-benzyne dissociation<sup>iv</sup> although there is significant disagreement at high temperatures.

## B. 2-Methylfuran



little attention.<sup>vii</sup> Simmie<sup>ix</sup> has studied dissociation of 2-MF theoretically and used a master equation analysis to obtain rate coefficients for the principle steps. The dissociation is a complex multichannel process initiated by loss of an H-atom. The radicals formed can undergo internal H-atom transfers before dissociating to the products shown in the above reaction scheme.

Dissociation of chlorobenzene generates a large quantity of Cl atoms that readily abstract H-atoms from the parent molecule, again resulting ultimately in C<sub>6</sub>H<sub>2</sub>. The Cl abstraction reactions also produce HCl. Thus it is not possible from DFST/TOF-MS experiments alone to determine the branching ratio  $k_{2a}/k_{2b}$  as the observed HCl, Fig. 1b, is likely coming from reaction (2a) and the Cl abstraction reactions.

A model has been developed that accurately simulates the experimental density gradients from both the chloro and fluorobenzene LS experiments. The model builds on that used for phenyl iodide pyrolysis<sup>i</sup> with appropriate substitutions for C<sub>6</sub>H<sub>5</sub>F/Cl and dissociation of *o*-benzyne. At the very highest temperatures a sub-mechanism for dissociation of acetylene is also included. The rate coefficients for the reverse

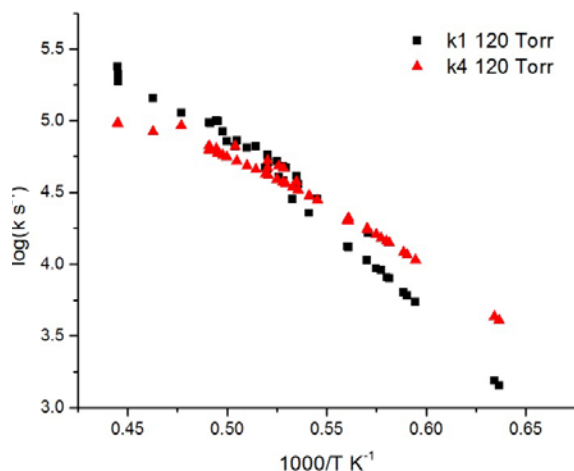


**Figure 2** First order rate coefficients at 120 Torr from LS experiments with 2% 2-MF dilute in krypton.

considerably reduced sensitivity to reaction (2) due to the much smaller heat of reaction even though the estimated rate coefficient is similar to that of reaction (1). Additionally, the products of reaction (2) are stable on the timescales of the LS experiments and have little influence on the secondary chemistry. Similarly, reaction (3) generates stable products and contributes little to the observed density gradients. The derived  $k_1$  and  $k_4$  at 120 Torr (1% and 2% 2-MF dilute in krypton) are shown in Fig. 2. The C-H scission channel, reaction (1), starts to dominate above about 1900 K but at lower temperatures reaction (4) is most important. Reaction (1) generates an H-atom and reaction (4) leads to the acetyl radical which readily dissociates to  $\text{CH}_3 + \text{CO}$ . Consequently, attack by H-atoms and  $\text{CH}_3$  radicals on the parent molecule are significant at all temperatures of the current work. Good comparison between the simulation results and the experimental data are obtained across the complete range of experimental results and the rate coefficients for reactions (1) and (4) show strong pressure dependencies.

### C. Cyclopentane and 1-pentene

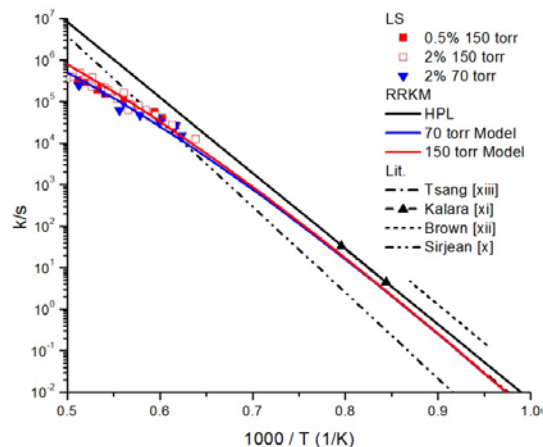


**Figure 4:** 1<sup>st</sup> order rate coefficients for dissociation of cyclopentane. For the RRRKM model  $E_0 = 78.5$  kcal/mol,  $\Delta E_{\text{down}} = 250\text{cm}^{-1}$  and reaction path degeneracy = 5.

and shape of the simulated density gradient profiles is strongly dependent upon the rates and reaction paths of these reactions. In the current work a wide range of initial reagent concentrations was used with the lowest concentrations giving sufficient signal while minimizing the influence of secondary reactions.

Pyrolysis of 2-MF has been studied by DFST/LS ( $1550 < T_2 < 2200$  K;  $P_2=30, 60$  and 120 Torr) and rate coefficients obtained for the main initial dissociation steps. Interpreting LS experiments for such a complex initial dissociation is challenging and tractable only in combination with reasonable estimates of rate coefficients and mechanism. Rate coefficients were estimated for the non-elementary reactions, (1-4) in the above scheme, from Simmie's calculations assuming the slowest step in the pathway was rate determining. The LS experiments are particularly sensitive to reactions (1) and (4) due to their relatively large heats of reaction and modeling of the complete density gradient profile for each experiment in the broad range covered allows reliable estimates to be made for  $k_1$  and  $k_4$ . The LS experiments show

Dissociation of cyclopentane has been studied theoretically and experimentally<sup>x-xiii</sup> and there is general agreement that the primary route is ring opening resulting in 1-pentene. As to whether this occurs via a diradical mechanism or similar to cyclohexene by simultaneous C-C bond breaking and intramolecular H-atom transfer is not clear. Dissociation of cyclopentane and 1-pentene have been studied by DFST/LS, the later molecule providing detail about the secondary chemistry of cyclopentane pyrolysis. At the conditions of the cyclopentane studies the 1-pentene dissociates almost immediately to ethyl and allyl radicals. A particular difficulty with simulating dissociation of cyclopentane is that ethyl radicals immediately dissociate to generate H-atoms that readily attack the parent molecule and they also react with the allyl radicals that are also present in large concentrations. Thus the secondary chemistry

This has allowed a model to be developed that provides good simulation over a broad range of conditions. Rate coefficients for dissociation of cyclopentane are shown in Fig. 4 where they are compared with literature values and the results of a RRKM model. Again  $E_0$  and  $\Delta E_{\text{down}}$  were treated as adjustable parameters and modified to fit the current work and data of Kalara et al. The preferred  $E_0$  (78.5 kcal/mol) is 4 kcal/mol lower than the calculated value of 82.4 kcal/mol from Sirjean et al.<sup>x</sup>

### III. Future Work

The current DFST/TOF-MS studies of fluorobenzene and chlorobenzene will be expanded and supplemented with experiments with bromobenzene as a precursor for phenyl and *o*-benzyne radicals. This will result in a comprehensive study of pyrolysis of halobenzenes and the recombination and dissociation reactions of important PAH building blocks. Additional experiments are planned to study reactions of phenyl and *o*-benzyne radicals with small molecules such as  $C_2H_2$  and  $CH_3$ . Further investigations of PAH formation are planned with studies of the H-atom catalyzed conversion of fulvene to benzene. Investigations of the mechanisms and kinetics of high temperature dissociation of cyclic molecules are ongoing and will include dissociation of cycloheptane and 2-DMF. Additional work related to dissociation of biofuels will be performed by studying dissociation of methyl acetate by DFST/LF complementing recent work by Michael and co-workers.<sup>xiv</sup>

### IV. References

- i. Tranter R. S., Klippenstein S. J., Harding L. B., Giri B. R., Yang X., Kiefer J. H. *J. Phys. Chem. A* **2010**, *114*, 8240
- ii. Kern R.D., Xie K., Chen H., *Combust. Sci. Technol.*, **1992**, *85*, 77.
- iii. Rao V. S., Skinner G. B., *J. Phys. Chem.* **1988**, *92*, 2442
- iv. Xu, C.; Braun-Unkhoff, M.; Naumann, C.; Frank, P. *Proc. Combust. Inst.* **2007**, *31*, 231.
- v. Zhang, X.; Maccarone, A. T.; Nimlos, M. R.; Kato, S.; Bierbaum, V. M.; Ellison, G. B.; Ruscic, B.; Simmonett, A. C.; Allen, W. D.; Schaefer, H. F.; III *J. Chem. Phys.* **2007**, *126* (4), 044312-044320
- vi. Moskaleva, L., Madden, L., Lin, M., *Phys. Chem. Chem. Phys.*, **1999**, *1*, 3967.
- vii. Wang, H., Laskin, A., Moriarty, N., Frenklach, M. *Proc. Combust. Inst.*, **2000**, *28*, 1545.
- viii. Lifshitz A., Tamburu C., Shashua R., *J. Phys. Chem. A*, **1997**, *101*, 108
- ix. Simmie J. *Private communication*
- x. Sirjean B., Glaude P. A., Ruiz-Lopez M. F., Fournet R., *J. Phys. Chem. A*, **2006**, *110*, 12693.
- xi. Kalara B. L., Feinstein S. A., Lewis D. K., *Can J Chem*, **1979**, *57*, 1324.
- xii. Brown T. C., King K. D., Nguyen T. T., *J. Phys. Chem.*, **1986**, *90*, 419.
- xiii. Tsang W, *Int. J. Chem. Kinet.*, **1978**, *10*, 599.
- xiv. Peukert S. L., Sivaramakrishnan R., Su M. C., Michael J. V., *Combust. Flame*, **159**, 7, 2312.

### V. Publications and submitted journal articles supported by this project 2011-2013

1. Tranter R. S., Lynch P. T., Yang X., 'Dissociation of dimethyl ether at high temperatures' *Proc. Combust. Inst.* **34**, 591-598 (2013)
2. Tranter R. S., Lynch P. T., Annesley C. J., 'Shock tube investigation of  $CH_3 + CH_3OCH_3$ ' *J. Phys. Chem. A*, **116**, 7287-7292 (2012)
3. Yang X., Kiefer J. H., Tranter R. S. 'Thermal dissociation of ethylene glycol vinyl ether' *Phys. Chem. Chem. Phys.* **13**, 21288-21300 (2011)
4. Yang X., Tranter R. S. 'High temperature dissociation of ethyl radicals and ethyl iodide' *Intl. J. Chem. Kinet.* **44**, 433-443 (2012)
5. Tranter R. S., Yang X., Kiefer, J. H. 'Dissociation of  $C_3H_3I$  and rates for recombination of  $C_3H_3$  high temperatures' *Proc. Combust. Inst.*, **33**, 259 (2011).
6. Yang X., Jasper A. W., Giri B. R., Kiefer J. H., Tranter R. S., 'A shock tube and theoretical study on the pyrolysis of 1,4-dioxane' *13*, 3686-3700 (2011).

## Variational Transition State Theory

Donald G. Truhlar

Department of Chemistry, University of Minnesota  
207 Pleasant Street SE, Minneapolis, Minnesota 55455  
truhlar@umn.edu

### Program scope

This project involves the development of variational transition state theory (VTST) [Garrett and Truhlar 2005] including optimized multidimensional tunneling (OMT) contributions and its application to gas-phase reactions with a special emphasis on developing reaction rate theory in directions that are important for applications to combustion. The further development of VTST/OMT as a useful tool for combustion kinetics also involves (i) developing and applying new methods of electronic structure calculations for the input potential energy surface, which is typically an implicit surface defined by a level of electronic structure theory, (ii) methods to interface reaction-path and reaction-swath dynamics calculations with electronic structure theory, and (iii) methods to treat vibrational anharmonicity and vibration–rotation coupling. The project also involves the development and implementation of practical techniques and software for applying the theory to various classes of reactions and transition states and applications to specific reactions, with special emphasis on combustion reactions and reactions that provide good test cases for methods needed to study combustion reactions.

The application of VTST to gas-phase reactions is carried out by direct dynamics [Truhlar and Gordon 1990, Truhlar 1995], and it involves electronic structure calculations of potential energy surfaces and the use of these surfaces to calculate generalized free energies of activation and multidimensional tunneling probabilities. A key emphasis is the interface of electronic structure calculations with dynamics algorithms as achieved in the POLYRATE computer program and its various RATE interfaces to electronic structure packages. The methods employed in POLYRATE are described in a review article [Fernandez-Ramos 2007].

### Recent progress

The atomistic simulation of reactions of complex molecules, such as those involved in combustion, requires one to treat anharmonic, coupled torsions in both reactants and transition states, along with the accompanying torsional anharmonicity, and to consider reaction along more than one reaction path. In the past year, our major accomplishments are the development of an internal coordinate method for including multiple structures and torsional anharmonicity of torsions coupled to each other and to overall rotation and for including multiple reaction paths in reaction rate calculations that include both variationally optimized transition states and multi-dimensional tunneling. These methods have been incorporated in a computer code called *MSTor* that is now available to the community at no charge in an international program library and on our Web site. We have applied the method to calculate thermochemical quantities for many molecules, radicals, and transition states, and to calculate reaction rates of combustion reactions. Examples are given in the references below. We have recently developed a coupled version of the theory that is more accurate along reaction paths.

## Software distribution

We have developed several software packages for applying variational transition state theory with optimized multidimensional tunneling coefficients to chemical reactions. These packages are well documented and distributed with manuals, installation scripts, and test suites. The license requests that we fulfilled during the period Jan. 1, 2010–March 5, 2013, for RATE packages developed under DOE support is as follows:

	<i>Total</i>	<i>academic</i>	<i>government//DoD/non-profit/industry</i>
POLYRATE	450	508	42
GAUSSRATE	244	227	17
6 other RATE programs	94	77	17

The total number of requests fulfilled for all RATE programs since we began keeping statistics in 1995 is 2553. In 2012, we began distributing *MSTor* through both the *Computer Physics Communications* web site (<http://www.cpc.cs.qub.ac.uk>) and own web site ([t1.chem.umn.edu/truhlar/index.htm#software](http://t1.chem.umn.edu/truhlar/index.htm#software)). So far 68 copies have been distributed by the former and 18 by the latter.

## Future plans

The general objective of this project is to develop and employ improved methods for calculating the rate constants of gas-phase chemical reactions. Our current plans are as follows:

(1) First, we aim to make the combination of *MSTor* with *POLYRATE* more user friendly and more powerful. We are presently working on greatly improved versions of *POLYRATE* and *GAUSSRATE* with new capabilities for microcanonical rate constants and pressure dependence.

(2) We are especially interested in developing methods applicable to radicals, reactive intermediates, and complex and unsaturated organic molecules, as required for modeling combustion of real fuels, fuel additives, and their combustion-generated intermediates.

(3) We plan to calculate benchmark converged partition functions for molecules with multiple torsions and to use them to test approximation schemes.

(4) We will calculate rate constants for specific applications that are important in combustion.

## References Cited

- [Garrett and Truhlar 2005] "Variational Transition State Theory," B. C. Garrett and D. G. Truhlar, in *Theory and Applications of Computational Chemistry: The First Forty Years*, edited by C. E. Dykstra, G. Frenking, K. Kim, and G. Scuseria (Elsevier, Amsterdam, 2005), pp. 67-87.
- [Fernandez-Ramos 2007] "Variational Transition State Theory with Multidimensional Tunneling," A. Fernandez-Ramos, B. A. Ellingson, B. C. Garrett, and D. G. Truhlar, in *Reviews in Computational Chemistry*, Vol. 23, edited by K. B. Lipkowitz and T. R. Cundari (Wiley-VCH, Hoboken, NJ, 2007), pp. 125-232.
- [Truhlar and Gordon 1990] "From Force Fields to Dynamics: Classical and Quantal Paths," D. G. Truhlar and M. S. Gordon, *Science* **249**, 491–498 (1990).
- [Truhlar 1995] "Direct Dynamics Method for The Calculation of Reaction Rates," D. G. Truhlar, in *The Reaction Path in Chemistry: Current Approaches and Perspectives*, edited by D.

Heidrich (Kluwer, Dordrecht, 1995), pp. 229–255. [Understanding Chem. React. **16**, 229–255 (1995).]

### Publications supported by this grant, 2011-present

1. “Minimally Augmented Karlsruhe Basis Sets,” J. Zheng, X. Xu, and D. G. Truhlar, *Theoretical Chemistry Accounts* **128**, 295-305 (2011).  
[dx.doi.org/10.1007/s00214-010-0846-z](https://doi.org/10.1007/s00214-010-0846-z)
2. “Convergent Partially Augmented Basis Sets for Post-Hartree-Fock Calculations of Molecular Properties and Reaction Barrier Heights,” E. Papajak and D. G. Truhlar, *Journal of Chemical Theory and Computation* **7**, 10-18 (2011). [dx.doi.org/10.1021/ct1005533](https://doi.org/10.1021/ct1005533)
3. “Kinetic Isotope Effects for the Reactions of Muonic Helium and Muonium with H<sub>2</sub>,” D. G. Fleming, D. J. Arseneau, O. Sukhorukov, J. H. Brewer, S. L. Mielke, G. C. Schatz, B. C. Garrett, K. A. Peterson, and D. G. Truhlar, *Science* **331**, 448-450 (2011).  
[dx.doi.org/10.1126/science.1199421](https://doi.org/10.1126/science.1199421)
4. “Computational Study of the Reactions of Methanol with the Hydroperoxyl and Methyl Radicals. Part I: Accurate Thermochemistry and Barrier Heights,” I. M. Alecu and D. G. Truhlar, *Journal of Physical Chemistry A* **115**, 2811–2829 (2011).  
[dx.doi.org/10.1021/jp110024](https://doi.org/10.1021/jp110024)
5. “High-Level Direct-Dynamics Variational Transition State Theory Calculations Including Multidimensional Tunneling of the Thermal Rate Constants, Branching Ratios, and Kinetic Isotope Effects of the Hydrogen Abstraction Reactions from Methanol by Atomic Hydrogen,” R. Meana-Pañeda, D. G. Truhlar and A. Fernández-Ramos, *Journal of Chemical Physics* **134**, 094302/1-14. [dx.doi.org/10.1063/1.3555763](https://doi.org/10.1063/1.3555763)
6. “Practical Methods for Including Torsional Anharmonicity in Thermochemical Calculations of Complex Molecules: The Internal-Coordinate Multi-Structural Approximation,” J. Zheng, T. Yu, E. Papajak, I. M. Alecu, S. L. Mielke, and D. G. Truhlar, *Physical Chemistry Chemical Physics* **13**, 10885-10907 (2011). [dx.doi.org/10.1039/C0CP02644A](https://doi.org/10.1039/C0CP02644A)
7. “How Well Can Modern Density Functionals Predict Transition State Bond Distances?” X. Xu, I. M. Alecu, and D. G. Truhlar, *Journal of Chemical Theory and Computation* **7**, 1667-1676 (2011). [dx.doi.org/10.1021/ct2001057](https://doi.org/10.1021/ct2001057).
8. Multi-Structural Variational Transition State Theory. Kinetics of the 1,4-Hydrogen Shift Isomerization of the Pentyl Radical with Torsional Anharmonicity,” T. Yu, J. Zheng, and D. G. Truhlar, *Chemical Science* **2**, 2199-2213 (2011). [dx.doi.org/10.1039/C1SC00225B](https://doi.org/10.1039/C1SC00225B)
9. “Thermodynamics of C–H Bond Dissociation in Hexane and Isohexane Yielding Seven Isomeric Hexyl Radicals,” J. Zheng, T. Yu, and D. G. Truhlar, *Physical Chemistry Chemical Physics* **13**, 19318-19324 (2011). [dx.doi.org/10.1039/C1CP21829H](https://doi.org/10.1039/C1CP21829H)
10. “Statistical Thermodynamics of the Isomerization Reaction Between n-Heptane and Isoheptane,” T. Yu, J. Zheng, and D. G. Truhlar, *Physical Chemistry Chemical Physics* **14**, 482-494 (2011). [dx.doi.org/10.1039/c1cp22578b](https://doi.org/10.1039/c1cp22578b).
11. “Kinetics of the Reaction of the Heaviest Hydrogen Atom with H<sub>2</sub>, the <sup>4</sup>Heμ + H<sub>2</sub> → <sup>4</sup>HeμH + H reaction: Experiments, Accurate Quantal Calculations, and Variational Transition State Theory, Including Kinetic Isotope Effects for a Factor of 36.1 in Isotopic Mass,” D. G. Fleming, D. J. Arseneau, O. Sukhorukov, J. H. Brewer, S. L. Mielke, D. G. Truhlar, George C. Schatz, B. C. Garrett, and K. A. Peterson, *Journal of Chemical Physics* **135**, 184310/1–18 (2011).  
[dx.doi.org/10.1063/1.3657440](https://doi.org/10.1063/1.3657440)

12. "Computational Study of the Reactions of Methanol with the Hydroperoxyl and Methyl Radicals. 2. Accurate Thermal Rate Constants," I. M. Alecu, and D. G. Truhlar, *Journal of Physical Chemistry A* **115**, 14599-14611 (2011). [dx.doi.org/10.1021/jp209029p](https://doi.org/10.1021/jp209029p)
13. "Multipath Variational Transition State Theory. Rate Constant of the 1,4-Hydrogen Shift Isomerization of the 2-Cyclohexylethyl Radical," T. Yu, J. Zheng, and D. G. Truhlar, *Journal of Physical Chemistry A* **116**, 297-308 (2012). [dx.doi.org/10.1021/jp209146b](https://doi.org/10.1021/jp209146b)
14. "Multi-Structural Variational Transition State Theory: Kinetics of the 1,5-Hydrogen Shift Isomerization of 1-Butoxyl Radical Including All Structures and Torsional Anharmonicity," X. Xu, E. Papajak, J. Zheng, and D. G. Truhlar, *Physical Chemistry Chemical Physics* **14**, 4204-4216 (2012). [dx.doi.org/10.1039/c2cp23692c](https://doi.org/10.1039/c2cp23692c).
15. "Multi-path Variational Transition State Theory for Chemical Reaction Rates of Complex Polyatomic Species: Ethanol + OH Reactions," J. Zheng and D. G. Truhlar, *Faraday Discussions* **157**, 59-88 (2012). [dx.doi.org/10.1039/C2FD20012K](https://doi.org/10.1039/C2FD20012K).
16. "MSTor: A program for calculating partition functions, free energies, enthalpies, entropies, and heat capacities of complex molecules including torsional anharmonicity," J. Zheng, S. L. Mielke, K. L. Clarkson, and D. G. Truhlar, *Computer Physics Communications* **183**, 1803-1812 (2012). [dx.doi.org/10.1016/j.cpc.2012.03.007](https://doi.org/10.1016/j.cpc.2012.03.007)
17. "A Product Branching Ratio Controlled by Vibrational Adiabaticity and Variational Effects: Kinetics of the H + trans-N<sub>2</sub>H<sub>2</sub> Reactions," J. Zheng, R. J. Rocha, M. Pelegrini, L. F. A. Ferrão, E. F. V. Carvalho, O. Roberto-Neto, F. B. C. Machado, and D. G. Truhlar, *Journal of Chemical Physics* **136**, 184310/1-10 (2012). [dx.doi.org/10.1063/1.4707734](https://doi.org/10.1063/1.4707734)
18. "What are the Most Efficient Basis Set Strategies for Correlated Wave Function Calculations of Reaction Energies and Barrier Heights?" E. Papajak and D. G. Truhlar, *Journal of Chemical Physics* **137**, 064110/1-8 (2012). [dx.doi.org/10.1063/1.4738980](https://doi.org/10.1063/1.4738980)
19. "Thermochemistry of Radicals Formed by Hydrogen Abstraction from 1-Butanol, 2-Methyl-1-propanol, and Butanal," E. Papajak, P. Seal, X. Xu, and D. G. Truhlar, *Journal of Chemical Physics* **137**, 104314/1-13 (2012). [dx.doi.org/10.1063/1.4742968](https://doi.org/10.1063/1.4742968)
20. "Role of Conformational Structures and Torsional Anharmonicity in Controlling Chemical Reaction Rates and Relative Yields: Butanal + HO<sub>2</sub> Reactions," J. Zheng, P. Seal, and D. G. Truhlar, *Chemical Science* **4**, 200-212 (2013). [dx.doi.org/10.1039/c2sc21090h](https://doi.org/10.1039/c2sc21090h)
21. "Multi-Structural Variational Transition State Theory: Kinetics of the Hydrogen Abstraction from Carbon-2 of 2-Methyl-1-propanol by Hydroperoxyl Radical Including All Structures and Torsional Anharmonicity," X. Xu, T. Yu, E. Papajak, and D. G. Truhlar, *Journal of Physical Chemistry A* **116**, 10480-10487 (2012). [dx.doi.org/10.1021/jp307504](https://doi.org/10.1021/jp307504)
22. "Biofuel Combustion. Energetics and Kinetics of Hydrogen Abstraction from Carbon-1 in *n*-Butanol by the Hydroperoxyl Radical Calculated by Coupled Cluster and Density Functional Theories and Multi-Structural Variational Transition State Theory with Multidimensional Tunneling," I. M. Alecu, J. Zheng, E. Papajak, T. Yu, and D. G. Truhlar, *Journal of Physical Chemistry A* **116**, 12206-12213 (2012). [dx.doi.org/10.1021/jp308460y](https://doi.org/10.1021/jp308460y)
23. "Quantum Thermochemistry: Multi-Structural Method with Torsional Anharmonicity Based on a Coupled Torsional Potential," J. Zheng and D. G. Truhlar, *Journal of Chemical Theory and Computation*, online as Article ASAP. [dx.doi.org/10.1021/ct3010722](https://doi.org/10.1021/ct3010722)

## **SISGR: Developing a predictive model for the chemical composition of soot nanoparticles: Integrating Model and Experiment**

Lead PI: A. Violi  
University of Michigan  
Ann Arbor, MI  
avioli@umich.edu

Co-PI's: N. Hansen, H. Michelsen  
Combustion Research Facility - Sandia National Laboratories

Co:PI: K. Wilson  
Lawrence Berkeley National Laboratory  
Berkeley

### **I. Program Scope**

Mechanisms of soot formation have been studied for quite some time, and there is a general consensus that polycyclic aromatic hydrocarbons (PAH) are key intermediates: their growth leads to nucleation of particles and the latter continue to add mass via surface growth. Even though we are now able to predict the rate of soot formation to some degree of accuracy due to the development of detailed soot models, key uncertainties remain. Particularly, the mechanisms of soot nucleation and mass growth remain phenomenological.

The research program described here focuses on the development of predictive models for nanoparticle formation from combustion sources. An important part of this project is to study the nucleation process. The kinetics of nucleation control the number of nascent particles and the coagulation of these particles determine the evolution of particle number density. Various pathways have been proposed for the formation of first soot nuclei and in several landmark papers key kinetic and thermodynamic arguments were made that established the central role of condensed PAH. In this work, we use atomistic simulations to investigate the chemical and physical phenomena related to the formation of PAH dimers, their nucleation, and further growth into nanoparticles.

This project is developed in collaboration with the research group composed by Dr. Michelsen and Dr. Hansen at Sandia National Laboratories and Wilson at Lawrence Berkeley National Laboratory to develop the next generation of soot models, which allow the prediction of chemical compositions of nanoparticles produced in flames of different fuels.

### **II. Recent Progress**

The majority of work on soot formation has been driven by the need of developing predictive models for soot formation and oxidation arising from principles of kinetics and thermodynamics. Various pathways have been proposed for the formation of first soot nuclei [1-11] and in several landmark papers key kinetic and thermodynamic arguments were made that established the central role of condensed PAH. The majority of numerical studies performed with detailed models of soot formation invoke irreversible dimerization of pyrene molecules as initial nucleation step for the condensed phase [12-16]. The choice of pyrene dimerization for initiating particle nucleation was motivated by the great thermodynamic stability of this molecule [17]. The purpose of this study is to determine the thermodynamic driving forces for the formation of PAH dimers using molecular dynamics (MD) simulations.

Our recent work has focused on determining the free energy of interactions of various hydrocarbons using atomistic models.

The MD results discard the hypothesis of dimerization of small peri-condensed aromatics in flame conditions, and suggest the importance of aromatics with saturated and unsaturated chains as monomers that can lead to the formation of stable dimers. The presence of aliphatic chains favor proximity of molecules that can react or collide with other species, suggesting a more complex scenario for soot nucleation than the simple stacking of small-sized PAH.

The Helmholtz free energies of dimerization of several PAHs were computed employing molecular dynamics simulations coupled with the well-tempered Metadynamics algorithm [19]. Metadynamics is a technique used to improve the sampling of a system and reconstruct the free energy landscape. The algorithm assumes that the system can be described by a few collective variables, which discern the states (initial, final and intermediates) of the system, as well as the slow events that are relevant to the process of interest.

The following procedure was adopted to study the systems of PAH: for each pair of molecules a canonical simulation was performed for 1 ns at the target temperature (either 500 K or 1000 K). For the interaction potential, the parameters introduced by Herdmann and Miller [6] for the non-bonded potential of the aromatic rings and the all atom version of the Optimized Potentials for Liquid Simulations (OPLS-AA) force field [20] for all the other parameters were employed. Figure 1 shows the pool of molecules considered in this study.

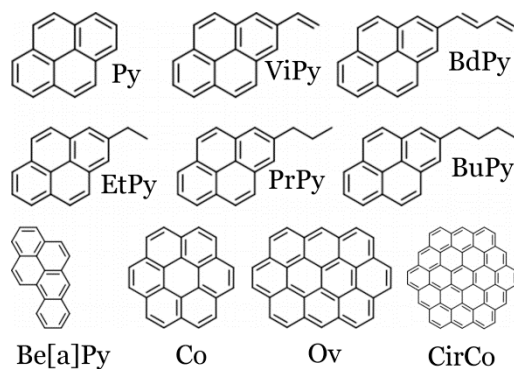


**Fig. 1.** Pool of molecules analyzed in this study

In addition to peri-condensed aromatics, we included substituted PAH with unsaturated and saturated chains to assess the role of aliphatic substituents during the clustering process. These compounds have been detected in flames and some of them are key intermediates in the HACA mechanism to describe the growth of aromatics.

Figure 2 reports the free energy profiles of pyrene substituted molecules with unsaturated and saturated chains at 500K. The plots in Fig. 2a show that there is a small increase in dimerization propensity when a vinyl chain is attached to pyrene (ViPy), but the change in the free energy curve is mostly at short distances. On the other hand, the addition of another C<sub>2</sub>H<sub>2</sub> to the system, which leads to the formation of 1,3 butadiene pyrene (BdPy), modifies the whole free energy curve. To understand the source of these effects, we simulated three dimerization processes that involve pyrene substituted with a similar but saturated aliphatic chain (*i.e.*, ethyl, *n*-propyl and *n*-butyl chains). Since these chains are more flexible and, at the same time there is no double bond that can resonate with the aromatic ring, we expect an increase in the importance of the entropic contributions and a decrease in the strength of the interaction, when compared with molecules with unsaturated chains.

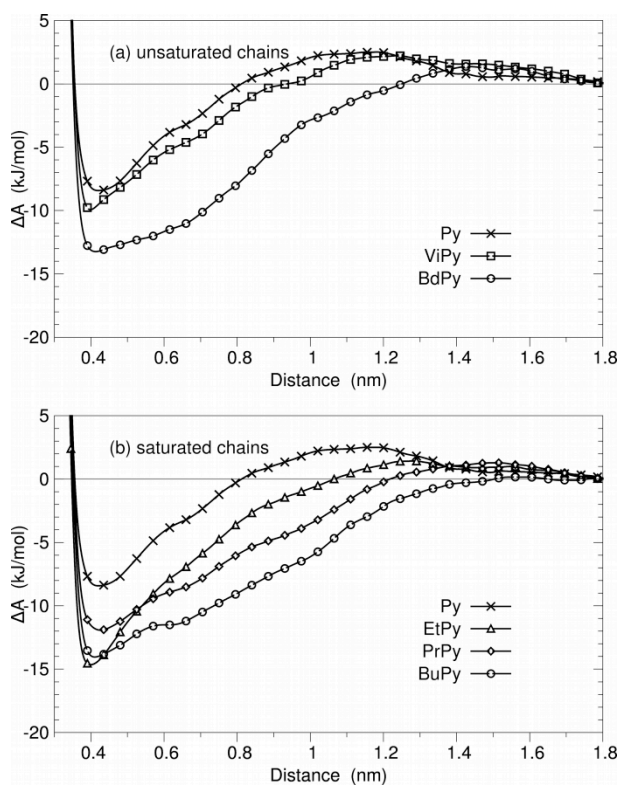


**Fig. 2.** Free energy of the dimerization of different PAHs as a function of the distance between their center of mass at (a) 500 K and (b) 1000 K. The error is less than 0.5 kJ/mol.

As shown in Fig. 2b, we can distinguish a short range ( $<0.55$  nm) effect, which mostly causes a stabilization of the dimer, and long range effects (up to about 1.2 nm), which decrease the free energy of the configurations of the two approaching monomers. The comparison between ViPy and EtPy show that the saturated compound (ETPy) has a minimum more than 3 kJ/mol deeper than the unsaturated ViPy, suggesting that the entropic effect is the most important factor contributing to the stabilization of the dimers, already at this temperature. This correlation becomes more evident if we compare BuPy with BdPy, demonstrating that the presence of a saturated chain in BuPy leads to a more stable dimer.

The results in Fig. 2 also speak to the effect of the chain length on the dimerization process. Two classes of effects influence the free energy profiles; the addition of a short flexible chain markedly increases the dimer stability by increasing the number of configurations that are available when the aromatic sites of the molecules get close (and therefore have a limited number of energetically favorable configurations). As the length of the chain increases, at short range the resulting hindrance reduces the stability and at long distances, it lowers the free energy profile. As another carbon is added to the chain, i.e. BuPy, the stabilization of the dimer from the contributions of entropy and potential energy, compensates for the increased volume of the side chain, producing a lower free energy profile as compared with the previous cases. However, a telltale mark of the steric hindrance is still visible in the shift of the minimum of BuPy to slightly longer distances.

While these simulations do not describe the dynamics of the system and therefore quantities like the lifetime of the aggregates should be computed by other means, the stabilization of loose aggregates (for which the distance between the aromatic rings is  $> 0.6$  nm), suggests that these configurations can play a role in the preliminary phase of soot formation.

### III. References

- [1] Homann KH. *Angewandte Chemie-International Edition*. **1998**, 37(18), 2435.
- [2] D'Anna A. *Proceedings of the Combustion Institute*. **2009**, 32, 593.
- [3] Frenklach M, Wang H. **1991**, 23(1), 1559.
- [4] Miller JH. *Symposium (International) on Combustion*. **1991**, 23(1), :91.
- [5] Herdman JD, Miller JH. *Journal of Physical Chemistry A*. **2008**, 112(28), 6249.
- [6] Richter H, Benish TG, Mazyar OA, Green WH, Howard JB. *Proceedings of the Combustion Institute*. **2000**, 28, 2609.
- [7] Apicella B, Ciajolo A, Suelves I, Morgan TJ, Herod AA, Kandiyoti R. *Combustion Science and Technology*. **2002**, 174(11-2), 345.
- [8] Chung SH, Violi A. *Journal of Chemical Physics*, **2011**, 132.
- [9] Chung SH, Violi A. *Carbon*. **2007**, 45(12), 2400.
- [10] Izvekov S, Violi A. *Journal of Chemical Theory and Computation*, **2006** May;2(3):504-12.
- [11] Violi A, Izvekov S. *Proceedings of the Combustion Institute*. **2007** 2007;31:529-37.
- [12] Kazakov A, Wang H, Frenklach M. *Combustion and Flame*, **1995**, 100(1-2):111-20.
- [13] Appel J, Bockhorn H, Frenklach M. *Combustion and Flame*, **2000** Apr;121(1-2):122-36.
- [14] Marquardt M, Mauss F, Jungfleisch B, Suntz R, Bockhorn H. *Twenty-Sixth Symposium on Combustion* **1996**:2343-50.
- [15] Bai XS, Balthasar M, Mauss F, Fuchs L. *Twenty-Seventh Symposium* **1998**:1623-30.
- [16] Davis SG, Wang H, Brezinsky K, Law CK. *Twenty-Sixth Symposium* **1996**:1025-33.
- [17] Schuetz CA, Frenklach M. *Proceedings of the Combustion Institute*. **2002**;29:2307-14.
- [18] Wang H. *Proceedings of the Combustion Institute*. **2011**, 33, 41.
- [19] Barducci A, Bussi G, Parrinello M. *Physical Review Letters*. **2008**, 100(2), 020603.
- [20] Jorgensen WL, Maxwell DS, Tirado-Rives J. *J. American Chemical Society*. **1996**, 118(45), 11225.

### IV. Publications and submitted journal articles supported by this project

1. S.H. Chung, A. Violi “Nucleation of Fullerenes as a Model for Examining the Formation of Soot”, *J. Chem. Phys.* 132(17): 174502 (2010).
2. S.H. Chung, A. Violi “Pericondensed aromatics with aliphatic chains as key intermediates for the nucleation of aromatic hydrocarbons” *Proc. Combust. Inst.* 33(1), 693-700, (2011).
3. S.A. Skeen, H.A. Michelsen, Kevin R. Wilson, Denisia M. Popolan, A. Violi, N. Hansen, “Near-Threshold Photoionization Mass Spectra of Combustion-Generated High-Molecular-Weight Soot Precursors”, *J. Aerosol Science*, (2013), <http://dx.doi.org/10.1016/j.jaerosci.2012.12.008>
4. S.A. Skeen, B. Yang, H.A. Michelsen, J.A. Miller, A. Violi, N. Hansen “Studies of laminar opposed-flow diffusion flames of acetylene at low-pressures with photoionization mass spectrometry”, *Proceedings of the Combustion Institute* 34 (2013), pp. 1067-1075.
5. P. Elvati, A. Violi “Thermodynamics of poly-aromatic hydrocarbon clustering and the effects of substituted aliphatic chains” *Proceedings of the Combustion Institute* 34 (2013), pp. 1837-1843.

# PRESSURE DEPENDENCE OF COMBUSTION REACTIONS: QUANTUM INELASTIC DYNAMICS ON AUTOMATICALLY GENERATED POTENTIAL ENERGY SURFACES

Albert Wagner  
Chemical Sciences and Engineering Division  
Argonne National Laboratory  
9700 South Cass Avenue  
Argonne, IL 60439  
Email: [wagner@anl.gov](mailto:wagner@anl.gov)

## PROJECT SCOPE

This program is aimed both at developing improved ways to automatically construct a reliable potential energy surface (PES) and at using such surfaces to carry out inelastic quantum dynamics studies on pressure effects. Among several methods capable of growing a PES, this program is especially interested in the interpolative moving least squares (IMLS) method with a local error estimator based on contending basis sets. Among the several inelastic quantum dynamics methods, this program is investigating the infinite order sudden approximation in the context of time dependent quantum dynamics.

## RECENT PROGRESS

In collaboration with R. Dawes (Missouri University of Science and Technology) and D. Thompson (University of Missouri), we have compared the ground state  $^2A''$  HO<sub>2</sub> IVR, isomerization, and dissociation dynamics determined by classical trajectories on an IMLS PES,<sup>1</sup> a spline fit PES (XXZLG<sup>2</sup>), and a double many body expansion PES (DMBE-IV<sup>3</sup>). The underlying electronic structure theory for the IMLS and XXZLG PESs are similar MRCI calculations with IMLS incorporating larger basis sets effects. The XXZLG PES also has small artifacts in the isomerization region due to ringing of the spline and incomplete mirror symmetry about the perpendicular bisector of the O-O bond. The pioneering DMBE-IV PES uses

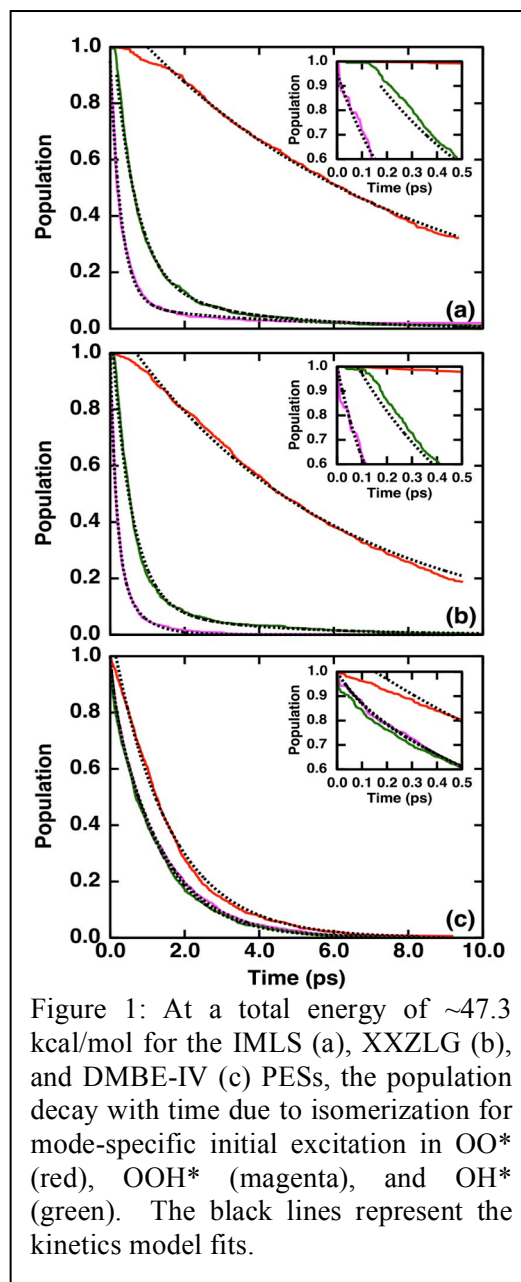


Figure 1: At a total energy of  $\sim 47.3$  kcal/mol for the IMLS (a), XXZLG (b), and DMBE-IV (c) PESs, the population decay with time due to isomerization for mode-specific initial excitation in OO\* (red), OOH\* (magenta), and OH\* (green). The black lines represent the kinetics model fits.

experimental information and lower quality ab initio information. IMLS and XXZLG PESs produce similar but not identical results as seen in Fig. 1 for isomerization at the same total energy but with one of the three vibrational modes excited while the other two modes are at their zero point energy. For IMLS and XXZLG, isomerization is highly mode specific; IVR is not fast enough to erase initial condition effects prior to isomerization. The early time behavior and bi-exponential character of the decay curves on these two PESs are related to the strong local mode character of the O-O stretch. Close inspection of the inserts will reveal “ballistic” type isomerization for OOH\* excitation where isomerization directly occurs without any intervening vibrational turning points. In contrast, isomerization dynamics on DMBE-IV is much less mode specific and single exponential in character. This contrast between DMBE-IV and IMLS/XXZLG is also present in IVR and unimolecular dissociation. Interestingly, the strong local mode character of the O-O stretch on the IMLS and XXZLG PESs means that the as yet un-isomerized HO<sub>2</sub> population becomes progressively enriched in OO\* excitation as time goes on. Presumably the reactive chemistry of this population would be different from the isomerized population.

In collaboration with the Thompson group, we have carried out trajectory studies of isomerization and dissociation for C<sub>2</sub>H<sub>5</sub> at energies at which very long unimolecular dissociation times (~100 nanoseconds) have been experimentally reported<sup>4,5</sup> from photoexcitation experiments where the electronically excited C<sub>2</sub>H<sub>5</sub>\* is presumed to intersystem cross to and dissociate on the ground state. An AIREBO<sup>6</sup> molecular mechanics PES was used that was significantly modified to reproduce key features of ab initio CBS-QB3 dissociation and isomerization saddle points. This is the first application of AIREBO for gas phase reactions and the minor computational cost in evaluating this PES enables batches of 10,000 trajectories to be run until all dissociate. At the lowest energies of the experimental range, all trajectories dissociated in ~100 ps with dissociation times consistent with RRKM values and several orders of magnitude less than experimental values. In addition, Fig. 2(a) shows that at the higher end of the

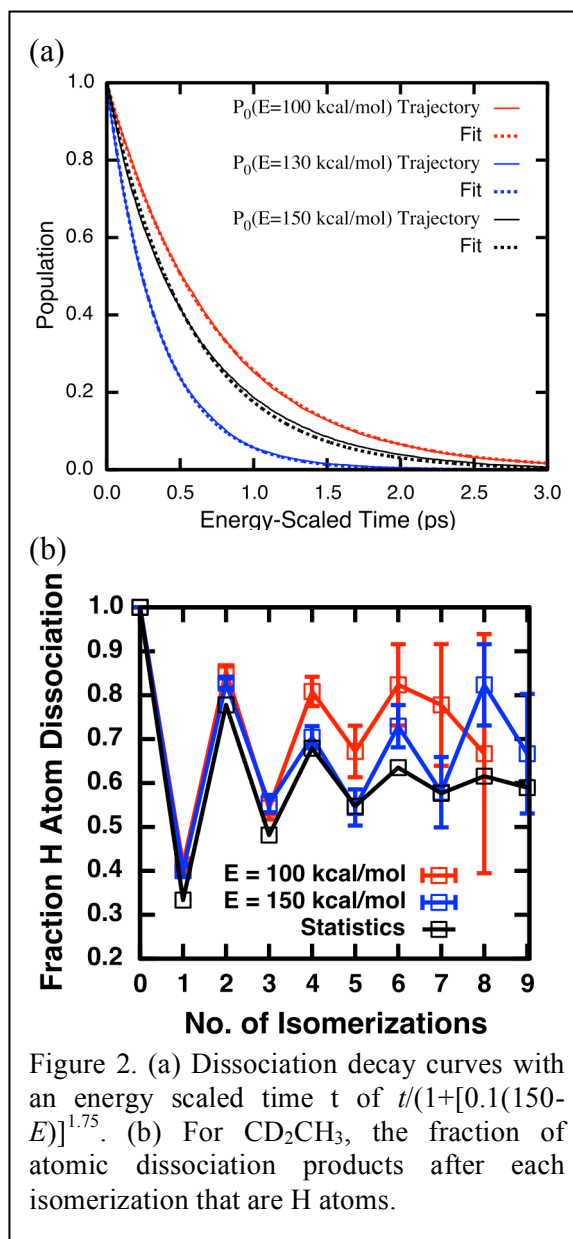


Figure 2. (a) Dissociation decay curves with an energy scaled time  $t$  of  $t/(1+[0.1(150-E)]^{1.75})$ . (b) For CD<sub>2</sub>CH<sub>3</sub>, the fraction of atomic dissociation products after each isomerization that are H atoms.

experimental range of energies, a single exponential fit to the dissociation begins to fail. Modeling suggests that failure is due to an IVR bottleneck at higher energies. (Energy scaling of time allows the three decay curves at different energies to have comparable resolution on the plot.) In Fig. 2(b), the fraction of H dissociation of  $\text{CD}_2\text{CH}_3$  as a function of the number of isomerizations is shown to be largely statistical (black line) with some additional bias for H dissociation relative to D. Interestingly, on this PES the difference in energy dependence of the isomerization rate versus the dissociation rate leads to a dip in the overall dissociation isotope effect as a function of energy. However the one available experimental measurement in this energy range (more than a factor of two about the dissociation energy) shows this PES allows too much isomerization.

In collaboration with the Dawes group, H. Guo (U. New Mexico), and R. Continetti (UC San Diego), we are reproducing the Continetti modeling<sup>7</sup> of his HOCO tunneling measurements but using ab initio PESs instead of a model potential and multidimensional tunneling via POLYRATE and SCTST<sup>8</sup> instead of a one dimensional semiclassical tunneling. As suspected in Ref. 7, the widely used LTSH PES<sup>9</sup> cannot reproduce the experimental results. However the CCSD-3/d PES<sup>10</sup> by the Guo and Bowman groups in combination with POLYRATE tunneling does compare well with experiment as seen in Fig. 3. Similar results are found for a CASPT2 PES under development. Comparisons between POLYRATE and SCTST tunneling calculations for this application are in progress.

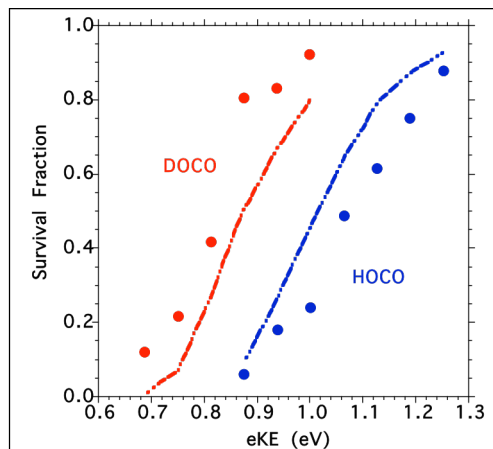


Figure 3. The fraction of H(D)OCO created from the anion by photodetachment that reaches the detector without tunneling to products: measurements (circles), CCSD-3/d POLYRATE calculations (lines).

## FUTURE PLANS

In the development of PESs, the  $\text{HO}_2$  and HOCO PESs will be extended to include rare gas and other colliders. Since an IMLS approach can operate on ab initio information over an irregular array of geometries, spatial and/or compositional extensions of a PES are relatively straightforward. For the  $\text{C}_2\text{H}_5$  work, M05 DFT calculations will be compared to the modified AIREBO PES to test its usefulness as a zeroth order PES. If so, IMLS-type methods need only be applied to correct AIREBO and would presumably require fewer ab initio calculations. In collaboration with Y. Suleymanov and W. Green (MIT), we are pursuing the application of IMLS methods to automatically grow that portion of the PES needed for ring polymer molecular dynamics (RPMD) calculations of abstraction and insertion rate constants. RPMD methods can extract from specially formulated classical trajectory calculations quantum dynamics information including tunneling.

The second aspect of this program is the application of quantum dynamics calculations of the inelastic properties of chemically activated molecular complexes. Such studies can

address the effects of zero point energy and the details of mode specificity. The starting point of this program is the parallelized four atom time dependent quantum dynamics codes<sup>11</sup> of S. Gray (Argonne). This code will be modified for the infinite order sudden (IOS) approximation to make the calculations more tractable. Essentially all past quantum treatments of pressure effects in combustion reactions used this approximation and it should apply because typically rotations are significantly slower than vibrational motion. Time-dependent quantum dynamics is a natural framework for this problem because the initial wavepacket can be constructed with a collider component possessing a thermal translational energy profile and with a chemically activated molecular component with filtered eigenstates in a specific energy grain. In this application, the goal is to filter the eigenstates only sufficiently to distinguish one energy grain from another. This incomplete filtering will make the calculations more practical and also more applicable to Master Equation modeling.

- <sup>1</sup> A. Li, D. Xie, R. Dawes, A. W. Jasper, J. Ma, and H. Guo, *J. Chem. Phys.* **133**, 144306 (2010).
- <sup>2</sup> C. Xu, D. Xie, P. Honvault, S. Y. Lin, and H. Guo, *J. Chem. Phys.* **127**, 024304 (2007).
- <sup>3</sup> M. R. Pastrana, L. A. M. Quintales, J. Brandão, and A. J. C. Varandas, *J. Chem. Phys.* **94**, 8073 (1990).
- <sup>4</sup> Gilbert, T.; Gerbner, T. L.; Fischer, I.; Chen, P. *J. Chem. Phys.* **1999**, *110*, 5485-5488.
- <sup>5</sup> Steinbauer, M.; Giegerich, J.; Fischer, K. H.; Fischer, I. *J. Chem. Phys.* **2012**, *137*, 014303.
- <sup>6</sup> A. Liu and S. J. Stuart, *J. Comp. Chem.* **29**, 601 (2008).
- <sup>7</sup> C. J. Johnson, B. L. J. Poad, B. B. Shen and R. E. Continetti, *J. Chem. Phys.* **134**, 171106 (2011).
- <sup>8</sup> As developed by T. L. Nguyen, J. F. Stanton, and J. R. Barker and contained in Multiwell at <http://aoss-research.engin.umich.edu/multiwell/>
- <sup>9</sup> M. Lakin, D. Troya, G. Schatz, and L. Harding, *J. Chem. Phys.* **119**, 5848 (2003).
- <sup>10</sup> J. Li, Y. Wang, B. Jiang, J. Ma, R. Dawes, D. Xie, J. M. Bowman, and H. Guo, *J. Chem. Phys.* **136**, 041103 (2012).
- <sup>11</sup> E.M. Goldfield and S.K. Gray, *J. Chem. Phys.* **117**, 1604 (2002); J. Mayneris, M. Gonzalez, and S. K. Gray, *Comp. Phys. Comm.* **179**, 741 (2008).

## DOE-SPONSORED PUBLICATIONS SINCE 2011

R. Sivaramakrishnan, J. V. Michael, A. F. Wagner, R. Dawes, A. W. Jasper, L. B. Harding, Y. Georgievskii, and S. J. Klippenstein  
ROAMING RADICALS IN THE THERMAL DECOMPOSITION OF DIMETHYL ETHER: EXPERIMENT AND THEORY  
*Comb. Flame* **158**, 618 (2011).

A. F. Wagner, L. A. Rivera, D. Bachelierie, J. W. Perry, and D. L. Thompson  
A CLASSICAL TRAJECTORY STUDY OF THE DISSOCIATION AND ISOMERIZATION OF C<sub>2</sub>H<sub>5</sub>  
*J. Phys. Chem. A.* (online DOI: 10.1021/jp3099889)

# Ultrafast Structural Dynamics in Combustion Relevant Model Systems

Peter M. Weber  
Department of Chemistry  
Brown University, Providence, Rhode Island 02912  
Peter\_Weber@brown.edu

## I. Program Scope

The binding energy of an electron in a Rydberg state, that is, the energy difference between the Rydberg level and the ground state of the molecular ion, has been found to be a uniquely powerful tool to characterize the molecular structure. To rationalize the structure sensitivity we invoke a picture from electron diffraction: when it passes the molecular ion core, the Rydberg electron experiences a phase shift compared to an electron in a hydrogen atom. This phase shift requires an adjustment of the binding energy of the electron, which is measurable. As in electron diffraction, the phase shift depends on the molecular, geometrical structure, so that a measurement of the electron binding energy can be interpreted as a measurement of the molecule's structure.

Building on this insight, we have developed a structurally sensitive spectroscopy: the molecule is first elevated to the Rydberg state, and the binding energy is then measured using photoelectron spectroscopy. The molecule's structure is read out as the binding energy spectrum. Since the photoionization can be done with ultrafast laser pulses, the technique is inherently capable of a time resolution in the femtosecond regime.

For the purpose of identifying the structures of molecules during chemical reactions, and for the analysis of molecular species in the hot environments of combustion processes, there are several features that make the Rydberg ionization spectroscopy uniquely useful. First, the Rydberg electron's orbit is quite large and covers the entire molecule for most molecular structures of combustion interest. Secondly, the ionization does not change vibrational quantum numbers, so that even complicated and large molecules can be observed with fairly well resolved spectra. In fact, the spectroscopy is blind to vibrational excitation of the molecule. This has the interesting consequence for the study of chemical dynamics, where the molecules are invariably very energetic, that the molecular structures are observed unobstructed by the vibrational congestion that dominates other spectroscopies. This implies also that, as a tool to probe the time-dependent structural dynamics of chemically interesting molecules, Rydberg spectroscopy may well be better suited than electron or x-ray diffraction. With recent progress in calculating Rydberg binding energy spectra, we are approaching the point where the method can be evolved into a structure determination method.

To implement the Rydberg ionization spectroscopy we use a molecular beam based, time-resolved pump-probe multi-photon ionization/photoelectron scheme in which a first laser pulse excites the molecule to a Rydberg state, and a probe pulse ionizes the molecule. A time-of-flight detector measures the kinetic energy spectrum of the photoelectrons. The photoelectron spectrum directly provides the binding energy of the electron, and thereby reveals the molecule's time-dependent structural fingerprint. Only

the duration of the laser pulses limits the time resolution. With a new laser system, we have now reached time resolutions better than 100 fs, although very deep UV wavelengths (down to 190 nm) have slightly longer instrument functions. The structural dynamics of molecules in Rydberg-excited states is obtained by delaying the probe ionization photon from the pump photon; the structural dynamics of molecules in their ground state or excited valence states is measured by inducing the dynamics using a near UV laser pulse, and employing a multi-photon ionization scheme via the Rydberg states as a probe process. Thus, the technique is capable of measuring the reaction dynamics in any electronic state of neutral molecules.

## II. Recent Progress

Progress has been made in the past year in the study of several model systems, including the reaction dynamics of 1,3-cyclohexadiene and the charge delocalization reaction in dimethyl piperazine. We have further observed a very intriguing wavelength dependence in the molecular dynamics in dimethylisopropylamine. The following provides a snapshot of some of the results.

*The electrocyclic ring-opening of 1,3-cyclohexadiene: still full of surprises!*

The ring-opening reaction of 1,3-cyclohexadiene (CHD) is a textbook example for a general class of electrocyclic reactions that play an important role in the photochemical opening and closing of organic ring structures. Those reactions are of importance to the understanding of the formation of soot in flames. As a prototypical example, numerous investigations have been made on CHD to elucidate the details of the molecular reaction. Just as we thought we pretty much understand how it works, we have now obtained data that put into question some of this understanding.

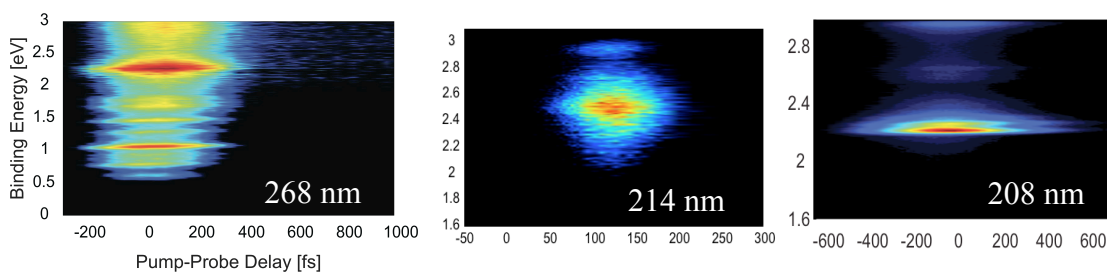


Figure 1: Time-resolved spectra of 1,3-cyclohexadiene excited at 268 nm, 214 nm and 208 nm. The ionization is with a 400 nm pulse at time delays as plotted on the horizontal axis. The binding energy spectrum upon excitation at 268 nm represents the well-known path of the molecule from the B state to the 2A state, followed by a crossing through a conical intersection to the ground state. The spectra at shorter wavelengths are markedly different, suggesting a reaction path distinct from that at 268 nm.

Figure 1 shows the time resolved photoelectron spectra of CHD at several wavelengths across the near UV absorption spectrum of CHD. The longer wavelength is in the general absorption band of the  $S_0 \rightarrow S_1$  transition, while at the shorter wavelengths, there are admixtures of other electronic states, notably the Rydberg states. As is clear from Figure 1, the appearance of the time resolved spectra depends dramatically on the

excitation energy: rather than being similar albeit with a little more energy, higher excitation energies appear to be associated with a reaction mechanism that does not involve the transition to the 2A state that is so apparent in the spectrum with 268 nm excitation. Ongoing work seeks to better understand the reaction mechanism and the pathway of this interesting molecular model.

#### *Delocalization of a charge in dimethyl piperazine: rate limited by structural motions*

Dimethyl piperazine (DMP) is a heterocyclic 6-ring with two nitrogen groups in para position. In its ground electronic state, the nitrogen atoms are too far apart to allow for substantial delocalization of the lone pair electrons.

However, in the Rydberg states and the ground state of the ion, the positive charge is delocalized between the two nitrogens. Excitation from the ground state to the Rydberg state involves at first one charge, followed by the delocalization of the charge between the nitrogen charge centers. Figure 2 shows the time-dependent electron binding energy spectrum of the system: upon rapid decay of the initially prepared 3p Rydberg state at 2.2 eV, the molecule

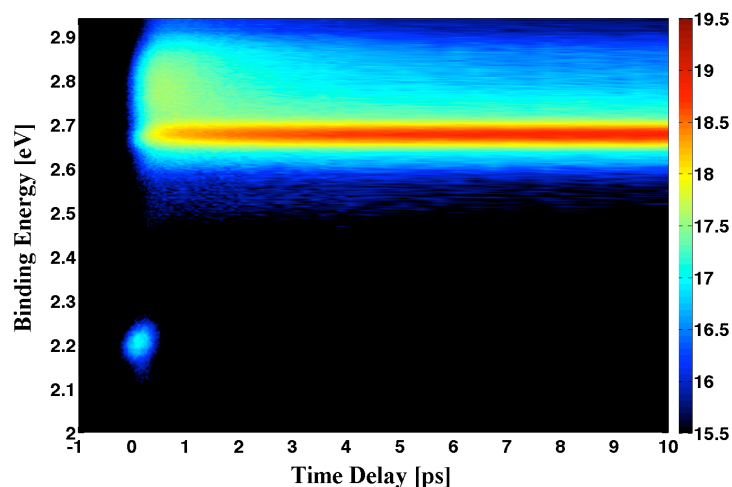


Figure 2: Photoelectron binding energy spectra obtained upon two-color photoionization of dimethyl piperazine with 208 nm pump pulses and 416 nm probe pulses. The one-color contributions to the spectra are subtracted. The initial excitation prepares DMP in 3p (2.2 eV), from where it relaxes quickly to the 3s (2.6 to 2.9 eV).

arrives at the 3s level partially in a broad peak, from 2.6 to 2.9 eV, that we attribute to a state with a localized charge and partially in a sharp peak near 2.7 eV that likely belongs to the delocalized charge state. Within the 3s level, we observe a slow reaction from the localized to the delocalized state on a picosecond time scale. While of course the motions of the electrons can be very fast, the rate of the reaction in DMP is confined to the picosecond regime by the structural rearrangements of the ring skeleton that are required to place the system into a geometry that is conducive to charge delocalization.

### III. Future Plans

Ongoing work continues to explore the chemical dynamics of reactive species using Rydberg ionization spectroscopy. We continue to explore model systems that are relevant to combustion and that test the limits of applicability of the method. In order to develop the range of applications further, we are collaborating with theorists to calculate the Rydberg electron binding energies using DFT methods. Our current state of the art is a level of accuracy in the range of 100 meV. This is already quite useful to assign the time dependent spectra that we observe, but not quite sufficient to a-priori identify a

molecular structure based on a match between theory and experiment. Continuing effort is directed toward improving the computational tools so as to develop the Rydberg ionization spectroscopy into a structure determination method.

#### IV. Publications resulting from DOE sponsored research (2009 - 2013)

1. “Ultrafast Electron Microscopy for Chemistry, Biology and Material Science” S.A. Aseyev, P.M. Weber and A.A. Ischenko, *Journal of Analytical Sciences, Methods and Instrumentation*, in print (2013).
2. “Ultrafast structural and isomerization dynamics in the Rydberg-excited Quadricyclane – Norbornadiene System,” Fedor Rudakov and Peter M. Weber, *The Journal of Chemical Physics*, 136, 1343031 - 7 (2012).
3. “The Far-UV Photochemical Bond Cleavage of n-Amyl Nitrite: Bypassing a Repulsive Surface” M. P. Minitti, Y. Zhang, M. Rosenberg, R. Y. Brogaard, S. Deb, T. I. Sølling and P. M. Weber; *J. Phys. Chem. A* **2012**, 116, 810 – 819.
4. “Structural Dynamics and Energy Flow in Rydberg-Excited Clusters of N,N-Dimethylisopropylamine,” S. Deb, M. P. Minitti, and P. M. Weber, *The Journal of Chemical Physics* 135, 044319 (2011). See also *Virtual Journal of Ultrafast Science*, August 2011.
5. “Ultrafast Dynamics of 1,3-Cyclohexadiene in Highly Excited States,” Christine C. Bühler, Michael P. Minitti, Sanghamitra Deb, Jie Bao, Peter M. Weber, *Journal of Atomic, Molecular, and Optical Physics*, Vol. 2011, Article ID 637593, 6 pages, **2011**. doi:10.1155/2011/637593.
6. “Structural Dynamics in Floppy Systems: Ultrafast Conformer Motions in Rydberg-Excited Triethylamine,” Brian Bayes, Sanghamitra Deb, Michael P. Minitti and Peter M. Weber, *J. Phys. Chem. A* **2011**, 115, 1804–1809.
7. “Dissociative energy flow, vibrational energy redistribution and conformer structural dynamics in bifunctional amine model systems,” Joseph C. Bush, Michael P. Minitti and Peter M. Weber, *J. Phys. Chem. A* **2010**, 114, 11078–11084.
8. “The Ultrafast Pathway of Photon-Induced Electrocyclic Ring Opening Reactions: The case of 1,3-cyclohexadiene” Sanghamitra Deb and Peter M. Weber, *Annu. Rev. Phys. Chem.* **2011**, 62, 19–39.
9. “Electron Diffraction with Bound Electrons: the Structure Sensitivity of Rydberg Fingerprint Spectroscopy” Xiao Liang, Michael G. Levy, Sanghamitra Deb, Joseph D. Geiser, Richard M. Stratt, and Peter M. Weber, *Journal of Molecular Structure* 978 (2010), pp. 250-256.
10. “Probing the Lifetimes of Internally Excited Amyl Nitrite Cations” Martin Rosenberg, Michael P. Minitti, Nerijus Rusteika, Christer Z. Bisgaard, Sanghamitra Deb, Peter M. Weber, Theis I. Sølling, *J. Phys. Chem. A* **2010**, 114, 7021–7025.
11. “Ultrafast Formation of an Intramolecular Cation-Pi Bond,” Joseph C. Bush, Michael P. Minitti and Peter M. Weber. *Journal of Photochemistry and Photobiology A: Chemistry* 213 **2010**, 70–72.
12. “Ultrafast Curve Crossing Dynamics through Conical Intersections in Methylated Cyclopentadienes,” Fedor Rudakov and Peter M. Weber, *J. Phys. Chem. A*, **2010**, 114 (13), pp 4501–4506.
13. “Ground State Recovery and Molecular Structure upon Ultrafast Transition through Conical Intersections in Cyclic Dienes,” Fedor Rudakov and Peter M. Weber, *Chemical Physics Letters* 470, **2009** 187-190.
14. “Excited-state ions in femtosecond time-resolved mass spectrometry: An investigation of highly excited chloroamines”, R. Y. Brogaard, N. Rusteika and T. I. Sølling, F. M. Rudakov and P. M. Weber, *J. Phys. Chem. A*, **2009**, 113 (1), pp 40–43.

Detailed Studies of Hydrocarbon Radicals:  
C<sub>2</sub>H Dissociation Dynamics

Curt Wittig  
Department of Chemistry  
University of Southern California  
Los Angeles, CA 90089-1062  
wittig@usc.edu

### Program Scope

This program examines C<sub>2</sub>H excited state properties and dynamics throughout the energy range that begins at dissociation threshold, D<sub>0</sub>(C<sub>2</sub>-H), and extends as far above D<sub>0</sub> as possible. The central role played by this species in hydrocarbon chemistry cannot be overstated. It is also an excellent prototype for examining important properties and phenomena: electronic states; curve crossings and associated nonadiabatic transitions; intramolecular and dissociation dynamics; and so on. It is small enough to provide experimental parent and product state resolution, and it is tractable at a high level of theory — electronic structure and quantum mechanical nuclear dynamics, including nonadiabatic couplings. It is an example of systems in which more than two conical-type intersections need to be taken into account simultaneously.

### Recent Progress

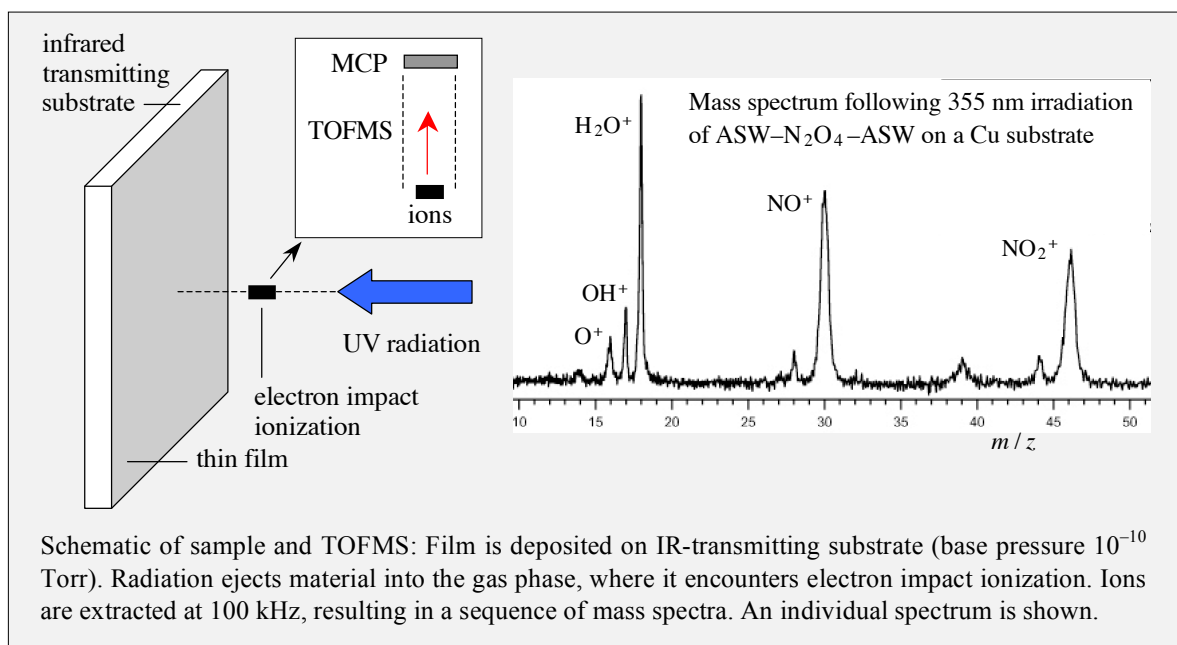
To determine the UV absorption spectrum of gaseous C<sub>2</sub>H, it is helpful to have cold samples that are, to the extent possible, free of contaminants. The term "contaminant" refers to species that interfere with the UV absorption spectrum of C<sub>2</sub>H. Thus an arrangement was prepared in which 193 nm photolysis of expansion-cooled C<sub>2</sub>H<sub>2</sub> served as a clean C<sub>2</sub>H precursor. There are other possible precursors (e.g., CF<sub>3</sub>C<sub>2</sub>H), but C<sub>2</sub>H<sub>2</sub> is particularly clean, so it was our first choice. Species were detected using a time-of-flight mass spectrometer (TOFMS) using electron bombardment with variable eKE operating at 100 kHz, i.e., a complete spectrum is recorded at 10 μs intervals. Many variations were explored: depletion of C<sub>2</sub>H<sub>2</sub><sup>+</sup>, appearance and enhancement of C<sub>2</sub>H<sup>+</sup> and C<sub>2</sub><sup>+</sup>, and tests with other molecules. It was hoped that, under high fluence conditions, photodissociation could be detected through C<sub>2</sub>H<sub>2</sub><sup>+</sup> depletion and/or C<sub>2</sub>H<sup>+</sup> appearance. The latter is potentially more sensitive because the C<sub>2</sub>H<sup>+</sup> signal that is present without C<sub>2</sub>H<sub>2</sub> photodissociation can be almost eliminated. For example, it was shown that C<sub>2</sub>H could be isolated by turning down eKE to the extent that, for all practical purposes, no C<sub>2</sub>H<sup>+</sup> daughter ions derived from electron impact ionization of C<sub>2</sub>H<sub>2</sub>. In other words, conditions can be arranged such that there is no C<sub>2</sub>H<sup>+</sup> background. The system was tested with H<sub>2</sub>S and large depletion signals were observed. However, with C<sub>2</sub>H<sub>2</sub>, no C<sub>2</sub>H<sup>+</sup> was observed, despite C<sub>2</sub>H<sub>2</sub> clearly being dissociated. It was determined that the 193 nm absorption cross-section of cooled C<sub>2</sub>H<sub>2</sub> is smaller by an order of magnitude than that of room temperature C<sub>2</sub>H<sub>2</sub>. This confounds measurement of the UV absorption spectrum because the high fluence needed to dissociate a reasonable percentage of the C<sub>2</sub>H<sub>2</sub> virtually guarantees that any C<sub>2</sub>H product will itself be photodissociated.

### Future Plans

An alternate strategy has been developed and is being implemented. The C<sub>2</sub>H is obtained through photolysis of C<sub>2</sub>H<sub>2</sub> embedded in a thin matrix (few hundred layers) under UHV conditions. Small dissociation yield is countered by varying sample thickness. Though gaseous H<sub>2</sub>O has a modest 193 nm absorption cross section, this is down considerably with condensed water because the ground state is stabilized (hydrogen bonding). The matrix enables the H atom photoproduct to diffuse through the sample and enter the gas phase, leaving behind C<sub>2</sub>H. A CO<sub>2</sub> host is a reasonable first choice, as the

$C_2H$  product will not react with the substrate. Between laser pulses (10 Hz) it is expected that the H atoms will leave the thin film, though some will recombine:  $H + C_2H \rightarrow C_2H_2$  and  $H + H \rightarrow H_2$ . The latter is more likely than the former because H is labile whereas  $C_2H$  is not. Note that  $HCO_2$  has a local minimum for the T-shaped geometry with the H atom near the carbon; this is interesting but has no direct bearing on  $C_2H$  production. Note also that a water host is likely to result in  $C_2H + H_2O \rightarrow C_2H_2 + OH$  or worse.

The TOFMS extraction region is approximately 1 cm above the film. This enables efficient detection of species that enter the gas phase. It will be possible to accumulate enough  $C_2H$  (and perhaps  $C_2$ ) to observe this with the TOFMS, e.g., in temperature programmed desorption (TPD) or photo-ejection. To give an idea of what kind of signals are possible, an earlier result is shown in the figure. These data have nothing to do with  $C_2H$ . They are presented only to provide a sense of single-shot S/N. In TPD, effluent leaves the surface over periods of seconds, so  $> 10^5$  spectra will be summed.



With ample  $C_2H$  density, this species is easily detected via its well-known  $A \leftarrow X$  infrared feature using FTIR. This is significantly more sensitive and at higher frequency than a vibrational transition. This provides an unambiguous signature of  $C_2H$ . Measurement of the UV absorption spectrum of the sample is then used to establish the  $C_2H$  spectrum. We do not currently have capability to reach temperatures below 80 K, and even 80 K requires bubbling He through the LN<sub>2</sub> reservoir. At these temperatures, there is little contribution from vibrationally excited  $C_2H$ . Correlation of the IR and UV spectra (under different experimental conditions) will be used to establish the identity of the UV absorbing species. This will settle some controversy concerning the excited states, and permit us to advance to the next stage, i.e., the gas phase studies.

A theoretical paper (invited but refereed) was published on the topic of geometric phase and conical intersections.

### Reference

C. Wittig, Geometric phase and gauge connection in polyatomic molecules, PCCP **14**, 6409 (2012).

# Experimental Ignition Studies of Oxygenated Hydrocarbons

Margaret S. Wooldridge

Departments of Mechanical and Aerospace Engineering, University of Michigan

Ann Arbor, MI 48109-2121

mswool@umich.edu

## I. Program Scope

The chemical physics of oxygenated fuels is an area which, until recently, has seen little scrutiny from the fundamental combustion science community. The chemistry of oxygenates presents an exciting area to apply our learning from hydrocarbons and adapt our methods to develop a similar level of predictive capabilities for elementary reaction theory and combustion reaction mechanisms. This research program uses ignition studies to investigate combustion and flame chemistry from the initiation and fuel oxidation phase to the heat release phase of combustion. Ignition delay time data provide valuable information on fuel reactivity for a range of state conditions, and speciation data provide direct insight into the dominant reaction pathways. The University of Michigan (UM) rapid compression facility (RCF) is used to create the temperature and pressure conditions of interest for the ignition studies. UM RCF studies focus on intermediate temperatures (600 – 1200 K) and high pressures (1-25 atm) where there are high uncertainties in the combustion chemistries.

During the past year, we completed ignition and speciation studies of *n*-heptane and of a blend of *n*-heptane with *n*-butanol. Ignition delay time data were acquired using the UM RCF for over a range of state and mixture conditions. Mass sampling and gas chromatography were applied to quantify the stable intermediates present during ignition of *n*-heptane and the perturbation of *n*-heptane combustion chemistry that occurs with the addition of increasing amounts of *n*-butanol.

## II. Recent Progress

The long test times of the UM RCF allow application of rapid gas sampling methods to simultaneously measure a large number of stable species during ignition experiments. Details on the dimensions, components and performance characterization of the UM RCF can be found in Donovan *et al.* [1]. Previous UM RCF studies have considered iso-octane ignition [2] and radical growth during iso-octane ignition [3], H<sub>2</sub>/CO ignition [4], particle nucleation [5], and C<sub>5</sub> ester ignition [6]. Previous gas sampling studies on iso-octane can be found in He *et al.* [7] and on methyl butanoate in Walton *et al.* [8].

Since these earlier studies, the UM RCF gas sampling system has been modified to allow multiple sampling events to occur within one ignition experiment, and the trapped residual volume in the gas sampling system has been reduced to improve the accuracy of the species measurements. In the 2011 progress report, the results of ignition and speciation studies of *n*-butanol were reported. The results of the *n*-butanol study are summarized in Karwat *et al.* [9]. We subsequently conducted a study to characterize the combustion chemistry of *n*-heptane in detail at low temperatures [10]. These studies established baseline understanding of the ignition chemistry of the two fuels in isolation. We then focused on understanding fuel interactions in studies of *n*-heptane/*n*-butanol blends. The details of the fuel blend study are provided in Karwat *et al.* [11]. This progress report presents a brief summary of the *n*-heptane/*n*-butanol fuel blend studies.

Chemical interactions between fuel components are another interesting and challenging topic for predictive combustion chemistry. In our recent RCF ignition studies of two important fuel reference compounds, *n*-heptane and *n*-butanol, we documented both expected and unexpected behaviors [9,10]. The ignition studies of blends of these two fuels revealed additional discoveries. Two fuel blend ratios, 80%-20% and 50%-50% (mole basis) of *n*-heptane and *n*-butanol, were compared with experimental and computational results for 100% *n*-heptane and 100% *n*-butanol. When compared with 100% *n*-heptane ignition results, the experimental data show that *n*-butanol slows the reactivity of *n*-heptane. In addition, speciation results of *n*-butanol concentrations show that *n*-heptane causes *n*-butanol to react at temperatures where *n*-butanol in isolation would not be considered reactive. These trends were

anticipated, and the chemical kinetic mechanism developed for the blend accurately predicted the trends observed for species such as carbon monoxide, methane, propane, 1-butene and others. However, the mechanism predicted a higher amount of *n*-heptane consumed at the first stage of ignition compared to the experimental data. Consequently, many of the species concentration predictions show a sharp rise at the first stage of ignition; a trend that was not observed experimentally. We have subsequently revised the *n*-heptane reaction mechanism to address some of the uncertainties that were revealed in the low temperature chemistry [10].

The basis of an important discovery of the fuel blend study is presented in **Figures 1** and **2**. The measured and predicted time histories for two heptene species are presented in the figures. The time domain is normalized to the first stage of ignition ( $t = 1.0$ ) and autoignition ( $t = 2.0$ ). The two panels in each figure present the absolute values [ppm] (left panels) and the results normalized to the initial amount of *n*-heptane in the mixture (right panels). Since the predicted *n*-C<sub>7</sub>H<sub>16</sub> consumption rates were much higher than observed experimentally, it is not surprising that the modeling results for 2-C<sub>7</sub>H<sub>14</sub> and 3-C<sub>7</sub>H<sub>14</sub> are much higher (twenty times higher for 2-C<sub>7</sub>H<sub>14</sub> and a factor of 3 higher for 3-C<sub>7</sub>H<sub>14</sub>) than the experimental data. What is more important and interesting is the experimental data show the presence of *n*-butanol suppresses the formation of these heptene isomers, even when normalized to the initial amount of *n*-heptane present in the reactants. Computationally, the opposite trends are predicted. Comparison of 50%-0% and 80%-0% simulations, where the initial amount of *n*-butanol in the mixture has been removed, with their 50%-50% and 80%-20% counterparts are also presented in **Figures 1** and **2**. The computational results show that *n*-butanol actually increases the predicted concentrations of 2-C<sub>7</sub>H<sub>14</sub> and 3-C<sub>7</sub>H<sub>14</sub> from the *n*-heptane. In other words, the model predicts a change in the branching fractions of *n*-heptane decomposition with the addition of *n*-butanol. The results for these large linear alkenes including heptenes, hexenes, and pentenes, show the addition of *n*-butanol affects the fundamental chemical pathways of *n*-heptane during ignition in ways that we currently do not understand and which are the subject of current work.

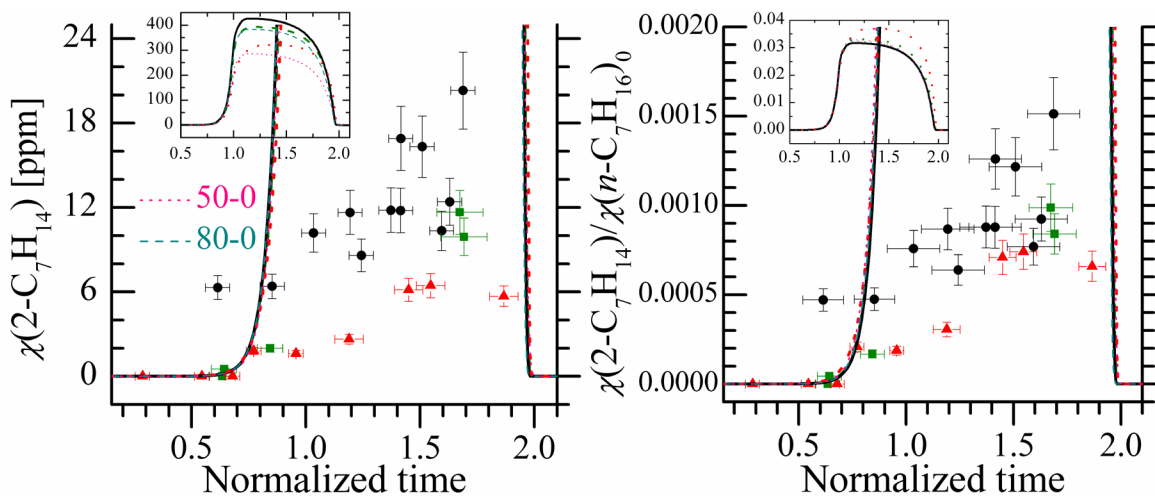


**Figure 1.** Experimental time-histories of 2-C<sub>7</sub>H<sub>14</sub> for stoichiometric mixtures of 100%-0% *n*-heptane/*n*-butanol fuel blends (black circles), 80%-20% % *n*-heptane/*n*-butanol fuel blends (green squares), and 50%-50% % *n*-heptane/*n*-butanol fuel blends (red triangles) blends. Also shown are predictions using the fuel blend mechanism developed as part of the study (with black, red and green lines representing the calculations for the three fuel blends), as well as predictions where the *n*-C<sub>4</sub>H<sub>9</sub>OH has been removed from the initial reactant mixture (i.e. 80–20 → 80–0 (cyan lines) and 50–50 → 50–0 (pink lines)). Nominal experimental conditions were 700 K and 9 atm for the three blends.

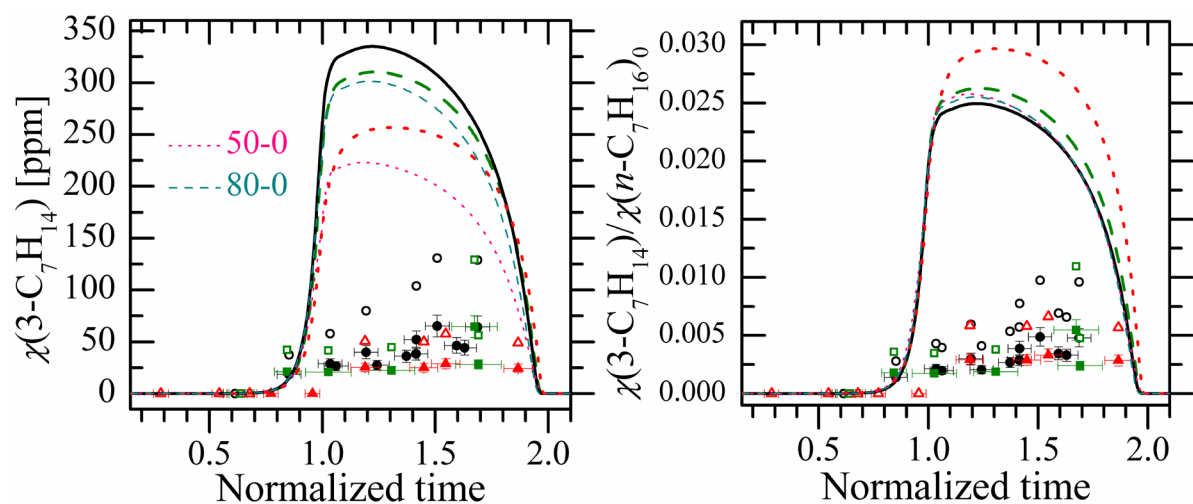


**Figure 2.** Experimental time-histories of 3-C<sub>7</sub>H<sub>14</sub> for stoichiometric mixtures of 100%-0% *n*-heptane/*n*-butanol fuel blends (black circles), 80%-20% *n*-heptane/*n*-butanol fuel blends (green squares), and 50%-50% *n*-heptane/*n*-butanol fuel blends (red triangles) blends. An upper bound for the measurements which is due to uncertainties in the calibration standard for 3-C<sub>7</sub>H<sub>14</sub> is presented as the open symbols. Also shown are predictions using the fuel blend mechanism developed as part of the study (with black, red and green lines representing the calculations for the three fuel blends), as well as predictions where the *n*-C<sub>4</sub>H<sub>9</sub>OH has been removed from the initial reactant mixture (i.e. 80–20 → 80–0 (cyan lines) and 50–50 → 50–0 (pink lines)). Nominal experimental conditions were 700 K and 9 atm for the three blends.

### III. Future Work

Our future work includes ignition and speciation studies of unsaturated hydrocarbons to clarify the uncertainties raised in this class of compounds during our previous studies. We continue to work with Dr. Westbrook to develop a more accurate understanding of the intermediates formed during ignition of hydrocarbon and oxygenated hydrocarbon. We also plan to upgrade our gas-sampling system to allow studies of higher pressure in partnership with Dr. Robert Tranter of Argonne National Laboratories. We will modify Dr. Tranter's high repetition rate valve design for application in UM RCF studies. The effects of pressure on low temperature combustion chemistry remain an area of considerable interest, particularly with the current shift in power train systems to more boosted engine designs.

### IV. References

1. Donovan, M.T., He, X., Zigler, B.T., Palmer, T.R., Wooldridge, M.S., Atreya, A. (2004) "Demonstration of a Free-Piston Rapid Compression Facility for the Study of High Temperature Combustion Phenomena" *Combust. Flame* **137** 351.
2. He, X., Donovan, M.T., Zigler, B.T., Palmer, T.R., Walton, S.M., Wooldridge, M.S., Atreya, A., (2005) "An Experimental and Modeling Study of Iso-octane Ignition Delay Times under Homogeneous Charge Compression Ignition Conditions," *Combust. Flame* **142** 266.
3. He, X., Zigler, B.T., Walton, S.M., Wooldridge, M.S., Atreya, A., (2006) "A Rapid Compression Facility Study of OH Time Histories During Iso-octane Ignition," *Combust. Flame* **145** 552.
4. Walton, S.M., He, X., Zigler, B.T., Wooldridge, M.S., (2007) "An Experimental Investigation of the Ignition Properties of Hydrogen and Carbon Monoxide Mixtures for Syngas Turbine Applications," *Proc. Combust. Inst.* **31** 3147.

5. Donovan, M.T., He, X., Zigler, B.T., Palmer, T.R., Walton, S.M., Wooldridge, M. S., (2005) "Experimental Investigation of Silane Combustion and Particle Nucleation Using a Rapid Compression Facility," *Combust. Flame* **141** 360.
6. Walton, S. M., Wooldridge, M. S., and Westbrook, C. K., (2009) "An Experimental Investigation of Structural Effects on the Auto-Ignition Properties of Two C5 Esters" *Proc. Combust. Inst.* **32** 255.
7. He, X., Walton, S.M., Zigler, B.T., Wooldridge, M.S., Atreya, A., (2007) "An Experimental Investigation of the Intermediates of Iso-octane During Ignition," *Int. J. Chem. Kinet.* **39** 498.
8. Walton, S.M., Karwat, D.M., Teini, P.D., Gorny, A., and Wooldridge, M.S., (2011) "Speciation Studies of Methyl Butanoate Ignition," *Fuel* **90** 1796.
9. Karwat, D. M. A., Wagnon, S. W., Teini, P. D., Wooldridge, M. S., "On the Chemical Kinetics of n-Butanol: Ignition and Speciation Studies," *J. Phys. Chem. A* **115** (2011) 4909-4921.
10. Karwat, D. M. A., Wagnon, S., Wooldridge, M. S., Westbrook, C. K., "Chemical Kinetics of n-Heptane Ignition in a Rapid Compression Facility," submitted to *Combustion and Flame*, in review (2013).
11. Karwat, D. M. A., Wagnon, S., Wooldridge, M. S., Westbrook, C. K., (2012) "On the Combustion Chemistry of n-Heptane and n-Butanol Blends," *Journal of Physical Chemistry A*, DOI 10.1021/jp3093 58h, **116**, pp. 12406-12421.

#### **V. Publications and submitted journal articles supported by this project 2006-2008**

1. Karwat, D. M. A., Wagnon, S., Wooldridge, M. S., Westbrook, C. K., Chemical Kinetics of n-Heptane Ignition in a Rapid Compression Facility, submitted to *Combustion and Flame*, in review (2013).
2. Karwat, D. M. A., Wagnon, S., Wooldridge, M. S., Westbrook, C. K., (2012) "On the Combustion Chemistry of n-Heptane and n-Butanol Blends," *Journal of Physical Chemistry A*, DOI 10.1021/jp3093 58h, **116**, pp. 12406-12421.
3. Karwat, D. M. A., Wagnon, S., Teini, P. D., Wooldridge, M. S. (2011) "On the Chemical Kinetics of n-Butanol: Ignition and Speciation Studies," *Journal of Physical Chemistry A*, **115**, pp. 4909-4921.
4. Wagnon, S. W., Karwat, D. M. A., and Wooldridge, M. S., "On the ignition chemistry of methyl trans-3-hexenoate," Central States Meeting of the Combustion Institute, Dayton, Ohio, April 2012.
5. Walton, S. M., Karwat, D. M., Teini, P. D., Gorny, A., and Wooldridge, M. S., (2011) "Speciation Studies of Methyl Butanoate Ignition," *Fuel*, **90**, pp. 1796-1804.
6. Wagnon, S., Karwat, D. M. A., Wooldridge, M. S., "Chemical Kinetics of an Unsaturated Ester: Methyl Trans-3-hexenoate," 7<sup>th</sup> U.S. National Combustion Meeting, Atlanta, Georgia, March 2011.
7. Karwat, D. M. A., Wagnon, S., Lai, J. Y. W., Wooldridge, M. S., Westbrook, C. K. "An Experimental and Computational Investigation of n-Dodecane Ignition and Chemical Kinetics," AIAA Conference, Orlando, Florida, January 2011.

THEORETICAL STUDIES OF THE REACTIONS AND SPECTROSCOPY OF RADICAL SPECIES RELEVANT TO  
COMBUSTION REACTIONS AND DIAGNOSTICS

DAVID R. YARKONY

DEPARTMENT OF CHEMISTRY, JOHNS HOPKINS UNIVERSITY, BALTIMORE, MD 21218  
yarkony@jhu.edu

## Overview

### A. Photoionization Spectra

We continued our work on anion photoelectron and photoionization spectra that describe states of a residual molecule (the species left after the electron is removed) that are strongly coupled by conical intersections. We are nearing completion of our simulation of the photoionization spectrum of propyne, where the combined effects of the Jahn-Teller and spin-orbit interactions require clarification.

### B. Nonadiabatic Dynamics

Using our algorithm for representing adiabatic potential energy surfaces coupled by conical intersections in processes involving bond breaking we are developing an accurate representation of the  $1,2,3^2A$  potential energy surfaces of  $H_3O$  needed to describe the electronic quenching  $OH(A^2\Sigma^+) + H_2 \rightarrow H_2O + H_2$  or  $OH(A^2\Pi) + H_2$ . To date we have surveyed, for the first time, the nonplanar regions of the conical intersection seams and established the significance of a region where Rydberg states form Jahn-Teller symmetry required conical intersections.

We have teamed with Marsha Lester at the University of Pennsylvania in a combined experimental and computational study of the quenching reaction,  $OH(A^2\Sigma^+) + CO \rightarrow CO_2 + H$ ,  $OH(A^2\Pi) + CO$  or  $HCO + O(^3P)$ .

We have extended our above noted algorithm for representing adiabatic potential energy surfaces coupled by conical intersections to handle systems comprised of a mixture of bound and dissociative modes. We are in the process of using that algorithm to describe photodissociation of phenol.

### WORK COMPLETED

A.  $OH(A^2\Sigma^+) + CO \rightarrow CO_2 + H$ ,  $OH(A^2\Pi) + CO$  or  $HCO + O(^3P)$  (Ref. [1])

We have teamed with Marsha Lester at the University of Pennsylvania in a combined

experimental and computational study of the quenching reaction,  $OH(A^2\Sigma^+) + CO \rightarrow CO_2 + H$ ,  $OH(A^2\Pi) + CO$  or  $HCO + O(^3P)$ . The theoretical studies identified four regions of strong nonadiabatic coupling accessible from the  $OH(A^2\Sigma^+) + CO$  asymptote and determined energy minimized conical intersections in those regions. For three of the conical intersections, the O-side of OH points toward CO and likely leads to  $H + CO_2$  reaction products and/or nonreactive quenching. A seam of intersection originating at the  $OH(A^2\Sigma^+) + CO$  asymptote and running along a barrierless path to a fourth energy minimized crossing has a very different nuclear configuration. In this case, the H-side of an elongated OH points toward CO in a bent configuration, and is likely the origin of the dominant  $O + HCO$  product channel. Dynamical calculations are needed to evaluate the branching between multiple reactive and nonreactive product channels.

### B. *Electronic Structure of the HydroxymethoxyRadical.* (Ref. [2])

Our study of electronic structure of the  $1,2^2A$  states of hydroxymethoxy  $(HO)CH_2O$  focused on nonadiabatic interactions attributable to a seam of conical intersections, extending a previous high quality analysis of this molecule which *ignored the possibility of such interactions*. [3] Illuminating comparisons were made between hydroxymethoxy and ethoxy and isopropoxy, all of which can be thought of as substitutional isomers of the methoxy radical. The results of the analysis were surprising. The electronic structure of hydroxymethoxy was shown to be dramatically different from that of ethoxy, isopropoxy or methoxy, a dissimilarity attributable to the differing interactions of the methyl (in the alkoxides) and the hydroxyl (in hydroxymethoxy) groups.

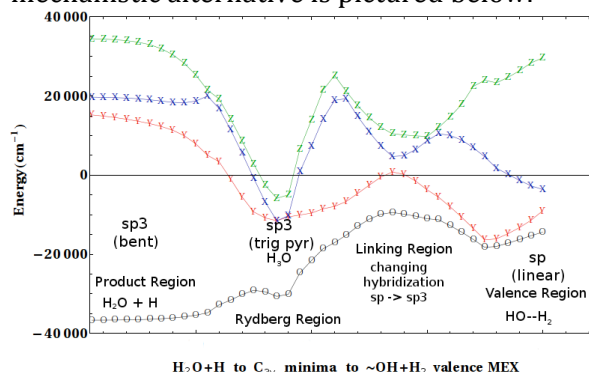
Also considered was the feasibility of representing the coupled  $1,2^2A$  adiabatic electronic states of hydroxymethoxy within the vibronic coupling approximation using a quasi-diabatic  $\mathbf{H}^d$  and subsequently using that representation to simulate the photoelectron spectrum of the hydroxymethoxide anion. That approach had previously proved very effective in representing the  $1,2^2A$  states of ethoxy and isopropoxy and in simulating the corresponding anion electron detachment spectra. The  $\mathbf{H}^d$ s for ethoxy and isopropoxy had been constructed using 2<sup>nd</sup> order polynomials, the standard second order vibronic coupling model. Here polynomials through 4<sup>th</sup> and 8<sup>th</sup> order were required although only a small subset of higher order coefficients,  $<10^3$  as opposed to  $\sim 10^6$  if the full 8<sup>th</sup> order representation were used. The  $\mathbf{H}^d$  with 8<sup>th</sup> order polynomials provided a uniformly accurate representation of the *ab initio* data from which it was derived, except for the region where the hydroxyl hydrogen torsion angle,  $\varphi \rightarrow \pm 180^\circ$ . In this region, which is accessed when unhindered rotation of the hydroxyl hydrogen, a prototypical large-amplitude motion, is energetically feasible, the electronic energy in the vibronic coupling model necessarily approaches  $+\infty$ , while the *ab initio* results exhibit the requisite periodicity. The effects of this limitation on the ability of  $\mathbf{H}^d$  to accurately represent vibronic states of hydroxymethoxy were addressed. In a future work, the reported  $\mathbf{H}^d$  will be used as the basis for a determination of the photoelectron spectrum of hydroxymethoxide anion. The hydroxymethoxide photoelectron spectrum has not been experimentally measured but it is hoped that this work will serve to motivate such an investigation.

C.  $OH(A^2\Sigma^+) + H_2 \rightarrow H_2O + H, OH(X^2\Pi)+H_2$ , Part 1- A survey of the conical intersection seams[4]

The captioned reaction is of fundamental importance as an archetypical nonadiabatic reaction involving more than one exit channel, and has been studied in the DoE supported laboratories of Lester[5] at University of Pennsylvania and Davis[6] at Cornell. It is

small enough to be amenable to highly accurate fully quantum mechanical treatments and for that reason has attracted considerable theoretical interest including Bowman's DoE supported work.[7, 8] Although this reaction has long been known to be driven by conical intersections,[9] knowledge of the locus of the seams of conical intersection is actually quite limited. Most discussions focused on the planar portion of the  $2,3^2A$  conical intersection seam. The  $1,2^2A$  seam, which, as in the case of  $NH_3$ , only exists for planar structures, has not been well discussed.

As part of our work in progress to represent these coupled potential energy surfaces using the quasi-diabatic representation noted above,[10] a careful mapping of the seams of conical intersection has been carried out.[4] This study reports for the first time a region in which Rydberg states form  $C_{3v}$  symmetry required conical intersections which are expected to play a role in the nonadiabatic quenching. This Rydberg region is accessible from a linking region on the  $2^2A$  potential energy surface, AFTER passing through a  $2,3^2A$  intersection in the well described valence region, providing an alternative quenching pathway not previously reported. This mechanistic alternative is pictured below.



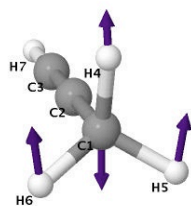
A manuscript describing these new mechanistic insights is being prepared for publication. Our coupled quasi-diabatic state representation and mechanistic insights will complement a recent study by Collins and coworkers.[11]

### Work almost ready for publication

#### A. Propyne Photoionization spectrum

Propyne,  $CH_3C \equiv CH$ , is an important intermediate in combustion chemistry being known to participate in the formation of

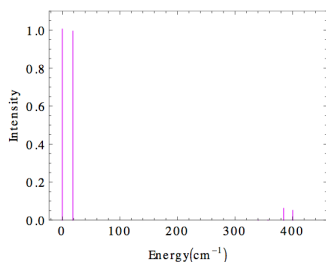
polycyclic aromatic hydrocarbons.[12]



Propyne has a  $\tilde{X}^1A_1$  ( $C_{3v}$ ) ground electronic state, whereas the ionized species, the propyne cation, pictured above together with its g-vector has an  $\tilde{X}^2E$  ground state, which exhibits a Jahn-Teller distortion. The  ${}^2E$  state is also split by the spin-orbit interaction, producing  ${}^2E_{1/2}$  and  ${}^2E_{3/2}$  states. Grant and coworkers have recorded and analyzed a nonresonant two-photon pulsed field ionization-photoelectron (PFI-PE) spectrum[13] of propyne,  $C_3H_4^+(\tilde{X}^2E_{1/2, 3/2}) \leftarrow C_3H_4(\tilde{X}^1A_1)$ . They conclude that the spin-orbit (A) constant for this  ${}^2E$  state is the same as that for the acetylene cation  ${}^2\Pi_{1/2,3/2}$ , which is  $A = -30.9 \text{ cm}^{-1}$ , as determined by Pratt *et. al.*[14]. Using this value of the spin-orbit constant, they report good agreement for their measured rotational profile and a structure very little altered by Jahn-Teller distortion.

More recently Ng and coworkers, have used the IR-VUV-PFI-PE method,[15, 16] to analyze the  $C_3H_4^+(\tilde{X}^2E, \nu_1^+) \leftarrow C_3H_4(\tilde{X}^1A_1, \nu_1)$ . These authors very carefully compared, measured and simulated spectra and find  $A = -13.9 \pm 0.2 \text{ cm}^{-1}$  and a ratio of the photoionization cross sections  $E_{1/2}:E_{3/2} = 4:1$ . These results are not consistent with those of Grant and coworkers in Ref. [13].

Using methods developed as part of prior DoE funding,[17] we have nearly completed a simulation of the photoionization spectrum of propyne designed to address these discrepancies.

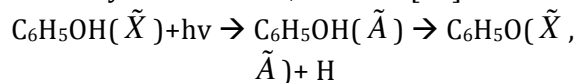


The results are summarized in the above figure. The first two lines in the spectrum provide the  ${}^2E_{1/2}$ - ${}^2E_{3/2}$  splitting and line strengths. The separation of  $18.5 \text{ cm}^{-1}$  represents an  $\sim 30\%$  Ham reduction of the computed raw spin-orbit interaction  $28.3 \text{ cm}^{-1}$  to due the Jahn-Teller effect, in (agreement with Ng). But the photoionization cross section is clearly approximately equal for the  ${}^2E_{1/2}$  and  ${}^2E_{3/2}$  states which is significantly different than the inference of Ng and unlikely to be changed by a more precise treatment.

### Work in Progress

#### A. Representing potential energy surfaces coupled by conical intersections for complex molecules using Fragment Coordinates

As noted above, we recently developed a quasi-adiabatic Hamiltonian,  $\mathbf{H}^d$ , that represents adiabatic potential energy surfaces coupled by conical intersections.[10, 18] Since the Hamiltonian is expressed in terms of exponentially decaying functions of internuclear distances,  $r_{j,k} = |\mathbf{R}_j - \mathbf{R}_k|$ , the number of coordinates grows like  $N^{atom}(N^{atom} - 1)/2$  (quadratically). Many nonadiabatic processes involve molecules that decompose into intact fragments. In this case, the fragments can be described, using local coordinates, connected by decaying exponential coordinates to describe the dissociation of the fragments. The scaling is improved since the number of internal coordinates grows only like  $3N^{atom}-6$  (linearly). Introduction of this hybrid coordinate system is facilitated by our use of redundant coordinates in our representation of  $\mathbf{H}^d$ , which allows for the arbitrary union of unrelated coordinates. Point group symmetry is replaced by complete nuclear permutation group inversion symmetry. The program to construct this fit has been written. Our initial application will consider photodissociation of phenol studied in Crim's group at the University of Wisconsin, Madison[19]



These calculations, in addition to validating the mixed coordinates approach will provide very reliable coupled potential energy surfaces for

studying the nonadiabatic photodissociation of phenol.

#### References

- [1] J. H. Lehman, M. I. Lester, and D. R. Yarkony, *J. Chem. Phys.* **137**, 094312 (2012).  
[2] J. Dillon, and D. R. Yarkony, *J. Chem. Phys.* **137**, 154315(2012).  
[3] W. Eisfeld, and J. Francisco, *J. Chem. Phys.* **131**, 134313(2009).  
[4] J. Dillon, and D. R. Yarkony, *J. Phys. Chem. A*, submitted(2013).  
[5] R. A. Loomis, and M. I. Lester, *Annu. Rev. Phys. Chem.* **48**, 643(1997).  
[6] M. Ortiz-Suárez, M. F. Witinski, and H. F. Davis, *J. Chem. Phys.* **124**, 201106 (2006).  
[7] B. Fu, E. Kamarchik, and J. M. Bowman, *J. Chem. Phys.* **133**, 164306(2010).  
[8] E. Kamarchik, B. Fu, and J. M. Bowman, *J. Chem. Phys.* **132**, 091102(2010).  
[9] B. C. Hoffman, and D. R. Yarkony, *J. Chem. Phys.* **113**, 10091(2000).  
[10] X. Zhu, and D. R. Yarkony, *J. Chem. Phys.* **137**, 22A511(2012).  
[11] M. A. Collins, O. Godsi, S. Liu, and D. H. Zhang, *J. Chem. Phys.* **135**, 234307(2011).  
[12] X. Xing, M.-K. Bahng, B. Reed, C. S. Lam, K.-C. Lau, and C. Y. Ng, *J. Chem. Phys.* **128**, 094311(2008).  
[13] H. Matsui, Y.-F. Zhu, and E. R. Grant, *Laser Chem.* **16**, 161(1996).  
[14] S. T. Pratt, P. M. Dehmer, and J. L. Dehmer, *J. Chem. Phys.* **99**, 6233(1993).  
[15] C. Y. Ng, *J. Electron Spectrosc. Rela. Phenom.* **142**, 179(2005).  
[16] H. K. Woo, P. Wang, K. C. LAu, X. Xing, C. Chang, and C. Y. Ng, *J. Chem. Phys.* **119**, 9333(2003).  
[17] M. S. Schuurman, D. E. Weinberg, and D. R. Yarkony, *J. Chem. Phys.* **127**, 104309(12 pages)(2007).  
[18] X. Zhu, and D. R. Yarkony, *J. Chem. Phys.* **136**, 174110(2012).  
[19] M. L. Hause, Y. H. Yoon, A. S. Case, and F. F. Crim, *J. Chem. Phys.* **128**, 194307 (2008).

#### PUBLICATIONS ACKNOWLEDGING (EXCLUSIVELY) CURRENT DOE SUPPORT (2010-2012)

- 1. On the Role of Conical Intersections and their Local Topography in the Photodissociation of 1-Hydroxyethyl Radical*,  
Kousik Samanta and David R. Yarkony, *Chem. Phys.* 378, 110-117 (2010)
- 2. A Lippmann – Schwinger Approach for the Determination of Photoionization and Photodetachment Cross Sections Based on a Partial Wave Green's Function Expansion and Configuration Interaction Wave Functions*.  
Seungsuk Han and David R. Yarkony, *Mol. Phys.* 110, 845-859 (2012).
- 3. Nonadiabatic Effects in Substitutional Isomers of Jahn-Teller Molecules. The Strange Case of Hydroxymethoxy*  
Joseph Dillon and David R. Yarkony, *J. Chem. Phys.* **137**, 154315 (2012)
- 4. Reactive quenching of OH A  $^2\Sigma^+$  by O<sub>2</sub> and CO: Experimental and nonadiabatic theoretical studies of H- and O-atom product channels*  
Julia H. Lehman, Marsha I. Lester, and David R. Yarkony, *J. Chem. Phys.* 137, 094312 (2012)

# GAS-PHASE MOLECULAR DYNAMICS: THEORETICAL STUDIES IN SPECTROSCOPY AND CHEMICAL DYNAMICS

Hua-Gen Yu (hgy@bnl.gov)

Chemistry Department, Brookhaven National Laboratory, Upton, NY 11973-5000

## Program Scope

The main goal of this program is the development and application of computational methods for studying chemical reaction dynamics and molecular spectroscopy in the gas phase. We are interested in developing rigorous quantum dynamics algorithms for small polyatomic systems and in implementing approximate approaches for complex ones. Particular focus is on the dynamics and kinetics of chemical reactions and on the rovibrational spectra of species involved in combustion processes. This research also explores the potential energy surfaces of these systems of interest using state-of-the-art quantum chemistry methods, and extends them to understand some important properties of materials in condensed phases and interstellar medium as well as in combustion environments.

## Recent Progress

### The ring opening pathways in the reaction of morpholinyl radicals with O<sub>2</sub>

In this research, we have explored the ring opening pathways in the reaction of morpholinyl radicals with O<sub>2</sub> using high level *ab initio* methods. Here morpholine is used to mimic future transportation fuels and diesels, produced largely from non-traditional sources such as oil shales, sand oils and biomass. These fuels often contain N and O atoms, and have higher concentration of cyclic compounds than in current fuels. Results show that morpholinyl radicals have a strong reactivity with O<sub>2</sub>, as the addition reaction of O<sub>2</sub> to the radicals has no apparent activation barrier, and is considerably exothermic. The resulting adduct has two main paths to decomposition. A 1,4-H shift isomerization reaction is likely to produce a stable cyclic epoxy intermediate, whereas a 1,5-H shifting isomerization leads to ring-opened products. These two isomerization reactions will compete owing to their comparable barrier heights along the reaction pathway. In particular, as shown in Fig. 1, the 1,5-H shifting reaction pathway involves an energy barrier that is merely 4.85 kcal/mol higher than the reactant dissociation limit, and the overall ring opening reaction can produce significant amount of heat. These novel findings provide valuable insights for the

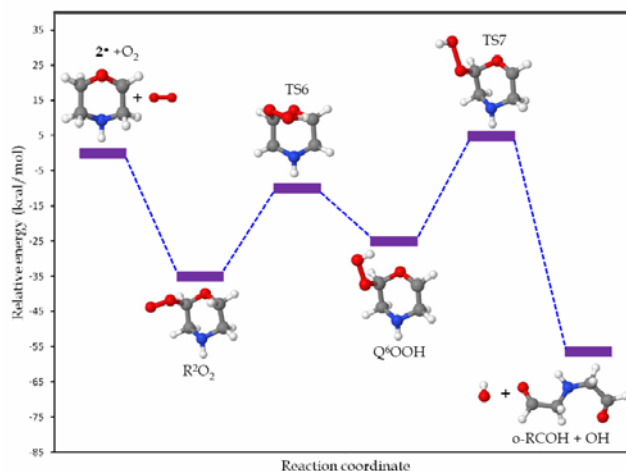


**Figure 1:** Relative energy diagram at the CCSD(T)/aug-cc-pVTZ level for the reaction of morpholinyl radical (2•) with O<sub>2</sub> through a low barrier pathway for the ring opening process.

development of mechanisms for low-temperature combustion of morpholine and similar cyclic O- and N-containing fuels.

### Quantum dynamics of cold collisions of CH<sub>2</sub> + He in a magnetic field

A rigorous quantum dynamics study has been performed for the low-temperature collisions of polyatomic molecular radicals with <sup>1</sup>S<sub>0</sub> atoms in the presence of an external magnetic field using CCSD(T) *ab initio* and scaled potential energy surfaces. The He-CH<sub>2</sub>(X<sup>3</sup>B<sub>1</sub>) interaction potential is weakly anisotropic. Quantum scattering calculations show that collision-induced spin relaxation of the prototypical methylene radical CH<sub>2</sub>(X<sup>3</sup>B<sub>1</sub>) and nine other triatomic radicals in cold <sup>3</sup>He gas occurs at a slow rate, demonstrating that cryogenic buffer-gas cooling and magnetic trapping of those molecules is feasible with current technology. The calculations also suggest that it may be possible to create ultracold gases of polyatomic molecules by sympathetic cooling with alkaline-earth atoms in a magnetic trap. This work was done in collaboration with Tscherbul and Dalgarno at Harvard, and Alexander at Uni. Maryland.

### Time-dependent wavepacket study of photo-initiated dissociation of O<sub>2</sub> on TiO<sub>2</sub>

Recently, we have carried out a TDDFT study of the photo-initiated dissociation of O<sub>2</sub> on rutile TiO<sub>2</sub> nanocluster, motivated by the research at the BNL Surface Chemical Dynamics Group. Results show that the most stable configuration is O<sub>2</sub> adsorbed parallel at the bridging row vacancy site of reduced TiO<sub>2</sub> cluster in a state of O<sub>2</sub><sup>2-</sup>. According to this observation, we have built a one-dimensional five-state model as shown in Fig. 2, and carried out a time-dependent wavepacket (TDWP) dynamics calculation. The TDWP results show that the photo-initiated dissociation of O<sub>2</sub> at TiO<sub>2</sub> occurs via a direct dissociation mechanism. The lifetime of excited O<sub>2</sub> molecules was predicted to be about 266 fs. It was noticed that the non-adiabatic effects among the singlet electronic states have played an important role in the dissociation reaction. However, the spin-orbit effect on the dynamics was found to be negligible. In neat future, we are going to understand the dynamics of photoinduced O<sub>2</sub> desorption processes from TiO<sub>2</sub> surface, especially, the translational distribution of O<sub>2</sub> measured by White's group at BNL.

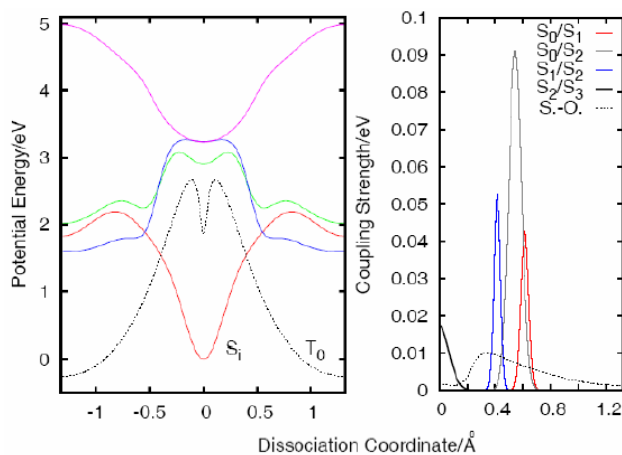


**Figure 2:** Diabatic potential energy curves formed by the four lowest singlet and the ground triplet states (left panel), and their coupling strengths and spin-orbit interactions between S<sub>0</sub> and T<sub>0</sub> (right panel) of O<sub>2</sub>/TiO<sub>2</sub> system.

## Future Plans

### Non-adiabatic molecular dynamics studies of polyatomic molecular reactions

Electronically excited species such as <sup>1</sup>CH<sub>2</sub> also play an important role in combustion chemistry. However, the studies of their reactivity are rather limited, partially due to the

non-adiabatic dynamics effects because those reactions often occur on multiple potential energy surfaces. In this research, we will extend the surface hopping direct *ab initio* molecular dynamics algorithm, developed for the SECH MD studies, to simulate the bimolecular reactions and the photo-dissociation chemistry. The first application would be the photodissociation dynamics of acetone at 193-230 nm. This system has been investigated by Suits et al. using a universal ion imaging technique. The photon excited acetones produce two major types of products:  $\text{CH}_3\text{CO} + \text{CH}_3$  and  $\text{CO} + 2\text{CH}_3$ . The latter products result from poorly understood dissociation mechanisms. Here we will attempt to explore the dissociation pathways of acetone on its three low-lying electronic states.

### **Calculations of vibrational spectra of polyatomic systems**

In this proposal, we aim to develop computational algorithms to accurately calculate the vibrational spectra of polyatomic molecules, and to assist experimentalists to understand their observed spectra. For polyatomic systems beyond six-atom, the challenge in rigorous quantum dynamics calculations comes from the huge basis size owing to high-dimensional problems. The Lanczos method is an iterative eigensolver capable of solving the eigenvalue problem of a large sparse matrix with a size up to  $N \sim 10^7$ , which might be equivalent to a chemical system with six degrees of freedom. In order to overcome this difficulty, we may try to reduce the basis size by using a compact basis set. The reduction of the basis size is the crucial idea of the sequential truncation approach widely used in direct diagonalization methods. This approach however requires too much CPU time and fast memory to be tractable for polyatomic molecules beyond five-atom molecules. During the past decade, several methods to obtain a compact basis set have been developed, e.g., the pruned basis functions.

Instead, in this proposal, we will use our recently developed ZDVR method to build a compact basis set. The ZDVR is a multi-dimensional PO-DVR method so that the ZDVR basis is very compact, which can substantially reduce the basis size. Numerical tests also demonstrated that it has the Gauss convergence speed with the basis size. Importantly, the ZDVR is a grid basis representation. As a result, the matrix representation of system Hamiltonian in ZDVR is often very sparse, which guarantees the efficiency of an iterative diagonalization method as well as the low memory requirement.

We will apply the algorithm to study the vibrational spectra of combustion-related radicals such as vinyl ( $\text{C}_2\text{H}_3$ ) and propargyl ( $\text{C}_2\text{H}_5$ ) radicals, in collaboration with Sears and Hall in the GPMD group of BNL. They are going to measure the overtones of both radicals using high-resolution near infrared spectroscopy. Currently, the Hamiltonian in normal mode coordinates has been numerically tested with propargyl radical in full dimension. The full coupled potential energy surface is used. Results obtained are very promising.

### **Publications since 2011**

T.V. Tscherbul, H.-G. Yu, and A. Dalgarno, *Sympathetic cooling of polyatomic molecules with S-state atoms in a magnetic trap*, Phys. Rev. Lett. **106**, 073201 (2011).

H.-G. Yu, *An ab initio molecular dynamics study of the roaming mechanism of the  $\text{H}_2 + \text{HOC}^+$  reaction*, Physica Scripta **84**, 028104 (2011).

- S.-Y. Du, T. Germann, J. Francisco, K. Peterson, H.-G. Yu, and J. Lyons, *The kinetics study of the  $S + S_2 \rightarrow S_3$  reaction by the Chaperon mechanism*, J. Chem. Phys. **134**, 154508 (2011).
- H.-G. Yu, *An optimal density functional theory method for GaN and ZnO*, Chem. Phys. Lett. **512**, 231 (2011).
- W.-Q. Han, H.-G. Yu, Z. Liu, *Convert graphene sheets to boron nitride and boron nitride-carbon sheets via a carbon-substitution reaction*, App. Phys. Lett. **98**, 203112 (2011).
- H.-G. Yu and G. Nyman, *The infrared and UV-visible spectra of polycyclic aromatic hydrocarbons containing (5,7)-member ring defects: A theoretical study*, Astrophys. J., **751**, 3 (2012).
- P.P Dholabhai and H.-G. Yu, *Exploring the ring opening pathways in the reaction of morpholinyl radicals with oxygen molecule*, J. Phys. Chem. A, **116**, 7123 (2012).
- T.V. Tscherbul, T.A. Grinev, H.-G. Yu, A. Dalgarno, J. Klos, L. Ma and M.H. Alexander, *Cold collisions of polyatomic molecular radicals with S-state atoms in a magnetic field: An ab initio study of  $He + CH_2(X^3B_1)$* , J. Chem. Phys. **137**, 104302 (2012).
- G. Nyman and H.-G. Yu, *Quantum approaches to polyatomic reaction dynamics*, Int. Rev. Phys. Chem., **32**, 000 (2013).
- P.P Dholabhai and H.-G. Yu, *Electronic structure and quantum dynamics of photoinitiated dissociation of  $O_2$  on rutile  $TiO_2$  nanocluster*, J. Chem. Phys., (submitted, 2013).

# Chemical Kinetics of Elementary Reactions

Judit Zádor

Combustion Research Facility, Mail Stop 9055, Sandia National Laboratories

Livermore, CA 94551-0969

jzador@sandia.gov

## I. PROGRAM SCOPE

My program focuses on the theoretical determination of rate coefficients and branching fractions relevant to combustion chemistry. Specifically, the formation and dissociation of primary radicals derived from various fuel molecules, and the pressure- and temperature-dependent formation and reactions of peroxyalkyl radicals associated with low-temperature autoignition processes are studied. A particular aspect of the program is the close collaboration with experimental groups to minimize the effects of inherent uncertainties in the theoretical methods, and also to reveal the parts of our current theoretical models that cause most of these uncertainties. The work involves quantum chemical calculations, application of transition-state theory, solution of the master equation, and modeling of small reaction systems related to the experimental conditions.

## II. RECENT PROGRESS

### A. Primary radical formation reactions: H-abstraction from fuel molecules

**Propanol + OH and butanol + OH** In collaboration with Jim Miller, hydrogen-abstraction rate coefficients were calculated for the *n*- and *i*-propanol and *n*-butanol + OH reactions. We found high sensitivity to the level of theory applied. Also, the analysis of the 2D hindering potentials revealed that the strong interaction between the alcoholic and the radical OH groups leads to significant coupling between the rotors. This causes the overestimation of the number and densities of states. We also showed that higher energy conformers with larger entropy (compared to the lowest energy conformer) also contribute significantly to the rate coefficients, therefore, the separable 1-D hindered rotor approximation is not accurate enough for these types of reactions.

Theoretical methods to obtain rate coefficients are essential to fundamental combustion chemistry research, yet the associated uncertainties are greatly unexplored in a systematic manner. In an exploratory work, in collaboration with Habib Najm, we focused on the parametric uncertainties for the hydrogen-atom-abstraction reaction,  $\text{CH}_3\text{CH}(\text{OH})\text{CH}_3 + \text{OH} \rightarrow \text{CH}_3\text{C}(\text{OH})\text{CH}_3 + \text{H}_2\text{O}$ . The barrier height, one of the lowest vibrational frequencies at the transition state, and the imaginary frequency were identified as the parameters causing the most significant uncertainty in the rate-coefficient calculations. Bayesian inference was employed to determine the joint probability distribution function of these parameters using the experimental data of Dunlop and Tully on isopropanol + OH.<sup>i</sup>

We found that although most of the commonly used high-level ab initio calculations result in not more than a factor of two difference in the rate coefficient for this specific reaction in the 293-745 K temperature range, significant uncertainties remain in these types of calculations. We have clearly demonstrated that it is not necessarily true that the lion's share of the uncertainty in the calculated rate coefficient arises solely due to the uncertainties in the barrier height, and the presented methodology provided a transparent way of assessing the various quantum chemical methods.

### B. Unimolecular dissociation of primary fuel radicals

**Alkene + OH reactions, and the unimolecular dissociation of the hydroxypropyl and propoxy radicals**

Propene is an important intermediate in many combustion mechanisms and is also a prototype alkene, which exhibits richer combustion chemistry than ethene and yet is simple enough to permit a detailed theoretical analysis. In our previous work<sup>ii</sup> we investigated the rich chemistry of the propene + OH reaction by high-level quantum chemical methods coupled to multiwell master equation methodology, which provided excellent agreement with the literature experimental results.

In our more recent work, in collaboration with Craig Taatjes and Matthias Olzmann (Karlsruhe Institute of Technology), we investigated the behavior of this interesting reaction focusing on the ~650-700 K temperature range, where addition to the double bond, backdissociation of the adducts to propene + OH, and H-abstraction interact. We devised a method to decompose the biexponential OH LIF signals to extract the backdissociation and the abstraction rate coefficients directly in this previously unexplored temperature region. We also provided a simplified parameterization of this reaction to be used in combustion modeling. An interesting aspect of the work was the kinetic isotope effect (KIE) of the abstraction reaction. We have shown that the dislocation of the energy maximum along the reaction coordinate relative to the electronic saddle point on the adiabatic potential energy surface (PES) plays the major role in the KIE, and other variational effects are negligible.

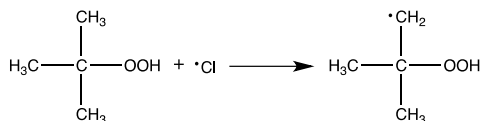
We also calculated dissociation rate coefficients based on the propene + OH PES in collaboration with Jim Miller. The C<sub>3</sub>H<sub>7</sub>O isomers found on this surface correspond to the isomers obtained from propanol by H-abstraction and are inherently important in setting the stage for propanol combustion. All rate coefficients were obtained with internal consistency with particular attention paid to shallow wells. After minor adjustments very good agreement with the experimental results on *i*-propoxy dissociation<sup>iii</sup> was obtained. Several interesting pathways were uncovered, such as the catalytic dehydration, well-skipping reactions, and reactions forming enols. Our work quantitatively described the dissociation pathways from the radicals derived from propanol, which can be used for both the improvement of propanol models as well as to make better predictions for larger alcohols.

### C. Low-temperature autoignition chemistry

**Alkene + HO<sub>2</sub> reactions** It is well known that OH radicals play a central role in combustion, especially at lower temperatures, where it is the main chain carrier and is ultimately responsible for autoignition. HO<sub>2</sub>, although a much less reactive radical, weighs in by being produced in much larger quantities. In our study, in collaboration with Stephen Klippenstein and Jim Miller, we have shown that HO<sub>2</sub> + alkene reactions can provide an important pathway in which HO<sub>2</sub> radicals are converted into the more reactive OH ones.

We have investigated seven HO<sub>2</sub> + unsaturated molecule reactions. Despite the belief, it is generally not true that the alkene + HO<sub>2</sub> reaction leads mostly to oxirane and OH. At low temperatures the formation of the alkylperoxy radical is favored due to the lower barrier height, while at higher temperatures the hydroperoxyalkyl and/or oxirane + OH formation is faster because of the looser transition state structure. An important exception is 2-butene, where the QOOH formation is both entropically and energetically favorable. Allylic abstraction is non-negligible from alkenes by HO<sub>2</sub> and competes with the addition reactions. This influences the effect that alkene + HO<sub>2</sub> reactions have on autoignition. The example of vinyl alcohol + HO<sub>2</sub> showed that substituted alkenes produce a completely different chemistry: instead of OH formation, a simple HO<sub>2</sub>-assisted isomerization is predicted. Recent mechanisms overpredict the ethenol concentration in flames compared to experimental results.<sup>iv</sup> This reaction can be one that corrects for that discrepancy. However, the effect has to be tested numerically, because the rate coefficient is small.

**Direct investigation of QOOH radicals** The single largest obstacle when studying ephemeral species such as QOOH radicals is their generation in sufficient quantities and purity. QOOH radicals are very short-lived transients in the R + O<sub>2</sub> → ROO → QOOH → P sequence, and, therefore, are never present in high enough concentrations when starting with an alkyl radical. We devised a new experimental strategy to make QOOH radicals: we reacted stable tert-butyl hydroperoxide (TBHP) molecules with photolytically generated Cl atoms at room temperature.



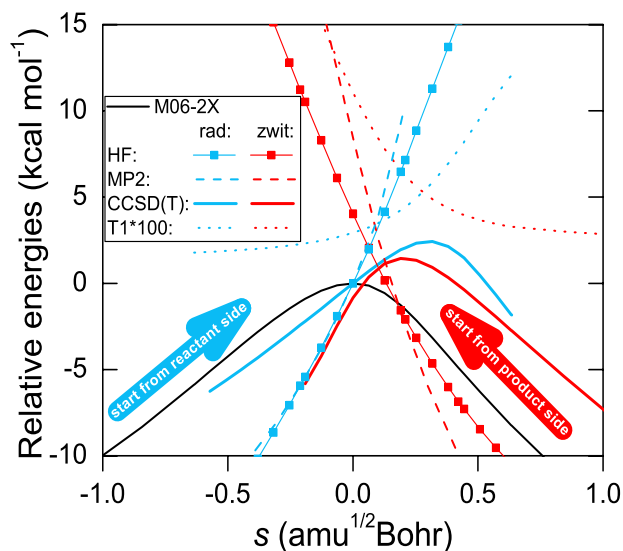
The QOOH radical that is produced, 2-hydroperoxy-2-methylprop-1-yl, dissociates exclusively to form the corresponding cyclic ether (2,2-dimethyl oxirane) + OH. The formation of QOOH was indeed demonstrated by multiplexed photoionization mass spectrometry (MPIMS) measurements by observing the formation of this cyclic ether as the major product species. However, we did not observe the PIE spectrum of this QOOH radical itself, because the structure of the neutral and cation are very different, leading to a poor Frank-Condon overlap. In the presence of oxygen, however, we were able to detect the related OOQOOH radical and record its PI spectrum. This is the first such PIE spectra in the literature. We have also determined the ionization mechanism of this substituted alkylperoxy radical, which was found to be fundamentally different from that of small unsubstituted alkylperoxy radicals.

In another set of experiments we measured OH concentration–time profiles using direct absorption, and were able to derive directly from the experiments rate coefficients for both the pressure dependent decomposition of this QOOH radical as well as for its association reaction with oxygen. The results were compared to, and confirmed by high-level theoretical kinetics calculations. This work breaks fresh ground for further studies on QOOH radicals, and helps build more accurate autoignition models, which critically depend on the chemistry of these short-lived species. These results have been submitted for publication.

**Unconventional peroxy chemistry and the role of low-lying zwitterionic states.** For the detailed modeling of combustion chemistry the possibility of unknown pathways is of continual concern, especially for biofuels, where the presence of oxygen atoms can significantly alter the chemical pathways. In our recent work we characterized a low-lying water elimination pathway from key QOOH radicals derived from alcohols. The corresponding saddle-point structure involves the interaction of radical and zwitterionic electronic states. This interaction presents extreme difficulties for electronic structure characterizations, as most standard methods produce two completely different potential curves depending on whether one starts with the corresponding orbital guesses from the reactant side or the product side. On the reactant side, the ROHF HOMO has the character of a carbon-centered radical orbital, while on the product side the HOMO has the character of an OO  $\sigma^*$  orbital associated with the breaking OO bond. The latter is a zwitterionic state and has a large dipole moment.

We demonstrated that the properties of this saddle point can be well captured by M06-2X and CCSD(T) methods, which methods produce comparable and low barrier heights. In the HF, MP2, CCSD and CCSD(T) progression the character of the calculated radical and zwitterionic states converge to each other, indicating the importance of excited states.

Experimental evidence for the existence and relevance of this pathway was shown using recently reported MPIMS data from our group on the low-temperature oxidation of isopentanol and isobutanol. In these systems, water elimination is a major pathway, and is likely ubiquitous in low-temperature alcohol oxidation. These findings will substantially alter current alcohol oxidation mechanisms. Moreover, the methods described will be useful for the more general phenomenon of interacting radical and zwitterionic states.



Electronic energy profiles along the M06-2X/6-311++G(d,p) IRC around the TS structure using either the radical (“rad”) or the zwitterionic (“zwit”) ROHF orbital guesses.

### III. FUTURE WORK

We continue our efforts to calculate more rigorous and accurate kinetic parameters to be used in combustion models. We plan to make progress on reactions involving OH radicals, especially in the

context of oxygenated biofuels, where hydrogen-bonding influences the kinetics. We also plan to explore possibilities to efficiently calculate state densities for coupled hindered rotors with multiple important minima in order to improve our results on the *n*-butanol + OH calculations. Also, in collaboration with Leonid Sheps and based on the propene + OH study, we started to study the reactions of the various butene isomers with OH, which can extend our knowledge on butanol chemistry. Another area of recent interest that we plan to contribute to is the oxidation of heterocycles,<sup>v</sup> where ring-opening pathways can result in significantly different reactivity compared to acyclic compounds.

The current work on uncertainty is only a first step towards understanding the uncertainty in the currently used models. In the future we would like to consider all of the parameters in a screening procedure to select the most important candidates systematically for the Bayesian inference study. Moreover, it would be important to explore better the inherent correlation of the molecular parameters as obtained from electronic structure calculations, and if possible, use this information both in the forward uncertainty propagation and the inference step. These correlations would be employed in the construction of the joint prior on the parameters. Such correlation will reduce the uncertainty predictions, and also point to weak points in the model more directly.

Building on my past LDRD project, I would like to bring to the program computational capabilities, which would enable the automated exploration of stationary points on potential energy surfaces for at least common reaction types encountered in combustion, and enable systematic studies on larger molecules.

#### IV. References

- i. Dunlop, J. R.; Tully, F. P., *J. Phys. Chem.* **1993**, *97*, 6457-6464.
- ii. Zádor, J.; Jasper, A. W.; Miller, J. A., *Phys. Chem. Chem. Phys.* **2009**, *11*, 11040-11053.
- iii. Devolder, P.; Fittschen, C.; Frenzel, A.; Hippler, H.; Poskrebshev, G.; Striebel, F.; Viskolcz, B., *Phys. Chem. Chem. Phys.* **1999**, *1*, 675-681.
- iv. Hansen, N.; Harper, M. R.; Green Jr., W. H., *Phys. Chem. Chem. Phys.* **2011**, *13*, 20262-20274.
- v. Roman-Leshkov, Y.; Barrett, C. J.; Liu, Z. Y.; Dumesic, J. A., *Nature* **2007**, *447*, 982-U985.

#### V. DOE supported publications, 2011-present

1. Zádor, J.; Huang, H.; Welz, O.; Zetterberg, J.; Osborn, D. L.; Taatjes, C. A. Directly measuring reaction kinetics of QOOH – a crucial but elusive intermediate in hydrocarbon autoignition. **submitted**.
2. Welz, O.; Klippenstein, S. J.; Harding, L. B.; Taatjes, C. A.; Zádor, J. Unconventional peroxy chemistry in alcohol oxidation: The water elimination pathway. *J. Phys. Chem. Lett.* **2013**, *4*, 350.
3. Zádor, J.; Miller, J. A., Unimolecular dissociation of hydroxypropyl and propoxy radicals. *Proc. Combust. Inst.* **2013**, *34*, 519-526.
4. Prager, J.; Najm, N. H.; Zádor, J., Uncertainty quantification in the ab initio rate-coefficient calculation for the  $\text{CH}_3\text{CH}(\text{OH})\text{CH}_3 + \text{OH} \rightarrow \text{CH}_3\text{C}(\text{OH})\text{CH}_3 + \text{H}_2\text{O}$  reaction. *Proc. Combust. Inst.* **2013**, *34*, 583-590.
5. Welz, O.; Zádor, J.; Savee, J. D.; Ng, M. Y.; Meloni, G.; Fernandes, R. X.; Sheps, L.; Simmons, B. A.; Lee, T. S.; Osborn, D. L.; Taatjes, C. A., Low-temperature combustion chemistry of biofuels: pathways in the initial low-temperature (550 K-750 K) oxidation chemistry of isopentanol. *Phys. Chem. Chem. Phys.* **2012**, *14*, 3112-3127.
6. Zádor, J.; Taatjes, C. A.; Fernandes, R. X., Kinetics of elementary reactions in low-temperature autoignition chemistry. *Prog. Energy Comb. Sci.* **2011**, *37*, 371-421.
7. Kappler, C.; Zádor, J.; Welz, O.; Fernandes, R. X.; Olzmann, M.; Taatjes, C. A., Competing channels in the propene + OH reaction: Experiment and validated modeling over a broad temperature and pressure range. *Z. Phys. Chem.* **2011**, *225*, 1271-1293.
8. Zádor, J.; Klippenstein, S. J.; Miller, J. A., Pressure-Dependent OH Yields in Alkene plus HO<sub>2</sub> Reactions: A Theoretical Study. *J. Phys. Chem. A* **2011**, *115*, 10218-10225.

# Isomer-specific Spectroscopy and Isomerization in Aromatic Fuels

*Timothy S. Zwier*

Department of Chemistry, Purdue University, West Lafayette, IN 47907-2084  
zwier@purdue.edu

## Program Definition and Scope

Under fuel-rich conditions, reactions that lead toward soot formation occur, with aromatic molecules and resonance-stabilized radicals playing key roles as intermediates. A key objective of this research program is to develop and utilize novel methods to characterize the spectroscopy and isomerization of conformational and structural isomers of aromatic derivatives, resonance-stabilized free radicals that play a role in combustion. We are also characterizing the spectroscopy of model lignin compounds both as neutrals and ions, with the goal of providing deeper insight to the chemistry involved in the combustion and pyrolysis of wood and biofuels. Double-resonance laser spectroscopies are being used to record single-conformation IR and UV spectra of the molecules and radicals, including UV-UV hole-burning and resonant ion-dip infrared (RIDIR) schemes. The scope of methods is expanding to include broadband microwave and cryocooled ion traps to explore reactive intermediates both as neutrals and ions.

## Recent Progress

### A. Toward a first principles model of the alkyl CH stretch region

The alkyl CH stretch region of the infrared is a region rich in information content, but a challenge to assign, due to the ubiquitous presence of strong Fermi resonance mixing between the alkyl CH stretch and CH bend overtone levels. Conformational assignments based on a comparison of the observed alkyl CH stretch spectra with *ab initio* predictions of harmonic frequencies often fail in spectacular fashion due to these Fermi resonances, which shift and split bands to the point that comparison with harmonic calculations is fruitless. Working in collaboration with Ned Sibert (UW-Madison), we are developing a first-principles model of the alkyl CH stretch region built around a reduced dimension Hamiltonian in which anharmonic CH stretches and scissor modes are Fermi coupled. Using IR-UV double resonance spectroscopy of jet-cooled molecules, our group is recording single-conformation infrared spectra of hydrocarbons containing alkyl and ether chains that serve as benchmark data for comparison with theory. The phenyl capped alkyl and alkoxy chains present in 1,2-diphenylethane ( $C_6H_5-CH_2-CH_2-C_6H_5$ , DPE) and 1,2-diphenoxyethane ( $C_6H_5-O-CH_2-CH_2-O-C_6H_5$ , DPOE) have served as initial model conformationally flexible chains, which contain only  $CH_2$  groups, and therefore are easier to model theoretically. We have obtained high-quality infrared spectra extending from the alkyl CH stretch region down to about  $1000\text{ cm}^{-1}$ , thereby encompassing both the scissors fundamentals and the alkyl CH stretch/scissor overtone regions. The theoretical model is able to account for the experimental CH stretch spectra of both molecules in significant detail. Two manuscripts describing this work were recently completed (papers 6, 7).

### B. Vibronic coupling in near-degenerate excited states

Beyond their role in modeling alkyl CH stretch spectra, the flexible bichromophore DPOE have served a dual purpose as a benchmark system in which to study vibronic coupling involving the two aromatic chromophores present in the molecules. We have carried out a detailed spectroscopic characterization of DPOE in the region of its  $S_1/S_2$  states. Using a combination of resonant two-photon ionization (R2PI), UV-holeburning, and dispersed fluorescence spectra, we

have characterized the unusual spectroscopic consequences of vibronic coupling on the vibronic spectroscopy. Based on the vibronic level data of both the all  $^{12}\text{C}$  and singly  $^{13}\text{C}$ -substituted molecules, when combined with high resolution UV data taken in collaboration with David Plusquellic at NIST, we have determined that the two conformers of DPOE have electronic origins that are split by no more than  $1\text{ cm}^{-1}$  from one another. Despite the symmetric environments of the two chromophores in the conformers, even a single  $^{13}\text{C}$  atom induces sufficient asymmetry in the zero-point energies of the two rings to significantly localize the electronic excitation on one or the other ring. DPOE is thus in the extreme limit of weak vibronic coupling. We see these studies as relevant to the more general circumstance in which two potential energy surfaces are in close proximity over extended regions of the surface, as occurs, for instance, anytime two surfaces share the same asymptote.

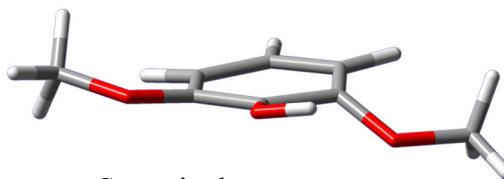
In these symmetric bichromophores, the vibronically coupled states are best treated in an adiabatic model in which the excitonic splitting is treated as a tunneling splitting between  $|A^*B\rangle$  and  $|AB^*\rangle$  on the double minimum potential well associated with the lower adiabatic surface. The magnitude of this tunneling splitting is determined by vibronic effects associated with the nuclear reorganization and electronic energy transfer between the two aromatic rings. A manuscript describing this work is currently nearing completion.

### C. Resonance-stabilized radicals

We also continue to pursue isomer-specific and conformation-specific spectroscopy of resonance-stabilized radicals. We have had for some time now a beautiful data set of R2PI, LIF excitation, dispersed fluorescence, and alkyl CH stretch infrared spectra of  $\alpha$ -methylbenzyl radical  $\text{C}_6\text{H}_5\text{-}\dot{\text{C}}\text{H-CH}_3$  in both ground and excited states. Our interest in this radical is fueled by the fact that the methyl radical rocks against the primary radical site of this resonance-stabilized radicals. We have fit the internal rotor structure present in the radical to determine both ground and excited state barriers to methyl internal rotation. The best-fit methyl rotor potential in the ground electronic state ( $D_0$ ) is a flat-topped three-fold potential ( $V_3'' = 151\text{ cm}^{-1}$ ,  $V_6'' = 34\text{ cm}^{-1}$ ) while the  $D_1$  state has a lower barrier ( $V_3' = 72\text{ cm}^{-1}$ ,  $V_6' = 15\text{ cm}^{-1}$ ) with  $\Delta\phi = \pi$ , indicating that the preferred methyl orientation flips between ground and excited state. Completion of this work has been slowed by the exceptional challenge associated with prediction of the barriers to internal rotation in excited states of radicals, especially in this case where  $D_1$  and  $D_2$  states are in close proximity. We are currently collaborating with Lyudmila Slipchenko on excited state calculations that are poised to bring this work to completion.

### D. Model lignin compounds and biofuels

Lignin is an aromatic-rich biopolymer that is second in natural abundance only to cellulose. It encases cellulose, providing an architectural framework for the plant, providing needed resistance to degradation, but also hindering the extraction of biofuels from the plant material. Its complex structure belies the fact that it is composed of only three monomers: p-coumaryl alcohol, coniferyl alcohol, and sinapyl alcohol. Enzyme-catalyzed radical polymerization of these monomers leads to a variety of chemical linkages. Among the important degradation products in the combustion and pyrolysis of wood are methoxyphenols, the aromatic chromophore pervasive to lignin, shared by the three monolignols. The spectroscopy of a series of simple methoxyphenols shows a striking sensitivity to the position and number of OH and/or  $\text{OCH}_3$  groups on the aromatic ring. As the figure to the right shows, in



$S_1$  excited state structure of 2,6-dimethoxyphenol.

the  $S_1$  excited state of 2,6-dimethoxyphenol (the chromophore of sinapyl alcohol), the aromatic ring and substitutions buckle out-of-plane, producing long Franck-Condon progressions in the UV characteristic of the large geometry change. We have extensive data sets on the UV spectroscopy of a series of model methoxyphenols, two lignin dimers, sinapic acid, and sinapoyl malate, all of which are pervasive in plants and relevant to lignin degradation. These results are in various stages of preparation for publication.

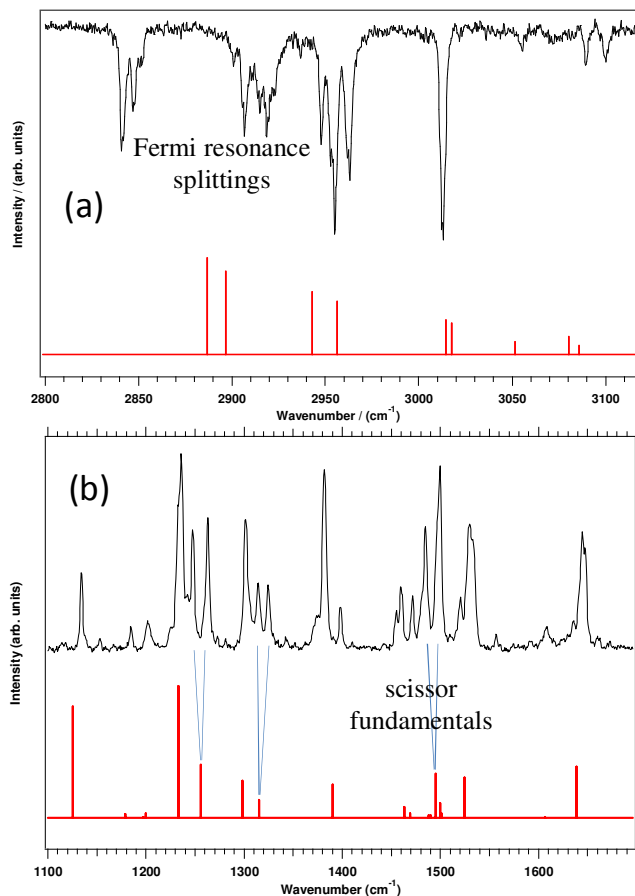


Figure 1. (a) Alkyl CH stretch and (b) mid-IR RIDIR spectra of 2,6-dimethoxyphenol.

## Future Work

The methoxyphenols will serve as a starting point for extending the alkyl CH stretch models to include the methyl group. We have both mid-IR and alkyl CH stretch spectra of a series of methoxyphenols with high signal-to-noise ratio (see, e.g., Figure 1).

We are pursuing several new directions that we hope will add significantly to the scope and impact of our DOE research. A hyperthermal nozzle has been built and tested as a source for new radicals and reactive combustion intermediates. This nozzle can be used to study the pyrolysis of model biofuels, and to characterize the spectroscopy of the intermediates. As an illustration, Figure 2 shows a series of VUV photoionization mass spectra of the pyrolysis of 2,5-dimethylfuran, a model biofuel, using the hyperthermal nozzle.

We plan to combine the hyperthermal nozzle with chirped-pulse Fourier transform microwave (CP-FTMW) detection of the pyrolysis intermediates, with a bandwidth from 7.5-

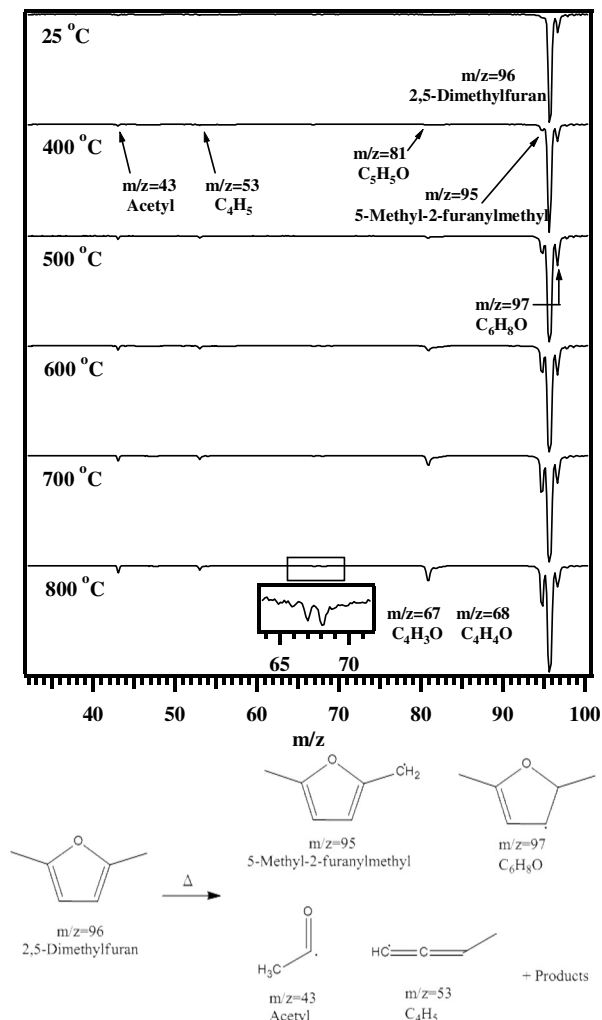


Figure 2. 118 nm VUV photoionization TOFMS of pyrolysis of 2,5-dimethylfuran.

18.5 GHz. This general and powerful detection scheme is complementary to LIF or R2PI detection in not requiring an electronic chromophore, and is ideally suited for detection of reactive intermediates via their rotational spectra. We have initiated a collaboration with the G.B. Ellison and John Stanton groups to use the hyperthermal nozzle/CP-FTMW instrument to obtain spectra of a series of isotopomers of cyclopentenone, with the goal of obtaining atomic positions for all its atoms via Kraitchman analysis.

Finally, a new multi-stage mass spectrometer with a cryo-cooled 22-pole ion trap is now in full operation, opening up a vast array of ions to conformation-specific infrared and ultraviolet spectroscopy. To date, we have recorded UV photofragment spectra of protonated peptide ions that demonstrate cooling down to  $\sim 10$  K, and have obtained single-conformation infrared spectra using IR depletion of the photofragment signal. We hope soon to begin exploring the UV and conformation-specific IR spectra of model lignin oligomer ions as a part of our DOE project. Our longer-term goal is to see whether wavelength-selective photofragmentation can be used to diagnose sequences of lignin oligomers, using the unique absorption properties of the multiple chromophores present in the oligomers to selectively excite and fragment at different positions along the lignin backbone.

## Publications acknowledging DOE support, 2011-present

1. Joshua A. Sebree, Nathan Kidwell, Evan G. Buchanan, Marek Zgierski, and Timothy S. Zwier, "Spectroscopy and Ionization Thresholds of  $\pi$ -Isoelectronic 1-Phenylallyl and Benzylallenyl Resonance Stabilized Radicals", *Chemical Science*, **2**, 1746-1754 (2011).
2. Chirantha P. Rodrigo, William H. James III, and Timothy S. Zwier, "Single-conformation ultraviolet and infrared spectra of jet-cooled monolignols: p-coumaryl alcohol, coniferyl alcohol, and sinapyl alcohol", *J. Am. Chem. Soc.* **133**, 2632-2641 (2011).
3. Chirantha P. Rodrigo, Christian W. Müller, Nathan R. Pillsbury, William H. James III, Timothy S. Zwier, and David F. Plusquellic, "Conformer-specific vibronic spectroscopy and vibronic coupling in a flexible bichromophore: bis-(4-hydroxyphenyl)methane", *J. Chem. Phys.* **134**, 164312 (2011).
4. Shin G. Chou, Chirantha P. Rodrigo, Christian W. Müller, Kevin O. Douglass, Timothy S. Zwier, and David F. Plusquellic, "Rotationally resolved  $C_2$  symmetric conformers of bis-(4-hydroxyphenyl)-methane: Prototypical examples of Excitonic coupling in the  $S_1$  and  $S_2$  Electronic States", *J. Phys. Chem. A* **115**, 9643-9652 (2011).
5. Jacob C. Dean, Deepali Mehta, William H. James III, and Timothy S. Zwier, "Conformation-specific spectroscopy and populations of diastereomers of a model monolignol derivative: Chiral effects in a triol chain", *J. Phys. Chem. A* **115**, 8464-8478 (2011).
6. Evan G. Buchanan, Jacob C. Daen, Timothy S. Zwier, and Edwin L. Sibert III, "Towards a first-principles model of Fermi resonances in the alkyl CH stretch region: Application to 1,2-diphenylethane and 2,2,2-paracyclophane", *J. Chem. Phys.* **134**, 064308 (2013). 11 pages.
7. Evan G. Buchanan, Edwin L. Sibert III, and Timothy S. Zwier, "Ground state conformational preferences and CH stretch-bend coupling in a model alkoxy chain: 1,2-diphenoxyethane", *J. Phys. Chem. A* (accepted).